Life cycle of the Cabo Verde Archipelago: Growth and denudation of seamounts and islands

Dissertation
zur Erlangung des Doktorgrades Dr. rer. nat.
der Mathematisch-Naturwissenschaftlichen Fakultät
der Christian-Albrechts-Universität zu Kiel

vorgelegt von

Lisa Katharina Samrock

Kiel, October 2022

Erster Gutachter und Betreuer:	PD Dr. Thor Hansteen
Zweiter Gutachter:	Prof. Dr. Romain Bousquet
Eingereicht am:	10. Oktober 2022
Tag der Disputation:	14. Dezember 2022

Eidesstattliche Erklärung

Hiermit erkläre ich, dass die vorliegende Abhandlung, abgesehen von der Beratung durch meine Betreuer, nach Inhalt und Form die eigene Arbeit ist.

Teile dieser Arbeit wurden bereits in wissenschaftlichen Fachzeitschriften veröffentlicht, und Kurzfassungen mit gleichem wissenschaftlichem Inhalt wurden im Rahmen von Konferenzbeiträgen veröffentlicht. Diese oder eine ähnliche Arbeit wurde weder in Teilen noch in ganzer Form einer anderen Abteilung oder Hochschule im Rahmen eines Prüfungsverfahrens vorgelegt.

Ferner versichere ich, dass diese Arbeit unter Einhaltung der Regeln der guten wissenschaftlichen Praxis der Deutschen Forschungsgemeinschaft entstanden ist.

Es wurde kein akademischer Grad entzogen.

Ravensburg, 10. Oktober 2022 Lisa Katharina Samrock

Summary

Ocean island archipelagos consist of islands and seamounts that originate from hot spot related volcanism. The evolution of ocean island archipelagos is determined by a complex interplay between plume dynamics, geodynamic and magmatic processes, and external factors such as sea level changes. Their study provides an important insight into processes and dynamics in Earth's mantle and crust. As they are prone to natural hazards, the understanding of ocean islands and their development over time is important for the prediction of hazards and risk management in ocean island archipelagos. It is therefore important to combine different data sets from various evolutionary stages and different locations in order to understand the geological evolution of an archipelago over time.

The Cabo Verde Archipelago, located in the Atlantic Ocean off the west coast of Africa, offers a unique location to study ocean island volcanism: The islands and seamounts are in different stages of evolution and mature islands are well-eroded, exposing also early stages of volcanism. Therefore, they represent an excellent location to study a hot spot related archipelago. So far, studies on the geology of the Cabo Verdes focused on the different islands of the archipelago. Little is known about the submarine realm of the archipelago due to its limited accessibility. Especially geochronological data is only available for the islands. Understanding of the temporal evolution of the archipelago is therefore limited and incomplete.

Aim of this thesis was to take a regional approach and to combine data and observations from both, Cabo Verde Seamounts and Islands, to gain a better understanding of the geological and geodynamic evolution of the archipelago. Both, the early magmatic-tectonic evolution as well as the later Pliocene phases of evolution, were investigated using selected samples and observations from submarine and subaerial edifices.

To study the submarine part of the Cabo Verde Archipelago, five lava samples from the phonolitic Cadamosto Seamount located in the SW of the archipelago, were ^{40}Ar-^{39}Ar dated (Samrock et al. 2019, Chapter 2). Sanidine, nepheline and sodalite-group minerals were dated and the chemical zonation patterns in these minerals were determined by electron microprobe analyses. The combined geochronological and petrological observations reveal young sanidine eruption ages at Cadamosto Seamount preserved in phenocrysts with a combined mean age of 21.14 ± 0.62 ka (2σ errors). This volcanic eruption period falls in the Last Glacial Maximum, a period dominated by sea level lowstands. We therefore suggest enhanced submarine eruption activity due to rapid unloading of the crust. Maximum eruption ages of 51.8± 2.4 ka and 97± 14 ka are recorded in some samples with complex zoned sanidines with antecrystic resorbed cores and phenocrystic rims. Older magmatic events are also recorded in sanidine and nepheline antecrysts in theses samples, with antecryst minimum ages extending back to 1.5215± 0.0083 Ma.

To study the early magmatic-tectonic evolution of the Cabo Verde seamounts, the extinct Nova Holanda (Senghor) Seamount in the NE of the archipelago was investigated. Sanidines and phlogopites from a pillow lava sample yield a ^{40}Ar-^{39}Ar weighted mean age of 14.872 ± 0.027 Ma (2σ; Kwasnitschka et al. in prep.).

To reconstruct the evolution of a mature ocean island, Maio Island (East) was investigated. Field observations were combined with ^{40}Ar-^{39}Ar geochronology, biostratigraphy, structural geology and petrology. Maio Island comprises uplifted Early-Mesozoic mid-ocean ridge basalt-type pillow lavas (Batalha Formation) and exposes the only deep-sea sedimentary sequences of the archipelago (Morro and Carqueijo Formations), representing early Atlantic Ocean floor. Investigations of the fossil assemblages and a revision of the biostratigraphy suggest that the Batalha Formation has an Early Cretaceous age (Chapter 5). The overlying pelagic limestones of the Morro Formation contain a Valanginian to Early Aptian fauna attributed to the widespread Maiolica facies of the Western Tethys Ocean. The overlying limestones and marls of the Carqueijo Formation yield Aptian to Cenomanian nannofossils and record important information on the evolution and paleo-oceanographic conditions of the young evolving Atlantic Ocean.

The pre-volcanic sequences are unconformably overlain and intruded by Miocene igneous rocks. New phlogopite ^{40}Ar-^{39}Ar ages from nosean nephelinite dykes cutting the Mesozoic strata, combined

with existing K-Ar and ^{40}Ar-^{39}Ar ages, confirm a period of intense growth of an igneous core complex in the middle to upper crust between ~16 and 8.7 Ma. This period is characterized by numerous intrusive events and is associated with semi-circular doming and disruption of the Mesozoic strata. Extensive polymict conglomerates occur below the Late Miocene Monte Penoso Formation. They are re-interpreted as landslide deposits with a maximum ^{40}Ar–^{39}Ar age of 8.666 ± 0.0274 Ma, confining a period of large-scale flank collapses and erosion to between 8.7 to 6.7 Ma. This erosive period may have rejuvenated the igneous activity due to decompressional melting, i.e., resulting in the formation of the Tortonian/Messinian Monte Penoso and Malhada Pedra Formations (Samrock et al. 2022, Chapter 3). A recent phase of uplift is recorded in a Pleistocene large-scale fossil dune located in the East of Maio Island. The dune consists of carbonaceous sandstones and arenites (Samrock et al. 2018, Chapter 4). Changes in the cross-stratification and dune geometry patterns from the lower and upper part of the dune recorded changes in the paleo-environmental conditions.

The 14.872 ± 0.027 Ma age from Nova Holanda (Senghor) Seamount in the NE of the archipelago suggests that this seamount was in a late evolutionary stage, while Maio was in a period of intense growth and enhanced magmatic activity. In combination with the Pleistocene ages from Cadamosto Seamount and current seismic and volcanic activity patterns in the West of the archipelago, these old Nova Holanda (Senghor) Seamount ages support the NE-SW oriented age progression of magmatism observed in the Cabo Verde Archipelago.

The thesis provides the first geochronological data of the Cabo Verde seamounts. The observations from both the submarine and subaerial study locations provide important insights to different phases of the magmatic-tectonic evolution of the archipelago and add to a better understanding of ocean island evolution worldwide.

Kurzfassung

Ozeaninselarchipele bestehen aus Inseln und Seamounts (Seebergen), die durch Hot Spot Vulkanismus entstanden sind. Die Entwicklung von Inselarchipelen wird durch ein komplexes Zusammenspiel von Mantelplumedynamik, Geodynamik und magmatischen Prozessen sowie externen Einflüssen wie Meeresspiegelschwankungen bestimmt. Ihre Untersuchung liefert wichtige Einblicke in die Prozesse und Dynamik von Erdmantel und Kruste. Da Ozeaninseln anfällig für Naturgefahren sind, ist es essenziell ihre Entstehung zu verstehen, um Gefahrenabschätzungen und das Risikomanagement auf Inselarchipelen besser gestalten zu können. Für die Rekonstruktion der geologische Entwicklung der Inselarchipele ist es wichtig, verschiedene Datensätze der einzelnen Entwicklungsstufen von unterschiedlichen Lokalitäten zu kombinieren.

Die im Atlantik vor der Westküste Afrikas gelegene Inselgruppe der Kapverden bietet einen einzigartigen Standort zur Untersuchung des Inselvulkanismus: Die Inseln und Seamounts befinden sich in unterschiedlichen Entwicklungsstadien und die älteren Inseln sind stark erodiert, so dass auch frühe Stadien des Vulkanismus freigelegt sind. Daher sind sie ein ausgezeichnete Region, um Hot Spot Vulkanismus zu. Bisher lag der Schwerpunkt geologischer Studien der Kapverden auf der Untersuchung der Landflächen. Über den submarinen Bereich des Archipels ist aufgrund der begrenzten Zugänglichkeit nur wenig bekannt. Da geochronologische Daten bisher nur für die Landflächen der Inseln vorliegen, ist das Wissen über die zeitliche Entwicklung des Archipels begrenzt und unvollständig.

Ziel dieser Dissertation war ein regionaler Ansatz, bei dem verschiedene Datensätze und Beobachtungen sowohl von kapverdischen Inseln als auch Seamounts kombiniert wurden, um die geologische und geodynamische Entwicklung des Archipels besser zu verstehen. Sowohl die frühe magmatisch-tektonische Entwicklung als auch die späten Pliozänen Entwicklungsphasen wurden mit Hilfe ausgesuchter Proben und Beobachtungen von submarinen und subaerischen Vulkangebäuden untersucht.

Um den submarinen Teil des Archipels zu untersuchen, wurden fünf Lavaproben des phonolitische Cadamosto Seamount im SW der Kapverden ^{40}Ar-^{39}Ar datiert (Samrock et al. 2019, Kapitel 2). Sanidine, Nepheline und Sodalith-Gruppen Minerale wurden datiert und ihre chemischen Zonierungsmuster wurden mit der Elektronenstrahlmikrosonde analysiert. Die geochronologischen und petrologischen Beobachtungen offenbaren junge Sanidin-Eruptionsalter des Cadamosto Seamount, die in Phänokristallen mit einem Durchschnittsalter von 21.14 ± 0.62 ka (2σ Fehler) enthalten sind. Diese vulkanische Eruptionsphase fällt in das letzte glaziale Maximum, eine Phase niedriger Meeresspiegel. Dies deutet darauf hin, dass die schnelle Entlastung der Erdkruste zu erhöhter submariner Eruptionsaktivität geführt hat. Maximale Eruptionsalter von 51.8± 2.4 ka und 97± 14 ka wurden in einigen Proben verzeichnet, die komplex zonierte Sanidine mit antekristischen resorbierten Kernen und phenokristischen Rändern enthalten. In diesen Proben wurden auch ältere magmatische Ereignisse in Sanidin- und Nephelin-Antekristallen verzeichnet, deren Mindestalter bis zu 1.5215± 0.0083 Ma zurück reicht.

Um die frühe magmatisch-tektonische Entwicklung der kapverdischen Seamounts zu untersuchen, wurde der erloschene Nova Holanda (Senghor) Seamount im NE des Archipels gewählt. Sanidine und Phlogopite einer Kissenlava liefern ein gewichtetes mittleres ^{40}Ar-^{39}Ar-Alter von 14.872 ± 0.027 Ma (2σ; Kwasnitschka et al. in prep.).

Um die verschiedenen Entwicklungsstufen einer ausgewachsenen Ozeaninsel zu untersuchen, wurde die Insel Maio im Osten des Archipels erforscht. Geländebeobachtungen wurden mit ^{40}Ar-^{39}Ar Geochronologie, Biostratigraphie, Strukturgeologie und Petrologie kombiniert. Die Insel Maio umfasst gehobene Frühmesozoische MORB-Kissenlaven (Batalha-Formation) und die einzigen sedimentären Abfolgen der Tiefsee im Archipel (Morro- und Carqueijo-Formationen), die den frühen atlantischen Meeresboden darstellen. Untersuchungen des Fossilienbestands und eine Überprüfung der Biostratigraphie deuten darauf hin, dass die Batalha-Formation ein frühes kreidezeitliches Alter hat (Kapitel 5). Die überlagernden pelagischen Kalksteine der Morro-Formation enthalten eine Fauna des Valangin bis frühen Apt, die der weit verbreiteten Maiolica-Fazies des westlichen Tethys-Ozeans zugeordnet wird. Die überlagernden Kalksteine und Mergel der Carqueijo-Formation enthalten

Nannofossilien aus dem Aptikum bis Cenomanium und liefern wichtige Informationen über die Entwicklung und die paläoozeanografischen Bedingungen des jungen, sich entwickelnden Atlantiks.

Die prävulkanischen Abfolgen werden von magmatischen Gesteinen des Miozän diskordant überlagert und intrudiert. Neue ^{40}Ar-^{39}Ar Alter von Phlogopit in Nosean-Nephelinit-Gängen, die die mesozoischen Schichten schneiden, kombiniert mit existierenden K-Ar und ^{40}Ar-^{39}Ar Altern, bestätigen einen Zeitraum intensiven Wachstums eines magmatischen Kernkomplexes in der mittleren bis oberen Kruste zwischen ~16 und 8.7 Ma. Diese Phase ist durch zahlreiche Intrusionen gekennzeichnet und steht im Zusammenhang mit einer halbkreisförmigen Wölbung und Störung der mesozoischen Schichten. Ausgedehnte polymiktische Konglomerate, die unter der Monte Penoso-Formation des späten Miozän liegen, werden als Ablagerungen von Erdrutschen interpretiert. Diese haben ein ^{40}Ar-^{39}Ar-Höchstalter von 8.666 ± 0.0274 Ma, was großskalige Flankenstürze und Phasen der Erosion auf einen Zeitraum von 8.7 bis 6.7 Ma eingrenzt. Diese erosive Phase könnte die jüngere magmatische Aktivität durch Dekompressionsschmelze ausgelöst haben, was zur Bildung der tortonisch/messinianischen Monte Penoso- und Malhada Pedra-Formationen führte (Samrock et al. 2022, Kapitel 3).

In einer großflächigen pleistozänen Düne, die sich im Osten der Insel Maio befindet, ist eine jüngere Phase der Hebung zu verzeichnen. Die fossile Düne besteht aus karbonatischem Sandstein und Areniten (Samrock et al. 2018, Kapitel 4). Veränderungen der Schrägschichtungs- und Dünengeometriemuster im unteren und oberen Teil der Düne dokumentieren Änderungen der Paläo-Umweltbedingungen.

Das Alter von 14.872 ± 0.027 Ma für den Nova Holanda (Senghor) Seamount im Nordosten des Archipels deutet darauf hin, dass sich dieser Seamount in einer späten Entwicklungsphase befand, während sich die Insel Maio in einer Phase intensiven Wachstums und erhöhter magmatischer Aktivität befand. Kombiniert mit den pleistozänen Altern des Cadamosto Seamounts und den aktuellen seismischen und vulkanischen Aktivitäten im westlichen Teil des Archipels stützen diese alten Nova Holanda (Senghor) Seamount Alter eine NO nach SW ausgerichtete Altersentwicklung des Magmatismus im Kapverden Archipel.

Diese Dissertation präsentiert die ersten geochronologischen Daten für kapverdische Seamounts. Die Ergebnisse von sowohl submarinen als auch subaerialen Forschungslokalitäten liefern wichtige Einblicke in die verschiedenen Phasen der magmatisch-tektonischen Entwicklung des Archipels und können daher zu einem besseren Verständnis der Entwicklung von Ozeaninseln weltweiten beitragen.

List of Abbreviations

$^{40}Ar/^{36}Ar_i$	Initial $^{40}Ar/^{36}Ar$ ratio
$^{40}Ar^*$	Radiogenic ^{40}Ar
AI	$^{36}Ar/^{39}Ar$ alteration index
a.s.l.	Above sea level
AMS	Accelerator mass spectrometry
BSE image	Backscattered electron image
b.s.l	Below sea level
CIC	Central Intrusive Complex
DMM	Depleted MORB mantle
EM1	Enriched mantle 1
EMP	Electron microprobe
Fm.	Formation
GMRT	Global Multi-Resolution Topography
HIMU	High μ ($^{206}Pb/^{204}Pb$ ratios > 19.5)
High-T	High temperature
MCTF	Multi-crystal total-fusion
MORB	Mid-ocean ridge basalt
MSWD	Mean square weighted deviation
Mte.	Monte (portuguese for mount)
Or	Mol% orthoclase
P	Probability
Rib.	Ribeira (portuguese for creek)
ROV	Remote operated vehicle
SCTF	Single-crystal total-fusion
SF	Spreading factor
SH	Step-heating
SRTM	Shuttle Radar Topographic Mission
TCS2	Taylor Creek sanidine 2
WD	Wavelength dispersive
WMA	Weighted mean age
Wt% K (EMP)	Weight % K (derived from EMP data)
Wt% K (^{39}Ar)	Weight % K (derived from $^{39}Ar_K$ ^{40}Ar-^{39}Ar analyses)

List of Content

1 Introduction

Intraplate ocean islands are of volcanic origin and therefore provide a unique opportunity to study Earth's interior, including crustal processes and mantle dynamics. Many ocean islands are associated with mantle plumes that transport material from the deep mantle to the surface, and are thus indirectly related to recycling of subducted lithosphere. However, a large number of ocean islands are not directly associated with thermal mantle anomalies and may originate from a combination of tectonic processes and compositional mantle heterogeneities.

Ocean islands typically occur in archipelagos, which consist of both, subaerial islands and submarine seamounts. The latter are usually less studied due to their limited accessibility. The Cabo Verde Archipelago, located in the Atlantic Ocean, is a prominent example of an oceanic archipelago and the focus area of this thesis. Other well-studied examples include the Canary Islands and Azores in the Atlantic Ocean, and the Hawaiian Archipelago in the Pacific Ocean.

The evolution of islands and seamounts of major archipelagos is influenced by a complex interplay between plume dynamics, tectonics, magmatic processes and external factors such as sea level changes over time. It is therefore essential to combine data from different research fields and from different evolutionary stages of islands and seamounts in order to understand the archipelago evolution over time. Understanding the different processes involved in the growth and destruction of ocean islands also helps to understand the natural hazards and risks prevailing at different evolutionary stages. Potential hazards common on ocean islands are volcanic eruptions, landslides and flank collapses. These hazards not only regionally affect the archipelagos, but may also encompass ocean basin scales through potential tsunamis. Ocean islands are exceptional places to live, and provide unique terrestrial and marine ecosystems.

1.1 Evolutionary stages of ocean islands

Several evolutionary stages of ocean islands are distinguished, which relate to changing magma production rates, magma composition, and the changing balance between growth and erosion rates. They were first defined for the Hawaiian Archipelago (e.g., Clague and Dalrymple 1987, Moore and Clague 1992), which is one of the most prominent examples of ocean island archipelagos. Later, the Hawaiian model has been refined and modified for the Atlantic Ocean archipelagos to account for differences, in factors such as in the speed of plate motions, magma supply and composition at different stages, or rates of subsidence (e.g., Carracedo 1999, Ramalho 2011).

The general model for volcanic ocean islands usually distinguishes the following eight different stages of evolution (Ramalho 2011, Kwasnitschka et al. in prep.):

1) Seamount stage:

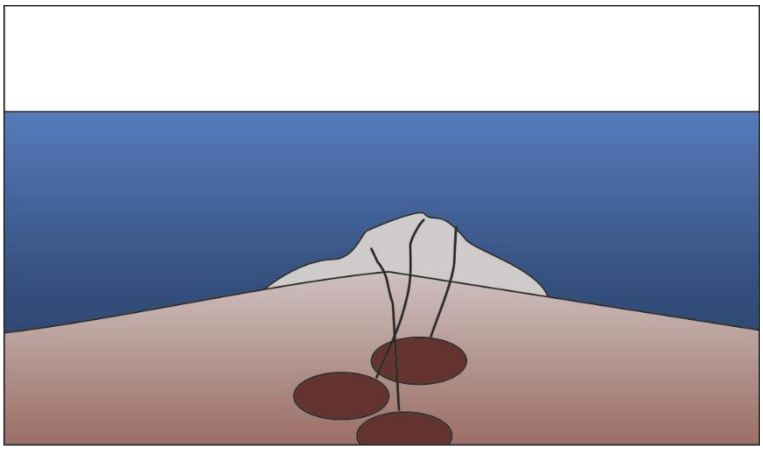

In the seamount stage, volcanism is initiated and an edifice starts to grow at the seafloor. If volcanism takes place below the critical depth for explosive volcanism, eruptions are characterized by effusive products (lava flows). At intermediate and shallow water depths, the vesicularity of lavas increases and explosive activity is possible, leading to deposition of hyaloclastites and pyroclastic material. In some occasions (e.g., in the Canaries and Cabo Verdes) remnant seamounts can be found on deeply eroded mature ocean islands, but further volcanic activity may overprint the remnants of this early evolutionary stage. In that case, studying the submarine stage of an archipelago is limited to the submarine realm.

2) Emergent island stage:

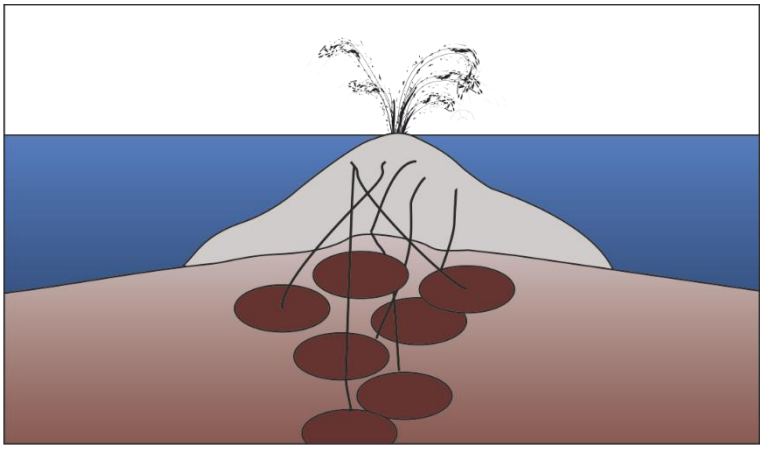

If a seamount edifice reaches the water surface (or just below), a complex interplay between volcanic activity and marine erosion shapes the edifice at the emergent island stage. Typical deposits of this stage are volcaniclastic deposits that originate from surtseayan-type eruptions, transport and re-sedimentation processes. Remnants are usually overprinted by later-stage volcanic activity.

3) Shield building stage:

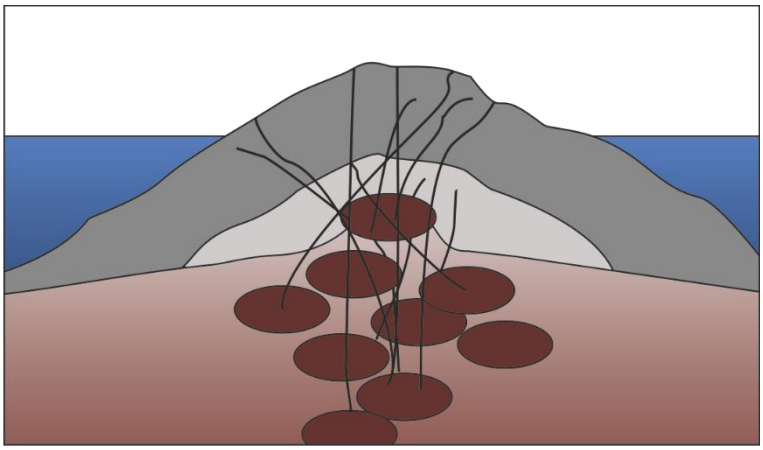

At the shield building stage, an island has developed and subaerial volcanic activity prevails. This subaerial volcanism is characterized by Strombolian- and/or Hawaiian-type effusive activity. Thick sequences of interlayered lava flows lead to massive growth of the island flanks. Where subaerial lava flows meet the shoreline, lava deltas form and produce pillow lavas and hyaloclastites. Intrusive activity and the emplacement of dykes further leads to growth of the edifice from the inside (Barker et al. 2021). Remnants of the shield building stage can be studied on mature ocean islands and during their active phase.

4) Capping stage

The capping stage may occur at the end of the shield building stage, if abrupt changes in magma composition or eruption rates occur. However, this stage cannot always be distinguished from the shield building stage in the Atlantic archipelagos. It is more pronounced in some Hawaiian examples, where the tholeiitic shield-stage volcanism shifts to alkalic magmas at the capping/post-shield stage (Silva and Lindsay 2015). In the Atlantic archipelagos (Canaries, Cabo Verdes), magma compositions are variable in all stages and do not necessarily show such a strong contrast as in the Hawaiian Archipelago (Carracedo 1999).

5) Erosional stage:

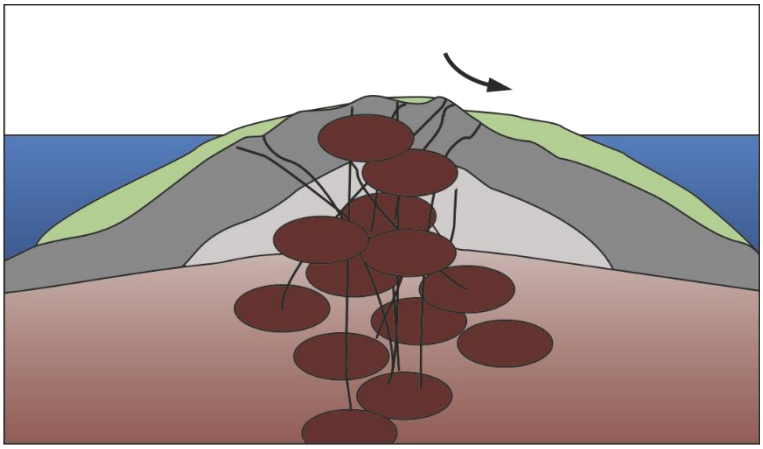

Once the productive volcanic activity of the shield building stage (or capping stage) has ceased, a phase of volcanic quiescence and erosion begins. This is associated with erosive landforms shaping the islands. Flank collapse events may occur, gradually destroying the edifice.

6) Rejuvenated (post-erosional) stage:

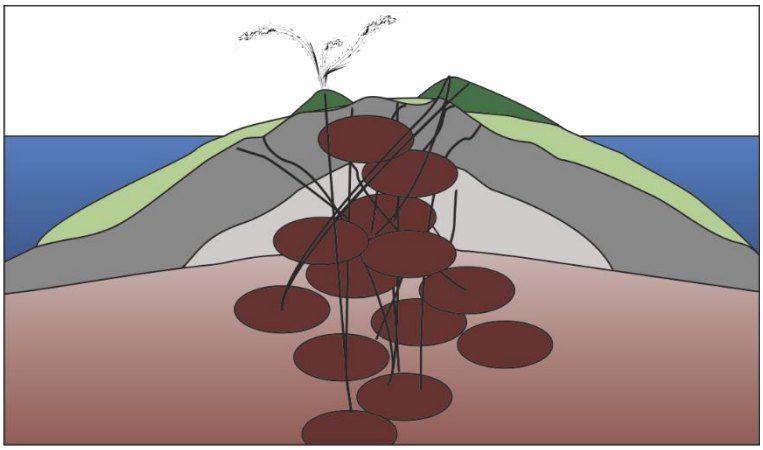

The erosional stage is ended by renewed volcanism, representing the rejuvenated or post-erosional stage. In some locations, several cycles of rejuvenated volcanism can be observed. The rejuvenated stage is characterized by comparatively low volumes of alkalic magmas that form valley-filling sequences and coastal lava deltas (Carracedo 1999).

7) Razed island (atoll) stage:

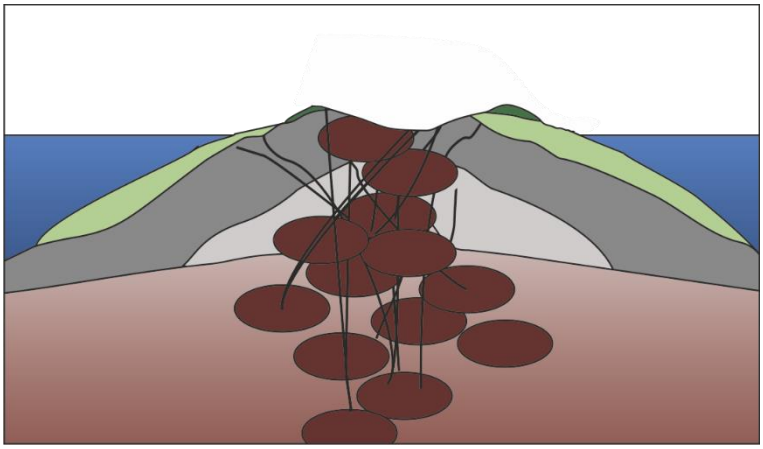

After volcanic activity has ceased, the edifice is slowly ablated and eroded. Fluvial and marine erosion lead to flat, razed island morphologies with only little relief. If the edifice subsides, coral growth may lead to the formation of atolls.

8) Drowned island (guyot) stage:

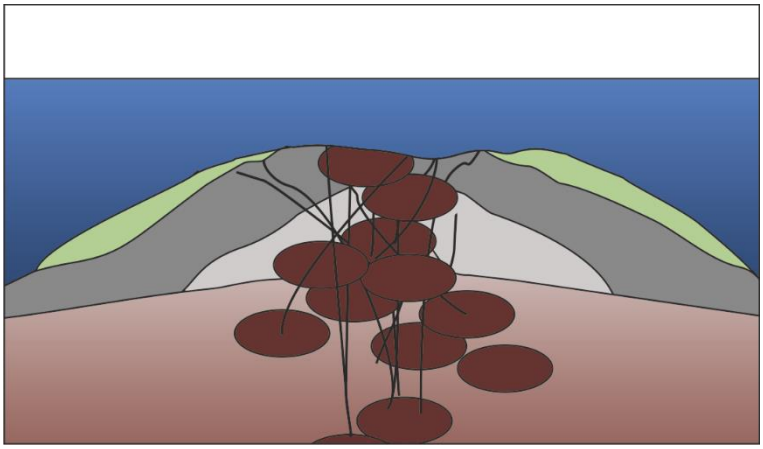

A guyot is formed, if subsidence or erosion cause the former islands to submerge below sea level. In case subsidence is not significant, erosion is the dominant process: Once the former island has been truncated by long term erosion, marine erosion forms a wave cut morphology. Eventually, the island submerges and a flat-topped guyot is formed.

Parallel volcanic activity on several islands and seamounts can be observed for example in the Atlantic archipelagos (Canaries, Cabo Verdes), whereas only the youngest end of the volcanic chain is active in the Hawaiian Archipelago, leading to a linear age distribution (e.g., Carracedo 1999). This observation has been attributed to the slow-moving plate in the Atlantic Ocean and is especially pronounced in the Cabo Verde Archipelago. Further differences that led to amendment of the Hawaiian model of evolution are the different time scales of processes and island life spans. While the shield building stage in the Canaries lasts for a time span of several million years, the Hawaiian shield building stage is much shorter, lasting only up to 1 Ma (Carracedo 1999). In addition, the lack of significant subsidence in the Atlantic archipelagos exposes islands much longer at the surface, so remnants of early evolutionary stages (e.g., seamount stage) and as old as 20 Ma can be studied in outcrop locations (Carracedo 1999).

1.2 The Cabo Verde Archipelago

The Cabo Verde Archipelago is located in the Atlantic Ocean off the west coast of Africa and comprises 10 islands and numerous islets and seamounts. The islands and seamounts of the Cabo Verde Archipelago are of volcanic origin associated with intraplate (hot spot) volcanism, similar to other ocean island archipelagos in the Atlantic Ocean, for example the Canary Islands, Madeira or the Azores. Although similar to other ocean archipelagos in the Atlantic, volcanism in the Cabo Verde Archipelago is characterized by some peculiarities. These include the situation on one of the world's largest bathymetric anomalies (the Cape Verde Rise; **Fig. 1.1**), the distribution of islands in two separate chains, the highly alkaline compositions of rocks, and the chemical mantle plume signatures (e.g., Barker et al. 2010, 2012, 2014, Holm 2006, Duprat et al. 2007, Holm et al. 2008). The Cabo Verde Islands and Seamounts are in different stages of evolution, and therefore represent an excellent location to study the evolution of a hot spot related archipelago.

The islands are distributed in two chains that are about 180 km apart and SE-NW trending in a sub-parallel, horseshoe-like structure that is open towards the West (**Figs. 1.1, 1.2**). Morphologically, the eastern islands show low topographies (razed islands), while the western islands show high reliefs. Holocene and Quaternary volcanism occurred in the SW and NW of the archipelago. While Fogo Island (SW) is volcanically active (last eruption 2015), the islands Brava and Santo Antão and several seamounts located in the W (Charlels Darwin Volcanic Field, Nola (Noroeste), Sodade and Cadamosto) are seismically active (Grevemeyer et al. 2010, Faria and Fonseca 2014, Mata et al. 2017, Leva et al. 2019, Klügel et al. 2020; Bruno Faria, pers. comm. 2019).

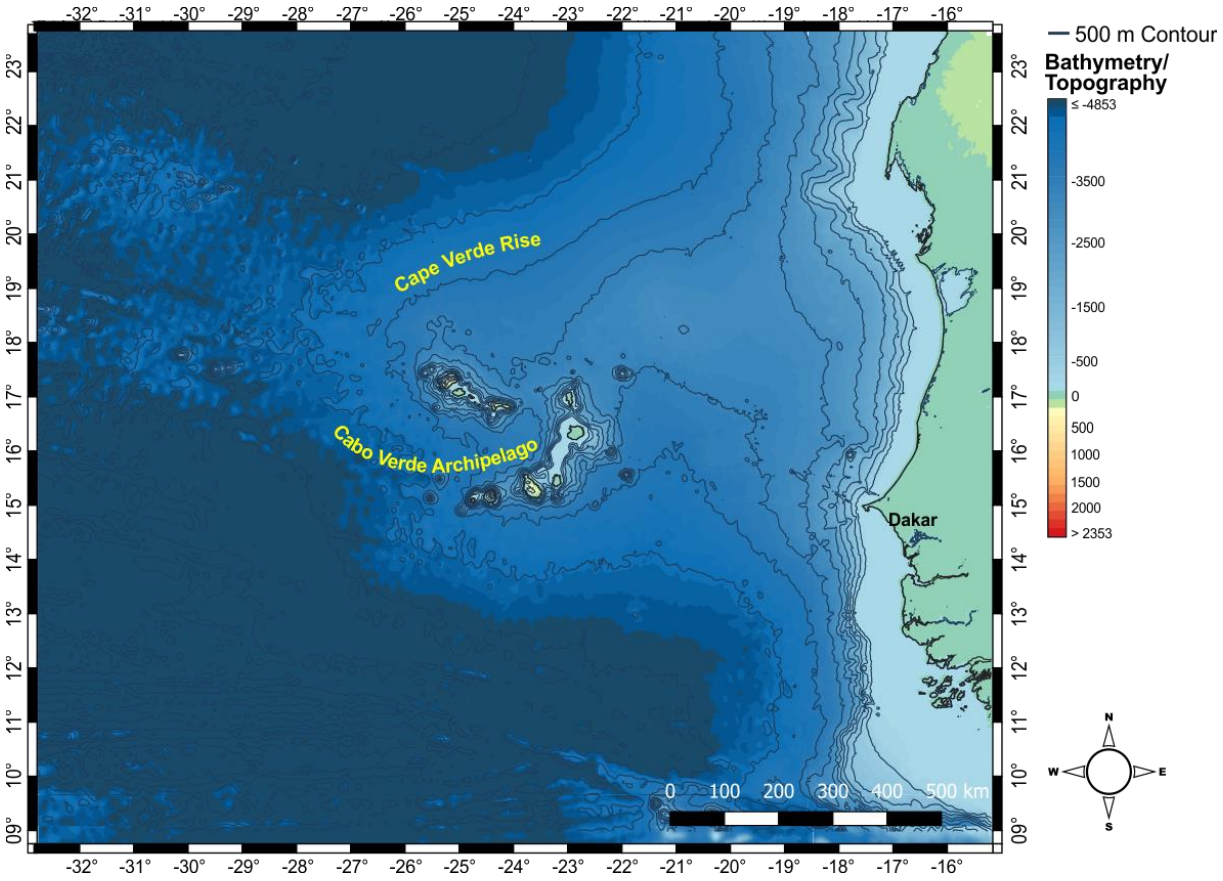

Figure 1.1 The Cabo Verde Archipelago is located in the Atlantic Ocean off the coast of Senegal (W-Africa). It is situated on one of the world's largest bathymetric anomalies, the Cape Verde Rise, rising about 4000 m from the surrounding sea floor (data: GMRT).

Combined morphological observations and geochronological (K-Ar and ^{40}Ar-^{39}Ar) data indicate a rough synchronous age progression from E to W in both island chains (Holm et al. 2008). Volcanism started at about 22 Ma at the northeastern islands Sal, Boa Vista and Maio, with most activity in the Miocene and Pliocene, while the southwestern and northwestern islands developed mainly during the Pliocene (Holm et al. 2008). However, a pronounced age progression as seen on other ocean island chains (e.g., Hawaii, Canary Islands) cannot be observed on the Cabo Verdes. This may be at odds with the classical mantle plume model. Previous studies explained the less pronounced age progression with the proximity of the archipelago to the pole of rotation of the African plate (Holm et al. 2008, Pollitz 1991). However, these studies were limited to observations and geochronological data from the islands, and a regional investigation of the Cabo Verde Archipelago that includes the submarine part of the archipelago is still missing.

Cabo Verde volcanism is characterized by highly alkaline magmatism. Rock compositions range from primitive basanites and nephelinites, to highly evolved tephrites and phonolites, with a comparatively high abundance of carbonatites. Geochemical analyses suggest geochemical differences between the two island chains that may be explained by a zoned mantle plume (Holm 2006, Barker et al. 2010, 2012, Mourão et al. 2012a, 2012b). Such a zoned mantle plume may explain the unusually high temperatures in the upper mantle and associated geoid anomalies (Courtney and White 1986, Carvalho et al. 2019). The magmatic plumbing system shows complex magma-crust interactions below the islands (Millet et al. 2008, Barker et al. 2019). The controls and mechanisms on the spatial distribution of the edifices, such as the distribution in two separate island chains, remain poorly understood.

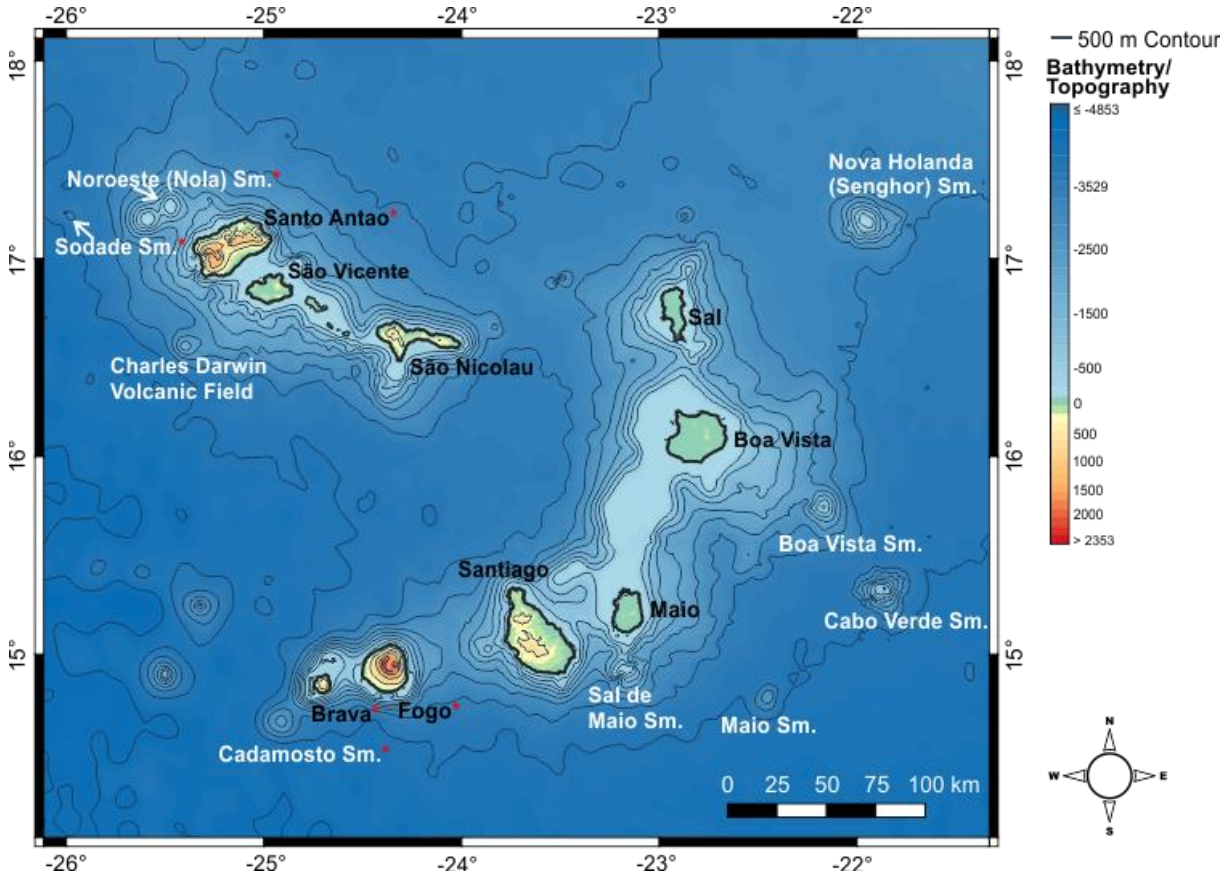

Figure 1.2 The islands (black labels) and seamounts (white labels) of the Cabo Verde Archipelago are distributed in two island chains. Seismically and/or volcanically active regions are located in the western part of both chains (marked with a red asterisk). The eastern islands show low topographies, while the western islands (e.g. Fogo, Santo Antão) show a high relief (source of data: GMRT).

1.3 Objectives and research questions

In order to understand the geodynamic evolution of an archipelago it is necessary to study both its subaerial and submarine parts. Until now, most studies of the geological evolution of Cabo Verde focussed on islands and islets, and on the evolution of the Cape Verde Rise. A main motivation for this thesis was therefore to integrate observations and data from both seamounts and islands to open up to a more holistic view of the archipelago.

To better constrain the spatio-temporal evolution of Cabo Verde, this thesis investigate three widely spaced locations, of which one is located in a currently volcanically active region and two in the presumably oldest regions of the archipelago. The submarine locations comprise the active Cadamosto Seamount in the SW and the presumably old and extinct Nova Holanda (Senghor) Seamount to the extreme NE. These locations were also chosen due to the occurrence of the K-rich minerals sanidine (Cadamosto) and phlogopite (Nova Holanda) in the local rocks, which are essential for obtaining precise ages using the ^{40}Ar-^{39}Ar dating method. Detailed field work on the extinct Maio Island in the E, including age dating of key sequences, were used to refine our understanding of the subaerial evolution of Cabo Verde. Maio Island is one of the older islands of the archipelago with a reasonably well studied stratigraphy and a well exposed igneous core complex.

Both the Miocene and earlier magmatic-tectonic evolution as well as the Pliocene phases of evolution were investigated, using selected samples and observations from submarine and subaerial edifices. An important objective of this thesis was to establish absolute ages for the submarine evolution of the Cabo Verde Archipelago, and to compare with the subaerial evolution. For this purpose, ^{40}Ar-^{39}Ar geochronology was combined with petrological data, field observations, and structural analyses.

The following research questions were addressed in this thesis:

1. How old and how active is the morphologically young Cadamosto Seamount in the SW of the Cbo Verde Archipelago?
2. How did the presumably old Maio Island in the East of the archipelago evolve during the Miocene and when was it volcanically active?
3. How did Maio Island evolve after volcanism ceased?
4. What is the age of the youngest pre-archipelago seafloor, which was uplifted and is now exposed on Maio, and which must be present below the other Cabo Verde Islands?
5. What is the oldest seamount age at Cabo Verde?

1.4 Structure of the thesis

The thesis is divided into different chapters (chapters 2 to 5). Each chapter has been published in a peer-reviewed journal or was prepared for publication. The papers and manuscripts address research questions 1-4. Appendices to the different chapters are listed in Chapter 9. Some of the data and results obtained in the framework of the present thesis were presented at international conferences. The different conference abstracts are listed in Appendix 9.1.

Research question 5 was approached in the framework of this thesis. The determined age will be published within context in a paper on detailed morphological descriptions of all Cabo Verde seamounts: Kwasnitschka et al. (in prep.). The main radiometric dating results from a pillow lava from the extinct Nova Holanda (Senghor) Seamount in the NE of the archipelago is a weighted mean ^{40}Ar-^{39}Ar age of 14.872 ± 0.027 Ma (2σ) from sanidines and phlogopites. It represents an important time marker for the submarine part of the Cabo Verde Archipelago.

Chapter 2 addresses research question 1 and has been published in *Lithos*:

Samrock LK, Wartho J-A, Hansteen TH (2019) ^{40}Ar-^{39}Ar geochronology of the active phonolitic Cadamosto Seamount, Cape Verde. Lithos 344-345:464–481. doi:10.1016/j.lithos.2019.07.003.

To reveal the age of Cadamosto Seamount, five submarine lava samples from Cadamosto Seamount that were collected by dredging or by Remotely Operated Vehicles (ROV) during several

research cruises with *RV Meteor* and *RV Poseidon* were analysed. This paper presents high quality radiometric ages and therefore provides the first record of absolute ages for the submarine part of the Cabo Verde Archipelago. Petrological observations and ^{40}Ar-^{39}Ar ages were combined to investigate the age of Cadamosto Seamount and timescales and dynamics of igneous processes. The results suggest young eruption ages (all <100 ka), with the youngest combined eruption age at 21.14 ± 0.62 ka, and a long-lived magma plumbing system recorded in antecrysts of the phonolite lava samples.

Studies on Maio Island are presented in **Chapters 3 to 5**, of which each chapter focuses on different periods of activity on Maio Island, respectively.

In **Chapter 3**, the Miocene evolution of Maio was investigated, addressing research question 2. The manuscript has been published in *International Journal for Earth Sciences (Geologische Rundschau)* under a Creative Commons Attribution 4.0 International License:

Samrock, L.K.; Hanstseen, T.H., Dullo. W.C., Wartho, J.A. (2022) Internal igneous growth, doming and rapid erosion of a mature ocean island: The Miocene evolution of Maio (Cabo Verde). Int J Earth Sci (Geol Rundsch) 111:1129–1148. doi:10.1007/s00531-022-02160-x

In this paper, structural analyses and ^{40}Ar-^{39}Ar ages from dyke intrusions and a conglomerate clast were combined in order to constrain the Miocene evolution of Maio. A period of intense island growth at 16 to ~8.7 Ma is confirmed. A landslide deposit is described, suggesting a period of large-scale collapse and erosion between 8.7 and 6.7 Ma, preceding the final volcanic activity on Maio. A new model for the Miocene evolution of Maio Island is presented.

Chapter 4 provides a brief description of fossil dunes exposed in the East of Maio. This study addresses research question 3 and has been published in *International Journal for Earth Sciences (Geologische Rundschau)*:

Samrock L.K., Dullo W.-C., Hansteen T.H. (2018) Large-scale fossil dune on Maio, Cape Verdes. Int J Earth Sci (Geol Rundsch) 107(8):2931–2932. doi:10.1007/s00531-018-1622-x

In this GEOSITE article (an arctivle series featuring interesting geological locations), uplifted Early to Middle Pleistocene fossil dunes that are located in the East of Maio Island are described. These dunes are composed of well-cemented carbonaceous sandstones and arenites and show changes in the type and direction of cross-stratification, suggesting changes in paleo-environmental conditions.

Research question 4 was addressed in **Chapter 5**, which is a manuscript describing the biostratigraphy of the Mesozoic marine sediments on Maio Island. The chapter is a revised version of a manuscript that was submitted to the journal *Newsletters in Stratigraphy* in 2019:

Samrock L.K., Dullo C.W., Hansteen T.H. (2019) Early biostratigraphy and facies of Mesozoic marine sediments on Maio (Cabo Verde) revisited: Witnesses of the Early Atlantic Ocean.

In Chapter 5, field observations were combined with findings of macro-, micro- and nannofossils from the MORB-type pillow lavas and Mesozoic sedimentary rock successions that are exposed in the centre of Maio, forming a circular structure around the Central Intrusive Complex. The manuscript confirms that the former seafloor is of Early Cretaceous age.

This manuscript has been reviewed by a member of the editorial board of *Newsletters in Stratigraphy* and the authors were invited to resubmit the manuscript for an additional review round after revising the manuscript. During the revision of the manuscript, a study with similar research questions and similar conclusions was published (Casson et al. 2020), which made the publication of this manuscript obsolete. The manuscript is hence only included as a chapter in the present thesis. However, some of the results and figures from Chapter 5 were included and published in Samrock et al. (2022; Chapter 3).

1.5 Contributions to the papers and manuscripts

The following people contributed to Chapter 2 (Samrock et al. 2019):

- Lisa Samrock and Thor Hansteen designed and conceptualized the study;
- Thor Hansteen was responsible for sampling;
- Lisa Samrock prepared the samples for analyses and carried out the Electron Microprobe analyses;
- Jo-Anne Wartho performed radiometric dating;
- Lisa Samrock and Jo-Anne Wartho created figures;
- Lisa Samrock drafted the first version of the manuscript. Afterwards, all authors were involved in preparing the manuscript for publication.

The following people contributed to Chapter 3 (Samrock et al. 2022):

- Lisa Samrock, Thor Hansteen and Wolf-Christian Dullo designed and conceptualized the study, carried out field work and sampling;
- Lisa Samrock prepared the samples for analyses;
- Jo-Anne Wartho performed radiometric dating;
- Lisa Samrock and Jo-Anne Wartho prepared the figures;
- Lisa Samrock drafted the first version of the manuscript. Afterwards, all authors were involved in preparing the manuscript for publication.

The following people contributed to Chapter 4 (Samrock et al. 2018):

- Lisa Samrock, Wolf-Christian Dullo and Thor Hansteen, carried out field work and sampling, discussed and interpreted the data.
- Lisa Samrock and Wolf-Christian Dullo analysed the samples;
- Lisa Samrock prepared the figures;
- Lisa Samrock drafted the first version of the manuscript. Afterwards, all authors were involved in preparing the manuscript for publication.

The following people contributed to Chapter 5:

- Lisa Samrock, Thor Hansteen and Wolf-Christian Dullo designed and conceptualized the study, carried out field work and sampling. All authors were involved in interpretation of data, writing and discussions.
- Lisa Samrock prepared the samples for analyses and created figures for the manuscript;
- Lisa Samrock and Wolf-Christian Dullo carried out the SEM analyses at Kiel University;
- Daniel Bernoulli provided feedback on the manuscript and unpublished material;
- Lisa Samrock drafted the first version of the manuscript. Afterwards, all authors were involved in preparing the manuscript for publication.

2 ^{40}Ar-^{39}Ar geochronology of the active phonolitic Cadamosto Seamount, Cape Verde

This article was published in the peer-reviewed journal *Lithos* with the following bibliography:

Samrock LK, Wartho J-A, Hansteen TH (2019) ^{40}Ar-^{39}Ar geochronology of the active phonolitic Cadamosto Seamount, Cape Verde. Lithos 344-345:464–481. doi:10.1016/j.lithos.2019.07.003.

Highlights

- Extensive set of 170 ^{40}Ar-^{39}Ar single-crystal ages for Cadamosto Seamount.
- Volcanic eruption ages at Cadamosto Seamount are all young (<100 ka).
- Three samples dominated by sanidine phenocrysts preserve a 21.04 ± 0.62 ka age.
- Sanidine antecrysts in two samples show complex chemical zonation patterns.
- Antecryst ages suggest long-lived magmatic activity in the seamount, up to 1.52 Ma.

Abstract

Cadamosto Seamount is located in the SW of the Cape Verde Archipelago in the central Atlantic Ocean off the west coast of Africa. Many radiometric dates exist for the islands in the archipelago, however, no geochronological information has been obtained from the numerous seamounts. The timescales for igneous processes in the submarine realm are thus poorly understood.

In this study, we investigated five lavas that were sampled by dredging and ROV (remotely operated vehicle) from the flanks and summit areas of the largely phonolitic Cadamosto Seamount during two different research cruises. Chemical zonation patterns of minerals were determined by electron microprobe, and radiometric ages were obtained from single-crystal total-fusion and single-/multi-grain step-heating ^{40}Ar-^{39}Ar analyses of sanidine, nepheline and sodalite-group minerals.

Our ^{40}Ar-^{39}Ar results reveal young sanidine eruption ages (all <100 ka) at Cadamosto Seamount: (1) Three western flank/summit lavas have a relatively simple petrology dominated by phenocrysts, and overlap with mean sanidine ages of 20.98 ± 0.87 ka, 21.44 ± 0.80 ka and 22.3 ± 2.0 ka, with a combined mean age of 21.04 ± 0.62 ka from the three samples (all uncertainties are quoted at 2σ). The remaining two samples from the summit/NE flank are dominated by complex zoned sanidines with resorbed antecrystic cores and phenocrystic rims. These samples yield older sanidine ages of 51.8 ± 2.4 ka and 97 ± 14 ka, which are interpreted to be maximum eruption ages. This is due to the dominance of antecrysts in these two samples and the possibility that the analyzed sanidine grains may be a mixture of older antecrystic cores and younger phenocrystic rims.

The older ^{40}Ar-^{39}Ar ages of many sanidine and nepheline antecrysts also give us clues regarding older magmatic events at Cadamosto Seamount, despite these grains having undergone resorption and phenocrystic rim overgrowths, resulting in some radiogenic ^{40}Ar loss during entrainment in the subsequent magmas. The antecrysts minimum ages extend back to 1.5215 ± 0.0083 Ma, which supports the age progression of magmatism observed in the southern islands chain of the Cape Verde Archipelago.

The youngest volcanic eruption period (21.14 ± 0.62 ka) occurred during the Last Glacial Maximum, a period of global sea level lowstands. We suggest that the comparatively rapid unloading leading up to the lowstand may have reduced pressure conditions within the Cadamosto Seamount magma plumbing system, and thus led to enhanced submarine eruption activity.

Keywords: Cape Verde · Cadamosto Seamount · ^{40}Ar-^{39}Ar · Sanidine · Nepheline · Volcanism

2.1 Introduction

The Cape Verde Archipelago consists of 10 islands and several seamounts that have a volcanic origin. The volcanism in the archipelago differs from some other ocean island archipelagos in that it is (1) split into two island chains, (2) it is dominated by highly alkaline magmatic rocks and an unusually high abundance of carbonatites, and (3) there is evidence of a zoned mantle plume characterized by HIMU & DMM (e.g., high $^{206}Pb/^{204}Pb$ ratios of > 19.5, high εNd values (>+3), and negative $\Delta^{208}Pb/^{204}Pb$ ratios) signatures in the northern islands and Cadamosto Seamount, and EM1 & HIMU (lower $^{206}Pb/^{204}Pb$ ratios, lower εNd values, and positive $\Delta^{208}Pb/^{204}Pb$ ratios) signatures in the southwestern islands (e.g., Holm 2006, Barker et al. 2010, 2012). The majority of mafic and felsic rocks range from basanites and nephelinites, to tephrites and phonolites. Examples of other mantle plume related alkaline ocean islands in the Atlantic include the nearby Canary Islands, Azores and Madeira Islands (e.g., Schmincke 1973).

Based on a variety of K-Ar and ^{40}Ar-^{39}Ar radiometric data plus morphological observations on the Cape Verde volcanic islands, Holm et al. (2008) suggested that volcanic activity in the archipelago started in the NE (Sal, Boavista and Maio), and later synchronously progressed towards the NW and SW in the northern and southern island chains in a NE-SW and SE-NW trending direction (**Fig. 2.1**). In contrast, the ages and timescales for formation of the the submarine stages of the islands and the 10 major seamounts are unknown.

The aim of this study was to obtain the first ^{40}Ar-^{39}Ar geochronological analyses of submarine lavas from the seismically active Cadamosto Seamount and to address the absolute eruption ages and timescales of magmatic processes in this large submarine phonolite volcano. We therefore combined detailed petrologic data with geochronology. The suggested age progression in the Cape Verde islands (Holm et al. 2008) further predicts very young magmatic ages (< 1 Ma). The high K contents of the Cadamosto Seamount rocks facilitate single-crystal ^{40}Ar-^{39}Ar dating of these presumably very young samples, in a geochronological realm that overlaps with the AMS ^{14}C dating technique (up to ~50 ka). The sanidine crystals present in these Cadamosto Seamount lavas allow determination of volcanic eruption ages. Petrologically-identified antecrysts of sanidine and nepheline, which may have undergone some $^{40}Ar^*$ loss, also allow the estimation of minimum ages for older magmatic events within this submarine seamount.

2.2 Geological Setting

The Cape Verde Archipelago is located in the Atlantic Ocean, 450-600 km off the west coast of Africa. The islands and seamounts are distributed between two distinct island chains; a SE-NW trending northern chain (São Nicolau in the SE to Santo Antão in the NW), and a NE-SW-trending southern chain (Sal in the NE to Brava in the SW; **Fig. 2.1**). In both volcanic chains, the western islands have higher relief while the eastern islands have lower topographies, which is due to the effects of erosion and decreasing volcanic activity.

Most of the volcanic rocks from the Cape Verde islands have been dated using K-Ar, ^{40}Ar-^{39}Ar, and ^{3}He cosmogenic techniques, including rocks from Sal, Boa Vista, Maio, Santiago, Fogo, São Nicolau, São Vicente, and Santo Antão (Bernard-Griffiths et al. 1975, Grunau et al. 1975, Mitchell et al. 1983, Plesner et al. 2002, Torres et al. 2002, Madeira et al. 2005, 2010, Duprat et al. 2007, Holm et al. 2008, Foeken et al. 2009, Dyhr and Holm 2010, Ancochea et al. 2010, 2012, 2014, 2015).

The age progression in the Cape Verde Archipelago is less pronounced than for other Atlantic volcanic island chains, possibly because of its proximity to the African plate's pole of rotation (e.g., Pollitz 1991). While the southern chain shows a NE-SW age progression from ~26 Ma to present, the northern chain shows younger more synchronous ages from ~10 Ma to present and no clear age progression (Holm et al. 2008; **Fig. 2.1B**). The oldest dated volcanic activity occurred on the island of Sal at ~26 Ma, with the majority of the volcanic activity throughout the southern chain occurring at different stages from ~19-2 Ma (**Fig. 2.1B**; Bernard-Griffiths et al. 1975, Grunau et al. 1975, Mitchell et al. 1983, Plesner et al. 2002, Torres et al. 2002, Madeira et al. 2005, 2010, Duprat et al. 2007, Holm et al. 2008, Foeken et al. 2009, Dyhr and Holm 2010, Ancochea et al. 2010, 2012, 2014, 2015).

The Cape Verde Archipelago is dominated by mafic silica under-saturated rocks with moderate to high alkali contents, ranging in composition from foidites and nephelinites, to tephrites and

phonolites (e.g., Mitchell-Thomé 1972, Gerlach et al. 1988, Holm 2006, and references therein). The mantle plume below the archipelago has been suggested to be zoned, with dominantly HIMU/DM signatures in the northern islands and Cadamosto Seamount, and mainly EM1-like/HIMU signatures in the southwestern islands (Holm 2006, Barker et al. 2010).

Seismic activity indicating present day magmatic activity has been recorded on the islands of Fogo, Brava, and Santo Antão, and offshore on the Nola, Sodade, and Cadamosto seamounts (**Fig. 2.1A**; Grevemeyer et al. 2010, Faria and Fonseca 2014). In historic times, Fogo has been the only active volcano in the archipelago; it erupts on average every 20 years, which makes it one of the most active volcanic islands in the Atlantic Ocean (last eruption: 2014/2015; Mata et al. 2017). Due to recently observed seismic activity on Brava, it has been suggested that this island is still volcanically active and could erupt in the near future (Faria and Fonseca 2014).

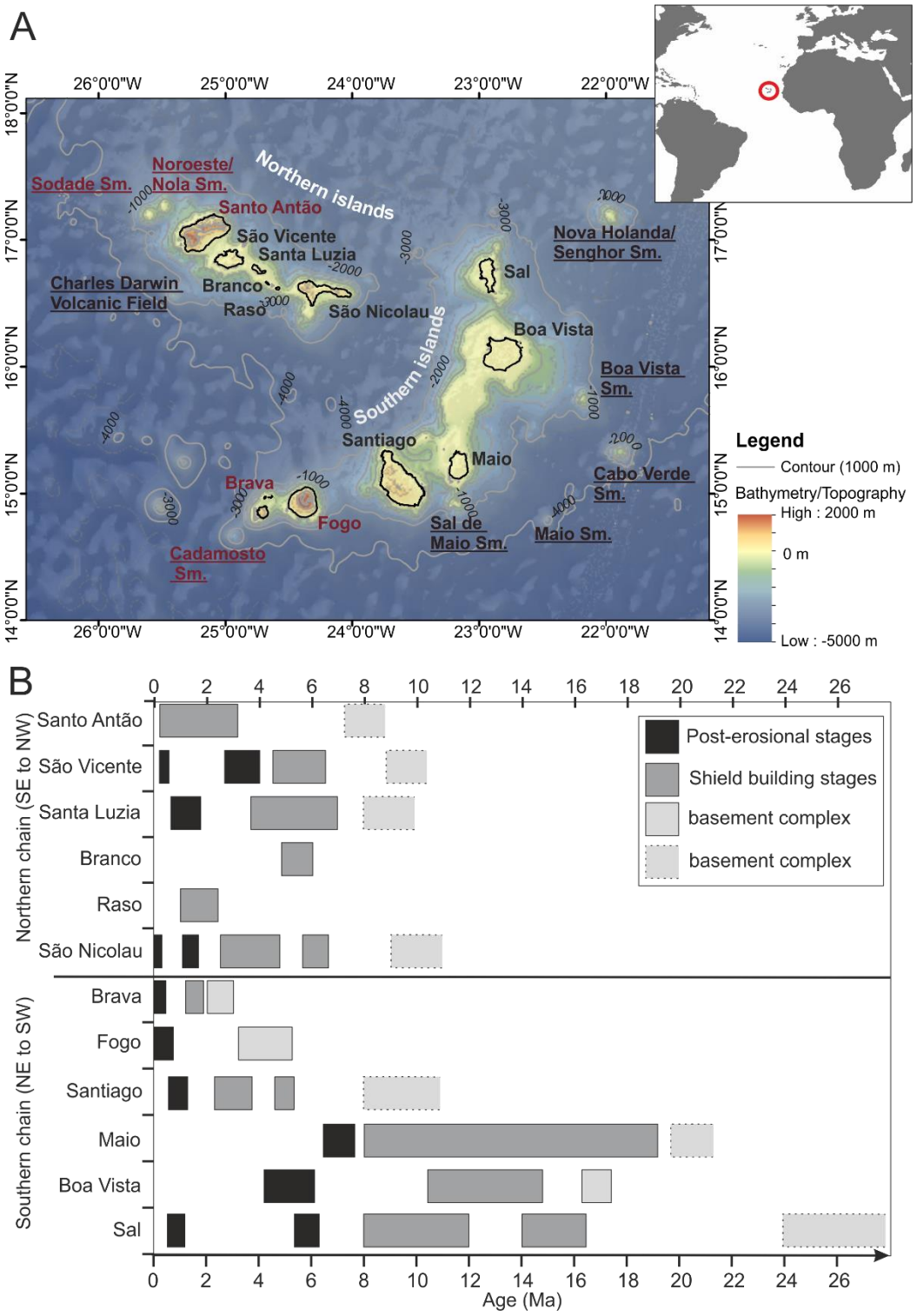

Figure 2.1 Overview map of the Cape Verde Archipelago showing the islands (black/red) and some of the seamounts (Sm.; black/red underlined; topography from Ryan et al. 2009). The red labels mark seismically and/or volcanically active areas of the archipelago. The insert map shows the location of the archipelago (red circle) in the central Atlantic Ocean, off the African west coast. Cadamosto Seamount is located in the SW of the Cape Verde Archipelago. B: Distribution of volcanic activity in the northern and southern chains of the Cape Verde Archipelago. The southern chain indicates an age progression from NE to W, while the volcanic activity in the northern chain is more or less synchronous since the Late Miocene, but also overlaps with the easternmost islands of the southern chain. The boxes with solid lines indicate relatively well constrained K-Ar and ^{40}Ar-^{39}Ar ages, and the boxes with dashed lines show poorly defined ages (K-Ar analyses of a few samples or from geological relationships). This figure is modified from Ramalho (2011) based on data from Bernard-Griffiths et al. (1975); Grunau et al. (1975); Mitchell et al. (1983); Torres et al. (2002); Plesner et al. (2002), Madeira et al. (2005, 2010), Duprat et al. (2007), Holm et al. (2008), Foeken et al. (2009), Dyhr and Holm (2010), Ancochea et al. (2010, 2012, 2014, 2015).

2.2.1 *Cadamosto Seamount*

The Cadamosto Seamount is situated at the southwestern end of the southern chain of the Cape Verde Archipelago, ~25 km SW of Brava (**Fig. 2.1A**). It occurs at depths of ~3300 m to 1500 m below sea level (b.s.l.), and has a basal diameter of ~15 km (**Fig. 2.2**). Several smaller volcanic cones occur on the north-eastern flank of the seamount and on the seafloor between Brava and Cadamosto (**Fig. 2.2**). Morphologic analyses and ROV dives revealed at least three major eruptive centers in the summit region of Cadamosto Seamount (**Fig. 2.2**), each appearing morphologically young and well-preserved (Hansteen et al. 2014). Each of these centers comprises fresh lavas with little sedimentary cover, and some crater structures contain hydrothermally altered rocks, which are suggestive of recent igneous activity. Probable flank collapse escarpments are evident on three sides of the seamount (**Fig. 2.2**; Hansteen et al. 2014). The rocks of Cadamosto Seamount have broadly phonolitic compositions, with occasional clinopyroxene nephelinites.

Two tephra layers (C1 and C7) sampled from five different gravity cores located up to 67 km N and SW of Cadamosto Seamount, were attributed to Cadamosto Seamount, based on the chemical composition of glass shards preserved within these tephra layers (Eisele et al. 2015). The authors obtained a tephrachronological age of ~17 ka for layer C1, and ~40 ka for layer C7.

We analyzed five phonolitic samples from Cadamosto Seamount that were collected either by the remotely operated vehicle ROV *Kiel6000*, (sample 035ROV-12), or by dredging (samples 149-2, 149-6, 152-1, 037DR-2) during the expeditions of *RV Poseidon* POS320/2 in 2005 (Kraus 2005) and *RV Meteor* M80/3 in 2010 (Hansteen et al. 2014; **Fig. 2.2; Table 2.1**). Two samples were dredged from the southwestern flanks of the seamount (149-2 and 149-6), one was dredged from the NE flank (037DR-2), and two samples originate from the summit area where they were dredged (152-1) and collected by ROV (035ROV-12; **Fig. 2.2, Table 2.1**).

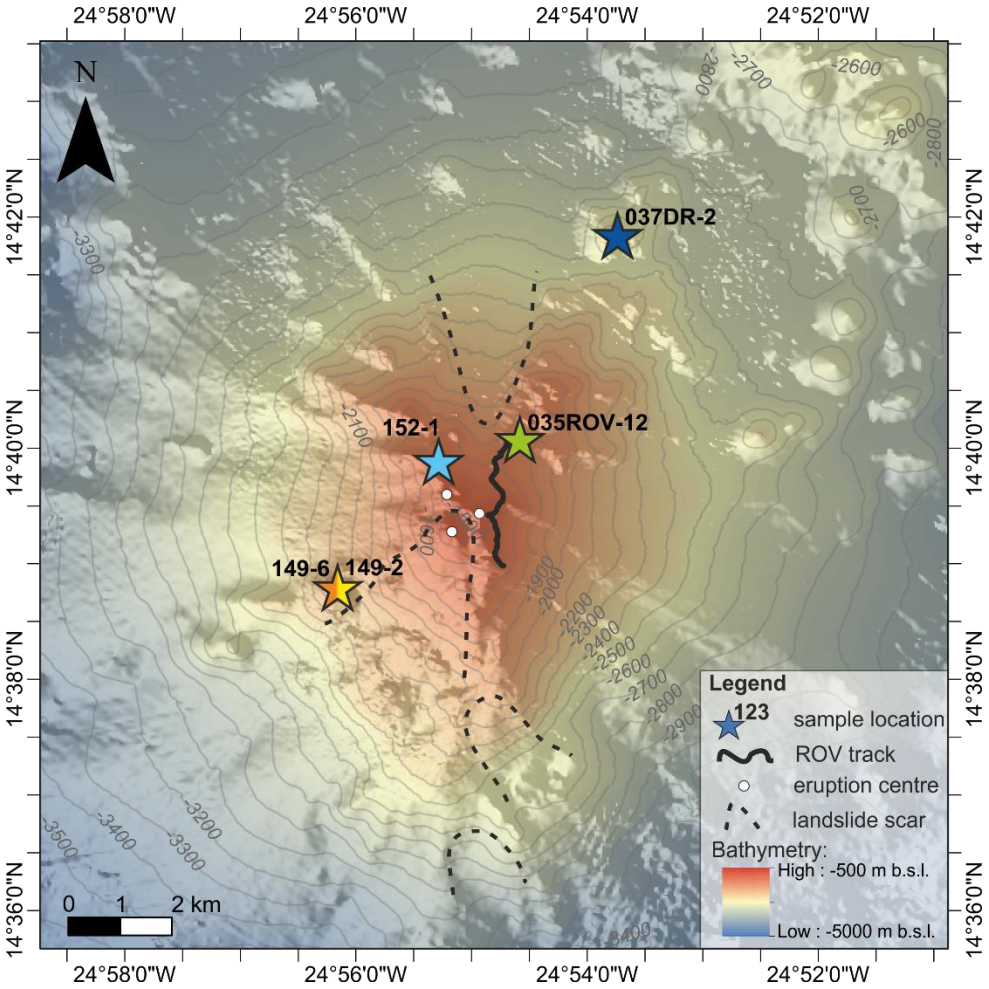

Figure 2.2 Close-up bathymetric map of the Cadamosto Seamount. The seamount ranges from ~1500 m to ~3300 m b.s.l. The stars mark the locations of the analyzed samples. Landslide scars and eruption centers are also marked (Hansteen et al. 2014).

2.3 Analytical Methods

Petrological observations were made on thin-sections from all five Cadamosto Seamount samples using a polarized-light microscope.

Major element mineral compositions were analyzed on carbon-coated polished thin-sections, using a JEOL JXA 8200 wavelength dispersive (WD) electron microprobe (EMP) at GEOMAR, fitted with five WD spectrometers, and calibrated with international natural and synthetic standards (Jarosewich 2002). We used a constant acceleration voltage of 15 kV. For feldspar mineral analyses, the beam current was 20 nA and peak counting times 20 s (30 s for K), with a focused beam (<1µm diameter). In high resolution profiles, peak counting times were 30 s for Fe, and 60 s for Ba. For the feldspathoids, we used varying beam currents of 20-30 nA, peak counting times of 20 s (30 s for S, Cl and K), and a beam diameter of 5 µm. Backscattered electron (BSE) photomicrographs were also obtained using the EMP. Linear interpolation was used to correct data if the measured standard differed by more than ± 1 % from the standards data. Before plotting, all the data sums were normalized to 100. The EMP data are presented in Appendix 9.2.2.

To prepare the samples for the laser ^{40}Ar-^{39}Ar analyses, the rocks were crushed, dry sieved to obtain fractions of 250-500 µm, 500-1000 µm, and >1 mm. Four of the five samples were hot HCl/HNO_3 acids/distilled water leached in an ultrasonic bath (Koppers 2002) to remove feldspathoids, allowing hand-picking of sanidine crystals using an optical microscope. These sanidine crystals were subsequently HF acid leached and cleaned. The samples were irradiated at the Oregon State University reactor, and analysed at the GEOMAR Argon Geochronology in Oceanography Laboratory (ARGO) in Kiel, Germany. The isotopic analyses were corrected using the K decay constants and atmospheric air ratio of (Steiger and Jäger 1977). The J values were determined using age standard TCS2 (27.87 ± 0.04 Ma, 1σ; M.A. Lanphere, pers. comm). The ^{40}Ar-^{39}Ar data corrections, weighted mean ages, and plateau and inverse isochron plots for the individual samples and combined samples were all made using the ArArCALC Excel macro program (v. 2.5.2; Koppers 2002). All ages in the text and figures are quoted with 2σ internal errors, and include analytical, J value, and irradiation correction factor errors. Weighted mean ages with MSWD values >1 were assigned larger errors, using error magnification factors calculated by multiplying the mean ages by the square root of the MSWD (Appendix 9.2.3). $^{36}Ar/^{39}Ar$ alteration index (AI) values were used to gauge the alteration/freshness of the sanidine ^{40}Ar-^{39}Ar analyses, and were calculated using the criteria of Baksi (2007) with the $^{36}Ar/^{39}Ar$ AI-cut-off value of < 0.00006 for K-feldspar (van den Bogaard 2013). Additional analytical details for the laser ^{40}Ar-^{39}Ar single-crystal total-fusion (SCTF) and single/multi-grain step-heating analyses are described in Appendix 9.2.1, and the ^{40}Ar-^{39}Ar data and plots are presented in Appendix 9.2.3.

Table 1. Table of the sample names and sampling locations from Cadamosto Seamount, plus the respective grain size fractions used for ^{40}Ar-^{39}Ar dating.

Cruise	Sample	Sampling Method	Location		Depth [m b.s.l.]	Grain size fraction dated [mm]
			Latitude (N)	Longitude (W)		
POS 320/2	149-2	Dredging	14°38'44.40"/ 14°38'45.6"	24°56'11.4"/ 24°56'00.6"	2025/ 2012	0.5-2
POS 320/2	149-6	Dredging	14°38'44.40"/ 14°38'45.6"	24°56'11.4"/ 24°56'00.6"	2025/ 2012	0.5-1
POS 320/2	152-1	Dredging	14°39'46.19"/ 14°39'43.2"	24°55'13.8"/ 24°54'58.79"	1518/ 1682	1-2
M80/3	035ROV-12	ROV	14°40'03.96"	24°54'37.71"	1733,4	1- 2
M80/3	037DR-2	Dredging	14°41'43.8"/ 14°41'49.2"	24°53'43.8"/ 24°53'51.60"	2455.6/ 2457,2	0.25-0.5 & 0.5-1

2.4 Results

2.4.1 Sample descriptions, petrology and mineralogy

Five phonolitic samples were used for ^{40}Ar-^{39}Ar dating of the Cadamosto Seamount, and are described in detail below. In the following sections, we use the term "phenocryst" to describe a crystal that apparently grew in the final magma prior to eruption, and "antecryst" to describe a crystal entrained in the final magma or introduced by magma mixing before eruption. More specifically, the term "antecryst" is used here for crystals that belong to the magmatic system below and within Cadamosto Seamount, but originate from different magma batches than the final host magma. However, we cannot exclude the possible presence of xenocrysts originating from external sources (e.g., wall rock material), but their presence is comparatively unlikely (e.g., Jerram et al. 2018). Please note that for the purposes of simplicity we use the term "normal zonation" to describe sanidine crystals that have lower Or contents in the rim compared to the core, as crystal fractionation may lead to different zonation patterns (e.g., Nekvasil et al. 2000).

Sample 149-2

Sample 149-2 was dredged from a water depth of ~2000 m below sea level (b.s.l.) from the southwestern flank of the seamount (**Fig. 2.2; Table 2.1**). Crystals are up to 3 mm in diameter and make up ~10% of the rock volume, set in a glassy matrix with vesicles. The dominant crystal cargo comprises feldspathoids (nepheline, sodalite, nosean-haüyne and leucite), sanidine, and additional minor apatite, Fe-Ti oxide, titanite, and rounded green aegirine-augite (**Fig. 2.3A-B**). Vesicles make up ~10% of the rock volume and are unfilled. The glassy matrix contains microlites of feldspathoids. The sanidines are idiomorphic and optically unzoned, which suggests that they are phenocrysts, with compositions ranging from Or 72 to 81 (average = Or 78; **Fig. 2.6**).

Sample 149-6

A second sample, 149-6, was collected from the same dredge haul as 149-2 (**Fig. 2.2; Table 2.1**). This sample is also dominated by feldspathoids (nepheline, sodalite and nosean-haüyne) and sanidine crystals in a microcrystalline groundmass, but unlike sample 149-2 it lacks leucite. Additional minor minerals include Fe-Ti oxide, apatite, and rounded green aegirine-augite (**Fig. 2.3C-F**). Vesicles constitute up to ~15% of the rock volume, are rounded as well as elongated, and are unfilled. Nepheline grains are up to 3 mm in diameter, and are also present in the groundmass (up to 250 µm diameter). Some nepheline crystals (0.5 to 3 mm diameter) preserve normal (high to low temperature formation) and reverse zonation patterns with partially resorbed cores and thin nepheline overgrowth rims (up to 75 µm wide), which suggests that they may be antecrysts (**Fig. 2.3C-F**). Others nepheline crystals do not show any chemical zonation or signs of resorption and overgrowth, suggesting they may be phenocrysts (**Fig. 2.3C-D**). Sanidine grains are up to 2 mm in diameter and are also present in the groundmass (up to 250 µm in diameter), ranging in composition from Or 74 to 79 (average = Or 77 **Fig. 2.6**). The sanidines show little or no evidence of chemical zonation or resorbed cores/overgrowth rims, which suggests they are phenocrysts. Sodalite-group crystals occur as phenocrysts and as microlites in the groundmass. They are idiomorphic and zoned, with some zones containing dark inclusions (**Fig. 2.3C-D**). Some grains are composed of different sodalite-group minerals (nosean-haüyine and sodalite), suggesting strong zonation.

Sample 152-1

Sample 152-1 was dredged from the western summit area of Cadamosto Seamount at water depths of 1500-1700 m b.s.l. (**Fig. 2.2; Table 2.1**). This sample also mainly comprises feldspathoid (nepheline, sodalite, and nosean-haüyne) and sanidine crystals, but vesicles are mostly absent. Additional minor phases include Fe-Ti oxide, apatite and titanite. Sanidine occurs as idiomorphic crystals up to 3 mm in diameter, often in aggregates with other sanidine and feldspathoid grains (**Fig. 2.3G-H**). The Or component in these sanidines varies from 77 to 81 (average = Or 79). Most of the EMP-analyzed sanidine crystals do not show significant chemical and optical zonation or only slight normal zonation patterns with a maximum rim width of 29 µm (**Fig. 2.3G-I**). Resorbed cores cannot be observed. This suggests that the majority of the crystals are phenocrysts, but some of the larger sanidine crystals may be antecrysts (**Figs. 2.3I, 2.6**).

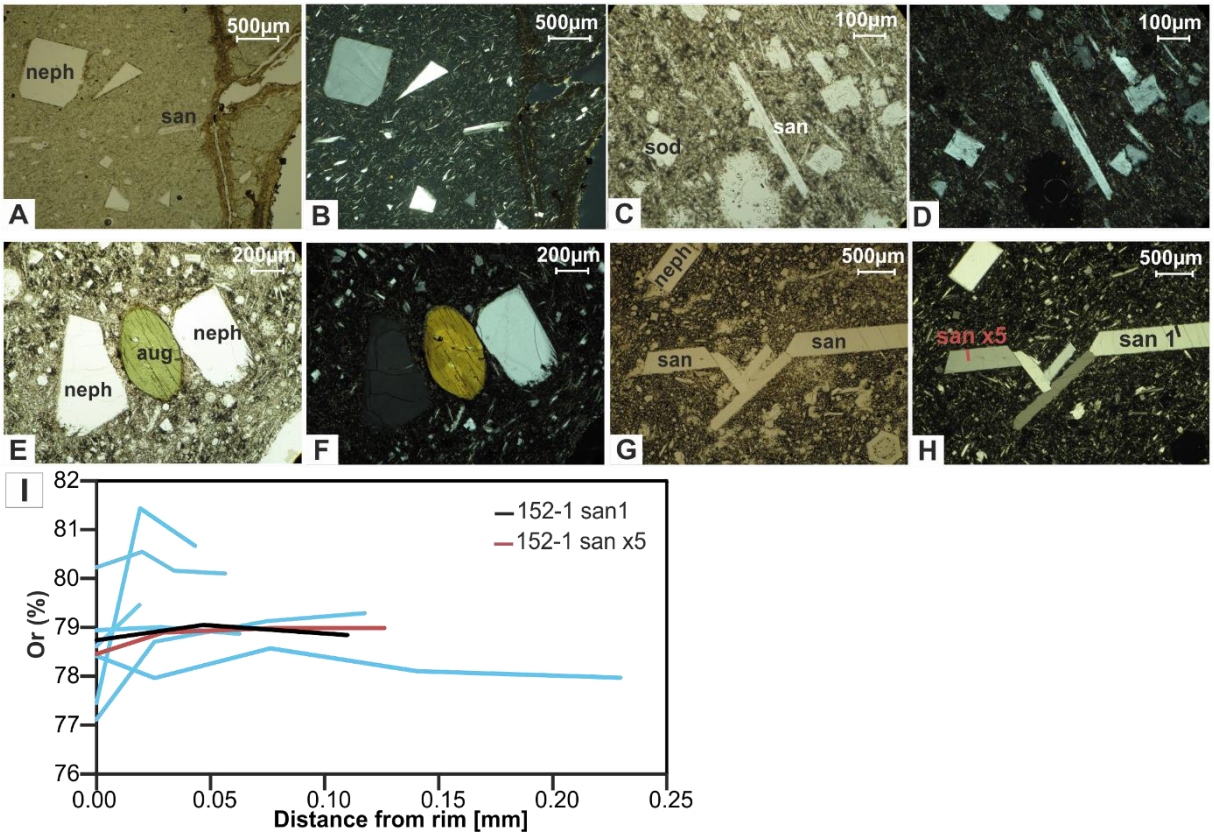

Figure 2.3 Thin section images of the dated Cadamosto samples in plain polarized light (left) and crossed polars (right). **A-B**: Sample 149-2 contains nepheline (neph) and sanidine (san) crystals marked. **C–F**: Sample 149-6 contains feldspathoids (e.g., sodalite (sod), and nepheline), sanidine, and rounded, aegirine-augite (aug). Note the resorbed nepheline crystals in **E** and **F**. **G-H**: Sample 152-1 contains feldspathoids and larger sanidine crystals. **I**: Plot showing mol% Or versus distance from crystal rim to core for selected profiles (blue lines) in sanidines from 152-1. Some profile locations (red/black lines) are marked in **H**.

Sample 035ROV-12

Sample 035ROV-12 was recovered from the NE summit area at a water depth of 1730 m b.s.l. (**Fig. 2.2; Table 2.1**). This sample differs from the previously described samples in several respects. Crystals make up ~25% of the rock volume, including sanidine, feldspathoids (sodalite, nepheline, and nosean-haüyne), clinopyroxene (mainly diopside, and minor amounts of aegirine-augite and green-core clinopyroxene), resorbed biotite crystals, and minor apatite, titanite, Fe-Ti oxides, and pyrite (**Fig. 2.4**). The crystals are set in a microcrystalline groundmass, and unfilled elongated vesicles (up to 20 mm in diameter) make up to 15% of the rock. In addition, this sample also contains mm-sized carbonatite enclaves (calcite dominated) inter-grown with apatite, feldspathoids, titanite and biotite crystals (**Fig. 2.4A-B**). Centimeter-sized mafic enclaves, with a higher degree of crystallinity than the host rock, are also present and mainly consist of biotite, clinopyroxene, Fe-Ti oxides, with minor feldspathoids (**Fig. 2.4E-F**). Both these types of enclaves do not contain any vesicles.

The sanidine crystals are up to 5 mm in diameter, are hypidiomorphic to xenomorphic, with rounded edges, and many of the larger sanidine crystals contain fluid, melt and mineral inclusions (e.g., feldspathoids and biotite; **Fig. 2.4C-F**). The sanidines preserve resorbed cores that are either rounded or irregularly serrated, and/or several zones of growth and resorption (e.g., **Fig. 2.4F-H**). The chemical compositions of the sanidines in the 035ROV-12 sample are variable. Some sanidines do not show significant variations in Or contents, but zonation patterns are visible in BSE images (e.g., san3 in **Fig. 2.4F, I**). These zonations are recorded by minor elements, e.g., Ba and Fe (**Fig. 2.4K-L**). Reverse, normal, patchy, and oscillatory zoned sanidines are also present in this sample, with some of the multiple overgrowth zones showing signs of resorption. The sanidines

have thin magmatic overgrowth rims of 5 µm to 20 µm thickness. The maximum thickness between the innermost antecrystic absorbed core and the final rim is 1.64 mm (**Fig. 2.4F**).

At least two different types of rim compositions can be observed: 1) Or contents ranging from 64 to 69, and 2) Or 59 to 63 (**Fig. 2.4I**). The sanidine core compositions can be further divided into at least three different groups: 1) Or 65-70, 2) Or 61 to 63, and 3) Or 55 to 60 (**Fig. 2.4I**). Even small sanidines present in the groundmass (up to 50 µm in diameter) show resorbed cores, and are part of the first compositional core group (Or 65 to 70). We thus interpret the sanidine crystals in sample 035ROV-12 to be entrained antecrysts.

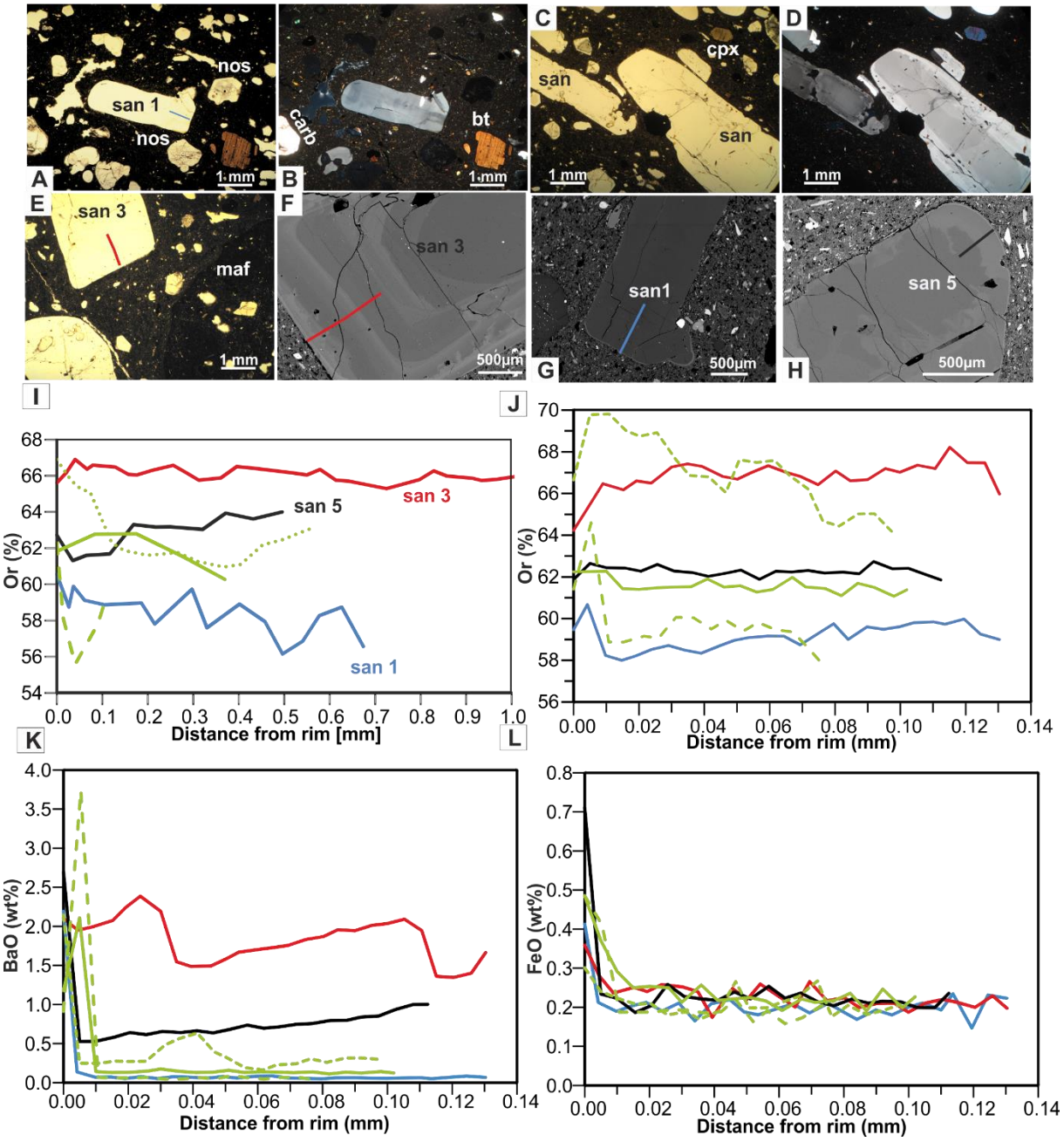

Figure 2.4 Sample 035ROV-12. **A-F**: Thin section images in plain (**A, C, E**) and crossed-polarized light (B**, D, F**), showing numerous rounded sanidine antecrysts (san), as well as feldspathoids (nosean-hauyin; nos), and biotite (bt). Note the carbonatite enclave (carb) in **A-B**, and the mafic enclave (maf) in images **E-F. G-H**: BSE images of rounded and zoned sanidine crystals. The sanidine antecryst core in **H** is serrated. **I-L**: Plots of selected sanidines (green lines), with some of the profiles marked in the BSE and thin section images(blue, black and red lines). The sanidine profiles are plotted from rim (left) to core (right), and show mol% Or composition (low resolution in **I**, high resolution in **J**), and normalized wt%; BaO (**K**) and normalized wt% FeO (**L**) values.

Sample 037DR-2

Sample 037DR-2 was dredged from a small cone on the lower NNE flank of Cadamosto Seamount, at a water depth of 2450 m b.s.l. (**Fig. 2.2; Table 2.1**). This sample has the highest crystal content with up to 35% of the rock volume and vesicles are rare. The sample comprises feldspathoids (nepheline, and nosean-haüyne), sanidine, and aegirine-augite, with the latter mineral accounting for up to 10% of the rock volume (**Fig. 2.5**). Additional phases include titanite, apatite, and minor amounts of biotite, Fe-Ti oxides, and pyrite, in a microcrystalline groundmass. Carbonatite enclaves (mm-sized and calcite dominated) are also present in this sample, are inter-grown with apatite, feldspathoids, and titanite, and carbonatite surrounded by rims of aegirine-augite crystals. The sanidine crystals in this sample are idiomorphic to hypidiomorphic and up to 4 mm in diameter, but are also found in the groundmass (up to 70 µm in diameter).

Typical sanidines have one or two (nested) resorbed and rounded cores that have partly-irregular boundaries, with final overgrowth rims that are 25 µm to 85µm wide. The maximum thickness between the antecrystic cores and overgrowth rims is 960 µm (**Fig. 2.5A**). Biotite and feldspathoid inclusions are frequently observed in sanidine cores and show cellular textures, but some of the cores are free of inclusions (e.g., **Fig. 2.5C-F**). Groundmass microlites occur as inclusions in the rims of sanidine crystals (e.g., **Fig. 2.5A-B**). The sanidines are all reversely zoned, with core compositions of Or ~67 to 77 (average = Or 71) and rim compositions of Or 76 to 82 (average = Or 80; **Figs. 2.5G, 2.6**). This relatively uniform reverse zonation pattern in the sanidines is not observed in any of the other four samples. Groundmass sanidines have the same Or 80 compositions as the rims of the larger crystals (**Fig. 2.6**). Therefore, we suggest that the cores of the larger sanidines are antecrysts with phenocrystic overgrowth rims, and the smaller groundmass sanidines are phenocrysts.

In summary, three of the phonolite samples (149-2, 149-6 and 152-1; **Figs. 2.3-2.5,** Appendix 9.2.2) are similar in composition and mineral chemistry, and are all dominated by feldspathoids. The sanidine crystals have comparable compositions of Or 72 to 81 and show either no or slight normal zoning (e.g., **Figs. 2.3I, 2.6**), indicating that most of the crystal cargo consists of phenocrysts.

The remaining two samples yield more complex compositions and contain two or more crystal generations: Sample 035ROV-12 also contains mafic enclaves, and several groups of sanidine crystals that display resorbed cores and complex zoning patterns (normal, reverse, patchy and oscillatory; **Figs. 2.4, 2.6**). This suggests several entrained crystal generations of antecrysts. Sample 037DR-2 contains sanidine grains that display reverse zoning with resorbed cores (average Or = 71) and overgrowth rims up to 85 µm wide, with average compositions of Or 80 that are interpreted to be antecrystic sanidines with phenocrystic overgrowth rims (**Figs. 2.5, 2.6;** Appendix 9.2.2).

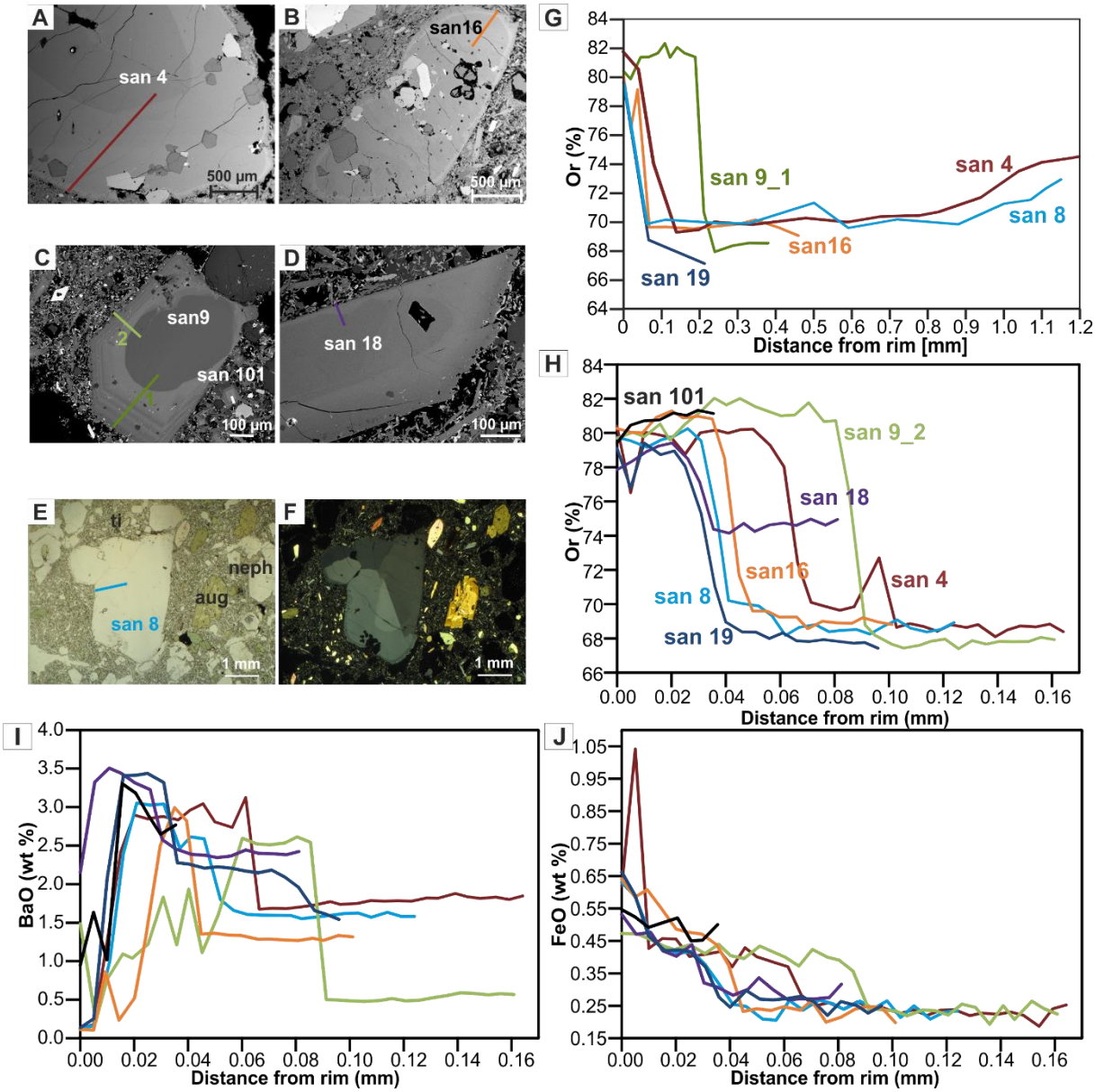

Figure 2.5 Sample 037DR-2. **A-D**: BSE images of sanidine crystals showing absorbed antecryst cores and phenocrystic overgrowth rims, as well as cellular textures (**B**) and mineral inclusions (A-B). E-F: Thin section images in plain (**E**) and crossed-polarized light (**F**), showing the sanidine (san) antecrysts and minor minerals titanite (ti), aegirine-augite (aug), and feldspathoids (nepheline; neph). **G-J**: Selected sanidine profiles from rim (left) to core (right), vs. mol% Or (low resolution in **G**, high resolution in **H**), and normalized wt% BaO (**I**) and wt%FeO (**H**). Some of the profile lines are marked in the BSE and thin section images (**A-F**).

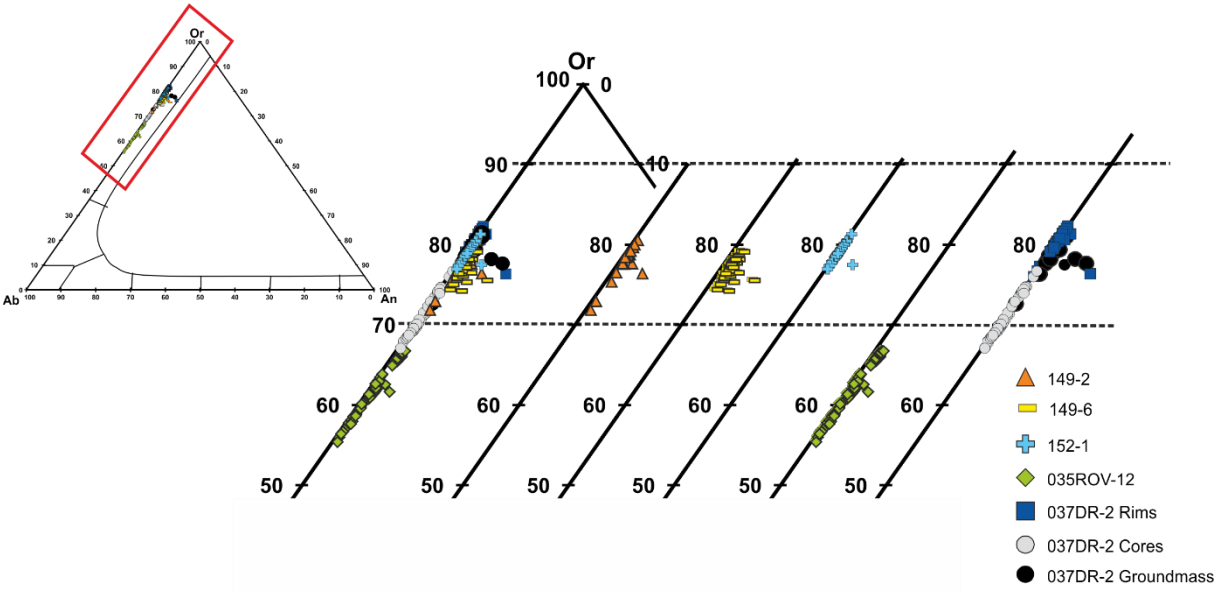

Figure 2.6 Ternary plot (insert) for the orthoclase (Or), albite (Ab) and anorthite (An) contents of the sanidines from five Cadamosto Seamount samples. The main plot shows details of the ternary plot (red rectangle) showing the range of mol% Or 50-100 values.

2.4.2 *^{40}Ar-^{39}Ar dating results*

^{40}Ar-^{39}Ar laser SCTF analyses of sanidine, nepheline and sodalite crystals from five Cadamosto Seamount samples provide an extensive set of 170 ages, which are summarized in **Figs. 2.7** and **2.8A-B.** Additionally, ^{40}Ar-^{39}Ar multi- and single-grain step-heating analyses were undertaken on four samples, and the data tables, age spectra and inverse isochrons are presented in Appendix 9.2.3. Weighted mean, plateau and inverse isochron ages from the SCTF and step-heated ^{40}Ar-^{39}Ar analyses are presented in **Table 2.2**. The weighted mean SCTF ages were determined using either the Excel-macro software *Isoplot* (v. 4.15; Ludwig 2011) that can identify statistical outliers, and/or examination of the ^{40}Ar-^{39}Ar data via inverse isochron plots. Statistical outliers or inverse isochron data that did not plot within 2σ errors of the inverse isochron were excluded in the determination of the 149-2, 149-6, 152-1 and 035ROV-12 SCTF weighted mean ages (Appendix 9.2.3). For the more complex Cadamosto Seamount sample (sample 037DR-2), the youngest ^{40}Ar-^{39}Ar analyses were selected from the smallest grain fraction, where some of the wt% K (^{39}Ar) values corresponded to wt % K (EMP) values obtained from sanidine phenocrysts or sanidine phenocrystic overgrowth rims (**Fig. 2.8B**).

The sanidine SCTF ^{40}Ar-^{39}Ar ages for all five samples range from 11.5 ± 6.5 ka to 611.9 ± 8.8 ka (n = 140). The SCTF sanidine ages from samples 149-2 and 149-6 are similar and range from 12.5 ± 8.0 ka to 29.8 ± 10.6 ka (n = 23), and 11.5 ± 6.5 ka to 29.0 ± 1.4 ka (n = 15), respectively.

The sanidine SCTF weighted mean age for sample 149-2 is 22.3 ± 2.0 ka (MSWD = 0.98; P = 49%; n = 22), with an inverse isochron age of 22.9 ± 2.9 ka (MSWD = 1.02; P = 44%; SF = 65%; ^{40}Ar/^{36}Ar$_i$ = 292 ± 13; n = 22; **Fig. 2.7; Table 2.2**). The multi-grain ^{40}Ar-^{39}Ar step-heating sanidine plateau age of sample 149-2 is 20.1 ± 1.0 ka (MSWD = 0.66; P = 73%; 100% ^{39}Ar), which is consistent with the inverse isochron age of 18.1 ± 5.8 ka (MSWD = 0.69; P = 68%; SF = 54%) with an initial ^{40}Ar/^{36}Ar (^{40}Ar/^{36}Ar$_i$) ratio of 322 ± 87 that is within 2σ errors of the atmospheric ^{40}Ar/^{36}Ar ratio of 295.5 (Steiger and Jäger 1977; **Table 2.2**).

Sample 149-6 was analyzed in 2011 by Paul van den Bogaard and the ^{40}Ar-^{39}Ar data were renumber-crunched in 2017, before analyses of the subsequent four samples in 2017-2018. The 149-6 sample yields a wide range of SCTF ages ranging from 11.5 ± 6.5 ka to 106352.2 ± 889.8 ka. Wt% K values were calculated using the K-derived ^{39}Ar isotopic analyses and measured grain weights (wt% K (^{39}Ar)), which suggested that three different minerals had been analyzed in the 2011 SCTF study of sample 149-6. The sanidine, nepheline and sodalite analyses in sample 149-6 yield wt% K(^{39}Ar) values

of 9.5-10.6, 3.9-4.6, and 1.4-1.5, respectively, which were corroborated by EMP wt% K values of 10.3-11.5, 3.1-5.3 and 0.4-1.6, respectively (**Figs. 2.8A**).

It was difficult to distinguish between these transparent minerals during hand-picking, as the crystals do not show pronounced crystal habits or colour differences, hence the array of different minerals that were analyzed in the 2011 study of sample 149-6. Therefore, 65°C HCl and HNO_3 acid leaching treatment in an ultrasonic bath was adopted for the remaining four samples, as this allowed complete dissolution of many transparent minerals. This included carbonates, leucite, sodalite, and the HCl acid treatment turns nepheline to a gel, which was separated from the unaffected sanidines. This hot HCl/HNO_3 acid treatment was suggested by Koppers et al. (2000) to remove alteration products from basaltic groundmass samples. We adapted the method to apply to our phonolite samples, to allow the preparation of pure sanidine mineral separates. As for altered basaltic groundmass samples, the 3.5 M HCl acid treatment was not found to impart any Cl contamination problems in the sanidine minerals separates. Routine monitoring of baseline mass 35.5 showed no increase from background levels, compared to increases at mass 35.5 that are observed during analyses of Cl-rich basaltic samples. The majority of $^{36}Ar/^{39}Ar$ AI values from the SCTF all indicate that fresh sanidines were analysed (Appendix 9.2.3).

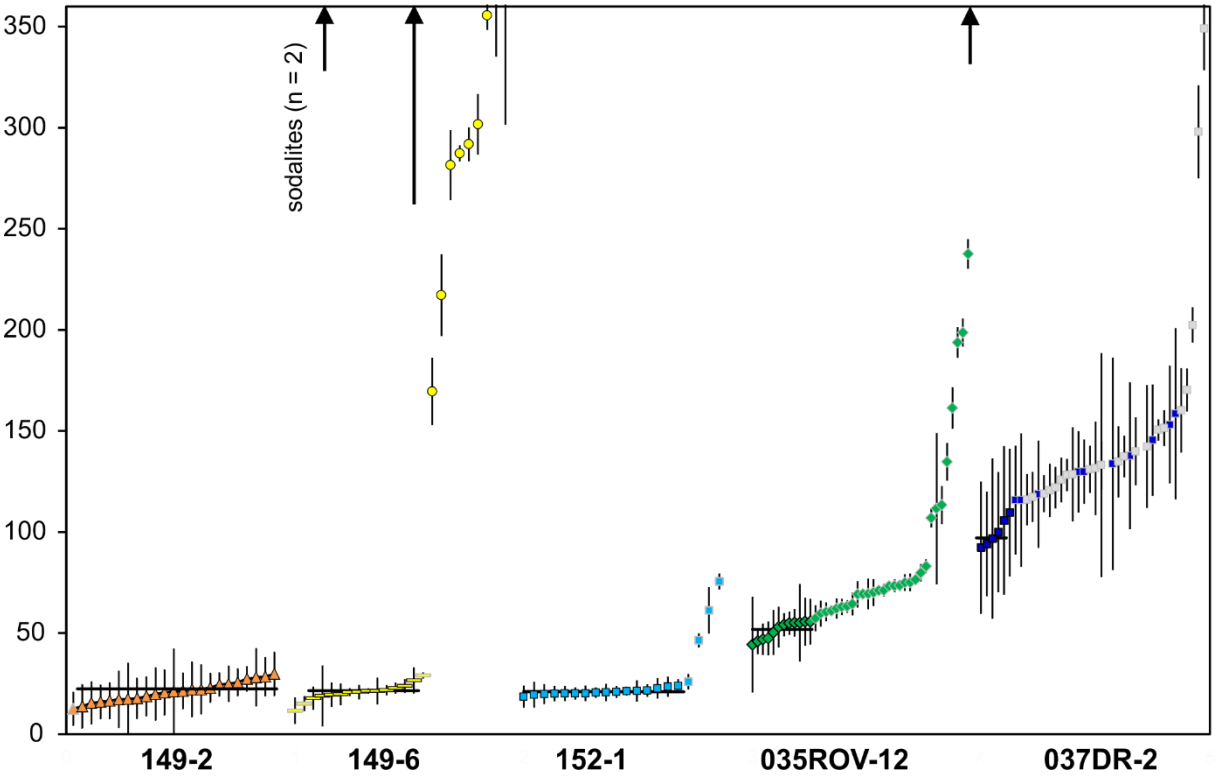

Figure 2.7 Stacked ages plot for the ^{40}Ar-^{39}Ar SCTF sanidine, nepheline and sodalite analyses from five Cadamosto samples, with 2σ uncertainties. The black horizontal lines and ages show the inverse-variance weighted mean ages (2σ errors), where the black-outlined symbols indicate selected analyses, and the grey-outlined symbols shown unselected analyses.

The sanidine SCTF weighted mean age for sample 149-6 is similar to sample 149-2, being 21.44 ± 0.80 ka (MSWD = 0.80, P = 64%; *n* = 12), with an inverse isochron age of 20.6 ± 1.4 ka (MSWD = 0.67; P = 76%, SF = 32%; $^{40}Ar/^{36}Ar_i$ = 300.2 ± 6.3; *n* = 12; for sample 149-6; **Fig. 2.7; Table 2.2**). No laser step-heating was undertaken on a single-/multi-crystal sample of sample 149-6. The nepheline SCTF ^{40}Ar-^{39}Ar ages from sample 149-6 appear to be at least one order of magnitude older than the 149-6 sanidine ages, ringing from 169.5 ± 16.5 ka to 1521.5 ± 8.3 ka (*n* = 27; **Fig. 2.8A**). Due to the large spread of ages in the nepheline analyses, we were only able to determine one inverse isochron from *n* = 3 analyses, with ages ranging from 355.5 ± 7.1 ka to 383.0 ± 81.4 ka. They yielded an inverse isochron age of 356.7 ± 7.3 ka (MSWD = 0.72; P = 40%; SF = 84%; *n* = 3) with a $^{40}Ar/^{36}Ar_i$ ratio of 297.3 ± 5.3, within 2σ errors of the atmospheric $^{40}Ar/^{36}Ar$ ratio (Appendix 9.2.3). Two sodalite SCTF analyses from sample 149-6 yield even older ages of 105549 ± 489 ka and 106352 ± 890 ka (**Fig. 2.8A**). No inverse isochron could be plotted from these two sodalite analyses.

The SCTF ages from sample 152-1 from the western Cadamosto Seamount summit area range from 18.5 ± 5.3 ka to 75.6 ± 3.8 ka (n = 20), yielding a weighted mean age of 20.98 ± 0.87 ka (MSWD = 0.50; P = 94%; *n* = 16; **Fig. 2.7**), with an inverse isochron age of 20.7 ± 1.4 ka (MSWD = 0.50, P = 93%, SF = 53%; $^{40}Ar/^{36}Ar_i$ = 301 ± 17; **Table 2.2**). The weighted mean age is within 2σ errors of the multi-grain step-heating sanidine plateau age of 22.3 ± 1.1 ka (MSWD = 1.23; 93% ^{39}Ar). The inverse isochron age from the plateau steps is 22.9 ± 3.1 ka (MSWD = 1.79; P = 17%, SF = 53%; $^{40}Ar/^{36}Ar_i$ = 245 ± 320; **Table 2.2**).

The SCTF sanidine ages from sample 035ROV-12 are generally older, ranging from 44.3 ± 23.5 ka to 611.9 ± 8.8 ka (*n* = 43), yielding a youngest group weighted mean age of 51.8 ± 2.4 ka (MSWD = 0.98; P = 46%; *n* = 12; **Fig. 2.7**). The SCTF inverse isochron age from this youngest group is 48.3 ± 5.5 ka (MSWD = 0.86; P = 57%, SF = 44%; $^{40}Ar/^{36}Ar_i$ = 341 ± 71; **Table 2.2**. The weighted mean age is within 2σ errors of the single-grain (2.8 x 1.5 x 0.5 mm) sanidine step-heating plateau age of 56.8 ± 4.4 ka (MSWD = 1.01; P = 39%; 71%^{39}Ar). The inverse isochron age from the plateau steps is 51 ± 14 ka (MSWD = 0.90; P = 41%; SF = 89%; $^{40}Ar/^{36}Ar_i$ = 452 ± 477; **Table 2.2**).

Sample 037DR-2 preserves the oldest SCTF sanidine ages, ranging from 92.3 ± 32.6 ka to 349.0 ± 20.4 ka (*n* = 40; **Fig. 2.7**). The SCTF youngest group weighted mean age is 97 ± 14 ka (; MSWD = 0.10; P = 98%; *n* = 5). The youngest group SCTF analyses yield a poorly defined inverse isochron age of 90 ± 46 ka (MSWD = 0.093; P = 96%; SF = 20%; $^{40}Ar/^{36}Ar_i$ = 306 ± 61; *n* = 5; **Table 2.2**), with low MSWD and < 40 % spreading factor values (Jourdan et al. 2009). The SCTF weighted mean age is younger than two overlapping sanidine multi-grain step-heating high-temperature weighted mean and plateau ages of 131.9 ± 3.7 ka (MSWD = 1.25; P = 29%; 33% ^{39}Ar), and 126.6 ± 3.3 ka (MSWD = 1.23; P = 29%; 87% ^{39}Ar), for the 037DR-2 0.25-0.5 mm and 0.5-1.0 mm size fractions, respectively. The inverse isochrons from these two step-heated fraction sizes yield poorly defined ages of 99 ± 49 ka (MSWD = 1.41; P = 24%; SF = 33%; $^{40}Ar/^{36}Ar_i$ = 714 ± 2480) for the finer 0.25-0.5 mm size fraction, and 138 ± 13 ka (MSWD = 0.97; P = 43%; SF = 35%; $^{40}Ar/^{36}Ar_i$ = 259 ± 41) for the coarser 0.5-1.0 mm size fraction, with low < 40% spreading factors (Jourdan et al. 2009;**Table 2.2**).

Due to the measurement of small quantities of ^{40}Ar and ^{39}Ar from SCTF analyses in these Pleistocene Cadamosto Seamount samples, the ^{40}Ar-^{39}Ar errors can be large (e.g., 0.5% up to101% 2σ; **Appendix 9.2.3**). The larger errors are most noticeable in the younger analyses and those from finer grain fractions, e.g., the 0.25-0.5 mm fraction of in sample 037DR-2 (compared to SCTF analyses from the larger 0.5-1 mm size fractions of 037DR-2 (**Fig. 2.8B**). It should be noted that the youngest eight SCTF sanidine ages (92.3 ± 32.6 ka to 115.7 ± 32.8 ka) for sample 037DR-2 all originate from the 0.25-0.5 mm size fraction. Five of these ^{40}Ar-^{39}Ar sanidine ages yield the 97 ± 14 ka youngest age for this 037DR-2 sample. Three of these five analyses also yield wt% K(^{39}Ar) values within 2σ errors of the wt% K(EMP) values from the sanidine phenocrysts and phenocrystic overgrowth rims (**Fig. 8B**). In contrast the five oldest SCTF ages (160.2 ± 20.8 ka to 349.0 ± 20.4 ka) in sample 037DR-2 all originate from the coarser 0.5-1.0 mm size fraction, and nearly all have wt% K(^{39}Ar) values within 2σ errors of the wt% K (EMP) of the sanidine antecrystic cores (**Fig. 2.8B**).

Table 2.2 Eruption ages from single-crystal total-fusion sanidine ^{40}Ar-^{39}Ar analyses

Sample #	Mineral	Size fraction (mm)	Weighted mean age ± 2σ (ka)	MSWD	P (%)	*n*	Inverse isochron age ± 2σ (ka)	Initial $^{40}Ar/^{36}Ar$	MSWD	P (%)	SF (%)	*n*
149-2	K-feldspar	0.5-1	22.3 ± 2.0	0.98	49	22	22.9 ± 2.9	292 ± 13	1.02	44	65	22
149-6	K-feldspar	0.5-2	21.44 ± 0.80	0.80	64	12	20.6 ± 1.4	300.2 ± 6.3	0.67	76	*32*	12
152-1	K-feldspar	>1	20.98 ± 0.87	0.50	94	16	20.7 ± 1.4	301 ± 17	0.50	93	53	16
035ROV-12	K-feldspar	>1	51.8 ± 2.4	0.98	46	12	48.3 ± 5.5	341 ± 71	0.86	57	44	12
037DR-2	K-feldspar	0.25-0.5 & 0.5-1	97 ± 14	*0.10*	98	5	90 ± 46	306 ± 61	*0.093*	96	*20*	5

Combined single-crystal total-fusion K-feldspar ages from samples 149-2, 149-6 and 152-1

Sample #	Mineral	Size fraction (mm)	Weighted mean age ± 2σ (ka)	MSWD	P (%)	*n*	Inverse isochron age ± 2σ (ka)	Initial $^{40}Ar/^{36}Ar$	MSWD	P (%)	SF (%)	*n*
149-2, 149-6 & 152-1	K-feldspar	0.5 to >1	21.14 ± 0.62	1.30	7	53	20.56 ± 0.90	299.1 ± 5.3	1.30	9	74	53

Multi- and single-grain step-heating sanidine ^{40}Ar-^{39}Ar analyses

Sample #	Mineral	Size fraction (mm)	Plateau age ± 2σ (ka)	MSWD	P (%)	% ^{39}Ar	Inverse isochron age ± 2σ (ka)	Initial $^{40}Ar/^{36}Ar$	MSWD	P (%)	SF (%)	Steps
149-2	K-feldspar	0.5-1	20.1 ± 2.0	0.66	73	100	18.1 ± 5.8	322 ± 87	0.69	68	54	1-9
152-1	K-feldspar	> 1 (7 grains)	22.3 ± 1.1	1.23	30	93	22.9 ± 3.1	245 ± 320	1.79	17	53	5-8
035ROV-12	K-feldspar	2.8 x 1.5 x 0.5 (1 grain)	56.8 ± 4.4	1.01	39	71	51 ± 14	452 ± 477	0.90	41	89	1-4
037DR-2	K-feldspar	0.25-0.5	131.9 ± 3.7*	1.25	29	*33*	99 ± 49	714 ± 2480	1.41	24	*13*	5-8
037DR-2	K-feldspar	0.5-1	126.5 ± 3.3	1.23	29	87	138 ± 13	259 ± 41	0.97	43	*35*	3-9

Abbreviations: *MSWD* Mean Square Weighted Deviation, *P* Probability (%), *n* number of analyses, *SF* Spreading factor.
Values in italics = statistically invalid values showing overestimated errors (MSWD < 0.30 or P values of < 5%), or SF values of < 40%.
Plateau, weighted mean and inverse isochron ages include analytical and J value and correction factor errors, plus error magnification for MSWD values > 1.0.
*Pseudo plateau (40-49% total ^{39}Ar) or high-temperature weighted mean (< 39% total ^{39}Ar) ages.

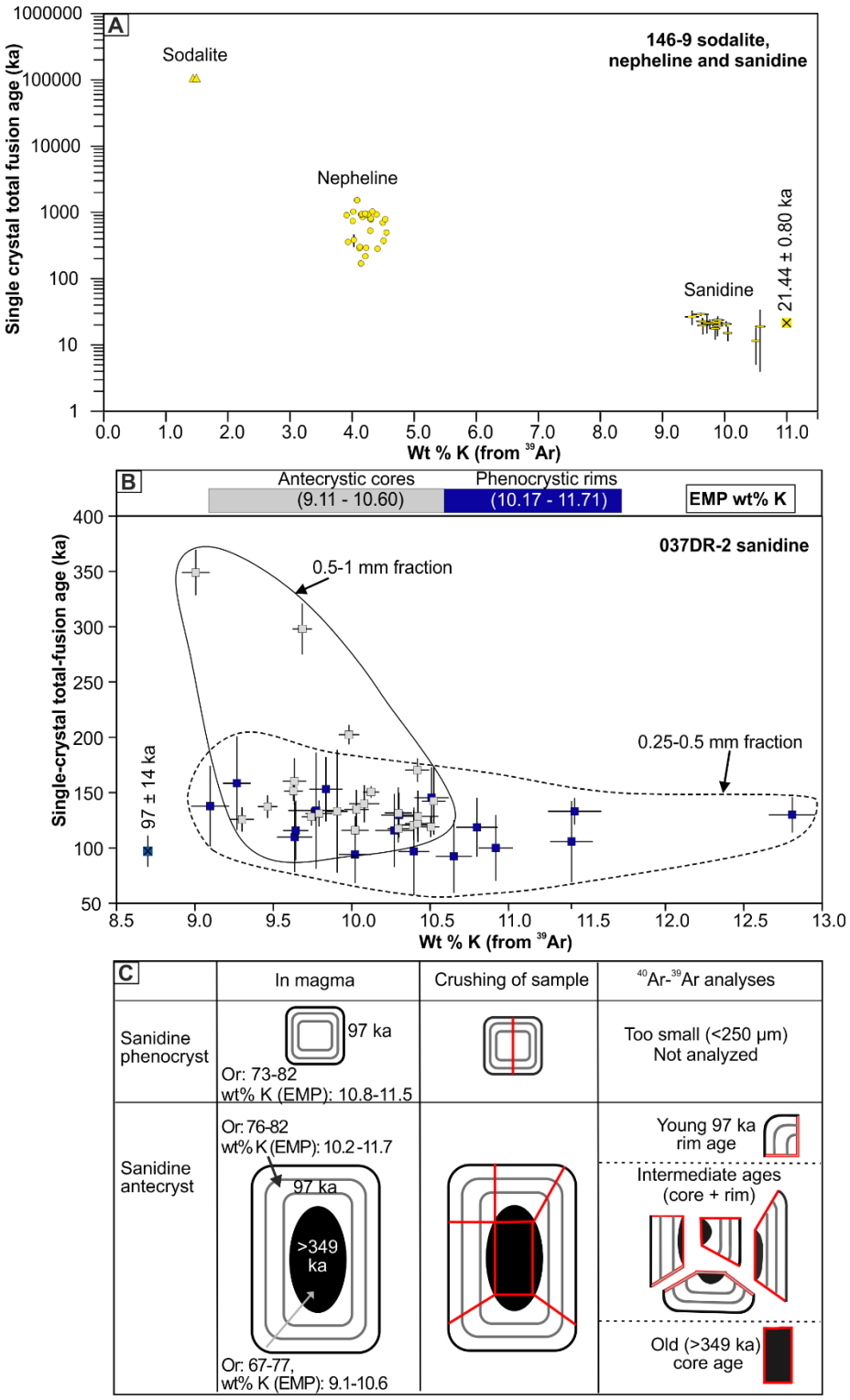

Figure 2.8 A: Wt% K(^{39}Ar) vs. SCTF ages for sodalites, nephelines and sanidines from sample 149-6. The yellow crossed box shows the 21.44 ± 0.80 ka sanidine eruption age for this sample. **B**: Wt% K(^{39}Ar) vs. SCTF ages for sanidines from two size fractions - 0.25-0.5 mm (blue squares) and 0.5-1 mm (grey squares) - from sample 037DR-2. The upper box shows the range of wt% K(EMP) values obtained from sanidine antecrystic cores and phenocrystic rims, for comparison with the ^{40}Ar-^{39}Ar data. The blue crossed box shows the 97 ± 14 ka sanidine eruption age for sample 037DR-2. The x- and y-axes error bars in **A-B** show 2σ errors associated with the ^{39}Ar measurements and ^{40}Ar-^{39}Ar ages, respectively. **C**: Schematic diagram showing the possible sources for the myriad of SCTF sanidine ages obtained from sample 037DR-2. The maximum eruption age of 97 ± 14 ka may be sourced from phenocrystic overgrowth rims. The multitude of intermediate SCTF sanidine ages in sample 037DR-2 may originate from a mixture of partially degassed antecrystic cores and overgrowth rims. The oldest SCTF sanidine age of 349.0 ± 20.4 ka should be considered a minimum antecryst core age, as the antecrysts may have undergone some ^{40}Ar* loss during entrainment in the final magma.

2.5 Discussion

2.5.1 Magma chamber processes at Cadamosto Seamount

Based on their mineralogy and mineral zonation patterns, the analyzed samples from Cadamosto Seamount indicate a variety of igneous processes occurring in the magma plumbing system within and below the seamount, all of which should be taken into consideration in the interpretation of the ^{40}Ar-^{39}Ar dating results.

Samples 149-2, 149-6 and 152-1 show petrologic similarities and are mainly composed dominated by sanidine phenocrysts. The mineral chemistry of the large sanidines and smaller groundmass sanidine crystals are similar (**Fig. 2.6;** Appendix 9.2.2). Some of the larger sanidines preserve weak normal zonation patterns (**Fig. 2.3I**), which indicates that closed system crystal fractionation was the dominant process. However, the presence of sanidine antecrysts in these three samples cannot be completely excluded. Some of the larger nepheline crystals (0.5-3 mm in diameter) in sample 149-6 preserve resorbed cores and thin overgrowth rims, which suggests that they may be antecrysts. This observation is confirmed by the presence of older ^{40}Ar-^{39}Ar nepheline ages in sample 149-6 (**Figs. 2.7, 2.8A**).

Sample 035ROV-12 reflects a more complex magmatic history. The highly crystalline mafic enclaves suggest magma mixing of a more mafic magma batch into the phonolite magma, probably inducing enhanced crystallization of the more mafic magma due to cooling. The presence of rounded minerals (e.g., biotites, **Figs. 2.4A-B**), further indicates reaction and dissolution due to changes in the chemical/physical conditions within the magma. The large sanidines in sample 035ROV-12 are not uniform and show various textures. Some sanidines preserve one resorbed core and only a thin overgrowth rim. A second group has absorbed cores that show an irregular serrated pattern, a second resorbed core, and a thin overgrowth rim, and a third group of sanidines that preserves several growth zones, of which some also show additional resorption textures (**Fig. 2.4**). These hypidiomorphic- and xenomorphic-shaped sanidines with resorbed cores and/or resorbed rims (**Figs. 2.4, 2.6;** Appendix 9.2.2), indicate repeated episodes of dissolution and growth (e.g., Triebold et al. 2006). Normal, reverse and oscillatory zonation patterns in the sanidines, and the presence of different groups of sanidines in 035ROV-12 suggest that these crystals are antecrysts from two or more batches of magma (**Fig. 2.4**). Already incorporated in the final magma, some of these antecrystic sanidines may have experienced changes in chemical and physical crystallization conditions. This is also reflected by the composition of these sanidines, as zonation patterns are recorded by the minor elements Ba and Fe, which preserve different growth zones and show a pronounced rise at the outermost 5 µm to 20 µm overgrowth rim (**Fig. 2.4K-L**). This indicates replenishment with a more mafic magma and/or convection within the magma shortly before eruption (Ginibre et al. 2007). These complexities may result in the preservation of a series of complex sanidines, which is confirmed by the presence of variable ^{40}Ar-^{39}Ar sanidine ages in this 035ROV-12 sample (**Figs. 2.4, 2.7**).

Compared to sample 035ROV-12, the sanidines in sample 037DR-2 are more uniform in composition (**Fig. 2.5;** Appendix 9.2.2). The 037DR-2 groundmass sanidine phenocrysts and the overgrowth rims on the larger antecrystic sanidines show similar Or contents (Or 80). Together with observed inclusions of groundmass crystals and matrix minerals within the sanidine overgrowth rims (e.g. **Fig. 2.5D**), this indicates that the sanidine phenocrysts and the overgrowth rims on the resorbed sanidine antecrysts crystallized under similar conditions. The antecrystic sanidine cores are commonly resorbed, indicating dissolution occurred before the formation of overgrowth rims. Dissolution is also suggested by cellular textures and mineral inclusions in some larger sanidine antecrysts (Streck 2008). A distinct compositional change is reflected in the major element compositions (e.g., K) by a steep increase from Or 71 in the cores to an average of Or 80 in 25µm to 85µm thick overgrowth rims. Minor elements (e.g., Fe and Ba) preserve the same pattern, with a steep increase from core to rim. The outermost few microns of the rim preserve a rapid decrease in Ba, which is probably due to exhaustion of Ba in the host melt. The Ba zonation pattern indicates a replenishment from a more mafic magma and/or convection within the magma, rather than changes in pressure/temperature conditions or the flushing of additional volatiles into the magma (cf., Ginibre et al. 2007, Ruprecht and Wörner 2007; **Fig. 2.5I-K;** Appendix 9.2.2). The chemical compositions of the sanidine rims from sample 037DR-2 from the NE flank of Cadamosto Seamount,

and the sanidine phenocrysts from the three western summit/flank samples (149-2, 149-6 and 152-1) are relatively similar with average Or contents of 77-80% (**Figs. 2.3, 2.5, 2.6**), testifying to an origin from largely similar and homogenous magma batches. However, the antecrystic core compositions in some sanidines from sample 037DR-2 overlap with some sanidine compositions in sample 035ROV-12 (**Fig. 2.6**). The complex crystal zonation patterns and resorption features in sanidines from these two samples strongly suggest a comparatively complicated magma evolution. This may involve two or more magmatic evolutionary stages, and thus two or more generations of sanidine crystals. One explanation for this variety of crystal generations could be the interaction between two magmas that partly exchange crystals (e.g., Triebold et al. 2006), the incorporation of antecrystic material into the magmas, or a combination of both these processes.

The presence of overgrowth rims on sanidine antecrysts in samples 035ROV-12 and 037DR-2 that preserve similar compositions to phenocrysts in the groundmass suggests that these antecrysts spent some time in the final magma before eruption. To calculate these residence times, we used the sanidine overgrowth rim thicknesses (from analyzed EMP compositional profiles, and BSE images), and a sanidine crystal growth rate of ~1.2×10^{-10} cm s^{-1} (Zellmer and Clavero 2006). This sanidine growth rate was estimated for a magmatic temperature of 875°C, and we have also used this temperature as an estimate of the phonolite magma temperature, which is similar to the temperature of 900°C reported by Stoppa et al. (2017). This sanidine growth rate is consistent with other feldspar growth rates, e.g., plagioclase growth rates of 10^{-10} to 10^{-11}cm s^{-1} in shallow magmatic systems (Cashman 1993). In sample 035ROV-12, the final overgrowth rims range from 5 µm to 20µm. Assuming that the sanidine overgrowth rims grew in the final magma before eruption, the antecrystic sanidines spent 48 to 193 days in the final magma before eruption (**Appendix 9.2.4**). Magma residence durations in sample 037DR-2 with final overgrowth rim widths of 25 µm to 85 µm have been calculated at 241 to 820 days (**Appendix 9.2.4**). These magma residence times are similar to the timescales required for processes such as magma degassing (hours-decades), magma ascent (hours-milleniums), and magma mixing, assimilation and recharge (hours-centuries; e.g., Turner and Costa 2007).

2.5.2 Timing of magmatic events at Cadamosto Seamount

In the following section we discuss the SCTF sanidine, nepheline and sodalite ages, and sanidine single-/multi-grain step heating results from five Cadmosto Seamount samples. We use the term "eruption age" to refer to the youngest group of SCTF sanidine ages in each individual sample (**Table 2.2**). In samples that are dominated by sanidine phenocrysts (i.e., 149-2, 149-6, and 152-1), we suggest that this youngest group of ages records the timing of the final magma eruption event. In samples dominated by sanidine antecryts with phenocrystic overgrowth rims (035ROV-12 and 037DR-2) that were incorporated prior to eruption, the youngest group of ages may represent maximum eruption ages. Given the observed presence of generations of sanidine and nepheline antecrysts in three of the Cadamosto Seamount samples (149-6, 035ROV-12 and 037DR-2), the older ^{40}Ar-^{39}Ar SCTF ages are hereby termed "antecryst ages". However, due to the possible effects of ^{40}Ar* loss during entrainment into the final eruptive magma, these antecryst ages are considered to be minimum ages. We will also discuss the ^{40}Ar-^{39}Ar ages obtained from these five Cadamosto Seamount phonolites in terms of the published phonolitic magma ages from other volcanic islands in the Cape Verde Archipelago.

Volcanic eruption ages at Cadamosto Seamount

The majority of ^{40}Ar-^{39}Ar SCTF sanidine ages for samples 149-2, 149-6 and 152-1, and the sanidine multi-grain step-heating plateau ages (149-2 and 152-1) are young and overlap within 2σ uncertainties (**Fig. 2.7; Table 2.2**). Therefore, the phenocrystic sanidines in these three samples are interpreted to be yield eruption ages, which is in agreement with our petrological observations.

Sample 152-1 predominantly comprises sanidine phenocrysts, however this sample does yield four older SCTF sanidine ages (26.0 ± 3.7 ka to 75.6 ± 3.8 ka; **Fig. 2.7)**, which may be due to the presence of some sanidine antecrysts. Each of these three samples (149-2, 149-6 and 152-1) yield overlapping statistically-valid SCTF weighted mean eruption ages of 22.3 ± 2.0 ka (149-2), 21.44 ± 0.80 ka (149-6), and 20.98 ± 0.87 ka (152-1), which allows the determination of a combined weighted mean age of 21.14 ± 0.62 ka (**Fig. 2.7; Table 2.2**). These SCTF weighted mean ages are additionally

confirmed by sanidine step-heating plateau ages of 20.1 ± 2.0 ka (149-2), and 22.3 ± 1.1 ka (152-1), with comparable inverse isochron ages and $(^{40}Ar/^{36}Ar)_i$ values within 2σ errors of the atmospheric $^{40}Ar/^{36}Ar$ ratio (**Table 2.2**). This combined weighted mean age of 21.14 ± 0.62 ka may record a pronounced eruption activity period that overlapped in time for at least two different eruption centers, i.e., the western flank (samples 149-2 and 149-6), and the western summit area (sample 152-1; **Fig. 2.2**).

Sample 035ROV-12 preserves an older SCTF ^{40}Ar-^{39}Ar eruption age of 51.8 ± 2.4 ka, which is within 2σ errors of a single-grain step-heating plateau age of 56.8 ± 4.4 ka (**Table 2.2**). As this sample is shown to contain several different groups of sanidine antecrysts, the 51.8 ± 2.4 ka age is considered to be a maximum age for this eruption event.

Sample 037DR-2 yields a SCTF eruption age of 97 ± 14 ka (**Table 2.2**), which is derived from five analyses of the smallest grain size fraction (0.25-0.5 mm). Three of these five ages have wt% K(^{39}Ar) values that overlap with the wt% K(EMP) concentrations from the sanidine phenocrystic overgrowth rims (**Fig. 2.8B**). However, as this 037DR-2 sample is shown to contain abundant sanidine antecrysts with final overgrowth rims up to 85 μm wide , the majority of the SCTF ages from the 0.25-0.5 and 0.5-1 mm size fractions are most likely due to mixing of sanidine antecrysts and phenocrystic overgrowth rims (shown schematically in **Fig. 2.8C**). Therefore the 97 ± 14 ka eruption age for sample 037DR-2 is considered to be a maximum age for eruption.

Sanidine antecryst ^{40}Ar-^{39}Ar ages and possible $^{40}Ar^*$ loss

In contrast to the relatively simple nature of the sanidine phenocrysts in sample 149-2, 149-6 and 152-1, two Cadamosto samples (035ROV-12 and 037DR-2) preserve a multitude of older ^{40}Ar-^{39}Ar SCTF sanidine ages ranging from 57.3 ± 6.3 ka to 611.9 ± 8.8 ka (n = 31), and 110 ± 31 ka to 349 ± 20 ka (n = 35), respectively (**Fig. 2.7**). Petrological observations of 035ROV-12 and 037DR-2 suggest that these sanidine crystals underwent dissolution with subsequent multiple generations of sanidine overgrowth rims (**Figs. 2.4-2.6**). The total overgrowth rims are thus 1.64 mm (035ROV-12) and 0.96 mm (037DR-2) wide (**Figs. 2.4F, 2.5A**). Therefore, the older SCTF ages are interpreted to be due to the presence of sanidine antecrysts, which were entrained and heated during possibly multiple magmatic events. This entrainment and continued heating of sanidine antecrysts in the multiple magmas may have resulted in $^{40}Ar^*$ loss and resetting of the original ^{40}Ar-^{39}Ar ages. To gauge this potential effect, we modelled the % of $^{40}Ar^*$ diffusive loss and the resetting of sanidine ^{40}Ar-^{39}Ar ages in two samples, using an author-written MathCAD program. We used the Ar diffusion parameters of Benson Mines orthoclase (note that orthoclase and sanidines shre similar Ar diffusion parameters; Cassata and Renne 2013), an estimated phonolite magma temperature of 875°C, and the minimum to maximum magma residence times 48 days to 43 years (035ROV-12), and 191 days to 25 years (037DR-2; **Fig. 2.9A;** Appendix 9.2.4).

The magma residence times versus model $\%^{40}Ar^*$ losses in the antecrystic sanidines from samples 035ROV-12 and 037DR-2 are plotted in **Fig. 2.9A**. In addition, we used the oldest ^{40}Ar-^{39}Ar SCTF sanidine ages of 237 ka and 612 ka from samples 035ROV-12 and 037DR-2, respectively, to plot the magma residence times versus the ^{40}Ar-^{39}Ar modeled resetting age windows for the largest sanidine antecrysts (**Fig. 2.9B**). We also show the SCTF antecryst ages with 2σ errors for direct comparison with the modelled ages (**Fig. 2.9B**).

Fig. 2.9A shows modeled $\%^{40}Ar^*$ losses of 18 to 100% (035ROV-12) and 46 to 100% (037DR-2), using estimated maximum grain diameters of 5 mm and 4 mm, respectively. **Fig. 2.9B** shows that our SCTF sanidine ages match very well with the modeled ages from the partially-reset 4-5 mm sanidine crystals. This modeling suggests that our sanidine SCTF ages may be partially reset antecrysts, with the relatively large amounts of $^{40}Ar^*$ loss being the result of long residence times in entraining magma(s), prior to eruption.

In summary, the large range in SCTF sanidine ages in samples 035ROV-12 and 037DR-2 may be the result of (1) relatively un-degassed antecryst cores from large grains yielding minimum antecryst ages; (2) partially degassed antecryst core ages, (3) young eruption ages from phenocrystic overgrowth rims and/or fully degassed antecrysts, or (4) a mixture of all these components (**Fig. 2.9**; shown schematically for sample 037DR-2 in **Fig. 2.8C**). The two multi-grain step-heating sanidine age spectra from sample 037DR-2 are discordant and yield a high-temperature weighted mean age of 131.9 ± 3.7 ka from the 0.25-0.5 mm size fraction, and a plateau age of 126.5 ± 3.3 ka from the 0.5-

1 mm size fraction (**Table 2.2;** Appendix 9.2.3). These two step-heating ages overlap within 2σ errors, but are both older than the SCTF sanidine maximum eruption age of 97 ± 14 ka (**Table 2.2**). These step-heating results suggest that the multi-grain sanidine aliquots contained a mixture of crushed sanidine material from partially degassed antecrysts and phenocrystic overgrowth rims, resulting in discordant age spectra, and geologically meaningless ages. This underlines the importance of careful examination of samples before selecting the appropriate ^{40}Ar-^{39}Ar technique to use, i.e., total-fusion or step-heating.

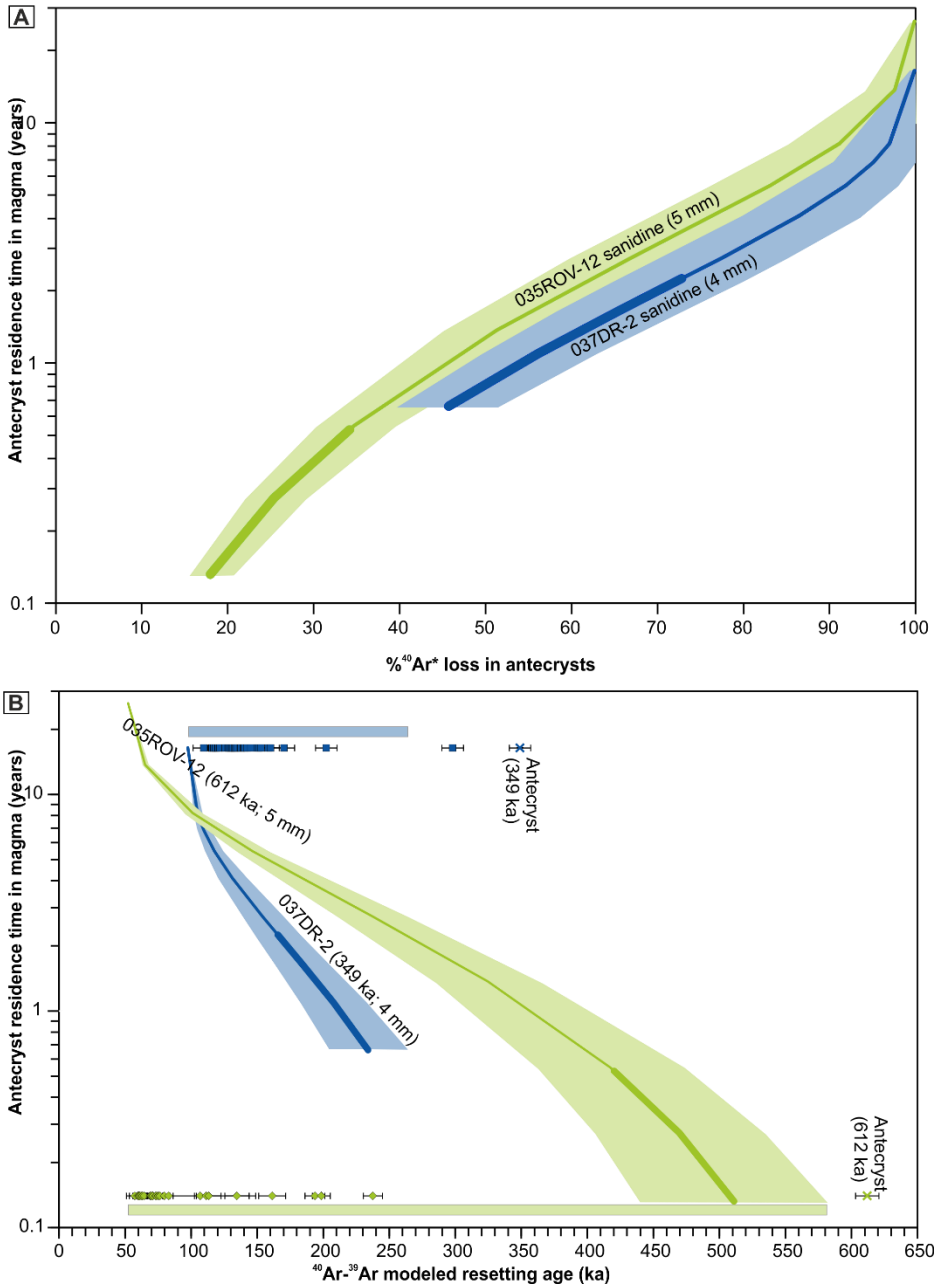

Figure 2.9 Modeling of the potential effects of entrainment of sanidine antecrysts into subsequent magma(s) for Cadamosto Seamount samples 035ROV-12 and 037DR-2. **A**: Modeled %^{40}Ar* loss vs. residence time in magma (log scale) for sanidine antecrysts (colored lines: The thin and thick lines are from estimated ^{40}Ar* losses associated with total and final phenocrystic overgrowth rim widths, respectively, and the shaded areas around the lines show 2σ errors associated with the Ar diffusion parameters from Cassata and Renne (2013)). **B**: ^{40}Ar-^{39}Ar modeled resetting ages using the %^{40}Ar* loss determinations vs. antecrysts residence time in the magma (log scale). The thin and thick lines estimated from reset ages associated with total and final phenocrystic overgrowth rim widths, repectively, and the shaded areas around the lines show 2σ errors associated with the Ar diffusion parameters from Cassata and Renne (2013). The same assumptions are used as in A, and for the purposes of the modeling we have used the oldest sanidine ages for each sample as these will be minimum sanidine antecryst ages (X symbols). The colored squares and diamonds show the SCTF ^{40}Ar-^{39}Ar sanidine ages, with 2σ error bars. The shaded rectangles indicate the range of modeled reset ages associated with the grain sizes and minimum to maximum magma residence times, for easy comparison with the ^{40}Ar-^{39}Ar SCTF sanidine data.

Nepheline and sodalite $^{40}Ar/^{39}Ar$ SCTF ages and the possibility of excess ^{40}Ar

The ^{40}Ar-^{39}Ar SCTF ages of nepheline antecrysts (169.5 ± 16.5 ka to 155.15 ± 8.3 ka) and sodalite phenocrysts (105.55 ± 0.49 Ma and 106.35 ± 0.89 Ma) in sample 149-6 are orders of magnitude older than the sanidine phenocryst eruption age of 21.44 ± 0.80 ka in the same sample (**Fig. 2.8A**). The nepheline and sodalite ages may indicate either (1) the full or partial preservation of very old antecrystic sodalite and nepheline ages indicating evidence of a long-lived magma plumbing system below Cadamosto Seamount, or (2) the presence of excess ^{40}Ar in these minerals.

Excess Ar is defined as ^{40}Ar that is not associated with atmospheric ^{40}Ar, and is incorporated into samples by processes other than the *in situ* radiogenic decay of ^{40}K (e.g., McDougall and Harrison 1999). Inverse isochron plots can reveal the presence of excess Ar in samples, as shown by initial $^{40}Ar/^{36}Ar$ ratios that are greater than the $^{40}Ar/^{36}Ar$ atmospheric ratio.

Due to the large variation in SCTF nepheline ages in sample 149-6, we could only produce one inverse isochron on three nepheline grains (355.5 ± 7.1 ka to 383.0 ± 81.4 ka). This plot yields an inverse isochron age of 356.6 ± 7.3 ka (MSWD = 0.72, P = 40%, SF = 84%) with an initial $^{40}Ar/^{36}Ar$ ratio of 297.3 ± 5.3, which is within 2σ errors of the $^{40}Ar/^{36}Ar$ atmospheric ratio (**Appendix 9.2.3**). This suggests that the older nepheline SCTF ages in sample 149-6 do not appear to be due to the contaminating effects of excess ^{40}Ar, and may indeed be robust antecryst ages.

Unfortunately, only two SCTF analyses were undertaken on sodalite crystals in sample 149-6 so no inverse isochron could be plotted to confirm the presence of excess ^{40}Ar. It is difficult to explain the ~106 Ma SCTF sodalite ages being antecrysts ages for the following reasons. Considering that the crustal basement age in the Cadamosto Seamount is ~120 Ma (Müller et al. 2008) and sodalite has relatively fast Ar diffusion properties (Kopelevich and Chang 2001), any sodalite antecrysts entrained in a magma would rapidly lose their $^{40}Ar^*$ and yield reset ~21 ka ages. For example, a 0.5 mm diameter sodalite crystal would lose 95% of its $^{40}Ar^*$ in only 4.5 days in a 875°C entraining magma, compared to 39 days for a similarly-sized sanidine or nepheline antecryst under the same conditions (assuming that nepheline has similar Ar diffusion properties to orthoclase/sanidine (Wartho et al. 1999)). The crystal lattice of sodalite (a six-ring structure) allows the incorporation of large amount of chemically unbound material, making them potential reservoirs for excess ^{40}Ar (Barrer and Vaughan 1971, Lippolt et al. 1990). Our SCTF sodalite ages are nearly 5,000 times older than the SCTF phenocrystic sanidine eruption age of 21.44 ± 0.80 ka in sample 149-6 (**Fig. 2.8A**). K-Ar studies (York et al. 1969, Lippolt et al. 1990) also found sodalite ages that are 1.4-2.7 and 27-29 times older than the respective geologically-meaningful biotite and nepheline ages, and sanidine ages from the same samples. In addition, excess ^{40}Ar contamination has been observed in other Cape Verde islands (e.g., Brava and Santo Antão (Plesner et al. 2002, Madeira et al. 2010). Therefore, as has been noted in other studies, our ~106 Ma SCTF sodalite ages are more likely due to the contaminating effects of excess ^{40}Ar, and provide no geochronologically relevant information on Cadamosto Seamount.

The reasons for the presence of excess ^{40}Ar in the sodalites but not in the sanidines and nephelines from sample 149-6 are probably due to: (1) the low K contents in sodalites making the effects of excess ^{40}Ar more noticeable compared to the higher K contents in sanidines and nephelines, (2) higher Ar solubility values in sodalite due to its open crystal structure, compared to K-feldspar and nepheline (Wartho et al. 1999), and (3) faster Ar diffusion in sodalite (Kopelevich and Chang 2001) compared to K-feldspar and nepheline (Wartho et al. 1999, Cassata and Renne 2013). In fact, the sodalites in sample 149-6 may have actively partitioned $^{40}Ar^*$ due to the degassing of the older nepheline antecrysts in the entraining magma.

Linking Cadamosto Seamount magmatism with phonolite eruptive activity on other volcanic islands in the Cape Verde Archipelago

The ^{40}Ar-^{39}Ar sanidine eruption ages recorded from Cadamosto Seamount are all young (<100 ka). The presence of antecrysts in our five samples also gives us minimum estimates for older magmatic episodes within Cadamosto Seamount. For example, sanidine antecryst SCTF ages from samples 037DR-2 and 035ROV-12 suggest minimum ages of 349.0 ± 20.4 ka and 611.9 ± 8.8 ka, respectively. Nepheline SCTF ages from sample 149-6 suggest the presence of even older antecrysts up to 1.5215 ± 0.0083 Ma (**Fig. 2.8A**). This range of SCTF ages seems to suggest a long lived magma plumbing system below the 15 km wide Cadamosto Seamount, with activity for up to 1.52 Ma.

Currently recorded seismic activity at the seamount indicates that the seamount is still active at present day (Grevemeyer et al. 2010).

These young Cadamosto Seamount ages are expected, as this seamount is located at the SW tip of southern chain of islands in the Cape Verde Archipelago. Similar <100 ka Pleistocene ^{40}Ar-^{39}Ar, cosmogenic ^{3}He and tephrachronological ages are also found on the nearby volcanic islands of: (1) Brava (a poorly constrained groundmass age of 33.9 ± 21.3 ka; Madeira et al. 2010), and (2) Fogo (continuous volcanism from ~11-63 ka, and multiple extensive marine ash layers from ~18-114 ka; Foeken et al. 2009, Eisele et al. 2015; **Fig. 2.1B**). Poorly constrained Pleistocene ages of 57.8 ± 38.3 ka and 63.5 ± 45.5 ka have also been obtained from the northern chain island of São Nicolau (**Fig. 2.1A**).

The minimum nepheline antecryst age of 1.52 Ma from Cadamosto Seamount is similar to other Pleistocene ages on the islands of Brava in the southern chain (Madeira et al. 2010), and the northern chain islands of São Nicolau, Raso, Santa Luzia, and Santo Antão (Plesner et al. 2002, Duprat et al. 2007, Holm et al. 2008, Ancochea et al. 2015; **Fig. 2.1B**).

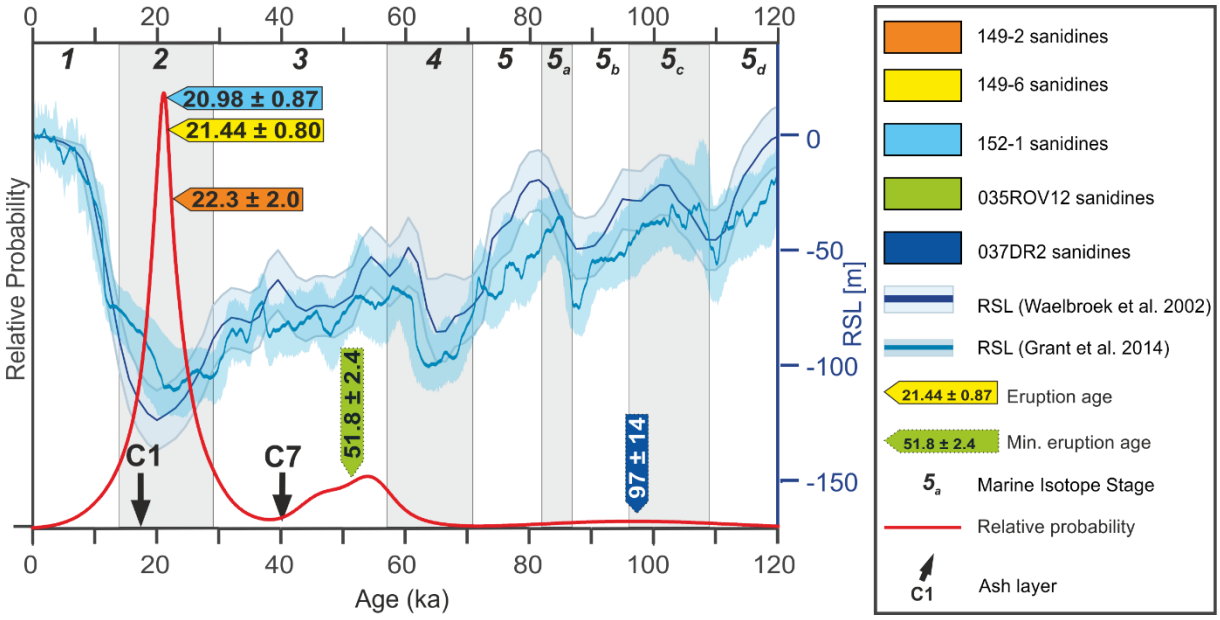

Figure 2.10 Probability density function plot (red line) of ^{40}Ar-^{39}Ar SCTF sanidine eruption ages from Cadamosto Seamount, and relative sea level (RSL; blue lines) caused by global climate changes due to orbital forcing for the past 120 ka. Marine Isotope Stages (MIS) are marked with grey vertical lines and bold numbers 1-7 (Lisiecki and Raymo 2005). Global and Red Sea relative sea level curves are from Waelbroeck et al. (2002) and Grant et al. (2014). The ~17 ka (C1) and ~40 ka (C7) marine ash layers from Eisele et al. (2015) are also shown.

Cadamosto Seamount volcanism and a potential relationship with global sea level changes

The youngest and most prominent SCTF age at Cadamosto Seamount is the combined weighted mean age of 21.14 ± 0.62 ka, derived from three samples (149-2, 149-6 and 152-1; **Fig. 2.7; Table 2.2**). This youngest Cadamosto Seamount eruption age overlaps with the Last Glacial Maximum at ~26.5-19 ka, a geological period that is characterized by a rapid change in global climate, including rapid changes in the global relative sea level (Waelbroeck et al. 2002, Grant et al. 2014; **Fig. 2.10**). The Last Glacial Maximum is within Marine Isotope Stage (MIS) 2, and includes a global relative sea level fall that resulted in a sea level lowstand (i.e., a period of low sea levels) of up to -136 m below the current sea level occured at ~22-18 ka, due to the formation of large ice sheets (Waelbroeck et al. 2002, Lisiecki and Raymo 2005; **Fig. 2.10**). The Cadamosto Seamount magmatic activity period at 21.14 ± 0.62 ka, recorded in three samples, appears to be correlated to MIS 2 and spans the entire period of the Last Glacial Maximum (**Fig. 2.10**).

Rapid sea level changes and lowstands can result in regional crustal loading and unloading, and a relationship between sea level changes and magmatism has been observed in the Mediterranean during the Messinian salinity crisis, 5-6 Ma ago (Sternai et al. 2017). In addition, global and local

volcanic activity levels in the Pleistocene-Holocene have been linked to Milankovitch frequencies and ice mass redistribution/sea level changes (e.g., Paterne et al. 1990, Kutterolf et al. 2013). We suggest that a similar situation may be occurring at Cadamosto Seamount, where a rapid change in sea level would have resulted in ocean crust depressurization, which can in turn affect pressure conditions within the Cadamosto Seamount magma plumbing system. Thus the period at 21.14 ± 0.62 ka is an obvious candidate for enhanced magmatic activity during the Last Glacial Maximum. As the ages from the other two samples (035ROV-12 and 037DR-2) are mixed ages due to the presence of antecrystic cores, the maximum eruption ages of these samples cannot be directly linked to sea level changes.

During the Last Glacial Maximum, the sea level dropped from approximately -75 m below current sea level at ~40 ka, to -136 m below current sea level at ~22-18 ka. Assuming that a change of 10 m in sea level correlates to 1 bar change in pressure at the seafloor, this would result in a depressurization value of of 6.3 bar (0.63 MPa) during a period of ~20 ka. At the end of the Last Glacial Maximum (~18 ka), the sea level rose from -136 m to about -10 m below current sea level within a period of ~10 ka, resulting in a re-pressurization of the magmatic system below Cadamosto Seamount by 13.2 bar (1.3 MPa). This depressurization and subsequent re-pressurization may have affected the magmatic plumbing system in volcanic islands and submarine volcanoes. An overpressure on the order of 1 MPa in a highly viscous magma can either lead to internal crack formation and volatile re-distribution, or promote degassing leading to magma movements within a reservoir (e.g., Sparks 1997, Spieler et al. 2004).

Two different mechanisms can be envisioned to explain enhanced volcanic activity at Cadamosto Seamount during the Last Glacial Maximum: 1) Increased fluid exsolution in volatile-saturated magmas, resulting in pressurization of the magma plumbing system. This in turn may induce crack formation, renewed depressurization and enhanced degassing, and concomitant pressure buildup, ultimately leading to magma movements. Alternatively, 2) enhanced crack formation in the volcanic edifice occurred due to crustal unloading, effectively leading to magma degassing, pressurization and further crack formation. The two proposed mechanisms would have a similar net effect of enhancing magma movement, and probably result in volcanic eruptions. These scenarios are supported by model determinations of Hasenclever et al. (2017), which predict that a falling sea level should result in enhanced pressure-release melting in the uppermost oceanic mantle. Our proposed scenario of enhanced magma degassing in the oceanic crust should be similarly efficient and result in more efficient magma movements and thus a higher eruption probability.

Enhanced volcanic activity at Cadamosto Seamount during the last sea level low stand is further supported by an external data set. The 21.14 ± 0.62 ka ^{40}Ar-^{39}Ar sanidine age is similar to the 17 ka age of a marine ash layer (C1) that was attributed to Cadamosto Seamount by Eisele et al. (2015) (**Fig. 2.10**). Our Cadamosto eruptive ages of 22.3 ± 2.0 ka, 21.44 ± 0.8 ka, and 20.98 ± 0.87 ka for samples 149-2, 149-6 and 152-1, respectively, and the combined sample young ^{40}Ar-^{39}Ar weighted mean age of 21.14 ± 0.62 ka are all older than the ~17 ka age of the distal C1 tephra layer. The Eisele et al. (2015) 17 ka age for ash layer C1 has no uncertainty associated to it, and the uncertainties of individual ages in samples 149-2, 149-6 and 152-1 are large. Although there is no statistical overlap, these events may therefore be related and the ash layer does provide further evidence for a peak in submarine (explosive) volcanic activity at Cadamosto Seamount during this 17-22 ka period.

2.6 Conclusions

In this study, we present petrological and ^{40}Ar-^{39}Ar analyses of sanidines, nephelines and sodalities from five phonolitic lavas from the flanks and summit area of Cadamosto Seamount, Cape Verde. The 170 sanidine, nepheline and sodalite SCTF and sanidine single-/multi-grain step-heating ages are used to decipher timescales of magmatic processes at Cadamosto Seamount.

1. Three samples from the western flank and summit (149-2, 149-6, and 152-1) have a relatively simple petrology mainly containing phenocrystic sanidines that show no or slight normal chemical zonation. The remaining two samples from the summit and eastern flank of the seamount (035ROV-12 and 037DR-2) contain zoned sanidine antecrysts, which preserve resorbed antecrystic cores and phenocrystic overgrowth rims. Zonation patterns recorded by

minor elements Fe and Ba suggest replenishment with more mafic magma and/or convection within the magma shortly before eruption.

2. The Cadamosto Seamount ^{40}Ar-^{39}Ar eruption ages are all <100 ka. Phenocrystic sanidines from three samples yield overlapping eruption ages of 20.98 ± 0.87 ka, 21.44 ± 0.8 ka and 22.3 ± 2.0 ka, resulting in a combined eruption age of 21.14 ± 0.62 ka. Sanidines from the remaining two samples that preserve antecrystic cores with phenocrystic overgrowth rims yield older maximum eruptive ages of 51.8 ± 2.4 ka and 9.7 ± 14 ka.
3. SCTF sanidine and nepheline ages of antecrysts in three samples suggest minimum antecryst ages up to at least 1.5215 ± 0.0083 Ma, suggesting a long lived magma plumbing system below Cadamosto Seamount.
4. The youngest eruption age (21.14 ± 0.62 ka) from Cadamosto Seamount coincides with the Last Glacial Maximum (~26.5-19 ka), a period of sea level lowstand of -136 m at ~22-18 ka. A ~17 ka marine ash layer that is geochemically linked to Cadamosto Seamount provides further evidence for pronounced volcanic activity during this period (Eisele et al. 2015). Based on the observed correlation between volcanic activity at Cadamosto Seamount versus a known global sea level lowstand and rapid sea level changes during the Last Glacial Maximum we suggest that rapid changes and lowstands of sea levels may have affected pressure conditions within the Cadamosto Seamount magma plumbing system. This suggested external forcing may have implications for the coupling between global relative sea level changes and submarine or near-coastal eruptive activity.

Acknowledgements

The authors would like to thank Thorsten Lux and Karin Junge for help and assistance with sample preparation. We would like to acknowledge sample preparation and analysis of sample 149-6 by Paul van den Bogaard. Jan Sticklus is thanked for his invaluable help with dating the samples. Mario Thöner assisted with EMP analyses. We would also like to acknowledge the ships crews and scientific parties at RV Meteor and RV Poseidon during the cruises M80/3 and POS320/2, respectively. Mladen Nedimovic is thanked for discussion. Meike Klischies commented on an early version of this manuscript. We would like to thank Abigail Barker and David Phillips for their reviews that helped to improve this manuscript, and also thank our editor Andrew Kerr. The authors also acknowledge the MuHS-V February 2018 writing retreat in Osten, Germany (organized and funded by Prof. Colin Devey). LKS would also like to acknowledge funding from the Helmholtz Research School for Ocean System Science and Technology (HOSST). The funding source was not involved in the study design, analyses, data interpretation, writing, and in the decision to submit the article for publication.

3 Internal igneous growth, doming and rapid erosion of a mature ocean island: the Miocene evolution of Maio (Cabo Verde)

This paper was published as an OpenAccess-Original Paper with a Creative Commons Attribution 4.0 International License in the peer-reviewed *International Journal of Earth Sciences (Geologische Rundschau):*

Samrock, L.K.; Hanstseen, T.H., Dullo. W.C., Wartho, J.A. (2022) Internal igneous growth, doming and rapid erosion of a mature ocean island: The Miocene evolution of Maio (Cabo Verde). Int J Earth Sci (Geol Rundsch) 111:1129–1148. doi:10.1007/s00531-022-02160-x

Abstract

Maio Island (Cabo Verde Archipelago) is composed of uplifted Early Mesozoic MORB-type pillow lavas and deep-sea sediments, unconformably overlain and intruded by Miocene igneous rocks. Combined structural analyses and ^{40}Ar-^{39}Ar dating were used to constrain the Miocene evolution of Maio. Structures and ages of uplifted Mesozoic sequences and crosscutting Miocene dykes showed that numerous intrusive events were associated with the intense growth of an igneous core complex in the middle to upper crust, causing semi-circular doming and partial disruption of the Mesozoic strata. Two nosean nephelinite dykes cut the Valanginian Batalha Formation and yielded phlogopite ^{40}Ar-^{39}Ar ages of 10.405 ± 0.033 Ma and 10.570 ± 0.053 Ma (2σ errors). A nosean nephelinite dyke that cuts the overlying Valanginian to Early Aptian Morro Formation yielded an age of 9.273 ± 0.020 Ma. Combined with existing K-Ar and ^{40}Ar-^{39}Ar ages, this confirmed a main period of island growth between ~16 and 8.7 Ma. We re-interpreted extensive polymict conglomerates, which occur below the Late Miocene Monte Penoso Formation, as landslide deposits. A nephelinite lava clast yielded a phlogopite ^{40}Ar-^{39}Ar age of 8.666 ± 0.0274 Ma, which represents a maximum age for these landslides and thus confined a period of large-scale flank collapses and erosion to between 8.7 and 6.7 Ma. Flank collapses and further mass wasting during this period may have rejuvenated the igneous activity, i.e., resulting in the formation of the Tortonian/Messinian Monte Penoso and Malhada Pedra Formations, due to decompression-induced melting at upper mantle depths. Such interaction between flank collapses and rejuvenated volcanism may be a key to better understand ocean island evolution worldwide.

Keywords: ^{40}Ar-^{39}Ar dating · Ocean island volcanism · Doming · Flank collapse · Cabo Verde

3.1 Introduction

Volcanic ocean islands show a typical pattern of growth stages, starting with a submarine seamount stage, followed by a shield building stage, collapse of parts of the shield volcano, final volcanism during a rejuvenation stage, and in many cases the final guyot phase (Clague and Dalrymple 1987). The volcanic Cabo Verde Archipelago hosts islands and seamounts in various growth stages, ranging from the seamount stage (e.g., Cadamosto Seamount; Samrock et al. 2019), to the rejuvenation stage (e.g., São Vicente; Ancochea et al. 2010). Maio Island, situated in the E of the archipelago, is one of the oldest islands in the archipelago and is volcanically inactive (**Fig. 3.1**).

Large-scale landslides or the collapse of island flanks are typical for volcanic edifices and have a large hazard potential, especially if associated with catastrophic tsunamis (Masson et al. 2008, Watt et al. 2014, Ramalho et al. 2015, van Wyk de Vries and Davies 2015, Madeira et al. 2020). Several landslide and collapse events have been discovered in the Cabo Verde Archipelago, for example on Santo Antão and Fogo (Day et al. 1999, Masson et al. 2008, Ramalho et al. 2015). The interplay between volcanic growth and destruction by flank collapses is still poorly understood (Cornu et al. 2021).

Similar to the neighbouring island of Boa Vista, Maio is deeply eroded and mostly dominated by gentle hills, with only a few topographic highs up to 436 m in elevation (e.g., Monte (Mte) Penoso; **Figs. 3.1, 3.2**). Maio comprises a basement of uplifted Mesozoic mid-ocean ridge basalt (MORB) lavas and dykes (Batalha Formation). Cretaceous deep-sea sedimentary rocks (Morro and Carqueijo Formations) are overlain by a series of Miocene to Pliocene volcanic rocks and conglomerates of the Casas Velhas, Pedro Vaz, Malhada Perdra and Mte Penoso Formations and are partially displaced by the Miocene Central Intrusive Complex (CIC) (Paepe et al. 1974, Stillman et al. 1982; **Fig. 3.1**). Large volumes of the Miocene volcanic rocks are eroded, exposing the uplifted seafloor and intrusive basement of the island. The Miocene evolution and processes of doming, collapse and erosion on Maio are still debated and poorly understood, although this deeply eroded island allows the study of different phases of growth, intensive erosion and collapse in great detail.

During two field campaigns on Maio in 2017 and 2018, we found new evidence for an intense erosive phase, pre-dating the youngest volcanic activity on Maio. In this study, we present new field observations of the Miocene intrusive and erosive units, their structural and stratigraphical relationships, and new ^{40}Ar-^{39}Ar ages. This allows re-evaluation of the ages of intrusive growth of the island, phases of erosion and collapse, and structural processes that shaped the current topography on Maio. In addition, we present a refined model of the stratigraphy and geological evolution of Maio.

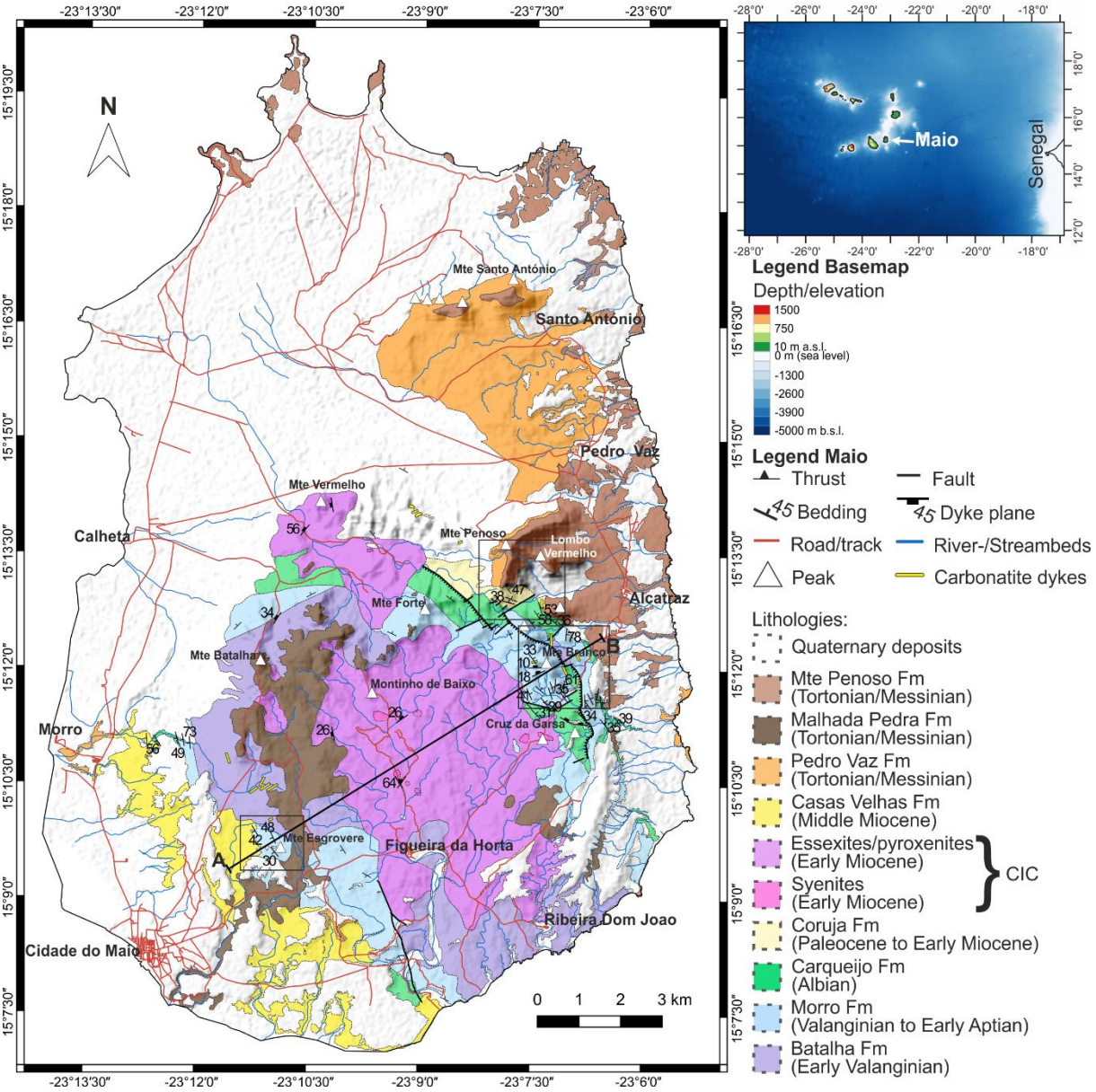

Figure 3.1 Geological map of Maio, modified after Serralheiro (1970) and Stillman et al. (1982), including our new field observations and mapping. The topographical shading is based on Shuttle Radar Topography Mission (SRTM) data, and the basemap is from OpenStreetMap. The black line (A, B) marks the profile shown in **Fig. 3.2a**, and the black boxes indicate areas enlarged in **Fig. 3.2b-d**. Top right: Insert map of the Cabo Verde Archipelago, showing the location of Maio (bathymetry data from General Bathymetric Chart of the Oceans (GEBCO) and topography data from SRTM).

3.2 Geological setting

The Cabo Verde Archipelago, which comprises 10 islands, several islets and seamounts in two volcanic chains, is situated on one of Earth's most prominent bathymetric anomalies, the Cape Verde Rise (**Fig. 3.1**). It rises ~2000 m from the surrounding seafloor and is associated with geoid, gravity, and thermal anomalies that are thought to originate in the deep mantle (Dash et al. 1976, Crough 1982, Courtney and White 1986, Ali et al. 2003, Pim et al. 2008, Wilson et al. 2010). The archipelago has been volcanically active since the Oligocene, with the oldest subaerial volcanic activity reported from Sal at ~26 Ma (Torres et al. 2002).

The eastern islands in both volcanic chains are deeply eroded, while the western islands have higher topographies (e.g., Ramalho et al. 2010c). Maio is located on the seafloor between paleomagnetic Chrons M11 (~136 Ma) and M16 (~141 Ma; Gradstein 2012). The islands show a flexural moat due to volcanic loading that has been filled with sediments, which are tilted away from the islands due to uplift of the edifices (Ali et al. 2003).

The geological units on Maio have been mapped by Serralheiro (1970) and further refined and named by Stillman et al. (1982). The oldest rocks on Maio are MORB-type pillow lavas and dykes of the Early Cretaceous (Valanginian) Batalha Formation (Paepe et al. 1974, Stillman et al. 1982, Robertson 1984, Casson et al. 2020). The upper part of the Batalha Formation contains intercalated sediments that include Early Valanginian calpionellids (Azéma et al. 1990, Fourcade et al. 1990, Casson et al. 2020).

The Batalha Formation rocks are overlain by Cretaceous siliceous pelagic nannofossil limestones and marls of the Morro Formation (Valanginian to Barremian/Early Aptian), which were formed in a deep-sea environment (**Figs. 3.1, 3.2, 3.3**). Based on the assemblages of macrofossils (e.g., ammonites and aptychi) and nannofossils (e.g., radiolaria and *Nannoconus*) the Morro Formation is attributed to the Maiolica facies (Stahlecker 1934, Robertson and Bernoulli 1982, Robertson 1984, Casson et al. 2020). The Albian Carqueijo Formation appears to conformably overlie the Morro Formation sequences; however, biostratigraphic analyses suggest a hiatus between these formations (**Fig. 3.3**; Robertson 1984, Casson et al. 2020. The Carqueijo Formation is seen as the equivalent to Mid-Cretaceous black shale deposits in the Central Atlantic Ocean (**Fig. 3.1**; Stillman et al. 1982, Robertson 1984, Fourcade et al. 1990, Casson et al. 2020. All these Cretaceous units formed on the seafloor prior to island formation, underwent uplift, and now form a circular structure dipping away from the Miocene CIC. Thrusting results in local repetition of the Cretaceous sedimentary units, especially in the NE of Maio (Monte Branco area; Robertson and Bernoulli 1982).

The CIC contains alkaline, silica-undersaturated rocks (essexites, pyroxenites, syenites and some carbonatites; **Figs. 3.1, 3.2**; Serralheiro 1970, Stillman et al. 1982). The Batalha Formation, limestones of the Morro Formation, the Carqueijo Formation, and the CIC form the Basement Complex (**Fig. 3.3**; Stillman et al. 1982).

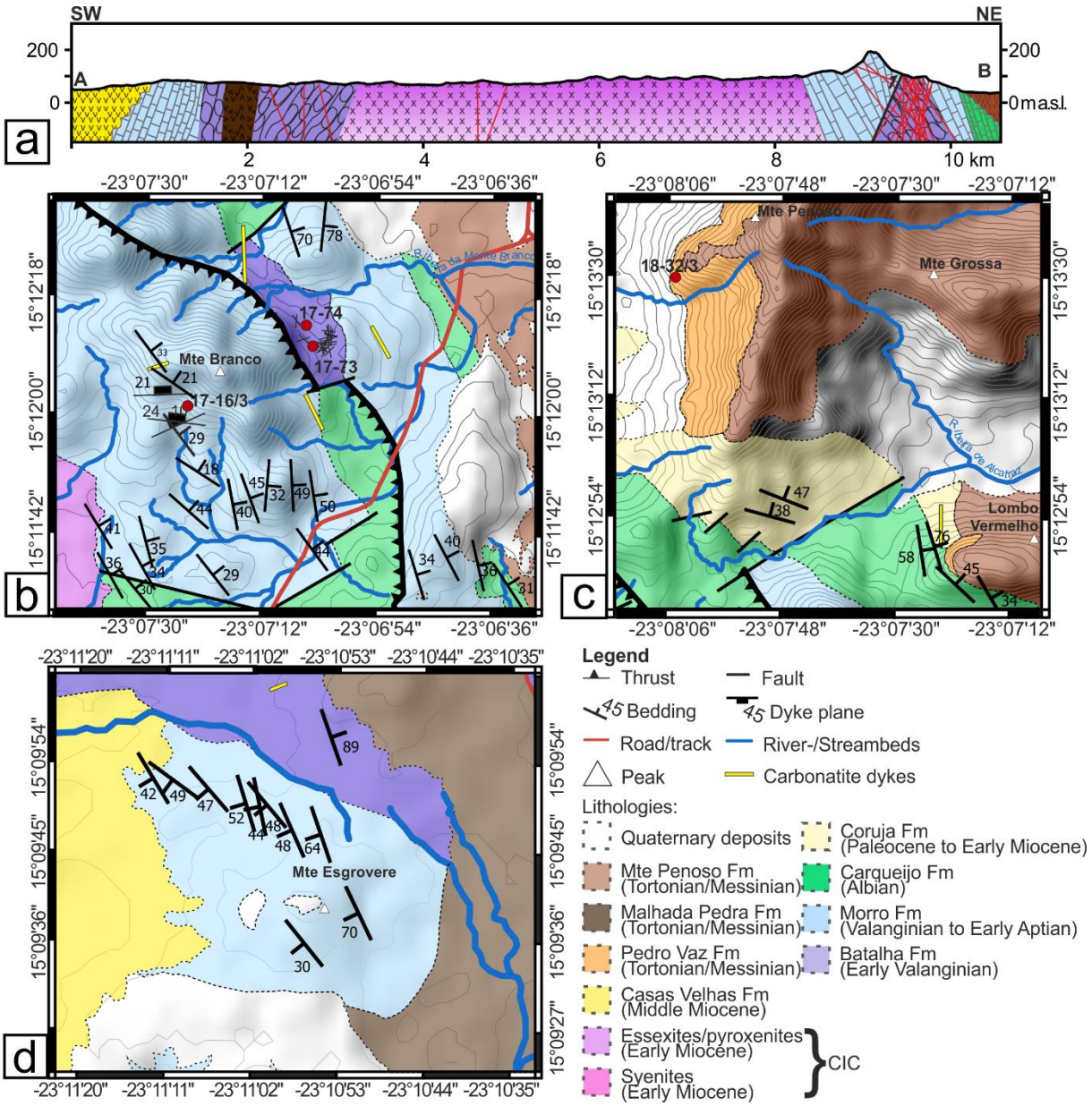

Figure 3.2 Geological profile across Maio (**a**) and enlargements from **Fig. 1** geological map (**b-d**). Sampling locations and dykes intruding the Batalha Formation below the Mte Branco Thrust (**b**), the study locations for the conglomerate below Mte Penoso Formation rocks (**c**), and enlarged image of the Mte Esgrovere area in the SW (**d**). Red circles = ^{40}Ar-^{39}Ar sampling locations.

Intrusive and volcanic activity on Maio started at ~19 Ma with the formation of the CIC and dyke intrusions in the Cretaceous sedimentary rocks (Mitchell et al. 1983). The Mesozoic units of the Basement Complex are apparently conformably overlain by volcaniclastic sediments (tuffs, sandstones, and conglomerates) of the Coruja Formation (**Figs. 3.1, 3.2, 3.3**; Stillman et al. 1982, Robertson 1984). Although rare planktonic foraminifera suggest a Paleocene to Early Miocene age for the Coruja Formation, it is difficult to determine the onset of extrusive volcanism on Maio (Robertson 1984, Bernoulli et al. 2007). The formations of the Basement Complex are unconformably overlain by ankaramite lavas of the subaerial Miocene Casas Velhas Formation, in the SW of Maio, and by sedimentary and volcaniclastic units of the Pedro Vaz Formation in the NE of Maio (**Fig. 3.3**; Serralheiro 1970, Stillman et al. 1982). The Casas Velhas Formation is dated by K-Ar at 9.8 ± 0.8 Ma (all errors are quoted at the 2σ level; Mitchell et al. 1983), and by ^{40}Ar-^{39}Ar at 11.9 ± 1.0 Ma (Ramalho 2011). Volcanic activity continued with the eruption of Malhada Pedra lava flows, dated by K-Ar at 7.3 ± 0.4 and 6.5 ± 1.2 Ma, and the formation of the Monte Penoso stratovolcano, dated by K-Ar at 6.9 ± 0.4 and 6.7 ± 0.4 Ma (**Fig. 3.3**; Stillman et al. 1982, Mitchell et al. 1983). The remnants of this volcano now form the highest elevation on the island, at ~436 m above sea level (a.s.l.). Extensive

Pliocene and Quaternary marine terraces, with elevations up to 100 m a.s.l., cover large areas, especially on the coastal regions of Maio. These marine terraces occur at different elevation levels and suggest several phases of uplift and subsidence (Serralheiro 1970, Ramalho et al. 2010c, Samrock et al. 2018). The coastal areas of Maio additionally exhibit numerous Pleistocene tsunami deposits (Madeira et al. 2020).

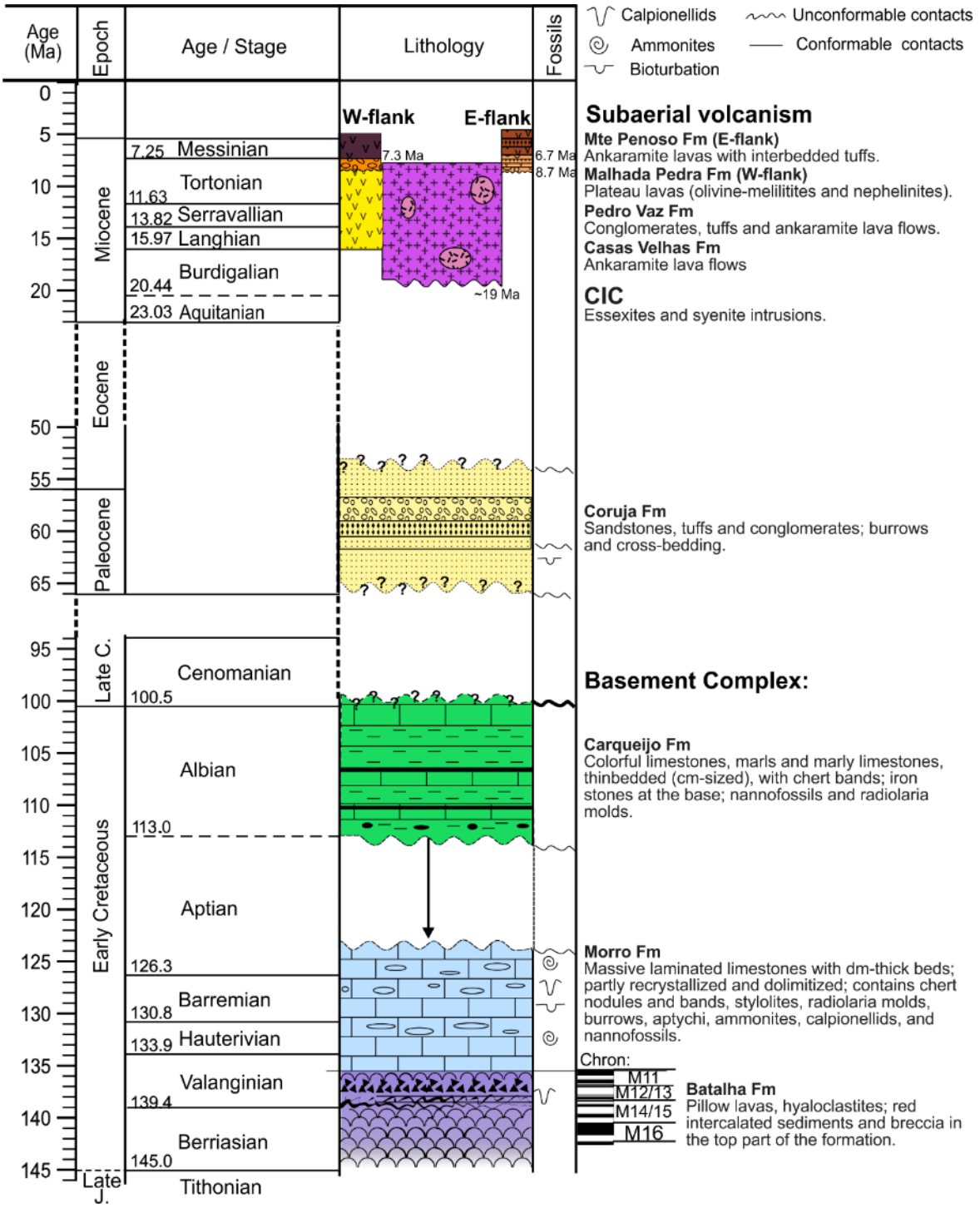

Figure 3.3 Simplified stratigraphic column of the Maio sequences, separated by the eastern and western flanks of Maio. K-Ar and ^{40}Ar-^{39}Ar ages for the Miocene formations are notated in the lithology and fossil columns and were based on this study and data from Bernard-Griffiths et al. (1975) and Mitchell et al. (1983). The geological timescale and Chrons were modified after Gradstein (2012). The arrow between the Morro and Carqueijo Formations indicates a hiatus of apparently conformably overlying rocks.

3.3 Methods

This study integrated field observations with ^{40}Ar-^{39}Ar geochronology and structural analyses. Structural measurements were taken with the Lambert App (Appel 2017), quoted with dip direction/dip angles. Structural plots were created with Stereonet v.11 (Allmendinger et al. 2012, Cardozo and Allmendinger 2013).

Phlogopite crystals from three dyke samples within the Morro and Batalha Formations, and phlogopite from a nephelinite lava clast in a conglomerate from the landslide deposits directly below Mte Penoso were dated using the ^{40}Ar-^{39}Ar technique. The ^{40}Ar-^{39}Ar sample locations are detailed in **Table 3.1** (**Figs. 3.2, 3.3, 3.4, 3.5**). Sample descriptions are summarized in **Appendix 9.3.1**. The samples were prepared for dating by crushing, sieving and washing in distilled water in an ultrasonic bath. Phlogopite separates in the 0.25-0.5 mm and 0.5-1 mm size-fractions were separated and handpicked under a binocular microscope, and cleaned in acetone before drying in an oven at 50℃ overnight. The samples were loaded into an aluminum cannister, and irradiated with fast neutrons in a Cadmium-Lined In-Core Irradiation Tube (CLICIT) reactor for four hours at the Oregon State University nuclear reactor, Corvallis, USA. The samples were analyzed at the GEOMAR Argon Geochronology in Oceanography (ArGO) Laboratory in Kiel, Germany. The isotopic analyses were corrected using the total K decay constant and atmospheric air ratio of Steiger and Jäger (1977); using the recommendation of Fleck et al. (2019), and $\mathcal{J}$ values were determined using the Taylor Creek sanidine (TCR-2) age standard (28.344 ± 0.0114 Ma, 1σ; Fleck et al. 2019). A summary of the ^{40}Ar-^{39}Ar data are shown in **Table 3.2**, and the full ^{40}Ar-^{39}Ar data are shown in Appendix 9.3.2. All our ^{40}Ar-^{39}Ar ages in the text and figures are quoted with 2σ internal errors, and include analytical, $\mathcal{J}$ value, and irradiation correction factor errors. A complete description of the laser step-heating and single-/multi-grain laser total fusion ^{40}Ar-^{39}Ar methods are given in Samrock et al. (2019).

Table 3.1 Sample numbers and location coordinates of samples dated by the ^{40}Ar-^{39}Ar technique

Sample #	Sample type	Sampling location	Sampling coordinates	
			Latitude	Longitude
17-16/3	Nosean nephelinite dyke in Morro Formation limestones	SW-flank of Mte Branco	15.200262	-23.123276
17-73	Nephelinite dyke in Batalha Formation pillow lavas	NE of Mte Branco	15.202839	-23.117849
17-74	Nephelinite dyke in Batalha Formation pillow lavas	NE of Mte Branco	15.203719	-23.118145
18-32/3	Nosean nephelinite clast in Pedro Vaz Formation conglomerate	SW-flank of Mte Penoso	15.224898	-23.134683

The ^{40}Ar-^{39}Ar corrections, age determinations, and plateau and inverse isochron plots were made using the ArArCALC Excel macro (v. 2.5.2) developed by Koppers (2002). The single-crystal total-fusion weighted mean plots were obtained using the Excel Isoplot macro v. 4.15 (Ludwig 2011), and the ^{40}Ar-^{39}Ar data and plots are presented in Appendix 9.3.2. Plateau ages were determined using the criteria of Lanphere and Dalrymple (1978), where the plateau was comprised of at least 3 consecutive heating steps that were within 2σ errors of each other, and where a significant proportion of the ^{39}Ar release (>50%) is represented in the plateau steps. $^{36}Ar/^{39}Ar$ alteration index (AI) values were used as a guide to gauge the alteration/freshness of the phlogopite samples, calculated using the criteria of Baksi (2007), with a cut-off value of $^{36}Ar/^{39}Ar$ AI < 0.0013 for the single-/multi-crystal total-fusion analyses, and < 0.0005 for the step-heated samples.

3.4 Results

In the following section, we (a) present field observations from the Pre-Miocene Basement Complex and the Miocene sequences, and (b) combine the structural relationships for four dykes intruded into the Basement Complex at two key locations (see **Fig. 3.2b-c**) with new ^{40}Ar-^{39}Ar data (**Table 3.2**). In addition, we (c) describe a newly discovered mass wasting deposit, which we ascribe to the Mid- to Late Miocene Pedro Vaz Formation.

3.4.1 Field observations

Pre-Miocene Basement Complex

The Basement Complex comprises Early Cretaceous pillow lavas of the Batalha Formation, the Early Cretaceous pelagic limestones of the Morro and Carqueijo Formations, the probably Paleocene to Eocene Coruja Formation, and the Miocene CIC. The Batalha Formation pillow lavas are exposed along the southern coast of Maio and north of Mte Esgrovere, plus at the western flanks of Mte Batalha and in a small sliver exposed on the NE flank of Mte Branco (**Figs. 3.1, 3.2**). North of Mte Esgrovere, red ferrigenous sediments are found intercalated with the pillow lavas in the upper part of the Batalha Formation, and these sediments are strongly folded and dip vertically (89°). A sample from these intercalated sediments contains a dense, hematite-dominated band and a pelagic protozoan amphore-shaped fossil ?*Calpiollenites darderi* (COLOM 1934) COLOM 1948, which confirms similar findings by Azéma et al. (1990), Fourcade et al. (1990) and Casson et al. (2020; **Appendix 9.3.3**). In the upper part of the Batalha Formation in the Mte Esgrovere area, additional breccias are observed above the red intercalated sediments that contain angular fragments and altered sedimentary rocks, which may have originated from the underlying red sediments (**Fig. 3.3**; **Appendix 9.3.3**). Brecciation of lithified sediments during magmatic growth of the Batalha Formation suggests that MORB-type magmatic activity in this area covered a considerable time span.

The limestones of the Morro and Carqueijo Formations are observed in some of the hills surrounding the CIC, e.g., Mte Branco and Mte Carqueijo to the NE and N, respectively (**Fig. 3.1**). Limestone beds are tilted away from the CIC, seemingly uplifted and tilted by CIC intrusions during the Miocene, and dip towards the NE at Mte Branco, SW at Mte Esgrovere, W at Ribeira (Rib) do Morro, and E at Rib da Baia (**Figs. 3.1, 3.2**). At Mte Esgrovere, the units dip with an average value of 49° towards the SW, but dip angles are steeper (up to 70°) closer to the CIC (**Fig. 3.2d**). At Rib do Morro in the W, the units have an average dip angle of 51°, but numerous meter-scale upright folds are observed with fold axes trending to the SE. At the top of Mte Branco, the limestone beds of the Morro Formation dip almost vertically and are thrust towards the NE (Mte Branco Thrust; **Fig. 3.2b**). Other outcrop locations are heavily intruded by dykes or covered by alluvium.

The Morro Formation consists of up to ~3 dm-thick beds of grey limestones that contain cm-sized chert lenses and bands, and show fine and swirly lamination. Stylolites are common and bioturbation is observed in the form of burrows, up to 2 cm in diameter and often associated with diagenetic dolomite rhombs (**Appendix 9.3.3**). Thin sections of the Morro Formation rocks reveal radiolaria (in the form of calcite-filled solution-molds), and rare fragments of gastropods, sponge spicules, echinoid fragments, radiolaria (*Nasselaria*) and foraminifera. At Mte Esgrovere, we found ammonites and aptychi, ~150 m above the stratigraphic base of the Morro Formation (Latitude/Longitude: 15.162936, -23.182217). Some of these ammonites are well preserved and were identified as *Phylloceras* cf. *infundibulum* (D'ORBIGNY 1840) and *Neocomites neocomiensis* (D'ORBIGNY 1841) (**Appendix 9.3.3**), which indicates a Valanginian to early Hauterivian age (136.4-130 Ma; Fossilworks.org) and supports similar ammonite findings at Mte Esgrovere by Casson et al. (2020). At Rib do Morro, we also found ammonites exposed on a bedding surface ~140 m above the Morro Formation stratigraphic base. These ammonites are unfortunately not well preserved, but confirm the first descriptions of ammonites from this location by Stahlecker (1934)that were revised by Casson et al. (2020). Additionally, the Morro Formation rocks contain Early Cretaceous nannofossils of biostratigraphic value (listed in **Appendix 9.3.3**), which support Valanginian to Early Aptian ages as quoted by Casson et al. (2020).

The Carqueijo Formation overlies the Morro Formation rocks and consists of cm-thick limestone beds, alternating with cm-thick elongated chert bands (usually 2-3 cm thick, locally up to 10 cm

thick), soft marls, and marly and shaley limestones. Bright purple and green coloration of these rocks suggest hydrothermal alteration, which is commonly observed, as well as the occurrence of dyke intrusions. Macrofossils are rare, but thin sections reveal abundant calcite filled solution molds of radiolaria, and some samples yield nannofossils of biostratigraphic value (listed in **Appendix 9.3.3**).

The Coruja Formation successions contain tuffs and conglomerates, which overlay the Carqueijo Formation and were mapped for large areas in the N and NW of the Basement Complex, and W of Mte Penoso (Serralheiro 1970, Stillman et al. 1982). However, we found that especially flat areas are covered by Quaternerary sediments, plus re-forestation and deposition of recent sediments cover many of the originally described outcrop locations. We were able to confirm the occurrence of Coruja Formation outcrops at the southern foot of Mte Penoso, and at the SW flank of Lombo Vermelho, where the formation is composed of orange weathered tuffs, bioturbated sandstones, and conglomerates (**Appendix 9.3.3**). The conglomerates contain wavy-cross-bedding and channel structures. Conglomerate clasts are strongly altered, and the original mineralogy was replaced by secondary minerals, despite partly retaining the original igneous textures. Unfortunately, these clasts were too altered to be used for ^{40}Ar-^{39}Ar dating.

Miocene deposits

The Early Miocene CIC is exposed in the southern central part of Maio island, where it forms a relatively flat, almost bowl-shaped, topography (**Figs. 3.1, 3.2**). It is composed of intrusions of essexites, syenites, and pyroxenites, cut by numerous basanitic, ankaramitic, trachytic, and carbonatite dykes. These Miocene units intruded the Early Cretaceous pillow lavas of the Batalha Formation, and the Early Cretaceous pelagic limestones of the Morro and Carqueijo Formations, which were uplifted and partly tilted during magmatic intrusion activity. The rocks of the Basement Complex are also discordantly overlain by Miocene volcanic deposits. The Casas Velhas Formation, composed of ankaramite lava flows, is exposed in river sections in the S and SW of Maio (**Fig. 3.1**). In the NE of Maio, the sediment-dominated Pedro Vaz Formation is exposed (**Fig. 3.1**), and is typically composed of conglomerates that contain (sub-) rounded igneous clasts, with clast diameters of up to 40 cm. Locally, pyroclastic deposits (tuffs and ignimbrites) and ankaramite lavas appear as lenticular bodies in sections within this formation. This agrees well with observations of Stillman et al. (1982), suggesting that the Pedro Vaz Formation crops out mainly between the Mte Penoso and Mte Santo António.

In the W and SE of Maio, the olivine-nephelinites and melilitites of the Malhada Pedra Formation are exposed (**Fig. 3.1**). These rocks are thickest at Mte Batalha and inclined to the SE. In the NE of Mte Esgrovere, these rocks are exposed in an open pit mine, where they form columns. Along the road towards Figueira da Horta, pillow lavas are also exposed, suggesting partial formation during periods of sea-level highstands.

The youngest volcanic rocks on Maio belong to the Mte Penoso Formation, which is exposed on Mte Penoso and Mte Santo António in the N of Maio (**Fig. 3.1**). Ankaramite lava flows are interbedded with tuffs and other pyroclastic deposits. The Mte Penoso Formation once formed a stratovolcano, with units dipping towards the NE (Stillman et al. 1982). The Mte Penoso Formation rests unconformably on rocks of the Coruja Formation at the southern flanks of Mte Penoso and Lombo Vermelho (**Fig. 3.2c**), and on conglomerates and pyroclastics of the Pedro Vaz Formation. Feeder dykes to the former stratovolcano are observed in the northern part of the island, where they cross-cut underlying rock units.

All formations on Maio are cross-cut by dykes, especially in the older parts of the island, where the dyke density is very high and obscures former rock units. Carbonatite dykes are present, especially in the pelagic limestones and intrusive rocks of the CIC. A larger complex of carbonatites is present E of Mte Vermelho and NW of Mte Penoso (**Fig. 3.1**).

3.4.2 ^{40}Ar-^{39}Ar ages of dykes and tectonic structures in the Basement Complex

A small area of Batalha Formation rocks is exposed at the NE flank of Mte Branco (**Figs. 3.2b, 3.4**). At this location, the shape of the pillows is still visible, but they were heavily intruded by dykes

(**Fig. 3.4a**). These dykes are all truncated by the Mte Branco Thrust (**Fig. 3.4b, c**), and faults and fractures parallel to this thrust were subsequently filled with calcite.

We obtained 100 structural measurements (dip direction/dip) of dykes intruding the Batalha Formation (**Fig. 3.4d-f;** Appendix 9.3.4). Dip angles vary between 25° and 90°. One third of the measured dykes are almost vertical with dip angles of >80°, and the majority (60%) have dip angles between 50° and 79° (**Fig. 3.4**). The steep dykes (>80°) dip towards the NW, NNE and SSE (**Fig. 3.4d, f**). The moderately-dipping dykes (25-79°) have a larger variation in orientations, but also show a similar NW dipping component (**Figs. 4d-e**). However, there is also an additional group of ENE and E dipping dykes, and a minor SSE dipping component (**Fig. 3.4d, e**). Dykes dipping towards the SW are completely absent (**Fig. 3.4d**). In two cases, the age relationships of the dykes were recorded by cross-cutting relationships. The older dykes are inclined towards the W and NW (275/58 and 341/63), while the younger dykes cross-cut the old dykes and dip towards the NE (053/53 and 044/59).

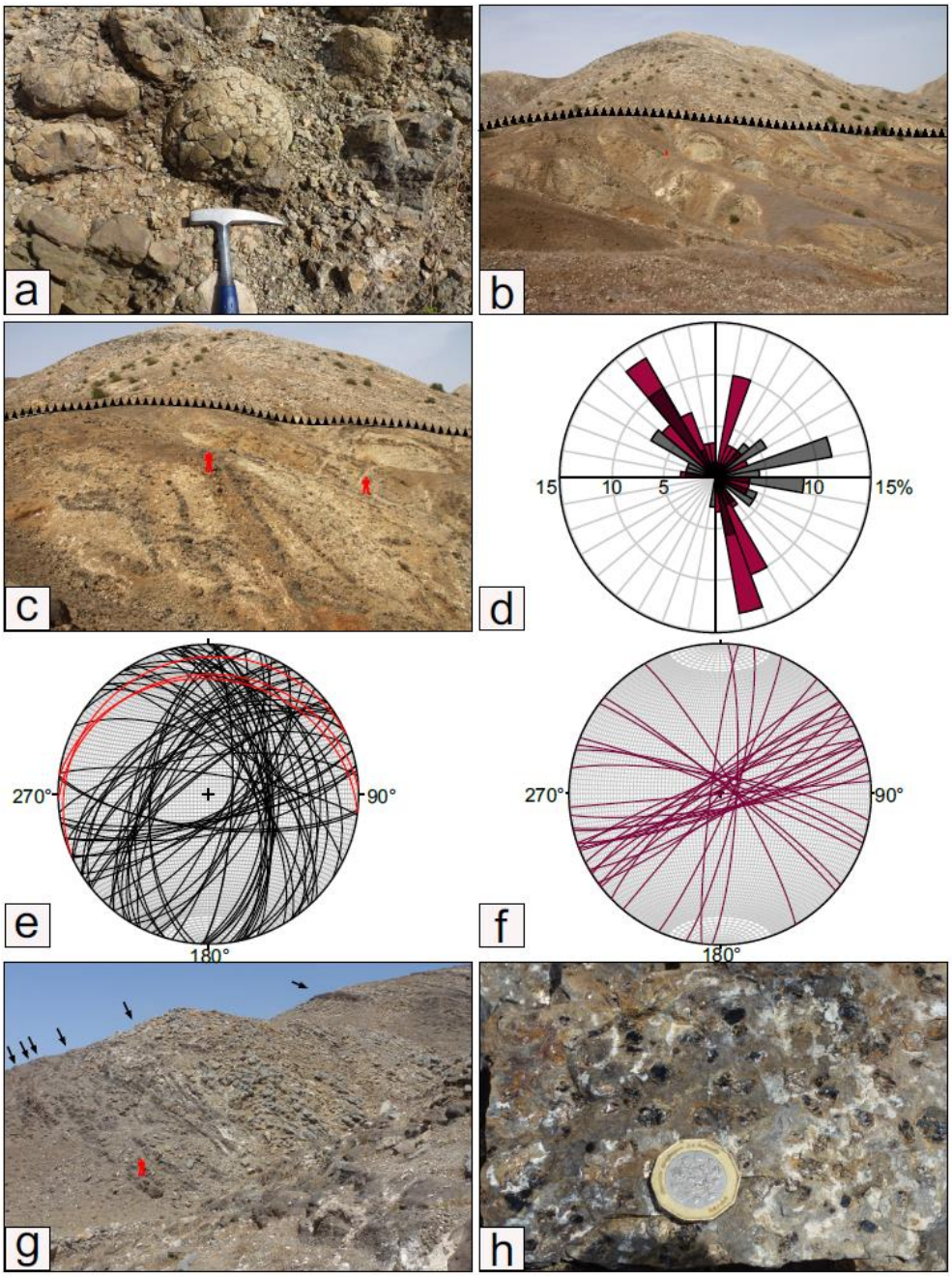

Figure 3.4 Dyke intrusions in the Basement Complex. Rocks of the Batalha Formation (pillow lavas; **a**) were heavily intruded by dykes that were truncated by the Mte Branco Thrust (**b-c**). Rose diagram (**d**) of the dip directions of the dykes: Almost vertical dykes (≥ 80°, n = 30) dip towards the NW, NNE and SSE; while all the other dykes (with dips of 25-79°, n = 70) show an additional group of ENE and southward dipping dykes. Stereoplots of dykes intruding the Batalha Formation, separated by moderate (25-79°, n = 70; **e**) and high (≥80°, n = 30; **f**) dip angles, showing a slight dominance in the NE-SW and NNE-SSW trends. The Morro Formation limestones at Mte Branco are also intruded by undulating dykes (**g**). A phlogopite-bearing sample (17-16/3) was used for ^{40}Ar-^{39}Ar dating (**h**). A hammer (**a**), red people (**b, c** and **g**) and coin (**h**) are shown for scale.

Two nephelinite dykes were sampled from the Batalha Formation (**Table 3.1**). Sample 17-73 yields a phlogopite ^{40}Ar-^{39}Ar single-crystal total-fusion weighted mean age of 10.570 ± 0.053 Ma (Mean Square of Deviation (MSWD) = 1.49, Probability (P) = 8%, *n* = 20, excluding the 4 youngest ages (8.95-9.61 Ma) that contained some of the highest ^{36}Ar/^{39}Ar AI values, which may indicate some radiogenic ^{40}Ar (^{40}Ar*) loss; **Table 3.2;** Appendix 9.3.2). Sample 17-74 yields a phlogopite ^{40}Ar-^{39}Ar single-crystal total-fusion weighted mean age of 10.405 ± 0.033 Ma (MSWD = 1.12, P = 32%, *n* = 22, excluding the 2 youngest ages (9.70 and 10.15 Ma) that may have suffered some ^{40}Ar* loss; **Table 3.2;** Appendix 9.3.2). Multi-grain step-heating of these two phlogopite samples yields disturbed staircase-rising age spectra, which suggest possible ^{40}Ar* loss as a result of alteration. However, the high-temperature step ages of 10.466 ± 0.070 Ma (29.9% ^{39}Ar, MSWD = 1.94, P = 7%; sample 17-74) and 10.61 ± 0.13 Ma (18.7% ^{39}Ar, MSWD = 4.39, P = 0%; sample 17-73) are within 2σ errors of the single-crystal total-fusion ages (**Table 3.2;** Appendix 9.3.2).

At the SW flank of Mte Branco, above the Mte Branco Thrust, the dm-thick banks of massive pelagic limestones from the Cretaceous Morro Formation were intruded by alkaline dykes (**Fig. 3.4g**). These dykes dip with angles of 10° to 24° towards the N with undulating orientations (dip direction/dip: 336/10, 007/24, 358/21), and show an angle of ~45° to the bedding of the Morro Formation that dips towards the NE. In contrast, the dykes that intruded the underlying Batalha Formation are mostly steeper dipping (25° to 90°). Two phlogopite grain fractions from one nosean nephelinite dyke sample (17-16/3) in the Morro Formation (**Fig. 3.4h; Table 3.1**) were dated by the single-crystal total-fusion ^{40}Ar-^{39}Ar technique, yielding 2σ-error overlapping ages of 9.292 ± 0.028 Ma (0.25-0.5 mm, MSWD = 1.31, P = 15%, *n* = 24), and 9.268 ± 0.028 Ma (0.5-1 mm, MSWD = 0.88, P = 62%, *n* = 23; **Table 3.2**). Combining the data from both phlogopite size fractions yields a ^{40}Ar-^{39}Ar single-crystal total-fusion weighted mean age of 9.282 ± 0.022 Ma (MSWD = 1.13, P = 26%, *n* = 47), which is within 2σ errors of the multi-grain step-heating plateau age of 9.263 ± 0.024 Ma (0.25-0.5 mm fraction, MSWD = 1.22, P = 23%, 100% ^{39}Ar; **Table 3.2;** Appendix 9.3.2). Thus, a combined ^{40}Ar*/^{39}Ar single-crystal total-fusion and step-heating age of 9.273 ± 0.020 Ma (MSWD = 1.17, P = 16%, *n* = 67) was calculated, using the approach of Heath et al. (2018) for sample 17-16/3.

Table 3.2 Summary of the Maio single-/multi-crystal total fusion and step-heating ^{40}Ar-^{39}Ar ages

Sample #	Sample type	Material/size fraction	Laboratory						*n* = steps/ analyses
			ID #	Age ± 2σ (Ma)	Analyses/age type	% ^{39}Ar	MSWD	P %	
17-73	Nephelinite dyke in Batalha Formation	Phlogopite (0.25-0.5 mm)	1773b	10.61 ± 0.13	SH - High-T WMA	18,7	4.39	0	15-20
17-73	Nephelinite dyke in Batalha Formation	Phlogopite (0.25-0.5 mm)	1773b	10.570 ± 0.053	SCTF/MCTF - WMA	-	1.49	8	20 of 24
17-74	Nephelinite dyke in Batalha Formation	Phlogopite (0.5-1mm)	1774b	10.466 ± 0.070	SH - High-T WMA	29,9	1.94	7	14-20
17-74	Nephelinite dyke in Batalha Formation	Phlogopite (0.5-1mm)	1774b	10.405 ± 0.033	SCTF - WMA	-	1.12	32	22 of 24
17-16/3	Nosean nephelinite dyke in Morro Formation	Phlogopite (0.25-0.5 mm)	163bs	9.263 ± 0.024	SH - Plateau	100,0	1.22	23	1-20
17-16/3	Nosean nephelinite dyke in Morro Formation	Phlogopite (0.25-0.5 mm)	163bs	9.292 ± 0.028	SCTF - WMA	-	1.31	15	24 of 24
17-16/3	Nosean nephelinite dyke in Morro Formation	Phlogopite (0.5-1 mm)	163bl	9.268 ± 0.028	SCTF - WMA	-	0.88	62	23 of 23
17-16/3	Nosean nephelinite dyke in Morro Formation	Phlogopite (0.25-1 mm)	163bs & 163bl	9.282 ± 0.022	SCTF - WMA	-	1.13	26	47 of 47
17-16/3	Nosean nephelinite dyke in Morro Formation	Phlogopite (0.25-1 mm)	163bs & 163bl	9.273 ± 0.020*	Combined SCTF/SH*	-	1.17	16	67
18-32/3	Nosean nephelinite clast in Pedro Vaz Formation	Phlogopite (0.25-0.5 mm)	323bs	8.707 ± 0.045	SCTF - WMA	-	1.18	30	11 of 12
18-32/3	Nosean nephelinite clast in Pedro Vaz Formation	Phlogopite (0.5-1 mm)	323bl	8.654 ± 0.029	SCTF - WMA	-	1.42	12	18 of 24
18-32/3	Nosean nephelinite clast in Pedro Vaz Formation	Phlogopite (0.25-1 mm)	323bs & 323bl	8.666 ± 0.027	SCTF - WMA Group 1	-	1.48	5	29 of 36
18-32/3	Nosean nephelinite clast in Pedro Vaz Formation	Phlogopite (0.25-1 mm)	323bs & 323bl	8.825 ± 0.062	SCTF - WMA Group 2	-	0.19	83	3 of 36
18-32/3	Nosean nephelinite clast in Pedro Vaz Formation	Phlogopite (0.25-1 mm)	323bs & 323bl	9.68 ± 0.13 to 11.75 ± 0.34	SCTF - Group 3	-	-	-	4 of 36

Table 3.2 (continued)

Sample #	Inverse isochron		MSWD	P %	SF %	n/Steps	% radiogenic	Wt% K	Analyses /steps with fresh material	Details
	Age ± 2σ (Ma)	Initial $^{40}Ar/^{36}Ar$					^{40}Ar range	(from $^{39}Ar_K$)		
17-73	10.78 ± 0.31	236 ± 102	4.48	0	7.6	15-20	26-97	5,9	3-20	Staircase age spectrum, some fresh material
17-73	10.572 ± 0.086	295 ± 18	1.57	6	23.9	20	73-98	5.4-9.4	23	Excluding 4 youngest ages (8.95-9.61 Ma), some fresh material
17-74	10.42 ± 0.11	326 ± 56	1.79	11	20.8	14-20	14-98	6,0	5-20	Staircase age spectrum, some fresh material
17-74	10.414 ± 0.046	294.2 ± 4.9	1.16	28	41.8	22	55-96	5.9-7.1	22	Excluding 2 youngest ages (9.70-10.15 Ma)
17-16/3	9.270 ± 0.029	292.77± 5.9	1.23	22	86.5	1-20	10-98	5.9	4-20	Staircase age spectrum, some fresh material
17-16/3	9.241 ± 0.049	311 ± 13	1.06	39	25.8	24	71-95	5.5-7.0	24	All fresh material
17-16/3	9.246 ± 0.040	300.3 ± 6.1	0.81	71	39.7	23	58-97	3.8-10.0	23	All fresh material
17-16/3	9.260 ± 0.031	301.1 ± 5.4	1.05	37	39.7	47	58-97	3.8-10.0	47	All fresh material
17-16/3	-	-	-	-	-	-	-	3.8-10.0	67	All fresh material
18-32/3	8.706 ± 0.077	296 ± 17	1.31	22	22.2	11	73-95	6.2-7.9	12	Excluding 1 oldest age (10.89 Ma), all fresh material
18-32/3	8.659 ± 0.056	294 ± 18	1.51	9	14.8	18	81-96	3.0-6.3	24	Excluding 6 oldest ages (8.81-11.75 Ma), all fresh material
18-32/3	8.661 ± 0.046	297 ± 13	1.53	4	23.0	29	73-96	5.6-7.9	36	Excluding Groups 2 and 3 ages, all fresh material
18-32/3	8.80 ± 0.13	301 ± 23	0.17	68	14.7	3	79-93	5.5-6.3	3	Excluding Groups 1 and 3 ages, all fresh material
18-32/3	-	-	-	-	-	-	54-63	3.0-4.5	4	Excluding Groups 1 and 2 ages, all fresh material

Abbreviations: *ID #* identification number, *SH* step-heating, *SCTF* single crystal total-fusion, *MCTF* multi-crystal total-fusion (2 grains maximum), *High-T* high-temperature, *WMA* weighted mean age, *MSWD* Mean Square Weighted Deviation, *P* probability, *SF* spreading factor, and *Wt%* weight %.

Numbers in red indicate statistically invalid values (i.e., MSWD < 0.3 (overestimated error); P < 5 %, and SF = < 40%).

Values in **bold** indicate preferred ages.

* The combined SCTF/SH weighted mean age for sample 17-16/3 was calculated using the $^{40}Ar^*/^{39}Ar$ ratios, after the approach of Heath et al. (2018), and includes the analytical and *J* value errors.

3.4.3 *Miocene mass wasting deposit and its ^{40}Ar-^{39}Ar age*

At the base of Mte Penoso and at the southern flank of Lombo Vermelho, conglomerates are found that had not previously been described in detail (**Figs. 3.2c, 3.5**). The two main outcrop areas are separated by more than 1 km across an erosional valley. Below Mte Penoso, exposed to the W and S, this ~50 m thick conglomerate sequence is exposed from ~200 m a.s.l. in the valley to ~250 m asl and was laterally traced for ~1 km along the base of the hill. It is overlain by lava flows and pyroclastic deposits of the Mte Penoso Formation (**Fig. 3.5a**). The conglomerate is polymict and poorly sorted, with clasts typically ranging from centimetres to several decimetres in diameter. Clast sizes vary by more than one order of magnitude at any location. The clast contents range between ~25 to 50 volume %, resulting in both matrix-supported and clast-supported fabrics on an outcrop scale (**Fig. 3.5b-d**). Some areas comprise subunits or flow units identified by difference in dominant grain size, typically separated by a thin indistinct transition zone. The individual clasts range from angular through sub-angular and sub-rounded to well rounded and are set in a weathered matrix that locally shows signs of hydrothermal alteration. Similar sequences have been characterized as debris flow or flank collapse deposits (e.g., Nemec and Steel 1984). The clasts represent a wide range of rock fragments, including alkali-basaltic and nephelinitic fragments ranging from dense to vesicle-rich, ankaramite, phonolite lava, and subordinate alkaline plutonic fragments, which closely resemble the Miocene igneous rocks on Maio. Many clasts are weathered and some show possible hydrothermal alteration. Locally, pyroclastic, lenticular units and occasional small lava flows are also identified and the deposit is therefore multi-phase, testifying to intermittent volcanism during this erosional period.

At Lombo Vermelho, such conglomerates also crop out discordantly above units of the Carqueijo and Coruja Formations, which were in turn intruded by numerous dykes. The Lombo Vermelho conglomerate is also overlain by lava flows and pyroclastic deposits of the Mte Penoso Formation (**Fig. 3.5e**), but at this location the conglomerates are thinner (~20 m to 30 m thick) compared to the Mte Penoso outcrop area (~50 m thick). Clasts have been derived from various lithologies as described above for Mte Penoso, but additionally include subordinate limestone and sedimentary rocks from the underlying Carqueijo Formation. The lower part of this conglomerate was strongly hydrothermally altered and shows a network of secondary mineralized cracks.

To ^{40}Ar-^{39}Ar date this unit, fresh phlogopites of 0.25 to 0.5 mm and 0.5 to 1 mm grain sizes were separated from a slightly altered nosean nephelinite clast (sample 18-32/3; **Table 3.1**), collected below the base of Mte Penoso. This clast yields ^{40}Ar-^{39}Ar ages ranging from 8.51 ± 0.12 Ma to 11.75 ± 0.34 Ma for both size fractions, with 2σ-error overlapping weighted mean ages of 8.707 ± 0.045 Ma (MSWD = 1.18, P = 30%, n = 11) and 8.654 ± 0.029 Ma (MSWD – 1.42, P =12%, n = 18) for the 0.25-0.5 mm and 0.5-1 mm size fractions, respectively. This broad range of ages in both size fractions may be explained by the presence of different generations of antecrysts or xenocrysts. Based on their weight % (wt%) K contents and ^{40}Ar-^{39}Ar ages, three different groups of phlogopites were identified from the two combined size fraction data: (1) the youngest group of 29 phlogopites yielded a weighted mean age of 8.666 ± 0.027 Ma (MSWD = 1.48, P = 5%, n = 29) with high wt% K (5.6-7.9) and % $^{40}Ar^*$ (73-95) contents; (2) a slightly older group of three phlogopite grains that yielded a weighted mean age of 8.825 ± 0.062 Ma (MSWD = 0.19, P = 83%, n = 3) with high wt% K (5.5-6.3) and % $^{40}Ar^*$ (79-93) contents; and (3) the oldest group of four phlogopites (9.68 ± 0.13 to 11.75 ± 0.34 Ma) that contained low wt% K (3.0-4.5) and % $^{40}Ar^*$ (54-78) contents (**Table 3.2**). The Group 1 (8.666 ± 0.027 Ma) phlogopites were interpreted as being phenocrysts, whilst the Group 2 (8.825 ± 0.062 Ma) phlogopites were possibly antecrysts or xenocrysts from an older local magma that were picked up during ascent of the erupted younger magma. The low wt% K contents in the older Group 3 (9.68 ± 0.13 to 11.75 ± 0.34 Ma) phlogopites may indicate the presence of composite grains (i.e., phlogopite crystals finely interlayered with a low-K mineral) that can result in anomalous ^{40}Ar-^{39}Ar ages due to ^{39}Ar recoil effects (Di Vincenzo et al. 2003). Alternatively, the four older phlogopite grains may have been xeno-/antecrysts that suffered some weathering or hydrothermal alteration, resulting in some K and $^{40}Ar^*$ loss and disturbed ^{40}Ar-^{39}Ar ages.

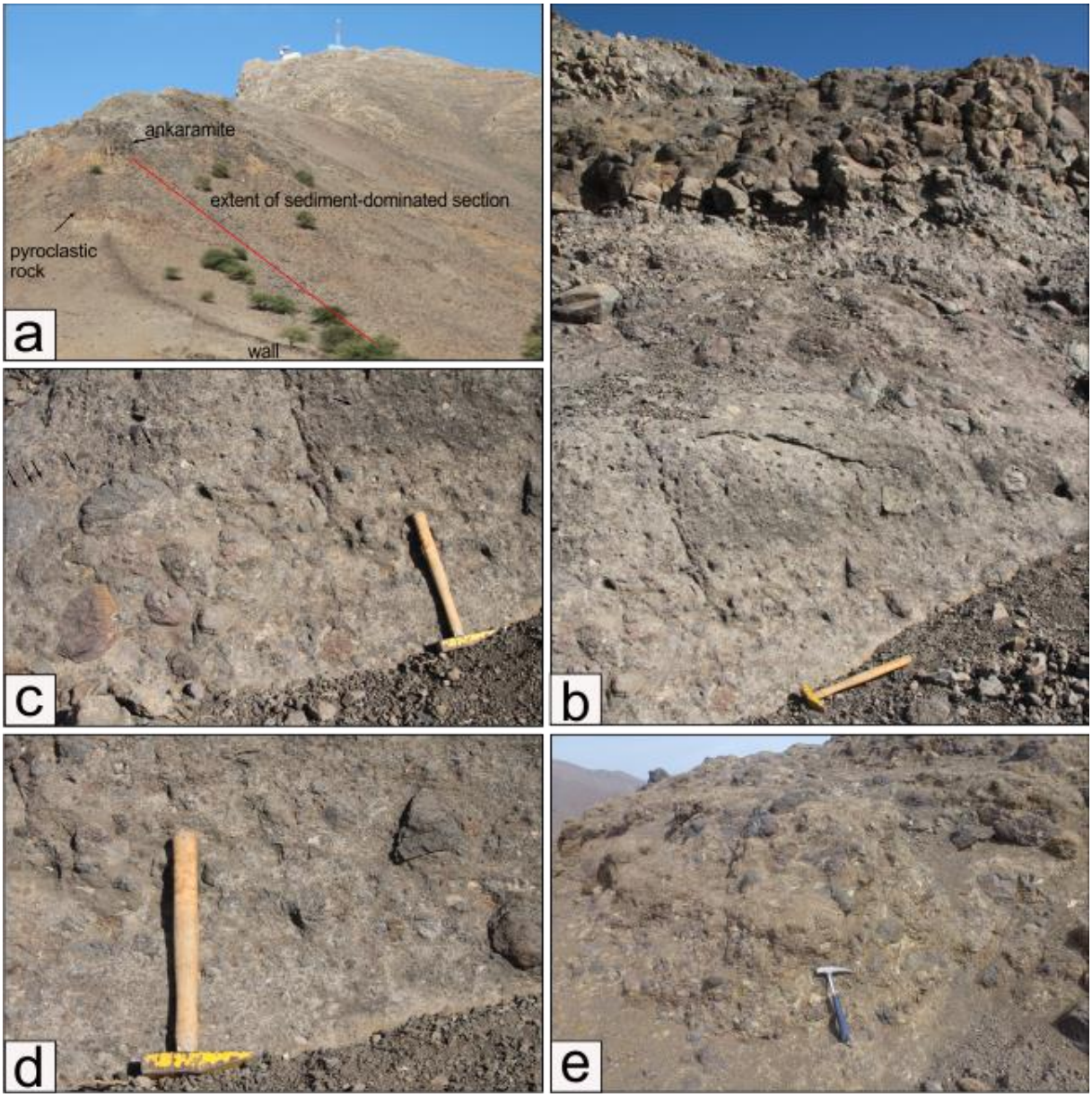

Figure 3.5 Polymict conglomerates cropped out at the base of Mte Penoso (**a-d**) and at Lombo Vemelho (**e**). The successions recorded multiple mass wasting and pyroclastic events, indicated by local lenticular pyroclastic units (**a**). The conglomerate successions were overlain by ankaramite lava flows of the Mte Penoso Formation (**a**). Clasts were well rounded to angular, varied in grain sizes from cm to dm in diameter, and were composed of various lithologies, including alkali-basalt, ankaramite, phonolite lava and alkaline plutonic rocks (**b-d**). At Lombo Vermelho (**e**), fragments of the Mesozoic limestone units were also found. These clasts were poorly sorted and set in a matrix that showed signs of hydrothermal alteration. The conglomerate varied between matrix- and clast-supported textures (**b-e**).

3.5 Discussion

3.5.1 Age of intrusive growth, dyke emplacement and tectonic activity at Mte Branco

Two of our nephelinite dyke samples were found intruding Batalha Formation rocks below the Mte Branco Thrust (**Fig. 3.4**), yielding ^{40}Ar-^{39}Ar ages of 10.570 ± 0.053 Ma and 10.405 ± 0.033 Ma (**Table 3.2**). On the southern coast of Maio, dykes intruding the Batalha Formation yield various K-Ar ages ranging from 12.2 to 9.1 Ma (12.2 ± 0.4 Ma, 11.1 ± 0.6 Ma, 10.8 ± 0.4 Ma and 9.1 ± 0.4 Ma; Mitchell et al. 1983), which partly overlap with our ^{40}Ar-^{39}Ar ages for the Monte Branco area further north (**Fig. 3.6**). Our new ^{40}Ar-^{39}Ar phlogopite ages overlap within 2σ errors with 2 of the 3 literature K-Ar ages (11.0 ± 0.6 Ma, 10.8 ± 2.2 Ma and 9.9 ± 0.4 Ma) from alkaline lamprophyre dykes cutting the nearby Albian Carqueijo Formation (Mitchell et al. 1983) and 2 of the youngest K-Ar ages from dyke intrusions in the CIC (10.9 ± 0.8 Ma to 10.0 ± 0.8 Ma; **Fig. 3.6**). In addition, they overlap within 2σ errors with a K-Ar age from a Casas Velhas Formation ankaramite lava (9.8 ± 0.8 Ma; Mitchell et al. 1983).

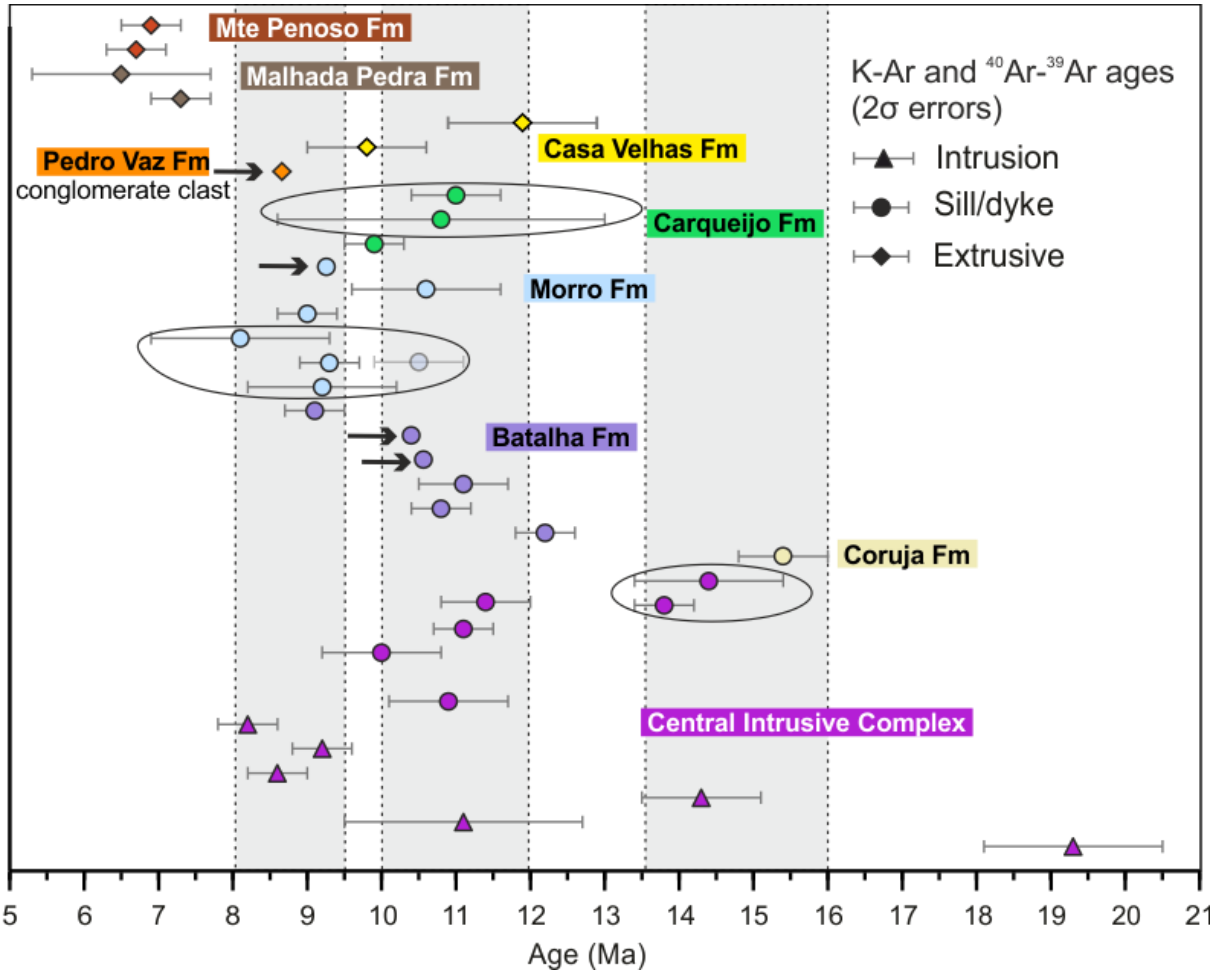

Figure 3.6 Compilation of available Miocene K-Ar and ^{40}Ar-^{39}Ar ages (all with 2σ errors) from Maio, Cabo Verde (Bernard-Griffiths et al. 1975, Mitchell et al. 1983, Ramalho 2011), including new ^{40}Ar-^{39}Ar ages presented in this study (marked by black arrows). The colors of the data points are based on the colors of the rock formations in the geological map (**Fig. 3.1**). Grey shaded areas indicate suggested phases of volcanic activity. Data that originated from one sample but yielded different K-Ar or ^{40}Ar-^{39}Ar ages are encircled. The small 2σ errors for our new ^{40}Ar-^{39}Ar ages are smaller than the symbol sizes.

The preferred ^{40}Ar-^{39}Ar age of 9.273 ± 0.020 Ma for our Morro Formation dyke sample from the Mte Branco region overlaps within 2σ errors with all 4 K-Ar ages (9.3 ± 0.4 to 8.1 ± 1.2 Ma) obtained from two samples of Mte Branco basanite and ankaramite intrusions presented by Mitchell et al. (1983; **Fig. 3.6**). However, Mitchell et al. (1983) obtained an older ^{40}Ar-^{39}Ar plateau age (10.5 ± 0.6 Ma) from a split of the same Morro Formation/Mte Branco basanite sill that also yielded younger 3 K-Ar sample split ages of 9.3 ± 0.5 to 8.1 ± 1.2 Ma. This 10.5 Ma older age is similar to a Bernard-

Griffiths et al. (1975) K-Ar age of 10.6 ± 1.0 Ma for micas from a carbonatite dyke sample at Mte Branco (**Fig. 3.6**). Mitchell et al. (1983) suggest that the formation age of their basanite sill is 10.5 Ma and their three younger K-Ar ages may have been reset by a younger event, even though their samples are fresh and show no evidence of thermal overprinting. It is difficult to confirm the Mitchell et al. (1983) 10.5 ± 0.6 Ma ^{40}Ar-^{39}Ar age, as no accompanying isochron or inverse isochron data are presented to confirm this plateau age. Given the very fresh nature of the phlogopites from our Morro Formation nosean nephelinite dyke sample and reproducible ^{40}Ar-^{39}Ar single-crystal total-fusion and inverse isochron ages, we are confident that the 9.273 ± 0.020 Ma is a magmatic formation age.

The context of multiple phases of intrusive growth is verified by the new and published geochronology ages. The overall distribution of new and published dyke K-Ar and ^{40}Ar-^{39}Ar ages suggest the preservation of several phases of intrusive growth in the different rock formations of Maio (**Fig. 3.6**; Grunau et al. 1975, Bernard-Griffiths et al. 1975, Mitchell et al. 1983, Ramalho 2011). Gabbros, essexites, pyroxenites and syenites from the CIC yield K-Ar ages of 8.2 ± 0.4 up to 21.6 ± 12.6 Ma (Grunau et al. 1975, Mitchell et al. 1983). However, the 2σ errors are large for some of these ages, therefore we chose to reject the three Grunau et al. (1975) K-Ar ages with the largest 2σ errors of 12.5 ± 4.8 Ma, 14.0 ± 8.0 Ma and 21.6 ± 12.6 Ma, as these cannot be used for any time discrimination in such a young age interval. Based on the combined ^{40}Ar-^{39}Ar and K-Ar age data of dyke and sill intrusions we tentatively suggest different periods of intense intrusive activity and by inference correspondingly high volcanic activity in Maio: (1) a first phase from ~16 Ma to 13.5 Ma is recorded in dykes that intrude CIC and Coruja Formation rocks; (2) a second phase from ~12 Ma to 10 Ma is obtained primarily in dykes that intruded the CIC, Batalha and Carqueijo Formations; and (3) a final phase from ~9.5 to 8 Ma is recorded mainly in dykes that intrude Morro Formation rocks (**Fig. 3.6**). We emphasise that the second and third phases partly overlap in time, but represent a geographical shift in dyking and intrusion activity. All three phases are recorded in dykes/sills and overlap within 2σ errors with the K-Ar and ^{40}Ar-^{39}Ar ages recorded in the CIC intrusive rocks (**Fig. 3.6**). The second (~12-10 Ma) phase is previously mentioned by Mitchell et al. (1983) as a period of intense intrusive activity on Maio. It is interesting to note that this ~12-10 Ma phase mainly records dyke/sill emplacement in the CIC, Batalha, and Carqueijo Formations, whereas the third phase (~9.5-8 Ma) is mainly recorded in dykes that intrude Morro Formation rocks in the Mte Branco area. The different geographical and lithological distributions of ages could be explained by a geographical shift in volcanic activity or be caused by tectonic activity. Both the second and third phases overlap with K-Ar and ^{40}Ar-^{39}Ar ages of ankaramite lavas from the Casas Velhas Formation (11.9 ± 1.0 Ma and 9.8 ± 0.8 Ma; Mitchell et al. 1983, Ramalho 2011).

At one of our study locations, N of Mte Branco, the pillow lavas are intensely intruded by numerous dykes that are all truncated by the Mte Branco Thrust. The variation in dip angles from vertical to 25° suggests different groups of intrusions, varying from steep dykes to inclined sheets. The dip directions of the moderately dipping dykes (25° to 79°) suggest conjugate extension (dipping twoards NW and ESE; **Fig. 3.4 d-e**), which may be due to a doming process caused by magmatic underplating and thermal uplift (e.g., Klügel et al. 2005). However, we cannot exclude the possibility that the orientations of the Batalha Formation rocks were also changed due to tectonic activity.

In general, the dykes that intruded the Morro Formation are younger than the Batalha Formation dykes below the Mte Branco Thrust and they also show different orientations: While the dykes in the Morro Formation dip towards the North and are relatively flat (336/10, 007/24 and 358/21), the dykes in the Batalha Formation below the thrust show various orientations (NW, ENE and SSE for the moderately dipping dykes and NW, NNE and SSE for the almost vertical dykes) The different orientations of dykes suggest different pulses of magma and therefore different phases of intrusive activity, which could be related to various growth stages in the CIC. However, the dyke orientations may have changed due to the thrusting and tectonic activity and therefore cannot be used to establish former eruption centres.

3.5.2 Miocene erosive activity – conglomerates

The conglomerates at the base of Mte Penoso and at the southern flank of Lombo Vermelho are variable in composition, rounding and grain sizes of clasts, and in facies types. This variability is typical for complex volcanic landslide and debris avalanche deposits (e.g., Bernard et al. 2009, Roverato et al. 2014, van Wyk de Vries and Delcamp 2015). In general, overloading, over-steepening, uplift and subsidence, magma emplacement in the crust and erosion can destabilize a volcanic edifice. Furthermore, debris avalanches and flank collapse events may be triggered by magmatic (intrusive or extrusive), seismogenic (tectonic/volcanic earthquakes), or environmental (sea level changes, precipitation) events (McGuire 1996).

According to Serralheiro (1970) and Stillman et al. (1982), the Pedro Vaz Formation crops out mainly between Mte Penoso and Mte Santo António and in small patches in the SW of Maio (e.g., Rib do Morro, close to Barreiro; **Fig. 3.1**). It contains "rudites" or matrix-supported conglomerates, interbedded with fine "tuffs" and ankaramite lava flows, separated by thin "arenites", and is intruded by numerous ankaramite dykes (Stillman et al. 1982). Locally confined, it apparently includes material from the underlying Casas Velhas Formation (Stillman et al. 1982). The deposits presented in this study are mainly composed of polymict conglomerates and contain dispersed pyroclastic rocks and lava flows, which agrees well with the descriptions of Stillman et al. (1982). Based on their stratigraphic position and the resemblance to previous descriptions, we therefore suggest that the conglomerates presented in our study are part of the Pedro Vaz Formation. An overlap in ages between the Pedro Vaz and Casas Velhas Formations is also noted by Casson et al. (2020; **Fig. 3.3**).

The Pedro Vaz Formation multi-phase deposits represent a period of both rapid erosion (landslides and flank collapses) and simultaneous moderate volcanic growth (pyroclastic flows and lavas), which most likely coincides with the onset of rejuvenated magmatic activity. Such periods of simultaneous volcano growth and destruction are common worldwide (e.g., Tutucapa volcano, Peru (Valderrama Murillo 2016); Stromboli, Italy (Romagnoli et al. 2009); Mount St. Helens, USA (McEwen and Malin 1989); Augustine volcano, Alaska (Begét and Kienle 1992); Tenerife, Canary Islands (Hunt et al. 2011, 2013, 2018); and Montserrat (Cassidy et al. 2014)). The shield stage of an ocean island volcano is defined as the period with highest magma supply rates and thus the most rapid growth. Intense erosion processes dominate the morphologic evolution of the mature edifice, as magma extrusion and intrusion rates diminish towards the end of the shield stage (Carracedo 1999, Ramalho et al. 2013). Such erosional phases are well-documented worldwide and include gravity sliding on both local and regional scales (e.g., Hunt et al. 2018, Urlaub et al. 2018). For example, in the Cabo Verde Archipelago, several large landslides and flank collapses have been described (Day et al. 1999, Le Bas et al. 2007, Masson et al. 2008, Martínze-Moreno et al. 2018, Barrett et al. 2020, Ancochea et al. 2010). Land slide deposits on São Vicente can also be compared to the conglomerates on Maio (Ancochea et al. 2010)

Our new 8.7 Ma ^{40}Ar-^{39}Ar age data combined with literature K-Ar and ^{40}Ar-^{39}Ar ages of the overlying Malhada Pedra and Monte Penoso Formations (Bernard-Griffiths et al. 1975, Mitchell et al. 1983) confine the Miocene erosional phase at Maio to between 8.7 and 6.7 Ma (base of Monte Penoso Formation), coinciding with dispersed and rejuvenated volcanism of the temporally overlapping Malhada Pedra and Pedro Vaz Formations. We additionally suggest that flank collapse activity and rapid mass wasting in the Tortonain/Messinian (8.7 to 6.7 Ma) may have enhanced the rejuvenated igneous activity on Maio, due to decompression-induced melting at upper mantle depths (Manconi et al. 2009, Cassidy et al. 2015, Hunt et al. 2018). It remains unclear what caused the presented multiphase flank collapse events. They may have been emplaced contemporaneously with fault activity along the Mte Branco Thrust, which was possibly active between 9 and 8.7 Ma, following the final dyke intrusions at Mte Branco. However, the collapse events could also have been influenced by early rejuvenated activity of Malhada Pedra and/or Monte Penoso Formations, which may have formed the local pyroclastic sequences within the conglomerate sequences.

The well constrained ^{40}Ar-^{39}Ar phlogopite age of 8.666 ± 0.027 Ma obtained from a nosean nephelinite clast within the conglomerate directly underlying the Mte Penoso Formation is regarded as a maximum age for this conglomerate deposit and a minimum age for previous igneous units (i.e., the Casas Velhas Formation). The presence of two older age groups of phlogopites within this sample may indicate the presence of older phlogopite antecrysts and/or xenocrysts, which are

distinguished by their ages and wt.% K contents (**Table 3.2;** Appendix 9.3.2). Xeno-/antecrysts in igneous rocks are typical for Cabo Verde rocks and the plumbing system below the islands and seamounts (e.g., Samrock et al. 2019, Barker et al. 2019, 2021) and is further supported by the presence of rounded phlogopites in the sample (Appendix 9.3.1).

3.5.3 Refined geological model of Maio

Based on field observations and new ^{40}Ar-^{39}Ar dating of dykes and a conglomerate clast, we present a refined model of the geological evolution of Maio (**Fig. 3.7**).

Initially, Early Cretaceous pillow lavas of the Batalha Formation and Early Cretaceous pelagic limestones from the Morro and Carqueijo Formations are deposited on the sea floor (**Fig. 3.7a;** e.g., Robertson 1984, Casson et al. 2020). We confirm descriptions of red intercalated sediments that include calpionellids in the upper Batalha Formation at Mte Esgrovere (Fourcade et al. 1990, Casson et al. 2020). Our ammonite findings and microfossil assemblages in the Morro Formation matches the previously proposed Valanginian to Early Aptian ages for the Morro Formation and the Albian age for the overlying Carqueijo Formation (Casson et al. 2020).

It is unclear when subaerial volcanism on Maio started, as there is little data for the rare outcrops of the Coruja Formation. Mitchell et al. (1983)published K-Ar ages for Coruja Formation igneous clasts in a conglomerate, yielding Late Jurassic to Late Cretaceous ages (157.8 ± 8.0, 99.8 ± 4.4, and 73.2 ± 2.4 Ma). Rare planktonic foraminifera suggest a Paleocene to Early Miocene age for the Coruja Formation, but the precise age of these units, and therefore the age of the first subaerial volcanism on Maio, remains weakly constrained (Robertson 1984). Gravity data suggests that an eruptive center is located in the SE of Maio (Represas et al. 2012). In this area, dyke density is high and rocks of the Miocene CIC are mainly preserved, and most successions of sedimentary units of the Basement Complex have been removed by erosion. However, early volcanic units are absent, therefore it is not clear if there is an early volcanic center in SE Maio. Volcanic ash layers in marine sediments NE of the Cabo Verde Archipelago suggest the onset of volcanism on the Cabo Verde Islands during the early Middle Miocene (DSDP Site 368; Lancelot et al. 1978b).

During the Early Miocene (at or before 19.3 ± 1.2 Ma; Mitchell et al. 1983) the CIC begins to form with the emplacement of shallow intrusions in the middle and upper crust, i.e., the formation of an intrusive core complex (**Fig. 3.7b-c**). Such pronounced intrusion activity is typically associated with volcanic activity and we also assume this in this case for Maio. Emplacement of plutonic rocks led to mechanical and thermal uplift and doming, which induced the semi-circular dip of the former seafloor units (**Fig. 3.7b**; Serralheiro 1970), and stoping probably led to the disruption of strata above the intrusive complex (e.g., Klügel et al. 2005, 2015, Montanari et al. 2017). This intrusive period may have lasted only a few million years, leading to a rapid flare up and accompanying uplift of the edifice (Klügel et al. 2005). Such comparatively rapid uplift has also been recorded from other Cabo Verde islands, e.g., Santiago (Marques et al. 2020). It has been shown that locally confined intrusive activity at crustal levels is responsible for distinct island uplift in the region (Ramalho et al. 2010a, 2010b, Ramalho 2011). The intrusive activity also caused crustal thickening, with the thickest crust being present below the older eastern islands of the Cabo Verde Archipelago, such as Sal and Maio (Lodge and Helffrich 2006)

At a later stage of intrusive island growth (from ~12 to 8 Ma; **Fig. 3.7d-e**), dyke emplacement plays a more important role. Some dykes probably stalled, leading to edifice growth at depth, while others reached the surface, feeding eruptions and extrusive growth and emplacement of the Casas Velhas Formation. The importance of dyke emplacement to the growth of volcanic edifices has been shown previously (e.g., Annen et al. 2001, Kervyn et al. 2009). The Casas Velhas Formation may be regarded as rocks from a 'Lower Volcanic Complex' and is possibly associated with a shield building stage, which may have started prior to ~11.9 Ma and overlaps with the last intrusive activity in the CIC that phased out at ~8 Ma (**Fig. 3.7d-e**; Ramalho 2011). The three high activity intrusive phases recorded in dykes (16 to 13.5 Ma, 12 to 10 Ma, and 9.5 to 8 Ma; **Fig. 3.6**) overlap with ages recorded in intrusive rocks from the CIC, which may partly be due to the overprinting of older rocks (Bernard-Griffiths et al. 1975, Mitchell et al. 1983).

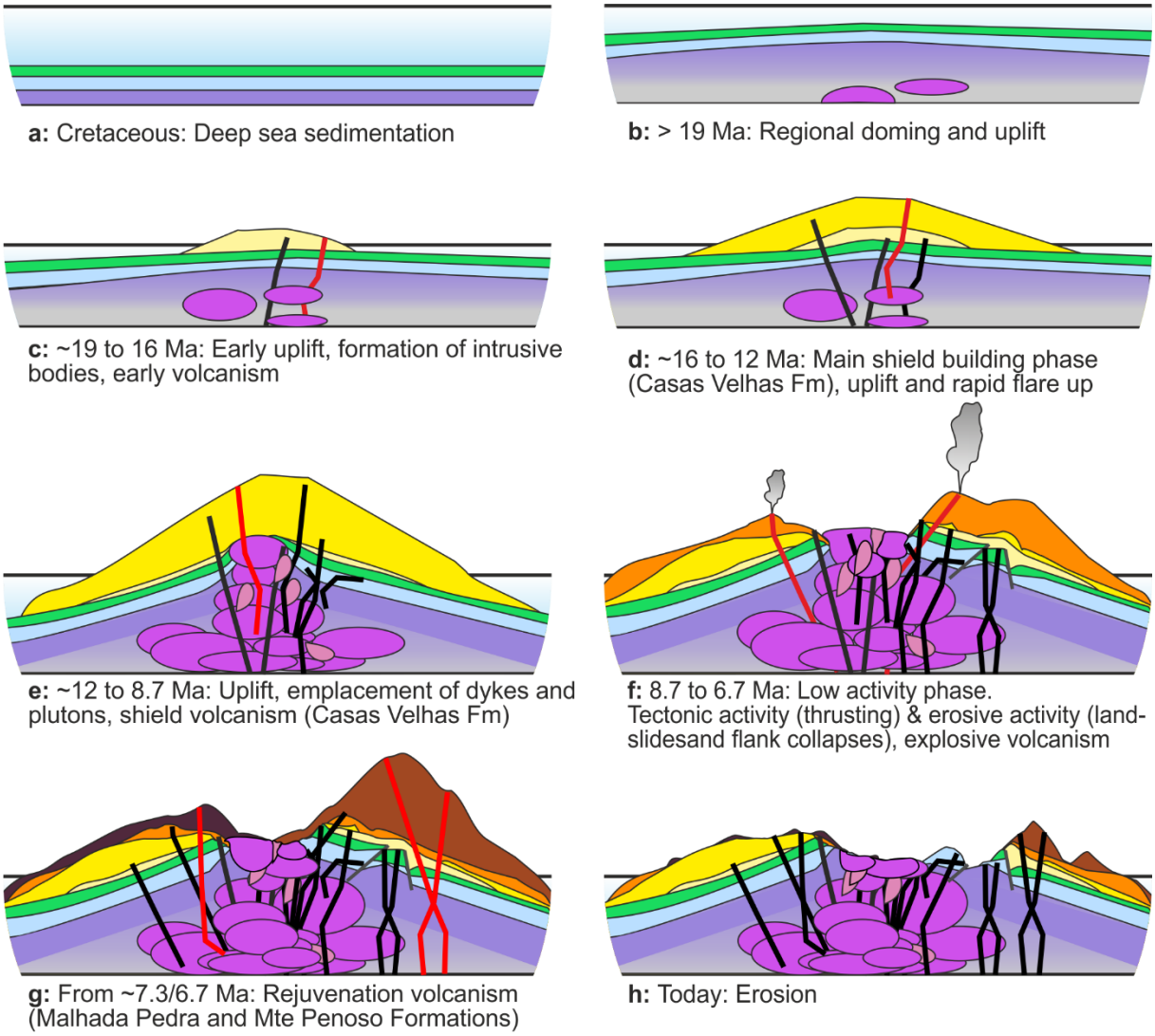

Figure 3.7 Cartoon of a simplified Maio geological evolution model (**a-h**; not drawn to scale and omitting sea level changes). Red lines = active dykes, black lines = cooled dykes.

Intrusive activity not only led to edifice growth from the inside, but also to extrusive activity and growth on the outside. Dyke K-Ar and ^{40}Ar-^{39}Ar ages from the second and third intrusive phases (12 to 10 Ma and 9.5 to 8 Ma) correspond with K-Ar ages from the subaerial Casas Velhas Formation lava flows and pyroclastic rocks, which are preserved in the S and SW parts of the island, mainly in river sections (Mitchell et al. 1983; **Fig. 3.1**). Casas Velhas Formation rocks are not preserved in the N and NE parts of Maio, possibly due to the later flank collapse events, but dykes of similar ages are present in these regions. An ankaramite lava from the base of the Casas Velhas Formation in the S of Maio yields a K-Ar age of 9.8 ± 0.4 Ma (Mitchell et al. 1983), although the authors suggest that the age may be older as the dyke may have been thermally overprinted due to the high dyke density at the sampling location. Mitchell et al. (1983) additionally observed petrological similarities between the youngest group of plutonic rocks from the CIC in the NW of Maio (Mte Vermelho) and lavas from the Casas Velhas Formation. This suggests that parts of the CIC and dykes cutting the Basement Complex rocks are the intrusive counterpart of the extrusive volcanics in the Casas Velhas Formation, with some of the dykes feeding surface eruptions. The ^{40}Ar-^{39}Ar age of 8.666 ± 0.027 Ma for a conglomerate clast from the Pedro Vaz Formation additionally overlaps with CIC and Casas Velhas Formation ages, further constraining igneous activity during the Tortonian.

A period of strong erosion and low volcanic activity followed the deposition of the Casas Velhas Formation lava flows, as shown by the emplacement of massive conglomerates and sparse pyroclastic deposits and the removal of large volumes of the previous volcanic edifice (**Figs. 3.2c, 3.3, 3.7f**). The 8.666 ± 0.027 Ma ^{40}Ar-^{39}Ar phlogopite age from a nephelinite clast from the Pedro Vaz Formation conglomerate, and the 6.7 ± 0.4 Ma K-Ar age from an ankaramite from the base of Mte Penoso (Mitchell et al. 1983), can be used to confine this erosive period to the Tortonian/Messinian. The sediment-dominated Pedro Vaz Formation is described as locally overlying the volcanic-dominated Casa Velhas Formation and incorporated rocks from the Casas Velhas Formation rocks in its base (i.e., in the western part of Rib do Morro and N of Barreiro; Serralheiro 1970, Stillman et al. 1982). Similar sedimentary deposits, which are locally confined and heterogenous, are difficult to differentiate and therefore it is hard to constrain their relative ages. This is especially true in this sequence of laterally heterogeneous units. We suggest that the younger parts of both the volcanic-dominated Casas Velhas Formation in the SW and the sediment-dominated Pedro Vaz Formation in the NE show similar features (i.e., conglomerates with pyroclastic layers) and they may overlap in age.

Previously published ages of the Pedro Vaz Formation are based on foraminifera findings from siltstones collected in the Pedro Vaz area (Rigassi 1972), who suggested an open sea environment and a planktonic zone N12 of Middle Miocene age. Reexamination of the Rigassi (1972)list of foraminifera reveals that only *Globorotalia fohsi robusta* and *G. fohsi lobata* are currently relevant for biostratigraphy and are now listed as modifications of *Fohsella fohsi (*s.l.) (J. Schönfeld, pers. comm.; Wade et al. 2011). This supports planktonic zone N12 (reclassified as M9a-M9b) with ages of 13.41 to 11.79 Ma (Wade et al. 2011). The Rigassi (1972) Pedro Vaz Formation microfossils have been previously used to confirm Miocene (>12 Ma) ages for the underlying Casas Velhas Formation. However, Stillman et al. (1982) states that the intercalation of open-sea rocks with subaerial lavas and conglomerates is problematic and thus these interpretations should be treated with caution.

Tectonic activity on the Mte Branco Thrust must post-date the intrusive activity in the Batalha Formation, as the dykes are all truncated by the thrust, which must therefore be younger than 10.405 ± 0.033 Ma. It is not clear if one of the Mitchell et al. (1983) samples from Mte Branco, yielding a K-Ar age of 9.0 ± 0.4 Ma, comes from the hanging or the foot wall of the thrust, but Mitchell et al. (1983) mention that it is truncated by the thrust, therefore the age of this thrust must also be younger than 9.0 Ma. Such reverse faults are common in volcanic settings around the world and typically occur at the end of the doming process caused by shallow magmatic intrusions (Montanari et al. 2017). Tectonic activity may have triggered the major Late Miocene erosive events, thus leading to the formation of sedimentary deposits overlying the Basement Complex Rocks (below Mte Penoso, in the Pedro Vaz Formation) and may therefore be contemporaneous in age (Tortonian/Messinian; **Fig. 3.7f**).

The eruption of Malhada Pedra Formation rocks (olivine melilitites) and Mte Penoso Formation nephelinite lavas mark the final phase of volcanism (**Fig. 3.7g**). Both formations are physically separated due to the deep erosion levels in the central part of Maio, but have overlapping ages: The Malhada Pedra olivine melilitite lavas yield K-Ar ages of 7.3 ± 0.4 Ma and 6.5 ± 1.2 Ma, whereas ankaramites from the base of the Mte Penoso lava pile and from Mte Santo António give K-Ar ages of 6.7 ± 0.4, and 6.9 ± 0.4 Ma, respectively (**Fig. 3.6**; Mitchell et al. 1983). While the Mte Penoso lavas dip towards the NE, the Malhada Pedra lavas dip towards the SE, indicating that they may originate from a restricted area in the W-central part of Maio. A missing systematic record of dyke directions, as well as faulting and thrusting of units complicates the effort to establish the positions of former eruptive centers. An eruptive center origin in the NW central region of Maio would fit well with a source area from the NW part of the deeper intrusive complex or island core, as deduced from gravity data (Represas et al. 2012), which again implies that this area is a younger part of the CIC. This is consistent with the youngest K-Ar ages (8.6 ± 0.4 Ma and 9.2 ± 0.4 Ma) of CIC intrusive rocks from the Monte Vermelho area (Mitchell et al. 1983). We additionally suggest that flank collapse activity in the Tortonian/Messinian (8.7 to 6.7 Ma) could have enhanced rejuvenated igneous activity of Malhada Pedra and Monte Penoso Formations on Maio, due to decompression-induced melting in the upper mantle.

After the final phase of volcanism (**Fig. 3.7g**), erosion was the dominant process shaping Maio. The topography has been flattened and only competent rocks remain as hills (**Fig. 3.7h**). Lava flows of the final volcanic phase capped the underlying conglomeratic units, protecting the last remnants from erosion. Quaternary dunes, alluvium and beach sediments are the youngest sediments on Maio.

3.6 Conclusions

Based on field observations, structural data and ^{40}Ar-^{39}Ar dating, we can refine the Miocene evolution of Maio Island in the Cabo Verde Archipelago.

Intrusive magmatic growth of Maio probably started in the Early Miocene with the emplacement of shallow plutonic rocks. Edifice growth was dominated by several phases of dyke intrusions and accompanying effusive activity in the Middle Miocene, leading to rapid growth of the island. The associated flare up and uplift is recorded in dyke orientations and resulted in semi-circular dips, deformation and disruption of Mesozoic marine sedimentary successions.

A newly discovered series of conglomerates, interwoven with local pyroclastic units, is interpreted as a flank collapse dominated phase of the Pedro Vaz Formation. The flank collapse events mark a period of rapid erosion in the Tortonian/Messinian (8.7 to 6.7 Ma), was possibly triggered by tectonic activity (i.e., the Mte Branco Thrust) and corresponds to the onset of rejuvenated volcanic activity. Mass wasting may have induced rejuvenated volcanism of the Malhada Pedra and Monte Penoso Formations due to decompression-induced melting in the upper mantle.

Acknowledgements

The authors would like to thank Thorsten Lux and Karin Junge for help in the labs and with sample preparation. Jan Sticklus is thanked for his invaluable help with ^{40}Ar-^{39}Ar dating of our samples. Dani Bernoulli is thanked for literature, unpublished material and valuable discussions on the geological (stratigraphical) evolution of Maio. Alistair Robertson is thanked for providing literature that was not publicly available. Ricardo Ramalho and Abigail Barker are thanked for their thorough reviews and comments, as well as topic editor Sascha Flögel for his hints, which greatly improved this manuscript. We are grateful for the hospitality and help we received from Dominique Gautherot on Maio, and for logistic help we received from OSCM Mindelo, especially from Cordula Zenk and Ivanice Monteiro. LKS would like to acknowledge financial support from the Helmholtz Research School for Ocean System Science and Technology (HOSST).

Funding

Open Access funding enabled and organized by Projekt DEAL. LKS was supported financially by the Helmholtz Research School for Ocean System Science and Technology (HOSST). The funding source was not involved in the study design, analyses, data interpretation and writing.

4 Large-scale fossil dune on Maio, Cape Verdes

The present paper was published as a GEOSITES-article in the peer-reviewed *International Journal of Earth Sciences (Geologische Rundschau)*:

Samrock L.K., Dullo W.-C., Hansteen T.H. (2018) Large-scale fossil dune on Maio, Cape Verdes. Int J Earth Sci (Geol Rundsch) 107(8):2931–2932. doi:10.1007/s00531-018-1622-x

This GEOSITE features an impressive fossil dune outcrop, which is one of the largest cemented dunes found on the eastern Atlantic islands (**Fig. 4.1**). The large scale fossil dune is located on Maio, an island in the eastern part of the Cape Verde archipelago. The archipelago is of volcanic origin and comprises ten islands, several islets, and ten volcanic seamounts. Maio is one of the oldest islands and has a complex history of volcanic activity and erosion, uplift and subsidence: The island consists of uplifted Jurassic and Cretaceous seafloor pre-dating volcanism, a Miocene intrusive complex, Miocene volcanic units, Mio-Pliocene calcarenites, and Quaternary sediments mainly consisting of uplifted beach terraces and alluvial/colluvial deposits (e.g., Serralheiro 1968, 1970, Stillman et al. 1982, Mitchell et al. 1983). Recent unconsolidated dunes can be found in windy areas along the coasts of the Cape Verde islands.

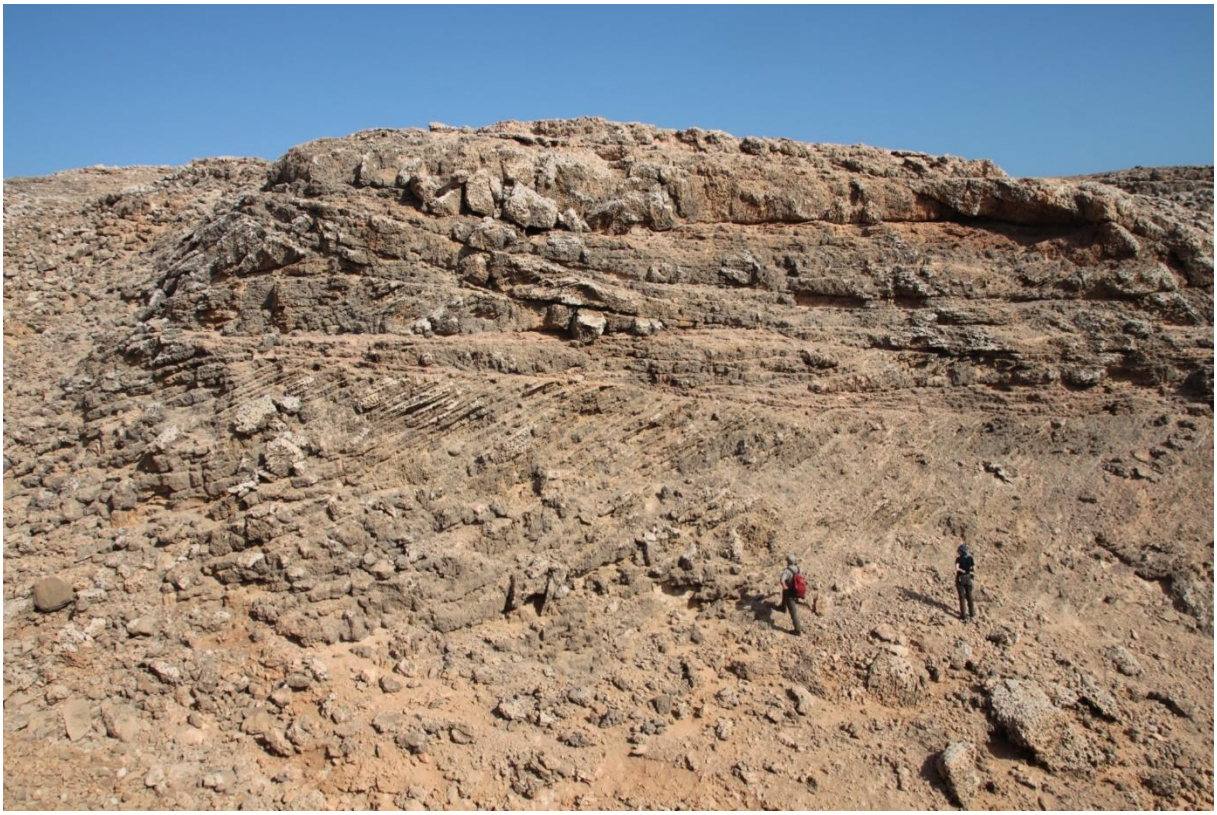

Figure 4.1 The large-scale fossil dune on Maio (Cape Verdes), looking North. The base of the image is about 30 m wide (Photo: T. Hansteen).

The large scale fossil dune is located in the East of Maio (15.19497N, -23.11072W), approximately 80-100 m above sea level, forming the highest terrace of uplifted beach sediments there. It overlies the colorful hydrothermally altered marls of the Late Cretaceous Coruja Formation (Fm.) and the ankaramite lava flows of the Miocene Mte Penoso Fm. in the vicinity of Cretaceous pelagic limestones (Morro Fm., Stillman et al. 1982). The fossil dune was first described by Serralheiro (1970), who identified several marine terraces that are located around the coasts of the island at elevations between 2-6 and 80-100 m a.s.l. Ramalho et al. (2010c) suggested seven main terrace levels at elevations 2-6, 8-12, 15-20, 30-40, 55-65, 65-75, and 80-100 m. The uppermost terraces have been dated to Middle-Late Pleistocene (Serralheiro 1970). Similar coastal marine terraces can be also found on the neighboring island Boa Vista and on Sal. Based on their ages and topographic location,

Ramalho et al. (2010c) suggested a recent phase of uplift by at least 45 m for Maio Island, following a phase of subsidence.

According to our own observations the outcropping dune consists of carbonaceous sandstones and arenites that are composed of coarse grained carbonate sands that formed locally by reworked bioclastic material from the Cape Verdean coasts, fine grained volcaniclastic material, and Sahara dust. The grains have ooidal carbonate crusts and are well cemented. Subaerial exposure led to intensive dissolution at the surface. Beds are usually several centimeters to decimeters thick, with single beds up to half a meter in thickness. The lower part of the dune dips 23° towards W (280/23) and shows tubular and wedge cross-stratification (**Fig. 4.2**). About 5 m above the base of the outcrop, trough cross-stratification is dominant, which forms sets of up to 3 m in thickness and is oriented in N-S wind-direction. This change in cross-stratification suggests a change in paleo-wind-directions and sedimentary geometry: The lower part of the dune was produced in a two-

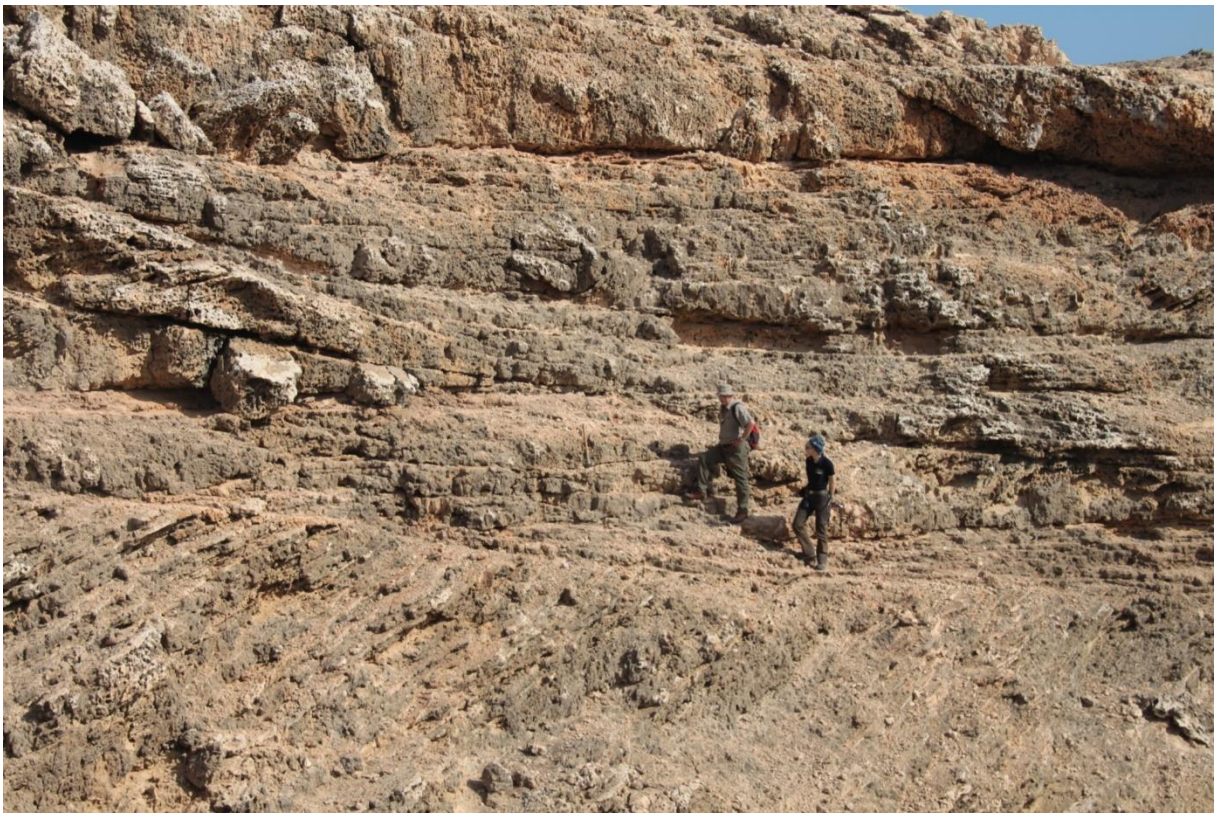

Figure 4.2 Close-up of fossil dune, showing the shift of cross-stratification from tabular-shaped (bottom) to trough cross-stratification (top), indicating changes in dune geometry and paleo-wind directions. The irregular trough-shapes become apparent especially on the left side of the image (Photo: T. Hansteen).

dimensional dune by easterly paleo-winds (the observer looks normal to the dominating paleo-wind direction). The upper part, on the other hand, indicates a shift to northerly paleo-wind directions and three-dimensional dune geometries (the observer looks parallel to the paleo-wind direction). Similar forms of large-scale cross-stratification were described for the Bahamas (see e.g., Fig. 21 in McKee and Ward 1983; Figs. 5-24 in Cheel 2005). Changes in paleoenvironmental conditions can also be observed in Quaternary aeolian deposits from Lanzarote and Fuerteventura (Canary Islands, Spain; e.g., Ortiz et al. 2006, Faust et al. 2015, Roettig et al. 2017).

Acknowledgements:

LKS would like to acknowledge funding from Helmholtz Research School for Ocean System Science and Technology (HOSST). The authors thank two anonymous reviewers and the editor, Sascha Flögel, for their comments.

5 Early biostratigraphy and facies of Mesozoic marine sediments on Maio (Cabo Verde) revisited: Witnesses of the early Atlantic Ocean

Lisa K. Samrock, Wolf-Christian Dullo, Thor H. Hansteen

Abstract

Maio Island, located in the south-eastern part of the Cabo Verde Archipelago, exposes the only pre-volcanic sedimentary sequences of all Cabo Verde islands. The sedimentary rocks of the Mesozoic Morro Formation and Carqueijo Formation, which consist of limestones and marls, surround the island's Miocene intrusive complex and overly MORB-type pillow lavas of the Batalha Formation representing early Atlantic Ocean floor.

It has previously been debated whether the sedimentary sequences are of Late Jurassic or Early Cretaceous age. Here we present new data on fossil assemblages together with a revised biostratigraphy of the Maio pre-volcanic sequences. Findings of *Calpionellites darderi* (Colom) in sediments intercalated between pillow lavas of the Batalha Formation suggest an Early Cretaceous age for the Maio oceanic basement. The overlying pelagic limestones of the Morro Formation contain a Valanginian to early Aptian fauna, including new findings of the ammonites *Phylloceras* cf. *infundibulum* (d'Orbigny 1840) and *Neocomites neocomiensis* (d'Orbigny 1841) that indicate a Valanginian to early Hauterivian age for the middle part of the Morro Formation. In addition, a new finding of *Tintinnopsella* cf. gr. *carpathica* (Murgeanu & Filipescu) and several calcareous nannofossils (e.g., *Nannoconus*, coccoliths) suggest an Early Cretaceous age for the Morro Formation. The overlying Carqueijo Formation yields nannofossils that suggest an Aptian to Cenomanian age.

The Morro Formation has been attributed to the widespread Maiolica facies (e.g., Robertson and Bernoulli 1982), which can be found in the Caribbean, Central Atlantic and Alpine-Mediterranean regions of the Western Tethys Ocean. Sediments of the Batalha Formation and especially the Carqueijo Formation contain turbidites from the W-African continental shelf. The absence of black shales on Maio, contrary to many sites in the Central Atlantic Ocean, could indicate active deep ocean circulation in the Early Cretaceous in the Cabo Verde archipelago. The sedimentary rocks of the Maio basement therefore yield important information on the evolution and paleo-oceanographic conditions of the young evolving Atlantic Ocean.

Keywords: Cabo Verde · Maio · Biostratigraphy · Maiolica · Cretaceous ·Atlantic Opening

5.1 Introduction

Maio Island is situated in the SE of the Cabo Verde (Cape Verde) Archipelago, about 600 km off the west coast of Senegal (**Fig. 5.1a**). Together with the islands Boa Vista and Sal to the North, Maio belongs to the oldest part of the archipelago (**Fig. 5.1b**; Holm et al. 2008).

Maio comprises the only exposed pre-volcanic sedimentary sequences of all Cabo Verde Islands. These segments surround the islands' Miocene intrusive complex, from which they dip away. The pre-volcanic sequence overlies MORB-type pillow lavas formed in the Mesozoic early Atlantic Ocean, and is composed of a thick succession of siliceous limestones and marls (Paepe et al. 1974). These units were uplifted from the seafloor before and/or during volcanic and intrusive activity, and deep erosion has removed large parts of the overlying younger volcanic sequences. The occurrence of these pre-volcanic units is unique for Cabo Verde, but similar, less complete pre-volcanic sequences have been reported from other volcanic oceanic islands, e.g., Fuerteventura (Canary Islands; Steiner et al. 1998). For the most part, the facies encountered can be compared to Mesozoic facies of the Maiolica from the Central Atlantic and Tethyan realm in terms of facies and age (e.g., Bernoulli 1972, Robertson and Bernoulli 1982, Bernoulli and Jenkyns 2009).

The age of the lowest part of the sedimentary sequences on Maio has been debated for decades: while some authors suggested a Late Jurassic origin (e.g., Stillman et al. 1982, Robertson 1984, and references therein), others argued for an Early Cretaceous age instead (Azéma et al. 1990, Fourcade et al. 1990). In this study we present new data on fossil assemblages and a resulting biostratigraphy of the pre-volcanic sedimentary sequences on Maio, and review them in the light of previous studies. This study improves the understanding of the composition and formation of pre-volcanic basement of an old volcanic ocean island and the opening and evolution of the early Atlantic Ocean.

5.2 Geological Setting

The Cabo Verde Archipelago comprises 10 islands and smaller islets and seamounts that are distributed between two island chains; a SE-NW trending northern chain, and a NE-SW trending southern chain (**Fig. 5.1b**; Gerlach et al. 1988).

The archipelago is situated on one of Earth's most prominent bathymetric anomalies, the Cape Verde Rise, rising ~2000 m from the surrounding seafloor. The Cape Verde Rise is associated with geoid, gravity, and thermal anomalies that are thought to originate in the deep mantle (Dash et al. 1976, Crough 1982, Courtney and White 1986, Ali et al. 2003, Pim et al. 2008, Wilson et al. 2010). The oceanic crust beneath the Cabo Verde islands and seamounts is ~115-147 Ma old, located between the Cretaceous Magnetic Quiet Zone (CMQZ) in the West, and Chrons M0 (120.6-121.0 Ma) to M21 (146.56-147.06 Ma) towards the East (Channell et al. 1995; Bird et al. 2007; Müller et al. 2008). The eastern islands in both chains are deeply eroded, while the western islands have higher topographies. The Cabo Verde archipelago has been volcanically active since the Oligocene, with the oldest subaerial volcanic activity reported from Sal at ~26 Ma (Torres et al. 2002).

Maio is located on the seafloor between paleomagnetic Chrons M11 (~136 Ma) and M16 (~141 Ma; Gradstein 2012) and has an area of ~273 km² (**Fig. 5.1b**). The geological units have been mapped by Serralheiro (1970) and further refined and named by Stillman et al. (1982).

The oldest rocks on Maio are MORB-type pillow lavas of the Batalha Formation (Paepe et al. 1974, Stillman et al. 1982) that are overlain by siliceous pelagic limestones and marls of the Morro Formation and the Carqueijo Formation (Stillman et al. 1982). These units were formed on the seafloor prior to island formation and were uplifted, now forming a circular structure dipping away from a Miocene Central Intrusive Complex (CIC), which contains alkaline, silica-undersaturated rocks (essexites, pyroxenites, syenites and some carbonatites; **Figs. 5.1c, 5.2**; Serralheiro 1970, Stillman et al. 1982). Together, these unites (Batalha Formation, limestones and CIC) form the Basement Complex (Stillman et al. 1982).

Intrusive and volcanic activity on Maio started at about 20 Ma with the formation of the Central Intrusive Complex and dyke intrusions (Grunau et al. 1975, Bernard-Griffiths et al. 1975, Mitchell et al. 1983; **Fig. 5.2**). The formations of the Basement Complex are unconformably overlain by ankaramite lavas of the subaerial Casas Velhas Formation, and by coarse conglomerates, tuffs, and

ankaramite lavas of the Pedro Vaz Formation (Stillman et al. 1982). Volcanic activity continued with the eruption of Malhada Pedra lava flows until the formation of the Monte Penoso stratovolcano ~7 Ma (Stillman et al. 1982, Mitchell et al. 1983). Its remnants now form the highest elevation on the island ~400 m above sea level (asl). Extensive Quaternary marine terraces cover large areas, especially the exterior of the island, up to elevations of 100 m asl. These marine terraces at different elevation levels suggest several phases of uplift and subsidence (Serralheiro 1970, Ramalho et al. 2010c, Samrock et al. 2018).

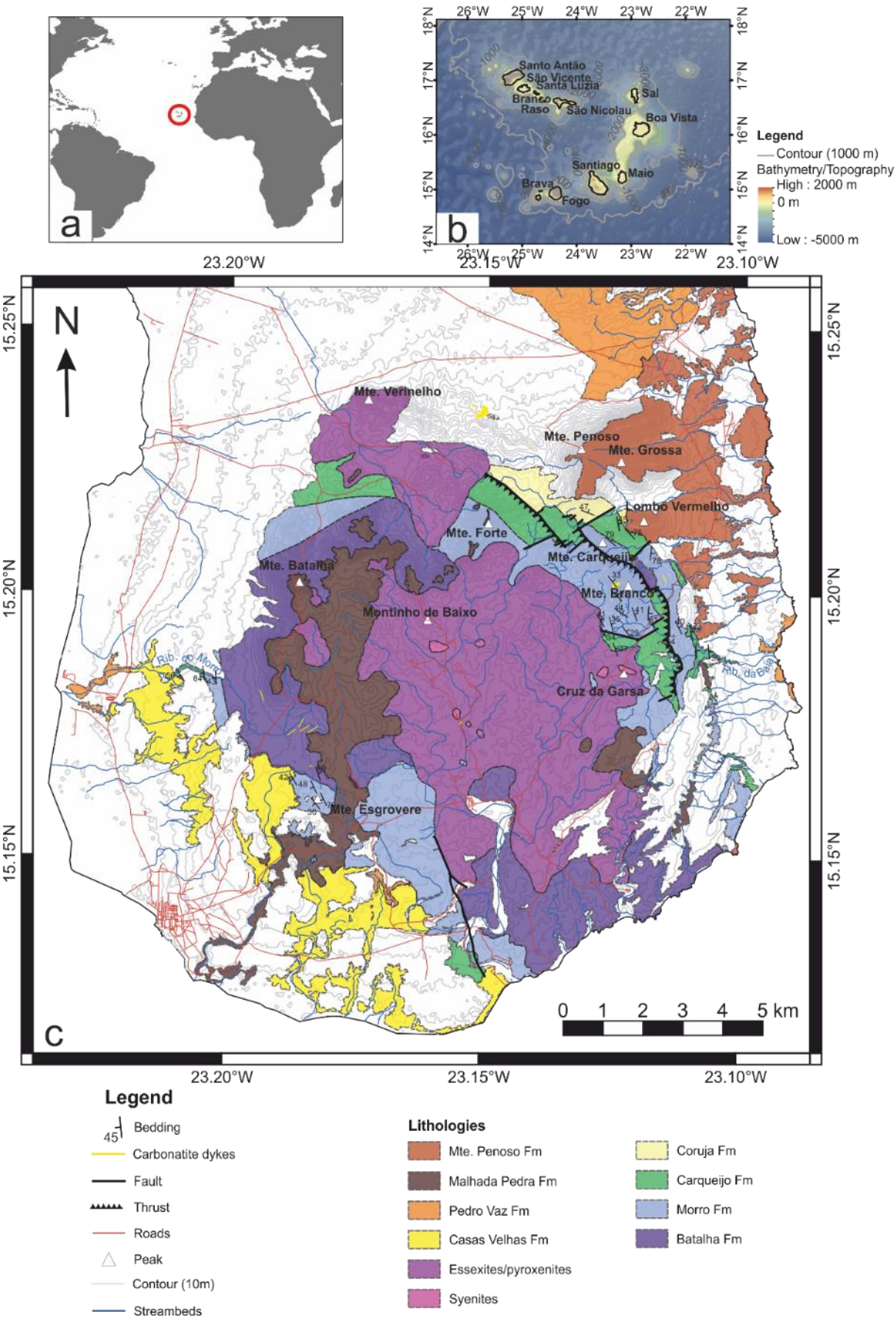

Figure 5.1 Section of the simplified geological map of Maio (**c**, modified after Serralheiro 1970, Stillman et al. 1982 and Represas et al. 2012) with small overview maps in **a** and **b**.

5.3 *Pre-volcanic sedimentary stratigraphy on Maio – own observations and current state of knowledge*

The following paragraphs present our own observations of the different units defined by Stillman et al. (1982), and review the current stage of knowledge regarding the facies and biostratigraphy of the pre-volcanic sedimentary successions on Maio. Species and their age ranges were identified and checked using Fossilworks.org and Nannotax3 (Young et al. 2017).

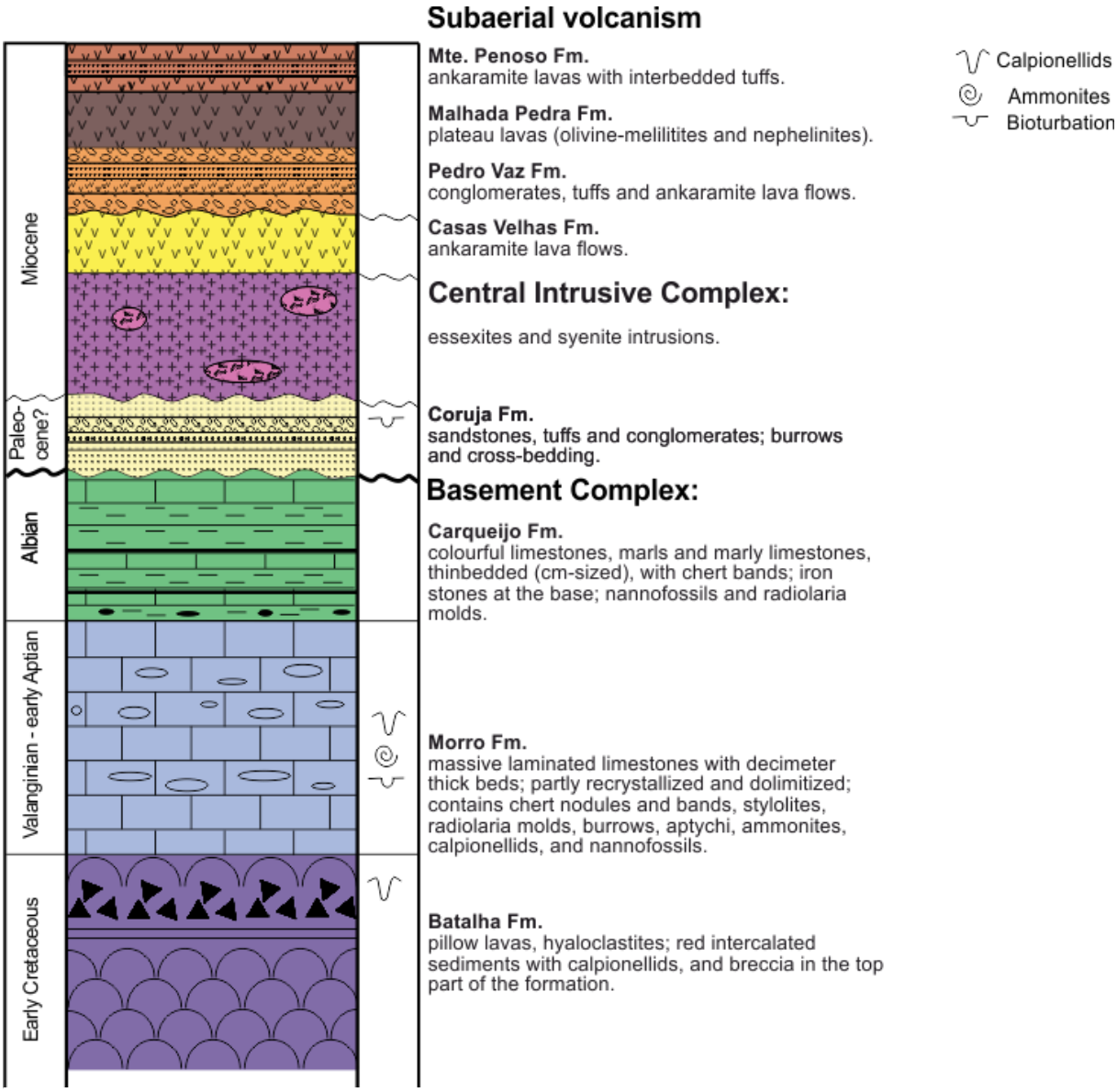

Figure 5.2 Simplified stratigraphic column of the mapped units on Maio, Cabo Verde. Not to scale

5.3.1 *Batalha Formation*

The Batalha Formation is dominated by basaltic pillow lavas, lava breccias and hyaloclastites, commonly strongly altered under greenschist-facies conditions. It crops out below the Mte. Branco thrust at the northern flank of Mte. Branco, at the SE coast of the island, N of Mte. Esgrovere, and at the western flanks of Monte Batalha (**Fig. 5.1c**). In many locations, the formation is strongly modified by dyke intrusions, and commonly only fragments of weathered/altered pillow lavas can be observed (**Fig. 5.3a**). The pillow lavas have MORB character (Paepe et al. 1974), and are characterized by the presence of calcic plagioclase, olivine and augite, a general composition of tholeiitic basalt, and a depleted LREE pattern, in contrast to the strongly alkaline silica-undersaturated rocks of the CIC (Paepe et al. 1974, Klerkx and Paepe 1976). As the pillow lavas are generally not well preserved, only the coastal outcrops allow a more detailed investigation of the

rocks. In many locations it is therefore difficult to decide if hyaloclastites are present, or if the physical appearance is due to strong alteration.

NE of Mte. Esgrovere, sediments are intercalated between pillow lavas (**Fig. 5.3b; Table 5.1**). These sediments are of a distinct red colour, are folded and are vertically dipping. In thin-section, a fine lamination comprising opaque material (oxides, organic matter), lithoclasts and pseudomorphs of igneous minerals, all crosscut by microfaults, can be observed. These intercalated sediments were also mentioned by Stillman et al. (1982), Robertson (1984), Azéma et al. (1990) and Fourcade et al. (1990), for the upper part of the Batalha Formation, especially E of Mte. Esgrovere. Robertson (1984) interpreted these sediments as terrigenous derived from turbidity currents from the West-African margin. Additionally, breccias occur in the upper part of the Batalha Formation, above the red intercalated sediments in the Mte. Esgrovere area (**Fig. 5.3 c, d; Table 5.1**). These breccias contain angular fragments of altered sedimentary rocks, possibly of the underlying red sediments, suggesting sufficient time for lithification of the sediments in the upper Batalha Formation before the last pulses of magmatic activity.

Biostratigraphy of the Batalha Formation

In one red organic rich sample of intercalated Batalha Formation north of Mte. Esgrovere, we found ?*Calpionellites darderi* (COLOM) (**Figs. 5.3e, f, 5.9, Table 5.1**; e.g., Grün and Blau 1997).

Azéma et al. (1990) found calpionellids in intercalated sediments of the upper Batalha Formation at the base of Mte. Esgrovere. With *Calpionellites darderi* (COLOM) and *Tintinnopsella longa* (COLOM), these sediments yield an early Valanginian age. Our finding of *Calpionellites darderi* (COLOM) therefore confirms the findings of Azéma et al. (1990). In addition to calpionellids, Fourcade et al. (1990) describe radiolarians: *Sethocapsa uterculus* PARONA 1890, *Angulobracchia portmanni* BAUMGARTNER 1984, and *Acanthocircus dicranacanthos* (SQUINABOL) (synonym according to GBIF Secretariat (2017): *Dicerosaturnalis dicranacanthos* (SQUINABOL)), and suggest an age not older than Valanginian for the Batalha Formation.

It is an ongoing debate if the Batalha Formation and the overlying lower Morro Formation are of Jurassic age (e.g., Stillman et al. 1982, Robertson and Bernoulli 1982, Robertson 1984) or of Early Cretaceous age. The suggestion of a Jurassic age by Stillman et al. (1982), Robertson and Bernoulli (1982), and Robertson (1984) is solely based on an unpublished report for the oil industry (Rigassi 1972) and a conference abstract (Rigassi 1975), of which extracts are available to us. Rigassi mentions the occurrence of *Saccocoma* sp., *Protoglobigerina,* and *Crassicollaria brevis* REMANE in rocks of the Morro Formation (above the Batalha Formation), and argues for Jurassic ages, but other authors (e.g., Robertson 1984, Fourcade et al. 1990) were not able to confirm these findings. Therefore, Rigassi's suggestion results in doubt and Valanginian is the most likely age.

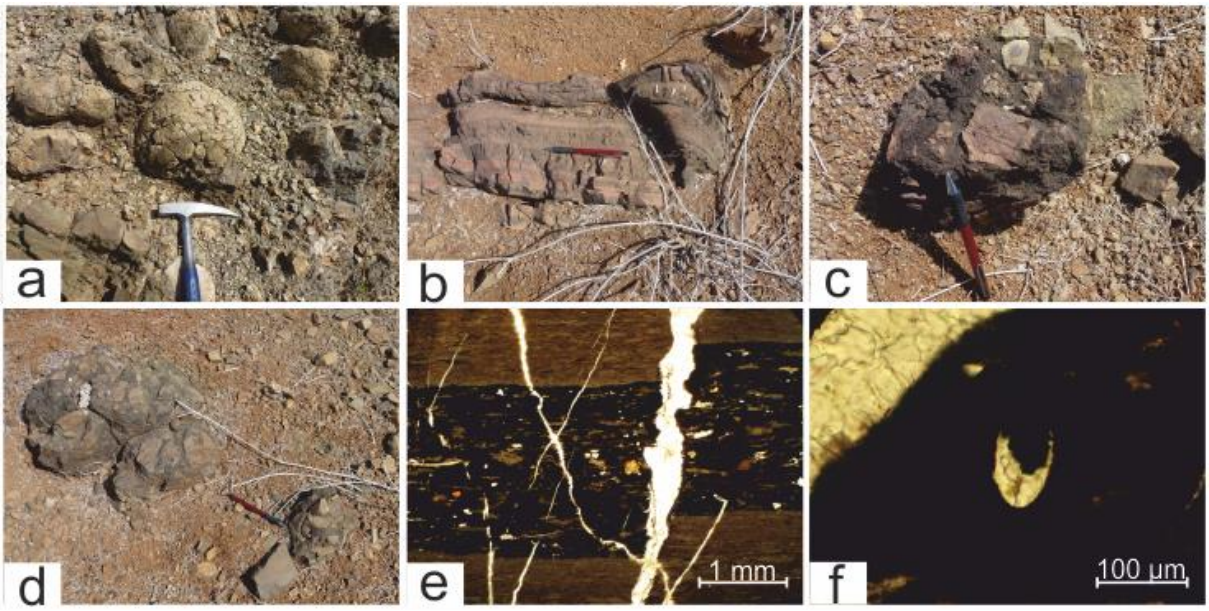

Figure 5.3 Batalha Formation. **a**: Pillow lava at the northern flank of Mte. Branco. Hammer for scale. **b**: red intercalated sediments in the upper Batalha Formation N of Mte. Esgrovere. Pencil for scale. **c, d**: Breccia in the upper part of the Batalha Formation N of Mte. Esgrovere, with angular fragments of altered sedimentary rocks. Pencil for scale. **e, f**: Thin section images of organic-rich red intercalated sediment (Mte. Esgrovere), showing a micro-fault (**e**) and ?*Calpionellites darderi* (COLOM) (**f**).

Table 5.1 Selected sample names, sampling locations, and bedding at these locations

Sample	Formation	Location Name	Description	Coordinates		Bedding (dip direction/ dip)
				Latitude	Longitude	
18-49	Batalha Formation.	N of Mte. Esgrovere	Pillow lava	15°09'57.14"N	23°10'52.22"W	
18-51	Batalha Formation	N of Mte. Esgrovere	Red intercalated sediment	15°09'57.25"N	23°10'53.72"W	
18-53	Batalha Formation	N of Mte. Esgrovere	Brecciated dyke	15°09'54.85"N	23°11'01.81"W	
18-40/8	Carqueijo Formation	N of Lomba da Vigia	Marl with iron stones above last beds of Morro Formation	15°11'37.42"N	23°06'37.07"W	078/36
18-69	Carqueijo Formation	Rib. do Morro	Marl with ironstones and nannofossils, just above Morro Formation	15°11'3.66"N	23°12'16.20"W	279/70
17-41	Coruja Formation	S flank of Mte. Penoso	Sandstone with burrows and cross-lamination	15°12'54.95"N	23°07'48.73"W	
17-43	Coruja Formation	S flank of Mte. Penoso	Sandstone with burrows, close to conglomerate	15°12'54.77"N	23°07'50.37"W	
17-75/5	Morro Formation	N of Mte. Branco	Pebble of Morro Formation limestone	15°12'14.09"N	23°07'6.78"W	
18-6	Morro Formation	S of Mte. Branco	Limestone with macrofossils	15°11'44.20"N	23°07'31.57"W	
18-14	Morro Formation	Mte. Branco	Pelagic limestone	15°11'42.47"N	23°07'14.28"W	076/36
18-42	Morro Formation	Rib. da Baia	Massive limestone with chert bands	15°11'19.85"N	23°06'30.63"W	074/23

18-62	Morro Formation	Mte. Esgrovere	Limestone with ammonites and aptychi	15°09'46.57"N	23°10'55.98"W	251/64
18-63	Morro Formation	Mte. Esgrovere	Limestone with ammonites and aptychi	15°09'38.37"N	23°10'51.74"W	245/70
18-64	Morro Formation	Mte. Esgrovere	Limestone, bioturbated	15°09'35.43"N	23°10'57.58"W	231/30
18-65	Morro Formation	Rib. do Morro	Limestone with ammonite remnants	15°11'1.08"N	23°12'8.58"W	264/43

5.3.2 Morro Formation

The Morro Formation has prominent outcrops at Monte Esgrovere, Monte Branco, NE of Lomba da Vigia, and in the river valleys Ribeira da Baia to the East and Ribeira do Morro to the West. Other locations (see **Fig. 5.1c**) are obscured by intensive dyke intrusions and/or alluvial material. In most locations, the limestones are mined by locals for road construction and building material: The small piles of rock cubes are indicative for the presence of Morro Formation limestones on Maio.

The Morro Formation is generally characterized by decimetre thick beds of grey pelagic limestones with various amounts of centimetre thick chert lenses and chert bands (**Fig. 5.4b, c**). The limestones show fine and swirly laminations. Stylolites are common (**Fig. 5.4d**), as well as burrows up to 2 cm in diameter. The limestones contain radiolaria in the form of calcite filled solution molds. In the lower parts of the unit, the limestones were intruded by dykes and fragments of limestone incorporated into these dykes (e.g., at Monte Esgrovere, southern coast). Diagenetic dolomite rhombs can be observed in some samples, especially associated to bioturbation. Such a selective dolomitization in burrows can be attributed to changes in permeability, porosity and grain size compared to the rest of the rock (e.g., Flügel and Munnecke 2010). Pyrite is present as individual crystals dispersed in the matrix.

At Monte Branco, numerous carbonatite dykes intrude the limestones. In addition, up to several meters thick undulating basanite sills intrude the sedimentary units more or less parallel to their bedding especially at the southern flanks of the mountain, with a few exceptions where these sills cross-cut the limestones with an angle up to 60°. (**Fig. 5.4a**). The limestones at Monte Branco are cut by several faults, including the Monte Branco thrust at the northern flank of Monte Branco. The limestone beds dip with an average of 35°, but become steeper towards the top of the mountain and the Monte Branco thrust (up to 60°). Because of the number of faults at Monte Branco, the thickness of sediments at this location is difficult to estimate, as tectonic repetition of units may have occurred (see e.g., Stillman et al. 1982). Most limestones at Monte Branco are grey-coloured and recrystallized, obscuring former fossil content and leaving only remnants of nannofossils.

Ribeira do Morro is the type section for the Morro Formation rocks and therefore one of its key locations. The first publications on the biostratigraphy of the Maio sedimentary rocks are based on samples from this dry river valley (e.g., Friedlaender 1913, Hennig 1913, Heinz 1935, Stahlecker 1934). However, during the past few decades, the river valley has been largely filled with sediment due to flood protection measures (stone walls). Only the upper meters of the outcrop can be studied, except for some active open pit mines that reach ~5 m down below the surface. These changes in outcrop conditions hamper the confirmation of previous findings. At Rib. do Morro, the units dip with an average of 55° towards the West. The Morro Formation at this location is outcropping over 200 to 350 m (calculated with dips of 30° to 55°). A thickness of 200 m is within the range of the one given by Robertson (1984), while a thickness of 350 m matches with the Rib. do Morro profile of Fourcade et al. (1990). The limestones here are also cut by dykes. Stylolites can be commonly observed and some of the rocks are recrystallized (**Fig. 5.4d; Table 5.1**). Colours vary between light grey and tan. Macro- and nannofossils are not well-preserved.

A third important outcrop location for the Morro Formation is Mte. Esgrovere in the SW of the island. Here, the Morro Formation dips with an average of 50° towards the SW (steeper at the base with up to 70°), and reaches a thickness of about 380 m. Thicknesses may become larger, if the

complete mapped area is considered. Most samples at Mte. Esgrovere contain well-preserved micro- and macrofossils. Colours vary between light grey and orange.

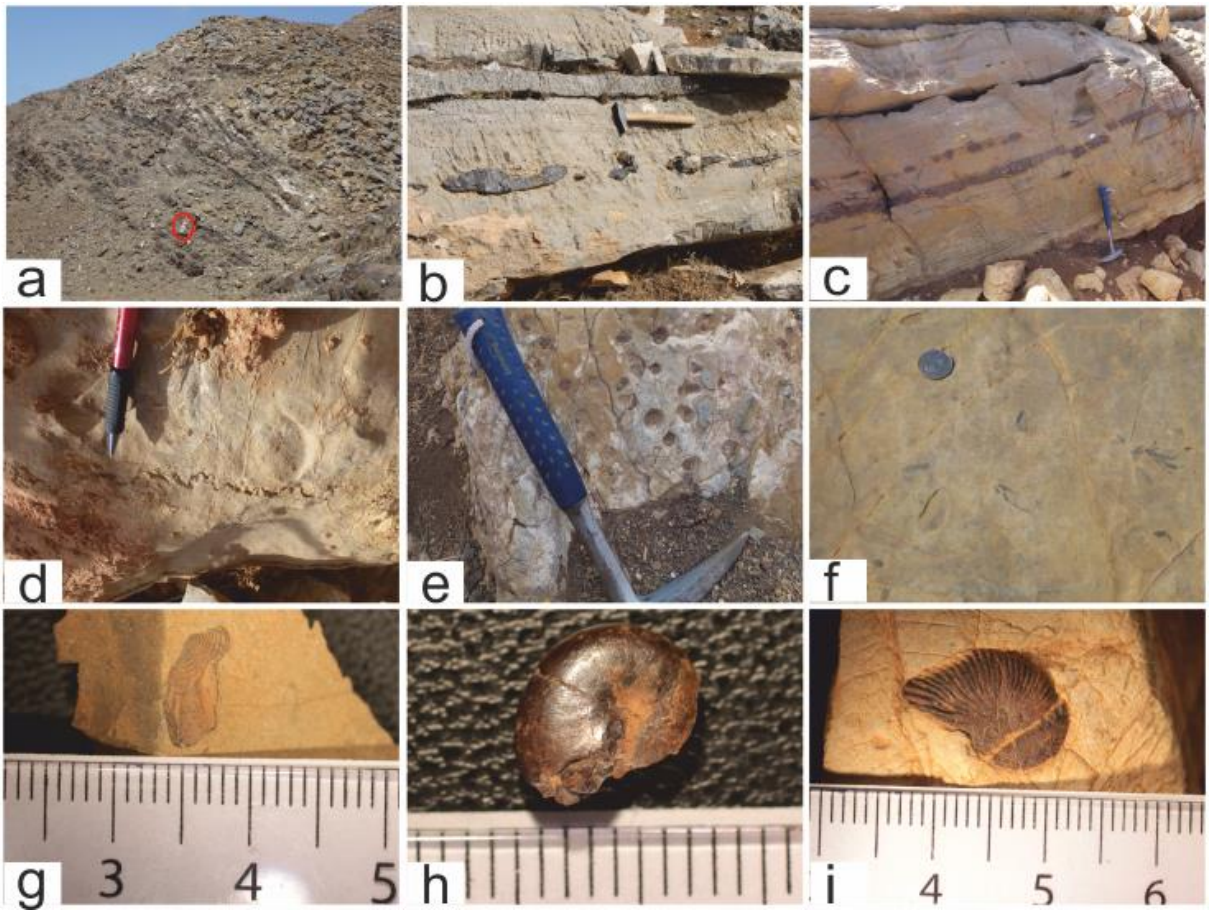

Figure 5.4 Morro Formation. **a**: Massive pelagic limestones, intruded by dykes (left side) at Mte. Branco. Person encircled in red for scale. **b, c**: Chert lenses in Morro Formation limestones at Mte. Branco (**b**) and Mte. Esgrovere (**c**). **d**: Stylolites in Morro limestones. e: Remnants of ammonites at Rib. do Morro. **f**: Macrofossils at Mte. Branco. g: Aptychus. **h, i**: Ammonites *Phylloceras cf. infundibulum* (d'Orbigny 1840) (**h**) and *Neocomites neocomiensis* (d'Orbigny 1841) in **i**.

Biostratigraphy of the Morro Formation

Ammonites

At Mte. Esgrovere, we found ammonites ~150 m from above the stratigraphic base of the Morro Formation. Some of these ammonites are well preserved and were identified as *Phylloceras* cf. *infundibulum* (d'Orbigny 1840) and *Neocomites neocomiensis* (d'Orbigny 1841) (**Figs. 5.4h, i, 5.9; Table 5.1**), which indicate a Valanginian to early Hauterivian age (136.4-130 Ma; Fossilworks.org). This is the first described record of ammonites at Mte. Esgrovere, all previous findings derive from Rib. do Morro. *Neocomites neocomiensis* (d'Orbigny 1841) has also been reported from Hauterivian units at DSDP Site 397 close to the Canary Islands (Wiedmann 1979), and from a turbidite sequence of Valanginian to Hauterivian age on Fuerteventura (Renz et al. 1992).

At Rib. do Morro, we found ammonites as well, exposed at a bedding surface ~140 m above the stratigraphic base (**Fig. 5.4e; Table 5.1**). These ammonites are unfortunately not well preserved, but confirm the first descriptions from Stahlecker (1934), who described abundant coin-sized cephalopods (>50 species), gastropods, and bivalves from Rib. Do Morro. Stahlecker (1934) divided the Morro Formation at this location into 14 different horizons, ranging from the Hauterivian-Barremian (horizon 1) to the Aptian (horizon 12). Since the thickness he proposed for the Morro Formation is 300 m and he described the first marls as occurring in the upper Barremian (above horizon 7), and colourful marls above horizon 14, we assume that most parts of his profile cover the Morro Formation and do not include the overlying Carqueijo Formation. *Phylloceras* cf.

infundibulum (D'ORBIGNY 1840), as we found at Mte. Esgrovere, was also described by Stahlecker (1934) from Rib. do Morro. The collection from Stahlecker (1934) was later reexamined by Fourcade et al. (1990), who confirmed Hauterivian to late Barremian ages for the series at Rib. do Morro, but he suggested that early Barremian might be absent as no ammonites of this period were found.

We also found aptychi, but were not able to determine the species (**Fig. 5.4f, g**). Aptychi were previously mentioned by Friedlaender (1913) for Rib. do Morro, and determined by Hennig (1913), who described *Aptychus atlanticus*, *Aptychus euglypticus*, and *Aptychus* sp., to which he assigned a Tithonian or even younger age. Additionally, Stahlecker (1934), described *Aptychus angulocostatus*. All these species were reinvestigated by Trauth (1936), who renamed Hennig's *Aptychus* sp. to *Laevilamellaptychus hennigi* TRAUTH (1936) and assorted all above mentioned aptychi to a Neocomian age (Berriasian-Hauterivian). These results where later questioned by Soares (1950) and Soares (1953), who attributed late Jurassic ages to his own findings of aptychi, but his results where debated and questioned (e.g., Mitchell-Thomé 1972, Mitchell-Thomé 1974). Therefore, our new biostratigraphic data from Mte. Esgrovere confirm Trauth's (1936) revision and proof an Early Cretaceous age (Valangian-Hauterivian).

Other fossils

In addition to ammonites and aptychi, rare remnants of gastropods, fragments of sponge spicules, echinoid fragments, *Nasselaria*, bivalve fragments (e.g., *Ostrea* sp., Stahlecker 1934), and foraminifera can be observed in rocks of Morro Formation (**Fig. 5.5**). Further calcified radiolarians are abundant **(Fig. 5.5)**. Robertson (1984) mentions radiolarians that are similar to *Dictyomitra* ZITTEL 1876, *Stichomitra* CAYEUX 1897, and Hagiastids. Two samples from Mte Esgrovere yield *Cadosina* **(Fig. 5.5g)**, which has previously been described by Fourcade et al. (1990) as *Cadosina lapidosa* VOGLER 1941 (Neocomian; Young et al. 2017). In the Monte Branco, Monte Grande and Rib. do Morro areas, Heinz (1935) also described various inoceramid bivalves of Early Cretaceous age (Barremian to Aptian). Rigassi (1972) mentions the occurrence of *Saccocoma* sp. (age range: 252.3 to 89.3 Ma; Fossilworks.org), *Protoglobigerina* (age range: 155.7 to 150.8 Ma; Fossilworks.org), and *Crassicollaria brevis* REMANE (~145-143 Ma; **Fig. 5.9**; Grün and Blau 1997) in rocks of the Morro Formation at Monte Branco, which would argue for Jurassic ages (Oxfordian to Tithonian), and mentions also traces of belemnites and rhyncholites (in addition to ammonites and aptychi). However, later investigations of the Morro Formation rocks did not confirm Rigassi's findings (e.g., Robertson 1984; Azéma et al. 1990, Fourcade et al. 1990). Stahlecker (1934) mentions rhyncholites ("Cephalopodenschnabel"), but stresses the complete absence of belemnites. Stahlecker (1934) also mentions the occurrence of remants of Teleostei.

Calpionellids

We found one pebble N of Monte Branco yielding *Tintinnopsella* cf. gr. *carpathica* (MURGEANU & FILIPESCU), which is of Early Cretaceous (Berriasian-Early Valanginian) age (Grün and Blau 1997; **Figs. 5.5c-f, 5.9**).

In addition to calpionellids from the Batalha Formation, Azéma et al. (1990) and Fourcade et al. (1990) described rare *Tintinnopsella* sp. and *Tintinnopsella longa* (COLOM) for the Morro Formation at Mte. Esgrovere (**Fig. 5.9**). Rigassi (1972) found *Tintinnopsella longa* (COLOM), *T.* gr. *carpathica* (MURGEANU & FILIPESCU), and *Calpionella alpina* LORENZ east of Lombo da Vigia and in the SE of Maio, suggesting Early Cretaceous (Berrias/Neocomian) ages. In addition, he mentions an occurrence of *Crassicollaria brevis* REMANE at Monte Branco, which led him to place the lower Morro Formation in the Jurassic (Tithonian). However, these findings are in conflict with the findings of Azéma et al. (1990) and Fourcade et al. (1990), who found only Early Cretaceous calpionellids in the underlying Batalha Formation. According to Grün and Blau (1997), *Crassicollaria brevis* REMANE

occurred from 145 Ma to 142.5 Ma, which would now plot into the Berriasian. We also only found Cretaceous calpionellids, there is therefore no indication for Jurassic calpionellids.

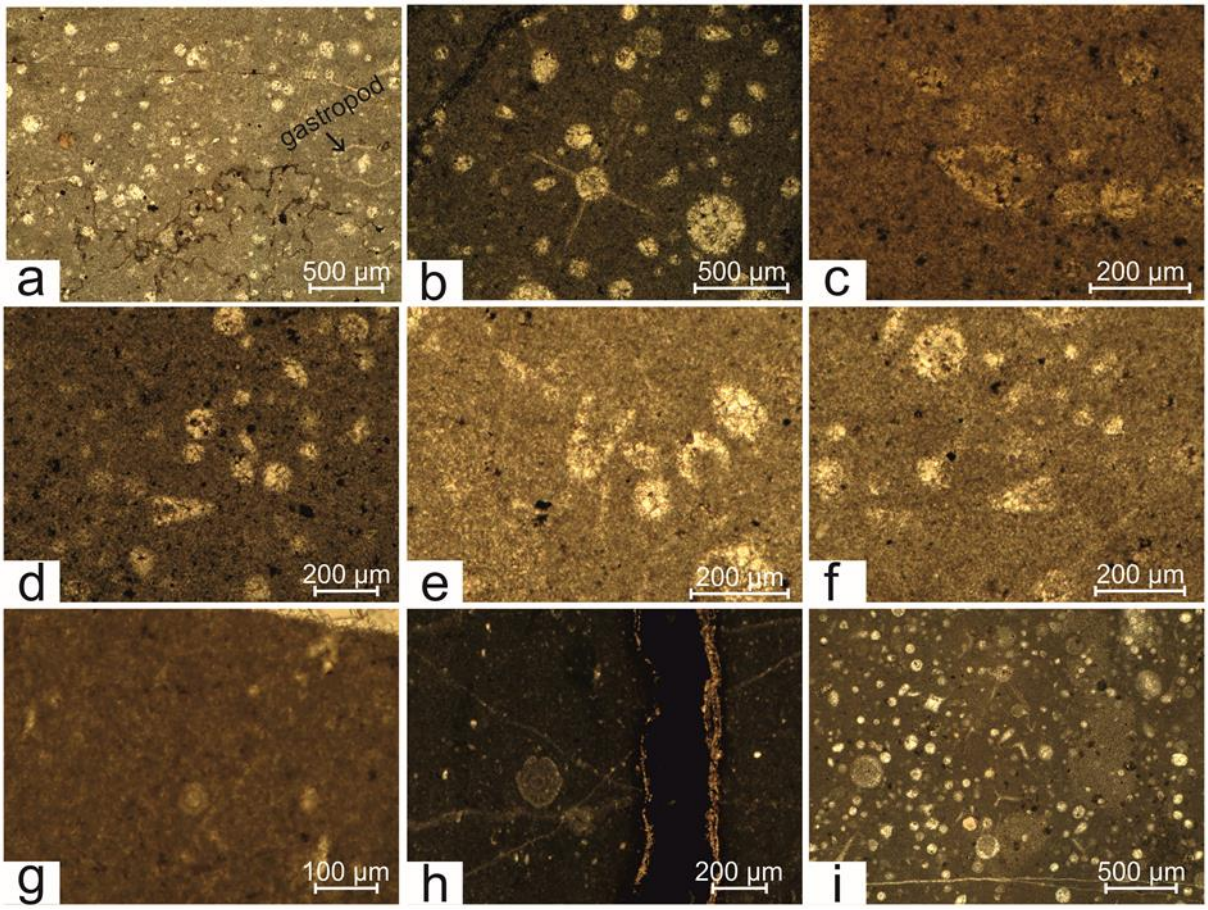

Figure 5.5 Thin section images of Morro Formation limestones. **a**: Gastropod and stylolites. **b**: radiolarians. **c-f**: calpionellids (*Tintinnopsella* cf. gr. *carpathica* (Murgeanu & Filipescu) in **c**). **g**: *Cadosina* sp. h: foraminifera (?) and organic-rich seam. **i**: Radiolaria and bioturbation, containing dolomite rhombs.

Nannofossils

Most samples of the Morro Formation are recrystallized micrites, especially from Mte. Branco and Rib. do Morro, which left only fragments of nannofossils. At Mte. Esgrovere, two samples yield well-preserved microfossils, which can be determined. An additional one was found at Rib. da Baia, which is located in the upper part of the Morro Formation just below the transition to the overlying Carqueijo Formation. *Nannoconus sp.* fragments can be frequently observed, but we did not confine a species (**Fig. 5.6a**). The samples contain *Watznaueria fossacincta* (Black 1971) Bown *in* Bown & Cooper, 1989, *Watznaueria britannica* (Stradner 1963) Reinhardt 1964, and *Cyclagelosphaera* cf. *argoensis* Bown 1992, all of which occur in the Late Jurassic and Early Cretaceous and are therefore not of high-resolution biostratigraphical value (**Figs. 5.6 b-d, 5.9**; Young et al. 2017). Rigassi (1972) found *Nannoconus colomi, N. steinmanni,* and *N. bucheri* (Early Cretaceous), as well as *Braarudosphaera discula* Bramlette & Riedel, 1954 (reclassified as *Micrantholithus disculus* (Bramlette & Riedel 1954) Bown 2005; Selandian to Late Oligocene; Young et al. 2017) and *Discolithus embergeri* (Noël) Stradner 1963 (reclassified as *Zeugrhabdotus embergeri* (Noël 1959) Perch-Nielsen 1984, Tithonian-Selandian stage; Young et al. 2017). Robertson (1984) mentions *Watznaueria barnesiae* (Black *in* Black & Barnes 1959) Perch-Nielsen 1968, *Cretarhabdus* sp., and *Cyclagelospahera deflandrei* (Manivit 1966) Roth, 1973 for the Monte Branco area, but these nannofossils do not allow a precise stratigraphic allocation. In addition, Robertson (1984) mentions findings of *Parhadolithus splendens* Deflandre 1953 (now reclassified as *Rhagodiscus splendens* (Deflandre 1953) Verbeek 1977; Young et al. 2017), and *P. asper* (Stradner) Manivit 1971 (reclassified as *Rhagodiscus asper* (Stradner 1963) Reinhardt 1967; Young et al. 2017), which would

place the formation in the Early Cretaceous. SEM photographs exhibit nannoconids that also indicate Early Cretaceous ages.

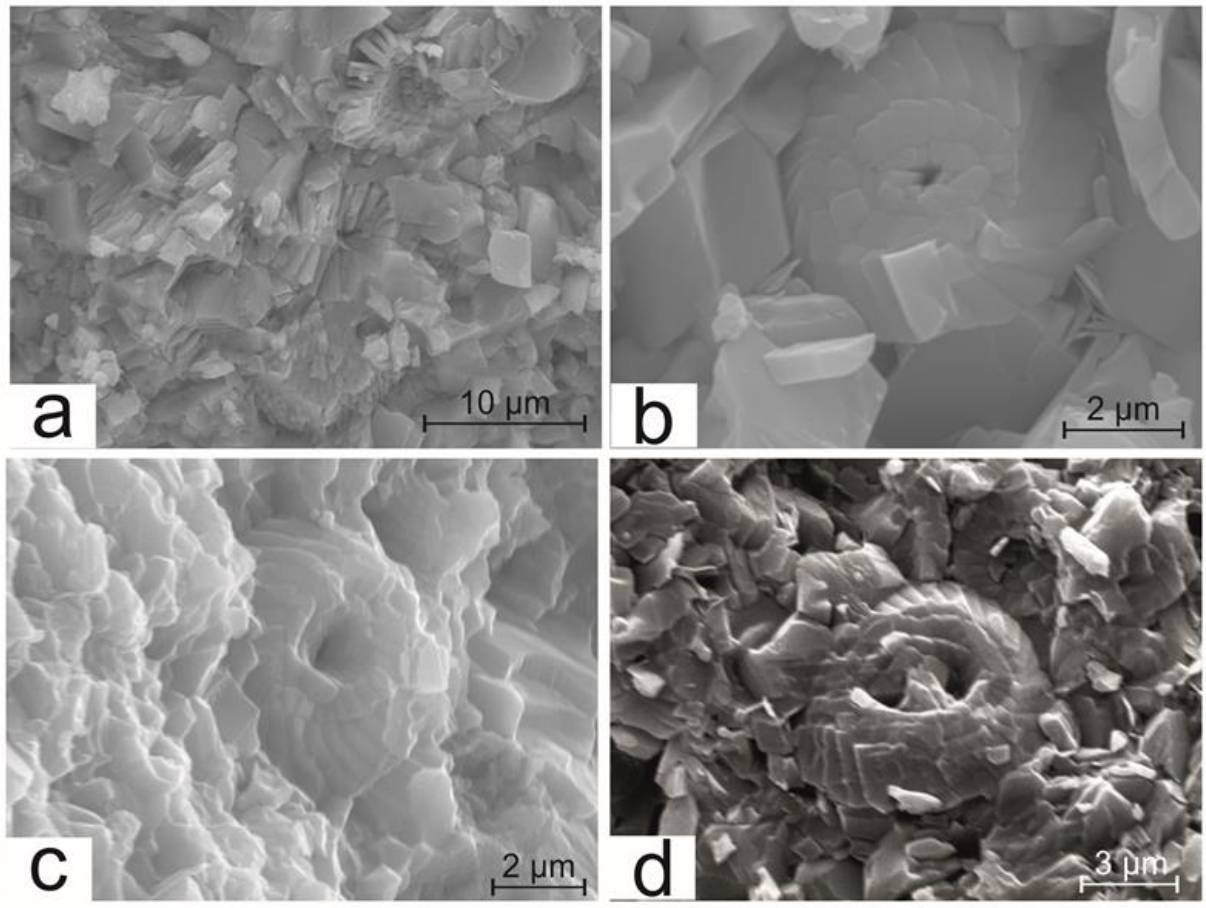

Figure 5.6 Microfossils in Morro Formation limestones: **a**: Remnants of *Nannoconus sp.* **b**: *Watznaueria fossacincta* (BLACK, 1971) BOWN *in* BOWN & COOPER, 1989. **c**: *Cylcagelosphaera cf. argoensis* BOWN 1992. **d**: *Watznaueria britannica* (STRADNER, 1963) REINHARDT, 1964.

5.3.3 Carqueijo Formation

The Carqueijo Formation concordantly overlays the Morro Formation and crops out at Rib. da Baia (E), Rib. do Morro (W), at the southern and eastern flanks of Mte. Branco, north of Mte. Carqueijo, north of Mte. Forte, NE and E of Lomba da Vigia, and at the SW flank of Lombo Vermelho (**Fig. 5.1c, Table 5.1**). This formation is characterized by limestone beds (cm-thick), alternating with softer marls and shaley and/or marly limestones (**Fig. 5.7a, b**). The sequence is characterized by a coarsening upward trend in connection with increasing amounts of siliciclastic sand. In the Mte. Branco area, the rocks are recrystallized. In many places (e.g., in the river valleys), the rocks of the Carqueijo Formation show bright purple-red and green colours, characteristic for hydrothermal alteration. Generally, bedding surfaces of the Carqueijo Formation are partly red, also in places that do not show intensive hydrothermal alteration. Dyke intrusions are abundant in many places (e.g., Rib. da Baia, Lombo Vermelho, N of Lomba da Vigia).

In contrast to the Morro Formation rocks, the lower part of the Carqueijo Formation contains cherts as elongated bands instead of round or lenticular inclusions, which are usually 2-3 cm thick (locally up to 10 cm). These decrease upward in the formation. A few meters above the transition from Morro to the Carqueijo Formation, red ellipsoidal nodules up to 10 cm in diameter occur (e.g., N of Mte. Carqueijo, N of Rib. da Baia, Rib. do Morro profile; **Fig. 5.7a, b; Table 5.1**). These nodules mainly consist of pyrite in the centre and iron oxides in both the centre and the rims, and can be either massive and compact, or porous and friable. Stahlecker (1934) first described similar objects in the uppermost 20 m of his profile, which he called “Brauneisensteine” (iron stones). Similar nodules

have been described from English Cretaceous cherts (e.g., Jeans et al. 2016). They probably formed close to the surface before compaction, during microbial decay of organic matter and slow sedimentation, during reworking of underlying sediments, or, however, less likely under covering of iron-rich sediments with organic-rich anoxic sediments (e.g., black shales; Schieber 2011 and references therein).

The Carqueijo Formation dips in average of 50° towards the NE between Mte. Carqueijo and Lombo Vermelho, where it reaches a thickness of ~300 m. At Rib. do Morro, it exhibits the same average dip towards the WSW and reaches a thickness of about 467 m, although the intermediate part of the profile is covered by Holocene sediments. In the lower part of the profile at Rib. do Morro, some folds can be observed in the units of the Carqueijo Formation, with fold axes dipping to the SE.

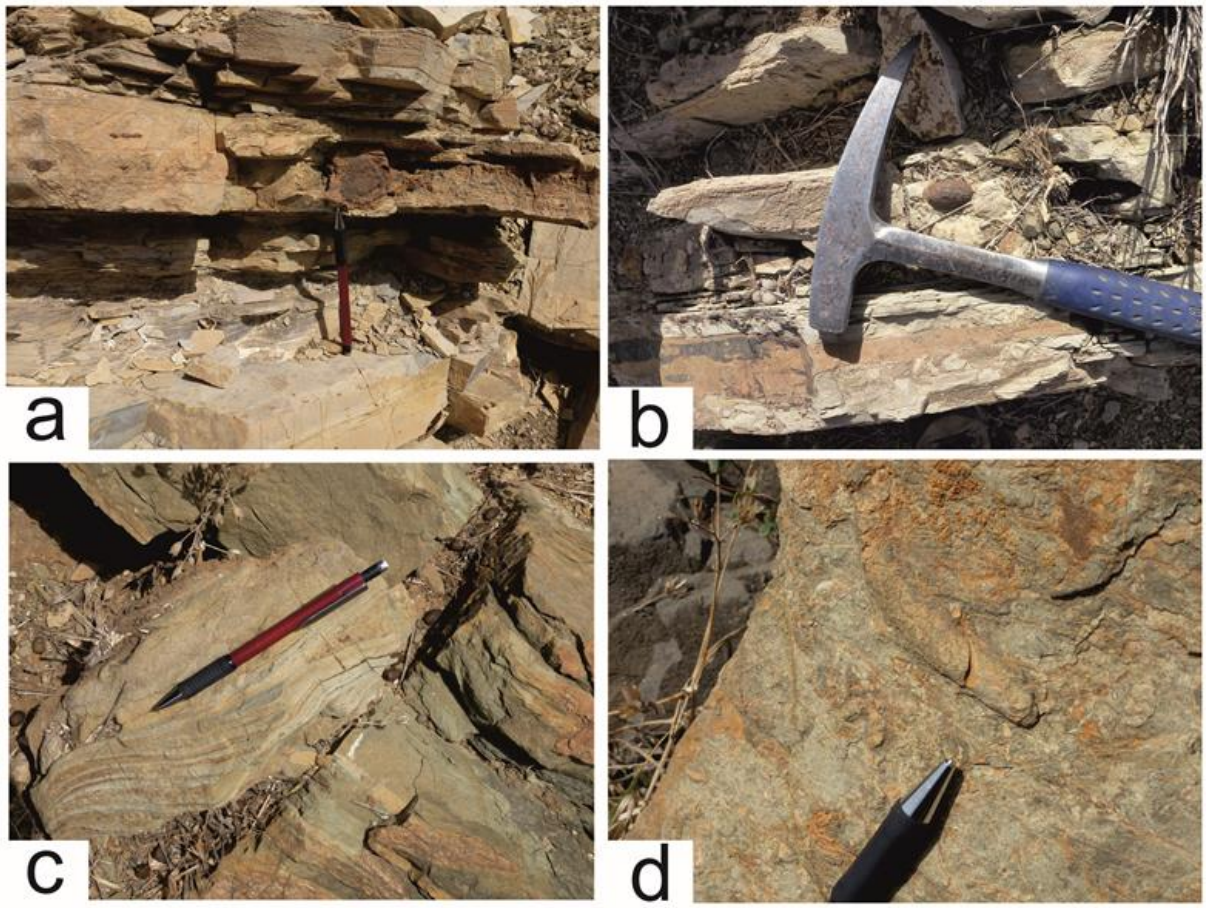

Figure 5.7 Marls and lime-mudstones of Carqueijo Formation, including iron-sulfide concretions (**a, b**); and images of Coruja Formation sandstones, incl. burrows (**c, d**).

Biostratigraphy of the Carqueijo Formation

Macrofossils are rare in rocks of the Carqueijo Formation. Similar to the rocks of the Morro Formation, calcite filled radiolarian molds can be found in thin section. Three samples of Carqueijo Formation rocks yield well preserved nannofossils (**Fig. 5.8**).

One sample (18-69/1), collected just above the base of the Carqueijo Formation in the Rib. do Morro, yields *Watznaueria* cf. *britannica* (Stradner, 1963) Reinhardt 1964, *Cyclagelospahera* cf. *argoensis* Bown 1992, *Prediscosphaera* cf. *cretacea* (Arkhangelsky 1912) Gartner 1968, and *Zeugarhabdotus* cf. *diplogrammus* (Deflandre *in* Deflandre & Fert, 1954) Burnett *in* Gale et al. 1996 (Young et al. 2017). In addition, this sample yields *Watznaueria* cf. *ovata* Bukry 1969, *Watznaueria fossacincta* (Black, 1971) Bown *in* Bown & Cooper, 1989, *Watznaueria* cf. *manivitae* Bukry 1973, which are not useful for high resolution biostratigraphy (Middle Jurassic to Late Cretaceous; **Fig. 5.9**).

Additionally two samples NE of Lomba da Vigia (E of the transmission mast) contain *Cyclagelospahera* cf. *argoensis* BOWN 1992 (Young et al. 2017).

Rigassi (1972) described (planktonic and benthonic) foraminifera *Hedbergella, Reophax* sp., *Trochammina* sp., and *Micula staurophora* GARDET 1955 ENE of Mte Branco/Lomba da Vigia, and *Rhizammina* sp., *Rotalipora* sp., and *Colomiella* BONET 1956 for the Rib. do Morro profile. Based on these findings, Rigassi (1972) suggested an Albian to Senonian-Turonian age for the eastern part of the formation, and an Albian to Cenomanian age for the western part of the formation (see also Robertson 1984). However, these results should be treated with caution. *Reophax* and *Trochammina* cannot be used for precise stratigraphic allocations. Based on nannofossils (*Watznaueria barnesiae* (BLACK *in* BLACK & BARNES 1959) PERCH-NIELSEN 1968, *Cretarhabdus crenulatus* BRAMLETTE & MARTINI, 1964 (now *Retecapsa crenulata* (BRAMLETTE & MARTINI 1964) GRÜN in GRÜN & ALLEMANN 1975; Young et al. 2017), *Braarudosphaera africana* STRADNER 1961) and radiolaria (*Archaeodictyomitra vulgaris* PESSAGNO 1977, *Thanarla veneta* SQUINABOL 1903) found at Rib. do Morro, Fourcade et al. (1990) suggested an Albian age for the Carqueijo Formation. In addition, Fourcade et al. (1990) suggested that the Aptian is very condensed or even absent, and that a hiatus therefore separates the Morro Formation from Carqueijo Formation at Rib. do Morro. However, an erosional hiatus cannot be observed at Rib. do Morro, and the biostratigraphic results are inconclusive. The question if a hiatus separates the Morro Formation from the Carqueijo Formation therefore remains unanswered. Albian ages are likely, Aptian and early Cenomanian ages are also possible for the Carqueijo Formation. Fourcade et al. (1990) also mentions findings of *Praeconocaryomma parvimamma* PESSAGNO and POISSON 1981for the Carqueijo Formation, but this species is limited to the Early Jurassic and therefore is in doubt (Fossilworks.org).

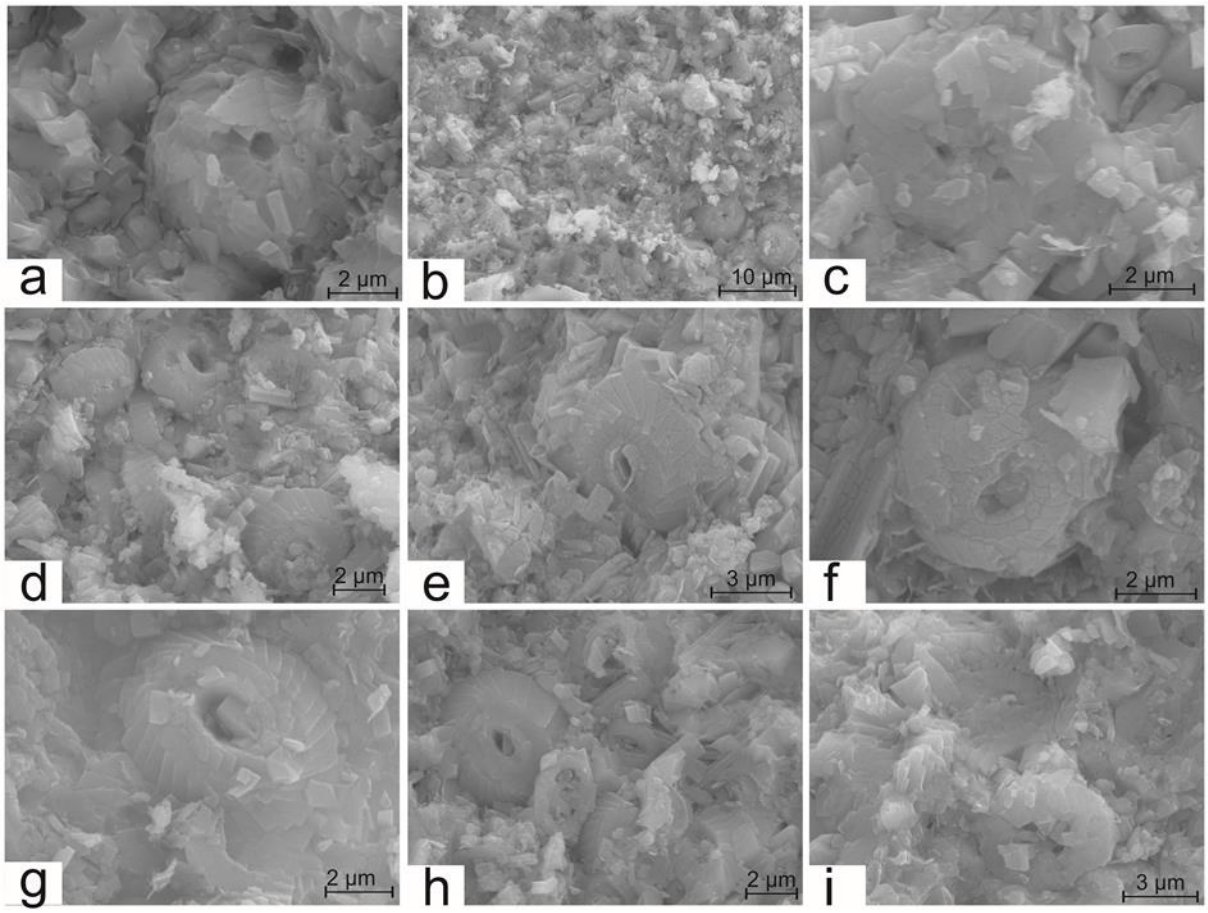

Figure 5.8 Microfossils of Carqueijo Formation. **a**: *Cyclagelosphaera* cf. *argoensis* BOWN 1992 (Lomba da Vigia). **b**: *Watznaueria britannica* (STRADNER 1963) Reinhardt 1964 (enlarged in **c**). **d**: *Watznaueria* cf. *britannica* (STRADNER 1963) REINHARDT 1964 and *Watznaueria fossacincta* (BLACK 1971) Bown *in* Bown & COOPER 1989. **f**: *Watznaueria* cf. *ovata* BUKRY 1969. **e, g**: *Watznaueria fossacincta* (BLACK 1971) BOWN *in* BOWN & COOPER 1989. **h**: *Watznaueria fossacincta* (BLACK 1971) BOWN *in* BOWN & COOPER, 1989 and *Zeugrhabdotus* cf. *diplogrammus* (DEFLANDRE *in* DEFLANDRE & FERT 1954) BURNETT *in* GALE et al. 1996. **i**: *Prediscosphaera* cf. *cretacea* (ARKHANGELSKY 1912) GARTNER 1968.

5.3.4 Coruja Formation

The rocks of the Coruja Formation have been mapped S of Mte. Penoso, extensively W of Mte. Penoso, at the base of Mte. Verinelho (Stillman et al. 1982), and has additionally been described from Rib. da Baia (Robertson 1984). However, the only outcrops we are confident to refer to as Coruja Formation rocks crop out at Mte. Coruja (S of Mte. Penoso), and at the NW flank of Lombo Vermelho (**Tablel 5.1**). The Coruja Formation is characterized by sandstones, strongly altered volcaniclastic rocks, and conglomerates that incorporate different igneous clasts up to a decimetre in diameter. The depositional layers are well to moderately sorted, and locally dominated by well-rounded clasts (**Fig. 5.7c, d**). The clasts show igneous textures, probably representing a mixture of fragmented and rounded rocks, of both volcanic and shallow plutonic origin (i.e. comparatively finegrained crystalline rocks). The clasts are heavily altered, but abundant clasts comprise characteristic pseudomorphs after olivine and clinopyroxene, now typically including fine-grained aggregates of e.g., chlorite and calcite, thus testifying to mafic rock compositions. We interpret the conspicuous layering and areal extent of the deposits to represent erosional products from a regional topographic high. The simplest interpretation would be to assign these deposits to erosion of a local seamount or island structure. Bioturbation and trace fossils can be observed in sandstones, as well as cross-lamination and ripple structures. The analysed sandstones do not contain any fossils, therefore an age assignment is difficult. Robertson (1984) reported rare planktonic foraminifera and suggested a Paleocene-Miocene age for the Coruja Formation. Stillman et al. (1982) suggested Turonian/Senonian ages for the Coruja Formation, but this was based on two tuff layers mentioned by Rigassi (1972, Rigassi) and Rigassi (1975) for the Rib. do Morro section, where the Coruja Formation is absent. Further investigations are necessary to map outcrop locations and extent, and to date the samples of this unit in more detail.

5.4 Discussion

5.4.1 Formation age of the Maio sedimentary basement rocks

The age of the sedimentary basement on Maio has been much debated. Stillman et al. (1982), Robertson and Bernoulli (1982) and Robertson (1984) argued for Jurassic ages for the formation of the seafloor and the oldest sedimentary rocks of Batalha Formation and the overlying lower Morro Formation, solely based on biostratigraphic descriptions from an unpublished report (Rigassi 1972) and a conference abstract (Rigassi 1975). While Fourcade et al. (1990) and Azéma et al. (1990), on the other hand, argued for an early Valanginian and therefore Early Cretaceous age for the upper part of the Batalha Formation (see also sections 5.3.1 and 5.3.2).

The location of Maio between Chrons M11(~136 Ma) in the West and M16 in the East (~141 Ma; Gradstein 2012), suggests that the entire sea floor below the island formed during the Valanginian and not already during the Jurassic. Considering both these magnetic lines and the biostratigraphic observations (our own and the ones in the literature, summarized in **Fig. 5.9**), the oldest rocks on Maio (Batalha Formation.) must be placed in the Early Cretaceous and not already in the Jurassic, as the sedimentary rocks were deposited on an oceanic magmatic basement of Early Cretaceous age. We can therefore confirm the conclusions of Fourcade et al. (1990).

Based on our biostratigraphic observations of Early Cretaceous nannoconids, calpionellids and nannofossils, the overlying pelagic limestones of the Morro Formation can be placed in the Late Valanginian-Barremian to early Aptian (**Fig. 5.9**). Previous authors (e.g., Serralheiro 1970; Robertson 1984) suggested age differences between eastern and western units of Morro and Carqueijo Formations. However, tectonic and igneous overprinting of the different locations due to the intrusion of the Miocene Central Igneous Complex (e.g., recrystallization of carbonates and faulting at Mte. Branco), hamper such an interpretation.

The Carqueijo Formation can be interpreted as the uppermost unit of the sedimentary part of the Maio Basement Complex. Fourcade et al. (1990) suggested an Albian age for this unit and proposed a hiatus between underlying Morro Formation (ending in the Barremian), with the Aptian being very condensed or even absent (**Fig. 5.9**). However, we cannot confirm such a hiatus. Based on stratigraphic observations, we suggest Aptian to early Cenomanian ages for the Carqueijo Formation (**Fig. 5.9**).

The Coruja Formation contains volcaniclastic rocks and conglomerates that are composed of igneous clasts that we interpret as erosional products from a regional topographic high such as a local seamount structure or even an emerging island. Based on sedimentological analyses, Robertson (1984) suggested a depositional depth of up to several hundred metres only, in line with our observations. This opens up for the possibility of extensive igneous activity and concomitant uplift already during the Paleocene. Volcanic ashes have been reported from the nearby DSDP Site 368, where they occur in discrete beds of Late Miocene age (Gardner et al. 1978). Older ashes have not been found at nearby drilling sites. In comparison, subaerial volcanic activity on the neighbouring islands of Boa Vista and Sal has been suggested to be younger than 17 Ma (Boa Vista; Ancochea et al. 2012) and 26 Ma (Sal; Torres et al. 2002), respectively. Considering that biostratigraphic observations of planktonic foraminifera also suggest Paleocene to Miocene ages (Robertson 1984), the Coruja Formation should be excluded from the Maio basement complex. However, further investigations are necessary to map outcrop locations and analyse the samples of this unit in more detail, in order to date this unit.

5.4.2 Black shales and turbidites in the Maio Basement Complex

Robertson (1984) mentions black shales that are now bleached due to prolonged oxidation as part of the Carqueijo Formation (still black in coastal outcrops), which are similar to the black shales found at DSDP sites 367 and 368 (Lancelot et al. 1978a, 1978b).

From the Aptian onwards, several global oceanic anoxic events (OAE) have been reported, characterized by high productivity, changes in water ventilation by circulation pattern changes, stratified water columns, and high sea surface temperatures (Leckie et al. 2002). These OAEs could be controlled by orbital variations (Leckie et al. 2002, Li et al. 2008). Along the W-African margin, IODP data suggests that black shales reach to the west of the Cabo Verde archipelago, but are restricted to a sea floor that is older than Turonian, whereas towards the present equator, they were deposited for another 10 Ma (Jones et al. 2007). Black shales have been reported east of the Cabo Verde Archipelago at DSDP Site 367 (Albian-Cenomanian, Unit 4a) and Site 368 (Cenomanian-Santonian, Unit 3; Lancelot et al. 1978a, 1978b). However, the distribution of black shales in the vicinity of the Cabo Verde islands is unclear (Jones et al. 2007). Two major global events, the OAE1 (Aptian-Albian), and OAE2 across the Cenomanian to Turonian transition (93.5 Ma) have been reported for the Late Cretaceous (Schlanger and Jenkyns 1976). OAE1 has been further divided into OAE1a (global event, 120.5 Ma, early Aptian), OAE1b (113-109 Ma; multiple discrete black shales across parts of the Tethys ocean, focused on Mexico and the North Atlantic); and OAE1d (99.5 Ma, late Albian, widespread in eastern and western Tethys; Leckie et al. 2002). At DSDP Sites 367, both OAE1 and OAE2 could be present, whereas at Site 368, the age of the black shales fits only with OAE2. The Carqueijo Formation could especially include OAE1 deposits. However, we did not identify any such deposits.

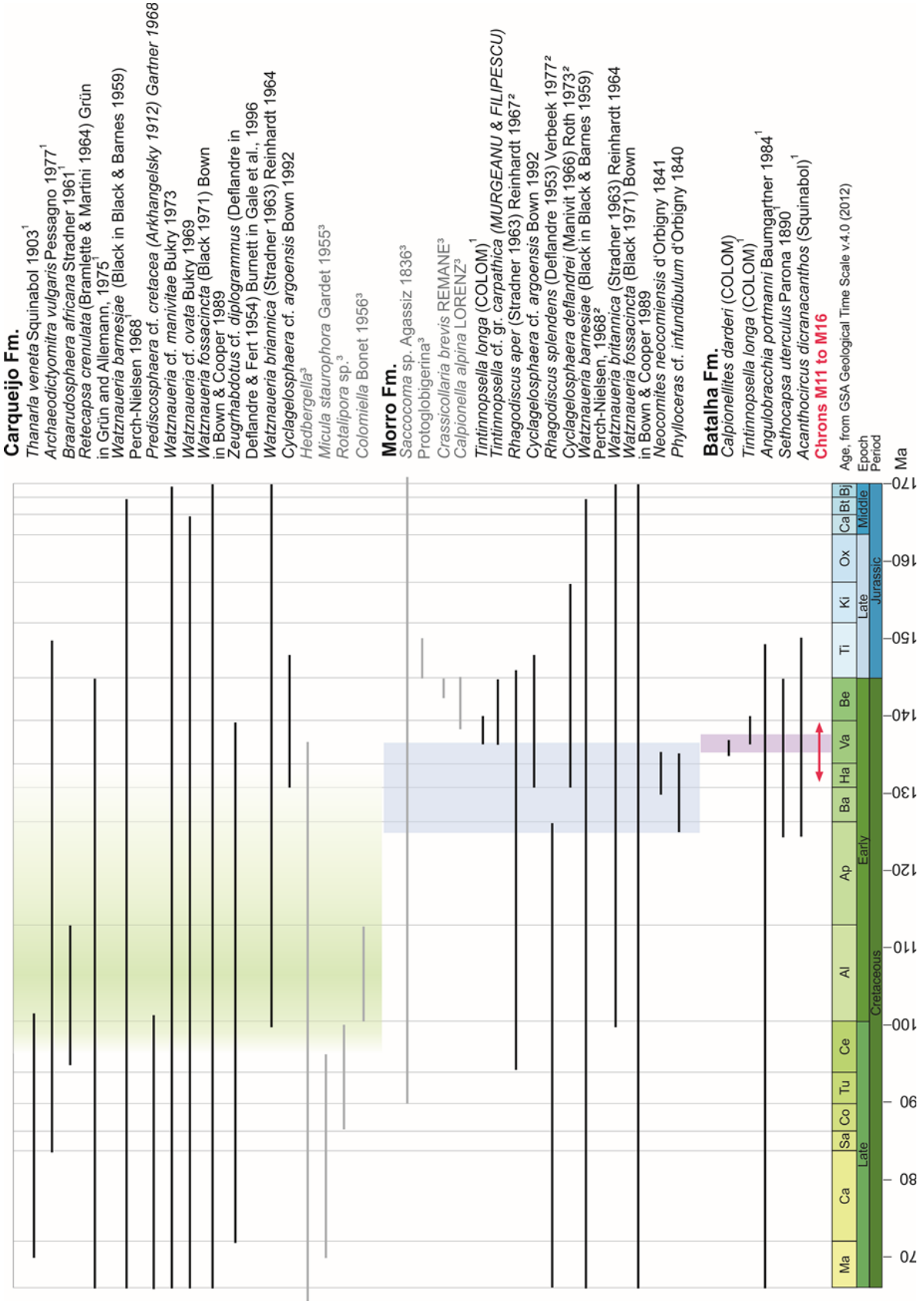

Figure 5.9 Compilation of the biostratigraphy (radiolarian, nannofossils, ammonites) of the sedimentary successions of the Maio Basement Complex, including findings of [1]: Fourcade et al. (1990) and [2]: Robertson (1984), and [3]: Rigassi (1972) (in gray, as these finding were not verified). Species that have a broader range of occurrence than shown are excluded, as they have no stratigraphic value. Age ranges after Sanfilippo and Riedel (1985) (Acanthocircus dicranacranthus); Grün and Blau (1997) (Calpionellids); Young et al. (2017) (nannofossils) and Fossilworks.org (all others), annotated on a GSA Geological time scale v.4.0 (2012) redrawn after Young et al. (2017).

Black shales fill topographic depressions within/adjacent to upwelling zones and sometimes can be preserved by rapid burial by turbidites, as evidenced by turbidite layers in black shales of DSDP 367 (Lancelot et al. 1978a, Gardner et al. 1978, Jones et al. 2007). Turbidites have been reported by Robertson (1984) for the sediments entrapped in the upper part of the Batalha Formation, which he interpreted originating from the West-African margin, and silt-turbidites for the Carqueijo Formation interpreted to be transported from W-Africa, or a topographic high close-by.

Paleogeographic and Paleo-oceanographic studies show that during the entire Cretaceous, the shelf edge of West-Africa was located further west than today, while the shore line was located further east than today due to higher sea levels (e.g., Miller 2009 and references therein, Mourlot et al. 2018). Maio island was therefore located about 800 km (Berriasian-Aptian) to 700 km (Turonian-Maastrichtian) from the shelf edge, and 1000 km (Berriasian-Aptian) to 1200 km (Turonian Maastrichtian) from the shore line (Mourlot et al. 2018). During the Early Cretaceous, deep-sea fan deposits and turbidites accumulated along the slope of West Africa, mostly off today's Senegal. Redeposition by bottom currents at paleo water depths >4000 m occurred in the distal part of the basin (Mourlot et al. 2018). During the Albian to Cenomanian, rivers and deltas transported large amounts of sediments from the African continent and drained into the basin. These were deposited as turbidites, other deep-sea fan deposits and stacked channel-levee complexes off Senegal (Jansa et al. 1978, Mourlot et al. 2018). Additionally, bottom current activity caused contourite drifts and migration of sediment waves along the base of the continental slope (Mourlot et al. 2018). So-called extrabasinal turbidites related to deltas and submarine fans, and especially hyperpycnal flows originating from river discharge can travel considerable distances of several hundred kilometres and transport land-derived material, including plant debris (Zavala and Arcuri 2016) and could have therefore affected sediments on Maio, especially in the Carqueijo Formation. During the Late Cretaceous, a transgression and a change in the circulation pattern during the early Turonian (94 Ma) caused mass transport complexes and an increasing number of sediment waves in the abyssal plain of the Senegal Basin, as well as contourite drifts off Mauretania, suggesting bottom water current activity not related to turbidites off Senegal (Mourlot et al. 2018). Generally, Mourlot et al. (2018) suggest an active deep oceanic circulation since the Early Cretaceous, and a well ventilated Central Atlantic Ocean, which is inconsistent with the hypothesis of stagnant conditions forming OAEs, and which could explain the absence of black shales on Maio. However, there is further evidence that intermediate and deep waters of the proto-North Atlantic were changing periodically during the Mid-Cretaceous between well-oxygenated and euxinic states due to biogeochemical processes (Wallmann et al. 2019). The sea floor in the Senegal Basin became successively shallower during the Cretaceous, ranging from up to 5700 m in the Early Berriasian, up to 5050 m in the Late Cretaceous (Mourlot et al. 2018).

The absence of black shales may also be explained by shallowing at the beginning of the development of the Cape Verde Rise. However, seismic and geomorphological studies suggests that the swell took 5 to 25 Myrs to develop, and that it began to form at 17 to 26 Ma (Ramalho et al. 2010a) during a single uplift event (Ali et al. 2003). Based on these studies, a Cretaceous uplift of the Maio Basement cannot be inferred, and therefore cannot explain the more continental influence or the lower carbonate content of Carqueijo Formation sediments.

5.4.3 Why are the early sediments at Maio important?

The sedimentary rocks of the Basement Complex on Maio have been attributed to the Maiolica Facies, which also occurs in the Central Atlantic, Cuba, Caribbean and Alpine-Mediterranean Tethys, and is also called Blake-Bahama Formation and White Limestone Unit (**Fig. 5.10**; e.g., Bernoulli 1972, Bernoulli and Jenkyns 1974, Jansa et al. 1978, 1979, Robertson and Bliefnick 1983, Robertson 1984, Wieczorek 1988, Fourcade et al. 1990, and references therein). The Maiolica facies was deposited over a period of 30 Ma and with the widest facies distribution in the Atlantic-Alpine Tethys and some of the branches of Neotethys to Oman and possibly beyond.

The Maiolica facies has been described from several DSDP sites (**Fig. 5.10**), e.g., site 367 in the Cape Verde Basin (Lancelot et al. 1978a), and sites 4 , 5, 99, 100, 101, 105, 387, 391, 534, and 603 (Caribbean and Atlantic Ocean W and NW of Cabo Verde, e.g. Cat Gap (site 4 ; Site 4: >60 m; Ewing et al. 1969a; and site 5, Ewing et al. 1969b; site 99A, Bernoulli 1972, Hollister et al. 1972c; and site 100,

Bernoulli 1972, Hollister et al. 1972a), the Hatterras Abyssal Plain (site 105, Hollister et al. 1972b), the Hatterras Outer Ridge (site 603, van Hinte et al. 1987, Ogg et al. 1987), the Bermuda Rise (site 387, Tucholke and Vogt 1979, Tucholke et al. 1979), and the Blake-Bahama Basin (site 391, Benson et al. 1978, Bourbon 1978, Robertson and Bliefnick 1983; and site 534 Sheridan et al. 1983, Robertson and Bliefnick 1983). In the eastern Atlantic, the Maiolica Facies can be found at the Moroccan continental margin (site 547; Hinz et al. 1984, Jansa et al. 1984). Maiolica-type facies has also been reported from the Romanche Fraction Zone to the South of Cabo Verde (Gasperini et al. 2001), and from Gorringe Bank towards the North (Conti et al. 2004).

The Maiolica facies varies in thickness across the Atlantic, ranging from 9 to 181 m in the Cat Gap area (sites 4, 5, 99A, 100; Ewing et al. 1969a, 1969b, Bernoulli 1972, Hollister et al. 1972c), 156 m at the Hatteras Abyssal Plain (site 105; Hollister et al. 1972b), 362 m at the Hatteras Outer Ridge (site 603, van Hinte et al. 1987, Ogg et al. 1987), >199-208 m at the Bermuda Rise; (site 387, Tucholke and Vogt 1979, Tucholke et al. 1979), 323 to 392 m in the Blake-Bahama Basin (sites 391 and 534, Benson et al. 1978, Bourbon 1978, Sheridan et al. 1983, Robertson and Bliefnick 1983), and 66 m at the Moroccan continental margin (site 547, Hinz et al. 1984, Jansa et al. 1984). At site 367 in the Cape Verde Basin, the Maiolica facies limestones reach a thickness of ~198 m (Lancelot et al. 1978a). The thicknesses of 200-380 m for the Morro Formation are within the range of mapped thicknesses of Maiolica facies across the Atlantic. We suggest larger thicknesses up to 500 m for the Mte. Esgrovere profile, but cannot exclude the existence of faults and therefore repetition of facies. This is commonly observed on Maio and, together with dyke intrusions, therefore hampers a precise determination of thickness.

The separation of the American and African continental plates began during the Early Jurassic and evolved at different spreading rates (Labails et al. 2010). The Morro Formation on Maio is part of this history of the opening of the Atlantic Ocean, as it was deposited directly on the oceanic crust forming at that time.

5.5 Conclusion

New and revised biostratigraphic data for the early sedimentary successions on Maio suggest Early Cretaceous ages for the Maio Basement Complex.

We present findings of Valanginian to early Hauterivian ammonites from a new location – Mte. Esgrovere – and therefore can confirm findings of ammonites by Stahlecker (1934) in Rib. do Morro. In addition, our findings of calpionellids in samples from the Batalha and Morro Formations, and additional nannofossils from Morro and Carqueijo Formation samples complement and refine previous biostratigraphic descriptions from Maio and strongly point towards Early Cretaceous ages for these units. Jurassic ages for the MORB-type pillow lavas and the overlying sediments of the Batalha and Morro Formations are therefore unlikely, especially in the light of Cretaceous ages for the underlying ocean floor. The volcaniclastic-dominated Coruja Formation is most probably of Paleocene to Miocene age, and may reflect the first emergence of Maio Island.

In addition, the sedimentary units of Maio give insights into the paleo-oceanography of the Early Atlantic Ocean. The absence of observations of black shales on Maio, contrary to Cretaceous units from DSDP sites in the Cape Verde Basin, Cape Verde Rise, and the Central Atlantic (e.g., sites 367 and 368, Lancelot et al. 1978a, 1978b; site 105 Hollister et al. 1972b; and site 387, Tucholke et al. 1979) suggest that active ventilation and circulation by bottom currents affected the Cabo Verde area during that period of time. Turbidites from the continental shelf of West Africa may have affected the Maio sedimentary units, especially during the Albian-Cenomanian, when rivers and deltas transported a high amount of sediment from the African continent and drained into the Senegal basin. The Morro Formation is part of the Maiolica facies, which formed across large parts of the Caribbean, Central Atlantic and Alpine-Mediterranean regions of the Western Tethys. It formed, while the central Western Tethys was rifting to form the Atlantic Ocean and while the Alpine-Mediterranean area already experienced closing.

Figure 5.10 Overview of known locations of the Maiolica facies (blue). DSDP drill sites are marked in red.

Acknowledgements

The authors would like to thank Daniel Bernoulli for his most valuable support, for comments and discussions on an early version of this manuscript, and for surrendering us literature and unpublished material. Alistair Robertson is thanked for providing literature that was not publicly available. We would like to thank Sascha Flögel for comments on the manuscript. Birgit Mohr from the Institute of Geosciences at University Kiel, and Christin Szillus from the Institute of Material Sciences at University Kiel are thanked for assistance with SEM imaging. We would also like to thank Thorsten Lux and Sophia Stavrakoudis for help in the labs. We are grateful for the hospitality and help we received from Dominique Gautherot on Maio. LKS would like to acknowledge financial support from the Helmholtz Research School for Ocean System Science and Technology (HOSST).

6 Conclusions and Outlook

This thesis combines observations from both submarine and subaerial study locations, and constrains both early and late phases of the temporal and magmatic-tectonic evolution of the Cabo Verde Archipelago.

The thesis provides the first ^{40}Ar-^{39}Ar ages for Cabo Verde seamounts. Both the Miocene part (Nova Holanda (Senghor) Seamount) as well as the younger part of the archipelago (Cadamosto Seamount) were investigated. The geochronology presented in this thesis, as well as the field observations from the different study locations, in combination with the known Cabo Verde geology, support a model of age progression in the archipelago of the two island chains from the NE (old) to the SW: Nova Holanda (Senghor) Seamount located in the NE with a weighted mean ^{40}Ar-^{39}Ar of 14.872 ± 0.027 Ma (2σ) was in a late evolutionary stage, while Maio Island in the E was as in its main growth phase (~16 and 8.7 M). The Pleistocene ages from Cadamosto Seamount, and recent seismic activity indicating present day magmatic activity from the islands of Fogo, Brava, and Santo Antão, and offshore on the Nola, Sodade, and Cadamosto seamounts (Grevemeyer et al. 2010, Faria and Fonseca 2014) support an overall age progression of the two Cabo Verde island and seamount chains from the NE to SW. The thesis therefore also contributes to a better understanding of seamount and ocean island evolution worldwide.

The weighted mean ^{40}Ar-^{39}Ar age of 14.872 ± 0.027 Ma (2σ) from sanidines and phlogopites from a Nova Holanda (Senghor) Seamount pillow lava sample is the oldest age for a seamount in the Cabo Verde Archipelago. It overlaps with ^{40}Ar-^{39}Ar and K-Ar ages obtained from the nearby islands of Sal and Maio. In particular, it overlaps with the main period of growth and enhanced igneous activity on Maio between ~16 and 8.7 Ma.

At Cadamosto Seamount, the extensive data set with 170 ^{40}Ar-^{39}Ar ages of sanidine, nepheline and sodalite minerals from phonolitic lavas allows to unravel timescales of magmatic processes at this seamount located in the SW of the archipelago. In combination with the petrological analyses of lava samples, changes in the magmatic plumbing system can be determined, such as replenishment, magma mixing and convection processes.

Phenocrystic sanidines from three out of five samples yield eruption ages of 20.98 ± 0.87 ka, 21.44 ± 0.8 0ka and 22.3 ± 2.0 ka, and a combined eruption age of 21.14 ± 0.62 ka. This youngest eruption episode coincides with the Last Glacial Maximum, suggesting enhanced eruptive activity due to pressure changes within the magma plumbing system caused by rapid sea level changes. This is interpreted as a coupling between global relative sea level changes and submarine eruptive activity.

Two other Cadamosto lava samples contain sanidines with resorbed antecrystic cores with phenocrystic overgrowth rims, yielding older maximum eruption ages of 51.8 ± 2.4 ka and 97 ± 14 ka, respectively. The zonation patterns of Ba and Fe in the minerals suggest replenishment with more mafic magma and/or convection and mixing within the magma prior to eruption. A long lived magma-plumbing system below Cadamosto Seamount is suggested based on sanidine and nepheline minimum antecryst ages up to at least 1.5215±0.0083Ma. Such a seamount lifetime of at least 1.5 Ma is comparable to, but on the low side of, those of the subaerial volcanoes.

The detailed study of the magmatic and temporal evolution of Cadamosto Seamounts provides important insights to the growth and evolution of a seamount, and therefore it contributes to the general understanding of seamount evolution.

The results of the complementary studies from Maio Island provide further insights in the evolution of a mature ocean island and therefore add to our understanding of the growth and decay processes that act on ocean islands. In addition, the different studies contribute to our knowledge on geological hazards such as landslides and flank collapse events.

The thesis introduces a refined model for the Miocene evolution of Maio Island. It helps to identify different stages during the evolution and erosion of the edifice: Intrusive magmatic growth on Maio Island started during the Early Miocene with the emplacement of shallow plutons. Several phases of dyke intrusions, associated with effusive activity and the emplacement of an igneous core

complex in the middle to upper crust, led to rapid growth of the island in the Middle Miocene. This main shield building phase was associated with magmatic flare-up and simultaneous uplift, which is recorded in dyke orientations. This rapid growth resulted in the tectonic deformation and disruption of the Mesozoic marine sedimentary strata (circular-dipping units, Monte Branco Thrust). The ^{40}Ar-^{39}Ar phlogopite ages of nosean nephelinite dykes cutting the Valanginian Batalha Formation (10.405 ± 0.033 Ma and 10.570 ± 0.053 Ma) and the Morro Formation (9.273 ± 0.020 Ma), respectively, confirm a main growth period between ~16 and 8.7 Ma.

The discovery of a series of polymict conglomerates below the youngest volcanic deposits on Maio Island fills a major gap in the evolution of the island. These conglomerates are located below the Late Miocene Monte Penoso Formation and are interwoven with local pyroclastic units. These conglomerates have not been described previously and are interpreted as flank collapse deposits of the Pedro Vaz Formation. A phlogopite ^{40}Ar–^{39}Ar age of 8.666 ± 0.0274 Ma (2σ) from a nephelinite lava clast represents a maximum age for the landslides. The main shield building stage on Maio was therefore followed by a period of rapid erosion in the Tortonian/ Messinian (8.7–6.7 Ma). The presence of pyroclastic units inbetween the conglomerates additionally suggests a phase of low but partly explosive volcanic activity. The erosive period was possibly triggered by tectonic activity (potentially associated to the Monte Branco Thrust). Flank collapses and mass wasting could have caused pressure changes in the upper mantle, that may have induced the rejuvenated volcanic activity of the Malhada Pedra and Monte Penoso Formations.

One of the geologically youngest sequences on Maio Island is a Quaternary fossil dune located in the East of the island. It is composed of carbonaceous standstones and arenites. The lower and upper part of this aeolian deposit show different cross-stratification patterns, which were produced due to changes in paleo-wind directions. The study of the dune adds to the understanding how the paleo-environmental conditions are recorded in such sedimentary deposits. It is also a good marker for uplift at a late stage of island evolution.

This thesis complements on our basic understanding on how the Early Atlantic Ocean developed. Pre-volcanic sedimentary sequences are exposed above the mid-ocean ridge basalt-type pillow lavas in the center of Maio and are the only place to study the pre-volcanic ocean floor in the Cabo Verde Archipelago. For this thesis, new data on fossil assemblages and high-quality SEM-images of nannofossils from the limestones and marls of the Mesozoic Morro and Carqueijo Formations were acquired and combined with field observations and a revision of the previously described biostratigraphy. Based on the finding of *Calpionellites darderi (*COLOM*)* in sediments intercalated between MORB-type pillow lavas in the uppermost part the Batalha Formation, an Early Cretaceous age is suggested for the Early Atlantic Ocean basement below Maio. The nannofossil assemblage and findings of ammonites *Phylloceras cf. infundibulum* (D'ORBIGNY 1840*)* and *Neocomites neocomiensis (*D'ORBIGNY 1841*)* within the pelagic limestone successions suggest Valanginian to early Aptian ages for the Morro Formation. The Carqueijo Formation is suggested to have an Aptian to Cenomanian age. The Morro Formation is attributed to the widespread Maiolica facies, which is also cropping out in several other regions on both sides of the Central Atlantic Ocean basin and in the Alpine-Mediterranean region, and which recorded paleo-oceanographic conditions of the Early Atlantic Ocean.

In conclusion, this thesis contributed to the basic research on the evolution of oceanic archipelagos in general and the Cabo Verde Archipelago in particular. By taking a regional approach that includes both subaerial (island) and submarine (seamount) investigations, early and late evolutionary stages, and rapid and slow processes, this thesis further contributes to more detailed understanding of the whole archipelago. It also adds to our basic understanding of different evolutionary stages on a mature ocean island, and especially the interplay between growth and destruction of volcanic islands. Nevertheless, there are several aspects which need to be further investigated:

1. The processes regarding coupling between sea level changes and eruptive activity are not fully understood yet. How significant the effects of pressure changes are to the magmatic plumbing systems is especially important to study with regard to the climate change. A combination of modelling and high-quality geochronology are necessary to further

investigate this point.
→ global approach.

2. Understanding the interaction of flank collapses and rejuvenated volcanism and the timescales of these processes are important for hazard mitigation. So far, it is not fully understood how these processes influence each other and therefore should be further investigated.
   → global and regional approach
3. This thesis added a significant contribution to the geochronology of the Cabo Verde Archipelago. However, the seamounts of the northern island and seamount chain remain undated and therefore hamper the interpretation of direction of evolution (E-W or NE-SW-directed plume propagation)?
   → regional approach
4. Additional research is necessary to complement the findings of this thesis from Maio Island. The conglomerates below the Monte Penoso Formation at the southern flanks of Monte Penoso should be further investigated, both with respect to their composition and their distribution. The analysis of conglomerate compositions will reveal insights into petrology and magmatic processes of the early edifice, whereas the distribution of the conglomerate deposit could help to understand the extend of the former edifice and the erosive processes. Additional geochronological data would help to further constrain the erosive phase on Maio Island.
   A systematic study of dyke orientations across the island could help to improve our understanding of the magma plumbing system and the location of former eruptive centres, and also on the temporal evolution of the magma plumbing system and the igneous growth of the island.
   → local approach
5. The geology of the Joao Valente platform, located NE of Maio Island and forming a saddle that connects Maio and Boa Vista, is a key to understand the early evolution of the Cabo Verde Archipelago. Also, it is unknow if this platform is a separate edifice or an extended part of the Maio edifice. However, it remains uninvestigated and therefore neither its age nor its compositions are known. The platform could contain flank collapse deposits from Maio and/or Boa Vista Islands. The investigation of these deposits could help to better constrain the erosive phases on these islands.
   → regional and local approach

7 References

Ali MY, Watts AB, Hill I (2003) A seismic reflection profile study of lithospheric flexure in the vicinity of the Cape Verde Islands. J Geophys Res Solid Earth 108(B5). doi:10.1029/2002JB002155

Allmendinger RW, Cardozo N, Fisher DM (2012) Structural geology algorithms. Vectors and tensors. New York; Cambridge University Press, Cambridge, Melbourne

Ancochea E, Hernán F, Huertas MJ, Brändle JL (2012) A basic radial dike swarm of Boa Vista (Cape Verde Archipelago); its significance in the evolution of the island. J Volcanol Geotherm Res 243-244:24–37. doi:10.1016/j.jvolgeores.2012.06.029

Ancochea E, Huertas MJ, Hernán F, Brändle JL (2010) Volcanic evolution of Sao Vicente, Cape Verde Islands: The Praia Grande landslide. J Volcanol Geotherm Res 198(1-2):143–157. doi:10.1016/j.jvolgeores.2010.08.016

Ancochea E, Huertas MJ, Hernán F, Brändle JL (2014) A new felsic cone-sheet swarm in the Central Atlantic Islands. The cone-sheet swarm of Boa Vista (Cape Verde). J Volcanol Geotherm Res 274:1–15. doi:10.1016/j.jvolgeores.2014.01.010

Ancochea E, Huertas MJ, Hernán F, Brändle JL, Alonso M (2015) Structure, composition and age of the small islands of Santa Luzia, Branco and Raso (Cape Verde Archipelago). J Volcanol Geotherm Res 302:257–272. doi:10.1016/j.jvolgeores.2015.07.015

Annen C, Lénat J-F, Provost A (2001) The long-term growth of volcanic edifices. Numerical modelling of the role of dyke intrusion and lava-flow emplacement. J Volcanol Geotherm Res 105(4):263–289. doi:10.1016/S0377-0273(00)00257-2

Appel P (2017) Lambert. Geocompass App for iPhone/iPad. Christian-Albrechts University Kiel, Kiel, Germany

Azéma J, Fourcade E, Wever P de (1990) Découverte de Valanginien inférieur a Calpionelles à Maio (République du Cap Vert): discussion de l'âge des sédiments associés aux laves de type MORB de ce secteur de l'Atlantique Central. C R Acad Sci Paris Sér IIA 310:277–283

Baksi AK (2007) A quantitative tool for detecting alteration in undisturbed rocks and minerals—I. Water, chemical weathering, and atmospheric argon. In: Foulger GR, Jurdy DM (eds) Plates, Plumes and Planetary Processes. Geol Soc Am Spec Pap, 430:285–303

Barker AK, Hansteen TH, Nilsson D (2019) Unravelling the crustal architecture of Cape Verde from the seamount xenolith record. Minerals 9(90):1–13. doi:10.3390/min9020090

Barker AK, Holm PM, Peate DW, Baker JA (2010) A 5 million year record of compositional variations in mantle sources to magmatism on Santiago, southern Cape Verde archipelago. Contrib Mineral Petrol 160(1):133–154. doi:10.1007/s00410-009-0470-x

Barker AK, Holm PM, Troll VR (2014) The role of eclogite in the mantle heterogeneity at Cape Verde. Contrib Mineral Petrol 168(3). doi:10.1007/s00410-014-1052-0

Barker AK, Rydeblad EM, Silva SMDM (2021) Magma Storage at Ocean Islands. In: Masotta M, Beier C, Mollo S (eds) Crustal magmatic system evolution. Anatomy, architecture, and physico-chemical processes. Wiley-American Geophysical Union, Hoboken, NJ, pp 45–78

Barker AK, Troll VR, Ellam RM, Hansteen TH, Harris C, Stillman CJ, Andersson A (2012) Magmatic evolution of the Cadamosto Seamount, Cape Verde. Beyond the spatial extent of EM1. Contrib Mineral Petrol 163(6):949–965. doi:10.1007/s00410-011-0708-2

Barrer RM, Vaughan DEW (1971) Trapping and diffusion of rare gases in phillipsite, zeolite K—M and other silicates. Trans. Faraday Soc. 67(0):2129–2136. doi:10.1039/TF9716702129

Barrett R, Lebas E, Ramalho R, Klaucke I, Kutterolf S, Klügel A, Lindhorst K, Gross F, Krastel S (2020) Revisiting the tsunamigenic volcanic flank collapse of Fogo Island in the Cape Verdes, offshore West Africa. Geol Soc Lond Spec Publ 500(1):13–26. doi:10.1144/SP500-2019-187

Begét JE, Kienle J (1992) Cyclic formation of debris avalanches at Mount St Augustine volcano. Nature 356(6371):701–704. doi:10.1038/356701a0

Benson WE, Sheridan RE, Enos P, Freeman T, Gradstein FM, Murdmaa IO, Pastouret L, Schmidt RR, Stuermer DH, Weaver FM, Worstell P (1978) Site 391. Blake-Bahama Basin. In: Benson W, Sheridan R (eds) DSDP Initial Reports vol. 44. U.S. Government Printing Office, Washington, USA, 153-336

Bernard B, van Wyk de Vries B, Leyrit H (2009) Distinguishing volcanic debris avalanche deposits from their reworked products. The Perrier sequence (French Massif Central). Bull Volcanol 71(9):1041–1056. doi:10.1007/s00445-009-0285-7

Bernard-Griffiths J, Cantagrel J-M, Matos Alves C, Mendes F, Serralheiro A, Rocha de Macedo J (1975) Données radiométriques potassium-argon sur quelques formations magmatiques des iles de l'archipel du Cap Vert. In: Gauthier-Villards (ed) Comptes rendus hebdomadaires des séances de l'Académie des sciences. Gauthier-Villars, Paris (France), pp 2429–2432

Bernoulli D (1972) North Atlantic and Mediterranean Mesozoic Facies. A Comparison. In: Hollister CD, Ewing JI (eds) DSDP Initial Reports vol. 11. U.S. Government Printing Office, Washington, USA, pp 801–871

Bernoulli D, Hottinger L, Spezzaferri S, Stille P (2007) Miocene shallow-water limestones from São Nicolau (Cabo Verde). Caribbean-type benthic fauna and time constraints for volcanism. Swiss J Geosci 100(2):215–225. doi:10.1007/s00015-007-1224-2

Bernoulli D, Jenkyns HC (1974) Alpine, Mediterranean, and Central Atlantic Mesozoic Facies in Relation to the Early Evolution of the Tethys. In: Dott RH, Shaver RH (eds) Modern and Ancient Geosynclinal Sedimentation. Society for Sedimentary Geology, Tulsa, Okla., U.S.A., pp 129–159

Bernoulli D, Jenkyns HC (2009) Ancient oceans and continental margins of the Alpine-Mediterranean Tethys. Deciphering clues from Mesozoic pelagic sediments and ophiolites. Sedimentology 56(1):149–190. doi:10.1111/j.1365-3091.2008.01017.x

Bird DE, Hall SA, Burke K, Casey JF, Sawyer DS (2007) Early Central Atlantic Ocean seafloor spreading history. Geosphere 3(5):282. doi:10.1130/GES00047.1

Bourbon M (1978) Mesozoic Evolution of Western North Atlantic and North Tethyan Margins. A Comparison. In: Benson W, Sheridan R (eds) DSDP Initial Reports vol. 44. U.S. Government Printing Office, Washington, USA, pp 949–969

Cardozo N, Allmendinger RW (2013) Spherical projections with OSXStereonet. Comput Geosci 51:193–205. doi:10.1016/j.cageo.2012.07.021

Carracedo JC (1999) Growth, structure, instability and collapse of Canarian volcanoes and comparisons with Hawaiian volcanoes. J Volcanol Geotherm Res 94(1-4):1–19. doi:10.1016/S0377-0273(99)00095-5

Carvalho J, Bonadio R, Silveira G, Lebedev S, Mata J, Arroucau P, Meier T, Celli NL (2019) Evidence for high temperature in the upper mantle beneath Cape Verde archipelago from Rayleigh-wave phase-velocity measurements. Tectonophysics 770:228225. doi:10.1016/j.tecto.2019.228225

Cashman KV (1993) Relationship between plagioclase crystallization and cooling rate in basaltic melts. Contrib Mineral Petrol 113(1):126–142. doi:10.1007/BF00320836

Cassata WS, Renne PR (2013) Systematic variations of argon diffusion in feldspars and implications for thermochronometry. Geochim Cosmochim Acta 112:251–287. doi:10.1016/j.gca.2013.02.030

Cassidy M, Trofimovs J, Watt SFL, Palmer MR, Taylor RN, Gernon TM, Talling PJ, Le Friant A (2014) Multi-stage collapse events in the South Soufrière Hills, Montserrat as recorded in marine sediment cores. In: Wadge, Robertson R, Voight B (eds) The Eruption of Soufrière Hills Volcano, Montserrat from 2000 to 2010, vol 39. Geological Society, London, pp 383–397

Cassidy M, Watt SFL, Talling PJ, Palmer MR, Edmonds M, Jutzeler M, Wall-Palmer D, Manga M, Coussens M, Gernon T, Taylor RN, Michalik A, Inglis E, Breitkreuz C, Le Friant A, Ishizuka O, Boudon G, McCanta MC, Adachi T, Hornbach MJ, Colas SL, Endo D, Fujinawa A, Kataoka KS, Maeno F, Tamura Y, Wang F (2015) Rapid onset of mafic magmatism facilitated by volcanic edifice collapse. Geophys Res Lett 42(12):4778–4785. doi:10.1002/2015GL064519

Casson M, Bulot LG, Jeremiah J, Redfern J (2020) Deep sea rock record exhumed on oceanic volcanic islands. The Cretaceous sediments of Maio, Cape Verde. Gondwana Res 81:252–264. doi:10.1016/j.gr.2019.11.007

Channell J, Erba E, Nakanishi M, Tamki K (1995) Late Jurassic-Early Cretaceous Time Scales and Oceanic Magnetic Anomaly Block Models. In: Berggren WA (ed) Geochronology, time scales, and global stratigraphic correlation. Society for Sedimentary Geology, Tulsa Oklahoma, pp 51–63

Cheel RJ (2005) Introduction to Clastic Sedimentology. https://brocku.ca/sedimentology/SedNotes/

Clague DA, Dalrymple GB (1987) The Hawaiian-Emperor volcanic Chain. Part 1, Geologic evolution. In: Decker R, Wright TL, Stauffer PH (eds) Volcanism in Hawaii, 1350(1). US Geol Surv Prof Pap, Hawaii, pp 5–54

Conti MA, Alteriis G de, Marino MC, Pallini G, Tonielli R (2004) Discovery of Late Jurassic fossils inside modern sediments at Gorringe Bank (Eastern Atlantic Ocean) and some geological implications. Terra Nova 16(6):331–337. doi:10.1111/j.1365-3121.2004.00570.x

Cornu M-N, Paris R, Doucelance R, Bachélery P, Bosq C, Auclair D, Benbakkar M, Gannoun A-M, Guillou H (2021) Exploring the links between volcano flank collapse and the magmatic evolution of an ocean island volcano: Fogo, Cape Verde. Sci Rep 11(1):17478. doi:10.1038/s41598-021-96897-1

Courtney RC, White RS (1986) Anomalous heat flow and geoid across the Cape Verde Rise. Evidence for dynamic support from a thermal plume in the mantle. Geophys J R Astr Soc 87(3):815–867. doi:10.1111/j.1365-246X.1986.tb01973.x

Crough ST (1982) Geoid height anomalies over the Cape Verde Rise. Mar Geophys Res 5(3):263–271. doi:10.1007/BF00305564

Dash BP, Ball MM, King GA, Butler LW, Rona PA (1976) Geophysical investigation of the Cape Verde Archipelago. J Geophys Res Solid Earth 81(29):5249–5259. doi:10.1029/JB081i029p05249

Day SJ, Heleno da Silva S, Fonseca, J. F. B. D. (1999) A past giant lateral collapse and present-day flank instability of Fogo, Cape Verde Islands. J Volcanol Geotherm Res 94(1-4):191–218. doi:10.1016/S0377-0273(99)00103-1

Di Vincenzo G, Viti C, Rocchi S (2003) The effect of chlorite interlayering on 40Ar?39Ar biotite dating: an 40Ar?39Ar laser-probe and TEM investigations of variably chloritised biotites. Contrib Mineral Petrol 145(6):643–658. doi:10.1007/s00410-003-0472-z

Duprat HI, Friis J, Holm PM, Grandvuinet T, Sørensen RV (2007) The volcanic and geochemical development of São Nicolau, Cape Verde Islands. Constraints from field and $^{40}Ar/^{39}Ar$ evidence. J Volcanol Geotherm Res 162(1-2):1–19. doi:10.1016/j.jvolgeores.2007.01.001

Dyhr CT, Holm PM (2010) A volcanological and geochemical investigation of Boa Vista, Cape Verde Islands; $^{40}Ar/^{39}Ar$ geochronology and field constraints. J Volcanol Geotherm Res 189(1-2):19–32. doi:10.1016/j.jvolgeores.2009.10.010

Eisele S, Reißig S, Freundt A, Kutterolf S, Nürnberg D, Wang KL, Kwasnitschka T (2015) Pleistocene to Holocene offshore tephrostratigraphy of highly explosive eruptions from the southwestern Cape Verde Archipelago. Mar Geol 369:233–250. doi:10.1016/j.margeo.2015.09.006

Ewing M, Worzel JL, Beall AO, Berggren AW, Bukry D, Burk CA, Fischer AG, Pessagno EA (1969a) Site 4. In: Ewing M, Worzel JL (eds) DSDP Initial Reports vol. 1. U.S. Government Printing Office, Washington, USA, 179-213

Ewing M, Worzel JL, Beall AO, Berggren AW, Bukry D, Burk CA, Fischer AG, Pessagno EA (1969b) Site 5. In: Ewing M, Worzel JL (eds) DSDP Initial Reports vol. 1. U.S. Government Printing Office, Washington, USA, pp 214–242

Faria B, Fonseca J (2014) Investigating volcanic hazard in Cape Verde Islands through geophysical monitoring. Network description and first results. Nat Hazards Earth Syst Sci 14(2):485–499. doi:10.5194/nhess-14-485-2014

Faust D, Yanes Y, Willkommen T, Roettig C, Richter D, Richter D, Suchodoletz Hv, Zöller L (2015) A contribution to the understanding of late Pleistocene dune sand-paleosol-sequences in Fuerteventura (Canary Islands). Geomorphology 246:290–304. doi:10.1016/j.geomorph.2015.06.023

Fleck RJ, Calvert AT, Coble MA, Wooden JL, Hodges K, Hayden LA, van Soest MC, Du Bray EA, John DA (2019) Characterization of the rhyolite of Bodie Hills and $^{40}Ar/^{39}Ar$ intercalibration with Ar mineral standards. Chem Geol 525:282–302. doi:10.1016/j.chemgeo.2019.07.022

Flügel E, Munnecke A (2010) Microfacies of carbonate rocks. Analysis, interpretation and application, 2nd edn. Springer, Berlin

Foeken JP, Day SJ, Stuart FM (2009) Cosmogenic ^{3}He exposure dating of the Quaternary basalts from Fogo, Cape Verdes. Implications for rift zone and magmatic reorganisation. Quat. Geochronol. 4(1):37–49. doi:10.1016/j.quageo.2008.07.002

Fossilworks.org Paleobiology Database Fossilworks. http://fossilworks.org/bridge.pl?a=home. Accessed 25 Mar 2019

Fourcade E, Azéma J, Wever P de, Busnardo R (1990) Contribution à la datation de la croûte océanique de l'Atlantique central: Age valanginien inférieur des basalts océaniques et âge néocomien des calcaires Maiolica de Maio (Iles du Cap Vert). Mar Geol 95:31–44

Friedlaender I (1913) Beiträge zur Kenntnis der Kapverdischen Inseln. Die Ergebnisse einer Studienreise im Sommer 1912 von Immanuel Friedlaender, Neapel. Mit einer Übersicht über die Gesteien der Kapverdischen Inseln von Professor Dr. W. Bergt in Leipzig. Dietrich Reimer (Ernst Vohsen), Berlin (Germany)

Gardner JV, Dean WE, Jansa L (1978) Sediments Recovered from the Northwest African Continental Margin, Leg 41, Deep Sea Drilling Project. In: Lancelot Y, Seibold E (eds) DSDP Initial Reports vol. 41. US Government Printing Office, Washington, USA, pp 1121–1134

Gasperini L, Bernoulli D, Bonatti E, Borsetti A, Ligi M, Negri A, Sartori R, Salis K von (2001) Lower Cretaceous to Eocene sedimentary transverse ridge at the Romanche Fracture Zone and the opening of the equatorial Atlantic. Mar Geol 176(1-4):101–119. doi:10.1016/S0025-3227(01)00146-3

GBIF Secretariat (2017) GBIF Backbone Taxnomy. https://doi.org/10.15468/39omei. Accessed via gbif.org on 17 Jul 2021

Gerlach DC, Cliff RA, Davies GR, Norry M, Hadgson N (1988) Magma sources of the Cape Verdes archipelago. Isotopic and trace element constraints. Geochim Cosmochim Acta 52(12):2979–2992. doi:10.1016/0016-7037(88)90162-7

Ginibre C, Wörner G, Kronz A (2007) Crystal Zoning as an Archive for Magma Evolution. Elements 3(4):261–266. doi:10.2113/gselements.3.4.261

Gradstein FM (2012) The Geologic Time Scale 2012. Elsevier, Amsterdam

Grant KM, Rohling EJ, Ramsey CB, Cheng H, Edwards RL, Florindo F, Heslop D, Marra F, Roberts AP, Tamisiea ME, Williams F (2014) Sea-level variability over five glacial cycles. Nat Commun 5:5076. doi:10.1038/ncomms6076

Grevemeyer I, Helffrich G, Faria BVE, Booth-Rea G, Schnabel M, Weinrebe W (2010) Seismic activity at Cadamosto seamount near Fogo Island, Cape Verdes - formation of a new ocean island? Geophys J Int 180(2):552–558. doi:10.1111/j.1365-246X.2009.04440.x

Grün B, Blau J (1997) New aspects of calpionellid biochronology: proposal for a revised calpionellid zonal and subzonal division. Revue Paléobiol (Revue de Paléobiologie) 16(1):197–214

Grunau HR, Lehner P, Cleintuar MR, Allenbach P, Bakker G (1975) New radiometric ages and seismic data from Fuerteventura (Canary Islands), Maio (Cape Verde Islands), and Sao Tomé (Gulf of Guinea). In: Borradaile GJ (ed) Progress in Geodynamics. Koninklijke Nederlandse Akademie van Wetenshappen, Amsterdam, pp 90–118

Hansteen T, Kwasnitschka T, Klügel A (2014) Cape Verde Seamounts - Cruise No. M80/3. December 29, 2009 - February 1, 2010 - Dakar (Senegal) - Las Palmas de Gran Canaria (Spain)(M80/3):1–42

Hasenclever J, Knorr G, Rüpke LH, Köhler P, Morgan J, Garofalo K, Barker S, Lohmann G, Hall IR (2017) Sea level fall during glaciation stabilized atmospheric CO2by enhanced volcanic degassing. Nat Commun 8:15867. doi:10.1038/ncomms15867

Heath M, Phillips D, Matchan EL (2018) An evidence-based approach to accurate interpretation of $^{40}Ar/^{39}Ar$ ages from basaltic rocks. Earth Planet Sci Lett 498:65–76. doi:10.1016/j.epsl.2018.06.024

Heinz R (1935) Unterkreide-Inoceramen von der Kapverden-Insel Maio. Neues Jahrbuch für Mineralogie und Geologie, Beilage-Band 73(B):302–311

Hennig E (1913) Aptychen von den Cap Verdeschen Inseln. Zeitschrift der Deutschen Geologischen Gesellschaft:151–158

Hinz K, Winterer EL, Baumgartner PO, Bradshaw MJ, Channell J, Jaffrezo M, Jansa LF, Moore JN, Rullkötter J, Schaftenaar CH, Steiger TH, Tuchev VT, Wiegand GE (1984) Site 547. In: Hinz K, Winterer EL (eds) DSDP Initial Reports vol. 79. U.S. Government Printing Office, Washington, USA, pp 223–361

Hollister CD, Ewing JI, Habib D, Hathaway JC, Lancelot Y, Luterbacher H, Paulus FJ, Poag CW, Wilcoxon JA, Worstell P (1972a) Site 100. Cat Gap. In: Hollister CD, Ewing JI (eds) DSDP Initial Reports vol. 11. U.S. Government Printing Office, Washington, USA, pp 75–104

Hollister CD, Ewing JI, Habib D, Hathaway JC, Lancelot Y, Luterbacher H, Paulus FJ, Poag CW, Wilcoxon JA, Worstell P (1972b) Site 105. Lower Continental Rise Hills. In: Hollister CD, Ewing JI (eds) DSDP Initial Reports vol. 11. U.S. Government Printing Office, Washington, USA, pp 219–312

Hollister CD, Ewing JI, Habib D, Hathaway JC, Lancelot Y, Luterbacher H, Paulus FJ, Poag CW, Wilcoxon JA, Worstell P (1972c) Site 99. Cat Gap. In: Hollister CD, Ewing JI (eds) DSDP Initial Reports vol. 11. U.S. Government Printing Office, Washington, USA, pp 51–73

Holm PM (2006) Sampling the Cape Verde Mantle Plume. Evolution of Melt Compositions on Santo Antao, Cape Verde Islands. J Petrol 47(1):145–189. doi:10.1093/petrology/egi071

Holm PM, Grandvuinet T, Friis J, Wilson JR, Barker AK, Plesner S (2008) An ^{40}Ar-^{39}Ar study of the Cape Verde hot spot:. Temporal evolution in a semistationary plate environment. J Geophys Res Solid Earth 113(B8). doi:10.1029/2007JB005339

Hunt JE, Cassidy M, Talling PJ (2018) Multi-stage volcanic island flank collapses with coeval explosive caldera-forming eruptions. Sci Rep 8(1):1146. doi:10.1038/s41598-018-19285-2

Hunt JE, Wynn RB, Masson DG, Talling PJ, Teagle DAH (2011) Sedimentological and geochemical evidence for multistage failure of volcanic island landslides. A case study from Icod landslide on north Tenerife, Canary Islands. Geochem Geophys Geosys 12(12):Q12007. doi:10.1029/2011GC003740

Hunt JE, Wynn RB, Talling PJ, Masson DG (2013) Turbidite record of frequency and source of large volume (>100 km^3) Canary Island landslides in the last 1.5 Ma. Implications for landslide triggers and geohazards. Geochem Geophys Geosys 14(7):2100–2123. doi:10.1002/ggge.20139

Jansa J, Gardner JV, Dean WE (1978) Mesozoic Sequences of the Central North Atlantic. In: Lancelot Y, Seibold E (eds) DSDP Initial Reports vol. 41. US Government Printing Office, Washington, USA, pp 991–1031

Jansa LF, Enos P, Tucholke BE, Gradstein FM, Sheridan RE (1979) Mesozoic-Cenozoic Sedimentary Formations of the North American Basin; Western North Atlantic. In: Talwani M, Hay WW, Ryan WBF (eds) Deep drilling results in the Atlantic Ocean. Continental margins and paleoenvironment. American Geophysical Union, Washington, pp 1–57

Jansa LF, Steiger TH, Bradshaw M (1984) Mesozoic Carbonate Deposition on the Outer Continental Margin off Morocco. In: Hinz K, Winterer EL (eds) DSDP Initial Reports vol. 79. U.S. Government Printing Office, Washington, USA, 857-891

Jarosewich E (2002) Smithsonian Microbeam Standards. J Res Natl Inst Stand Technol 107(6):681–685. doi:10.6028/jres.107.054

Jeans CV, Turchyn AV, Hu X-F (2016) Sulfur isotope patterns of iron sulfide and barite nodules in the Upper Cretaceous Chalk of England and their regional significance in the origin of coloured chalks. Acta Geologica Polonica 66(2):227–256. doi:10.1515/agp-2016-0010

Jerram DA, Dobson KJ, Morgan DJ, Pankhurst MJ (2018) The Petrogenesis of Magmatic Systems. Using Igneous Textures to Understand Magmatic Processes. In: Burchardt S (ed) Volcanic and Igneous Plumbing Systems. Understanding Magma Transport, Storage, and Evolution in the Earth's Crust. Elsevier, Amsterdam, Netherlands, pp 191–229

Jones EJW, Bigg GR, Handoh IC, Spathopoulos F (2007) Distribution of deep-sea black shales of Cretaceous age in the eastern Equatorial Atlantic from seismic profiling. Palaeogeo, Palaeoclim, Palaeoecol 248(1-2):233–246. doi:10.1016/j.palaeo.2006.12.006

Jourdan F, Renne PR, Reimold WU (2009) An appraisal of the ages of terrestrial impact structures. Earth Planet Sci Lett 286(1-2):1–13. doi:10.1016/j.epsl.2009.07.009

Kervyn M, Ernst GGJ, van Wyk de Vries B, Mathieu L, Jacobs P (2009) Volcano load control on dyke propagation and vent distribution. Insights from analogue modeling. J Geophys Res Solid Earth 114(B3):517. doi:10.1029/2008JB005653

Klerkx J, Paepe P de (1976) The main characteristics of the magmatism of the Cape Verde Islands. Annuales de la Société Géologique de Belgique 99:347–357

Klügel A, Day S, Schmid M, Faria B (2020) Magma Plumbing During the 2014–2015 Eruption of Fogo (Cape Verde Islands). Front Earth Sci 8:41. doi:10.3389/feart.2020.00157

Klügel A, Hansteen TH, Galipp K (2005) Magma storage and underplating beneath Cumbre Vieja volcano, La Palma (Canary Islands). Earth Planet Sci Lett 236(1-2):211–226. doi:10.1016/j.epsl.2005.04.006

Klügel A, Longpré M-A, García-Cañada L, Stix J (2015) Deep intrusions, lateral magma transport and related uplift at ocean island volcanoes. Earth Planet Sci Lett 431:140–149. doi:10.1016/j.epsl.2015.09.031

Kopelevich DI, Chang H-C (2001) Diffusion of inert gases in silica sodalite: Importance of lattice flexibility. J Chem Phys 115(20):9519–9527. doi:10.1063/1.1414373

Koppers A (2002) ArArCALC—software for $^{40}Ar/^{39}Ar$ age calculations. Comput Geosci 28(5):605–619. doi:10.1016/S0098-3004(01)00095-4

Koppers A, Staudigel H, Wijbrans JR (2000) Dating crystalline groundmass separates of altered Cretaceous seamount basalts by the $^{40}Ar/^{39}Ar$ incremental heating technique. Chem Geol 166(1-2):139–158. doi:10.1016/S0009-2541(99)00188-6

Kraus G (2005) Cruise Report R.V. POSEIDON P320_2, Kiel, Germany
Kutterolf S, Jegen M, Mitrovica JX, Kwasnitschka T, Freundt A, Huybers PJ (2013) A detection of Milankovitch frequencies in global volcanic activity. Geology 41(2):227–230. doi:10.1130/G33419.1
Kwasnitschka T, Hansteen TH, Ramalho RS, Devey CW, Klügel A, Samrock LK, Wartho J-A (in prep.) Morphology of Seamounts in the Cabo Verde Archipelago, and their Relation to Island Age and Evolution
Labails C, Olivet J-L, Aslanian D, Roest WR (2010) An alternative early opening scenario for the Central Atlantic Ocean. Earth Planet Sci Lett 297(3-4):355–368. doi:10.1016/j.epsl.2010.06.024
Lancelot Y, Seibold E, Cepek P, Dean WE, Eremeev VV, Gardner J, Jansa LF, Johnson D, Krasheninnikov V, Pflaumann U, Rankin JG, Trabant P, Bukry D (1978a) Site 367. Cape Verde Basin. In: Lancelot Y, Seibold E (eds) DSDP Initial Reports vol. 41. US Government Printing Office, Washington, USA, pp 163–232
Lancelot Y, Seibold E, Cepek P, Dean WE, Eremeev VV, Gardner J, Jansa LF, Johnson D, Krasheninnikov V, Pflaumann U, Rankin JG, Trabant P, Bukry D (1978b) Site 368: Cape Verde Rise. In: Lancelot Y, Seibold E (eds) DSDP Initial Reports vol. 41. US Government Printing Office, Washington, USA, pp 253–326
Lanphere MA, Dalrymple GB (1978) The use of $^{40}Ar/^{39}Ar$ data in evaluation of disturbed K-Ar systems. US Geol Surv Open-file Rep 78-701:141–148
Le Bas TP, Masson DG, Holtom RT, Grevemeyer I (2007) Slope Failures Of The Flanks Of The Southern Cape Verde Islands. In: Lykousis V, Locat J, Sakellariou D (eds) Submarine Mass Movements and Their Consequences. 3 International Symposium. Springer, Dordrecht, pp 337–345
Leckie RM, Bralower TJ, Cashman R (2002) Oceanic anoxic events and plankton evolution. Biotic response to tectonic forcing during the mid-Cretaceous. Paleoceanography 17(3):13-1-13-29. doi:10.1029/2001PA000623
Leva C, Rümpker G, Link F, Wölbern I (2019) Mantle earthquakes beneath Fogo volcano, Cape Verde: Evidence for subcrustal fracturing induced by magmatic injection. J Volcanol Geotherm Res 386:106672. doi:10.1016/j.jvolgeores.2019.106672
Li Y-X, Bralower TJ, Montañez IP, Osleger DA, Arthur MA, Bice DM, Herbert TD, Erba E, Premoli Silva I (2008) Toward an orbital chronology for the early Aptian Oceanic Anoxic Event (OAE1a, ~120 Ma). Earth Planet Sci Lett 271(1-4):88–100. doi:10.1016/j.epsl.2008.03.055
Lippolt HJ, Troesch M, Hess JC (1990) Excess argon and dating of Quaternary Eifel volcanism, IV. Common argon with high and lower-than-atmospheric $^{40}Ar/^{36}Ar$ ratios in phonolitic rocks, East Eifel, F.R.G. Earth Planet Sci Lett 101(1):19–33. doi:10.1016/0012-821X(90)90120-M
Lisiecki LE, Raymo ME (2005) A Pliocene-Pleistocene stack of 57 globally distributed benthic δ 18 O records. Paleoceanography 20(1):PA1003. doi:10.1029/2004PA001071
Lodge A, Helffrich G (2006) Depleted swell root beneath the Cape Verde Islands. Geol 34(6):449. doi:10.1130/G22030.1
Ludwig K (2011) User's Manual for Isoplot 4.15. a Geochronological Toolkit for Microsoft Excel 4:77p.
Madeira J, Mata J, Mourão C, Brum da Silveira A, Martins S, Ramalho RS, Hoffmann D (2010) Volcano-stratigraphic and structural evolution of Brava Island (Cape Verde) based on $^{40}Ar/^{39}Ar$, U-Th and field constraints. J Volcanol Geotherm Res 196(3-4):219–235. doi:10.1016/j.jvolgeores.2010.07.010
Madeira J, Munhá J, Tassinari C, Mata J, Brum da Silva A, Martins S (2005) K/Ar ages of carbonatites from the Island of Fogo (Cape Verde). Proceedings of the XIV semana de Geoquímica /VIII Congresso de Geoquímica dos Países de Língua Portuguesa Lisboa, Portugal:475–478
Madeira J, Ramalho RS, Hoffmann DL, Mata J, Moreira M, Costa P (2020) A geological record of multiple Pleistocene tsunami inundations in an oceanic island. The case of Maio, Cape Verde. Sedimentology 67(3):1529–1552. doi:10.1111/sed.12612
Manconi A, Longpre M-A, Walter TR, Troll VR, Hansteen TH (2009) The effects of flank collapses on volcano plumbing systems. Geol 37(12):1099–1102. doi:10.1130/G30104A.1
Marques FO, Hildenbrand A, Zeyen H, Cunha C, Victória SS (2020) The complex vertical motion of intraplate oceanic islands assessed in Santiago Island, Cape Verde. Geochem Geophys Geosys 21(3):2429. doi:10.1029/2019GC008754

Martínze-Moreno FJ, Monteira Santos FA, Madeira J, Pous J, Bernardo I, Soares A, Esteves M, Adao F, Ribeiro J, Mata J, Brum da Silva A (2018) Investigating collapse structures in oceanic islands using magnetotelluric survey: The case of Fogo Island in Cape Verde. J Volcanol Geotherm Res 357:152–162

Masson DG, Le Bas TP, Grevemeyer I, Weinrebe W (2008) Flank collapse and large-scale landsliding in the Cape Verde Islands, off West Africa. Geochem Geophys Geosys 9(7):Q07015. doi:10.1029/2008GC001983

Mata J, Martins S, Mattielli N, Madeira J, Faria BVE, Ramalho RS, Silva P, Moreira M, Caldeira R, Rodrigues J, Martins L (2017) The 2014–15 eruption and the short-term geochemical evolution of the Fogo volcano (Cape Verde). Evidence for small-scale mantle heterogeneity. Lithos 288-289:91–107. doi:10.1016/j.lithos.2017.07.001

McDougall I, Harrison TM (1999) Geochronology and Thermochronology by the ^{40}Ar-^{39}Ar Method, 2nd edn. Oxford University Press, New York (USA)

McEwen AS, Malin MC (1989) Dynamics of Mount St. Helens' 1980 pyroclastic flows, rockslide-avalanche, lahars, and blast. J Volcanol Geotherm Res 37(3-4):205–231. doi:10.1016/0377-0273(89)90080-2

McGuire WJ (1996) Volcano instability. A review of contemporary themes. Geol Soc Lond Spec Publ 110(1):1–23. doi:10.1144/GSL.SP.1996.110.01.01

McKee E, Ward WC (1983) Eolian Environment. In: Scholle PA, Bebout DG, Moore CH (eds) Carbonate depositional environments. American Association of Petroleum Geologists, Tulsa, Okla., U.S.A., pp 131–170

Miller KG (2009) Sea Level Change, Last 250 Million Years. In: Gornitz V (ed) Encyclopedia of Paleoclimatology and Ancient Environments. Springer Netherlands, Dordrecht, pp 879–887

Millet M-A, Doucelance R, Schiano P, David K, Bosq C (2008) Mantle plume heterogeneity versus shallow-level interactions. A case study, the São Nicolau Island, Cape Verde archipelago. J Volcanol Geotherm Res 176(2):265–276. doi:10.1016/j.jvolgeores.2008.04.003

Mitchell JG, Le Bas MJ, Zielonka J, Furnes H (1983) On dating the magmatism of Maio, Cape Verde Islands. Earth Planet Sci Lett 64:61–76

Mitchell-Thomé RC (1972) Outline of the geology of the Cape Verde Archipelago. Geol Rundsch 61(3):1087–1109. doi:10.1007/BF01820907

Mitchell-Thomé RC (1974) The sedimentary rocks of macaronesia. Geol Rundsch 63(3):1179–1216. doi:10.1007/BF01821329

Montanari D, Bonini M, Corti G, Agostini A, Del Ventisette C (2017) Forced folding above shallow magma intrusions: Insights on supercritical fluid flow from analogue modelling. J Volcanol Geotherm Res 345:67–80. doi:10.1016/j.jvolgeores.2017.07.022

Moore JG, Clague DA (1992) Volcano growth and evolution of the island of Hawaii. Geol Soc Am Bull 104(11):1471–1484. doi:10.1130/0016-7606(1992)104<1471:VGAEOT>2.3.CO;2

Mourão C, Mata J, Doucelance R, Madeira J, Millet M-A, Moreira M (2012a) Geochemical temporal evolution of Brava Island magmatism. Constraints on the variability of Cape Verde mantle sources and on carbonatite–silicate magma link. Chem Geol 334:44–61. doi:10.1016/j.chemgeo.2012.09.031

Mourão C, Moreira M, Mata J, Raquin A, Madeira J (2012b) Primary and secondary processes constraining the noble gas isotopic signatures of carbonatites and silicate rocks from Brava Island. Evidence for a lower mantle origin of the Cape Verde plume. Contrib Mineral Petrol 163(6):995–1009. doi:10.1007/s00410-011-0711-7

Mourlot Y, Calvès G, Clift PD, Baby G, Chaboureau A-C, Raisson F (2018) Seismic stratigraphy of Cretaceous eastern Central Atlantic Ocean. Basin evolution and palaeoceanographic implications. Earth Planet Sci Lett 499:107–121. doi:10.1016/j.epsl.2018.07.023

Müller RD, Sdrolias M, Gaina C, Roest WR (2008) Age, spreading rates, and spreading asymmetry of the world's ocean crust. Geochem Geophys Geosys 9(4):Q04006. doi:10.1029/2007GC001743

Nekvasil H, Simon A, Lindsley DH (2000) Crystal Fractionation and the Evolution of Intra-plate *hy*-normative Igneous Suites. Insights from their Feldspars. J Petrology 41(12):1743–1757. doi:10.1093/petrology/41.12.1743

Nemec W, Steel RJ (1984) Alluvial and coastsal conglomerates: Their significant features and some comments on gravelly mass-flow deposits. In: Koster EH, Steel RJ (eds) Sedimentology of Gravels and Conglomerates, Memoir 10, pp 1–31

Ogg JG, Haggerty J, Sarti M, Rad U von (1987) Lower Cretaceous Pelagic Sediments of Deep Sea Drilling Project Site 603, Western North Atlantic. A Synthesis. In: van Hinte J, Wise S, Jr. ea (eds) DSDP Initial Reports vol. 93. U.S. Government Printing Office, Washington, USA, 1305-1331

Ortiz JE, Torres T, Yanes Y, La Nuez J de, Ibánez M, Alonso MR (2006) Climatic cycles inferred from the aminostratigraphy and aminochronology of Quaternary dunes and palaeosols from the eastern islands of the Canary Archipelago. J Quaternary Sci 21(3):287–306

Paepe P de, Klerkx J, Hertogen J, Plinke P (1974) Oceanic tholeiites on the Cape Verde Islands: petrochemical and geochemical evidence. Earth Planet Sci Lett 22:347–354

Paterne M, Labeyrie J, Guichard F, Mazaud A, Maitre F (1990) Fluctuations of the Campanian explosive volcanic activity (South Italy) during the past 190,000 years, as determined by marine tephrochronology. Earth Planet Sci Lett 98(2):166–174. doi:10.1016/0012-821X(90)90057-5

Pim J, Peirce C, Watts AB, Grevemeyer I, Krabbenhoeft A (2008) Crustal structure and origin of the Cape Verde Rise. Earth Planet Sci Lett 272(1-2):422–428. doi:10.1016/j.epsl.2008.05.012

Plesner S, Holm PM, Wilson JR (2002) ^{40}Ar-^{39}Ar geochronology of Santo Antao, Cape Verde Islands. J Volcanol Geotherm Res 120:103–121

Pollitz FF (1991) Two-stage model of African absolute motion during the last 30 million years. Tectonophysics 194(1-2):91–106. doi:10.1016/0040-1951(91)90274-V

Ramalho RS (2011) Building the Cape Verde Islands. Springer Theses. Springer, Berlin, Heidelberg

Ramalho RS, Helffrich G, Cosca M, Vance D, Hoffmann D, Schmidt DN (2010a) Episodic swell growth inferred from variable uplift of the Cape Verde hotspot islands. Nat Geosci 3(11):774–777. doi:10.1038/NGEO982

Ramalho RS, Helffrich G, Cosca M, Vance D, Hoffmann D, Schmidt DN (2010b) Vertical movements of ocean island volcanoes: Insights from a stationary plate environment. Mar Geol 275(1-4):84–95. doi:10.1016/j.margeo.2010.04.009

Ramalho RS, Helffrich G, Schmidt DN, Vance D (2010c) Tracers of uplift and subsidence in the Cape Verde archipelago. J Geol Soc 167(3):519–538. doi:10.1144/0016-76492009-056

Ramalho RS, Quartau R, Trenhaile AS, Mitchell NC, Woodroffe CD, Ávila SP (2013) Coastal evolution on volcanic oceanic islands: A complex interplay between volcanism, erosion, sedimentation, sea-level change and biogenic production. Earth-Sci Rev 127:140–170. doi:10.1016/j.earscirev.2013.10.007

Ramalho RS, Winckler G, Madeira J, Helffrich GR, Hipólito A, Quartau R, Adena K, Schaefer JM (2015) Hazard potential of volcanic flank collapses raised by new megatsunami evidence. Sci Adv 1(9):e1500456. doi:10.1126/sciadv.1500456

Renz O, Bernoulli D, Hottinger L (1992) Cretaceous ammonites from Fuerteventura, Canary Islands. Geol Mag 129(06):763. doi:10.1017/S0016756800008487

Represas P, Catalão J, Montesinos FG, Madeira J, Mata J, Antunes C, Moreira M (2012) Constraints on the structure of Maio Island (Cape Verde) by a three-dimensional gravity model. Imaging partially exhumed magma chambers. Geophys J Int 190(2):931–940. doi:10.1111/j.1365-246X.2012.05536.x

Rigassi DA (1972) Geology and oil prospects of Cabo Verde Islands. Petroconsultants S.A., Geneva, Switzerland

Rigassi DA (1975) Micropaleontological investigations in Cabo Verde Archipelago. Colloquium of African Geology Annual Report of the Research Institute of African Geology:83

Robertson A, Bliefnick DM (1983) Sedimentology and origin of Lower Cretaceous pelagic carbonates and redeposited clastics, Blake-Bahama Formation, Deep Sea Drilling Project Site 534, Western Equatorial Atlantic. In: Sheridan RE, Gradstein FM (eds) DSDP Initial Reports vol. 76. U.S. Government Printing Office, Washington, USA, pp 795–828

Robertson AHF (1984) Mesozoic deep-water and Tertiary volcaniclastic deposition of Maio, Cape Verde Islands: Implications for Atlantic paleoenvironments and ocean island volcanism. Geol Soc Am Bull 95:433–453. doi:10.1130/0016-7606(1984)95<433:MDATVD>2.0.CO;2

Robertson AHF, Bernoulli D (1982) Stratigraphy, facies, and significance of Late Mesozoic and Early Tertiary sedimentary rocks of Fuerteventura (Canary Islands) and Maio (Cape Verde Islands). In: Rad U von, Hinz K, Sarnthein M, Seibold E (eds) Geology of the Northwest African continental margin. Springer, Berlin, Heidelberg, pp 498–525

Roettig C-B, Kolb T, Wolf D, Baumgart P, Richter C, Schleicher A, Zöller L, Faust D (2017) Complexity of Quaternary aeolian dynamics (Canary Islands). Palaeogeo, Palaeoclim, Palaeoecol 472:146–162. doi:10.1016/j.palaeo.2017.01.039

Romagnoli C, Kokelaar P, Casalbore D, Chiocci FL (2009) Lateral collapses and active sedimentary processes on the northwestern flank of Stromboli volcano, Italy. Mar Geol 265(3-4):101–119. doi:10.1016/j.margeo.2009.06.013

Roverato M, Cronin S, Procter J, Capra L (2014) Textural features as indicators of debris avalanche transport and emplacement, Taranaki volcano. Geol Soc Am Bull 127(1-2):3–18. doi:10.1130/B30946.1

Ruprecht P, Wörner G (2007) Variable regimes in magma systems documented in plagioclase zoning patterns. El Misti stratovolcano and Andahua monogenetic cones. J Volcanol Geotherm Res 165(3-4):142–162. doi:10.1016/j.jvolgeores.2007.06.002

Ryan WBF, Carbotte SM, Coplan JO, O'Hara S, Melkonian A, Arko R, Weissel RA, Ferrini V, Goodwillie A, Nitsche F, Bonczkowski J, Zemsky R (2009) Global Multi-Resolution Topography synthesis. Geochem Geophys Geosys 10(3):n/a-n/a. doi:10.1029/2008GC002332

Samrock LK, Dullo W-C, Hansteen TH (2018) Large-scale fossil dune on Maio, Cape Verdes. Int J Earth Sci (Geol Rundsch) 107(8):2931–2932. doi:10.1007/s00531-018-1622-x

Samrock LK, Hansteen TH, Dullo W-C, Wartho J-A (2022) Internal igneous growth, doming and rapid erosion of a mature ocean island: the Miocene evolution of Maio (Cabo Verde). Int J Earth Sci (Geol Rundsch) 111:1129–1148. doi:10.1007/s00531-022-02160-x

Samrock LK, Wartho J-A, Hansteen TH (2019) ^{40}Ar-^{39}Ar geochronology of the active phonolitic Cadamosto Seamount, Cape Verde. Lithos 344-345:464–481. doi:10.1016/j.lithos.2019.07.003

Schieber J (2011) Iron Sulfide Formation. In: Reitner J, Thiel V (eds) Encyclopedia of geobiology. Springer, Dordrecht, pp 486–502

Schlanger SO, Jenkyns HC (1976) Cretaceous Oceanic Anoxic Events: Causes and Consequences. Geologie En Mijnbouw 55(3-4):179–184

Schmincke H-U (1973) Magmatic Evolution and Tectonic Regime in the Canary, Madeira, and Azores Island Groups. Geol Soc Am Bull 84(2):633. doi:10.1130/0016-7606(1973)84<633:MEATRI>2.0.CO;2

Serralheiro A (1968) Formações sedimentares do arquipélago de Cabo Verde. Agrupamento Científico de Geologia da Universidade de Lisbôa da Junta de Investigações do Ultramar, Lisboa, Portugal

Serralheiro A (1970) Geologia da ilha de Maio (Cabo Verde). Junta de Investigações do Ultrama, Lisboa, Portugal

Sheridan RE, Gradstein FM, Barnard LA, Bliefnick DM, Habib D, Jenden PD, Kagami H, Keenan EM, Kostecki J, Kvenvolden K, Moullade M, Ogg JG, Roth PH, Shipley T (1983) Site 534. Blake-Bahama Basin. In: Sheridan RE, Gradstein FM (eds) DSDP Initial Reports vol. 76. U.S. Government Printing Office, Washington, USA, pp 141–340

Silva S de, Lindsay JM (2015) Primary Volcanic Landforms. In: Sigurdsson H (ed) Encyclopedia of volcanoes, Second edition. Academic Press, San Diego, pp 273–297

Soares JMP (1950) A propósito da estratigrafia da ilha de Maio (Archipélago de Cabo Verde). Imprensa Portuguesa, Porto

Soares JMP (1953) A propósito dos "Aptychi" da Ilha de Maio (Archipélago de Cabo Verde). Junta das Missoes Geográficas e de Investigacoes do Ultramar, Lisboa, Portugal

Sparks R (1997) Causes and consequences of pressurisation in lava dome eruptions. Earth Planet Sci Lett 150(3-4):177–189. doi:10.1016/S0012-821X(97)00109-X

Spieler O, Kennedy B, Kueppers U, Dingwell DB, Scheu B, Taddeucci J (2004) The fragmentation threshold of pyroclastic rocks. Earth Planet Sci Lett 226(1-2):139–148. doi:10.1016/j.epsl.2004.07.016

Stahlecker R (1934) Neocom auf der Kapverden-Insel Maio. N Jb Geol Paläont 73(2):265–301

Steiger RH, Jäger E (1977) Subcommission on geochronology. Convention on the use of decay constants in geo- and cosmochronology. Earth Planet Sci Lett 36(3):359–362. doi:10.1016/0012-821X(77)90060-7

Steiner C, Hobson A, Favre P, Stampfli GM, Hernandez J (1998) Mesozoic sequence of Fuerteventura (Canary Islands): Witness of Early Jurassic sea-floor spreading in the central Atlantic. Geol Soc America Bull 110(10):1304–1317

Sternai P, Caricchi L, Garcia-Castellanos D, Jolivet L, Sheldrake TE, Castelltort S (2017) Magmatic pulse driven by sea-level changes associated with the Messinian salinity crisis. Nat Geosci 10(10):783–787. doi:10.1038/ngeo3032

Stillman CJ, Furnes H, Le Bas MJ, Robertson AHF, Zielonka J (1982) The geological history of Maio, Cape Verde Islands. J Geol Soc 139(3):347–361. doi:10.1144/gsjgs.139.3.0347

Stoppa F, Principe C, Schiazza M, Liu Y, Giosa P, Crocetti S (2017) Magma evolution inside the 1631 Vesuvius magma chamber and eruption triggering. Open Geosci 9(1):1. doi:10.1515/geo-2017-0003

Streck MJ (2008) Mineral Textures and Zoning as Evidence for Open System Processes. Rev Mineral Geochem 69(1):595–622. doi:10.2138/rmg.2008.69.15

Torres P, Silva LC, Serralheiro A, Tassinari C, Munhá J (2002) Enquadramento geocronológico pelo método K/Ar das principais sequências vulcano-estratigráficas da Ilha do Sal—Cabo Verde. Garcia da Orta, Série Geol. 18(1/2):9–13

Trauth F (1936) Aptychenstudien VIII. Die Laevilamellaptychi des Oberjura und der Unterkreide. Annalen des Naturhistorischen Museums in Wien 47:127–145

Triebold S, Kronz A, Wörner G (2006) Anorthite-calibrated backscattered electron profiles, trace elements, and growth textures in feldspars from the Teide–Pico Viejo volcanic complex (Tenerife). J Volcanol Geotherm Res 154(1-2):117–130. doi:10.1016/j.jvolgeores.2005.09.023

Tucholke BE, Vogt PR (1979) Western North Atlantic. Sedimentary Evolution and Aspects of Tectonic History. In: Tucholke B, Vogt P (eds). U.S. Government Printing Office, pp 791–825

Tucholke BE, Vogt PR, Demars KR, Galehouse JS, Houghton RL, Kaneps A, Kendrick JW, McCave IN, McNulty CL, Murdmaa IO, Okada H, Rothe P (1979) Site 387. Cretaceous to Recent Sedimentary Evolution of the Western Bermuda Rise. In: Tucholke B, Vogt P (eds). U.S. Government Printing Office, pp 323–391

Turner S, Costa F (2007) Measuring Timescales of Magmatic Evolution. Elements 3(4):267–272. doi:10.2113/gselements.3.4.267

Urlaub M, Petersen F, Gross F, Bonforte A, Puglisi G, Guglielmino F, Krastel S, Lange D, Kopp H (2018) Gravitational collapse of Mount Etna's southeastern flank. Sci Adv 4(10):eaat9700. doi:10.1126/sciadv.aat9700

Valderrama Murillo P (2016) Origin and dynamics of volcanic debris avalanches: surface structure analysis of Tutucapa volcano (Peru). Doctoral Thesis, Université Blaise Pascal

van den Bogaard P (2013) The origin of the Canary Island Seamount Province - New ages of old seamounts. Sci Rep 3(1):58. doi:10.1038/srep02107

van Hinte JE, Wise SW, Biart B, Cowington JM, Dunn DA, Haggerty A, Johns MW, Meyers PA, Arbor A, Moullade MR, Muza JP, Ogg J, Okamura M, Sarti M, Rad U von (1987) Site 603. In: van Hinte J, Wise S, Jr. ea (eds) DSDP Initial Reports vol. 93. U.S. Government Printing Office, Washington, USA, pp 25–276

van Wyk de Vries B, Davies T (2015) Landslides, debris avalanches, and volcanic gravitational deformation. In: Sigurdsson H (ed) Encyclopedia of volcanoes, Second edition. Academic Press, San Diego, pp 665–685

van Wyk de Vries B, Delcamp A (2015) Volcanic debris avalanches. In: Davies T, Shroder JF (eds) Landslide hazards, risks, and disasters. Elsevier Science, Amsterdam, pp 131–157

Wade BS, Pearson PN, Berggren WA, Pälike H (2011) Review and revision of Cenozoic tropical planktonic foraminiferal biostratigraphy and calibration to the geomagnetic polarity and astronomical time scale. Earth-Sci Rev 104(1-3):111–142. doi:10.1016/j.earscirev.2010.09.003

Waelbroeck C, Labeyrie L, Michel E, Duplessy JC, McManus JF, Lambeck K, Balbon E, Labracherie M (2002) Sea-level and deep water temperature changes derived from benthic foraminifera isotopic records. Quat Sci Rev 21(1-3):295–305. doi:10.1016/S0277-3791(01)00101-9

Wallmann K, Flögel S, Scholz F, Dale AW, Kemena TP, Steinig S, Kuhnt W (2019) Periodic changes in the Cretaceous ocean and climate caused by marine redox see-saw. Nat Geosci 12(6):456–461. doi:10.1038/s41561-019-0359-x

Wartho J-A, Kelley SP, Brooker RA, Carroll MR, Villa IM, Lee MR (1999) Direct measurement of Ar diffusion profiles in a gem-quality Madagascar K-feldspar using the ultra-violet laser ablation microprobe (UVLAMP). Earth Planet Sci Lett 170(1-2):141–153. doi:10.1016/S0012-821X(99)00088-6

Watt S, Talling P, Hunt J (2014) New insights into the emplacement dynamics of volcanic island landslides. Oceanog 27(2):46–57. doi:10.5670/oceanog.2014.39

Wieczorek J (1988) Maiolica - a unique facies of the western tethys. Annales Societatis Geologorum Poloniae 58:255–276

Wiedmann J (1979) Early Cretaceous Mollusks from DSDP Hole 397A off Northwest Africa. In: Rad U von, Ryan W (eds) DSDP Initial Reports vol. 47. U.S. Government Printing Office, Washington, USA, pp 283–287

Wilson DJ, Peirce C, Watts AB, Grevemeyer I, Krabbenhoeft A (2010) Uplift at lithospheric swells - I. Seismic and gravity constraints on the crust and uppermost mantle structure of the Cape Verde mid-plate swell. Geophys J Int 182(2):531–550. doi:10.1111/j.1365-246X.2010.04641.x

York D, Macintyre RM, Gittins J (1969) Excess radiogenic ^{40}Ar in cancrinite and sodalite. Earth Planet Sci Lett 7(1):25–28. doi:10.1016/0012-821X(69)90006-5

Young JR, Bown PR, Lees JA (2017) Nannotax3 website. http://www.mikrotax.org/Nannotax3/. Accessed 01 Apr 2019

Zavala C, Arcuri M (2016) Intrabasinal and extrabasinal turbidites. Origin and distinctive characteristics. Sediment Geol 337:36–54. doi:10.1016/j.sedgeo.2016.03.008

Zellmer GF, Clavero JE (2006) Using trace element correlation patterns to decipher a sanidine crystal growth chronology. An example from Taapaca volcano, Central Andes. J Volcanol Geotherm Res 156(3-4):291–301. doi:10.1016/j.jvolgeores.2006.03.004

8 Acknowledgements

Working on this thesis was a great experience. There are many people who supported and encouraged me on my way to finishing this thesis, but also who made Kiel a wonderful place to live.

First of all, I would like to thank Thor Hansteen – thank you for your guidance and supervision during the last years. Your door was always open and I learned a lot during our numerous discussions and brainstorming sessions, thanks to your patient explanations. Our travels to volcanic islands and conferences were a great experience in many ways. Thank you for your encouragement to initiate expeditions and conference sessions, for your trust, commitment and support!

I would also like to thank Christian Dullo. It was an honour to be able to work and to travel to the Cabo Verdes with you. Thank you for your enthusiasm, especially in the field. Thank you also for your support and encouragement during the whole project and for all your inspiration!

Jo-Anne Wartho, thank you for helping me produce more ^{40}Ar-^{39}Ar ages than published in your own PhD thesis! You never lost your humour, despite all the challenges and frustrations in the lab! Thank you also for your thorough and detailed reviews of our manuscripts, which sometimes made me swear but always improved my writing, figures and analytical skills. Thank you also for one or the other "SplishySplashy"-Friday evening wine! Cheers, Jo!

Meike Klischies, thank you for countless coffees after lunch, discussions and conversations. Thank you also for your thorough revisions of early stage manuscripts and careful proof reading this thesis. I am glad you showed me that Kiel can be a great place to live.

This thesis was conducted within the framework of the Helmholtz Research School for Ocean System Science and Technology (HOSST), and in cooperation with the Canadian partner TOSST. First of all, I would like to thank the HOSST-speakers Christian Dullo and Colin Devey, and the TOSST-speakers Douglas Wallace and Markus Kienast, for initiating this research school. Thank you for financing my research, several visits of conferences, and summer schools. It was a wonderful experience and a huge opportunity to be part of such an interdisciplinary program. Christel van den Bogaard deserves a special thank you for coordinating the program and organising seminar series, great retreats and fantastic summer schools. Without you, most things would not have worked. I would also like to thank all fellow HOSSTies and TOSSTies for making this program such a memorable and fun time, for building bridges and foster friendships. Thank you, Mladen Nedimović, for being part of my thesis committee and your support from across the Atlantic!

Being part of the GEOMAR DokTeam was a fantastic experience and I am proud we actually achieved so much. Thank you, Meike, Dagmara, Jacky, Kristin, Luisa, Christian, Thea, and Caro for all your effort and commitment. We were great teams and it was fun working with you! It was also a great experience to be part of Helmholtz Juniors and represent the GEOMAR doctoral researchers. Thank you especially, Dagmara Rusiecka, who invited me to become part of this nationwide interdisciplinary network.

Mario Thöner is thanked for help with EMP analyses and several hours of calibrating measurements. Birgit Mohr from the Institute of Geosciences at University Kiel, and Christin Szillus from the Institute of Material Sciences at University Kiel are thanked for assistance with SEM imaging. Jan Stiklus is thanked for assistance in the ARGO-lab.

I would like to thank Daniel Bernoulli for his support for our biostratigraphy work on Maio, his input and comments and for providing unpublished material.

There are many people who supported the field work on Maio and our expeditions to the Cabo Verde Islands. I would like to thank Tatjana Cabral, Ivanice Monteiro and Bruno Faria for teaching more about the Cabo Verde geology, ecology and culture. I would also like to thank the OSCM in Mindelo and Cordula Zenk for logistical support.

Ricardo Ramalho, thank you for valuable discussions and your thorough revisions of some of my manuscripts. I learned a lot about Cabo Verdean geology from you! Thank you also for your

willingness to become my co-convener and your enthusiasm to organize an ocean island geology session at AGU in Washington DC, together with Thor Hansteen and Dennis Geist.

I would like to thank Abigail Barker for her encouragement and support, which actually made me move from Sweden to Kiel. Thank you also for your thorough manuscript reviews, which always improved my writing.

I would like to thank the whole FB4 at GEOMAR, especially muhs-v and mmr. It was great to work with and learn from you! Dominik Pałgan and Tatum Miko Herrero: it was a pleasure to share an office and a coffee machine with you! I hope you are doing well in your new positions. Torsten Lux, without your help with sample preparations, things would have taken much longer. Thank you for your careful lab work! I would also like to thank Karin Junge for help in the labs. Many more people at GEOMAR supported me and my work. Thank you for this great ocean science experience. I hope our paths cross again in the future!

Last but not least I would like to thank Mirco and Frederick for all their support. Thank you for letting me do "my thing" and travel the world. Thank you for countless hours on trains between Kiel and Berlin and numerous Vater-Sohn-Sunday afternoons. Without your love, support and tolerance, this thesis would never have come to an end..

9 Appendices

9.1 List of conference abstracts

Wartho, JA, **Samrock L** and Hansteen T (2019) Antecrysts – angels or devils in $^{40}Ar/^{39}Ar$ geochronology? Examples from Cape Verde seamounts. GeoMünster 2019; 22.-25.09.2019, Münster, Germany.

Barker A, Weis F, Khadhem L, **Samrock L**, Hansteen T (2019) Volatile Contents Explain High Vesicularity of Deep Sea Eruptions. Goldschmidt Conference 2019, 18.-23.08.2019, Barcelona, Spain.

Samrock L, Wartho JA, Hansteen TH, Dullo C (2018) Crumbling Away: ^{40}Ar-^{39}Ar Dating of a Large Miocene Mass Wasting Period on Maio Island (Cape Verde). AGU Fall Meeting 2018, 10.-14.12.2018, Washington, D.C., USA.

Samrock L, Hansteen TH and Wartho JA (2017) ^{40}Ar-^{39}Ar age clustering in the active phonolitic Cadamosto Seamount (Cape Verdes): Indications for periodic magmatic activity. AGU Fall Meeting 2017, 11.12.-15.12.2017, New Orleans, USA.

Eisele S, **Samrock L**, Freundt A, Hansteen TH, Barker AK, Kutterolf S, Kwasnitschka T, Grevemeyer I (2017) Widespread (>100 km) Tephra from a Deep-Sea (>3000 mbsl) Eruption at the Cape Verde Archipelago, Central-East Atlantic Ocean. AGU Chapman Conference on Submarine Volcanism, 29.01.-03.02.2017, Hobart, Tasmania, Australia.

9.2 Appendices and supplementary data to Chapter 2

The data was published alongside the article (Samrock et al. 2019). Original Excel spreadsheets (Appendix B to D) are available online at: https://doi.org/10.1016/j.lithos.2019.07.003.

9.2.1 Appendix A – ^{40}Ar-^{39}Ar analytical methods

The rocks were crushed, dry sieved to obtain fractions of 250-500 µm, 500-1000 µm, and > 1 mm, and cleaned with distilled water in an ultrasonic bath. Similar to the technique used by Koppers et al. (2000) for acid leaching on basaltic groundmass samples, our 149-2, 152-1, 035ROV-12 and 037DR-2 samples were treated for (1) one hour with 3.5 M HCl acid in an ultrasonic bath heated at 65°C, followed by (2) repeated rinsing of the sample with distilled water and one hour ultrasonic treatment at 65°C with distilled water, (3) drying in a 50°C oven overnight. The hot HCl acid treatment dissolved sodalite, decomposed leucite, and turned nepheline into a gel, yielding pure sanidine separates. The separates were carefully hand-picked under a binocular microscope. The mineral separates were then additionally treated for 10 minutes in 5% HF acid, rinsed with distilled water, cleaned with distilled water for four minutes using an ultrasonic stick, and dried overnight in a 50°C oven. Samples 149-2, 152-1, 035ROV-12 and 037DR-2 were finally cleaned in American Chemical Society (ACS) grade acetone, followed by rinsing in distilled water and drying at 50°C oven overnight.

Approximately 20-30 mg of each unknown sample was loaded into appropriately sized holes in 20 mm diameter 99.999% aluminum disks, which were stacked and bolted together, and then sealed within a 99.9 % Al canister to make up the irradiation package. Grains of Taylor Creek sanidine (TCR-2) age standard (27.87 ± 0.04 Ma, 1σ error; M.A. Lanphere, pers. comm.) were regularly interspersed in the aluminum disks with the unknown samples to monitor the fast neutron gradient. The samples mentioned in this study were irradiated in two different irradiation canisters, in two different reactors: Sample 149-6 was irradiated in the NRG Petten reactor (position P3) in The Netherlands for one hour in 2012. The second irradiation canister (samples 149-2, 152-1, 035ROV-12, and 037DR-2) was irradiated with fast neutrons in the Cadmium-Lined In-Core Irradiation Tube (CLICIT) reactor core position for seven minutes at the Oregon State University nuclear reactor, Corvallis, USA.

Upon return of the irradiation canisters, grains of the age standard (multi-grains) and samples (single grains) were loaded into ~2 mm holes in 142-hole aluminum laser palettes. A laser palette and glass coverslips were loaded into an ultra-high vacuum 4.5" laser chamber fitted with a Kovar viewport that was baked at 230°C, and the whole extraction line was baked in an oven at 195°C for eight hours, and then pumped for two days to remove adsorbed atmospheric argon from the samples and chamber walls.

A 25 W Coherent Sabre 25TSM argon ion laser (λ = 455-515 nm) with a computer-controlled isel X-Y stage, was used to totally fuse the single grain unknown and multi-grain age standard samples for 45 seconds, with a 0.25-1.0 mm diameter laser beam. The laser system was fitted with a binocular microscope and light source for sample illumination and X-Y stage calibration, and a camera for video recording of the laser heating of each sample.

The gases released by laser total fusion were cleaned for a total of three minutes using an automatically-refilling liquid nitrogen Dewar attached to a glass finger, and two SAES AP10 getter pumps (one at 400°C and one at room temperature) to remove all active gases. The remaining noble gases were equilibrated into a high sensitivity Mass Analyser Products (MAP) 216 mass spectrometer with a mass resolution of 237, fitted with a Bauer-Signer-type source, operated at an emission current of 240 µA, with a Becton Dickinson MM-1 Mesh electron multiplier, and a mass spectrometer sensitivity of 1.203 x 10^{-14} moles/V (samples 149-6, 149-2, 152-1, and 037DR-2), and 1.211 x 10^{-14} moles/V (sample 035ROV-12).

The five Ar isotopes (^{36}Ar to ^{40}Ar) and six baselines (masses 35.5 to 40.5) were measured for blanks, age standards, airs, and unknown samples via peak-hoping using a single electron multiplier. The extraction line to mass spectrometer equilibration time was 30 seconds, which was followed by peak centering routine(s) that took 15-22 seconds. The 11 cycles of raw intensity data were extrapolated back to time-zero (i.e., when the inlet valve between the extraction line and the mass

spectrometer opened). The fully automated laser heating, X-Y stage movement, automated valves operation, and data acquisition were computer controlled using a Turbo Pascal program. System blank Ar isotope measurements were obtained during the unknown sample analyses, after every five unknown analyses, and are shown in **Appendix 9.2.3**.

Unknown analyses were corrected for (1) peak tails from adjoining Ar peaks, (2) baselines, (3) blanks, (4) mass spectrometer discrimination using a power law mass discrimination factor of 1.0098 ± 0.21% (1σ) per atomic mass unit, measured from air pipette shots and modern glasses, and (5) nuclear interference correction factors (Wijbrans et al. 2007) for sample 149-6, and (Renne et al. 2013, 2015) for samples 149-2, 152-1, 035ROV-12 and 037DR-2; Appendix 9.2.3). Errors are quoted at %1σ and 2σ levels in Appendix 9.2.3, and the ^{40}Ar-^{39}Ar ages were calculated using the ^{40}K decay constants ($^{40}K_{\beta-}$ = 4.962 x 10^{-10} years, $^{40}K_e$ + $^{40}K_{e'}$ = 5.810 x 10^{-11} years, and a total ^{40}K λ = 5.543 x 10^{-10} years), a ^{40}K/K ratio of 0.01167, and a ^{40}Ar/^{36}Ar atmospheric ratio of 295.5 (Steiger and Jäger 1977). Other decay constants used include ^{39}Ar = 2.941 x 10^{-7} hours (± 0.558 % 1σ; Stoenner et al. 1965), ^{37}Ar = 8.262 x10^{-4} hours (± 0.229 % 1σ; Renne and Norman 2001), and ^{36}Cl = 2.257 x 10^{-6} years (± 0.65% 1σ; Renne et al. 2008). The ingrowth of ^{36}Ar from the decay of ^{36}Cl was corrected using the ^{36}Cl/^{38}Cl production ratio of 262.8 ± 1.7 (1σ; Renne et al. 2008). The $\mathcal{J}$ values and 1σ errors for each unknown sample are noted in the sample ^{40}Ar/^{39}Ar data tables in **Appendix 9.2.3**.

The corrections and age determinations, and plateau and inverse isochron plots for the individual samples and combined samples were all made using the ArArCALC Excel macro program (v. 2.5.2) developed by Koppers (2002). All errors in the manuscript are quoted at 2σ levels, unless otherwise stated, and include the $\mathcal{J}$ value errors and error magnification factors for MSWD values >1 (Appendix 9.2.3). Alteration index (AI) values were used as a guide to gauge the alteration/freshness of the sanidine analyses, and were calculated using the criteria of Baksi (2007), with the ^{36}Ar/^{39}Ar AI-cut-off value of < 0.00006 for K-feldspar (van den Bogaard 2013).

The weighted mean ages (**Table 2.2**; Appendix 9.2.3) were defined by statistical analysis of the ^{40}Ar-^{39}Ar data including; 1) outlier identification using the Isoplot software of Ludwig (2011), and/or 2) fits of the ^{40}Ar-^{39}Ar analyses to inverse isochron plots (Appendix 9.2.3). Statistical information is provided to verify the weighted mean and inverse isochron ages, including the Mean Square Weighted Deviation (MSWD) and Probability (P; in %) values, and the number of analyses in the weighted mean/inverse isochron age determination (*n*), plus the ^{40}Ar/^{36}Ar$_i$ ratios and the Spreading Factor (SF; in %; Jourdan et al. 2009) values for the inverse isochron data.

Our SCTF data is presented in stacked age plots with 2σ errors, and using inverse isochron plots (**Fig. 2.7;** Appendix 9.2.3). Data from the single-/multi-grain step heating analyses are shown in age spectra and inverse isochrons plots (Appendix 9.2.3).

References

Baksi AK (2007) A quantitative tool for detecting alteration in undisturbed rocks and minerals—I. Water, chemical weathering, and atmospheric argon. In: Foulger GR, Jurdy DM (eds) Plates, Plumes and Planetary Processes. Geol Soc Am Spec Pap, 430:285–303

Jourdan F, Renne PR, Reimold WU (2009) An appraisal of the ages of terrestrial impact structures. Earth Planet Sci Lett 286(1-2):1–13. doi:10.1016/j.epsl.2009.07.009

Koppers A (2002) ArArCALC—software for $^{40}Ar/^{39}Ar$ age calculations. Comput Geosci 28(5):605–619. doi:10.1016/S0098-3004(01)00095-4

Koppers A, Staudigel H, Wijbrans JR (2000) Dating crystalline groundmass separates of altered Cretaceous seamount basalts by the $^{40}Ar/^{39}Ar$ incremental heating technique. Chem Geol 166(1-2):139–158. doi:10.1016/S0009-2541(99)00188-6

Ludwig K (2011) User's Manual for Isoplot 4.15. a Geochronological Toolkit for Microsoft Excel 4:77p.

Renne PR, Deino AL, Hilgen FJ, Kuiper KF, Mark DF, Michell, W.S., Morgan, L.E., Mundil, R., Smit J (2013) Time scales of critical events around the Cretaceous-Paleogene boundary. Science 339:463–466. doi:10.1126/science.1230492

Renne PR, Norman EB (2001) Determination of the half-life of ^{37}Ar by mass spectrometry. Phys. Rev. C 63(047302):1–3. doi:10.1103/PhysRevC.63.047302

Renne PR, Sharp ZD, Heizler MT (2008) Cl-derived argon isotope production in the CLICIT facility of OSTR reactor and the effects of the Cl-correction in $^{40}Ar/^{39}Ar$ geochronology. Chem Geol 255(3-4):463–466. doi:10.1016/j.chemgeo.2008.07.014

Renne PR, Sprain CJ, Richards MA, Self S, Vanderkluysen L, Pande K (2015) State shift in Deccan volcanism at the Cretaceous-Paleogene boundary, possibly induced by impact. Science 350(6256):76–78. doi:10.1126/science.aac7549

Steiger RH, Jäger E (1977) Subcommission on geochronology. Convention on the use of decay constants in geo- and cosmochronology. Earth Planet Sci Lett 36(3):359–362. doi:10.1016/0012-821X(77)90060-7

Stoenner RW, Schaeffer OA, Katcoff S (1965) Half-Lives of Argon-37, Argon-39, and Argon-42. Science 148(3675):1325–1328. doi:10.1126/science.148.3675.1325

van den Bogaard P (2013) The origin of the Canary Island Seamount Province - New ages of old seamounts. Sci Rep 3(1):58. doi:10.1038/srep02107

Wijbrans J, Németh K, Martin U, Balogh K (2007) $^{40}Ar/^{39}Ar$ geochronology of Neogene phreatomagmatic volcanism in the western Pannonian Basin, Hungary. J Volcanol Geotherm Res 164(4):193–204. doi:10.1016/j.jvolgeores.2007.05.009

9.2.2 *Appendix B – EMP data for sanidines from five Cadamosto Seamount samples, and nepheline and sodalite data from sample 149-6*

EMP analyses of sample 149-2 sanidines

data: rim data (10µm from rim); or microcryst data (separate points within microcrysts, label: gm)

Sample	Oxide (wt%)									normalized values			
	Na2O	K2O	FeO	SiO2	CaO	MgO	Al2O3	TiO2	Sum	Or (mol%)	An (mol%)	Ab (mol%)	K (wt%)
149-2b_san7_rim1_2	2.24	13.51	0.38	64.14	0.02	0.00	18.98	0.04	99.30	79.80	0.09	20.11	11.29
149-2b_san7_rim2_3	3.00	12.46	0.54	64.55	0.03	0.00	19.04	0.04	99.67	73.10	0.16	26.74	10.38
149-2b_san8_rim1_1	2.46	13.34	0.44	64.36	0.01	0.00	18.98	0.04	99.63	78.08	0.04	21.88	11.12
149-2b_san8_rim2_2	2.34	13.29	0.45	63.88	0.00	0.00	19.14	0.02	99.13	78.89	0.00	21.11	11.13
149-2b_san13_rim1_1	2.16	13.78	0.49	64.25	0.02	0.00	19.06	0.04	99.79	80.69	0.08	19.23	11.46
149-2b_san13_rim2_2	2.37	13.21	0.52	63.88	0.21	0.00	19.16	0.21	99.57	77.77	1.03	21.20	11.02
149-2b_san15_gm1	2.21	13.60	0.48	64.37	0.01	0.00	18.94	0.04	99.66	80.14	0.07	19.79	11.33
149-2b_san15_gm2	2.32	13.36	0.53	64.18	0.05	0.00	18.81	0.06	99.31	78.92	0.25	20.82	11.17
149-2b_san15_gm3	2.33	13.22	0.51	63.91	0.05	0.01	19.29	0.02	99.34	78.68	0.24	21.08	11.04
149-2b_san16_rim1_1	2.33	13.38	0.48	64.33	0.02	0.00	19.08	0.04	99.66	78.99	0.11	20.90	11.15
149-2b_san17_gm3	2.44	13.14	0.53	63.95	0.07	0.01	19.29	0.02	99.45	77.73	0.33	21.94	11.10
149-2b_san18_gm1	2.67	12.69	0.56	64.28	0.07	0.00	19.24	0.05	99.55	75.51	0.33	24.15	10.58
149-2b_san18_gm2	2.44	13.08	0.61	63.99	0.04	0.00	19.25	0.00	99.41	77.77	0.19	22.05	10.92
149-2b_san18_gm3	2.54	12.78	0.57	64.08	0.04	0.00	19.15	0.02	99.17	76.64	0.20	23.16	10.69
149-2b_san20_gm1	2.36	13.45	0.48	64.08	0.03	0.00	19.19	0.03	99.62	78.84	0.14	21.03	11.21
149-2b_san20_gm2	2.34	13.01	1.01	63.52	0.52	0.18	18.82	0.05	99.46	76.52	2.56	20.91	10.86
149-2b_san20_gm3	2.36	13.26	0.59	63.87	0.02	0.00	19.25	0.03	99.38	78.62	0.12	21.26	11.08
149-2b_san20_gm4	3.11	12.26	0.62	63.81	0.05	0.00	19.22	0.06	99.13	71.99	0.25	27.76	10.26
149-2b_san23_rim1_3	2.43	13.53	0.50	64.37	0.01	0.00	18.93	0.04	99.81	78.54	0.03	21.43	11.26
149-2b_san23_rim2	2.30	13.50	0.51	63.92	0.02	0.00	19.08	0.03	99.36	79.36	0.10	20.54	11.28

EMP analyses of sample 149-6 sanidines

data: rim data (10µm from rim); core data (crystal center); or microcryst data (separate points within microcrysts, label: gm)

Sample	Oxide (wt%)									normalized values			
	Na_2O	K_2O	FeO	SiO_2	CaO	MgO	Al_2O_3	TiO_2	Sum	Or (mol%)	An (mol%)	Ab (mol%)	K (wt%)
149-6_san9_gm_p1	2.80	12.61	0.43	63.43	0.06	0.00	19.63	0.03	98.99	74.54	0.29	25.16	10.58
149-6_san9_gm_p3	2.69	12.54	0.48	63.76	0.05	0.00	19.38	0.02	98.92	75.18	0.28	24.54	10.52
149-6_san9_gm_p4	2.43	13.28	0.48	64.39	0.01	0.00	19.05	0.02	99.65	78.21	0.04	21.74	11.06
149-6_san11_gm_p2	2.57	12.82	0.49	64.82	0.07	0.00	19.25	0.02	100.04	76.41	0.33	23.27	10.64
149-6_san11_gm_p3	2.63	12.28	0.85	63.37	0.28	0.23	19.09	0.07	98.80	74.39	1.42	24.19	10.32
149-6_san11_gm_p5	2.45	13.51	0.48	65.42	0.00	0.02	19.02	0.05	100.95	78.38	0.00	21.62	11.11
149-6_san12_gm_p1	2.48	13.39	0.55	65.31	0.00	0.02	19.02	0.04	100.81	78.02	0.00	21.98	11.03
149-6_san12_gm_p2	2.63	12.99	0.75	64.82	0.27	0.07	19.01	0.04	100.57	75.48	1.31	23.21	10.72
149-6_san12_gm_p3	2.69	12.92	0.57	64.68	0.06	0.00	18.89	0.09	99.90	75.77	0.28	23.96	10.74
149-6_san12_gm_p4	2.65	12.91	0.60	64.77	0.04	0.00	19.12	0.04	100.13	76.09	0.17	23.73	10.70
149-6_san12_gm_p5	2.70	13.09	0.80	64.18	0.05	0.00	19.40	0.09	100.31	75.96	0.24	23.80	10.83
149-6_san14_gm_p1	2.48	13.25	0.53	65.16	0.00	0.00	18.96	0.03	100.41	77.81	0.02	22.18	10.95
149-6_san14_gm_p2	2.53	13.35	0.52	65.50	0.00	0.00	19.06	0.05	101.02	77.61	0.00	22.39	10.97
149-6_san14_gm_p3	2.47	13.36	0.48	65.54	0.01	0.02	18.96	0.04	100.87	78.06	0.05	21.89	10.99
149-6_san14_gm_p4	2.42	13.07	0.58	64.75	0.62	0.00	18.52	0.78	100.74	75.70	3.03	21.27	10.77
149-6_san14_gm_p5	2.54	13.22	0.54	65.25	0.00	0.00	18.95	0.05	100.55	77.36	0.00	22.63	10.91
149-6_san12b_gm_p1	2.34	13.23	0.43	64.02	0.01	0.00	18.99	0.01	99.03	78.81	0.03	21.16	11.09
149-6_san12b_gm_p2	2.50	12.54	0.50	63.82	0.12	0.00	19.56	0.02	99.06	76.26	0.59	23.15	10.51
149-6_san12b_gm_p3	2.33	13.17	0.52	64.13	0.03	0.00	19.39	0.01	99.59	78.68	0.16	21.16	10.98
149-6_san13_gm_p4	2.28	13.36	0.56	62.20	0.01	0.00	19.18	0.04	97.63	79.33	0.07	20.60	11.36

149-6_san13_gm_p5	2.29	12.79	0.84	63.48	0.04	0.49	18.57	0.04	98.54	78.42	0.20	21.38	10.77
149-6_san13_gm_p6	2.34	13.08	0.51	62.17	0.08	0.00	19.13	0.10	97.40	78.29	0.39	21.32	11.14
149-6_san15_gm_p1	2.48	12.94	0.53	63.63	0.03	0.00	19.32	0.03	98.96	77.30	0.17	22.53	10.85
149-6_san15_gm_p2	2.39	13.01	0.55	63.31	0.07	0.00	19.49	0.03	98.86	77.87	0.36	21.78	10.93
149-6_san15_gm_p3	2.28	13.45	0.51	63.21	0.07	0.00	19.15	0.06	98.72	79.25	0.35	20.41	11.31
149-6_san16_core_p1	2.54	13.17	0.63	63.63	0.02	0.01	18.95	0.03	98.98	77.26	0.11	22.62	11.05
149-6_san16_core_p2	2.52	13.26	0.56	63.80	0.01	0.00	18.76	0.03	98.94	77.57	0.04	22.39	11.12
149-6_san16_core_p3	2.48	13.00	0.62	63.36	0.23	0.00	18.78	0.26	98.74	76.64	1.16	22.20	10.93
149-6_san16_core_p4	2.57	12.89	0.65	63.25	0.05	0.00	19.33	0.04	98.77	76.57	0.26	23.17	10.83
149-6_san16_core_p5	2.55	12.96	0.47	63.84	0.04	0.01	19.33	0.01	99.19	76.88	0.17	22.95	10.85
149-6_san16_core_p6	2.61	12.99	0.46	63.83	0.01	0.00	19.18	0.03	99.12	76.54	0.06	23.39	10.88
149-6_san17_gm_p1	2.48	13.41	0.65	63.99	0.00	0.00	18.62	0.03	99.18	78.10	0.00	21.90	11.23
149-6_san17_gm_p2	2.51	13.27	0.55	64.00	0.00	0.01	18.68	0.04	99.07	77.63	0.02	22.35	11.12
149-6_san18_rim_p1	2.46	13.49	0.50	64.65	0.00	0.00	18.89	0.05	100.04	78.27	0.00	21.73	11.19
149-6_san18_core_p4	2.49	13.10	0.44	64.16	0.07	0.01	19.23	0.08	99.58	77.30	0.36	22.34	10.92
149-6_san18_core_p5	2.34	12.90	0.60	63.75	0.01	0.19	18.79	0.05	98.64	78.31	0.07	21.62	10.86

EMP analyses of sample 152-1 sanidines

data: profiles (rim to rim full transects)

Sample	Oxide (wt%)									normalized values				Full transects: profile distance to first rim (mm)
	Na2O	K2O	FeO	SiO2	CaO	MgO	Al2O3	TiO2	Sum	Or (mol%)	An (mol%)	Ab (mol%)	K (wt%)	
152-1_san1_prof1	2.39	13.45	0.48	64.41	0.00	0.00	18.39	0.01	99.13	78.74	0.00	21.26	11.26	0.00
152-1_san1_prof2	2.36	13.53	0.34	64.27	0.00	0.00	18.46	0.01	98.98	79.05	0.00	20.95	11.35	0.05
152-1_san1_prof3	2.38	13.48	0.31	64.74	0.00	0.00	18.45	0.02	99.39	78.84	0.00	21.16	11.26	0.11
152-1_san1_prof4	2.40	13.55	0.30	64.64	0.00	0.00	18.40	0.01	99.30	78.79	0.00	21.21	11.33	0.17
152-1_san1_prof5	2.37	13.51	0.22	64.54	0.00	0.00	18.33	0.01	98.98	78.95	0.00	21.05	11.33	0.21
152-1_san1_prof6	2.36	13.59	0.34	64.64	0.00	0.01	18.25	0.01	99.20	79.12	0.00	20.88	11.37	0.25
152-1_sanx4_prof1	2.38	13.56	0.46	64.44	0.00	0.00	18.55	0.02	99.41	78.94	0.00	21.06	11.32	0.00
152-1_sanx4_prof2	2.34	13.38	0.36	64.10	0.00	0.01	18.33	0.01	98.53	79.00	0.00	21.00	11.27	0.03

152-1_sanx4_prof3	2.38	13.50	0.30	64.30	0.00	0.00	18.46	0.01	98.96	78.87	0.00	21.13	11.33	0.06
152-1_sanx4_prof4	2.37	13.54	0.33	64.48	0.00	0.00	18.35	0.02	99.09	78.99	0.00	21.01	11.34	0.10
152-1_sanx4_prof5	2.42	13.60	0.29	64.60	0.00	0.00	18.57	0.02	99.50	78.71	0.00	21.29	11.35	0.13
152-1_sanx5_prof1	2.44	13.50	0.35	64.67	0.00	0.00	18.35	0.03	99.34	78.45	0.00	21.55	11.28	0.00
152-1_sanx5_prof2	2.39	13.58	0.38	64.73	0.00	0.00	18.66	0.02	99.76	78.90	0.00	21.10	11.30	0.03
152-1_sanx5_prof3	2.36	13.48	0.32	64.68	0.00	0.00	18.54	0.00	99.38	78.98	0.00	21.02	11.26	0.08
152-1_sanx5_prof4	2.36	13.48	0.34	64.46	0.00	0.00	18.44	0.02	99.10	78.98	0.00	21.02	11.29	0.13
152-1_sanx5_prof5	2.37	13.49	0.36	64.44	0.00	0.00	18.40	0.01	99.07	78.93	0.00	21.07	11.30	0.16
152-1_sanx5_prof6	2.38	13.51	0.33	64.61	0.00	0.00	18.40	0.01	99.24	78.88	0.00	21.12	11.30	0.20
152-1_sanx5_prof7	2.40	13.51	0.36	64.49	0.00	0.00	18.58	0.01	99.34	78.74	0.00	21.26	11.29	0.22
152-1_sanx8_prof1	2.56	13.37	0.72	64.30	0.00	0.00	18.73	0.04	99.71	77.46	0.01	22.54	11.13	0.00
152-1_sanx8_prof2	2.10	14.00	0.56	64.64	0.00	0.00	18.51	0.02	99.83	81.44	0.00	18.56	11.64	0.02
152-1_sanx8_prof3	2.17	13.76	0.52	64.50	0.00	0.00	18.60	0.04	99.59	80.67	0.00	19.33	11.47	0.04
152-1_sanx8_prof4	2.28	13.72	0.54	64.36	0.00	0.00	18.67	0.03	99.60	79.83	0.01	20.16	11.44	0.06
152-1_sanx8_prof5	2.34	13.54	0.54	64.12	0.41	0.00	18.16	0.09	99.21	77.62	2.00	20.39	11.33	0.08
152-1_sanx9_prof1	2.42	13.52	0.47	64.86	0.00	0.00	18.49	0.03	99.79	78.61	0.00	21.39	11.25	0.00
152-1_sanx9_prof2	2.30	13.52	0.53	64.62	0.00	0.00	18.46	0.01	99.44	79.46	0.00	20.54	11.29	0.02
152-1_sanx9_prof3	2.41	13.46	0.40	64.54	0.00	0.00	18.64	0.01	99.46	78.61	0.00	21.39	11.23	0.04
152-1_san10_prof1	2.40	13.49	0.42	64.57	0.01	0.00	18.55	0.02	99.46	78.41	0.00	21.59	11.03	0.00
152-1_san10_prof2	2.40	13.40	0.42	64.60	0.00	0.00	18.46	0.00	99.28	77.96	0.00	22.04	10.92	0.03
152-1_san10_prof3	2.36	13.41	0.37	64.40	0.00	0.00	18.45	0.01	99.00	78.57	0.00	21.43	11.05	0.08
152-1_san10_prof4	2.29	13.23	0.36	63.66	0.00	0.02	18.22	0.00	97.79	78.10	0.00	21.90	11.00	0.14
152-1_san10_prof5	2.35	13.47	0.31	64.61	0.00	0.00	18.26	0.02	99.02	77.97	0.00	22.03	10.99	0.23
152-1_san10_prof6	2.37	13.47	0.33	64.70	0.00	0.00	18.48	0.01	99.35	77.92	0.00	22.08	10.95	0.32
152-1_san10_prof7	2.38	13.50	0.31	64.57	0.00	0.00	18.38	0.01	99.15	77.98	0.00	22.02	10.93	0.48
152-1_san10_prof8	2.40	13.39	0.32	64.51	0.00	0.00	18.55	0.01	99.18	77.87	0.00	22.13	10.90	0.57
152-1_san10_prof9	2.43	13.31	0.52	64.05	0.00	0.00	18.80	0.01	99.13	77.55	0.00	22.45	10.88	0.62
152-1_sanx11_prof1	2.23	13.75	0.56	63.94	0.00	0.00	18.26	0.01	98.75	80.23	0.00	19.77	11.56	0.00
152-1_sanx11_prof2	2.19	13.78	0.49	63.98	0.00	0.00	18.17	0.02	98.63	80.55	0.00	19.45	11.60	0.02
152-1_sanx11_prof3	2.23	13.69	0.51	63.95	0.00	0.00	18.26	0.02	98.66	80.16	0.00	19.84	11.52	0.03
152-1_sanx11_prof4	2.23	13.64	0.51	63.55	0.00	0.01	18.65	0.03	98.62	80.10	0.00	19.90	11.48	0.06

152-1_sanx11_prof5	2.27	13.62	0.50	64.03	0.00	0.00	18.48	0.03	98.94	79.79	0.00	20.21	11.43	0.08
152-1_sanx11_prof6	2.29	13.56	0.55	64.29	0.00	0.00	18.47	0.03	99.19	79.58	0.00	20.42	11.35	0.10
152-1_sanx11_prof7	2.40	13.48	0.69	64.82	0.00	0.00	18.34	0.03	99.76	78.70	0.00	21.30	11.22	0.11
152-1_san14_prof1	2.57	13.18	0.68	63.86	0.01	0.01	18.34	0.03	98.67	77.11	0.03	22.85	11.09	0.00
152-1_san14_prof2	2.40	13.48	0.40	64.51	0.00	0.01	18.46	0.01	99.27	78.70	0.00	21.30	11.27	0.03
152-1_san14_prof3	2.34	13.48	0.30	64.65	0.00	0.00	18.32	0.01	99.10	79.12	0.00	20.88	11.29	0.07
152-1_san14_prof4	2.32	13.50	0.31	64.78	0.00	0.00	18.32	0.00	99.23	79.29	0.00	20.71	11.29	0.12
152-1_san14_prof5	2.35	13.52	0.33	64.68	0.00	0.00	18.42	0.01	99.32	79.10	0.00	20.90	11.30	0.16
152-1_san14_prof6	2.42	13.60	0.35	64.75	0.00	0.00	18.60	0.02	99.74	78.71	0.00	21.29	11.32	0.20
152-1_san14_prof7	2.36	13.53	0.36	64.58	0.00	0.00	18.49	0.00	99.32	79.05	0.00	20.95	11.31	0.23

EMP analyses of sample 035ROV-12 sanidines

data: profiles (rim to core)

Sample	Oxide (wt%)									normalized values				Distance to rim (mm)
	Na_2O	K_2O	FeO	SiO_2	CaO	MgO	Al_2O_3	TiO_2	Sum	Or (mol%)	An (mol%)	Ab (mol%)	K (wt%)	
035ROV12_san1_prof1	4.43	10.38	0.27	65.77	0.04	0.00	19.13	0.01	100.03	60.56	0.17	39.27	8.62	0.00
035ROV12_san1_prof2	4.66	10.11	0.23	65.72	0.02	0.00	19.17	0.01	99.91	58.73	0.11	41.16	8.40	0.03
035ROV12_san1_prof3	4.48	10.20	0.23	65.34	0.03	0.00	19.07	0.01	99.36	59.88	0.16	39.96	8.53	0.04
035ROV12_san1_prof4	4.62	10.18	0.22	65.63	0.03	0.00	19.14	0.01	99.84	59.11	0.14	40.75	8.47	0.06
035ROV12_san1_prof5	4.63	10.10	0.17	65.43	0.03	0.00	19.20	0.01	99.58	58.87	0.13	41.00	8.42	0.10
035ROV12_san1_prof6	4.61	10.11	0.20	65.54	0.04	0.00	19.16	0.03	99.69	58.97	0.18	40.85	8.42	0.19
035ROV12_san1_prof7	4.70	9.83	0.19	65.84	0.04	0.00	19.09	0.00	99.70	57.79	0.20	42.00	8.18	0.22
035ROV12_san1_prof8	4.51	10.22	0.17	65.94	0.04	0.00	19.10	0.00	99.99	59.73	0.22	40.05	8.49	0.30
035ROV12_san1_prof9	4.76	9.87	0.20	65.84	0.04	0.00	19.25	0.01	99.96	57.59	0.18	42.23	8.19	0.33
035ROV12_san1_prof10	4.64	10.13	0.21	66.23	0.02	0.00	19.15	0.00	100.38	58.90	0.10	41.00	8.38	0.40
035ROV12_san1_prof11	4.75	9.95	0.16	66.10	0.01	0.01	19.15	0.00	100.13	57.93	0.06	42.01	8.25	0.46
035ROV12_san1_prof12	4.95	9.66	0.13	66.00	0.03	0.00	18.99	0.00	99.76	56.15	0.12	43.73	8.04	0.50
035ROV12_san1_prof13	4.87	9.78	0.20	66.03	0.02	0.00	19.22	0.01	100.13	56.85	0.10	43.04	8.11	0.54
035ROV12_san1_prof14	4.68	9.95	0.20	65.62	0.02	0.00	18.98	0.01	99.47	58.27	0.09	41.64	8.31	0.58
035ROV12_san1_prof15	4.65	10.08	0.21	66.35	0.02	0.00	19.06	0.02	100.39	58.73	0.09	41.18	8.34	0.63

035ROV12_san1_prof16	4.90	9.72	0.20	66.36	0.02	0.00	18.96	0.00	100.15	56.56	0.08	43.35	8.05	0.67
035ROV12_san3_prof1	3.59	10.58	0.30	63.09	0.11	0.01	19.60	0.00	97.27	65.60	0.55	33.85	9.03	0.00
035ROV12_san3_prof2	3.45	10.45	0.16	62.46	0.12	0.00	19.74	0.00	96.38	66.15	0.65	33.20	9.00	0.02
035ROV12_san3_prof3	3.49	10.88	0.17	63.30	0.09	0.00	19.56	0.00	97.49	66.90	0.47	32.62	9.26	0.04
035ROV12_san3_prof4	3.51	10.70	0.19	63.43	0.11	0.00	19.61	0.00	97.55	66.37	0.55	33.08	9.11	0.07
035ROV12_san3_prof5	3.49	10.72	0.26	63.14	0.09	0.00	19.58	0.00	97.28	66.58	0.47	32.94	9.15	0.08
035ROV12_san3_prof6	3.55	10.86	0.28	63.72	0.09	0.01	19.68	0.00	98.18	66.48	0.48	33.04	9.18	0.13
035ROV12_san3_prof7	3.63	10.92	0.20	64.11	0.10	0.00	19.62	0.00	98.58	66.08	0.53	33.40	9.19	0.16
035ROV12_san3_prof8	3.59	10.79	0.20	63.73	0.11	0.00	19.65	0.00	98.06	66.04	0.56	33.40	9.13	0.18
035ROV12_san3_prof9	3.68	11.15	0.22	64.82	0.09	0.00	19.31	0.00	99.27	66.30	0.45	33.26	9.32	0.21
035ROV12_san3_prof10	3.68	11.26	0.16	64.84	0.07	0.00	19.32	0.00	99.33	66.57	0.35	33.07	9.41	0.26
035ROV12_san3_prof11	3.72	11.18	0.13	64.44	0.07	0.00	18.95	0.00	98.49	66.18	0.35	33.47	9.42	0.28
035ROV12_san3_prof12	3.75	11.08	0.18	64.78	0.09	0.00	19.35	0.00	99.23	65.75	0.42	33.82	9.27	0.31
035ROV12_san3_prof13	3.72	11.06	0.12	64.87	0.09	0.00	19.36	0.00	99.22	65.88	0.44	33.68	9.25	0.36
035ROV12_san3_prof14	3.67	11.21	0.25	64.70	0.08	0.00	19.25	0.00	99.15	66.51	0.38	33.11	9.38	0.40
035ROV12_san3_prof15	3.62	11.03	0.21	64.18	0.09	0.00	19.43	0.00	98.56	66.42	0.44	33.14	9.29	0.43
035ROV12_san3_prof16	3.66	11.02	0.17	63.86	0.09	0.00	19.49	0.00	98.29	66.16	0.44	33.40	9.31	0.52
035ROV12_san3_prof17	3.64	10.91	0.22	63.82	0.09	0.00	19.39	0.00	98.07	66.05	0.46	33.49	9.23	0.55
035ROV12_san3_prof18	3.57	10.84	0.18	63.46	0.09	0.00	19.40	0.00	97.54	66.34	0.46	33.20	9.23	0.58
035ROV12_san3_prof19	3.62	10.70	0.21	63.30	0.08	0.01	19.55	0.00	97.48	65.76	0.43	33.80	9.11	0.61
035ROV12_san3_prof20	3.64	10.73	0.19	63.56	0.08	0.00	19.56	0.00	97.76	65.71	0.42	33.87	9.11	0.64
035ROV12_san3_prof21	3.79	10.97	0.17	63.94	0.08	0.00	19.28	0.00	98.23	65.29	0.42	34.29	9.27	0.73
035ROV12_san3_prof22	3.71	10.97	0.20	64.20	0.08	0.00	19.49	0.00	98.64	65.78	0.40	33.82	9.23	0.80
035ROV12_san3_prof23	3.67	11.07	0.23	64.49	0.07	0.00	19.40	0.00	98.93	66.26	0.36	33.38	9.29	0.83
035ROV12_san3_prof24	3.72	11.08	0.15	64.31	0.07	0.00	19.29	0.00	98.63	66.00	0.34	33.67	9.33	0.86
035ROV12_san3_prof25	3.75	11.11	0.23	64.80	0.07	0.00	19.40	0.00	99.36	65.87	0.35	33.79	9.28	0.91
035ROV12_san3_prof26	3.75	11.07	0.22	64.86	0.08	0.00	19.34	0.00	99.32	65.74	0.42	33.84	9.25	0.93
035ROV12_san3_prof27	3.73	11.03	0.19	64.65	0.08	0.00	19.44	0.00	99.12	65.80	0.39	33.81	9.24	0.97
035ROV12_san3_prof28	3.71	11.04	0.18	64.23	0.08	0.00	19.42	0.00	98.65	65.94	0.38	33.68	9.29	1.01
035ROV12_san3_prof29	3.69	10.91	0.19	64.19	0.10	0.01	19.47	0.00	98.56	65.73	0.49	33.78	9.19	1.04
035ROV12_san5_prof1	3.81	9.98	0.31	63.01	0.17	0.00	19.77	0.00	97.04	62.72	0.89	36.40	8.54	0.00

035ROV12_san5_prof2	4.23	10.26	0.22	64.82	0.06	0.00	19.48	0.00	99.07	61.31	0.29	38.41	8.60	0.03
035ROV12_san5_prof3	4.17	10.23	0.21	64.99	0.05	0.00	19.44	0.00	99.10	61.60	0.25	38.15	8.57	0.07
035ROV12_san5_prof4	4.13	10.18	0.22	64.35	0.06	0.00	19.41	0.00	98.35	61.67	0.31	38.01	8.60	0.12
035ROV12_san5_prof5	4.11	10.79	0.18	65.67	0.01	0.00	19.08	0.02	99.87	63.30	0.07	36.64	8.97	0.17
035ROV12_san5_prof6	4.16	10.85	0.22	65.64	0.00	0.00	19.10	0.01	99.98	63.17	0.02	36.81	9.01	0.22
035ROV12_san5_prof7	4.16	10.87	0.18	65.78	0.01	0.00	19.04	0.02	100.06	63.18	0.07	36.75	9.02	0.25
035ROV12_san5_prof8	4.20	10.90	0.19	65.40	0.01	0.00	19.06	0.00	99.76	63.04	0.04	36.92	9.07	0.32
035ROV12_san5_prof9	4.07	10.97	0.18	65.72	0.00	0.00	18.99	0.02	99.94	63.93	0.02	36.05	9.11	0.37
035ROV12_san5_prof10	4.14	11.00	0.24	65.68	0.00	0.00	19.06	0.01	100.13	63.61	0.00	36.39	9.12	0.43
035ROV12_san5_prof11	4.08	11.03	0.17	65.48	0.00	0.00	19.12	0.00	99.88	64.00	0.02	35.98	9.17	0.50
035ROV12_san6_prof1	3.44	10.75	0.33	62.43	0.11	0.02	19.28	0.00	96.37	66.89	0.59	32.52	9.26	0.00
035ROV12_san6_prof2	3.79	11.17	0.17	64.92	0.07	0.00	19.25	0.00	99.37	65.75	0.34	33.92	9.33	0.03
035ROV12_san6_prof3	3.87	11.16	0.18	64.78	0.07	0.00	19.41	0.02	99.48	65.27	0.32	34.41	9.31	0.05
035ROV12_san6_prof4	3.87	11.08	0.18	64.86	0.08	0.00	19.36	0.02	99.45	65.08	0.37	34.55	9.25	0.07
035ROV12_san6_prof5	4.14	10.53	0.13	64.93	0.10	0.00	19.56	0.00	99.39	62.29	0.50	37.22	8.80	0.12
035ROV12_san6_prof6	4.19	10.45	0.21	64.59	0.09	0.00	19.45	0.01	99.00	61.86	0.45	37.69	8.76	0.15
035ROV12_san6_prof7	4.22	10.40	0.15	64.53	0.09	0.00	19.49	0.00	98.88	61.60	0.43	37.97	8.73	0.20
035ROV12_san6_prof8	4.19	10.38	0.22	65.11	0.08	0.00	19.47	0.02	99.47	61.74	0.39	37.86	8.67	0.27
035ROV12_san6_prof9	4.27	10.36	0.19	65.01	0.08	0.00	19.41	0.00	99.32	61.27	0.37	38.36	8.66	0.31
035ROV12_san6_prof10	4.35	10.41	0.18	65.25	0.07	0.01	19.56	0.01	99.84	60.95	0.35	38.70	8.66	0.37
035ROV12_san6_prof11	4.29	10.34	0.15	65.14	0.08	0.00	19.51	0.00	99.50	61.09	0.37	38.54	8.62	0.40
035ROV12_san6_prof12	4.22	10.62	0.27	65.12	0.06	0.00	19.54	0.02	99.84	62.18	0.27	37.55	8.83	0.45
035ROV12_san6_prof13	4.25	10.79	0.27	65.67	0.03	0.00	19.30	0.04	100.34	62.45	0.15	37.40	8.92	0.50
035ROV12_san6_prof14	4.13	10.66	0.33	65.51	0.04	0.00	19.22	0.05	99.94	62.81	0.21	36.98	8.85	0.53
035ROV12_san6_prof15	4.09	10.68	0.27	64.99	0.04	0.00	19.18	0.04	99.29	63.08	0.20	36.72	8.93	0.56
035ROV12_san7_prof1	4.16	10.52	0.18	64.26	0.06	0.00	19.22	0.00	98.41	62.27	0.32	37.41	8.88	0.00
035ROV12_san7_prof2	4.68	9.94	0.24	65.31	0.07	0.00	19.36	0.02	99.62	58.09	0.32	41.58	8.28	0.01
035ROV12_san7_prof3	4.96	9.49	0.17	65.86	0.06	0.00	19.45	0.02	100.00	55.57	0.27	44.16	7.87	0.04
035ROV12_san7_prof4	4.68	9.82	0.16	65.17	0.06	0.00	19.43	0.04	99.37	57.81	0.32	41.88	8.20	0.09
035ROV12_san7_prof5	4.62	10.08	0.17	65.35	0.05	0.00	19.37	0.03	99.68	58.80	0.25	40.95	8.40	0.10
035ROV12_san8_prof1	3.74	9.64	0.48	62.21	0.33	0.05	19.68	0.00	96.12	61.81	1.76	36.43	8.33	0.00

035ROV12_san8_prof2	4.18	10.71	0.18	65.37	0.00	0.00	19.03	0.01	99.48	62.77	0.00	37.23	8.94	0.08
035ROV12_san8_prof3	4.18	10.72	0.24	65.50	0.00	0.00	19.10	0.00	99.74	62.79	0.00	37.21	8.92	0.17
035ROV12_san8_prof4	4.33	10.54	0.22	65.37	0.01	0.00	19.15	0.00	99.62	61.51	0.07	38.42	8.78	0.28
035ROV12_san8_prof5	4.42	10.20	0.23	65.24	0.01	0.00	19.22	0.00	99.33	60.27	0.05	39.68	8.53	0.37

data:high resolution profiles (rim to core)

Comment	Oxide (wt%)										normalized values				Distance to rim (mm)	Classi-fication
	Na_2O	K_2O	FeO	SiO_2	CaO	MgO	BaO	Al_2O_3	TiO_2	Sum	Or (mol%)	An (mol%)	Ab (mol%)	K (wt%)		
Line 4 035_San_1	3.97	9.19	0.41	61.56	0.28	0.00	2.15	20.62	0.00	98.17	59.46	1.50	39.03	7.63	0.000	Rim
Line 5 035_San_1	4.39	10.34	0.21	64.51	0.03	0.00	0.13	19.33	0.02	98.96	60.68	0.16	39.16	8.58	0.004	Core
Line 6 035_San_1	4.70	10.00	0.19	65.10	0.04	0.00	0.07	19.41	0.01	99.52	58.22	0.20	41.58	8.30	0.010	Core
Line 7 035_San_1	4.74	9.99	0.20	65.11	0.04	0.00	0.07	19.29	0.01	99.45	57.99	0.20	41.81	8.29	0.015	Core
Line 8 035_San_1	4.71	10.01	0.21	64.52	0.04	0.00	0.05	19.33	0.01	98.87	58.20	0.20	41.60	8.31	0.019	Core
Line 9 035_San_1	4.64	10.00	0.19	65.08	0.04	0.00	0.07	19.37	0.01	99.40	58.52	0.18	41.31	8.30	0.024	Core
Line 10 035_San_1	4.66	10.09	0.21	65.15	0.02	0.00	0.05	19.29	0.03	99.51	58.70	0.09	41.21	8.38	0.029	Core
Line 11 035_San_1	4.70	10.11	0.16	64.81	0.04	0.00	0.07	19.32	0.01	99.23	58.48	0.19	41.33	8.40	0.034	Core
Line 12 035_San_1	4.72	10.09	0.21	64.70	0.04	0.00	0.07	19.41	0.03	99.27	58.33	0.20	41.47	8.38	0.039	Core
Line 13 035_San_1	4.69	10.17	0.22	65.03	0.04	0.00	0.06	19.42	0.00	99.63	58.69	0.18	41.13	8.44	0.045	Core
Line 14 035_San_1	4.65	10.18	0.19	65.03	0.03	0.00	0.08	19.08	0.02	99.25	58.95	0.15	40.90	8.45	0.049	Core
Line 15 035_San_1	4.64	10.21	0.18	64.92	0.03	0.00	0.06	19.20	0.02	99.25	59.09	0.14	40.77	8.48	0.054	Core
Line 16 035_San_1	4.65	10.26	0.19	64.72	0.03	0.00	0.08	19.11	0.00	99.04	59.16	0.13	40.71	8.52	0.059	Core
Line 17 035_San_1	4.64	10.25	0.21	64.85	0.02	0.00	0.09	19.35	0.01	99.42	59.15	0.11	40.74	8.51	0.064	Core
Line 18 035_San_1	4.65	10.17	0.18	64.34	0.09	0.02	0.06	19.16	0.01	98.68	58.73	0.41	40.85	8.44	0.069	Core
Line 19 035_San_1	4.60	10.24	0.21	64.73	0.04	0.00	0.05	19.27	0.01	99.14	59.31	0.18	40.51	8.50	0.075	Core
Line 20 035_San_1	4.55	10.31	0.19	64.97	0.04	0.00	0.05	19.22	0.01	99.33	59.75	0.18	40.07	8.56	0.080	Core
Line 21 035_San_1	4.68	10.28	0.17	64.84	0.03	0.00	0.06	19.52	0.02	99.60	59.00	0.16	40.84	8.53	0.084	Core
Line 22 035_San_1	4.60	10.36	0.19	64.91	0.04	0.00	0.06	19.35	0.02	99.52	59.60	0.18	40.22	8.60	0.090	Core

Line 23 035_San_1	4.59	10.28	0.18	64.60	0.03	0.00	0.06	19.30	0.03	99.06	59.49	0.16	40.36	8.53	0.095	Core
Line 24 035_San_1	4.58	10.31	0.20	64.79	0.04	0.00	0.05	19.29	0.03	99.30	59.61	0.21	40.18	8.56	0.100	Core
Line 25 035_San_1	4.54	10.32	0.21	64.42	0.04	0.00	0.06	19.23	0.02	98.84	59.80	0.19	40.00	8.57	0.104	Core
Line 26 035_San_1	4.55	10.37	0.19	64.37	0.05	0.00	0.06	19.30	0.00	98.90	59.84	0.25	39.91	8.61	0.110	Core
Line 27 035_San_1	4.56	10.34	0.23	64.28	0.05	0.00	0.05	19.43	0.01	98.95	59.72	0.24	40.03	8.59	0.114	Core
Line 28 035_San_1	4.55	10.39	0.15	64.69	0.02	0.00	0.07	19.41	0.00	99.29	59.97	0.12	39.91	8.63	0.120	Core
Line 29 035_San_1	4.61	10.23	0.23	64.78	0.03	0.00	0.08	19.48	0.01	99.46	59.25	0.15	40.59	8.49	0.124	Core
Line 30 035_San_1	4.66	10.24	0.22	64.97	0.04	0.00	0.07	19.28	0.00	99.48	58.99	0.20	40.81	8.50	0.130	Core
Line 3 035_San3	3.70	10.33	0.35	62.14	0.16	0.01	2.08	20.08	0.00	98.85	64.22	0.85	34.93	8.57	0.000	Rim
Line 4 035_San3	3.69	10.75	0.28	62.88	0.11	0.00	1.94	19.85	0.00	99.51	65.34	0.55	34.12	8.93	0.004	Rim
Line 5 035_San3	3.54	10.86	0.23	62.51	0.11	0.00	1.97	19.73	0.00	98.95	66.47	0.59	32.95	9.01	0.009	Core
Line 6 035_San3	3.59	10.84	0.25	62.59	0.10	0.00	2.06	19.96	0.00	99.40	66.18	0.52	33.30	9.00	0.015	Core
Line 7 035_San3	3.54	10.90	0.24	62.17	0.10	0.00	2.22	19.91	0.00	99.07	66.61	0.52	32.88	9.04	0.019	Core
Line 8 035_San3	3.52	10.80	0.25	61.54	0.12	0.00	2.35	19.98	0.00	98.56	66.50	0.60	32.91	8.97	0.024	Core
Line 9 035_San3	3.42	10.90	0.25	62.07	0.12	0.00	2.17	20.09	0.00	99.03	67.27	0.62	32.11	9.05	0.030	Core
Line 10 035_San3	3.54	11.27	0.24	62.58	0.09	0.01	1.53	19.70	0.00	98.95	67.42	0.44	32.14	9.36	0.035	Core
Line 11 035_San3	3.55	11.24	0.17	62.70	0.09	0.00	1.47	19.69	0.00	98.91	67.29	0.45	32.26	9.33	0.039	Core
Line 12 035_San3	3.60	11.14	0.25	62.73	0.08	0.00	1.48	19.76	0.00	99.03	66.82	0.40	32.78	9.25	0.046	Core
Line 13 035_San3	3.61	11.13	0.22	62.48	0.10	0.00	1.56	19.60	0.00	98.69	66.68	0.48	32.83	9.24	0.050	Core
Line 14 035_San3	3.57	11.19	0.26	62.36	0.10	0.00	1.65	19.72	0.00	98.85	66.99	0.49	32.52	9.29	0.054	Core
Line 15 035_San3	3.49	11.10	0.23	62.47	0.09	0.00	1.68	19.76	0.00	98.82	67.33	0.47	32.20	9.21	0.060	Core
Line 16 035_San3	3.54	11.12	0.20	62.35	0.11	0.00	1.71	19.86	0.00	98.88	67.02	0.54	32.45	9.23	0.065	Core
Line 17 035_San3	3.56	11.08	0.26	62.61	0.11	0.00	1.74	19.77	0.00	99.13	66.81	0.54	32.65	9.19	0.069	Core
Line 18 035_San3	3.61	11.03	0.22	62.58	0.11	0.00	1.82	20.07	0.00	99.44	66.42	0.54	33.04	9.16	0.075	Core
Line 19 035_San3	3.52	11.06	0.22	62.04	0.10	0.00	1.84	19.79	0.00	98.57	67.08	0.50	32.42	9.18	0.080	Core
Line 20 035_San3	3.61	11.11	0.20	62.23	0.10	0.00	1.94	19.99	0.00	99.19	66.60	0.53	32.87	9.23	0.085	Core

Line 21 035_San3	3.55	10.99	0.21	62.20	0.12	0.00	1.92	19.78	0.00	98.77	66.67	0.63	32.71	9.12	0.090	Core
Line 22 035_San3	3.48	11.03	0.21	62.37	0.12	0.00	1.99	19.59	0.00	98.79	67.19	0.63	32.18	9.16	0.095	Core
Line 23 035_San3	3.54	11.10	0.19	62.60	0.11	0.00	2.02	19.74	0.00	99.29	67.01	0.56	32.43	9.22	0.100	Core
Line 24 035_San3	3.47	11.08	0.21	62.26	0.11	0.00	2.07	19.89	0.00	99.09	67.36	0.55	32.09	9.20	0.105	Core
Line 25 035_San3	3.53	11.18	0.22	62.58	0.11	0.00	1.93	19.72	0.00	99.27	67.19	0.54	32.27	9.28	0.111	Core
Line 26 035_San3	3.47	11.49	0.21	63.00	0.09	0.00	1.35	19.70	0.00	99.31	68.22	0.44	31.34	9.53	0.115	Core
Line 27 035_San3	3.57	11.44	0.20	63.20	0.10	0.00	1.34	19.69	0.00	99.55	67.48	0.50	32.02	9.50	0.121	Core
Line 28 035_San3	3.58	11.44	0.23	62.90	0.09	0.00	1.39	19.69	0.00	99.32	67.47	0.42	32.11	9.50	0.126	Core
Line 29 035_San3	3.67	11.04	0.20	62.91	0.13	0.00	1.66	20.16	0.00	99.77	65.97	0.66	33.37	9.16	0.130	Core
Line 2 035_San7	4.16	10.39	0.48	62.75	0.25	0.00	0.90	20.17	0.00	99.10	61.40	1.23	37.37	8.62	0.000	Rim
Line 3 035_San7	3.47	9.95	0.41	60.54	0.22	0.00	3.69	20.63	0.00	98.90	64.59	1.19	34.21	8.26	0.005	Core
Line 4 035_San7	4.76	10.45	0.19	64.73	0.08	0.00	0.07	19.50	0.03	99.80	58.87	0.38	40.74	8.67	0.011	Core
Line 5 035_San7	4.72	10.34	0.19	64.87	0.07	0.00	0.06	19.61	0.02	99.88	58.87	0.34	40.79	8.59	0.015	Core
Line 6 035_San7	4.66	10.35	0.19	65.12	0.07	0.00	0.06	19.54	0.02	100.02	59.15	0.34	40.50	8.59	0.022	Core
Line 7 035_San7	4.71	10.41	0.19	64.96	0.07	0.00	0.07	19.48	0.03	99.92	59.06	0.32	40.63	8.64	0.026	Core
Line 8 035_San7	4.56	10.52	0.19	64.90	0.08	0.00	0.04	19.61	0.02	99.92	60.06	0.36	39.58	8.73	0.031	Core
Line 9 035_San7	4.56	10.49	0.18	64.81	0.07	0.01	0.05	19.51	0.04	99.73	60.03	0.33	39.64	8.71	0.037	Core
Line 10 035_San7	4.66	10.47	0.19	65.01	0.06	0.00	0.06	19.49	0.01	99.95	59.49	0.27	40.23	8.69	0.042	Core
Line 11 035_San7	4.60	10.51	0.22	65.05	0.06	0.00	0.05	19.61	0.03	100.12	59.91	0.27	39.82	8.73	0.047	Core
Line 12 035_San7	4.71	10.52	0.16	64.86	0.04	0.00	0.09	19.68	0.02	100.08	59.40	0.21	40.39	8.73	0.052	Core
Line 13 035_San7	4.64	10.54	0.19	64.84	0.05	0.00	0.06	19.21	0.04	99.56	59.81	0.21	39.98	8.75	0.056	Core
Line 14 035_San7	4.67	10.47	0.16	65.38	0.05	0.00	0.04	19.56	0.00	100.33	59.46	0.26	40.28	8.69	0.062	Core
Line 15 035_San7	4.66	10.42	0.17	65.09	0.06	0.00	0.07	19.47	0.04	99.98	59.35	0.28	40.37	8.65	0.067	Core
Line 16 035_San7	4.75	10.23	0.20	65.05	0.06	0.00	0.07	19.60	0.02	99.98	58.44	0.28	41.28	8.49	0.073	Core
Line 17 035_San7	4.86	10.15	0.22	65.08	0.08	0.00	0.04	19.43	0.02	99.88	57.66	0.36	41.98	8.43	0.077	Core
Line 2 035_San6	3.55	11.04	0.30	62.50	0.16	0.01	2.14	20.18	0.00	99.88	66.65	0.81	32.54	9.17	0.000	Rim
Line 3 035_San6	3.50	12.38	0.24	64.47	0.06	0.01	0.25	19.48	0.03	100.42	69.77	0.27	29.96	10.28	0.005	Core
Line 4 035_San6	3.48	12.31	0.22	64.43	0.04	0.00	0.25	19.35	0.01	100.08	69.81	0.20	29.99	10.22	0.011	Core
Line 5 035_San6	3.57	12.21	0.21	64.66	0.07	0.00	0.28	19.40	0.00	100.41	69.00	0.34	30.66	10.14	0.016	Core
Line 6 035_San6	3.57	12.08	0.21	64.43	0.07	0.00	0.27	19.32	0.01	99.96	68.75	0.35	30.90	10.02	0.020	Core
Line 7 035_San6	3.57	12.17	0.18	64.34	0.07	0.00	0.27	19.34	0.01	99.95	68.92	0.34	30.74	10.10	0.026	Core

Line 8 035_San6	3.66	11.78	0.19	64.27	0.09	0.00	0.48	19.29	0.00	99.76	67.61	0.43	31.95	9.78	0.031	Core
Line 9 035_San6	3.70	11.55	0.17	64.15	0.11	0.00	0.56	19.74	0.00	99.99	66.86	0.55	32.59	9.59	0.035	Core
Line 10 035_San6	3.67	11.45	0.19	64.01	0.12	0.00	0.63	19.51	0.00	99.58	66.80	0.60	32.60	9.50	0.041	Core
Line 11 035_San6	3.82	11.45	0.26	64.02	0.10	0.01	0.39	19.35	0.00	99.39	66.04	0.48	33.48	9.50	0.047	Core
Line 12 035_San6	3.71	11.89	0.20	64.27	0.07	0.00	0.31	19.37	0.00	99.81	67.61	0.34	32.05	9.87	0.051	Core
Line 13 035_San6	3.70	11.83	0.20	64.18	0.10	0.00	0.19	19.29	0.01	99.50	67.48	0.47	32.04	9.82	0.056	Core
Line 14 035_San6	3.69	11.81	0.21	64.46	0.07	0.00	0.16	19.41	0.00	99.82	67.58	0.36	32.06	9.81	0.062	Core
Line 15 035_San6	3.77	11.73	0.23	64.31	0.10	0.00	0.23	19.45	0.01	99.82	66.87	0.47	32.66	9.74	0.066	Core
Line 16 035_San6	3.77	11.36	0.27	64.17	0.09	0.00	0.24	19.79	0.01	99.69	66.20	0.42	33.38	9.43	0.072	Core
Line 17 035_San6	4.01	11.31	0.18	64.20	0.09	0.02	0.30	19.59	0.00	99.70	64.67	0.45	34.88	9.39	0.076	Core
Line 18 035_San6	4.02	11.23	0.20	64.14	0.11	0.00	0.26	19.69	0.02	99.67	64.43	0.55	35.02	9.32	0.081	Core
Line 19 035_San6	3.92	11.23	0.18	63.78	0.09	0.00	0.31	19.61	0.02	99.15	65.02	0.44	34.54	9.32	0.087	Core
Line 20 035_San6	3.90	11.21	0.19	64.07	0.11	0.01	0.31	19.58	0.00	99.38	65.03	0.54	34.43	9.30	0.092	Core
Line 21 035_San6	4.03	11.13	0.20	63.81	0.11	0.00	0.30	19.59	0.01	99.17	64.18	0.51	35.31	9.24	0.097	Core
Line 5 035_San5	3.61	9.82	0.71	61.76	0.67	0.16	2.68	20.09	0.00	99.50	61.86	3.52	34.61	8.15	0.000	Rim
Line 6 035_San5	4.15	10.67	0.23	64.71	0.06	0.00	0.53	19.47	0.00	99.83	62.64	0.31	37.05	8.86	0.005	Core
Line 7 035_San5	4.22	10.74	0.22	64.71	0.06	0.00	0.53	19.45	0.00	99.92	62.44	0.29	37.27	8.91	0.010	Core
Line 8 035_San5	4.24	10.79	0.19	64.34	0.06	0.00	0.58	19.72	0.00	99.91	62.43	0.31	37.26	8.95	0.016	Core
Line 9 035_San5	4.23	10.67	0.20	64.45	0.05	0.00	0.64	19.52	0.00	99.77	62.27	0.26	37.48	8.86	0.021	Core
Line 10 035_San5	4.16	10.66	0.26	64.50	0.07	0.00	0.61	19.47	0.00	99.73	62.59	0.33	37.08	8.85	0.026	Core
Line 11 035_San5	4.20	10.62	0.23	64.49	0.06	0.00	0.65	19.61	0.00	99.87	62.29	0.31	37.41	8.82	0.031	Core
Line 12 035_San5	4.22	10.63	0.22	64.53	0.06	0.01	0.64	19.41	0.00	99.72	62.20	0.29	37.51	8.83	0.036	Core
Line 13 035_San5	4.25	10.64	0.22	64.43	0.06	0.00	0.66	19.55	0.00	99.81	62.02	0.30	37.67	8.83	0.041	Core
Line 14 035_San5	4.22	10.60	0.24	64.35	0.05	0.00	0.63	19.78	0.00	99.88	62.16	0.24	37.60	8.80	0.046	Core
Line 15 035_San5	4.18	10.60	0.22	64.56	0.06	0.00	0.68	19.59	0.00	99.89	62.33	0.30	37.37	8.80	0.051	Core
Line 16 035_San5	4.26	10.60	0.25	64.64	0.06	0.00	0.74	19.57	0.00	100.11	61.88	0.28	37.84	8.80	0.057	Core
Line 17 035_San5	4.21	10.64	0.22	64.70	0.05	0.00	0.70	19.72	0.00	100.24	62.27	0.25	37.48	8.83	0.062	Core
Line 18 035_San5	4.21	10.63	0.24	64.41	0.05	0.00	0.71	19.62	0.00	99.88	62.23	0.27	37.50	8.82	0.067	Core
Line 19 035_San5	4.16	10.55	0.21	64.60	0.06	0.02	0.75	19.61	0.00	99.96	62.31	0.32	37.38	8.75	0.072	Core
Line 20 035_San5	4.12	10.38	0.20	64.69	0.06	0.01	0.76	19.79	0.00	100.01	62.19	0.29	37.53	8.62	0.077	Core
Line 21 035_San5	4.14	10.47	0.22	64.51	0.06	0.00	0.79	19.75	0.00	99.95	62.23	0.32	37.45	8.69	0.082	Core

Line 22 035_San5	4.20	10.55	0.21	64.51	0.06	0.00	0.80	19.68	0.00	100.00	62.15	0.28	37.57	8.76	0.087	Core
Line 23 035_San5	4.08	10.53	0.21	64.44	0.06	0.00	0.84	19.67	0.00	99.83	62.73	0.29	36.99	8.74	0.092	Core
Line 24 035_San5	4.17	10.59	0.21	64.34	0.06	0.00	0.85	19.59	0.00	99.81	62.39	0.29	37.31	8.79	0.097	Core
Line 25 035_San5	4.15	10.54	0.20	64.51	0.06	0.00	0.93	19.69	0.00	100.07	62.40	0.27	37.32	8.75	0.102	Core
Line 26 035_San5	4.13	10.37	0.20	64.45	0.07	0.01	1.00	19.75	0.00	99.98	62.09	0.35	37.57	8.61	0.108	Core
Line 27 035_San5	4.22	10.49	0.23	64.23	0.07	0.00	1.00	19.48	0.00	99.72	61.85	0.32	37.82	8.71	0.112	Core
Line 2 035_San8	3.88	10.11	0.48	62.66	0.27	0.00	1.16	20.07	0.01	98.64	62.25	1.39	36.36	8.39	0.000	Rim
Line 3 035_San8	3.97	10.11	0.37	62.40	0.12	0.00	2.09	20.05	0.00	99.10	62.26	0.61	37.13	8.39	0.005	Core
Line 4 035_San8	4.27	10.74	0.29	65.00	0.02	0.00	0.14	19.40	0.00	99.87	62.27	0.07	37.65	8.92	0.010	Core
Line 5 035_San8	4.38	10.60	0.25	65.55	0.01	0.00	0.13	19.23	0.00	100.15	61.43	0.02	38.55	8.80	0.015	Core
Line 6 035_San8	4.37	10.59	0.25	65.03	0.02	0.00	0.13	19.29	0.01	99.69	61.41	0.11	38.48	8.79	0.020	Core
Line 7 035_San8	4.35	10.55	0.25	64.95	0.00	0.00	0.15	19.31	0.01	99.57	61.48	0.02	38.50	8.76	0.026	Core
Line 8 035_San8	4.36	10.60	0.21	64.89	0.01	0.00	0.17	19.37	0.01	99.62	61.51	0.06	38.43	8.80	0.030	Core
Line 9 035_San8	4.37	10.63	0.26	65.18	0.01	0.00	0.14	19.36	0.00	99.95	61.52	0.05	38.43	8.83	0.036	Core
Line 10 035_San8	4.30	10.61	0.22	65.06	0.00	0.00	0.13	19.29	0.00	99.60	61.89	0.00	38.11	8.81	0.041	Core
Line 11 035_San8	4.35	10.59	0.22	65.01	0.02	0.00	0.13	19.22	0.01	99.55	61.51	0.10	38.40	8.79	0.046	Core
Line 12 035_San8	4.36	10.62	0.22	65.15	0.00	0.00	0.16	19.42	0.01	99.94	61.57	0.00	38.43	8.82	0.051	Core
Line 13 035_San8	4.38	10.55	0.21	64.98	0.01	0.00	0.13	19.23	0.00	99.50	61.27	0.05	38.68	8.76	0.056	Core
Line 14 035_San8	4.35	10.53	0.19	65.08	0.01	0.00	0.14	19.35	0.00	99.65	61.40	0.04	38.57	8.74	0.061	Core
Line 15 035_San8	4.27	10.59	0.22	65.04	0.01	0.00	0.13	19.27	0.02	99.55	61.97	0.05	37.98	8.79	0.067	Core
Line 16 035_San8	4.36	10.61	0.21	65.41	0.01	0.00	0.13	19.30	0.00	100.03	61.51	0.03	38.45	8.81	0.071	Core
Line 17 035_San8	4.39	10.62	0.22	65.29	0.00	0.00	0.14	19.48	0.00	100.13	61.44	0.00	38.56	8.82	0.077	Core
Line 18 035_San8	4.40	10.49	0.24	65.30	0.00	0.00	0.11	19.38	0.00	99.91	61.09	0.00	38.91	8.71	0.082	Core
Line 19 035_San8	4.32	10.56	0.19	66.22	0.00	0.00	0.14	19.39	0.00	100.82	61.69	0.00	38.31	8.77	0.087	Core
Line 20 035_San8	4.32	10.48	0.25	65.36	0.01	0.00	0.12	19.36	0.01	99.91	61.49	0.03	38.48	8.70	0.092	Core
Line 21 035_San8	4.38	10.46	0.20	65.33	0.02	0.00	0.14	19.16	0.00	99.68	61.07	0.09	38.84	8.68	0.098	Core
Line 22 035_San8	4.35	10.51	0.23	65.39	0.01	0.00	0.12	19.49	0.00	100.10	61.38	0.03	38.59	8.73	0.102	Core

EMP analyses of sample 037DR-2 sanidines

data: profiles (high and low resolution), and groundmass data (below)

Profiles (low resolution; rim to core)

Comment	Oxide (wt%)									normalized values				Dis-tance to rim (mm)	Class-ification
	Na_2O	K_2O	FeO	SiO_2	CaO	MgO	Al_2O_3	TiO_2	Sum	Or (mol%)	An (mol%)	Ab (mol%)	K (wt%)		
037DR-2_san4_prof1	2.07	14.13	0.79	64.66	0.00	0.00	18.57	0.02	100.24	81.78	0.01	18.21	11.70	0.00	Rim
037DR-2_san4_prof3	2.34	11.49	2.79	62.73	3.19	0.81	16.28	0.12	99.74	80.56	0.05	19.40	11.22	0.04	Rim
037DR-2_san4_prof4	2.08	13.13	0.46	62.42	0.01	0.00	19.01	0.00	97.11	74.00	0.30	25.70	10.37	0.08	Core
037DR-2_san4_prof5	2.77	12.12	0.18	62.66	0.06	0.00	19.27	0.00	97.06	69.23	0.33	30.44	9.64	0.14	Core
037DR-2_san4_prof6	3.26	11.27	0.24	62.98	0.06	0.00	19.22	0.00	97.03	69.41	0.27	30.33	9.61	0.20	Core
037DR-2_san4_prof7	3.24	11.27	0.21	63.37	0.05	0.01	19.18	0.00	97.33	69.95	0.28	29.77	9.60	0.24	Core
037DR-2_san4_prof8	3.15	11.25	0.24	63.21	0.05	0.00	19.37	0.00	97.27	69.76	0.31	29.93	9.71	0.34	Core
037DR-2_san4_prof9	3.19	11.30	0.23	62.68	0.06	0.00	19.19	0.00	96.65	70.22	0.22	29.55	9.70	0.48	Core
037DR-2_san4_prof10	3.14	11.34	0.23	63.06	0.04	0.01	19.21	0.00	97.04	69.93	0.23	29.84	9.67	0.59	Core
037DR-2_san4_prof11	3.17	11.29	0.26	62.96	0.04	0.00	19.20	0.00	96.93	70.33	0.24	29.43	9.74	0.68	Core
037DR-2_san4_prof12	3.13	11.37	0.22	62.92	0.05	0.00	19.27	0.00	96.95	70.40	0.19	29.40	9.74	0.78	Core
037DR-2_san4_prof13	3.13	11.39	0.26	63.09	0.04	0.01	19.13	0.00	97.04	70.64	0.30	29.06	9.81	0.83	Core
037DR-2_san4_prof14	3.10	11.45	0.23	62.84	0.06	0.00	19.17	0.00	96.85	71.64	0.15	28.21	9.92	0.94	Core
037DR-2_san4_prof15	3.00	11.58	0.24	63.04	0.03	0.00	18.99	0.00	96.88	73.47	0.09	26.44	10.29	1.04	Core
037DR-2_san4_prof16	2.87	12.12	0.20	63.45	0.02	0.00	19.08	0.00	97.74	74.08	0.05	25.88	10.49	1.10	Core
037DR-2_san4_prof17	2.88	12.53	0.24	64.41	0.01	0.01	19.09	0.00	99.16	74.40	0.03	25.58	10.56	1.18	Core
037DR-2_san4_prof18	2.85	12.60	0.22	64.43	0.01	0.00	18.95	0.00	99.06	74.75	0.02	25.23	10.60	1.25	Core
037DR-2_san4_prof19	2.80	12.61	0.13	64.27	0.00	0.00	18.94	0.00	98.75	74.24	0.02	25.74	10.55	1.30	Core
037DR-2_san4_prof20	2.87	12.58	0.22	64.28	0.00	0.00	19.04	0.00	99.00	74.50	0.05	25.46	10.56	1.38	Core
037DR-2_san8_prof2	2.17	12.91	0.45	62.52	0.03	0.00	18.98	0.00	97.07	79.51	0.17	20.31	11.04	0.00	Rim
037DR-2_san8_prof4	3.17	11.30	0.23	62.79	0.06	0.01	19.29	0.00	96.84	69.89	0.31	29.80	9.69	0.06	Core
037DR-2_san8_prof5	3.13	11.29	0.25	62.99	0.05	0.00	19.17	0.00	96.87	70.19	0.24	29.57	9.68	0.11	Core
037DR-2_san8_prof6	3.17	11.30	0.17	62.71	0.04	0.00	19.19	0.00	96.58	69.95	0.23	29.82	9.71	0.25	Core
037DR-2_san8_prof7	3.15	11.25	0.20	62.57	0.05	0.00	19.21	0.00	96.43	69.95	0.28	29.77	9.68	0.33	Core
037DR-2_san8_prof8	3.02	11.55	0.26	62.85	0.06	0.00	19.28	0.00	97.02	71.34	0.31	28.35	9.88	0.50	Core

037DR-2_san8_prof9	3.18	11.20	0.22	62.52	0.06	0.00	19.11	0.00	96.30	69.62	0.33	30.04	9.65	0.59	Core
037DR-2_san8_prof10	3.13	11.33	0.19	63.09	0.06	0.01	19.25	0.00	97.06	70.21	0.31	29.48	9.69	0.72	Core
037DR-2_san8_prof11	3.18	11.31	0.24	62.78	0.05	0.00	19.32	0.00	96.88	69.87	0.27	29.86	9.69	0.88	Core
037DR-2_san8_prof12	3.16	12.00	0.20	64.32	0.04	0.00	18.93	0.00	98.65	71.28	0.19	28.53	10.10	1.00	Core
037DR-2_san8_prof13	3.15	12.07	0.17	64.71	0.01	0.00	19.00	0.00	99.11	71.55	0.07	28.38	10.11	1.07	Core
037DR-2_san8_prof14	3.07	12.22	0.20	64.07	0.01	0.00	19.01	0.00	98.59	72.32	0.07	27.61	10.29	1.11	Core
037DR-2_san8_prof15	3.01	12.34	0.24	64.45	0.00	0.00	18.89	0.00	98.94	72.94	0.02	27.04	10.35	1.15	Core
037DR2_san9_1_prof1	2.21	13.89	0.67	64.65	0.03	0.00	18.62	0.03	100.09	80.43	0.12	19.45	11.52	0.00	Rim
037DR2_san9_1_prof2	2.22	13.46	0.45	63.57	0.02	0.00	18.94	0.00	98.66	79.88	0.09	20.03	11.32	0.02	Rim
037DR2_san9_1_prof3	2.06	13.69	0.43	63.95	0.00	0.00	19.10	0.00	99.23	81.38	0.01	18.61	11.46	0.05	Rim
037DR2_san9_1_prof4	2.00	13.33	0.43	62.73	0.01	0.00	19.14	0.00	97.64	81.41	0.03	18.56	11.33	0.07	Rim
037DR2_san9_1_prof5	2.00	13.54	0.44	63.13	0.00	0.00	19.07	0.00	98.18	81.67	0.00	18.33	11.45	0.09	Rim
037DR2_san9_1_prof6	1.97	13.96	0.38	63.67	0.00	0.00	18.99	0.00	98.97	82.34	0.00	17.66	11.71	0.11	Rim
037DR2_san9_1_prof7	1.96	13.54	0.48	62.96	0.15	0.02	19.03	0.00	98.14	81.36	0.74	17.90	11.45	0.12	Rim
037DR2_san9_1_prof8	1.92	13.37	0.38	62.32	0.00	0.00	18.91	0.00	96.89	82.07	0.01	17.92	11.45	0.14	Rim
037DR2_san9_1_prof9	1.94	13.14	0.36	62.03	0.00	0.00	18.95	0.00	96.42	81.67	0.01	18.32	11.31	0.16	Rim
037DR2_san9_1_prof10	1.98	13.16	0.33	62.36	0.00	0.00	18.88	0.00	96.71	81.39	0.00	18.61	11.30	0.19	Rim
037DR2_san9_1_prof11	3.22	11.86	0.18	64.50	0.02	0.01	19.18	0.00	98.96	70.71	0.11	29.19	9.95	0.21	Core
037DR2_san9_1_prof12	3.53	11.40	0.25	64.27	0.02	0.00	19.34	0.00	98.81	67.95	0.08	31.97	9.58	0.24	Core
037DR2_san9_1_prof13	3.46	11.41	0.25	64.12	0.02	0.00	19.21	0.00	98.46	68.37	0.11	31.52	9.62	0.29	Core
037DR2_san9_1_prof14	3.45	11.49	0.24	64.24	0.03	0.01	19.35	0.00	98.80	68.56	0.14	31.30	9.65	0.33	Core
037DR2_san9_1_prof15	3.44	11.46	0.23	64.31	0.03	0.00	19.18	0.00	98.65	68.55	0.16	31.28	9.64	0.38	Core
037DR-2_san16_prof1	2.25	13.82	0.61	64.08	0.01	0.00	18.52	0.04	99.33	80.12	0.05	19.83	11.55	0.00	Rim
037DR-2_san16_prof2	2.08	12.97	1.44	62.72	1.00	0.38	18.05	0.00	98.65	76.41	4.97	18.62	10.91	0.02	Rim
037DR-2_san16_prof3	2.20	12.70	0.42	61.98	0.00	0.00	18.78	0.00	96.08	79.16	0.00	20.84	10.97	0.04	Rim
037DR-2_san16_prof4	3.28	11.52	0.25	63.53	0.04	0.00	19.02	0.00	97.64	69.65	0.21	30.14	9.79	0.07	Core
037DR-2_san16_prof5	3.26	11.46	0.21	63.39	0.04	0.00	19.10	0.00	97.46	69.67	0.21	30.12	9.76	0.11	Core

037DR-2_san16_prof6	3.29	11.47	0.23	63.63	0.03	0.00	18.86	0.00	97.51	69.54	0.14	30.32	9.76	0.18	Core
037DR-2_san16_prof7	3.26	11.52	0.23	63.51	0.01	0.00	18.92	0.00	97.45	69.89	0.05	30.06	9.81	0.31	Core
037DR-2_san16_prof8	3.20	11.50	0.24	63.81	0.03	0.00	18.93	0.00	97.71	70.16	0.17	29.67	9.77	0.35	Core
037DR-2_san16_prof9	3.29	11.51	0.24	63.65	0.03	0.00	19.11	0.00	97.83	69.60	0.16	30.24	9.77	0.41	Core
037DR-2_san16_prof10	3.41	11.63	0.20	64.40	0.03	0.00	19.11	0.00	98.78	69.06	0.17	30.77	9.77	0.46	Core
037DR-2_san19_prof1	2.18	13.03	0.53	62.73	0.02	0.00	18.99	0.00	97.48	79.63	0.12	20.25	11.10	0.00	Rim
037DR-2_san19_prof2	3.29	11.07	0.21	62.60	0.03	0.00	19.07	0.00	96.28	68.76	0.18	31.06	9.55	0.07	Core
037DR-2_san19_prof3	3.44	10.76	0.26	62.34	0.04	0.00	19.29	0.00	96.14	67.14	0.23	32.62	9.29	0.21	Core

data: high resolution profiles (rim to core)

Comment	Oxide (wt%)										normalized values				Distance to rim (mm)	
	Na_2O	K_2O	FeO	SiO_2	CaO	MgO	BaO	Al_2O_3	TiO_2	Sum	Or (mol%)	An (mol%)	Ab (mol%)	K (wt%)		
Line 2 037_San8	2.29	13.70	0.63	64.43	0.01	0.00	0.12	18.71	0.00	99.88	79.74	0.03	20.23	11.37	0.000	Rim
Line 3 037_San8	2.29	13.51	0.59	65.07	0.00	0.00	0.16	18.99	0.03	100.64	79.54	0.00	20.46	11.22	0.005	Rim
Line 4 037_San8	2.28	13.19	0.46	63.27	0.01	0.02	1.00	19.35	0.00	99.58	79.16	0.07	20.77	10.95	0.011	Rim
Line 5 037_San8	2.16	12.82	0.43	62.66	0.00	0.00	2.40	19.68	0.00	100.15	79.58	0.01	20.41	10.64	0.016	Rim
Line 6 037_San8	2.10	12.64	0.41	61.87	0.00	0.00	3.05	19.83	0.00	99.91	79.81	0.02	20.17	10.49	0.021	Rim
Line 7 037_San8	2.06	12.73	0.42	62.23	0.00	0.00	3.03	19.64	0.00	100.11	80.25	0.00	19.75	10.57	0.026	Rim
Line 8 037_San8	2.12	12.54	0.38	62.13	0.00	0.00	3.04	19.80	0.00	100.01	79.52	0.02	20.46	10.41	0.031	Rim
Line 9 037_San8	2.67	12.09	0.30	62.24	0.02	0.00	2.45	19.53	0.00	99.30	74.82	0.10	25.08	10.04	0.037	Core
Line 10 037_San8	3.13	11.28	0.25	62.64	0.04	0.00	2.61	19.94	0.00	99.89	70.20	0.21	29.59	9.36	0.041	Core
Line 11 037_San8	3.15	11.26	0.25	62.73	0.04	0.00	2.59	20.06	0.00	100.08	70.03	0.21	29.76	9.35	0.046	Core
Line 12 037_San8	3.19	11.36	0.21	63.07	0.05	0.00	1.79	19.79	0.00	99.46	69.90	0.28	29.82	9.43	0.052	Core

Line 13 037_San8	3.29	11.40	0.20	63.14	0.05	0.00	1.65	19.86	0.00	99.60	69.32	0.26	30.42	9.46	0.057	Core
Line 14 037_San8	3.39	11.17	0.26	62.56	0.07	0.04	1.58	19.32	0.00	98.40	68.17	0.35	31.48	9.27	0.062	Core
Line 15 037_San8	3.36	11.30	0.24	63.35	0.06	0.00	1.59	19.64	0.00	99.53	68.64	0.31	31.05	9.38	0.067	Core
Line 16 037_San8	3.31	11.20	0.27	63.41	0.05	0.00	1.59	19.83	0.00	99.66	68.80	0.27	30.92	9.30	0.073	Core
Line 17 037_San8	3.39	11.28	0.26	63.26	0.07	0.00	1.59	19.85	0.00	99.69	68.38	0.34	31.28	9.36	0.078	Core
Line 18 037_San8	3.37	11.23	0.24	63.10	0.05	0.01	1.54	19.73	0.00	99.28	68.46	0.28	31.26	9.32	0.082	Core
Line 19 037_San8	3.37	11.27	0.26	63.46	0.06	0.00	1.57	19.68	0.00	99.68	68.52	0.30	31.18	9.36	0.088	Core
Line 20 037_San8	3.41	11.25	0.24	63.32	0.05	0.00	1.59	19.79	0.00	99.66	68.24	0.27	31.48	9.34	0.093	Core
Line 21 037_San8	3.34	11.26	0.26	63.23	0.06	0.00	1.61	19.65	0.00	99.41	68.70	0.30	31.00	9.35	0.098	Core
Line 22 037_San8	3.31	11.37	0.21	63.28	0.06	0.00	1.62	19.77	0.00	99.63	69.09	0.32	30.59	9.44	0.103	Core
Line 23 037_San8	3.35	11.24	0.25	63.31	0.06	0.01	1.56	19.71	0.00	99.49	68.60	0.30	31.10	9.33	0.108	Core
Line 24 037_San8	3.44	11.36	0.21	63.29	0.04	0.00	1.63	19.80	0.00	99.77	68.36	0.22	31.42	9.43	0.114	Core
Line 25 037_San8	3.36	11.23	0.23	63.09	0.06	0.00	1.57	19.72	0.00	99.26	68.52	0.29	31.19	9.32	0.119	Core
Line 26 037_San8	3.32	11.31	0.23	63.81	0.06	0.00	1.58	19.66	0.00	99.98	68.92	0.30	30.77	9.39	0.124	Core
Line 3 037_san4	2.22	13.81	0.62	64.42	0.00	0.00	0.12	18.63	0.02	99.82	80.40	0.00	19.60	11.46	0.000	Rim
Line 4 037_san4	2.36	13.17	1.03	63.28	0.55	0.22	0.18	18.33	0.09	99.21	76.50	2.68	20.82	10.93	0.005	Rim
Line 5 037_san4	2.15	13.14	0.42	63.20	0.00	0.00	1.25	19.12	0.00	99.29	80.04	0.02	19.94	10.91	0.010	Rim
Line 6 037_san4	2.12	12.86	0.45	62.21	0.01	0.00	2.40	19.37	0.00	99.43	79.90	0.06	20.04	10.68	0.015	Rim
Line 7 037_san4	2.12	12.71	0.46	62.14	0.01	0.00	2.90	19.75	0.00	100.09	79.71	0.06	20.23	10.55	0.020	Rim

Line 8 037_san4	2.25	12.73	0.40	61.89	0.03	0.00	2.84	19.63	0.00	99.76	78.75	0.14	21.11	10.57	0.025	Rim
Line 9 037_san4	2.11	12.88	0.41	62.12	0.01	0.00	2.88	19.65	0.00	100.06	80.00	0.05	19.94	10.69	0.031	Rim
Line 10 037_san4	2.09	12.85	0.42	62.44	0.00	0.00	2.84	19.55	0.00	100.19	80.16	0.00	19.84	10.67	0.036	Rim
Line 11 037_san4	2.10	12.77	0.37	62.27	0.00	0.00	2.96	19.47	0.00	99.95	79.99	0.00	20.01	10.60	0.041	Rim
Line 12 037_san4	2.09	12.88	0.43	61.78	0.00	0.00	3.04	19.62	0.00	99.84	80.19	0.01	19.80	10.69	0.046	Rim
Line 13 037_san4	2.08	12.85	0.40	62.42	0.00	0.00	2.81	19.51	0.00	100.07	80.22	0.03	19.75	10.67	0.050	Rim
Line 14 037_san4	2.16	12.63	0.38	62.04	0.02	0.00	2.72	19.50	0.00	99.46	79.27	0.09	20.64	10.48	0.056	Rim
Line 15 037_san4	2.31	12.46	0.37	62.06	0.00	0.00	3.13	19.82	0.00	100.14	78.04	0.00	21.96	10.34	0.061	Rim
Line 16 037_san4	2.94	11.85	0.28	63.24	0.04	0.00	1.67	19.62	0.00	99.65	72.43	0.23	27.34	9.84	0.066	Core
Line 17 037_san4	3.21	11.54	0.25	63.21	0.05	0.00	1.68	19.64	0.00	99.58	70.10	0.27	29.63	9.58	0.071	Core
Line 18 037_san4	3.24	11.53	0.26	63.28	0.06	0.00	1.68	19.78	0.00	99.83	69.87	0.28	29.85	9.57	0.076	Core
Line 19 037_san4	3.26	11.50	0.24	63.20	0.07	0.00	1.70	19.74	0.00	99.71	69.63	0.36	30.01	9.55	0.082	Core
Line 20 037_san4	3.23	11.48	0.26	63.00	0.06	0.00	1.72	19.62	0.00	99.37	69.84	0.29	29.87	9.53	0.087	Core
Line 21 037_san4	3.05	11.77	0.24	62.90	0.06	0.00	1.76	19.53	0.00	99.30	71.57	0.28	28.15	9.77	0.093	Core
Line 22 037_san4	2.91	11.91	0.24	63.17	0.05	0.00	1.73	19.63	0.00	99.65	72.71	0.27	27.02	9.89	0.096	Core
Line 23 037_san4	3.35	11.28	0.23	63.09	0.07	0.00	1.74	19.73	0.00	99.49	68.64	0.34	31.01	9.36	0.103	Core
Line 24 037_san4	3.33	11.29	0.24	63.09	0.05	0.00	1.78	19.80	0.00	99.58	68.86	0.24	30.89	9.37	0.108	Core
Line 25 037_san4	3.35	11.30	0.22	63.09	0.06	0.00	1.77	19.67	0.00	99.47	68.69	0.33	30.98	9.38	0.113	Core
Line 26 037_san4	3.37	11.21	0.23	62.86	0.06	0.01	1.77	19.66	0.00	99.17	68.41	0.29	31.29	9.31	0.118	Core

Line 27 037_san4	3.33	11.26	0.24	63.07	0.05	0.00	1.77	19.75	0.00	99.47	68.79	0.26	30.95	9.35	0.123	Core
Line 28 037_san4	3.37	11.32	0.22	62.96	0.06	0.00	1.81	19.71	0.00	99.44	68.63	0.28	31.09	9.40	0.129	Core
Line 29 037_san4	3.34	11.30	0.23	62.70	0.05	0.00	1.80	19.67	0.00	99.09	68.81	0.26	30.94	9.38	0.133	Core
Line 30 037_san4	3.34	10.97	0.22	62.27	0.07	0.00	1.84	19.31	0.00	98.02	68.09	0.37	31.54	9.11	0.139	Core
Line 31 037_san4	3.34	11.16	0.23	62.38	0.06	0.00	1.81	19.60	0.00	98.59	68.49	0.33	31.18	9.26	0.144	Core
Line 32 037_san4	3.33	11.23	0.22	62.83	0.05	0.02	1.80	19.69	0.00	99.17	68.72	0.28	31.00	9.32	0.148	Core
Line 33 037_san4	3.33	11.21	0.19	62.95	0.06	0.00	1.82	19.77	0.00	99.33	68.67	0.30	31.03	9.31	0.154	Core
Line 34 037_san4	3.24	10.99	0.23	61.70	0.06	0.01	1.75	19.19	0.00	97.18	68.83	0.33	30.84	9.12	0.159	Core
Line 35 037_san4	3.39	11.27	0.25	62.69	0.06	0.00	1.83	19.62	0.00	99.12	68.38	0.32	31.30	9.36	0.164	Core
Line 2 037_San16	2.22	13.69	0.64	63.82	0.00	0.00	0.11	18.82	0.03	99.33	80.26	0.00	19.74	11.36	0.000	Rim
Line 3 037_San16	2.22	13.53	0.58	64.14	0.01	0.00	0.10	18.81	0.04	99.43	80.04	0.04	19.92	11.23	0.005	Rim
Line 4 037_San16	2.18	13.35	0.60	63.20	0.02	0.00	0.85	19.09	0.00	99.30	80.02	0.09	19.90	11.08	0.009	Rim
Line 5 037_San16	2.10	13.65	0.54	63.13	0.03	0.00	0.23	18.45	0.02	98.15	80.91	0.16	18.94	11.33	0.014	Rim
Line 6 037_San16	2.07	13.68	0.48	63.26	0.00	0.00	0.52	19.27	0.00	99.28	81.28	0.01	18.71	11.36	0.020	Rim
Line 7 037_San16	2.07	13.38	0.47	62.62	0.02	0.00	1.29	19.38	0.00	99.23	80.88	0.09	19.03	11.11	0.024	Rim
Line 8 037_San16	2.01	13.00	0.47	61.66	0.00	0.01	2.47	19.44	0.00	99.06	80.97	0.00	19.03	10.79	0.030	Rim
Line 9 037_San16	2.01	12.87	0.44	61.65	0.00	0.00	2.98	19.60	0.00	99.55	80.82	0.00	19.18	10.68	0.035	Rim
Line 10 037_San16	2.26	12.55	0.37	61.73	0.00	0.00	2.80	19.43	0.00	99.14	78.54	0.00	21.46	10.42	0.039	Rim
Line 11 037_San16	3.06	11.84	0.23	63.00	0.04	0.00	1.34	19.57	0.00	99.07	71.70	0.18	28.12	9.83	0.045	Core

Line 12 037_San16	3.34	11.70	0.24	62.88	0.04	0.00	1.35	19.53	0.00	99.08	69.60	0.18	30.22	9.71	0.050	Core
Line 13 037_San16	3.30	11.55	0.23	62.84	0.04	0.00	1.32	19.44	0.00	98.72	69.59	0.18	30.24	9.59	0.055	Core
Line 14 037_San16	3.34	11.50	0.24	63.01	0.03	0.02	1.32	19.53	0.00	99.01	69.24	0.17	30.59	9.55	0.060	Core
Line 15 037_San16	3.35	11.53	0.23	62.96	0.03	0.00	1.27	19.54	0.00	98.92	69.25	0.14	30.61	9.57	0.066	Core
Line 16 037_San16	3.43	11.45	0.26	62.80	0.05	0.00	1.27	19.45	0.00	98.71	68.57	0.26	31.17	9.51	0.070	Core
Line 17 037_San16	3.36	11.45	0.20	62.83	0.04	0.00	1.26	19.54	0.00	98.67	69.00	0.19	30.81	9.51	0.076	Core
Line 18 037_San16	3.36	11.41	0.21	63.76	0.04	0.00	1.26	19.32	0.00	99.37	68.91	0.22	30.87	9.47	0.081	Core
Line 19 037_San16	3.35	11.34	0.24	63.81	0.03	0.00	1.29	19.37	0.00	99.44	68.88	0.17	30.95	9.41	0.086	Core
Line 20 037_San16	3.34	11.51	0.25	63.36	0.05	0.00	1.26	19.37	0.00	99.13	69.21	0.23	30.55	9.55	0.090	Core
Line 21 037_San16	3.37	11.46	0.25	63.76	0.04	0.00	1.33	19.49	0.00	99.70	68.96	0.18	30.86	9.51	0.096	Core
Line 22 037_San16	3.39	11.44	0.20	63.70	0.03	0.00	1.31	19.50	0.00	99.58	68.80	0.17	31.03	9.50	0.101	Core
Line 2 037_San19	2.36	13.57	0.66	63.43	0.00	0.00	0.13	18.96	0.02	99.13	79.11	0.00	20.89	11.27	0.000	Rim
Line 3 037_San19	2.58	13.08	0.59	63.41	0.03	0.00	0.25	19.50	0.00	99.45	76.79	0.16	23.05	10.86	0.005	Rim
Line 4 037_San19	2.16	12.76	0.46	62.37	0.03	0.00	2.07	19.67	0.00	99.52	79.40	0.14	20.46	10.59	0.010	Rim
Line 6 037_San19	2.15	12.29	0.42	61.51	0.01	0.01	3.40	19.76	0.00	99.55	78.94	0.05	21.01	10.20	0.021	Rim
Line 7 037_San19	2.26	12.27	0.42	61.32	0.01	0.00	3.42	19.76	0.00	99.46	78.06	0.04	21.90	10.19	0.025	Rim
Line 8 037_San19	2.55	11.82	0.37	61.03	0.01	0.00	3.28	19.71	0.00	98.76	75.27	0.04	24.69	9.81	0.031	Core
Line 9 037_San19	3.06	11.51	0.27	61.72	0.04	0.00	2.24	19.54	0.00	98.39	71.03	0.23	28.74	9.55	0.036	Core
Line 10 037_San19	3.30	11.21	0.24	62.52	0.04	0.00	2.24	19.48	0.00	99.03	68.95	0.21	30.84	9.31	0.040	Core

Line 11 037_San19	3.36	11.11	0.29	62.56	0.04	0.00	2.19	19.65	0.00	99.20	68.38	0.19	31.43	9.22	0.046	Core
Line 12 037_San19	3.34	11.05	0.27	62.70	0.04	0.00	2.21	19.71	0.00	99.32	68.37	0.23	31.40	9.17	0.051	Core
Line 13 037_San19	3.42	11.08	0.27	62.66	0.02	0.00	2.19	19.54	0.00	99.18	67.99	0.10	31.91	9.20	0.056	Core
Line 14 037_San19	3.37	11.11	0.27	62.40	0.04	0.01	2.15	19.67	0.00	99.01	68.32	0.19	31.49	9.22	0.061	Core
Line 15 037_San19	3.43	11.05	0.28	62.34	0.02	0.00	2.12	19.49	0.00	98.74	67.86	0.13	32.02	9.17	0.066	Core
Line 16 037_San19	3.45	11.12	0.26	62.17	0.04	0.00	2.16	19.73	0.00	98.93	67.82	0.19	31.99	9.23	0.071	Core
Line 17 037_San19	3.44	11.12	0.22	62.98	0.03	0.00	2.08	19.65	0.00	99.52	67.93	0.13	31.94	9.23	0.076	Core
Line 18 037_San19	3.45	11.10	0.26	63.20	0.03	0.00	1.95	19.53	0.00	99.52	67.82	0.13	32.04	9.21	0.081	Core
Line 19 037_San19	3.50	11.20	0.25	63.03	0.02	0.00	1.64	19.46	0.00	99.10	67.71	0.12	32.17	9.30	0.087	Core
Line 20 037_San19	3.49	11.19	0.23	63.24	0.02	0.00	1.60	19.57	0.00	99.34	67.76	0.12	32.13	9.29	0.091	Core
Line 21 037_San19	3.52	11.13	0.25	63.37	0.03	0.00	1.53	19.40	0.00	99.23	67.42	0.17	32.41	9.24	0.096	Core
Line 2 037_San18	2.32	12.53	0.53	62.31	0.04	0.00	2.14	19.46	0.00	99.33	77.85	0.22	21.94	10.40	0.000	Rim
Line 3 037_San18	2.20	12.25	0.47	61.05	0.05	0.00	3.29	19.71	0.00	99.02	78.33	0.29	21.38	10.17	0.005	Rim
Line 4 037_San18	2.09	12.29	0.47	60.68	0.14	0.04	3.46	19.56	0.00	98.72	78.90	0.74	20.37	10.20	0.011	Rim
Line 5 037_San18	2.14	12.47	0.42	61.24	0.02	0.00	3.42	19.78	0.00	99.49	79.23	0.12	20.65	10.35	0.015	Rim
Line 6 037_San18	2.12	12.43	0.40	61.55	0.01	0.00	3.30	19.71	0.00	99.51	79.41	0.03	20.56	10.32	0.020	Rim
Line 7 037_San18	2.24	12.45	0.44	61.38	0.01	0.01	3.21	19.78	0.00	99.51	78.49	0.04	21.47	10.34	0.026	Rim
Line 8 037_San18	2.40	12.37	0.32	62.17	0.03	0.00	2.56	19.54	0.00	99.39	77.10	0.14	22.77	10.27	0.030	Rim
Line 9 037_San18	2.70	12.09	0.30	62.00	0.07	0.00	2.44	19.73	0.00	99.34	74.38	0.38	25.25	10.04	0.035	Core

Line 10 037_San18	2.73	12.00	0.28	61.88	0.04	0.00	2.36	19.62	0.00	98.91	74.13	0.23	25.64	9.96	0.041	Core
Line 11 037_San18	2.67	12.05	0.30	61.97	0.03	0.00	2.35	19.66	0.00	99.02	74.72	0.13	25.15	10.00	0.047	Core
Line 12 037_San18	2.69	11.86	0.33	61.93	0.03	0.00	2.32	19.75	0.00	98.91	74.25	0.17	25.59	9.85	0.051	Core
Line 13 037_San18	2.67	11.99	0.30	62.01	0.03	0.00	2.34	19.61	0.00	98.94	74.62	0.13	25.24	9.95	0.056	Core
Line 14 037_San18	2.65	11.95	0.26	61.70	0.02	0.00	2.41	19.61	0.00	98.60	74.73	0.11	25.16	9.92	0.061	Core
Line 15 037_San18	2.68	12.02	0.27	62.06	0.03	0.00	2.38	19.71	0.00	99.15	74.59	0.15	25.26	9.98	0.066	Core
Line 16 037_San18	2.62	11.97	0.27	61.97	0.03	0.00	2.37	19.70	0.00	98.92	74.96	0.14	24.90	9.94	0.071	Core
Line 17 037_San18	2.68	12.02	0.27	62.37	0.03	0.00	2.37	19.71	0.00	99.45	74.61	0.13	25.26	9.98	0.077	Core
Line 18 037_San18	2.65	12.11	0.32	62.35	0.03	0.00	2.41	19.64	0.00	99.50	74.94	0.17	24.89	10.05	0.081	Core
Line 3 037_San9	2.15	12.81	0.47	62.79	0.01	0.15	1.47	19.21	0.00	99.05	79.68	0.04	20.28	10.63	0.000	Rim
Line 4 037_San9	2.24	13.67	0.47	63.56	0.01	0.01	0.21	18.83	0.01	99.01	80.03	0.06	19.91	11.35	0.006	Rim
Line 5 037_San9	2.21	13.41	0.45	62.97	0.05	0.01	0.76	19.20	0.00	99.06	79.78	0.27	19.95	11.13	0.010	Rim
Line 6 037_San9	2.08	13.31	0.43	62.76	0.06	0.04	1.08	19.02	0.00	98.78	80.53	0.31	19.16	11.05	0.016	Rim
Line 7 037_San9	2.24	13.34	0.42	62.55	0.03	0.01	1.02	19.03	0.00	98.63	79.58	0.14	20.28	11.07	0.019	Rim
Line 8 037_San9	2.14	13.50	0.43	62.49	0.00	0.00	1.21	19.24	0.00	99.02	80.54	0.01	19.45	11.21	0.025	Rim
Line 9 037_San9	2.02	13.32	0.41	62.36	0.00	0.00	1.82	19.43	0.00	99.36	81.26	0.00	18.74	11.06	0.031	Rim
Line 10 037_San9	1.97	13.67	0.43	62.29	0.00	0.00	1.20	19.25	0.00	98.82	82.03	0.00	17.97	11.35	0.036	Rim
Line 11 037_San9	1.98	13.40	0.40	62.05	0.01	0.00	1.92	19.44	0.00	99.20	81.63	0.03	18.34	11.12	0.040	Rim
Line 12 037_San9	1.97	13.66	0.39	62.55	0.00	0.00	1.10	19.41	0.00	99.08	82.01	0.01	17.98	11.34	0.045	Rim

Line 13 037_San9	1.99	13.41	0.43	62.03	0.02	0.01	1.57	19.61	0.00	99.07	81.53	0.08	18.39	11.13	0.051	Rim
Line 15 037_San9	2.02	13.15	0.40	61.36	0.02	0.00	2.57	19.53	0.00	99.04	81.00	0.08	18.92	10.92	0.060	Rim
Line 16 037_San9	2.02	13.17	0.37	61.29	0.01	0.00	2.50	19.68	0.00	99.04	81.05	0.05	18.90	10.93	0.065	Rim
Line 17 037_San9	1.94	13.21	0.42	61.52	0.00	0.00	2.49	19.58	0.00	99.16	81.76	0.00	18.24	10.97	0.070	Rim
Line 18 037_San9	2.06	13.14	0.40	61.42	0.02	0.00	2.51	19.42	0.00	98.97	80.66	0.11	19.23	10.91	0.076	Rim
Line 19 037_San9	2.04	12.98	0.39	61.62	0.00	0.00	2.59	19.46	0.00	99.08	80.72	0.00	19.28	10.78	0.080	Rim
Line 20 037_San9	2.48	12.33	0.35	61.93	0.02	0.00	2.52	19.52	0.00	99.16	76.51	0.12	23.38	10.24	0.085	Core
Line 21 037_San9	3.46	11.63	0.24	63.30	0.03	0.00	0.49	19.30	0.00	98.45	68.78	0.14	31.08	9.65	0.091	Core
Line 22 037_San9	3.53	11.55	0.23	63.27	0.03	0.00	0.49	19.14	0.00	98.24	68.18	0.15	31.66	9.59	0.095	Core
Line 23 037_San9	3.60	11.48	0.23	63.35	0.02	0.00	0.48	19.32	0.00	98.48	67.64	0.12	32.24	9.53	0.101	Core
Line 24 037_San9	3.64	11.51	0.22	63.55	0.03	0.00	0.47	19.31	0.00	98.73	67.43	0.15	32.42	9.55	0.105	Core
Line 25 037_San9	3.61	11.49	0.23	63.48	0.03	0.00	0.48	19.42	0.00	98.75	67.59	0.14	32.27	9.54	0.111	Core
Line 26 037_San9	3.59	11.56	0.23	63.36	0.03	0.00	0.51	19.32	0.00	98.60	67.83	0.16	32.01	9.60	0.116	Core
Line 27 037_San9	3.57	11.54	0.22	64.17	0.02	0.00	0.48	18.86	0.00	98.86	67.96	0.10	31.94	9.58	0.121	Core
Line 28 037_San9	3.67	11.57	0.25	62.57	0.02	0.00	0.48	19.34	0.00	97.91	67.39	0.12	32.49	9.60	0.126	Core
Line 29 037_San9	3.59	11.55	0.24	63.84	0.02	0.00	0.52	19.18	0.00	98.94	67.87	0.09	32.04	9.59	0.131	Core
Line 30 037_San9	3.59	11.45	0.19	64.08	0.02	0.00	0.55	19.34	0.00	99.22	67.66	0.12	32.22	9.51	0.136	Core
Line 31 037_San9	3.56	11.45	0.25	64.37	0.03	0.01	0.59	19.38	0.00	99.63	67.83	0.15	32.02	9.51	0.141	Core
Line 32 037_San9	3.57	11.45	0.21	64.05	0.02	0.00	0.58	19.31	0.00	99.18	67.81	0.09	32.10	9.51	0.145	Core

Line 33 037_San9	3.57	11.47	0.26	63.91	0.03	0.01	0.56	19.28	0.00	99.08	67.81	0.14	32.04	9.52	0.151	Core
Line 34 037_San9	3.54	11.49	0.24	63.94	0.02	0.01	0.57	19.30	0.00	99.11	68.05	0.12	31.82	9.54	0.156	Core
Line 35 037_San9	3.55	11.47	0.22	64.23	0.03	0.00	0.56	19.40	0.00	99.47	67.92	0.17	31.91	9.52	0.161	Core
Line 2 037_San101	2.22	13.23	0.54	62.75	0.07	0.00	0.94	19.40	0.00	99.15	79.40	0.34	20.25	10.98	0.000	Groundmass
Line 3 037_San101	2.07	13.04	0.52	62.86	0.03	0.00	1.63	19.64	0.00	99.79	80.45	0.17	19.39	10.83	0.005	Groundmass
Line 4 037_San101	2.08	13.29	0.49	62.52	0.02	0.00	1.00	19.41	0.00	98.81	80.70	0.12	19.17	11.03	0.010	Groundmass
Line 5 037_San101	1.96	12.62	0.50	61.14	0.04	0.00	3.28	19.74	0.00	99.28	80.76	0.22	19.02	10.48	0.016	Groundmass
Line 6 037_San101	1.95	12.85	0.52	61.65	0.01	0.00	3.17	19.51	0.00	99.67	81.16	0.07	18.77	10.67	0.021	Groundmass
Line 7 037_San101	1.99	12.88	0.45	61.49	0.00	0.00	2.85	19.38	0.00	99.03	81.02	0.00	18.98	10.69	0.026	Groundmass
Line 8 037_San101	1.95	12.93	0.45	62.12	0.00	0.00	2.64	19.63	0.00	99.73	81.32	0.00	18.68	10.73	0.030	Groundmass
Line 9 037_San101	1.98	13.03	0.50	61.69	0.02	0.01	2.75	19.41	0.00	99.39	81.13	0.09	18.78	10.82	0.035	Groundmass

Groundmass sanidines (measurements within core of microlites)

Comment	Oxide (wt%)									normalized values			
	Na_2O	K_2O	FeO	SiO_2	CaO	MgO	Al_2O_3	TiO_2	Sum	Or (mol%)	An (mol%)	Ab (mol%)	K (wt%)
037DR2_san1gm	2.43	13.21	0.56	63.70	0.03	0.00	19.32	0.00	99.54	78.03	0.16	21.81	11.05
037DR2_san2gm_1	2.30	13.45	0.62	64.41	0.03	0.00	18.83	0.04	99.97	79.27	0.13	20.60	11.20
037DR2_san2gm_2	2.08	13.42	0.53	63.40	0.00	0.01	18.86	0.00	98.58	80.94	0.00	19.06	11.33
037DR2_san2gm_3	2.13	13.40	0.58	63.61	0.01	0.00	18.89	0.00	98.90	80.52	0.03	19.45	11.28
037DR2_san3gm_2	2.25	13.24	0.61	63.19	0.02	0.04	18.55	0.00	98.17	79.40	0.09	20.51	11.22
037DR2_san3gm_3	2.24	13.46	0.65	64.15	0.02	0.00	18.86	0.00	99.66	79.73	0.10	20.16	11.24
037DR2_san5gm_1	2.24	13.75	0.63	65.10	0.00	0.01	18.64	0.04	100.67	80.15	0.00	19.85	11.37
037DR2_san5gm_2	2.04	12.88	0.52	62.29	0.00	0.00	19.19	0.00	97.18	79.97	0.13	19.90	11.14
037DR2_san5gm_3	2.14	13.07	0.42	62.88	0.03	0.00	18.91	0.00	97.71	80.76	0.00	19.24	11.29

037DR2_san5gm_4	2.08	13.27	0.42	62.75	0.00	0.01	19.06	0.00	97.85	77.79	0.17	22.04	10.80
037DR2_san6gm_2	2.06	12.81	0.80	62.31	0.49	0.16	18.62	0.00	97.50	78.33	2.53	19.14	10.94
037DR2_san6gm_3	2.10	13.41	0.49	63.60	0.01	0.00	19.12	0.00	98.99	80.73	0.06	19.22	11.27
037DR2_san6gm_4	2.12	13.12	0.45	62.42	0.01	0.00	19.17	0.00	97.56	80.24	0.06	19.70	11.20
037DR2_san6gm_5	2.34	13.54	0.52	63.96	0.01	0.00	18.79	0.03	99.45	79.15	0.05	20.80	11.33
037DR2_san7gm_1	2.26	13.82	0.60	64.70	0.00	0.00	18.82	0.03	100.50	80.09	0.00	19.91	11.45
037DR2_san7gm_4	2.03	13.01	1.05	62.80	0.75	0.29	18.62	0.00	98.80	77.77	3.79	18.45	10.96
037DR2_san7gm_5	2.02	13.60	0.40	63.66	0.00	0.00	19.02	0.00	98.96	81.57	0.01	18.42	11.44
037DR2_san7gm_6	2.04	13.51	0.48	63.13	0.00	0.01	19.05	0.00	98.48	81.33	0.00	18.67	11.42
037DR2_san7gm_8	2.27	13.28	0.54	63.54	0.02	0.00	19.10	0.00	99.01	79.31	0.09	20.60	11.17
037DR2_san10gm_3	2.60	13.02	0.51	63.48	0.07	0.01	19.34	0.00	99.24	76.48	0.32	23.20	10.92
037DR2_san11gm_2	2.41	13.54	0.58	63.81	0.00	0.00	18.96	0.02	99.53	78.70	0.01	21.29	11.32
037DR2_san11gm_3	2.21	12.97	0.50	62.60	0.05	0.00	19.09	0.00	97.63	79.23	0.25	20.52	11.05
037DR2_san12gm_2	1.97	13.37	0.48	62.38	0.02	0.00	19.22	0.00	97.66	81.64	0.08	18.28	11.39
037DR2_san12gm_3	2.20	13.44	0.50	63.37	0.04	0.00	18.87	0.00	98.65	79.91	0.22	19.87	11.34
037DR2_san13gm_1	2.08	13.54	0.52	63.46	0.04	0.00	18.98	0.00	98.83	80.92	0.19	18.89	11.40
037DR2_san13gm_4	2.41	13.44	0.36	62.81	0.07	0.02	19.09	0.00	98.41	78.31	0.35	21.34	11.36
037DR2_san13gm_6	2.27	13.72	0.52	64.39	0.04	0.00	18.90	0.02	100.07	79.73	0.22	20.05	11.40
037DR2_san14gm_1	2.13	13.70	0.43	64.01	0.00	0.00	18.94	0.00	99.42	80.89	0.00	19.11	11.46
037DR2_san14gm_3	1.98	13.18	0.48	62.55	0.07	0.01	19.04	0.00	97.51	81.12	0.36	18.52	11.24
037DR2_san14gm_5	1.96	13.27	0.43	62.27	0.00	0.00	19.20	0.00	97.33	81.67	0.00	18.33	11.34
037DR2_san14gm_8	2.22	13.50	0.51	63.98	0.00	0.00	19.09	0.00	99.50	80.00	0.00	19.99	11.29
037DR2_san14gm_9	3.18	12.94	0.64	62.19	0.01	0.00	19.28	0.02	98.46	72.77	0.06	27.18	10.93
037DR2_san14gm_10	2.22	13.45	0.55	63.98	0.12	0.00	18.95	0.07	99.55	79.49	0.58	19.93	11.24

EMP analyses of sample 149-6 feldspathoids

Data: Feldspathoid microlites (gm; within the crystal); rims (10µm from rim); cores; or profiles (rim to core).

Sample/Type	Oxide (wt%)										Sum	Distance to rim (mm)	K(wt%) (normalized value)	Classification
	Na_2O	SO_3	FeO	SiO_2	Cl	MgO	K_2O	Al_2O_3	CaO	TiO_2				
Sodalite														
149-6_foid1_gm_p1	18.45	2.93	0.95	38.82	4.31	0.06	0.60	33.97	0.80	0.03	100.91		0.49	Sodalite
149-6_foid1_gm_p2	21.17	2.84	0.76	37.83	4.36	0.01	1.33	32.89	0.87	0.01	102.07		1.08	Sodalite
149-6_foid1_gm_p3	22.82	1.16	1.08	38.18	6.25	0.06	0.63	33.22	0.23	0.03	103.65		0.50	Sodalite
149-6_foid1_gm_p4	20.42	3.68	0.62	36.85	3.36	0.00	1.55	31.84	1.06	0.03	99.41		1.29	Sodalite
149-6_foid1_gm_p5	20.53	2.24	0.87	38.24	5.24	0.07	0.87	33.25	0.57	0.04	101.92		0.71	Sodalite
149-6_foid3_gm_p1	23.08	1.16	0.83	37.95	6.23	0.01	0.89	32.88	0.31	0.01	103.35		0.72	Sodalite
149-6_foid3_gm_p2	21.58	1.50	0.80	38.56	5.58	0.07	0.87	32.51	0.43	0.00	101.89		0.71	Sodalite
149-6_foid3_gm_p4	21.36	1.73	0.77	37.84	5.69	0.03	1.16	33.49	0.51	0.02	102.60		0.94	Sodalite
149-6_foid5_rim1_p1	19.75	2.76	0.61	37.53	4.27	0.01	0.79	33.06	0.62	0.01	99.42		0.66	Sodalite
149-6_foid5_rim1_p2	18.00	3.38	1.09	38.06	3.60	0.34	0.80	32.51	0.71	0.07	98.56		0.68	Sodalite
149-6_foid5_rim1_p3	21.97	1.20	0.84	38.20	6.17	0.03	0.80	33.38	0.28	0.01	102.87		0.65	Sodalite
149-6_foid5_rim2_p5	18.59	1.75	0.77	39.09	5.66	0.05	0.76	34.79	0.51	0.00	101.96		0.62	Sodalite
149-6_foid5_rim2_p6	23.45	0.98	0.92	37.61	6.38	0.02	0.91	32.23	0.28	0.04	102.81		0.74	Sodalite
149-6_foid6_gm_p1	18.23	3.73	0.98	37.88	3.65	0.11	0.53	32.51	0.75	0.03	98.39		0.45	Sodalite
149-6_foid6_gm_p2	16.33	5.21	0.57	35.84	2.24	0.06	0.56	32.97	1.49	0.02	95.28		0.49	Sodalite
149-6_foid6_gm_p3	20.55	3.65	0.63	37.16	3.72	0.03	0.71	32.37	0.99	0.02	99.83		0.59	Sodalite
149-6_foid6_gm_p4	16.70	4.68	0.65	37.49	2.90	0.01	0.43	33.52	1.16	0.00	97.54		0.37	Sodalite
149-6_foid6_gm_p5	19.28	3.08	0.96	38.07	4.29	0.11	0.52	33.10	0.64	0.05	100.10		0.43	Sodalite
149-6_foid6_gm_p6	19.75	4.61	0.60	35.53	2.94	0.00	0.82	32.67	1.09	0.02	98.03		0.69	Sodalite
149-6_foid13_rim1_p1	20.44	3.71	0.73	38.07	3.18	0.02	1.87	32.16	0.78	0.01	100.96		1.54	Sodalite
149-6_foid13_rim1_p2	20.74	3.40	0.78	38.48	3.27	0.02	1.45	32.66	0.74	0.01	101.55		1.19	Sodalite
149-6_foid13_rim1_p3	20.70	3.34	0.70	38.34	3.29	0.00	1.92	32.10	0.71	0.01	101.11		1.58	Sodalite
149-6_foid13_rim2_p4	20.22	3.73	0.69	38.41	3.10	0.00	1.81	32.68	0.82	0.01	101.46		1.48	Sodalite
149-6_foid13_rim2_p5	19.04	3.60	0.71	38.26	3.27	0.01	0.92	33.14	0.80	0.01	99.76		0.76	Sodalite
Nepheline														
149-6_foid7_gm_p1	16.40	0.01	1.81	47.64	0.01	0.06	4.14	30.82	0.07	0.01	100.96		3.40	Nepheline

149-6_foid7_gm_p2	16.37	0.01	1.81	46.22	0.02	0.09	4.48	31.17	0.09	0.02	100.28		3.71	Nepheline
149-6_foid7_gm_p4	16.69	0.01	1.81	45.34	0.00	0.04	4.82	31.65	0.09	0.03	100.48		3.98	Nepheline
149-6_foid9_profile_1	16.81	0.00	1.91	43.48	0.01	0.02	4.68	31.60	0.10	0.03	98.65	0.00	3.93	Nepheline
149-6_foid9_profile_2	16.80	0.00	1.85	43.57	0.02	0.06	4.54	31.44	0.11	0.03	98.42	0.01	3.83	Nepheline
149-6_foid9_profile_3	15.91	0.00	1.86	48.34	0.01	0.07	4.23	29.97	0.07	0.00	100.45	0.02	3.49	Nepheline
149-6_foid9_profile_4	16.26	0.00	2.02	46.95	0.01	0.12	4.51	30.78	0.10	0.03	100.79	0.04	3.72	Nepheline
149-6_foid9_profile_5	15.68	0.01	1.74	47.75	0.01	0.06	5.09	30.44	0.09	0.01	100.88	0.05	4.19	Nepheline
149-6_foid9_rim1_p1	16.18	0.00	1.85	47.55	0.01	0.07	5.18	31.02	0.10	0.02	101.97		4.21	Nepheline
149-6_foid9_rim1_p2	16.44	0.01	1.92	46.84	0.00	0.05	4.70	31.39	0.10	0.03	101.48		3.84	Nepheline
149-6_foid9_rim2_p4	15.72	0.01	1.90	48.62	0.01	0.21	5.12	30.65	0.09	0.04	102.37		4.15	Nepheline
149-6_foid9_rim2_p5	12.92	0.01	1.60	49.44	0.00	0.04	5.25	31.65	0.09	0.02	101.02		4.31	Nepheline
149-6_foid9_rim2_p6	14.12	0.00	1.59	51.32	0.01	0.02	6.39	29.04	0.07	0.02	102.57		5.17	Nepheline
149-6_foid15_rim1_p3	16.72	0.00	1.66	45.57	0.03	0.02	4.71	31.67	0.10	0.01	100.50		3.89	Nepheline
149-6_foid15_rim2_p4	16.78	0.00	1.96	45.98	0.00	0.20	4.71	31.34	0.10	0.03	101.11		3.87	Nepheline
149-6_foid15_rim2_p6	14.09	0.02	2.97	48.79	0.07	0.40	4.95	29.04	0.15	0.15	100.64		4.08	Nepheline
149-6_foid16_rim1_p1	16.76	0.00	1.85	47.21	0.00	0.14	4.33	31.51	0.09	0.01	101.92		3.53	Nepheline
149-6_foid16_rim1_p2	16.87	0.00	1.59	46.87	0.01	0.07	4.21	31.63	0.07	0.01	101.33		3.45	Nepheline
149-6_foid16_rim1_p3	16.53	0.01	1.53	47.75	0.00	0.03	4.38	31.06	0.06	0.01	101.36		3.58	Nepheline
149-6_foid16_rim2_p4	15.56	0.00	1.95	49.70	0.02	0.39	4.57	30.48	0.11	0.03	102.80		3.69	Nepheline
149-6_foid16_rim2_p5	17.01	0.01	1.89	46.34	0.01	0.05	4.39	31.64	0.07	0.02	101.43		3.59	Nepheline
149-6_foid16_rim2_p6	16.87	0.00	1.88	45.74	0.00	0.04	4.75	31.75	0.13	0.06	101.23		3.89	Nepheline
149-6_foid16_profile1	16.86	0.01	1.68	48.25	0.01	0.04	4.21	31.54	0.08	0.01	102.69	0.00	3.40	Nepheline
149-6_foid16_profile2	16.88	0.02	1.70	47.31	0.01	0.05	4.07	31.31	0.08	0.02	101.44	0.01	3.33	Nepheline
149-6_foid16_profile3	13.37	0.00	1.40	50.75	0.02	0.04	6.45	28.32	0.07	0.04	100.46	0.03	5.33	Nepheline
149-6_foid16_profile4	14.44	0.03	1.74	49.22	0.02	0.18	6.29	30.01	0.13	0.06	102.12	0.07	5.11	Nepheline
149-6_foid16_profile5	16.51	0.00	1.95	46.67	0.00	0.05	4.75	31.43	0.09	0.03	101.47	0.10	3.89	Nepheline
149-6_neph1_rim1_p1	15.43		1.17	43.28		0.00	5.61	34.39	0.17	0.00	100.05		4.65	Nepheline
149-6_neph1_rim2_p4	15.38		0.94	43.47		0.00	5.58	34.17	0.15	0.00	99.70		4.65	Nepheline
149-6_neph1_rim2_p5	15.03		1.04	43.68		0.00	5.50	34.22	0.17	0.02	99.67		4.58	Nepheline
149-6_neph1_rim2_p6	14.15		1.69	46.65		0.03	4.57	33.08	0.10	0.02	100.28		3.78	Nepheline
149-6_neph2_rim1_p1	15.22		1.01	43.76		0.00	5.54	34.11	0.18	0.00	99.82		4.60	Nepheline

149-6_neph2_rim1_p3	15.26		1.05	44.00		0.00	5.42	34.55	0.14	0.01	100.43		4.47	Nepheline
149-6_neph2_rim2_p4	15.16		1.10	43.93		0.00	5.49	34.62	0.15	0.02	100.47		4.54	Nepheline
149-6_neph2_rim2_p5	14.68		0.96	44.21		0.00	5.34	34.45	0.13	0.01	99.78		4.44	Nepheline
149-6_neph2_rim2_p6	15.22		1.00	44.12		0.00	5.42	34.85	0.16	0.01	100.78		4.46	Nepheline
149-6_neph2_rim2_p7	15.21		1.06	43.32		0.00	5.52	34.08	0.18	0.01	99.38		4.61	Nepheline
149-6_neph3_rim1_p1	13.79		1.35	46.20		0.04	4.15	32.52	0.25	0.14	98.44		3.50	Nepheline
149-6_neph3_rim1_p2	14.90		1.49	47.06		0.02	4.36	31.76	0.07	0.03	99.70		3.63	Nepheline
149-6_neph3_rim1_p3	14.38		1.43	46.78		0.01	4.39	32.50	0.09	0.03	99.61		3.65	Nepheline
149-6_neph3_rim2_p4	14.40		1.40	46.99		0.01	4.26	32.24	0.08	0.03	99.40		3.55	Nepheline
149-6_neph3_rim2_p5	14.07		1.36	47.41		0.00	3.72	31.18	0.77	0.01	98.51		3.13	Nepheline
149-6_neph3_rim2_p6	14.45		1.45	47.83		0.03	3.94	32.77	0.07	0.02	100.55		3.25	Nepheline
149-6_neph3_rim2_p7	14.61		1.44	47.65		0.01	4.07	32.72	0.11	0.05	100.67		3.36	Nepheline
149-6_neph3_rim2_p8	14.09		1.40	48.40		0.02	3.87	32.36	0.07	0.00	100.20		3.20	Nepheline
149-6_neph4_rim1_p1	14.12		1.52	46.95		0.02	4.41	32.54	0.09	0.03	99.68		3.67	Nepheline
149-6_neph4_rim1_p3	13.55		1.51	47.80		0.06	5.08	32.15	0.12	0.03	100.29		4.20	Nepheline
149-6_neph4_rim2_p4	15.38		1.08	43.93		0.01	5.56	34.96	0.22	0.02	101.15		4.56	Nepheline
149-6_neph4_rim2_p6	15.30		0.94	43.57		0.00	5.56	34.74	0.22	0.02	100.35		4.59	Nepheline
149-6_neph4_rim2_p7	14.88		1.52	45.19		0.03	5.02	33.80	0.09	0.00	100.54		4.15	Nepheline
149-6_fsp6_profile1_p1	14.52		1.06	44.16		0.00	5.42	34.48	0.14	0.04	99.81	0.00	4.50	Nepheline
149-6_fsp6_profile1_p2	15.20		1.08	44.11		0.00	5.47	35.02	0.20	0.01	101.09	0.03	4.49	Nepheline
149-6_fsp6_profile1_p3	15.34		0.95	43.88		0.00	5.46	34.50	0.23	0.02	100.39	0.06	4.51	Nepheline
149-6_fsp6_profile1_p4	15.21		0.92	43.75		0.00	5.52	34.92	0.25	0.01	100.58	0.09	4.56	Nepheline
149-6_fsp6_profile1_p5	15.23		0.95	43.59		0.00	5.47	34.53	0.26	0.03	100.05	0.16	4.54	Nepheline
149-6_fsp6_profile1_p6	15.26		1.00	43.56		0.01	5.52	34.29	0.26	0.00	99.90	0.20	4.59	Nepheline
149-6_fsp6_profile1_p7	15.22		0.92	43.90		0.01	5.47	34.59	0.24	0.01	100.35	0.30	4.52	Nepheline
149-6_fsp6_profile1_p8	15.21		0.95	43.79		0.00	5.48	34.64	0.24	0.01	100.32	0.36	4.53	Nepheline
Strongly zoned sodalite group minerals														
149-6_foid2_profil_1	16.09	2.62	2.41	42.51	2.84	0.12	2.14	28.87	0.77	0.22	98.59	0.00	1.80	Sodalite
149-6_foid2_profil_2	18.96	5.81	0.59	37.34	1.74	0.00	0.93	33.17	0.76	0.00	99.30	0.01	0.78	Nosean-Haüyne
149-6_foid2_profil_3	19.86	5.98	0.53	36.91	1.63	0.00	0.93	32.75	0.84	0.01	99.44	0.02	0.77	Nosean-Haüyne
149-6_foid2_profil_4	19.21	6.70	0.53	36.71	1.40	0.00	0.87	32.79	1.23	0.01	99.44	0.02	0.73	Nosean-Haüyne

149-6_foid2_profil_5	19.70	5.88	0.53	36.96	1.70	0.00	0.95	33.00	0.78	0.01	99.51	0.03	0.79	Nosean-Haüyne
149-6_foid2_profil_7	22.25	0.84	1.42	38.11	6.57	0.13	0.72	33.41	0.14	0.06	103.65	0.05	0.57	Sodalite
149-6_foid4_rim1_p1	18.97	5.32	0.60	36.83	2.34	0.02	0.87	32.81	1.28	0.04	99.09		0.73	Nosean-Haüyne
149-6_foid4_rim1_p2	16.77	5.19	0.51	37.12	2.33	0.02	0.44	33.31	1.19	0.00	96.88		0.37	Nosean-Haüyne
149-6_foid4_rim1_p3	18.76	4.40	0.58	37.37	2.93	0.01	0.56	32.41	0.92	0.03	97.96		0.47	Nosean-Haüyne
149-6_foid4_rim2_p4	18.12	4.72	0.59	37.55	2.78	0.04	0.69	32.59	1.10	0.02	98.20		0.58	Nosean-Haüyne
149-6_foid4_rim2_p5	18.06	5.40	0.50	36.81	2.17	0.00	0.65	32.89	1.46	0.03	97.97		0.55	Nosean-Haüyne
149-6_foid4_rim2_p6	19.02	1.49	1.65	38.42	5.35	0.36	0.80	31.55	0.41	0.12	99.17		0.67	Sodalite
149-6_foid4_profil_1	16.05	2.12	2.12	40.18	4.41	0.39	0.67	31.56	0.50	0.11	98.12	0.00	0.57	Sodalite
149-6_foid4_profil_2	16.76	5.29	0.46	36.92	2.13	0.04	0.58	33.31	1.33	0.02	96.84	0.01	0.50	Nosean-Haüyne
149-6_foid4_profil_3	18.19	5.84	0.52	36.66	1.71	0.01	1.11	32.88	1.65	0.01	98.57	0.03	0.94	Nosean-Haüyne
149-6_foid4_profil_4	17.31	5.75	0.49	37.13	1.73	0.00	0.80	33.06	1.60	0.01	97.88	0.04	0.68	Nosean-Haüyne
149-6_foid5_profil_1	20.27	3.95	0.55	36.99	3.05	0.01	1.42	32.22	0.89	0.01	99.36	0.00	1.19	Nosean-Haüyne
149-6_foid5_profil_2	18.28	5.42	0.54	36.80	1.97	0.00	1.29	32.94	1.43	0.02	98.68	0.02	1.09	Nosean-Haüyne
149-6_foid5_profil_3	17.75	5.51	0.47	37.26	1.90	0.00	1.02	32.74	1.52	0.02	98.18	0.03	0.86	Nosean-Haüyne
149-6_foid5_profil_4	16.60	5.42	0.46	38.11	1.91	0.04	0.73	33.06	1.41	0.01	97.75	0.05	0.62	Nosean-Haüyne
149-6_foid5_profil_5	19.34	4.59	0.60	37.05	2.82	0.01	0.97	32.82	1.20	0.03	99.43	0.07	0.81	Nosean-Haüyne
149-6_foid5_profil_6	22.35	1.63	0.83	37.77	5.56	0.03	0.65	32.59	0.37	0.02	101.80	0.08	0.53	Nosean-Haüyne
149-6_foid8_rim1_p1	19.20	3.51	0.64	37.69	3.39	0.03	0.53	32.74	1.01	0.14	98.88		0.45	Sodalite
149-6_foid8_rim1_p2	19.86	3.80	0.70	37.18	3.17	0.01	0.85	32.20	1.34	0.01	99.12		0.71	Sodalite
149-6_foid8_rim1_p3	20.07	4.11	0.57	37.26	3.00	0.01	1.17	32.13	1.02	0.01	99.35		0.98	Sodalite
149-6_foid8_rim2_p4	19.73	4.13	0.61	37.29	3.00	0.00	0.84	32.52	1.03	0.01	99.16		0.70	Sodalite
149-6_foid8_rim2_p6	23.99	1.12	0.88	37.42	6.31	0.01	0.89	30.46	0.23	0.01	101.33		0.73	Sodalite
149-6_foid8_rim2_p7	22.11	1.06	1.00	37.06	6.10	0.07	0.90	30.68	0.29	0.04	99.31		0.75	Sodalite
149-6_foid8_profile_3	12.99	2.28	1.54	40.97	3.78	0.25	0.59	31.58	0.72	0.20	94.89	0.03	0.70	Nosean-Haüyne
149-6_foid8_profile_4	18.64	5.30	0.59	36.95	2.48	0.03	0.84	32.72	1.32	0.00	98.86	0.04	0.83	Nosean-Haüyne
149-6_foid8_profile_5	19.16	5.33	0.50	36.69	2.43	0.00	0.99	32.50	1.40	0.02	99.02	0.06	0.70	Nosean-Haüyne
149-6_foid8_profile_6	19.39	4.93	0.61	37.21	2.68	0.01	0.84	32.58	1.20	0.02	99.47	0.07	0.47	Sodalite

9.2.3 *Appendix C – 40Ar-39Ar data tables and inverse isochron plots from sanidine, nepheline and sodalite analyses of five samples from the Cadamosto Seamount*

ARGO Laboratory

GEOMAR Helmholtz Centre for Oceanographic Research Kiel, Kiel, Germany

149-2 sanidine total fusion

Relative Abundances	Laser power	[a]	36Ar [V]	%1σ	37Ar [V]	%1σ	38Ar [V]	%1σ	39Ar [V]	%1σ	40Ar [V]	%1σ	40(r)/39(k)[b] ± 2σ	Age ± 2σ (Ka)	40Ar(r) (%)	39Ar(k) (%)	K/Ca ± 2σ	Weight (mg)	Wt. % K[b]	$^{36}Ar/^{39}Ar$ Alt. Index[c]
C42BA078	15.00 W		0.0000455	29.162	0.0000782	184.733	0.0007120	2.207	0.0582289	0.324	0.0259542	3.469	0.21433 ± 0.13811	12.5 ± 8.0	48.09	4.12	380 ± 1403	0.602	11.6	*0.00000*
C42BB003	15.00 W	•	0.0004055	3.383	0.0011958	144.036	0.0005962	3.758	0.0444101	0.455	0.1302049	0.321	0.23543 ± 0.18386	13.7 ± 10.7	8.03	3.14	19 ± 55	0.446	11.9	*0.00003*
C42BA087	15.00 W	•	0.0001029	12.997	0.0000913	146.066	0.0005759	2.676	0.0457178	0.461	0.0425712	2.121	0.26533 ± 0.17733	15.4 ± 10.3	28.49	3.23	255 ± 746	0.471	11.6	*0.00001*
C42BB001	15.00 W	•	0.0003633	5.558	0.0017083	100.703	0.0010288	3.072	0.0847603	0.271	0.1304960	0.267	0.27402 ± 0.14112	15.9 ± 8.2	17.80	6.00	25 ± 51	0.903	11.2	*0.00002*
C42BA073	15.00 W	•	0.0001412	12.292	0.0001428	106.823	0.0008796	2.164	0.0694240	0.256	0.0614571	1.470	0.28346 ± 0.15010	16.5 ± 8.7	32.02	4.91	248 ± 530	0.786	10.5	*0.00001*
C42BB002	15.00 W	•	0.0000371	32.102	0.0013297	129.263	0.0003825	4.901	0.0296058	0.376	0.0196186	0.815	0.29570 ± 0.23791	17.2 ± 13.8	44.62	2.09	11 ± 29	0.316	11.2	*0.00000*
C42BA082	15.00 W	•	0.0000283	66.696	0.0000478	324.419	0.0004765	3.820	0.0375100	0.368	0.0196034	4.579	0.29895 ± 0.30109	17.4 ± 17.5	57.20	2.65	400 ± 2595	0.389	11.5	*0.00000*
C42BA074	15.00 W	•	0.0001831	11.434	0.0000888	148.926	0.0009169	2.605	0.0740350	0.364	0.0767087	1.208	0.30455 ± 0.16904	17.7 ± 9.8	29.39	5.24	425 ± 1267	0.81	10.9	*0.00001*
C42BA077	15.00 W	•	0.0004083	5.011	0.0001378	92.827	0.0009947	2.982	0.0749649	0.428	0.1447538	0.638	0.32103 ± 0.16326	18.6 ± 9.5	16.63	5.30	277 ± 515	0.789	11.3	*0.00002*
C42BB006	15.00 W	•	0.0000642	27.450	0.0003655	471.931	0.0005739	2.758	0.0473109	0.484	0.0350809	0.633	0.34031 ± 0.22050	19.8 ± 12.8	45.90	3.35	66 ± 623	0.49	11.5	*0.00001*
C42BA080	15.00 W	•	0.0003476	4.485	0.0001458	93.650	0.0006829	2.710	0.0499779	0.441	0.1204390	0.748	0.35390 ± 0.18801	20.6 ± 10.9	14.69	3.54	175 ± 327	0.552	10.8	*0.00002*
C42BA075	15.00 W	•	0.0000272	56.777	0.0000542	271.506	0.0003178	5.096	0.0259600	0.368	0.0174564	5.159	0.36210 ± 0.35855	21.0 ± 20.8	53.85	1.84	244 ± 1326	0.294	10.5	*0.00000*
C42BA083	15.00 W	•	0.0008178	4.057	0.0001136	119.079	0.0017429	1.688	0.1319606	0.292	0.2902314	0.320	0.36735 ± 0.14940	21.3 ± 8.7	16.70	9.34	593 ± 1411	1.376	11.5	*0.00002*
C42BA079	15.00 W	•	0.0000852	17.894	0.0001265	105.147	0.0005035	4.705	0.0399121	0.403	0.0403585	2.239	0.37972 ± 0.23034	22.1 ± 13.4	37.55	2.82	161 ± 338	0.436	10.9	*0.00001*
C42BA081	15.00 W	•	0.0000413	36.070	0.0000050	2630.977	0.0005043	3.159	0.0435252	0.488	0.0287708	3.117	0.38020 ± 0.20626	22.1 ± 12.0	57.52	3.08	4442 ± 233759	0.459	11.3	*0.00000*
C42BB005	15.00 W	•	0.0001725	6.436	0.0005226	330.485	0.0006984	4.218	0.0546947	0.283	0.0725081	0.308	0.39387 ± 0.12039	22.9 ± 7.0	29.71	3.87	53 ± 353	0.596	11.0	*0.00001*
C42BB004	15.00 W	•	0.0001766	6.877	0.0011186	154.018	0.0009279	2.809	0.0745578	0.274	0.0836302	0.288	0.42214 ± 0.09663	24.5 ± 5.6	37.63	5.27	34 ± 105	0.731	12.2	*0.00001*
C42BA076	15.00 W	•	0.0000457	37.509	0.0011725	11.512	0.0008880	3.146	0.0696443	0.394	0.0432431	2.132	0.42747 ± 0.14802	24.8 ± 8.6	68.84	4.93	30 ± 7	0.776	10.7	*0.00000*
C42BA072	15.00 W	•	0.0001648	9.169	0.0002399	50.530	0.0009858	1.980	0.0805558	0.319	0.0842344	1.098	0.44072 ± 0.11325	25.6 ± 6.6	42.15	5.70	171 ± 173	0.924	10.4	*0.00001*
C42BA088	15.00 W	•	0.0000779	17.665	0.0001221	107.913	0.0009769	2.087	0.0820519	0.330	0.0616295	1.461	0.46982 ± 0.10153	27.3 ± 5.9	62.55	5.80	343 ± 740	0.818	12.0	*0.00000*
C42BA084	15.00 W	•	0.0000055	331.899	0.0000899	128.930	0.0005625	3.009	0.0450479	0.397	0.0233939	3.871	0.48259 ± 0.24133	28.0 ± 14.0	92.93	3.19	255 ± 659	0.501	10.7	*0.00000*
C42BA085	15.00 W	•	0.0010269	2.544	0.0001717	67.675	0.0013557	2.461	0.0972734	0.321	0.3510261	0.278	0.48840 ± 0.16038	28.4 ± 9.3	13.53	6.88	289 ± 391	1.102	10.5	*0.00004*
C42BA086	15.00 W	•	0.0001356	11.682	0.0000741	188.203	0.0006463	3.550	0.0523754	0.297	0.0669493	1.354	0.51238 ± 0.18211	29.8 ± 10.6	40.08	3.71	361 ± 1358	0.575	10.9	*0.00001*
		Σ	0.0049039	1.730	0.0082921	51.332	0.0179298	0.613	1.4135047	0.077	1.9703191	0.194								

Procedure Blanks	Laser power	36Ar [V]	1σ	37Ar [V]	1σ	38Ar [V]	1σ	39Ar [V]	1σ	40Ar [V]	1σ
C42BA078	15.00 W	0.0002736	0.0000110	0.0020806	0.0000346	0.0001357	0.0000101	0.0002591	0.0000403	0.0043896	0.0008902
C42BB003	15.00 W	0.0001702	0.0000092	0.0014009	0.0003131	0.0000729	0.0000087	0.0001078	0.0000121	0.0016241	0.0001362
C42BA087	15.00 W	0.0002940	0.0000110	0.0021593	0.0000346	0.0001278	0.0000101	0.0001937	0.0000403	0.0030400	0.0008902
C42BB001	15.00 W	0.0001503	0.0000092	0.0012270	0.0003131	0.0000674	0.0000087	0.0000850	0.0000121	0.0015531	0.0001362
C42BA073	15.00 W	0.0002617	0.0000110	0.0020343	0.0000346	0.0001403	0.0000101	0.0002976	0.0000403	0.0051829	0.0008902
C42BB002	15.00 W	0.0001627	0.0000092	0.0013354	0.0003131	0.0000708	0.0000087	0.0000993	0.0000121	0.0015974	0.0001362
C42BA082	15.00 W	0.0002820	0.0000110	0.0021130	0.0000346	0.0001324	0.0000101	0.0002321	0.0000403	0.0038333	0.0008902
C42BA074	15.00 W	0.0002638	0.0000110	0.0020424	0.0000346	0.0001395	0.0000101	0.0002908	0.0000403	0.0050426	0.0008902
C42BA077	15.00 W	0.0002701	0.0000110	0.0020670	0.0000346	0.0001370	0.0000101	0.0002703	0.0000403	0.0046218	0.0008902
C42BB006	15.00 W	0.0001924	0.0000092	0.0015951	0.0003131	0.0000790	0.0000087	0.0001333	0.0000121	0.0017033	0.0001362
C42BA080	15.00 W	0.0002779	0.0000110	0.0020969	0.0000346	0.0001340	0.0000101	0.0002455	0.0000403	0.0041090	0.0008902
C42BA075	15.00 W	0.0002659	0.0000110	0.0020506	0.0000346	0.0001387	0.0000101	0.0002839	0.0000403	0.0049023	0.0008902
C42BA083	15.00 W	0.0002855	0.0000110	0.0021266	0.0000346	0.0001310	0.0000101	0.0002209	0.0000403	0.0036011	0.0008902
C42BA079	15.00 W	0.0002757	0.0000110	0.0020888	0.0000346	0.0001348	0.0000101	0.0002523	0.0000403	0.0042493	0.0008902
C42BA081	15.00 W	0.0002800	0.0000110	0.0021051	0.0000346	0.0001332	0.0000101	0.0002387	0.0000403	0.0039687	0.0008902
C42BB005	15.00 W	0.0001852	0.0000092	0.0015318	0.0003131	0.0000770	0.0000087	0.0001250	0.0000121	0.0016775	0.0001362
C42BB004	15.00 W	0.0001777	0.0000092	0.0014663	0.0003131	0.0000749	0.0000087	0.0001164	0.0000121	0.0016508	0.0001362
C42BA076	15.00 W	0.0002680	0.0000110	0.0020588	0.0000346	0.0001379	0.0000101	0.0002771	0.0000403	0.0047620	0.0008902
C42BA072	15.00 W	0.0002596	0.0000110	0.0020263	0.0000346	0.0001411	0.0000101	0.0003041	0.0000403	0.0053183	0.0008902
C42BA088	15.00 W	0.0002961	0.0000110	0.0021675	0.0000346	0.0001269	0.0000101	0.0001869	0.0000403	0.0028997	0.0008902
C42BA084	15.00 W	0.0002876	0.0000110	0.0021348	0.0000346	0.0001302	0.0000101	0.0002141	0.0000403	0.0034608	0.0008902
C42BA085	15.00 W	0.0002898	0.0000110	0.0021430	0.0000346	0.0001294	0.0000101	0.0002073	0.0000403	0.0033205	0.0008902
C42BA086	15.00 W	0.0002919	0.0000110	0.0021512	0.0000346	0.0001286	0.0000101	0.0002005	0.0000403	0.0031803	0.0008902

Sample Parameters	Laser power	Material	Location	Analyst	Watts	%1σ	J	%1σ	MDF	%1σ	Volume Ratio	Sensitivity (mol/volt)	Day	Month	Year	Hour	Min	Resist	Irradiation	Project	Experiment	Nmb	Standard Name
C42BA078	15.00 W	K-feldspar (0.5-1.0 mm)	Cadamosto, Cape Verdes	Jan Sticklus	15	0.14	0.0000322	0.31	1.0098	0.21	1	1.203E-14	3	FEB	2017	8	50	1	can42	Examples	c42it14ip4_1492F	01	TCS2
C42BB003	15.00 W	K-feldspar (0.5-1.0 mm)	Cadamosto, Cape Verdes	Jan Sticklus	15	0.14	0.0000322	0.31	1.0098	0.21	1	1.203E-14	6	MAR	2017	16	14	1	can42	Examples	c42it14ip4_1492F	01	TCS2
C42BA087	15.00 W	K-feldspar (0.5-1.0 mm)	Cadamosto, Cape Verdes	Jan Sticklus	15	0.14	0.0000322	0.31	1.0098	0.21	1	1.203E-14	3	FEB	2017	13	29	1	can42	Examples	c42it14ip4_1492F	01	TCS2
C42BB001	15.00 W	K-feldspar (0.5-1.0 mm)	Cadamosto, Cape Verdes	Jan Sticklus	15	0.14	0.0000322	0.31	1.0098	0.21	1	1.203E-14	6	MAR	2017	14	57	1	can42	Examples	c42it14ip4_1492F	01	TCS2
C42BA073	15.00 W	K-feldspar (0.5-1.0 mm)	Cadamosto, Cape Verdes	Jan Sticklus	15	0.14	0.0000322	0.31	1.0098	0.21	1	1.203E-14	3	FEB	2017	6	6	1	can42	Examples	c42it14ip4_1492F	01	TCS2
C42BB002	15.00 W	K-feldspar (0.5-1.0 mm)	Cadamosto, Cape Verdes	Jan Sticklus	15	0.14	0.0000322	0.31	1.0098	0.21	1	1.203E-14	6	MAR	2017	15	45	1	can42	Examples	c42it14ip4_1492F	01	TCS2
C42BA082	15.00 W	K-feldspar (0.5-1.0 mm)	Cadamosto, Cape Verdes	Jan Sticklus	15	0.14	0.0000322	0.31	1.0098	0.21	1	1.203E-14	3	FEB	2017	10	45	1	can42	Examples	c42it14ip4_1492F	01	TCS2
C42BA074	15.00 W	K-feldspar (0.5-1.0 mm)	Cadamosto, Cape Verdes	Jan Sticklus	15	0.14	0.0000322	0.31	1.0098	0.21	1	1.203E-14	3	FEB	2017	6	35	1	can42	Examples	c42it14ip4_1492F	01	TCS2
C42BA077	15.00 W	K-feldspar (0.5-1.0 mm)	Cadamosto, Cape Verdes	Jan Sticklus	15	0.14	0.0000322	0.31	1.0098	0.21	1	1.203E-14	3	FEB	2017	8	2	1	can42	Examples	c42it14ip4_1492F	01	TCS2
C42BB006	15.00 W	K-feldspar (0.5-1.0 mm)	Cadamosto, Cape Verdes	Jan Sticklus	15	0.14	0.0000322	0.31	1.0098	0.21	1	1.203E-14	6	MAR	2017	17	40	1	can42	Examples	c42it14ip4_1492F	01	TCS2
C42BA080	15.00 W	K-feldspar (0.5-1.0 mm)	Cadamosto, Cape Verdes	Jan Sticklus	15	0.14	0.0000322	0.31	1.0098	0.21	1	1.203E-14	3	FEB	2017	9	48	1	can42	Examples	c42it14ip4_1492F	01	TCS2
C42BA075	15.00 W	K-feldspar (0.5-1.0 mm)	Cadamosto, Cape Verdes	Jan Sticklus	15	0.14	0.0000322	0.31	1.0098	0.21	1	1.203E-14	3	FEB	2017	7	4	1	can42	Examples	c42it14ip4_1492F	01	TCS2
C42BA083	15.00 W	K-feldspar (0.5-1.0 mm)	Cadamosto, Cape Verdes	Jan Sticklus	15	0.14	0.0000322	0.31	1.0098	0.21	1	1.203E-14	3	FEB	2017	11	33	1	can42	Examples	c42it14ip4_1492F	01	TCS2
C42BA079	15.00 W	K-feldspar (0.5-1.0 mm)	Cadamosto, Cape Verdes	Jan Sticklus	15	0.14	0.0000322	0.31	1.0098	0.21	1	1.203E-14	3	FEB	2017	9	19	1	can42	Examples	c42it14ip4_1492F	01	TCS2
C42BA081	15.00 W	K-feldspar (0.5-1.0 mm)	Cadamosto, Cape Verdes	Jan Sticklus	15	0.14	0.0000322	0.31	1.0098	0.21	1	1.203E-14	3	FEB	2017	10	17	1	can42	Examples	c42it14ip4_1492F	01	TCS2
C42BB005	15.00 W	K-feldspar (0.5-1.0 mm)	Cadamosto, Cape Verdes	Jan Sticklus	15	0.14	0.0000322	0.31	1.0098	0.21	1	1.203E-14	6	MAR	2017	17	12	1	can42	Examples	c42it14ip4_1492F	01	TCS2
C42BB004	15.00 W	K-feldspar (0.5-1.0 mm)	Cadamosto, Cape Verdes	Jan Sticklus	15	0.14	0.0000322	0.31	1.0098	0.21	1	1.203E-14	6	MAR	2017	16	43	1	can42	Examples	c42it14ip4_1492F	01	TCS2
C42BA076	15.00 W	K-feldspar (0.5-1.0 mm)	Cadamosto, Cape Verdes	Jan Sticklus	15	0.14	0.0000322	0.31	1.0098	0.21	1	1.203E-14	3	FEB	2017	7	33	1	can42	Examples	c42it14ip4_1492F	01	TCS2
C42BA072	15.00 W	K-feldspar (0.5-1.0 mm)	Cadamosto, Cape Verdes	Jan Sticklus	15	0.14	0.0000322	0.31	1.0098	0.21	1	1.203E-14	3	FEB	2017	5	38	1	can42	Examples	c42it14ip4_1492F	01	TCS2
C42BA088	15.00 W	K-feldspar (0.5-1.0 mm)	Cadamosto, Cape Verdes	Jan Sticklus	15	0.14	0.0000322	0.31	1.0098	0.21	1	1.203E-14	3	FEB	2017	13	58	1	can42	Examples	c42it14ip4_1492F	01	TCS2
C42BA084	15.00 W	K-feldspar (0.5-1.0 mm)	Cadamosto, Cape Verdes	Jan Sticklus	15	0.14	0.0000322	0.31	1.0098	0.21	1	1.203E-14	3	FEB	2017	12	2	1	can42	Examples	c42it14ip4_1492F	01	TCS2
C42BA085	15.00 W	K-feldspar (0.5-1.0 mm)	Cadamosto, Cape Verdes	Jan Sticklus	15	0.14	0.0000322	0.31	1.0098	0.21	1	1.203E-14	3	FEB	2017	12	31	1	can42	Examples	c42it14ip4_1492F	01	TCS2
C42BA086	15.00 W	K-feldspar (0.5-1.0 mm)	Cadamosto, Cape Verdes	Jan Sticklus	15	0.14	0.0000322	0.31	1.0098	0.21	1	1.203E-14	3	FEB	2017	13	0	1	can42	Examples	c42it14ip4_1492F	01	TCS2

Irradiation Constants	Laser power	40/36(a)	%1σ	40/36(c)	%1σ	38/36(a)	%1σ	38/36(c)	%1σ	39/37(ca)	%1σ	38/37(ca)	%1σ	36/37(ca)	%1σ	40/39(k)	%1σ	38/39(k)	%1σ	36/38(cl)	%1σ	K/Ca	%1σ	K/Cl	%1σ	Ca/Cl	%1σ
C42BA078	15.00 W	295.5	0.169	0.018	35	0.1869	0.107	1.493	3	0.000702	1.71	0.000196	0.41	0.0002702	0.15	0.00073	12.33	0.01215	0.25	262.8	0.65	0.51	0	0	0	0	0
C42BB003	15.00 W	295.5	0.169	0.018	35	0.1869	0.107	1.493	3	0.000702	1.71	0.000196	0.41	0.0002702	0.15	0.00073	12.33	0.01215	0.25	262.8	0.65	0.51	0	0	0	0	0
C42BA087	15.00 W	295.5	0.169	0.018	35	0.1869	0.107	1.493	3	0.000702	1.71	0.000196	0.41	0.0002702	0.15	0.00073	12.33	0.01215	0.25	262.8	0.65	0.51	0	0	0	0	0
C42BB001	15.00 W	295.5	0.169	0.018	35	0.1869	0.107	1.493	3	0.000702	1.71	0.000196	0.41	0.0002702	0.15	0.00073	12.33	0.01215	0.25	262.8	0.65	0.51	0	0	0	0	0
C42BA073	15.00 W	295.5	0.169	0.018	35	0.1869	0.107	1.493	3	0.000702	1.71	0.000196	0.41	0.0002702	0.15	0.00073	12.33	0.01215	0.25	262.8	0.65	0.51	0	0	0	0	0
C42BB002	15.00 W	295.5	0.169	0.018	35	0.1869	0.107	1.493	3	0.000702	1.71	0.000196	0.41	0.0002702	0.15	0.00073	12.33	0.01215	0.25	262.8	0.65	0.51	0	0	0	0	0
C42BA082	15.00 W	295.5	0.169	0.018	35	0.1869	0.107	1.493	3	0.000702	1.71	0.000196	0.41	0.0002702	0.15	0.00073	12.33	0.01215	0.25	262.8	0.65	0.51	0	0	0	0	0
C42BA074	15.00 W	295.5	0.169	0.018	35	0.1869	0.107	1.493	3	0.000702	1.71	0.000196	0.41	0.0002702	0.15	0.00073	12.33	0.01215	0.25	262.8	0.65	0.51	0	0	0	0	0
C42BA077	15.00 W	295.5	0.169	0.018	35	0.1869	0.107	1.493	3	0.000702	1.71	0.000196	0.41	0.0002702	0.15	0.00073	12.33	0.01215	0.25	262.8	0.65	0.51	0	0	0	0	0
C42BB006	15.00 W	295.5	0.169	0.018	35	0.1869	0.107	1.493	3	0.000702	1.71	0.000196	0.41	0.0002702	0.15	0.00073	12.33	0.01215	0.25	262.8	0.65	0.51	0	0	0	0	0
C42BA080	15.00 W	295.5	0.169	0.018	35	0.1869	0.107	1.493	3	0.000702	1.71	0.000196	0.41	0.0002702	0.15	0.00073	12.33	0.01215	0.25	262.8	0.65	0.51	0	0	0	0	0
C42BA075	15.00 W	295.5	0.169	0.018	35	0.1869	0.107	1.493	3	0.000702	1.71	0.000196	0.41	0.0002702	0.15	0.00073	12.33	0.01215	0.25	262.8	0.65	0.51	0	0	0	0	0
C42BA083	15.00 W	295.5	0.169	0.018	35	0.1869	0.107	1.493	3	0.000702	1.71	0.000196	0.41	0.0002702	0.15	0.00073	12.33	0.01215	0.25	262.8	0.65	0.51	0	0	0	0	0
C42BA079	15.00 W	295.5	0.169	0.018	35	0.1869	0.107	1.493	3	0.000702	1.71	0.000196	0.41	0.0002702	0.15	0.00073	12.33	0.01215	0.25	262.8	0.65	0.51	0	0	0	0	0
C42BA081	15.00 W	295.5	0.169	0.018	35	0.1869	0.107	1.493	3	0.000702	1.71	0.000196	0.41	0.0002702	0.15	0.00073	12.33	0.01215	0.25	262.8	0.65	0.51	0	0	0	0	0
C42BB005	15.00 W	295.5	0.169	0.018	35	0.1869	0.107	1.493	3	0.000702	1.71	0.000196	0.41	0.0002702	0.15	0.00073	12.33	0.01215	0.25	262.8	0.65	0.51	0	0	0	0	0
C42BB004	15.00 W	295.5	0.169	0.018	35	0.1869	0.107	1.493	3	0.000702	1.71	0.000196	0.41	0.0002702	0.15	0.00073	12.33	0.01215	0.25	262.8	0.65	0.51	0	0	0	0	0
C42BA076	15.00 W	295.5	0.169	0.018	35	0.1869	0.107	1.493	3	0.000702	1.71	0.000196	0.41	0.0002702	0.15	0.00073	12.33	0.01215	0.25	262.8	0.65	0.51	0	0	0	0	0
C42BA072	15.00 W	295.5	0.169	0.018	35	0.1869	0.107	1.493	3	0.000702	1.71	0.000196	0.41	0.0002702	0.15	0.00073	12.33	0.01215	0.25	262.8	0.65	0.51	0	0	0	0	0
C42BA088	15.00 W	295.5	0.169	0.018	35	0.1869	0.107	1.493	3	0.000702	1.71	0.000196	0.41	0.0002702	0.15	0.00073	12.33	0.01215	0.25	262.8	0.65	0.51	0	0	0	0	0
C42BA084	15.00 W	295.5	0.169	0.018	35	0.1869	0.107	1.493	3	0.000702	1.71	0.000196	0.41	0.0002702	0.15	0.00073	12.33	0.01215	0.25	262.8	0.65	0.51	0	0	0	0	0
C42BA085	15.00 W	295.5	0.169	0.018	35	0.1869	0.107	1.493	3	0.000702	1.71	0.000196	0.41	0.0002702	0.15	0.00073	12.33	0.01215	0.25	262.8	0.65	0.51	0	0	0	0	0
C42BA086	15.00 W	295.5	0.169	0.018	35	0.1869	0.107	1.493	3	0.000702	1.71	0.000196	0.41	0.0002702	0.15	0.00073	12.33	0.01215	0.25	262.8	0.65	0.51	0	0	0	0	0

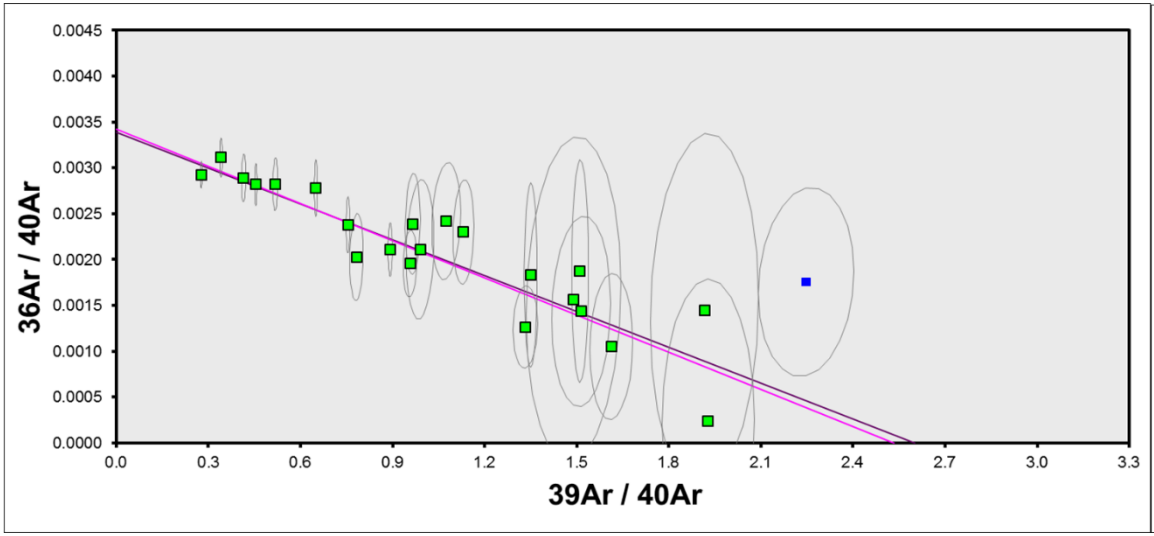
36Ar / 40Ar
39Ar / 40Ar
0.0045
0.0040
0.0035
0.0030
0.0025
0.0020
0.0015
0.0010
0.0005
0.0000
0.0
0.3
0.6
0.9
1.2
1.5
1.8
2.1
2.4
2.7
3.0
3.3

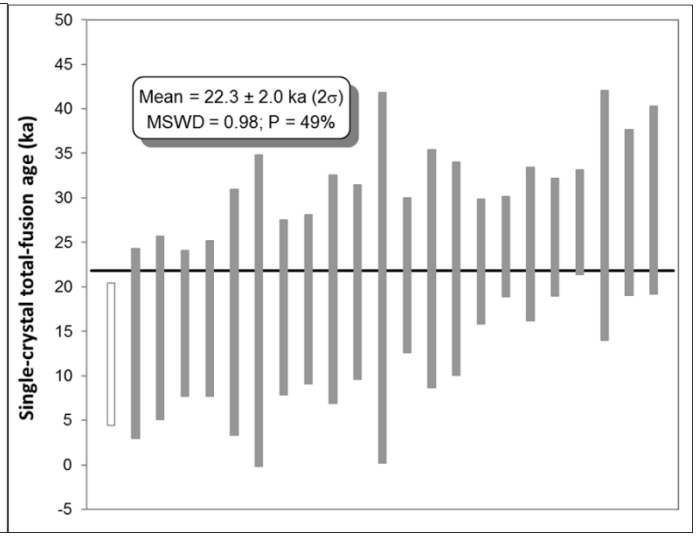
Single-crystal total-fusion age (ka)
Mean = 22.3 ± 2.0 ka (2σ)
MSWD = 0.98; P = 49%
50
45
40
35
30
25
20
15
10
5
0
-5

Information on Analysis and Constants Used in Calculations

Sample = 1492F
Material = K-feldspar
Location = Cadamosto, Cape Verdes
Analyst = Jan Sticklus
Project = EXAMPLES
Mass Discrimination Law = POW
Irradiation = can42
J = 0.00003220 ± 0.00000010
TCS2 = 27.870 ± 0.039 Ma
Heating = 45 sec
Instrument = MAP216

Age Equations = Conventional
Negative Intensities = Allowed
Decay Constant 40K = 5.543 ± 0.009 E-10 1/a
Decay Constant 39Ar = 2.940 ± 0.016 E-07 1/h
Decay Constant 37Ar = 8.230 ± 0.012 E-04 1/h
Decay Constant 36Cl = 2.257 ± 0.015 E-06 1/a
Atmospheric Ratio 40/36(a) = 295.50 ± 0.50
Atmospheric Ratio 38/36(a) = 0.1869 ± 0.0002
Production Ratio 39/37(ca) = 0.000702 ± 0.000012
Production Ratio 38/37(ca) = 0.000196 ± 0.000001
Production Ratio 36/37(ca) = 0.000270 ± 0.000000
Production Ratio 40/39(k) = 0.000730 ± 0.000090
Production Ratio 38/39(k) = 0.012150 ± 0.000030
Production Ratio 36/38(cl) = 262.80
Scaling Ratio K/Ca = 0.510

Results	40(a)/36(a) ± 2σ	40(r)/39(k) ± 2σ	Age ± 2σ (Ka)	MSWD	39Ar(k) (%,n)	K/Ca ± 2σ
Age Plateau		0.38455 ± 0.03364 ± 8.75%	22.3 ± 2.0 ± 8.77%	0.98	95.88	29 ± 7
		Minimal External Error ± 2.0		49%	22	
		Analytical Error ± 2.0		1.62	2σ Confidence Limit	
				1.0000	Error Magnification	
Total Fusion Age		0.36848 ± 0.03591 ± 9.75%	21.4 ± 2.1 ± 9.77%		23	87 ± 89
		Minimal External Error ± 2.1				
		Analytical Error ± 2.1				
Normal Isochron	297.42 ± 13.84 ± 4.65%	0.35056 ± 0.05919 ± 16.88%	20.4 ± 3.4 ± 16.90%	0.94	95.88	
		Minimal External Error ± 3.4		54%	22	
		Analytical Error ± 3.4		1.63	2σ Confidence Limit	
				1.0000	Error Magnification	
				24	Number of Iterations	
				0.0000021436	Convergence	
Inverse Isochron	292.39 ± 13.11 ± 4.49%	0.39482 ± 0.04981 ± 12.62%	22.9 ± 2.9 ± 12.63%	1.02	95.88	
		Minimal External Error ± 2.9		44%	22	
		Analytical Error ± 2.9		1.63	2σ Confidence Limit	
				1.0077	Error Magnification	
				3	Number of Iterations	
				0.0061242032	Convergence	
				65%	Spreading Factor	

[a] Blue dots in table indicate selected steps used to calculate the weighted mean and inverse isochron ages.
[b] Weight % K values calculated from $^{39}Ar_K$ values and weights of individual grains.
[c] Alteration Index values in italics indicate analyses from fresh material, normal font is from altered material (Baksi, 2007; van den Bogaard, 2013).
Values shown in red are negative values.
Abbreviations used in tables: (r) = radiogenic ^{40}Ar; (k) = Ar derived from K; (a) = atmospheric Ar; (ca) = Ar derived from Ca; (cl) = Ar derived from Ca; (c) = cosmogenic Ar; MDF = Mass Discrimination Factor.
Green squares in the inverse isochron plots indicate selected steps (blue dots in table), and blue squares are non-selected steps. Pink lines in the inverse isochron plot indicate a line fit through selected data, and the purple lines incidate a fit through an air $^{40}Ar/^{36}Ar$ ratio (295.5).
Stacked probability plot produced using Isoplot (Ludwig, 2011), where filled and unfilled 2σ error bars indicate selected/not selected data to calculate inverse-variance weighted mean age (black line), respectively.

149-6 total fusion

Relative Abundances	Laser power	[a]	36Ar [V]	%1σ	37Ar [V]	%1σ	38Ar [V]	%1σ	39Ar [V]	%1σ	40Ar [V]	%1σ	40(r)/39(k) ± 2σ	Age ± 2σ (Ka)	40Ar(r) (%)	39Ar(k) (%)	K/Ca ± 2σ	Weight (mg)	Wt. % K[b]	$^{36}Ar/^{39}Ar$ Alt. Index[c]
C36HA091	20.00 W		0.0001583	6.851	0.0029847	51.818	0.0052960	0.741	0.424113	0.233	0.05826	0.285	0.02697 ± 0.01515	11.5 ± 6.5	19.63	0.99	72.5 ± 75.1	0.654	10.50	*0.00001*
C36HA121	25.00 W		0.0005205	3.324	0.0081963	14.455	0.0149381	0.640	1.212482	0.218	0.19677	0.166	0.03527 ± 0.00846	15.1 ± 3.6	21.73	2.83	75.4 ± 21.8	1.954	10.05	*0.00001*
C36HA120	25.00 W	•	0.0008686	2.729	0.0052533	24.742	0.0136255	0.819	1.065267	0.221	0.30114	0.152	0.04146 ± 0.01320	17.8 ± 5.7	14.67	2.49	103.4 ± 51.2	1.752	9.85	*0.00002*
C36GC005	20.00 W	•	0.0006842	3.912	0.0006788	206.664	0.0056388	0.686	0.453663	0.218	0.22254	0.212	0.04420 ± 0.03497	18.9 ± 15.0	9.01	1.06	340.9 ± 1408.9	0.695	10.57	*0.00004*
C36HA119	25.00 W	•	0.0010362	2.653	0.0065411	24.343	0.0147631	0.710	1.183872	0.220	0.36033	0.147	0.04546 ± 0.01378	19.5 ± 5.9	14.93	2.76	92.3 ± 44.9	1.940	9.88	*0.00002*
C36GC100	25.00 W	•	0.0005210	4.082	0.0021081	86.425	0.0129722	0.706	1.035763	0.214	0.20222	0.515	0.04599 ± 0.01231	19.7 ± 5.3	23.56	2.42	250.6 ± 433.1	1.739	9.65	*0.00001*
C36GC104	25.00 W	•	0.0007460	2.727	0.0097528	21.946	0.0345007	0.506	2.797162	0.213	0.35764	0.289	0.04855 ± 0.00438	20.8 ± 1.9	37.97	6.53	146.3 ± 64.2	4.520	10.02	*0.00001*
C36GC106	25.00 W	•	0.0003849	3.782	0.0097853	20.932	0.0134244	0.713	1.087307	0.218	0.16667	0.615	0.04862 ± 0.00815	20.8 ± 3.5	31.72	2.54	56.7 ± 23.7	1.804	9.76	*0.00001*
C36HA122	25.00 W	•	0.0018267	1.506	0.0247142	5.382	0.0722566	0.457	5.784314	0.214	0.82955	0.086	0.04974 ± 0.00285	21.3 ± 1.2	34.68	13.50	119.4 ± 12.9	9.618	9.74	*0.00001*
C36HA117	25.00 W	•	0.0004007	5.167	0.0097898	15.045	0.0100242	0.618	0.810365	0.218	0.15858	0.271	0.04983 ± 0.01515	21.3 ± 6.5	25.46	1.89	42.2 ± 12.7	1.351	9.72	*0.00001*
C36GC103	25.00 W	•	0.0018669	1.926	0.0140216	13.714	0.0476596	0.565	3.731157	0.213	0.74267	0.138	0.05074 ± 0.00575	21.7 ± 2.5	25.49	8.71	135.7 ± 37.2	6.120	9.88	*0.00001*
C36HA118	25.00 W	•	0.0004240	2.883	0.0087973	17.279	0.0145290	0.619	1.176802	0.219	0.18783	0.171	0.05303 ± 0.00618	22.7 ± 2.6	33.22	2.75	68.2 ± 23.6	1.977	9.64	*0.00001*
C36GC101	25.00 W	•	0.0010277	1.658	0.0023691	79.584	0.0173904	0.742	1.354493	0.214	0.37965	0.301	0.05549 ± 0.00767	23.8 ± 3.3	19.80	3.16	291.6 ± 464.1	2.218	9.89	*0.00002*
C36GC105	25.00 W	•	0.0089829	1.033	0.0213425	9.282	0.0506497	0.528	3.728054	0.211	2.88622	0.051	0.06192 ± 0.01493	26.5 ± 6.4	8.00	8.70	89.1 ± 16.5	6.373	9.48	*0.00005*
C36GC102	25.00 W		0.0014689	1.272	0.0113907	16.759	0.0428666	0.649	3.381172	0.213	0.66482	0.162	0.06776 ± 0.00337	29.0 ± 1.4	34.46	7.89	151.4 ± 50.7	5.695	9.62	*0.00001*
C36HA088	25.00 W		0.0005848	3.138	0.0062818	23.802	0.0036517	1.426	0.282093	0.234	0.28415	0.115	0.39577 ± 0.03863	169.5 ± 16.5	39.29	0.66	22.9 ± 10.9	1.103	4.14	-
C36HA086	20.00 W		0.0003814	3.761	0.0023612	67.698	0.0022947	0.867	0.181446	0.270	0.20466	0.160	0.50704 ± 0.04702	217.1 ± 20.1	44.95	0.42	39.2 ± 53.1	0.697	4.22	-
C36GC002	25.00 W		0.0002250	7.093	0.0023381	57.441	0.0029133	1.007	0.236658	0.232	0.22207	0.165	0.65739 ± 0.04011	281.5 ± 17.2	70.06	0.55	51.6 ± 59.3	0.869	4.41	-
C36GC097	25.00 W		0.0005800	2.228	0.0152050	11.252	0.0112646	0.732	0.908978	0.217	0.78081	0.146	0.67099 ± 0.00927	287.3 ± 4.0	78.11	2.12	30.5 ± 6.9	3.573	4.12	-
C36HA092	25.00 W		0.0001893	4.515	0.0054146	27.291	0.0033085	1.343	0.270094	0.297	0.23978	0.131	0.68150 ± 0.01931	291.8 ± 8.3	76.77	0.63	25.4 ± 13.9	1.035	4.23	-
C36HA093	25.00 W		0.0002645	6.298	0.0053913	33.539	0.0036619	1.117	0.285276	0.230	0.27891	0.137	0.70456 ± 0.03479	301.7 ± 14.9	72.06	0.67	27.0 ± 18.1	1.120	4.13	-
C36HA090	25.00 W		0.0001082	10.027	0.0062726	28.261	0.0049962	0.976	0.405390	0.247	0.36835	0.113	0.83028 ± 0.01649	355.5 ± 7.1	91.38	0.95	33.0 ± 18.6	1.669	3.93	-
C36GC010	20.00 W		0.0000496	36.250	0.0030176	42.196	0.0015111	1.443	0.125857	0.284	0.12366	0.235	0.86733 ± 0.08465	371.4 ± 36.2	88.27	0.29	21.3 ± 18.0	0.452	4.51	-
C36GC099	25.00 W		0.0196809	0.887	0.0179529	11.196	0.0107402	0.910	0.552801	0.222	6.30907	0.039	0.89432 ± 0.19021	383.0 ± 81.4	7.84	1.29	15.7 ± 3.5	2.223	4.03	-
C36GC004	20.00 W		0.0002909	6.546	0.0047886	27.816	0.0031853	1.545	0.257211	0.236	0.38251	0.082	1.15358 ± 0.04419	494.0 ± 18.9	77.57	0.60	27.4 ± 15.2	0.915	4.55	-
C36HA094	20.00 W		0.0007911	3.073	0.0053516	25.374	0.0033444	1.542	0.260615	0.230	0.55385	0.090	1.22910 ± 0.05564	526.3 ± 23.8	57.83	0.61	24.8 ± 12.6	0.983	4.29	-
C36GC008	20.00 W		0.0001368	14.583	0.0066347	19.434	0.0017849	2.606	0.143241	0.335	0.27325	0.161	1.62837 ± 0.08328	697.2 ± 35.7	85.36	0.33	11.0 ± 4.3	0.516	4.50	-
C36GC096	25.00 W		0.0002072	6.508	0.0182052	11.522	0.0075751	0.714	0.614076	0.216	1.11767	0.096	1.72200 ± 0.01538	737.3 ± 6.6	94.61	1.43	17.2 ± 4.0	2.479	4.01	-
C36HA089	20.00 W		0.0001598	8.509	0.0110392	14.320	0.0030962	0.862	0.248654	0.261	0.49756	0.089	1.81396 ± 0.03389	776.7 ± 14.5	90.65	0.58	11.5 ± 3.3	0.936	4.30	-
C36GC009	20.00 W		0.0014629	2.677	0.0035492	39.987	0.0018373	1.783	0.128505	0.282	0.66847	0.113	1.83928 ± 0.18113	787.5 ± 77.5	35.36	0.30	18.5 ± 14.8	0.459	4.53	-
C36GC007	25.00 W		0.0002106	8.396	0.0081618	15.666	0.0027426	1.063	0.221094	0.256	0.48072	0.110	1.89496 ± 0.04852	811.4 ± 20.8	87.15	0.52	13.8 ± 4.3	0.832	4.30	-
C36GA001	25.00 W		0.0003592	4.874	0.0182411	7.373	0.0061299	0.869	0.505249	0.215	1.10308	0.060	1.97525 ± 0.02234	845.7 ± 9.6	90.47	1.18	14.1 ± 2.1	1.962	4.17	-
C36GC095	25.00 W		0.0011188	2.695	0.0614407	2.914	0.0190791	0.651	1.523902	0.218	3.54480	0.038	2.11169 ± 0.01501	904.1 ± 6.4	90.78	3.56	12.6 ± 0.7	6.308	3.91	-
C36HA087	25.00 W		0.0002831	5.927	0.0127448	12.674	0.0043567	1.192	0.343264	0.223	0.81322	0.051	2.12767 ± 0.03052	911.0 ± 13.1	89.81	0.80	13.7 ± 3.5	1.315	4.23	-
C36HA083	25.00 W		0.0001937	5.662	0.0118136	17.433	0.0035913	0.994	0.286727	0.230	0.67469	0.086	2.15614 ± 0.02504	923.2 ± 10.7	91.63	0.67	12.4 ± 4.3	1.120	4.15	-
C36GC003	25.00 W		0.0001768	9.028	0.0138655	10.167	0.0048109	1.274	0.391547	0.221	0.90040	0.077	2.16828 ± 0.02618	928.4 ± 11.2	94.29	0.91	14.4 ± 2.9	1.442	4.40	-
C36GC001	25.00 W		0.0003555	7.317	0.0116380	14.969	0.0044276	0.928	0.352810	0.240	0.87770	0.109	2.19191 ± 0.04516	938.5 ± 19.3	88.11	0.82	15.5 ± 4.6	1.342	4.26	-
C36GC098	25.00 W		0.0003123	6.068	0.0316307	5.499	0.0084267	0.861	0.681318	0.229	1.58872	0.068	2.19936 ± 0.01954	941.7 ± 8.4	94.32	1.59	11.0 ± 1.2	2.654	4.16	-
C36HA085	20.00 W		0.0002028	5.678	0.0095075	17.893	0.0030143	0.865	0.238810	0.258	0.58957	0.068	2.22032 ± 0.03095	950.6 ± 13.2	89.93	0.56	12.8 ± 4.6	0.918	4.21	-
C36GC094	25.00 W		0.0014800	2.572	0.0807040	2.916	0.0249043	0.556	1.952818	0.213	5.09111	0.027	2.38571 ± 0.01544	1021.4 ± 6.6	91.51	4.56	12.3 ± 0.7	7.864	4.02	-
C36GC006	25.00 W		0.0002149	10.738	0.0107662	11.196	0.0034837	1.550	0.279582	0.224	0.73383	0.064	2.39998 ± 0.05007	1027.5 ± 21.4	91.43	0.65	13.2 ± 3.0	1.046	4.33	-
C36GC093	25.00 W		0.0020245	1.589	0.0647117	2.820	0.0221103	0.602	1.603685	0.214	6.29379	0.021	3.55418 ± 0.01941	1521.5 ± 8.3	90.56	3.74	12.6 ± 0.7	6.364	4.08	-
C36HA116	25.00 W		0.0136909	1.014	0.1533759	3.037	0.1452107	0.448	0.281801	0.231	75.51704	0.012	253.80781 ± 1.21084	105549.5 ± 489.1	94.68	0.66	0.9 ± 0.1	3.171	1.44	-
C36HA084	20.00 W		0.0019352	1.778	0.0373295	7.996	0.0352699	0.470	0.066943	0.426	17.68284	0.013	255.79546 ± 2.20374	106352.2 ± 889.8	96.80	0.16	0.9 ± 0.1	0.726	1.49	-

Procedure Blanks	Laser power	36Ar [V]	1σ	37Ar [V]	1σ	38Ar [V]	1σ	39Ar [V]	1σ	40Ar [V]	1σ
C36HA091	20.00 W	0.0000919	0.0000058	0.0015969	0.0000265	0.0000487	0.0000059	0.0001396	0.0000187	0.0027368	0.0000555
C36HA121	25.00 W	0.0001262	0.0000074	0.0017518	0.0000149	0.0000659	0.0000050	0.0003088	0.0000236	0.0075875	0.0001600
C36HA120	25.00 W	0.0001262	0.0000074	0.0017518	0.0000149	0.0000659	0.0000050	0.0003088	0.0000236	0.0075875	0.0001600
C36GC005	20.00 W	0.0001048	0.0000139	0.0018238	0.0000344	0.0000485	0.0000096	0.0001812	0.0000256	0.0036907	0.0002204
C36HA119	25.00 W	0.0001262	0.0000074	0.0017518	0.0000149	0.0000659	0.0000050	0.0003088	0.0000236	0.0075875	0.0001600
C36GC100	25.00 W	0.0001386	0.0000091	0.0020699	0.0000485	0.0000852	0.0000079	0.0004663	0.0002074	0.0076277	0.0009805
C36GC104	25.00 W	0.0001576	0.0000091	0.0021553	0.0000485	0.0000866	0.0000079	0.0004594	0.0002074	0.0083598	0.0009805
C36GC106	25.00 W	0.0001577	0.0000091	0.0021959	0.0000485	0.0000750	0.0000079	0.0005153	0.0002074	0.0083375	0.0009805
C36HA122	25.00 W	0.0001262	0.0000074	0.0017518	0.0000149	0.0000659	0.0000050	0.0003088	0.0000236	0.0075875	0.0001600
C36HA117	25.00 W	0.0001262	0.0000074	0.0017518	0.0000149	0.0000659	0.0000050	0.0003088	0.0000236	0.0075875	0.0001600
C36GC103	25.00 W	0.0001551	0.0000091	0.0021355	0.0000485	0.0000891	0.0000079	0.0004493	0.0002074	0.0082869	0.0009805
C36HA118	25.00 W	0.0001262	0.0000074	0.0017518	0.0000149	0.0000659	0.0000050	0.0003088	0.0000236	0.0075875	0.0001600
C36GC101	25.00 W	0.0001437	0.0000091	0.0020864	0.0000485	0.0000878	0.0000079	0.0004573	0.0002074	0.0078620	0.0009805
C36GC105	25.00 W	0.0001585	0.0000091	0.0021755	0.0000485	0.0000820	0.0000079	0.0004805	0.0002074	0.0083782	0.0009805
C36GC102	25.00 W	0.0001485	0.0000091	0.0021041	0.0000485	0.0000894	0.0000079	0.0004502	0.0002074	0.0080581	0.0009805
C36HA088	25.00 W	0.0000919	0.0000058	0.0015969	0.0000265	0.0000487	0.0000059	0.0001396	0.0000187	0.0027368	0.0000555
C36HA086	20.00 W	0.0000919	0.0000058	0.0015969	0.0000265	0.0000487	0.0000059	0.0001396	0.0000187	0.0027368	0.0000555
C36GC002	25.00 W	0.0001045	0.0000139	0.0018259	0.0000344	0.0000446	0.0000096	0.0002072	0.0000256	0.0037588	0.0002204
C36GC097	25.00 W	0.0001236	0.0000091	0.0020233	0.0000485	0.0000716	0.0000079	0.0004750	0.0002074	0.0065303	0.0009805
C36HA092	25.00 W	0.0000919	0.0000058	0.0015969	0.0000265	0.0000487	0.0000059	0.0001396	0.0000187	0.0027368	0.0000555
C36HA093	25.00 W	0.0000919	0.0000058	0.0015969	0.0000265	0.0000487	0.0000059	0.0001396	0.0000187	0.0027368	0.0000555
C36HA090	25.00 W	0.0000919	0.0000058	0.0015969	0.0000265	0.0000487	0.0000059	0.0001396	0.0000187	0.0027368	0.0000555
C36GC010	20.00 W	0.0001052	0.0000139	0.0018209	0.0000344	0.0000539	0.0000096	0.0001453	0.0000256	0.0035967	0.0002204
C36GC099	25.00 W	0.0001306	0.0000091	0.0020457	0.0000485	0.0000793	0.0000079	0.0004786	0.0002074	0.0071680	0.0009805
C36GC004	20.00 W	0.0001047	0.0000139	0.0018247	0.0000344	0.0000467	0.0000096	0.0001930	0.0000256	0.0037218	0.0002204
C36HA094	20.00 W	0.0000919	0.0000058	0.0015969	0.0000265	0.0000487	0.0000059	0.0001396	0.0000187	0.0027368	0.0000555
C36GC008	20.00 W	0.0001051	0.0000139	0.0018220	0.0000344	0.0000518	0.0000096	0.0001596	0.0000256	0.0036343	0.0002204
C36GC096	25.00 W	0.0001219	0.0000091	0.0020150	0.0000485	0.0000680	0.0000079	0.0004599	0.0002074	0.0061778	0.0009805
C36HA089	20.00 W	0.0000919	0.0000058	0.0015969	0.0000265	0.0000487	0.0000059	0.0001396	0.0000187	0.0027368	0.0000555
C36GC009	20.00 W	0.0001052	0.0000139	0.0018215	0.0000344	0.0000529	0.0000096	0.0001524	0.0000256	0.0036155	0.0002204
C36GC007	25.00 W	0.0001050	0.0000139	0.0018226	0.0000344	0.0000507	0.0000096	0.0001668	0.0000256	0.0036531	0.0002204
C36GA001	25.00 W	0.0001066	0.0000130	0.0018521	0.0000353	0.0000600	0.0000112	0.0000952	0.0000176	0.0043596	0.0000978
C36GC095	25.00 W	0.0001230	0.0000091	0.0020066	0.0000485	0.0000635	0.0000079	0.0004066	0.0002074	0.0055682	0.0009805
C36HA087	25.00 W	0.0000919	0.0000058	0.0015969	0.0000265	0.0000487	0.0000059	0.0001396	0.0000187	0.0027368	0.0000555
C36HA083	25.00 W	0.0000919	0.0000058	0.0015969	0.0000265	0.0000487	0.0000059	0.0001396	0.0000187	0.0027368	0.0000555
C36GC003	25.00 W	0.0001046	0.0000139	0.0018253	0.0000344	0.0000456	0.0000096	0.0002002	0.0000256	0.0037406	0.0002204
C36GC001	25.00 W	0.0001044	0.0000139	0.0018268	0.0000344	0.0000428	0.0000096	0.0002190	0.0000256	0.0037899	0.0002204
C36GC098	25.00 W	0.0001266	0.0000091	0.0020334	0.0000485	0.0000754	0.0000079	0.0004803	0.0002074	0.0068541	0.0009805
C36HA085	20.00 W	0.0000919	0.0000058	0.0015969	0.0000265	0.0000487	0.0000059	0.0001396	0.0000187	0.0027368	0.0000555
C36GC094	25.00 W	0.0001266	0.0000091	0.0020051	0.0000485	0.0000621	0.0000079	0.0003532	0.0002074	0.0051912	0.0009805
C36GC006	25.00 W	0.0001049	0.0000139	0.0018232	0.0000344	0.0000496	0.0000096	0.0001740	0.0000256	0.0036719	0.0002204
C36GC093	25.00 W	0.0001329	0.0000091	0.0020066	0.0000485	0.0000622	0.0000079	0.0002809	0.0002074	0.0048132	0.0009805
C36HA116	25.00 W	0.0001262	0.0000074	0.0017518	0.0000149	0.0000659	0.0000050	0.0003088	0.0000236	0.0075875	0.0001600
C36HA084	20.00 W	0.0000919	0.0000058	0.0015969	0.0000265	0.0000487	0.0000059	0.0001396	0.0000187	0.0027368	0.0000555

Sample Parameters	Laser power	Material	Location	Analyst	Power	%1σ	J	%1σ	MDF	%1σ	Volume Ratio	Sensitivity (mol/volt)	Day	Month	Year	Hour	Min	Resist	Irradiation	Project	Experiment	Nmb	Standard Name
C36HA091	20.00 W	K-feldspar (0.5-2 mm)	Cadamosto, Cape Verdes	Jan Sticklus	20	0.14	2.37E-04	0.149	1.0098	0.21	1	1.203E-14	16	AUG	2012	14	22	1	can36	Examples	c36it2ip3_149-6	01	TCS2
C36HA121	25.00 W	K-feldspar (0.5-2 mm)	Cadamosto, Cape Verdes	Jan Sticklus	25	0.14	0.00023739	0.149	1.0098	0.21	1	1.203E-14	17	AUG	2012	7	21	1	can36	Examples	c36it2ip3_149-6	01	TCS2
C36HA120	25.00 W	K-feldspar (0.5-2 mm)	Cadamosto, Cape Verdes	Jan Sticklus	25	0.14	0.00023739	0.149	1.0098	0.21	1	1.203E-14	17	AUG	2012	6	52	1	can36	Examples	c36it2ip3_149-6	01	TCS2
C36GC005	20.00 W	K-feldspar (0.5-2 mm)	Cadamosto, Cape Verdes	Jan Sticklus	20	0.14	0.00023739	0.149	1.0098	0.21	1	1.203E-14	3	AUG	2012	10	11	1	can36	Examples	c36it2ip3_149-6	01	TCS2
C36HA119	25.00 W	K-feldspar (0.5-2 mm)	Cadamosto, Cape Verdes	Jan Sticklus	25	0.14	0.00023739	0.149	1.0098	0.21	1	1.203E-14	17	AUG	2012	6	23	1	can36	Examples	c36it2ip3_149-6	01	TCS2
C36GC100	25.00 W	K-feldspar (0.5-2 mm)	Cadamosto, Cape Verdes	Jan Sticklus	25	0.14	0.00023739	0.149	1.0098	0.21	1	1.203E-14	5	AUG	2012	13	19	1	can36	Examples	c36it2ip3_149-6	01	TCS2
C36GC104	25.00 W	K-feldspar (0.5-2 mm)	Cadamosto, Cape Verdes	Jan Sticklus	25	0.14	0.00023739	0.149	1.0098	0.21	1	1.203E-14	5	AUG	2012	15	34	1	can36	Examples	c36it2ip3_149-6	01	TCS2
C36GC106	25.00 W	K-feldspar (0.5-2 mm)	Cadamosto, Cape Verdes	Jan Sticklus	25	0.14	0.00023739	0.149	1.0098	0.21	1	1.203E-14	5	AUG	2012	16	32	1	can36	Examples	c36it2ip3_149-6	01	TCS2
C36HA122	25.00 W	K-feldspar (0.5-2 mm)	Cadamosto, Cape Verdes	Jan Sticklus	25	0.14	0.00023739	0.149	1.0098	0.21	1	1.203E-14	17	AUG	2012	7	50	1	can36	Examples	c36it2ip3_149-6	01	TCS2
C36HA117	25.00 W	K-feldspar (0.5-2 mm)	Cadamosto, Cape Verdes	Jan Sticklus	25	0.14	0.00023739	0.149	1.0098	0.21	1	1.203E-14	17	AUG	2012	5	7	1	can36	Examples	c36it2ip3_149-6	01	TCS2
C36GC103	25.00 W	K-feldspar (0.5-2 mm)	Cadamosto, Cape Verdes	Jan Sticklus	25	0.14	0.00023739	0.149	1.0098	0.21	1	1.203E-14	5	AUG	2012	15	5	1	can36	Examples	c36it2ip3_149-6	01	TCS2
C36HA118	25.00 W	K-feldspar (0.5-2 mm)	Cadamosto, Cape Verdes	Jan Sticklus	25	0.14	0.00023739	0.149	1.0098	0.21	1	1.203E-14	17	AUG	2012	5	35	1	can36	Examples	c36it2ip3_149-6	01	TCS2
C36GC101	25.00 W	K-feldspar (0.5-2 mm)	Cadamosto, Cape Verdes	Jan Sticklus	25	0.14	0.00023739	0.149	1.0098	0.21	1	1.203E-14	5	AUG	2012	13	48	1	can36	Examples	c36it2ip3_149-6	01	TCS2
C36GC105	25.00 W	K-feldspar (0.5-2 mm)	Cadamosto, Cape Verdes	Jan Sticklus	25	0.14	0.00023739	0.149	1.0098	0.21	1	1.203E-14	5	AUG	2012	16	3	1	can36	Examples	c36it2ip3_149-6	01	TCS2
C36GC102	25.00 W	K-feldspar (0.5-2 mm)	Cadamosto, Cape Verdes	Jan Sticklus	25	0.14	0.00023739	0.149	1.0098	0.21	1	1.203E-14	5	AUG	2012	14	17	1	can36	Examples	c36it2ip3_149-6	01	TCS2
C36HA088	25.00 W	Nepheline (0.5-2 mm)	Cadamosto, Cape Verdes	Jan Sticklus	25	0.14	0.00023739	0.149	1.0098	0.21	1	1.203E-14	16	AUG	2012	12	37	1	can36	Examples	c36it2ip3_149-6	01	TCS2
C36HA086	20.00 W	Nepheline (0.5-2 mm)	Cadamosto, Cape Verdes	Jan Sticklus	20	0.14	0.00023739	0.149	1.0098	0.21	1	1.203E-14	16	AUG	2012	11	39	1	can36	Examples	c36it2ip3_149-6	01	TCS2
C36GC002	25.00 W	Nepheline (0.5-2 mm)	Cadamosto, Cape Verdes	Jan Sticklus	25	0.14	0.00023739	0.149	1.0098	0.21	1	1.203E-14	3	AUG	2012	8	26	1	can36	Examples	c36it2ip3_149-6	01	TCS2
C36GC097	25.00 W	Nepheline (0.5-2 mm)	Cadamosto, Cape Verdes	Jan Sticklus	25	0.14	0.00023739	0.149	1.0098	0.21	1	1.203E-14	5	AUG	2012	11	34	1	can36	Examples	c36it2ip3_149-6	01	TCS2
C36HA092	25.00 W	Nepheline (0.5-2 mm)	Cadamosto, Cape Verdes	Jan Sticklus	25	0.14	0.00023739	0.149	1.0098	0.21	1	1.203E-14	16	AUG	2012	14	51	1	can36	Examples	c36it2ip3_149-6	01	TCS2
C36HA093	25.00 W	Nepheline (0.5-2 mm)	Cadamosto, Cape Verdes	Jan Sticklus	25	0.14	0.00023739	0.149	1.0098	0.21	1	1.203E-14	16	AUG	2012	15	20	1	can36	Examples	c36it2ip3_149-6	01	TCS2
C36HA090	25.00 W	Nepheline (0.5-2 mm)	Cadamosto, Cape Verdes	Jan Sticklus	25	0.14	0.00023739	0.149	1.0098	0.21	1	1.203E-14	16	AUG	2012	13	53	1	can36	Examples	c36it2ip3_149-6	01	TCS2
C36GC010	20.00 W	Nepheline (0.5-2 mm)	Cadamosto, Cape Verdes	Jan Sticklus	20	0.14	0.00023739	0.149	1.0098	0.21	1	1.203E-14	3	AUG	2012	12	36	1	can36	Examples	c36it2ip3_149-6	01	TCS2
C36GC099	25.00 W	Nepheline (0.5-2 mm)	Cadamosto, Cape Verdes	Jan Sticklus	25	0.14	0.00023739	0.149	1.0098	0.21	1	1.203E-14	5	AUG	2012	12	31	1	can36	Examples	c36it2ip3_149-6	01	TCS2
C36GC004	20.00 W	Nepheline (0.5-2 mm)	Cadamosto, Cape Verdes	Jan Sticklus	20	0.14	0.00023739	0.149	1.0098	0.21	1	1.203E-14	3	AUG	2012	9	23	1	can36	Examples	c36it2ip3_149-6	01	TCS2
C36HA094	20.00 W	Nepheline (0.5-2 mm)	Cadamosto, Cape Verdes	Jan Sticklus	20	0.14	0.00023739	0.149	1.0098	0.21	1	1.203E-14	16	AUG	2012	15	49	1	can36	Examples	c36it2ip3_149-6	01	TCS2
C36GC008	20.00 W	Nepheline (0.5-2 mm)	Cadamosto, Cape Verdes	Jan Sticklus	20	0.14	0.00023739	0.149	1.0098	0.21	1	1.203E-14	3	AUG	2012	11	38	1	can36	Examples	c36it2ip3_149-6	01	TCS2
C36GC096	25.00 W	Nepheline (0.5-2 mm)	Cadamosto, Cape Verdes	Jan Sticklus	25	0.14	0.00023739	0.149	1.0098	0.21	1	1.203E-14	5	AUG	2012	11	5	1	can36	Examples	c36it2ip3_149-6	01	TCS2
C36HA089	20.00 W	Nepheline (0.5-2 mm)	Cadamosto, Cape Verdes	Jan Sticklus	20	0.14	0.00023739	0.149	1.0098	0.21	1	1.203E-14	16	AUG	2012	13	24	1	can36	Examples	c36it2ip3_149-6	01	TCS2
C36GC009	20.00 W	Nepheline (0.5-2 mm)	Cadamosto, Cape Verdes	Jan Sticklus	20	0.14	0.00023739	0.149	1.0098	0.21	1	1.203E-14	3	AUG	2012	12	7	1	can36	Examples	c36it2ip3_149-6	01	TCS2
C36GC007	25.00 W	Nepheline (0.5-2 mm)	Cadamosto, Cape Verdes	Jan Sticklus	25	0.14	0.00023739	0.149	1.0098	0.21	1	1.203E-14	3	AUG	2012	11	9	1	can36	Examples	c36it2ip3_149-6	01	TCS2
C36GA001	25.00 W	Nepheline (0.5-2 mm)	Cadamosto, Cape Verdes	Jan Sticklus	25	0.14	0.00023739	0.149	1.0098	0.21	1	1.203E-14	2	AUG	2012	11	3	1	can36	Examples	c36it2ip3_149-6	01	TCS2
C36GC095	25.00 W	Nepheline (0.5-2 mm)	Cadamosto, Cape Verdes	Jan Sticklus	25	0.14	0.00023739	0.149	1.0098	0.21	1	1.203E-14	5	AUG	2012	10	17	1	can36	Examples	c36it2ip3_149-6	01	TCS2
C36HA087	25.00 W	Nepheline (0.5-2 mm)	Cadamosto, Cape Verdes	Jan Sticklus	25	0.14	0.00023739	0.149	1.0098	0.21	1	1.203E-14	16	AUG	2012	12	8	1	can36	Examples	c36it2ip3_149-6	01	TCS2
C36HA083	25.00 W	Nepheline (0.5-2 mm)	Cadamosto, Cape Verdes	Jan Sticklus	25	0.14	0.00023739	0.149	1.0098	0.21	1	1.203E-14	16	AUG	2012	10	12	1	can36	Examples	c36it2ip3_149-6	01	TCS2
C36GC003	25.00 W	Nepheline (0.5-2 mm)	Cadamosto, Cape Verdes	Jan Sticklus	25	0.14	0.00023739	0.149	1.0098	0.21	1	1.203E-14	3	AUG	2012	8	54	1	can36	Examples	c36it2ip3_149-6	01	TCS2
C36GC001	25.00 W	Nepheline (0.5-2 mm)	Cadamosto, Cape Verdes	Jan Sticklus	25	0.14	0.00023739	0.149	1.0098	0.21	1	1.203E-14	3	AUG	2012	7	38	1	can36	Examples	c36it2ip3_149-6	01	TCS2
C36GC098	25.00 W	Nepheline (0.5-2 mm)	Cadamosto, Cape Verdes	Jan Sticklus	25	0.14	0.00023739	0.149	1.0098	0.21	1	1.203E-14	5	AUG	2012	12	2	1	can36	Examples	c36it2ip3_149-6	01	TCS2
C36HA085	20.00 W	Nepheline (0.5-2 mm)	Cadamosto, Cape Verdes	Jan Sticklus	20	0.14	0.00023739	0.149	1.0098	0.21	1	1.203E-14	16	AUG	2012	11	10	1	can36	Examples	c36it2ip3_149-6	01	TCS2
C36GC094	25.00 W	Nepheline (0.5-2 mm)	Cadamosto, Cape Verdes	Jan Sticklus	25	0.14	0.00023739	0.149	1.0098	0.21	1	1.203E-14	5	AUG	2012	9	48	1	can36	Examples	c36it2ip3_149-6	01	TCS2
C36GC006	25.00 W	Nepheline (0.5-2 mm)	Cadamosto, Cape Verdes	Jan Sticklus	25	0.14	0.00023739	0.149	1.0098	0.21	1	1.203E-14	3	AUG	2012	10	40	1	can36	Examples	c36it2ip3_149-6	01	TCS2
C36GC093	25.00 W	Nepheline (0.5-2 mm)	Cadamosto, Cape Verdes	Jan Sticklus	25	0.14	0.00023739	0.149	1.0098	0.21	1	1.203E-14	5	AUG	2012	9	19	1	can36	Examples	c36it2ip3_149-6	01	TCS2
C36HA116	25.00 W	Sodalite (0.5-2 mm)	Cadamosto, Cape Verdes	Jan Sticklus	25	0.14	0.00023739	0.149	1.0098	0.21	1	1.203E-14	17	AUG	2012	4	38	1	can36	Examples	c36it2ip3_149-6	01	TCS2
C36HA084	20.00 W	Sodalite (0.5-2 mm)	Cadamosto, Cape Verdes	Jan Sticklus	20	0.14	0.00023739	0.149	1.0098	0.21	1	1.203E-14	16	AUG	2012	10	41	1	can36	Examples	c36it2ip3_149-6	01	TCS2

Irradiation Constants	Laser power	40/36(a)	%1σ	40/36(c)	%1σ	38/36(a)	%1σ	38/36(c)	%1σ	39/37(ca)	%1σ	38/37(ca)	%1σ	36/37(ca)	%1σ	40/39(k)	%1σ	38/39(k)	%1σ	36/38(cl)	%1σ	K/Ca	%1σ	K/Cl	%1σ	Ca/Cl	%1σ
C36HA091	20.00 W	295.5	0.169	0.018	35	0.1869	0	1.493	3	0.000699	0	0	0	0.00027	0	0.00183	0	0	0	0	0	0.51	0	0	0	0	0
C36HA121	25.00 W	295.5	0.169	0.018	35	0.1869	0	1.493	3	0.000699	0	0	0	0.00027	0	0.00183	0	0	0	0	0	0.51	0	0	0	0	0
C36HA120	25.00 W	295.5	0.169	0.018	35	0.1869	0	1.493	3	0.000699	0	0	0	0.00027	0	0.00183	0	0	0	0	0	0.51	0	0	0	0	0
C36GC005	20.00 W	295.5	0.169	0.018	35	0.1869	0	1.493	3	0.000699	0	0	0	0.00027	0	0.00183	0	0	0	0	0	0.51	0	0	0	0	0
C36HA119	25.00 W	295.5	0.169	0.018	35	0.1869	0	1.493	3	0.000699	0	0	0	0.00027	0	0.00183	0	0	0	0	0	0.51	0	0	0	0	0
C36GC100	25.00 W	295.5	0.169	0.018	35	0.1869	0	1.493	3	0.000699	0	0	0	0.00027	0	0.00183	0	0	0	0	0	0.51	0	0	0	0	0
C36GC104	25.00 W	295.5	0.169	0.018	35	0.1869	0	1.493	3	0.000699	0	0	0	0.00027	0	0.00183	0	0	0	0	0	0.51	0	0	0	0	0
C36GC106	25.00 W	295.5	0.169	0.018	35	0.1869	0	1.493	3	0.000699	0	0	0	0.00027	0	0.00183	0	0	0	0	0	0.51	0	0	0	0	0
C36HA122	25.00 W	295.5	0.169	0.018	35	0.1869	0	1.493	3	0.000699	0	0	0	0.00027	0	0.00183	0	0	0	0	0	0.51	0	0	0	0	0
C36HA117	25.00 W	295.5	0.169	0.018	35	0.1869	0	1.493	3	0.000699	0	0	0	0.00027	0	0.00183	0	0	0	0	0	0.51	0	0	0	0	0
C36GC103	25.00 W	295.5	0.169	0.018	35	0.1869	0	1.493	3	0.000699	0	0	0	0.00027	0	0.00183	0	0	0	0	0	0.51	0	0	0	0	0
C36HA118	25.00 W	295.5	0.169	0.018	35	0.1869	0	1.493	3	0.000699	0	0	0	0.00027	0	0.00183	0	0	0	0	0	0.51	0	0	0	0	0
C36GC101	25.00 W	295.5	0.169	0.018	35	0.1869	0	1.493	3	0.000699	0	0	0	0.00027	0	0.00183	0	0	0	0	0	0.51	0	0	0	0	0
C36GC105	25.00 W	295.5	0.169	0.018	35	0.1869	0	1.493	3	0.000699	0	0	0	0.00027	0	0.00183	0	0	0	0	0	0.51	0	0	0	0	0
C36GC102	25.00 W	295.5	0.169	0.018	35	0.1869	0	1.493	3	0.000699	0	0	0	0.00027	0	0.00183	0	0	0	0	0	0.51	0	0	0	0	0
C36HA088	25.00 W	295.5	0.169	0.018	35	0.1869	0	1.493	3	0.000699	0	0	0	0.00027	0	0.00183	0	0	0	0	0	0.51	0	0	0	0	0
C36HA086	20.00 W	295.5	0.169	0.018	35	0.1869	0	1.493	3	0.000699	0	0	0	0.00027	0	0.00183	0	0	0	0	0	0.51	0	0	0	0	0
C36GC002	25.00 W	295.5	0.169	0.018	35	0.1869	0	1.493	3	0.000699	0	0	0	0.00027	0	0.00183	0	0	0	0	0	0.51	0	0	0	0	0
C36GC097	25.00 W	295.5	0.169	0.018	35	0.1869	0	1.493	3	0.000699	0	0	0	0.00027	0	0.00183	0	0	0	0	0	0.51	0	0	0	0	0
C36HA092	25.00 W	295.5	0.169	0.018	35	0.1869	0	1.493	3	0.000699	0	0	0	0.00027	0	0.00183	0	0	0	0	0	0.51	0	0	0	0	0
C36HA093	25.00 W	295.5	0.169	0.018	35	0.1869	0	1.493	3	0.000699	0	0	0	0.00027	0	0.00183	0	0	0	0	0	0.51	0	0	0	0	0
C36HA090	25.00 W	295.5	0.169	0.018	35	0.1869	0	1.493	3	0.000699	0	0	0	0.00027	0	0.00183	0	0	0	0	0	0.51	0	0	0	0	0
C36GC010	20.00 W	295.5	0.169	0.018	35	0.1869	0	1.493	3	0.000699	0	0	0	0.00027	0	0.00183	0	0	0	0	0	0.51	0	0	0	0	0
C36GC099	25.00 W	295.5	0.169	0.018	35	0.1869	0	1.493	3	0.000699	0	0	0	0.00027	0	0.00183	0	0	0	0	0	0.51	0	0	0	0	0
C36GC004	20.00 W	295.5	0.169	0.018	35	0.1869	0	1.493	3	0.000699	0	0	0	0.00027	0	0.00183	0	0	0	0	0	0.51	0	0	0	0	0
C36HA094	20.00 W	295.5	0.169	0.018	35	0.1869	0	1.493	3	0.000699	0	0	0	0.00027	0	0.00183	0	0	0	0	0	0.51	0	0	0	0	0
C36GC008	20.00 W	295.5	0.169	0.018	35	0.1869	0	1.493	3	0.000699	0	0	0	0.00027	0	0.00183	0	0	0	0	0	0.51	0	0	0	0	0
C36GC096	25.00 W	295.5	0.169	0.018	35	0.1869	0	1.493	3	0.000699	0	0	0	0.00027	0	0.00183	0	0	0	0	0	0.51	0	0	0	0	0
C36HA089	20.00 W	295.5	0.169	0.018	35	0.1869	0	1.493	3	0.000699	0	0	0	0.00027	0	0.00183	0	0	0	0	0	0.51	0	0	0	0	0
C36GC009	20.00 W	295.5	0.169	0.018	35	0.1869	0	1.493	3	0.000699	0	0	0	0.00027	0	0.00183	0	0	0	0	0	0.51	0	0	0	0	0
C36GC007	25.00 W	295.5	0.169	0.018	35	0.1869	0	1.493	3	0.000699	0	0	0	0.00027	0	0.00183	0	0	0	0	0	0.51	0	0	0	0	0
C36GA001	25.00 W	295.5	0.169	0.018	35	0.1869	0	1.493	3	0.000699	0	0	0	0.00027	0	0.00183	0	0	0	0	0	0.51	0	0	0	0	0
C36GC095	25.00 W	295.5	0.169	0.018	35	0.1869	0	1.493	3	0.000699	0	0	0	0.00027	0	0.00183	0	0	0	0	0	0.51	0	0	0	0	0
C36HA087	25.00 W	295.5	0.169	0.018	35	0.1869	0	1.493	3	0.000699	0	0	0	0.00027	0	0.00183	0	0	0	0	0	0.51	0	0	0	0	0
C36HA083	25.00 W	295.5	0.169	0.018	35	0.1869	0	1.493	3	0.000699	0	0	0	0.00027	0	0.00183	0	0	0	0	0	0.51	0	0	0	0	0
C36GC003	25.00 W	295.5	0.169	0.018	35	0.1869	0	1.493	3	0.000699	0	0	0	0.00027	0	0.00183	0	0	0	0	0	0.51	0	0	0	0	0
C36GC001	25.00 W	295.5	0.169	0.018	35	0.1869	0	1.493	3	0.000699	0	0	0	0.00027	0	0.00183	0	0	0	0	0	0.51	0	0	0	0	0
C36GC098	25.00 W	295.5	0.169	0.018	35	0.1869	0	1.493	3	0.000699	0	0	0	0.00027	0	0.00183	0	0	0	0	0	0.51	0	0	0	0	0
C36HA085	20.00 W	295.5	0.169	0.018	35	0.1869	0	1.493	3	0.000699	0	0	0	0.00027	0	0.00183	0	0	0	0	0	0.51	0	0	0	0	0
C36GC094	25.00 W	295.5	0.169	0.018	35	0.1869	0	1.493	3	0.000699	0	0	0	0.00027	0	0.00183	0	0	0	0	0	0.51	0	0	0	0	0
C36GC006	25.00 W	295.5	0.169	0.018	35	0.1869	0	1.493	3	0.000699	0	0	0	0.00027	0	0.00183	0	0	0	0	0	0.51	0	0	0	0	0
C36GC093	25.00 W	295.5	0.169	0.018	35	0.1869	0	1.493	3	0.000699	0	0	0	0.00027	0	0.00183	0	0	0	0	0	0.51	0	0	0	0	0
C36HA116	25.00 W	295.5	0.169	0.018	35	0.1869	0	1.493	3	0.000699	0	0	0	0.00027	0	0.00183	0	0	0	0	0	0.51	0	0	0	0	0
C36HA084	20.00 W	295.5	0.169	0.018	35	0.1869	0	1.493	3	0.000699	0	0	0	0.00027	0	0.00183	0	0	0	0	0	0.51	0	0	0	0	0

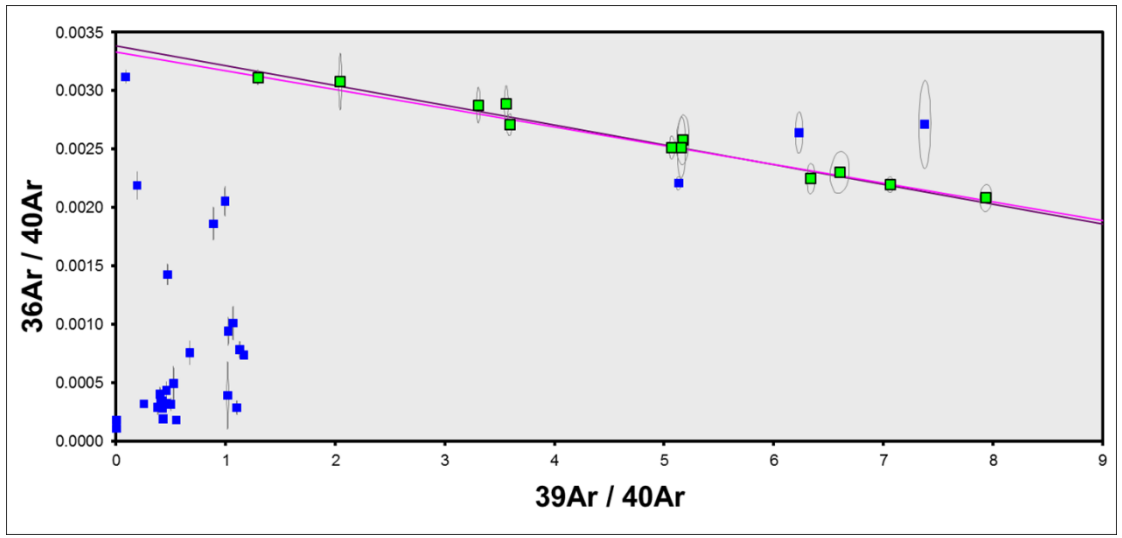
36Ar / 40Ar
39Ar / 40Ar
0.0035
0.0030
0.0025
0.0020
0.0015
0.0010
0.0005
0.0000
0
1
2
3
4
5
6
7
8
9

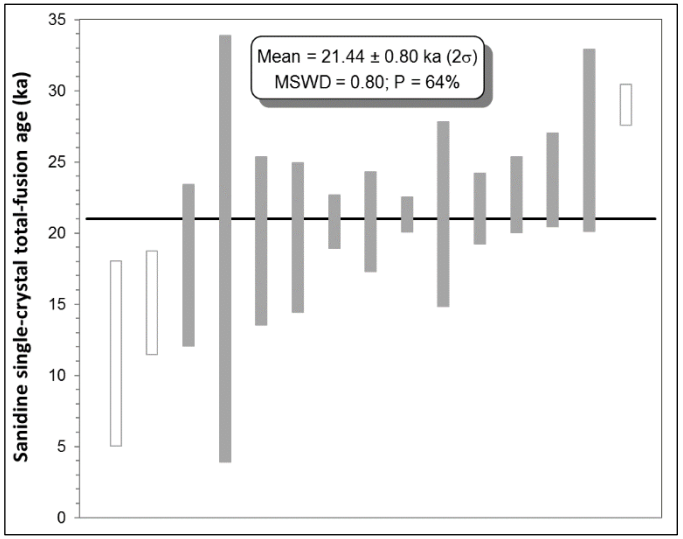
Sanidine single-crystal total-fusion age (ka)
Mean = 21.44 ± 0.80 ka (2σ)
MSWD = 0.80; P = 64%
35
30
25
20
15
10
5
0

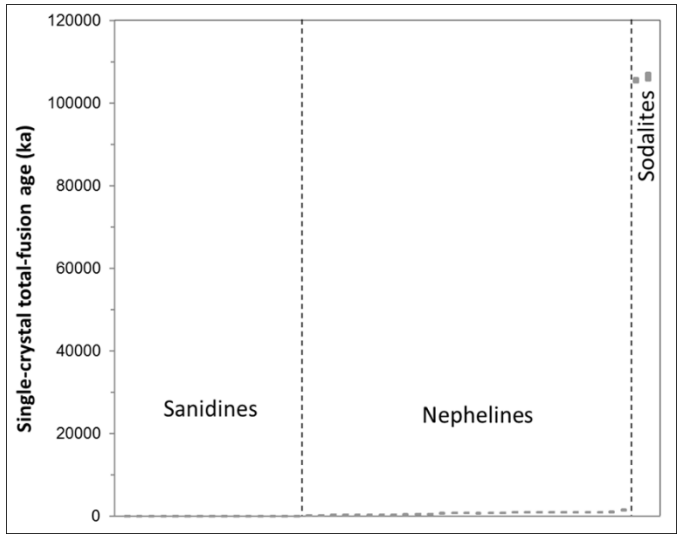
Single-crystal total-fusion age (ka)
120000
100000
80000
60000
40000
20000
0
Sanidines
Nephelines
Sodalites

Information on Analysis and Constants Used in Calculations

Sample = 149-6
Material = K-feldspar
Location = Cadamosto, Cape Verdes
Analyst = Jan Sticklus
Project = EXAMPLES
Mass Discrimination Law = POW
Irradiation = can36
J = 0.00023739 ± 0.00000035
TCS2 = 27.870 ± 0.039 Ma
Heating = 45 sec
Instrument = MAP216

Age Equations = Conventional
Negative Intensities = Allowed
Decay Constant 40K = 5.543 ± 0.009 E-10 1/a
Decay Constant 39Ar = 2.940 ± 0.016 E-07 1/h
Decay Constant 37Ar = 8.230 ± 0.012 E-04 1/h
Decay Constant 36Cl = 2.257 ± 0.015 E-06 1/a
Atmospheric Ratio 40/36(a) = 295.50 ± 0.50
Atmospheric Ratio 38/36(a) = 0.1869
Production Ratio 39/37(ca) = 0.000699
Production Ratio 36/37(ca) = 0.000270
Production Ratio 40/39(k) = 0.001830
Production Ratio 36/38(cl) = 262.80
Scaling Ratio K/Ca = 0.510

Results	40(a)/36(a) ± 2σ	40(r)/39(k) ± 2σ	Age ± 2σ (Ka)	MSWD	39Ar(k) (%,n)	K/Ca ± 2σ
Age Plateau		0.05005 ± 0.00185 ± 3.70%	21.44 ± 0.80 ± 3.71%	0.80	56.49	82.2 ± 20.1
				64%	12	
		Minimal External Error ± 0.8		1.85	2σ Confidence Limit	
		Analytical Error ± 0.8		1.0000	Error Magnification	
Total Fusion Age		2.69950 ± 0.00479 ± 0.18%	1155.7 ± 4.0 ± 0.35%		44	28.1 ± 0.9
		Minimal External Error ± 5.5				
		Analytical Error ± 2.0				
Normal Isochron	299.95 ± 6.27 ± 2.09%	0.04811 ± 0.00321 ± 6.68%	20.6 ± 1.4 ± 6.69%	0.69	56.49	
				74%	12	
		Minimal External Error ± 1.4		1.89	2σ Confidence Limit	
		Analytical Error ± 1.4		1.0000	Error Magnification	
				9	Number of Iterations	
				0.0000002080	Convergence	
Inverse Isochron	300.18 ± 6.28 ± 2.09%	0.04811 ± 0.00320 ± 6.64%	20.6 ± 1.4 ± 6.65%	0.67	56.49	
				76%	12	
		Minimal External Error ± 1.4		1.89	2σ Confidence Limit	
		Analytical Error ± 1.4		1.0000	Error Magnification	
				3	Number of Iterations	
				0.0011021917	Convergence	
				32%	Spreading Factor	

[a] Blue dots in table indicate selected steps used to calculate the weighted mean and inverse isochron ages.
[b] Weight % K values calculated from $^{39}Ar_K$ values and weights of individual grains. Based on the wt. % K values the following colours indicate the different minerals phases: yellow = K-feldspars, green = nephelines, and blue = sodalite grains.
[c] Alteration Index values in italics indicate analyses from fresh material, normal font is from altered material (Baksi, 2007; van den Bogaard, 2013).
Values shown in red are negative values.
Abbreviations used in tables: (r) = radiogenic ^{40}Ar; (k) = Ar derived from K; (a) = atmospheric Ar; (ca) = Ar derived from Ca; (cl) = Ar derived from Ca; (c) = cosmogenic Ar; MDF = Mass Discrimination Factor.
Green squares in the inverse isochron plots indicate selected steps (blue dots in table), and blue squares are non-selected steps. Pink lines in the inverse isochron plot indicate a line fit through selected data, and the purple lines incidate a fit through an air $^{40}Ar/^{36}Ar$ ratio (295.5).
Stacked probability plot produced using Isoplot (Ludwig, 2011), where filled and unfilled 2σ error bars indicate selected/not selected data to calculate inverse-variance weighted mean age (black line), respectively.

149-6 nepheline iochron

357 ka nepheline age group

Analysis #	Sample #	Mineral	Age (ka)	± 2σ (ka)	± % 2σ (ka)	Weighted mean age ± 2σ	Inverse isochron age ± 2σ
C36HA090	149-6	Nepheline	355.5	7.1	2.0	± ka	356.6 ± 7.3 ka
C36GC010	149-6	Nepheline	371.4	36.2	9.8	MSWD = , P = %, n =	MSWD = 0.72, P = 40%, SF = 84%, n = 3
C36GC099	149-6	Nepheline	383.0	81.4	21.3		Initial $^{40}Ar/^{36}Ar$ = 297.3 ± 5.3

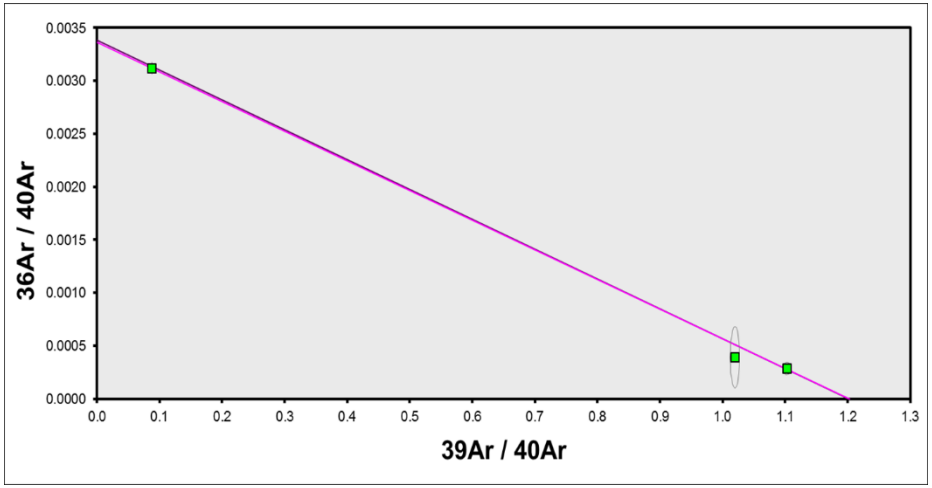

Inverse isochron plots: 2σ error ellipses; green squares = selected analyses; pink line = fit to data (green squares), purple line = line fit through atmospheric $^{40}Ar/^{36}Ar$ ratio.

152-1 total fusion

Relative Abundances	Laser power	a	36Ar [V]	%1σ	37Ar [V]	%1σ	38Ar [V]	%1σ	39Ar [V]	%1σ	40Ar [V]	%1σ	40(r)/39(k) ± 2σ	Age ± 2σ (Ka)	40Ar(r) (%)	39Ar(k) (%)	K/Ca ± 2σ	Weight (mg)	Wt. % K[a]	$^{36}Ar/^{39}Ar$ Alt. Index[b]
C42CA051	15.00 W	•	0.0000795	28.612	0.0003220	96.861	0.0018168	1.275	0.1497108	0.242	0.0703855	0.739	0.31263 ± 0.09010	18.5 ± 5.3	66.50	2.98	237 ± 459	1.52	11.55	*0.000002*
C42CA054	15.00 W	•	0.0001200	19.674	0.0002674	103.373	0.0016220	2.137	0.1304725	0.249	0.0785232	0.671	0.32945 ± 0.10728	19.5 ± 6.3	54.74	2.59	249 ± 514	1.276	11.99	*0.000004*
C42CA050	15.00 W	•	0.0000756	34.931	0.0001380	196.693	0.0022780	1.707	0.1919766	0.236	0.0867819	0.622	0.33495 ± 0.08147	19.8 ± 4.8	74.10	3.82	709 ± 2791	1.848	12.18	*0.000002*
C42CA060	15.00 W	•	0.0001419	18.803	0.0002403	122.246	0.0030928	1.236	0.2521465	0.227	0.1275143	0.416	0.33881 ± 0.06269	20.0 ± 3.7	67.00	5.01	535 ± 1309	2.461	12.01	*0.000002*
C42CA062	15.00 W	•	0.0011146	3.035	0.0019974	14.784	0.0041729	1.132	0.3249694	0.214	0.4397788	0.134	0.33957 ± 0.06173	20.1 ± 3.7	25.09	6.46	83 ± 25	3.352	11.37	*0.000013*
C42CA057	15.00 W	•	0.0001069	22.744	0.0003463	87.193	0.0036427	1.005	0.2987508	0.237	0.1332257	0.397	0.33959 ± 0.04825	20.1 ± 2.9	76.15	5.94	440 ± 767	2.963	11.82	*0.000001*
C42CA048	15.00 W	•	0.0003994	6.647	0.0000061	4056.087	0.0030852	1.287	0.2535969	0.227	0.2046008	0.255	0.34064 ± 0.06205	20.2 ± 3.7	42.22	5.04	21239 ± 1722940	2.448	12.14	*0.000006*
C42CA058	15.00 W	•	0.0004085	6.897	0.0002207	127.497	0.0049348	0.961	0.4008223	0.222	0.2602457	0.222	0.34742 ± 0.04169	20.6 ± 2.5	53.51	7.97	926 ± 2362	4.359	10.78	*0.000004*
C42CA065	15.00 W	•	0.0002512	11.610	0.0003444	80.150	0.0029751	1.392	0.2458081	0.250	0.1600057	0.343	0.34838 ± 0.07028	20.6 ± 4.2	53.52	4.89	364 ± 583	2.409	11.96	*0.000004*
C42CA049	15.00 W	•	0.0001656	14.873	0.0004959	55.227	0.0037906	0.995	0.3094615	0.225	0.1584453	0.321	0.35328 ± 0.04718	20.9 ± 2.8	69.00	6.15	318 ± 352	3.01	12.05	*0.000002*
C42CA052	15.00 W	•	0.0001329	18.549	0.0007458	47.285	0.0051031	1.390	0.4206175	0.226	0.1904475	0.289	0.35883 ± 0.03478	21.2 ± 2.1	79.25	8.36	288 ± 272	4.465	11.04	*0.000001*
C42CA067	15.00 W	•	0.0000776	32.094	0.0000355	987.604	0.0019774	1.854	0.1678147	0.253	0.0835292	0.616	0.36031 ± 0.08797	21.3 ± 5.2	72.39	3.34	2413 ± 47666	1.626	12.10	*0.000002*
C42CA056	15.00 W	•	0.0010196	3.282	0.0000381	849.994	0.0048589	0.817	0.3885575	0.220	0.4427705	0.155	0.36334 ± 0.05111	21.5 ± 3.0	31.89	7.72	5203 ± 88445	2.545	17.90	*0.000015*
C42CA063	15.00 W	•	0.0000934	27.177	0.0002083	148.338	0.0021385	1.543	0.1768883	0.263	0.0954620	0.605	0.38308 ± 0.08505	22.7 ± 5.0	70.98	3.52	433 ± 1285	1.771	11.71	*0.000002*
C42CA064	15.00 W	•	0.0003158	8.645	0.0000241	1179.194	0.0023636	1.156	0.1944446	0.231	0.1705450	0.313	0.39645 ± 0.08320	23.5 ± 4.9	45.20	3.86	4118 ± 97129	1.893	12.04	*0.000006*
C42CA047	15.00 W	•	0.0004324	5.789	0.0010364	34.525	0.0033899	1.218	0.2738050	0.246	0.2383084	0.219	0.40329 ± 0.05422	23.9 ± 3.2	46.34	5.44	135 ± 93	2.691	11.93	*0.000006*
C42CA053	15.00 W		0.0000871	29.482	0.0001992	136.044	0.0029482	1.470	0.2420241	0.248	0.1320874	0.369	0.43869 ± 0.06291	26.0 ± 3.7	80.38	4.81	620 ± 1686	2.378	11.93	*0.000001*
C42CA059	15.00 W		0.0001787	14.159	0.0001632	158.547	0.0031450	1.073	0.2594709	0.253	0.2565816	0.204	0.78467 ± 0.05791	46.4 ± 3.4	79.35	5.16	811 ± 2572	2.522	12.06	*0.000003*
C42CA066	15.00 W		0.0000749	32.764	0.0003010	96.928	0.0009195	2.028	0.0756754	0.293	0.1004651	0.527	1.03486 ± 0.19216	61.2 ± 11.4	77.95	1.50	128 ± 249	0.714	12.43	*0.000004*
C42CA061	15.00 W		0.0004994	5.975	0.0001032	246.398	0.0034529	1.052	0.2740306	0.233	0.4977353	0.139	1.27713 ± 0.06485	75.6 ± 3.8	70.31	5.45	1355 ± 6675	2.671	12.03	*0.000007*
		Σ	0.0057749	2.073	0.0067977	19.457	0.0617081	0.287	5.0310440	0.055	3.9274387	0.063								

Procedure Blanks	Laser power	36Ar [V]	1σ	37Ar [V]	1σ	38Ar [V]	1σ	39Ar [V]	1σ	40Ar [V]	1σ
C42CA051	15.00 W	0.0002021	0.0000234	0.0017957	0.0000283	0.0000851	0.0000115	0.0001309	0.0000112	0.0035664	0.0004814
C42CA054	15.00 W	0.0002053	0.0000234	0.0018008	0.0000283	0.0000860	0.0000115	0.0001449	0.0000112	0.0036987	0.0004814
C42CA050	15.00 W	0.0002008	0.0000234	0.0017952	0.0000283	0.0000856	0.0000115	0.0001255	0.0000112	0.0034877	0.0004814
C42CA060	15.00 W	0.0002081	0.0000234	0.0018176	0.0000283	0.0000912	0.0000115	0.0001516	0.0000112	0.0035556	0.0004814
C42CA062	15.00 W	0.0002090	0.0000234	0.0018240	0.0000283	0.0000916	0.0000115	0.0001489	0.0000112	0.0034584	0.0004814
C42CA057	15.00 W	0.0002071	0.0000234	0.0018096	0.0000283	0.0000890	0.0000115	0.0001512	0.0000112	0.0036570	0.0004814
C42CA048	15.00 W	0.0001977	0.0000234	0.0017961	0.0000283	0.0000878	0.0000115	0.0001127	0.0000112	0.0032632	0.0004814
C42CA058	15.00 W	0.0002075	0.0000234	0.0018122	0.0000283	0.0000898	0.0000115	0.0001517	0.0000112	0.0036271	0.0004814
C42CA065	15.00 W	0.0002104	0.0000234	0.0018291	0.0000283	0.0000892	0.0000115	0.0001432	0.0000112	0.0033859	0.0004814
C42CA049	15.00 W	0.0001994	0.0000234	0.0017954	0.0000283	0.0000865	0.0000115	0.0001195	0.0000112	0.0033873	0.0004814
C42CA052	15.00 W	0.0002038	0.0000234	0.0017974	0.0000283	0.0000850	0.0000115	0.0001383	0.0000112	0.0036538	0.0004814
C42CA067	15.00 W	0.0002119	0.0000234	0.0018305	0.0000283	0.0000851	0.0000115	0.0001382	0.0000112	0.0033828	0.0004814
C42CA056	15.00 W	0.0002064	0.0000234	0.0018054	0.0000283	0.0000875	0.0000115	0.0001492	0.0000112	0.0036913	0.0004814
C42CA063	15.00 W	0.0002094	0.0000234	0.0018260	0.0000283	0.0000912	0.0000115	0.0001473	0.0000112	0.0034276	0.0004814
C42CA064	15.00 W	0.0002099	0.0000234	0.0018278	0.0000283	0.0000904	0.0000115	0.0001454	0.0000112	0.0034028	0.0004814
C42CA047	15.00 W	0.0001959	0.0000234	0.0017974	0.0000283	0.0000896	0.0000115	0.0001055	0.0000112	0.0031193	0.0004814
C42CA053	15.00 W	0.0002046	0.0000234	0.0017989	0.0000283	0.0000854	0.0000115	0.0001419	0.0000112	0.0036837	0.0004814
C42CA059	15.00 W	0.0002078	0.0000234	0.0018149	0.0000283	0.0000906	0.0000115	0.0001519	0.0000112	0.0035927	0.0004814
C42CA066	15.00 W	0.0002111	0.0000234	0.0018300	0.0000283	0.0000874	0.0000115	0.0001408	0.0000112	0.0033788	0.0004814
C42CA061	15.00 W	0.0002084	0.0000234	0.0018202	0.0000283	0.0000916	0.0000115	0.0001509	0.0000112	0.0035178	0.0004814

Sample Parameter	Laser power	Material	Location	Analyst	Power	%1σ	J	%1σ	MDF	%1σ	Volume Ratio	Sensitivity (mol/volt)	Day	Month	Year	Hour	Min	Resist	Irradiation	Project	Experiment	Nmb	Standard Name
C42CA051	15.00 W	K-feldspar (>1 mm)	Cadamosto, Cape Verde	Jan Sticklus	15	0.144	0.0000328	0.305	1.0098	0.21	1	1.203E-14	23	MAR	2017	14	14	1	can42	Examples	c42it7ip3_1521F	01	TCS2
C42CA054	15.00 W	K-feldspar (>1 mm)	Cadamosto, Cape Verde	Jan Sticklus	15	0.144	0.0000328	0.305	1.0098	0.21	1	1.203E-14	23	MAR	2017	16	0	1	can42	Examples	c42it7ip3_1521F	01	TCS2
C42CA050	15.00 W	K-feldspar (>1 mm)	Cadamosto, Cape Verde	Jan Sticklus	15	0.144	0.0000328	0.305	1.0098	0.21	1	1.203E-14	23	MAR	2017	13	45	1	can42	Examples	c42it7ip3_1521F	01	TCS2
C42CA060	15.00 W	K-feldspar (>1 mm)	Cadamosto, Cape Verde	Jan Sticklus	15	0.144	0.0000328	0.305	1.0098	0.21	1	1.203E-14	23	MAR	2017	19	12	1	can42	Examples	c42it7ip3_1521F	01	TCS2
C42CA062	15.00 W	K-feldspar (>1 mm)	Cadamosto, Cape Verde	Jan Sticklus	15	0.144	0.0000328	0.305	1.0098	0.21	1	1.203E-14	23	MAR	2017	20	29	1	can42	Examples	c42it7ip3_1521F	01	TCS2
C42CA057	15.00 W	K-feldspar (>1 mm)	Cadamosto, Cape Verde	Jan Sticklus	15	0.144	0.0000328	0.305	1.0098	0.21	1	1.203E-14	23	MAR	2017	17	45	1	can42	Examples	c42it7ip3_1521F	01	TCS2
C42CA048	15.00 W	K-feldspar (>1 mm)	Cadamosto, Cape Verde	Jan Sticklus	15	0.144	0.0000328	0.305	1.0098	0.21	1	1.203E-14	23	MAR	2017	12	47	1	can42	Examples	c42it7ip3_1521F	01	TCS2
C42CA058	15.00 W	K-feldspar (>1 mm)	Cadamosto, Cape Verde	Jan Sticklus	15	0.144	0.0000328	0.305	1.0098	0.21	1	1.203E-14	23	MAR	2017	18	14	1	can42	Examples	c42it7ip3_1521F	01	TCS2
C42CA065	15.00 W	K-feldspar (>1 mm)	Cadamosto, Cape Verde	Jan Sticklus	15	0.144	0.0000328	0.305	1.0098	0.21	1	1.203E-14	23	MAR	2017	21	56	1	can42	Examples	c42it7ip3_1521F	01	TCS2
C42CA049	15.00 W	K-feldspar (>1 mm)	Cadamosto, Cape Verde	Jan Sticklus	15	0.144	0.0000328	0.305	1.0098	0.21	1	1.203E-14	23	MAR	2017	13	16	1	can42	Examples	c42it7ip3_1521F	01	TCS2
C42CA052	15.00 W	K-feldspar (>1 mm)	Cadamosto, Cape Verde	Jan Sticklus	15	0.144	0.0000328	0.305	1.0098	0.21	1	1.203E-14	23	MAR	2017	15	2	1	can42	Examples	c42it7ip3_1521F	01	TCS2
C42CA067	15.00 W	K-feldspar (>1 mm)	Cadamosto, Cape Verde	Jan Sticklus	15	0.144	0.0000328	0.305	1.0098	0.21	1	1.203E-14	23	MAR	2017	22	53	1	can42	Examples	c42it7ip3_1521F	01	TCS2
C42CA056	15.00 W	K-feldspar (>1 mm)	Cadamosto, Cape Verde	Jan Sticklus	15	0.144	0.0000328	0.305	1.0098	0.21	1	1.203E-14	23	MAR	2017	16	58	1	can42	Examples	c42it7ip3_1521F	01	TCS2
C42CA063	15.00 W	K-feldspar (>1 mm)	Cadamosto, Cape Verde	Jan Sticklus	15	0.144	0.0000328	0.305	1.0098	0.21	1	1.203E-14	23	MAR	2017	20	58	1	can42	Examples	c42it7ip3_1521F	01	TCS2
C42CA064	15.00 W	K-feldspar (>1 mm)	Cadamosto, Cape Verde	Jan Sticklus	15	0.144	0.0000328	0.305	1.0098	0.21	1	1.203E-14	23	MAR	2017	21	27	1	can42	Examples	c42it7ip3_1521F	01	TCS2
C42CA047	15.00 W	K-feldspar (>1 mm)	Cadamosto, Cape Verde	Jan Sticklus	15	0.144	0.0000328	0.305	1.0098	0.21	1	1.203E-14	23	MAR	2017	12	19	1	can42	Examples	c42it7ip3_1521F	01	TCS2
C42CA053	15.00 W	K-feldspar (>1 mm)	Cadamosto, Cape Verde	Jan Sticklus	15	0.144	0.0000328	0.305	1.0098	0.21	1	1.203E-14	23	MAR	2017	15	31	1	can42	Examples	c42it7ip3_1521F	01	TCS2
C42CA059	15.00 W	K-feldspar (>1 mm)	Cadamosto, Cape Verde	Jan Sticklus	15	0.144	0.0000328	0.305	1.0098	0.21	1	1.203E-14	23	MAR	2017	18	43	1	can42	Examples	c42it7ip3_1521F	01	TCS2
C42CA066	15.00 W	K-feldspar (>1 mm)	Cadamosto, Cape Verde	Jan Sticklus	15	0.144	0.0000328	0.305	1.0098	0.21	1	1.203E-14	23	MAR	2017	22	24	1	can42	Examples	c42it7ip3_1521F	01	TCS2
C42CA061	15.00 W	K-feldspar (>1 mm)	Cadamosto, Cape Verde	Jan Sticklus	15	0.144	0.0000328	0.305	1.0098	0.21	1	1.203E-14	23	MAR	2017	19	41	1	can42	Examples	c42it7ip3_1521F	01	TCS2

Irradiation Constants	Laser power	40/36(a)	%1σ	40/36(c)	%1σ	38/36(a)	%1σ	38/36(c)	%1σ	39/37(ca)	%1σ	38/37(ca)	%1σ	36/37(ca)	%1σ	40/39(k)	%1σ	38/39(k)	%1σ	36/38(cl)	%1σ	K/Ca	%1σ	K/Cl	%1σ	Ca/Cl	%1σ
C42CA051	15.00 W	295.5	0.169	0.018	35	0.1869	0.107	1.493	3	0.000702	1.71	0.000196	0.41	0.0002702	0.15	0.00073	12.33	0.01215	0.25	262.8	0.65	0.51	0	0	0	0	0
C42CA054	15.00 W	295.5	0.169	0.018	35	0.1869	0.107	1.493	3	0.000702	1.71	0.000196	0.41	0.0002702	0.15	0.00073	12.33	0.01215	0.25	262.8	0.65	0.51	0	0	0	0	0
C42CA050	15.00 W	295.5	0.169	0.018	35	0.1869	0.107	1.493	3	0.000702	1.71	0.000196	0.41	0.0002702	0.15	0.00073	12.33	0.01215	0.25	262.8	0.65	0.51	0	0	0	0	0
C42CA060	15.00 W	295.5	0.169	0.018	35	0.1869	0.107	1.493	3	0.000702	1.71	0.000196	0.41	0.0002702	0.15	0.00073	12.33	0.01215	0.25	262.8	0.65	0.51	0	0	0	0	0
C42CA062	15.00 W	295.5	0.169	0.018	35	0.1869	0.107	1.493	3	0.000702	1.71	0.000196	0.41	0.0002702	0.15	0.00073	12.33	0.01215	0.25	262.8	0.65	0.51	0	0	0	0	0
C42CA057	15.00 W	295.5	0.169	0.018	35	0.1869	0.107	1.493	3	0.000702	1.71	0.000196	0.41	0.0002702	0.15	0.00073	12.33	0.01215	0.25	262.8	0.65	0.51	0	0	0	0	0
C42CA048	15.00 W	295.5	0.169	0.018	35	0.1869	0.107	1.493	3	0.000702	1.71	0.000196	0.41	0.0002702	0.15	0.00073	12.33	0.01215	0.25	262.8	0.65	0.51	0	0	0	0	0
C42CA058	15.00 W	295.5	0.169	0.018	35	0.1869	0.107	1.493	3	0.000702	1.71	0.000196	0.41	0.0002702	0.15	0.00073	12.33	0.01215	0.25	262.8	0.65	0.51	0	0	0	0	0
C42CA065	15.00 W	295.5	0.169	0.018	35	0.1869	0.107	1.493	3	0.000702	1.71	0.000196	0.41	0.0002702	0.15	0.00073	12.33	0.01215	0.25	262.8	0.65	0.51	0	0	0	0	0
C42CA049	15.00 W	295.5	0.169	0.018	35	0.1869	0.107	1.493	3	0.000702	1.71	0.000196	0.41	0.0002702	0.15	0.00073	12.33	0.01215	0.25	262.8	0.65	0.51	0	0	0	0	0
C42CA052	15.00 W	295.5	0.169	0.018	35	0.1869	0.107	1.493	3	0.000702	1.71	0.000196	0.41	0.0002702	0.15	0.00073	12.33	0.01215	0.25	262.8	0.65	0.51	0	0	0	0	0
C42CA067	15.00 W	295.5	0.169	0.018	35	0.1869	0.107	1.493	3	0.000702	1.71	0.000196	0.41	0.0002702	0.15	0.00073	12.33	0.01215	0.25	262.8	0.65	0.51	0	0	0	0	0
C42CA056	15.00 W	295.5	0.169	0.018	35	0.1869	0.107	1.493	3	0.000702	1.71	0.000196	0.41	0.0002702	0.15	0.00073	12.33	0.01215	0.25	262.8	0.65	0.51	0	0	0	0	0
C42CA063	15.00 W	295.5	0.169	0.018	35	0.1869	0.107	1.493	3	0.000702	1.71	0.000196	0.41	0.0002702	0.15	0.00073	12.33	0.01215	0.25	262.8	0.65	0.51	0	0	0	0	0
C42CA064	15.00 W	295.5	0.169	0.018	35	0.1869	0.107	1.493	3	0.000702	1.71	0.000196	0.41	0.0002702	0.15	0.00073	12.33	0.01215	0.25	262.8	0.65	0.51	0	0	0	0	0
C42CA047	15.00 W	295.5	0.169	0.018	35	0.1869	0.107	1.493	3	0.000702	1.71	0.000196	0.41	0.0002702	0.15	0.00073	12.33	0.01215	0.25	262.8	0.65	0.51	0	0	0	0	0
C42CA053	15.00 W	295.5	0.169	0.018	35	0.1869	0.107	1.493	3	0.000702	1.71	0.000196	0.41	0.0002702	0.15	0.00073	12.33	0.01215	0.25	262.8	0.65	0.51	0	0	0	0	0
C42CA059	15.00 W	295.5	0.169	0.018	35	0.1869	0.107	1.493	3	0.000702	1.71	0.000196	0.41	0.0002702	0.15	0.00073	12.33	0.01215	0.25	262.8	0.65	0.51	0	0	0	0	0
C42CA066	15.00 W	295.5	0.169	0.018	35	0.1869	0.107	1.493	3	0.000702	1.71	0.000196	0.41	0.0002702	0.15	0.00073	12.33	0.01215	0.25	262.8	0.65	0.51	0	0	0	0	0
C42CA061	15.00 W	295.5	0.169	0.018	35	0.1869	0.107	1.493	3	0.000702	1.71	0.000196	0.41	0.0002702	0.15	0.00073	12.33	0.01215	0.25	262.8	0.65	0.51	0	0	0	0	0

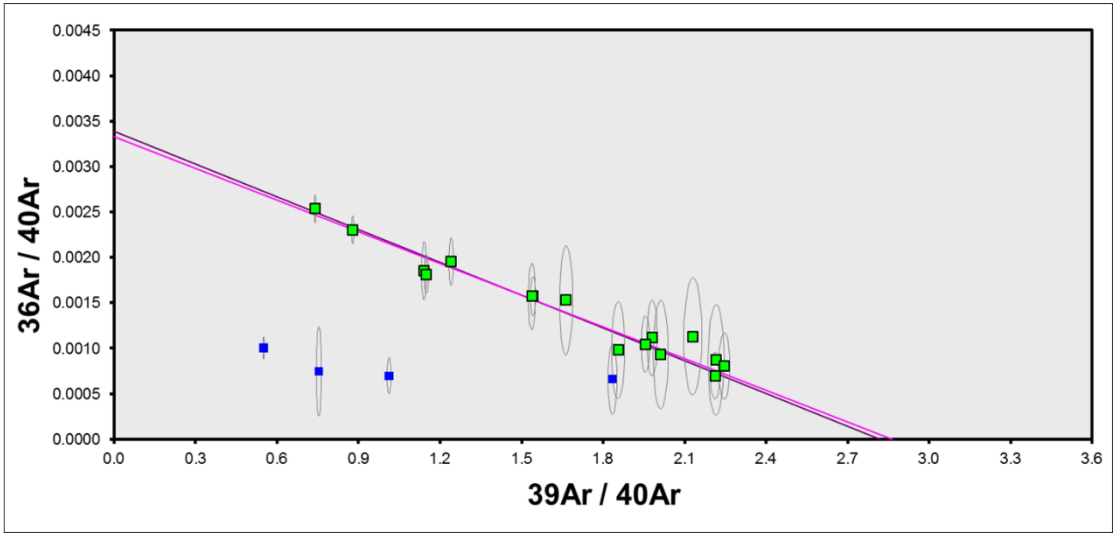
36Ar / 40Ar
39Ar / 40Ar
0.0045
0.0040
0.0035
0.0030
0.0025
0.0020
0.0015
0.0010
0.0005
0.0000
0.0
0.3
0.6
0.9
1.2
1.5
1.8
2.1
2.4
2.7
3.0
3.3
3.6

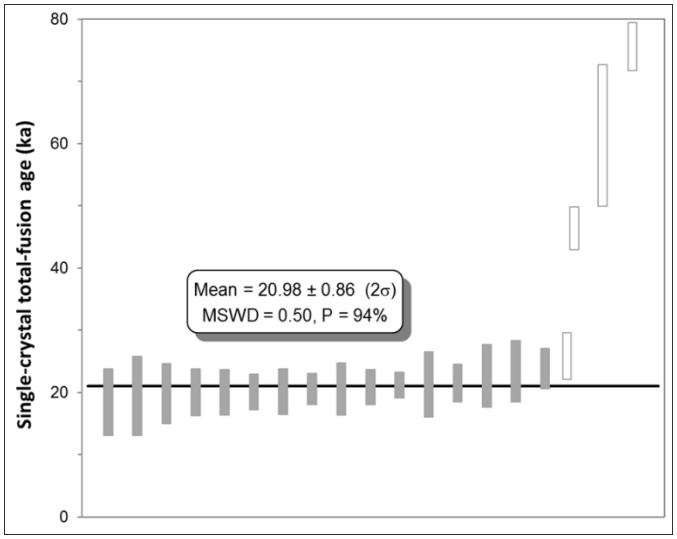
Single-crystal total-fusion age (ka)
80
60
40
20
0
Mean = 20.98 ± 0.86 (2σ)
MSWD = 0.50, P = 94%

Information on Analysis and Constants Used in Calculations

Sample = 1521F (POS 320/2 152-1)
Material = K-feldspar >1 mm
Location = Cadamosto, Cape Verde
Analyst = Jan Sticklus
Project = EXAMPLES
Mass Discrimination Law = POW
Irradiation = can42
J = 0.00003280 ± 0.00000010
TCS2 = 27.870 ± 0.040 Ma
Heating = 45 sec
Instrument = MAP216

Age Equations = Conventional
Negative Intensities = Allowed
Decay Constant 40K = 5.543 ± 0.009 E-10 1/a
Decay Constant 39Ar = 2.940 ± 0.016 E-07 1/h
Decay Constant 37Ar = 8.230 ± 0.012 E-04 1/h
Decay Constant 36Cl = 2.257 ± 0.015 E-06 1/a
Atmospheric Ratio 40/36(a) = 295.50 ± 0.50
Atmospheric Ratio 38/36(a) = 0.1869 ± 0.0002
Production Ratio 39/37(ca) = 0.000702 ± 0.000012
Production Ratio 38/37(ca) = 0.000196 ± 0.000001
Production Ratio 36/37(ca) = 0.000270 ± 0.000000
Production Ratio 40/39(k) = 0.000730 ± 0.000090
Production Ratio 38/39(k) = 0.012150 ± 0.000030
Production Ratio 36/38(cl) = 262.80
Scaling Ratio K/Ca = 0.510

Results	40(a)/36(a) ± 2σ	40(r)/39(k) ± 2σ	Age ± 2σ (Ka)	MSWD	39Ar(k) (%,n)	K/Ca ± 2σ
Age Plateau		0.35455 ± 0.01450 ± 4.09%	20.98 ± 0.87 ± 4.14%	0.50	83.08	
				94%	16	91 ± 23
		Minimal External Error ± 0.9		1.73	2σ Confidence Limit	
		Analytical Error ± 0.9		1.0000	Error Magnification	
Total Fusion Age		0.44083 ± 0.01411 ± 3.20%	26.09 ± 0.85 ± 3.26%		20	377 ± 147
		Minimal External Error ± 0.9				
		Analytical Error ± 0.8				
Normal Isochron	301.39 ± 16.86 ± 5.60%	0.34427 ± 0.02340 ± 6.80%	20.4 ± 1.4 ± 6.82%	0.48	83.08	
				94%	16	
		Minimal External Error ± 1.4		1.76	2σ Confidence Limit	
		Analytical Error ± 1.4		1.0000	Error Magnification	
				28	Number of Iterations	
				0.0000034213	Convergence	
Inverse Isochron	300.67 ± 16.84 ± 5.60%	0.34911 ± 0.02285 ± 6.55%	20.7 ± 1.4 ± 6.57%	0.50	83.08	
				93%	16	
		Minimal External Error ± 1.4		1.76	2σ Confidence Limit	
		Analytical Error ± 1.4		1.0000	Error Magnification	
				3	Number of Iterations	
				0.0000064246	Convergence	
				53%	Spreading Factor	

[a] Blue dots in table indicate selected steps used to calculate the weighted mean and inverse isochron ages.
[b] Weight % K values calculated from $^{39}Ar_K$ values and weights of individual grains.
[c] Alteration Index values in italics indicate analyses from fresh material, normal font is from altered material (Baksi, 2007; van den Bogaard, 2013).
Values shown in red are negative values.
Abbreviations used in tables: (r) = radiogenic ^{40}Ar; (k) = Ar derived from K; (a) = atmospheric Ar; (ca) = Ar derived from Ca; (cl) = Ar derived from Ca; (c) = cosmogenic Ar; MDF = Mass Discrimination Factor.
Green squares in the inverse isochron plots indicate selected steps (blue dots in table), and blue squares are non-selected steps. Pink lines in the inverse isochron plot indicate a line fit through selected data, and the purple lines incidate a fit through an air $^{40}Ar/^{36}Ar$ ratio (295.5).
Stacked probability plot produced using Isoplot (Ludwig, 2011), where filled and unfilled 2σ error bars indicate selected/not selected data to calculate inverse-variance weighted mean age (black line), respectively.

035ROV-12 total fusion

Relative Abundances	Laser power	a	36Ar [V]	%1σ	37Ar [V]	%1σ	38Ar [V]	%1σ	39Ar [V]	%1σ	40Ar [V]	%1σ	40(r)/39(k) ± 2σ	Age ± 2σ (Ka)	40Ar(r) (%)	39Ar(k) (%)	K/Ca ± 2σ	Weight (mg)	Wt. % K[a]	$^{36}Ar/^{39}Ar$ Alt. Index[b]
C42GA004	20.00 W	•	0.0000084	151.780	0.0035073	106.791	0.0002284	6.278	0.0189446	0.415	0.016935	0.987	0.74799 ±0.39722	44.3 ± 23.5	83.69	0.38	3 ± 6	0.484	9.54	*0.000002*
C42FA012	20.00 W	•	0.0001074	13.349	0.0001288	1157.521	0.0008734	1.984	0.0814926	0.301	0.095015	0.356	0.77557 ±0.10447	45.9 ± 6.2	66.52	1.66	323 ± 7470	2.153	-	*0.000040*
C42GA011	20.00 W	•	0.0000879	14.807	0.0008897	472.378	0.0006424	2.195	0.0595045	0.304	0.073242	0.305	0.79262 ±0.13002	46.9 ± 7.7	64.40	1.21	34 ± 322	1.373	10.56	*0.000005*
C42FA011	20.00 W	•	0.0000519	25.608	0.0009967	150.404	0.0006246	2.656	0.0567482	0.279	0.060732	0.546	0.80065 ±0.13904	47.4 ± 8.2	74.81	1.15	29 ± 87	1.613	-	*0.000003*
C42GA006	20.00 W	•	0.0000280	43.700	0.0034332	124.304	0.0004464	2.330	0.0391411	0.296	0.041802	0.410	0.84909 ±0.18558	50.2 ± 11.0	79.51	0.80	6 ± 14	0.902	10.57	*0.000003*
C42GA003	20.00 W	•	0.0000073	151.065	0.0040787	86.269	0.0004321	2.373	0.0385852	0.292	0.037028	0.603	0.89470 ±0.16939	52.9 ± 10.0	93.24	0.78	5 ± 8	0.937	10.03	*0.000001*
C42GA016	25.00 W	•	0.0000354	35.911	0.0001508	2686.136	0.0008977	2.021	0.0799244	0.278	0.083650	0.271	0.91483 ±0.09467	54.1 ± 5.6	87.41	1.62	270 ± 14521	1.642	11.86	*0.000002*
C42FA002	20.00 W	•	0.0001658	7.939	0.0005575	329.621	0.0008921	2.140	0.0822230	0.292	0.125288	0.286	0.92773 ±0.09525	54.9 ± 5.6	60.88	1.67	75 ± 496	2.169	-	*0.000006*
C42FA014	20.00 W	•	0.0001371	10.469	0.0008920	178.048	0.0007946	1.905	0.0743413	0.291	0.109668	0.307	0.93034 ±0.11469	55.1 ± 6.8	63.07	1.51	43 ± 151	1.935	-	*0.000006*
C42GA002	20.00 W	•	0.0000005	2724.637	0.0036194	110.066	0.0003149	2.511	0.0266739	0.295	0.024974	0.639	0.93051 ±0.32277	55.1 ± 19.1	99.40	0.54	4 ± 8	0.657	9.89	*0.000000*
C42GA005	20.00 W	•	0.0001093	12.420	0.0004405	911.032	0.0004761	3.241	0.0405834	0.390	0.070412	0.269	0.93960 ±0.19861	55.6 ± 11.8	54.16	0.82	47 ± 856	0.962	10.28	*0.000009*
C42GA008	20.00 W	•	0.0000437	24.881	0.0014616	297.289	0.0003726	2.613	0.0343528	0.324	0.045354	0.415	0.94026 ±0.18852	55.6 ± 11.2	71.22	0.70	12 ± 71	0.772	10.84	*0.000005*
C42FA001	20.00 W		0.0001866	9.088	0.0035136	48.480	0.0010400	2.076	0.0940985	0.283	0.146063	0.234	0.96861 ±0.10694	57.3 ± 6.3	62.40	1.91	14 ± 13	2.478	-	*0.000006*
C42GA001	20.00 W		0.0001751	6.905	0.0052739	74.271	0.0007233	2.543	0.0669769	0.249	0.119737	0.168	1.00815 ±0.10741	59.7 ± 6.4	56.40	1.36	6 ± 10	1.587	10.28	*0.000009*
C42FA005	20.00 W		0.0001528	8.218	0.0021551	64.535	0.0010177	1.897	0.0963869	0.279	0.143567	0.253	1.02202 ±0.07764	60.5 ± 4.6	68.61	1.96	23 ± 29	2.466	-	*0.000005*
C42CA070	15.00 W		0.0001570	9.658	0.0002331	152.004	0.0027792	0.824	0.2276687	0.246	0.281108	0.076	1.03027 ±0.03975	61.0 ± 2.4	83.44	4.63	498 ± 1514	2.964	9.00	*0.000002*
C42GA015	25.00 W		0.0000769	14.316	0.0024046	156.112	0.0009268	2.355	0.0804262	0.301	0.107337	0.199	1.04893 ±0.08166	62.1 ± 4.8	78.60	1.63	17 ± 53	1.801	10.88	*0.000003*
C42GA017	25.00 W		0.0000753	14.393	0.0058151	67.557	0.0011324	1.494	0.0978634	0.241	0.126873	0.143	1.06365 ±0.06604	62.9 ± 3.9	82.05	1.99	9 ± 12	2.149	11.09	*0.000003*
C42FA008	20.00 W		0.0004180	3.715	0.0013094	112.218	0.0019471	1.291	0.1806127	0.238	0.316250	0.135	1.06687 ±0.05136	63.1 ± 3.0	60.93	3.67	70 ± 158	4.730	-	*0.000007*
C42GA020	25.00 W		0.0019805	1.524	0.0019002	202.680	0.0024919	1.354	0.1936239	0.235	0.796306	0.038	1.08861 ±0.09299	64.4 ± 5.5	26.47	3.93	52 ± 211	4.209	11.21	*0.000038*
C42GA012	20.00 W		0.0001175	8.689	0.0016794	215.707	0.0006402	1.961	0.0563912	0.309	0.100525	0.203	1.16833 ±0.10805	69.1 ± 6.4	65.54	1.15	17 ± 74	1.230	11.17	*0.000008*
C42CA071	15.00 W		0.0003440	5.833	0.0012069	30.323	0.0040049	1.137	0.3360976	0.238	0.495487	0.090	1.17136 ±0.03584	69.3 ± 2.1	79.46	6.83	142 ± 86	4.109	9.59	*0.000003*
C42GA013	20.00 W		0.0001098	10.534	0.0025995	154.262	0.0006281	2.220	0.0543397	0.285	0.096382	0.211	1.17203 ±0.12675	69.4 ± 7.5	66.08	1.10	11 ± 33	1.200	11.03	*0.000007*
C42GA009	20.00 W		0.0000260	36.408	0.0011895	326.396	0.0005709	2.067	0.0509136	0.289	0.067869	0.316	1.18334 ±0.11105	70.0 ± 6.6	88.77	1.03	22 ± 142	1.168	10.62	*0.000002*
C42CA074	15.00 W		0.0001033	14.098	0.0008010	46.730	0.0028667	1.464	0.2349573	0.222	0.312726	0.102	1.20060 ±0.03713	71.0 ± 2.2	90.20	4.77	150 ± 140	3.043	9.05	*0.000001*
C42GA021	25.00 W		0.0005835	2.654	0.0025516	162.432	0.0021201	0.806	0.1820781	0.228	0.391589	0.055	1.20177 ±0.05086	71.1 ± 3.0	55.88	3.70	36 ± 118	4.072	10.89	*0.000011*
C42CA076	15.00 W		0.0001924	6.397	0.0010212	28.655	0.0026454	1.175	0.2190469	0.267	0.328092	0.138	1.23795 ±0.03412	73.3 ± 2.0	82.65	4.45	109 ± 63	2.649	9.69	*0.000003*
C42CA075	15.00 W		0.0003773	3.969	0.0007736	48.338	0.0020974	1.539	0.1738093	0.267	0.326996	0.117	1.23948 ±0.05159	73.3 ± 3.1	65.88	3.53	115 ± 111	2.205	9.24	*0.000007*
C42CA068	15.00 W		0.0002335	7.968	0.0005096	64.382	0.0030021	1.302	0.2482304	0.223	0.377513	0.057	1.24223 ±0.04470	73.5 ± 2.6	81.68	5.04	248 ± 320	3.172	9.17	*0.000003*
C42FA007	20.00 W		0.0001856	6.908	0.0004519	294.184	0.0012640	2.385	0.1140828	0.267	0.199599	0.219	1.26768 ±0.06726	75.0 ± 4.0	72.46	2.32	129 ± 758	2.799	-	*0.000005*
C42FA003	20.00 W		0.0002250	5.857	0.0022615	70.353	0.0011719	2.033	0.1081897	0.235	0.203726	0.161	1.26948 ±0.07255	75.1 ± 4.3	67.42	2.20	24 ± 34	2.632	-	*0.000007*
C42CA069	15.00 W		0.0002995	6.668	0.0009211	33.309	0.0042199	0.950	0.3505496	0.226	0.541212	0.061	1.29093 ±0.03423	76.4 ± 2.0	83.62	7.12	194 ± 129	4.454	9.23	*0.000003*
C42FA004	20.00 W		0.0001007	11.564	0.0018699	73.043	0.0010297	2.303	0.0995207	0.236	0.163846	0.251	1.34825 ±0.06995	79.8 ± 4.1	81.89	2.02	27 ± 40	2.914	-	*0.000003*
C42GA018	25.00 W		0.0003658	2.793	0.0003303	1222.772	0.0012993	1.393	0.1106080	0.254	0.263353	0.152	1.40316 ±0.05595	83.0 ± 3.3	58.93	2.25	171 ± 4176	2.608	10.33	*0.000011*
C42FA013	20.00 W		0.0002558	5.398	0.0000111	12676.007	0.0012025	2.080	0.1083342	0.243	0.271439	0.153	1.80713 ±0.07630	106.9 ± 4.5	72.12	2.20	4984 ± 1263664	2.684	-	*0.000008*
C42FA010	20.00 W		0.0116301	0.969	0.0024926	66.197	0.0033881	1.105	0.1074347	0.292	3.639110	0.036	1.88529 ±0.63079	111.6 ± 37.3	5.57	2.18	22 ± 29	2.739	-	0.000339
C42GA007	20.00 W		0.0000849	14.330	0.0031930	132.327	0.0005133	1.920	0.0458906	0.353	0.113274	0.199	1.91522 ±0.15828	113.3 ± 9.4	77.59	0.93	7 ± 19	1.101	10.15	*0.000006*
C42GA014	20.00 W		0.0001053	11.481	0.0016428	258.103	0.0005320	2.264	0.0462230	0.257	0.136499	0.174	2.27638 ±0.15603	134.7 ± 9.2	77.09	0.94	14 ± 74	1.041	10.82	*0.000008*
C42GA010	20.00 W		0.0000420	28.461	0.0002439	1512.268	0.0004501	2.999	0.0414981	0.375	0.125605	0.166	2.72657 ±0.17230	161.3 ± 10.2	90.08	0.84	87 ± 2625	1.000	10.11	*0.000003*
C42GA019	25.00 W		0.0029105	1.183	0.0037914	105.118	0.0023499	0.965	0.1643808	0.229	1.397980	0.040	3.27360 ±0.12635	193.7 ± 7.5	38.49	3.34	22 ± 46	3.886	10.31	*0.000060*
C42FA006	20.00 W		0.0003277	5.116	0.0015676	101.405	0.0009924	1.506	0.0882398	0.293	0.392976	0.090	3.35686 ±0.11439	198.6 ± 6.8	75.38	1.79	29 ± 58	2.323	-	*0.000011*
C42CA072	15.00 W		0.0009133	3.102	0.0009000	46.914	0.0018208	1.664	0.1392213	0.225	0.828832	0.053	4.01470 ±0.12196	237.5 ± 7.2	67.44	2.83	79 ± 74	1.701	9.60	*0.000021*
C42FA009	20.00 W		0.0028681	1.390	0.0041279	46.197	0.0023622	1.634	0.1711211	0.256	2.617126	0.048	10.34257 ±0.14930	611.9 ± 8.8	67.62	3.48	21 ± 20	4.202	-	*0.000055*
		Σ	0.0264053	0.590	0.0077934	246.056	0.0602256	0.260	4.9213313	0.045	16.213094	0.017								

Procedure Blanks	Laser power	36Ar [V]	1σ	37Ar [V]	1σ	38Ar [V]	1σ	39Ar [V]	1σ	40Ar [V]	1σ
C42GA004	20.00 W	0.0001926	0.0000089	0.0002227	0.0000141	0.0000907	0.0000060	0.0001968	0.0000218	0.0030038	0.0001487
C42FA012	20.00 W	0.0002535	0.0000088	0.0002105	0.0000100	0.0001163	0.0000076	0.0002260	0.0000398	0.0025750	0.0002950
C42GA011	20.00 W	0.0001966	0.0000089	0.0002171	0.0000141	0.0000975	0.0000060	0.0001897	0.0000218	0.0025756	0.0001487
C42FA011	20.00 W	0.0002503	0.0000088	0.0002104	0.0000100	0.0001158	0.0000076	0.0002327	0.0000398	0.0026590	0.0002950
C42GA006	20.00 W	0.0001940	0.0000089	0.0002218	0.0000141	0.0000962	0.0000060	0.0002022	0.0000218	0.0029966	0.0001487
C42GA003	20.00 W	0.0001915	0.0000089	0.0002219	0.0000141	0.0000879	0.0000060	0.0001911	0.0000218	0.0029084	0.0001487
C42GA016	25.00 W	0.0002013	0.0000089	0.0002198	0.0000141	0.0000898	0.0000060	0.0001766	0.0000218	0.0025047	0.0001487
C42FA002	20.00 W	0.0002527	0.0000088	0.0002068	0.0000100	0.0001074	0.0000076	0.0002424	0.0000398	0.0020218	0.0002950
C42FA014	20.00 W	0.0002660	0.0000088	0.0002116	0.0000100	0.0001191	0.0000076	0.0002223	0.0000398	0.0023249	0.0002950
C42GA002	20.00 W	0.0001900	0.0000089	0.0002201	0.0000141	0.0000847	0.0000060	0.0001829	0.0000218	0.0027351	0.0001487
C42GA005	20.00 W	0.0001933	0.0000089	0.0002227	0.0000141	0.0000931	0.0000060	0.0002003	0.0000218	0.0030376	0.0001487
C42GA008	20.00 W	0.0001947	0.0000089	0.0002198	0.0000141	0.0000982	0.0000060	0.0002000	0.0000218	0.0028560	0.0001487
C42FA001	20.00 W	0.0002452	0.0000088	0.0002024	0.0000100	0.0000996	0.0000076	0.0001932	0.0000398	0.0016777	0.0002950
C42GA001	20.00 W	0.0001861	0.0000089	0.0002142	0.0000141	0.0000788	0.0000060	0.0001625	0.0000218	0.0022293	0.0001487
C42FA005	20.00 W	0.0002552	0.0000088	0.0002108	0.0000100	0.0001146	0.0000076	0.0002794	0.0000398	0.0024803	0.0002950
C42CA070	15.00 W	0.0002102	0.0000110	0.0018510	0.0000362	0.0000862	0.0000058	0.0001258	0.0000152	0.0034470	0.0000452
C42GA015	25.00 W	0.0002006	0.0000089	0.0002188	0.0000141	0.0000912	0.0000060	0.0001779	0.0000218	0.0024811	0.0001487
C42GA017	25.00 W	0.0002018	0.0000089	0.0002208	0.0000141	0.0000885	0.0000060	0.0001760	0.0000218	0.0025365	0.0001487
C42FA008	20.00 W	0.0002499	0.0000088	0.0002112	0.0000100	0.0001160	0.0000076	0.0002661	0.0000398	0.0027402	0.0002950
C42GA020	25.00 W	0.0001995	0.0000089	0.0002225	0.0000141	0.0000875	0.0000060	0.0001788	0.0000218	0.0026088	0.0001487
C42GA012	20.00 W	0.0001974	0.0000089	0.0002169	0.0000141	0.0000965	0.0000060	0.0001866	0.0000218	0.0025236	0.0001487
C42CA071	15.00 W	0.0002102	0.0000110	0.0018510	0.0000362	0.0000862	0.0000058	0.0001258	0.0000152	0.0034470	0.0000452
C42GA013	20.00 W	0.0001983	0.0000089	0.0002171	0.0000141	0.0000952	0.0000060	0.0001837	0.0000218	0.0024888	0.0001487
C42GA009	20.00 W	0.0001951	0.0000089	0.0002188	0.0000141	0.0000985	0.0000060	0.0001977	0.0000218	0.0027750	0.0001487
C42CA074	15.00 W	0.0002102	0.0000110	0.0018510	0.0000362	0.0000862	0.0000058	0.0001258	0.0000152	0.0034470	0.0000452
C42GA021	25.00 W	0.0001971	0.0000089	0.0002217	0.0000141	0.0000889	0.0000060	0.0001808	0.0000218	0.0025754	0.0001487
C42CA076	15.00 W	0.0002102	0.0000110	0.0018510	0.0000362	0.0000862	0.0000058	0.0001258	0.0000152	0.0034470	0.0000452
C42CA075	15.00 W	0.0002102	0.0000110	0.0018510	0.0000362	0.0000862	0.0000058	0.0001258	0.0000152	0.0034470	0.0000452
C42CA068	15.00 W	0.0002102	0.0000110	0.0018510	0.0000362	0.0000862	0.0000058	0.0001258	0.0000152	0.0034470	0.0000452
C42FA007	20.00 W	0.0002515	0.0000088	0.0002114	0.0000100	0.0001161	0.0000076	0.0002737	0.0000398	0.0027026	0.0002950
C42FA003	20.00 W	0.0002548	0.0000088	0.0002087	0.0000100	0.0001107	0.0000076	0.0002613	0.0000398	0.0021985	0.0002950
C42CA069	15.00 W	0.0002102	0.0000110	0.0018510	0.0000362	0.0000862	0.0000058	0.0001258	0.0000152	0.0034470	0.0000452
C42FA004	20.00 W	0.0002556	0.0000088	0.0002100	0.0000100	0.0001130	0.0000076	0.0002733	0.0000398	0.0023515	0.0002950
C42GA018	25.00 W	0.0002017	0.0000089	0.0002222	0.0000141	0.0000871	0.0000060	0.0001763	0.0000218	0.0025902	0.0001487
C42FA013	20.00 W	0.0002586	0.0000088	0.0002109	0.0000100	0.0001174	0.0000076	0.0002222	0.0000398	0.0024637	0.0002950
C42FA010	20.00 W	0.0002488	0.0000088	0.0002106	0.0000100	0.0001156	0.0000076	0.0002413	0.0000398	0.0027160	0.0002950
C42GA007	20.00 W	0.0001944	0.0000089	0.0002208	0.0000141	0.0000974	0.0000060	0.0002016	0.0000218	0.0029339	0.0001487
C42GA014	20.00 W	0.0001997	0.0000089	0.0002180	0.0000141	0.0000928	0.0000060	0.0001797	0.0000218	0.0024704	0.0001487
C42GA010	20.00 W	0.0001960	0.0000089	0.0002175	0.0000141	0.0000982	0.0000060	0.0001929	0.0000218	0.0026425	0.0001487
C42GA019	25.00 W	0.0002010	0.0000089	0.0002226	0.0000141	0.0000870	0.0000060	0.0001773	0.0000218	0.0026096	0.0001487
C42FA006	20.00 W	0.0002531	0.0000088	0.0002114	0.0000100	0.0001159	0.0000076	0.0002789	0.0000398	0.0026395	0.0002950
C42CA072	15.00 W	0.0002102	0.0000110	0.0018510	0.0000362	0.0000862	0.0000058	0.0001258	0.0000152	0.0034470	0.0000452
C42FA009	20.00 W	0.0002488	0.0000088	0.0002110	0.0000100	0.0001159	0.0000076	0.0002572	0.0000398	0.0027522	0.0002950

Sample Parameters	Laser power	Material	Location	Analyst	Power	%1σ	J	%1σ	MDF	%1σ	Volume Ratio	Sensitivity (mol/volt)	Day	Month	Year	Hour	Min	Resist	Irradiation	Project	Experiment	Nmb	Standard Name
C42GA004	20.00 W	K-feldspar (>1 mm)	Cadamosto, Cape Verde	Jan Sticklus	20	0.14	0.0000328	0.3	1.0098	0.21	1	1.21E-14	13	SEP	2017	10	40	1	can42	Examples	C42GA004	03	TCS2
C42FA012	20.00 W	K-feldspar (>1 mm)	Cadamosto, Cape Verde	Jan Sticklus	20	0.14	0.0000328	0.3	1.0098	0.21	1	1.21E-14	8	AUG	2017	14	12	1	can42	Examples	C42FA001	02	TCS2
C42GA011	20.00 W	K-feldspar (>1 mm)	Cadamosto, Cape Verde	Jan Sticklus	20	0.14	0.0000328	0.3	1.0098	0.21	1	1.21E-14	13	SEP	2017	14	40	1	can42	Examples	C42GA004	03	TCS2
C42FA011	20.00 W	K-feldspar (>1 mm)	Cadamosto, Cape Verde	Jan Sticklus	20	0.14	0.0000328	0.3	1.0098	0.21	1	1.21E-14	8	AUG	2017	13	43	1	can42	Examples	C42FA001	02	TCS2
C42GA006	20.00 W	K-feldspar (>1 mm)	Cadamosto, Cape Verde	Jan Sticklus	20	0.14	0.0000328	0.3	1.0098	0.21	1	1.21E-14	13	SEP	2017	11	57	1	can42	Examples	C42GA004	03	TCS2
C42GA003	20.00 W	K-feldspar (>1 mm)	Cadamosto, Cape Verde	Jan Sticklus	20	0.14	0.0000328	0.3	1.0098	0.21	1	1.21E-14	13	SEP	2017	10	11	1	can42	Examples	C42GA004	03	TCS2
C42GA016	25.00 W	K-feldspar (>1 mm)	Cadamosto, Cape Verde	Jan Sticklus	25	0.14	0.0000328	0.3	1.0098	0.21	1	1.21E-14	13	SEP	2017	17	24	1	can42	Examples	C42GA004	03	TCS2
C42FA002	20.00 W	K-feldspar (>1 mm)	Cadamosto, Cape Verde	Jan Sticklus	20	0.14	0.0000328	0.3	1.0098	0.21	1	1.21E-14	8	AUG	2017	8	45	1	can42	Examples	C42FA001	02	TCS2
C42FA014	20.00 W	K-feldspar (>1 mm)	Cadamosto, Cape Verde	Jan Sticklus	20	0.14	0.0000328	0.3	1.0098	0.21	1	1.21E-14	8	AUG	2017	15	10	1	can42	Examples	C42FA001	02	TCS2
C42GA002	20.00 W	K-feldspar (>1 mm)	Cadamosto, Cape Verde	Jan Sticklus	20	0.14	0.0000328	0.3	1.0098	0.21	1	1.21E-14	13	SEP	2017	9	42	1	can42	Examples	C42GA004	03	TCS2
C42GA005	20.00 W	K-feldspar (>1 mm)	Cadamosto, Cape Verde	Jan Sticklus	20	0.14	0.0000328	0.3	1.0098	0.21	1	1.21E-14	13	SEP	2017	11	9	1	can42	Examples	C42GA004	03	TCS2
C42GA008	20.00 W	K-feldspar (>1 mm)	Cadamosto, Cape Verde	Jan Sticklus	20	0.14	0.0000328	0.3	1.0098	0.21	1	1.21E-14	13	SEP	2017	12	55	1	can42	Examples	C42GA004	03	TCS2
C42FA001	20.00 W	K-feldspar (>1 mm)	Cadamosto, Cape Verde	Jan Sticklus	20	0.14	0.0000328	0.3	1.0098	0.21	1	1.21E-14	8	AUG	2017	7	57	1	can42	Examples	C42FA001	02	TCS2
C42GA001	20.00 W	K-feldspar (>1 mm)	Cadamosto, Cape Verde	Jan Sticklus	20	0.14	0.0000328	0.3	1.0098	0.21	1	1.21E-14	13	SEP	2017	8	54	1	can42	Examples	C42GA004	03	TCS2
C42FA005	20.00 W	K-feldspar (>1 mm)	Cadamosto, Cape Verde	Jan Sticklus	20	0.14	0.0000328	0.3	1.0098	0.21	1	1.21E-14	8	AUG	2017	10	12	1	can42	Examples	C42FA001	02	TCS2
C42CA070	15.00 W	K-feldspar (>1 mm)	Cadamosto, Cape Verde	Jan Sticklus	15	0.14	0.0000328	0.3	1.0098	0.21	1	1.21E-14	24	MAR	2017	0	39	1	can42	Examples	c42it7ip6_3512F	01	TCS2
C42GA015	25.00 W	K-feldspar (>1 mm)	Cadamosto, Cape Verde	Jan Sticklus	25	0.14	0.0000328	0.3	1.0098	0.21	1	1.21E-14	13	SEP	2017	16	55	1	can42	Examples	C42GA004	03	TCS2
C42GA017	25.00 W	K-feldspar (>1 mm)	Cadamosto, Cape Verde	Jan Sticklus	25	0.14	0.0000328	0.3	1.0098	0.21	1	1.21E-14	13	SEP	2017	17	53	1	can42	Examples	C42GA004	03	TCS2
C42FA008	20.00 W	K-feldspar (>1 mm)	Cadamosto, Cape Verde	Jan Sticklus	20	0.14	0.0000328	0.3	1.0098	0.21	1	1.21E-14	8	AUG	2017	11	58	1	can42	Examples	C42FA001	02	TCS2
C42GA020	25.00 W	K-feldspar (>1 mm)	Cadamosto, Cape Verde	Jan Sticklus	25	0.14	0.0000328	0.3	1.0098	0.21	1	1.21E-14	13	SEP	2017	19	38	1	can42	Examples	C42GA004	03	TCS2
C42GA012	20.00 W	K-feldspar (>1 mm)	Cadamosto, Cape Verde	Jan Sticklus	20	0.14	0.0000328	0.3	1.0098	0.21	1	1.21E-14	13	SEP	2017	15	9	1	can42	Examples	C42GA004	03	TCS2
C42CA071	15.00 W	K-feldspar (>1 mm)	Cadamosto, Cape Verde	Jan Sticklus	15	0.14	0.0000328	0.3	1.0098	0.21	1	1.21E-14	24	MAR	2017	1	8	1	can42	Examples	c42it7ip6_3512F	01	TCS2
C42GA013	20.00 W	K-feldspar (>1 mm)	Cadamosto, Cape Verde	Jan Sticklus	20	0.14	0.0000328	0.3	1.0098	0.21	1	1.21E-14	13	SEP	2017	15	38	1	can42	Examples	C42GA004	03	TCS2
C42GA009	20.00 W	K-feldspar (>1 mm)	Cadamosto, Cape Verde	Jan Sticklus	20	0.14	0.0000328	0.3	1.0098	0.21	1	1.21E-14	13	SEP	2017	13	23	1	can42	Examples	C42GA004	03	TCS2
C42CA074	15.00 W	K-feldspar (>1 mm)	Cadamosto, Cape Verde	Jan Sticklus	15	0.14	0.0000328	0.3	1.0098	0.21	1	1.21E-14	24	MAR	2017	2	54	1	can42	Examples	c42it7ip6_3512F	01	TCS2
C42GA021	25.00 W	K-feldspar (>1 mm)	Cadamosto, Cape Verde	Jan Sticklus	25	0.14	0.0000328	0.3	1.0098	0.21	1	1.21E-14	13	SEP	2017	20	7	1	can42	Examples	C42GA004	03	TCS2
C42CA076	15.00 W	K-feldspar (>1 mm)	Cadamosto, Cape Verde	Jan Sticklus	15	0.14	0.0000328	0.3	1.0098	0.21	1	1.21E-14	24	MAR	2017	3	51	1	can42	Examples	c42it7ip6_3512F	01	TCS2
C42CA075	15.00 W	K-feldspar (>1 mm)	Cadamosto, Cape Verde	Jan Sticklus	15	0.14	0.0000328	0.3	1.0098	0.21	1	1.21E-14	24	MAR	2017	3	22	1	can42	Examples	c42it7ip6_3512F	01	TCS2
C42CA068	15.00 W	K-feldspar (>1 mm)	Cadamosto, Cape Verde	Jan Sticklus	15	0.14	0.0000328	0.3	1.0098	0.21	1	1.21E-14	23	MAR	2017	23	41	1	can42	Examples	c42it7ip6_3512F	01	TCS2
C42FA007	20.00 W	K-feldspar (>1 mm)	Cadamosto, Cape Verde	Jan Sticklus	20	0.14	0.0000328	0.3	1.0098	0.21	1	1.21E-14	8	AUG	2017	11	29	1	can42	Examples	C42FA001	02	TCS2
C42FA003	20.00 W	K-feldspar (>1 mm)	Cadamosto, Cape Verde	Jan Sticklus	20	0.14	0.0000328	0.3	1.0098	0.21	1	1.21E-14	8	AUG	2017	9	14	1	can42	Examples	C42FA001	02	TCS2
C42CA069	15.00 W	K-feldspar (>1 mm)	Cadamosto, Cape Verde	Jan Sticklus	15	0.14	0.0000328	0.3	1.0098	0.21	1	1.21E-14	24	MAR	2017	0	10	1	can42	Examples	c42it7ip6_3512F	01	TCS2
C42FA004	20.00 W	K-feldspar (>1 mm)	Cadamosto, Cape Verde	Jan Sticklus	20	0.14	0.0000328	0.3	1.0098	0.21	1	1.21E-14	8	AUG	2017	9	43	1	can42	Examples	C42FA001	02	TCS2
C42GA018	25.00 W	K-feldspar (>1 mm)	Cadamosto, Cape Verde	Jan Sticklus	25	0.14	0.0000328	0.3	1.0098	0.21	1	1.21E-14	13	SEP	2017	18	41	1	can42	Examples	C42GA004	03	TCS2
C42FA013	20.00 W	K-feldspar (>1 mm)	Cadamosto, Cape Verde	Jan Sticklus	20	0.14	0.0000328	0.3	1.0098	0.21	1	1.21E-14	8	AUG	2017	14	41	1	can42	Examples	C42FA001	02	TCS2
C42FA010	20.00 W	K-feldspar (>1 mm)	Cadamosto, Cape Verde	Jan Sticklus	20	0.14	0.0000328	0.3	1.0098	0.21	1	1.21E-14	8	AUG	2017	13	14	1	can42	Examples	C42FA001	02	TCS2
C42GA007	20.00 W	K-feldspar (>1 mm)	Cadamosto, Cape Verde	Jan Sticklus	20	0.14	0.0000328	0.3	1.0098	0.21	1	1.21E-14	13	SEP	2017	12	26	1	can42	Examples	C42GA004	03	TCS2
C42GA014	20.00 W	K-feldspar (>1 mm)	Cadamosto, Cape Verde	Jan Sticklus	20	0.14	0.0000328	0.3	1.0098	0.21	1	1.21E-14	13	SEP	2017	16	26	1	can42	Examples	C42GA004	03	TCS2
C42GA010	20.00 W	K-feldspar (>1 mm)	Cadamosto, Cape Verde	Jan Sticklus	20	0.14	0.0000328	0.3	1.0098	0.21	1	1.21E-14	13	SEP	2017	14	11	1	can42	Examples	C42GA004	03	TCS2
C42GA019	25.00 W	K-feldspar (>1 mm)	Cadamosto, Cape Verde	Jan Sticklus	25	0.14	0.0000328	0.3	1.0098	0.21	1	1.21E-14	13	SEP	2017	19	9	1	can42	Examples	C42GA004	03	TCS2
C42FA006	20.00 W	K-feldspar (>1 mm)	Cadamosto, Cape Verde	Jan Sticklus	20	0.14	0.0000328	0.3	1.0098	0.21	1	1.21E-14	8	AUG	2017	11	0	1	can42	Examples	C42FA001	02	TCS2
C42CA072	15.00 W	K-feldspar (>1 mm)	Cadamosto, Cape Verde	Jan Sticklus	15	0.14	0.0000328	0.3	1.0098	0.21	1	1.21E-14	24	MAR	2017	1	37	1	can42	Examples	c42it7ip6_3512F	01	TCS2
C42FA009	20.00 W	K-feldspar (>1 mm)	Cadamosto, Cape Verde	Jan Sticklus	20	0.14	0.0000328	0.3	1.0098	0.21	1	1.21E-14	8	AUG	2017	12	26	1	can42	Examples	C42FA001	02	TCS2

Irradiation Constants	Laser power	40/36(a)	%1σ	40/36(c)	%1σ	38/36(a)	%1σ	38/36(c)	%1σ	39/37(ca)	%1σ	38/37(ca)	%1σ	36/37(ca)	%1σ	40/39(k)	%1σ	38/39(k)	%1σ	36/38(cl)	%1σ	K/Ca	%1σ	K/Cl	%1σ	Ca/Cl	%1σ
C42GA004	20.00 W	295.5	0.178	0.018	35	0.1869	0.107	1.493	3	0.000702	1.71	0.000196	0.41	0.0002702	0.15	0.00073	12.33	0.01215	0.25	262.8	0.65	0.51	0	0	0	0	0
C42FA012	20.00 W	295.5	0.178	0.018	35	0.1869	0.107	1.493	3	0.000702	1.71	0.000196	0.41	0.0002702	0.15	0.00073	12.33	0.01215	0.25	262.8	0.65	0.51	0	0	0	0	0
C42GA011	20.00 W	295.5	0.178	0.018	35	0.1869	0.107	1.493	3	0.000702	1.71	0.000196	0.41	0.0002702	0.15	0.00073	12.33	0.01215	0.25	262.8	0.65	0.51	0	0	0	0	0
C42FA011	20.00 W	295.5	0.178	0.018	35	0.1869	0.107	1.493	3	0.000702	1.71	0.000196	0.41	0.0002702	0.15	0.00073	12.33	0.01215	0.25	262.8	0.65	0.51	0	0	0	0	0
C42GA006	20.00 W	295.5	0.178	0.018	35	0.1869	0.107	1.493	3	0.000702	1.71	0.000196	0.41	0.0002702	0.15	0.00073	12.33	0.01215	0.25	262.8	0.65	0.51	0	0	0	0	0
C42GA003	20.00 W	295.5	0.178	0.018	35	0.1869	0.107	1.493	3	0.000702	1.71	0.000196	0.41	0.0002702	0.15	0.00073	12.33	0.01215	0.25	262.8	0.65	0.51	0	0	0	0	0
C42GA016	25.00 W	295.5	0.178	0.018	35	0.1869	0.107	1.493	3	0.000702	1.71	0.000196	0.41	0.0002702	0.15	0.00073	12.33	0.01215	0.25	262.8	0.65	0.51	0	0	0	0	0
C42FA002	20.00 W	295.5	0.178	0.018	35	0.1869	0.107	1.493	3	0.000702	1.71	0.000196	0.41	0.0002702	0.15	0.00073	12.33	0.01215	0.25	262.8	0.65	0.51	0	0	0	0	0
C42FA014	20.00 W	295.5	0.178	0.018	35	0.1869	0.107	1.493	3	0.000702	1.71	0.000196	0.41	0.0002702	0.15	0.00073	12.33	0.01215	0.25	262.8	0.65	0.51	0	0	0	0	0
C42GA002	20.00 W	295.5	0.178	0.018	35	0.1869	0.107	1.493	3	0.000702	1.71	0.000196	0.41	0.0002702	0.15	0.00073	12.33	0.01215	0.25	262.8	0.65	0.51	0	0	0	0	0
C42GA005	20.00 W	295.5	0.178	0.018	35	0.1869	0.107	1.493	3	0.000702	1.71	0.000196	0.41	0.0002702	0.15	0.00073	12.33	0.01215	0.25	262.8	0.65	0.51	0	0	0	0	0
C42GA008	20.00 W	295.5	0.178	0.018	35	0.1869	0.107	1.493	3	0.000702	1.71	0.000196	0.41	0.0002702	0.15	0.00073	12.33	0.01215	0.25	262.8	0.65	0.51	0	0	0	0	0
C42FA001	20.00 W	295.5	0.178	0.018	35	0.1869	0.107	1.493	3	0.000702	1.71	0.000196	0.41	0.0002702	0.15	0.00073	12.33	0.01215	0.25	262.8	0.65	0.51	0	0	0	0	0
C42GA001	20.00 W	295.5	0.178	0.018	35	0.1869	0.107	1.493	3	0.000702	1.71	0.000196	0.41	0.0002702	0.15	0.00073	12.33	0.01215	0.25	262.8	0.65	0.51	0	0	0	0	0
C42FA005	20.00 W	295.5	0.178	0.018	35	0.1869	0.107	1.493	3	0.000702	1.71	0.000196	0.41	0.0002702	0.15	0.00073	12.33	0.01215	0.25	262.8	0.65	0.51	0	0	0	0	0
C42CA070	15.00 W	295.5	0.178	0.018	35	0.1869	0.107	1.493	3	0.000702	1.71	0.000196	0.41	0.0002702	0.15	0.00073	12.33	0.01215	0.25	262.8	0.65	0.51	0	0	0	0	0
C42GA015	25.00 W	295.5	0.178	0.018	35	0.1869	0.107	1.493	3	0.000702	1.71	0.000196	0.41	0.0002702	0.15	0.00073	12.33	0.01215	0.25	262.8	0.65	0.51	0	0	0	0	0
C42GA017	25.00 W	295.5	0.178	0.018	35	0.1869	0.107	1.493	3	0.000702	1.71	0.000196	0.41	0.0002702	0.15	0.00073	12.33	0.01215	0.25	262.8	0.65	0.51	0	0	0	0	0
C42FA008	20.00 W	295.5	0.178	0.018	35	0.1869	0.107	1.493	3	0.000702	1.71	0.000196	0.41	0.0002702	0.15	0.00073	12.33	0.01215	0.25	262.8	0.65	0.51	0	0	0	0	0
C42GA020	25.00 W	295.5	0.178	0.018	35	0.1869	0.107	1.493	3	0.000702	1.71	0.000196	0.41	0.0002702	0.15	0.00073	12.33	0.01215	0.25	262.8	0.65	0.51	0	0	0	0	0
C42GA012	20.00 W	295.5	0.178	0.018	35	0.1869	0.107	1.493	3	0.000702	1.71	0.000196	0.41	0.0002702	0.15	0.00073	12.33	0.01215	0.25	262.8	0.65	0.51	0	0	0	0	0
C42CA071	15.00 W	295.5	0.178	0.018	35	0.1869	0.107	1.493	3	0.000702	1.71	0.000196	0.41	0.0002702	0.15	0.00073	12.33	0.01215	0.25	262.8	0.65	0.51	0	0	0	0	0
C42GA013	20.00 W	295.5	0.178	0.018	35	0.1869	0.107	1.493	3	0.000702	1.71	0.000196	0.41	0.0002702	0.15	0.00073	12.33	0.01215	0.25	262.8	0.65	0.51	0	0	0	0	0
C42GA009	20.00 W	295.5	0.178	0.018	35	0.1869	0.107	1.493	3	0.000702	1.71	0.000196	0.41	0.0002702	0.15	0.00073	12.33	0.01215	0.25	262.8	0.65	0.51	0	0	0	0	0
C42CA074	15.00 W	295.5	0.178	0.018	35	0.1869	0.107	1.493	3	0.000702	1.71	0.000196	0.41	0.0002702	0.15	0.00073	12.33	0.01215	0.25	262.8	0.65	0.51	0	0	0	0	0
C42GA021	25.00 W	295.5	0.178	0.018	35	0.1869	0.107	1.493	3	0.000702	1.71	0.000196	0.41	0.0002702	0.15	0.00073	12.33	0.01215	0.25	262.8	0.65	0.51	0	0	0	0	0
C42CA076	15.00 W	295.5	0.178	0.018	35	0.1869	0.107	1.493	3	0.000702	1.71	0.000196	0.41	0.0002702	0.15	0.00073	12.33	0.01215	0.25	262.8	0.65	0.51	0	0	0	0	0
C42CA075	15.00 W	295.5	0.178	0.018	35	0.1869	0.107	1.493	3	0.000702	1.71	0.000196	0.41	0.0002702	0.15	0.00073	12.33	0.01215	0.25	262.8	0.65	0.51	0	0	0	0	0
C42CA068	15.00 W	295.5	0.178	0.018	35	0.1869	0.107	1.493	3	0.000702	1.71	0.000196	0.41	0.0002702	0.15	0.00073	12.33	0.01215	0.25	262.8	0.65	0.51	0	0	0	0	0
C42FA007	20.00 W	295.5	0.178	0.018	35	0.1869	0.107	1.493	3	0.000702	1.71	0.000196	0.41	0.0002702	0.15	0.00073	12.33	0.01215	0.25	262.8	0.65	0.51	0	0	0	0	0
C42FA003	20.00 W	295.5	0.178	0.018	35	0.1869	0.107	1.493	3	0.000702	1.71	0.000196	0.41	0.0002702	0.15	0.00073	12.33	0.01215	0.25	262.8	0.65	0.51	0	0	0	0	0
C42CA069	15.00 W	295.5	0.178	0.018	35	0.1869	0.107	1.493	3	0.000702	1.71	0.000196	0.41	0.0002702	0.15	0.00073	12.33	0.01215	0.25	262.8	0.65	0.51	0	0	0	0	0
C42FA004	20.00 W	295.5	0.178	0.018	35	0.1869	0.107	1.493	3	0.000702	1.71	0.000196	0.41	0.0002702	0.15	0.00073	12.33	0.01215	0.25	262.8	0.65	0.51	0	0	0	0	0
C42GA018	25.00 W	295.5	0.178	0.018	35	0.1869	0.107	1.493	3	0.000702	1.71	0.000196	0.41	0.0002702	0.15	0.00073	12.33	0.01215	0.25	262.8	0.65	0.51	0	0	0	0	0
C42FA013	20.00 W	295.5	0.178	0.018	35	0.1869	0.107	1.493	3	0.000702	1.71	0.000196	0.41	0.0002702	0.15	0.00073	12.33	0.01215	0.25	262.8	0.65	0.51	0	0	0	0	0
C42FA010	20.00 W	295.5	0.178	0.018	35	0.1869	0.107	1.493	3	0.000702	1.71	0.000196	0.41	0.0002702	0.15	0.00073	12.33	0.01215	0.25	262.8	0.65	0.51	0	0	0	0	0
C42GA007	20.00 W	295.5	0.178	0.018	35	0.1869	0.107	1.493	3	0.000702	1.71	0.000196	0.41	0.0002702	0.15	0.00073	12.33	0.01215	0.25	262.8	0.65	0.51	0	0	0	0	0
C42GA014	20.00 W	295.5	0.178	0.018	35	0.1869	0.107	1.493	3	0.000702	1.71	0.000196	0.41	0.0002702	0.15	0.00073	12.33	0.01215	0.25	262.8	0.65	0.51	0	0	0	0	0
C42GA010	20.00 W	295.5	0.178	0.018	35	0.1869	0.107	1.493	3	0.000702	1.71	0.000196	0.41	0.0002702	0.15	0.00073	12.33	0.01215	0.25	262.8	0.65	0.51	0	0	0	0	0
C42GA019	25.00 W	295.5	0.178	0.018	35	0.1869	0.107	1.493	3	0.000702	1.71	0.000196	0.41	0.0002702	0.15	0.00073	12.33	0.01215	0.25	262.8	0.65	0.51	0	0	0	0	0
C42FA006	20.00 W	295.5	0.178	0.018	35	0.1869	0.107	1.493	3	0.000702	1.71	0.000196	0.41	0.0002702	0.15	0.00073	12.33	0.01215	0.25	262.8	0.65	0.51	0	0	0	0	0
C42CA072	15.00 W	295.5	0.178	0.018	35	0.1869	0.107	1.493	3	0.000702	1.71	0.000196	0.41	0.0002702	0.15	0.00073	12.33	0.01215	0.25	262.8	0.65	0.51	0	0	0	0	0
C42FA009	20.00 W	295.5	0.178	0.018	35	0.1869	0.107	1.493	3	0.000702	1.71	0.000196	0.41	0.0002702	0.15	0.00073	12.33	0.01215	0.25	262.8	0.65	0.51	0	0	0	0	0

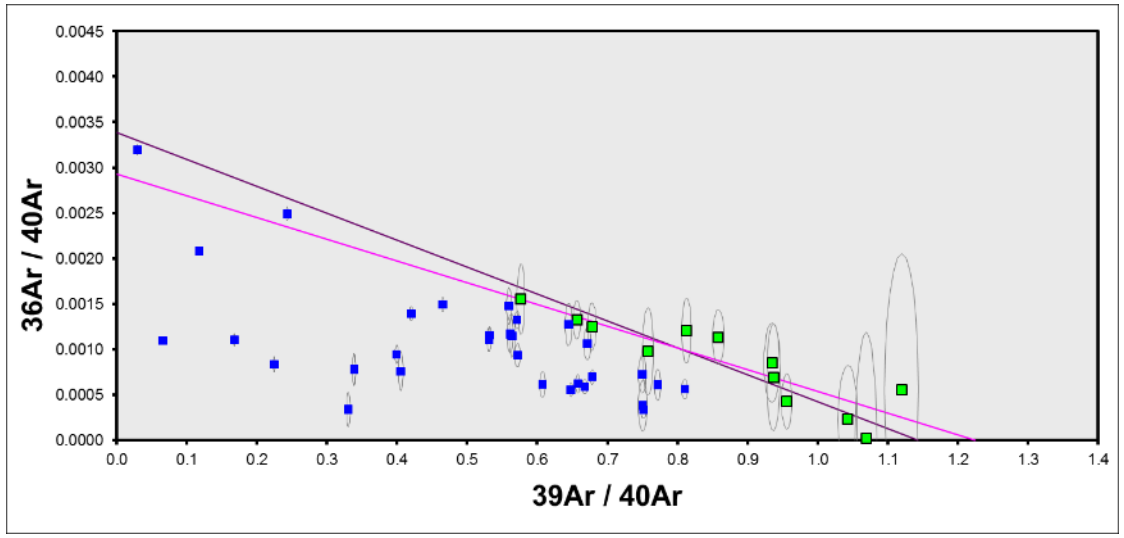
36Ar / 40Ar
39Ar / 40Ar
0.0045
0.0040
0.0035
0.0030
0.0025
0.0020
0.0015
0.0010
0.0005
0.0000
0.0
0.1
0.2
0.3
0.4
0.5
0.6
0.7
0.8
0.9
1.0
1.1
1.2
1.3
1.4

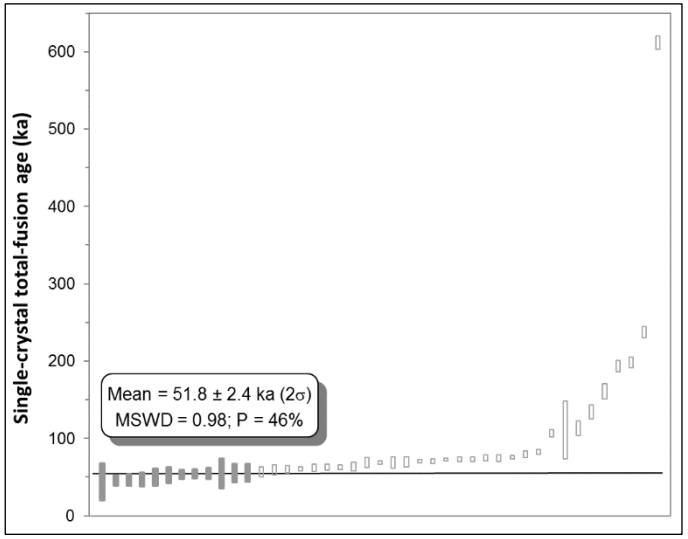
Single-crystal total-fusion age (ka)
600
500
400
300
200
100
0
Mean = 51.8 ± 2.4 ka (2σ)
MSWD = 0.98; P = 46%

Information on Analysis and Constants Used in Calculations

Sample = M80/3 035ROV-12 (3512F)
Material = K-feldspar (>1 mm)
Location = Cadamosto, Cape Verde
Analyst = Jan Sticklus
Project = EXAMPLES
Mass Discrimination Law = POW
Irradiation = can42
J = 0.00003280 ± 0.00000010
TCS2 = 27.870 ± 0.039 Ma
Heating = 45 sec
Instrument = MAP216

Age Equations = Conventional
Negative Intensities = Allowed
Decay Constant 40K = 5.543 ± 0.009 E-10 1/a
Decay Constant 39Ar = 2.940 ± 0.016 E-07 1/h
Decay Constant 37Ar = 8.230 ± 0.012 E-04 1/h
Decay Constant 36Cl = 2.257 ± 0.015 E-06 1/a
Atmospheric Ratio 40/36(a) = 295.50 ± 0.53
Atmospheric Ratio 38/36(a) = 0.1869 ± 0.0002
Production Ratio 39/37(ca) = 0.000702 ± 0.000012
Production Ratio 38/37(ca) = 0.000196 ± 0.000001
Production Ratio 36/37(ca) = 0.000270 ± 0.000000
Production Ratio 40/39(k) = 0.000730 ± 0.000090
Production Ratio 38/39(k) = 0.012150 ± 0.000030
Production Ratio 36/38(cl) = 262.80
Scaling Ratio K/Ca = 0.510

Results	40(a)/36(a) ± 2σ	40(r)/39(k) ± 2σ	Age ± 2σ (Ka)	MSWD	39Ar(k) (%,n)	K/Ca ± 2σ
Age Plateau		0.87464 ± 0.03973 ± 4.54%	51.8 ± 2.4 ± 4.58%	0.98	12.85	4 ± 4
		Minimal External Error ± 2.4		46%	12	
		Analytical Error ± 2.4		1.85	2σ Confidence Limit	
				1.0000	Error Magnification	
Total Fusion Age		1.70809 ± 0.01902 ± 1.11%	101.1 ± 1.3 ± 1.26%		43	322 ± 1585
		Minimal External Error ± 1.3				
		Analytical Error ± 1.1				
Normal Isochron	234.66 ± 82.30 ± 35.07%	0.93189 ± 0.09866 ± 10.59%	55.1 ± 5.8 ± 10.60%	3.43	12.85	
Error Chron		Minimal External Error ± 5.9		0%	12	
		Analytical Error ± 5.8		1.89	2σ Confidence Limit	
				1.8519	Error Magnification	
				1	Number of Iterations	
				0.0000039748	Convergence	
Inverse Isochron	341.48 ± 70.99 ± 20.79%	0.81640 ± 0.09227 ± 11.30%	48.3 ± 5.5 ± 11.32%	0.86	12.85	
		Minimal External Error ± 5.5		57%	12	
		Analytical Error ± 5.5		1.89	2σ Confidence Limit	
				1.0000	Error Magnification	
				3	Number of Iterations	
				0.0000626264	Convergence	
				44%	Spreading Factor	

[a] Blue dots in table indicate selected steps used to calculate the weighted mean and inverse isochron ages.
[b] Weight % K values calculated from $^{39}Ar_K$ values and weights of individual grains. The missing analyses (shown by "-" were analyses undertaken with an intermittenty functioning fan in the filament emission regulator unit, resulting in fluctuations to the mass spectrometer sensitivity). There was no effect on the age of these analyses (confirmed by analyses of TCS2-2 K-feldspar).

[c] Alteration Index values in italics indicate analyses from fresh material, normal font is from altered material (Baksi, 2007; van den Bogaard, 2013).
Values shown in red are negative values.
Abbreviations used in tables: (r) = radiogenic ^{40}Ar; (k) = Ar derived from K; (a) = atmospheric Ar; (ca) = Ar derived from Ca; (cl) = Ar derived from Ca; (c) = cosmogenic Ar; MDF = Mass Discrimination Factor.
Green squares in the inverse isochron plots indicate selected steps (blue dots in table), and blue squares are non-selected steps. Pink lines in the inverse isochron plot indicate a line fit through selected data, and the purple lines incidate a fit through an air $^{40}Ar/^{36}Ar$ ratio (295.5).
Stacked probability plot produced using Isoplot (Ludwig, 2011), where filled and unfilled 2σ error bars indicate selected/not selected data to calculate inverse-variance weighted mean age (black line), respectively.

037DR-2 total fusion

Relative Abundances	Laser power	a	36Ar [V]	%1σ	37Ar [V]	%1σ	38Ar [V]	%1σ	39Ar [V]	%1σ	40Ar [V]	%1σ	40(r)/39(k) ± 2σ	Age ± 2σ (Ka)	40Ar(r) (%)	39Ar(k) (%)	K/Ca ± 2σ	Weight (mg)	Wt. % K[a]	$^{36}Ar/^{39}Ar$ Alt. Index[b]
C42CA034	15.00 W	•	0.0002448	6.698	0.0003082	87.135	0.0002533	5.527	0.0174654	0.533	0.0998261	0.294	1.57374 ± 0.55644	92.3 ± 32.6	27.53	1.26	28.9 ± 50.4	0.194	10.65	*0.000049*
C42CA030	15.00 W	•	0.0000974	10.551	0.0002858	121.066	0.0001678	10.228	0.0138908	0.514	0.0510508	0.637	1.60485 ± 0.43998	94.1 ± 25.8	43.67	1.01	24.8 ± 60.0	0.164	10.02	*0.000023*
C42CA043	15.00 W	•	0.0002801	6.354	0.0006861	40.212	0.0002533	7.572	0.0156413	0.470	0.1085367	0.330	1.65011 ± 0.67451	96.7 ± 39.5	23.78	1.13	11.6 ± 9.4	0.178	10.40	0.000060
C42CA037	15.00 W	•	0.0002028	7.057	0.0002621	95.750	0.0002141	6.260	0.0167972	0.494	0.0885376	0.341	1.70467 ± 0.50517	99.9 ± 29.6	32.34	1.22	32.7 ± 62.6	0.182	10.92	*0.000043*
C42CA033	15.00 W	•	0.0002897	6.033	0.0001697	149.986	0.0002608	4.867	0.0165759	0.593	0.1155399	0.377	1.80357 ± 0.62611	105.7 ± 36.7	25.88	1.20	49.8 ± 149.4	0.172	11.40	0.000065
C42CA027	15.00 W		0.0000633	22.687	0.0002741	85.290	0.0001735	11.082	0.0158814	0.578	0.0483933	0.566	1.86973 ± 0.53614	109.6 ± 31.4	61.36	1.15	29.5 ± 50.4	0.195	9.64	*0.000012*
C42CA026	15.00 W		0.0001662	8.751	0.0005652	53.167	0.0002379	9.923	0.0188275	0.417	0.0862481	0.389	1.97379 ± 0.45841	115.7 ± 26.9	43.09	1.36	17.0 ± 18.1	0.231	9.64	*0.000028*
C42CA041	15.00 W		0.0002757	5.438	0.0004008	69.773	0.0002371	7.804	0.0158885	0.594	0.1128201	0.307	1.97413 ± 0.56024	115.7 ± 32.8	27.80	1.15	20.2 ± 28.2	0.183	10.27	*0.000058*
C42CA003	15.00 W		0.0002975	4.861	0.0005047	45.742	0.0005492	3.775	0.0399810	0.431	0.1669702	0.125	1.97759 ± 0.21486	115.9 ± 12.6	47.35	2.90	40.4 ± 37.0	0.472	10.02	*0.000024*
C42CA022	15.00 W		0.0002564	5.297	0.0002073	171.717	0.0004923	3.061	0.0383826	0.330	0.1526241	0.222	2.00116 ± 0.21041	117.3 ± 12.3	50.33	2.78	94.4 ± 324.3	0.441	10.30	*0.000022*
C42CA038	15.00 W		0.0001841	7.825	0.0000436	571.482	0.0002647	5.548	0.0189836	0.607	0.0928317	0.396	2.02396 ± 0.45084	118.7 ± 26.4	41.39	1.37	222.1 ± 2538.4	0.208	10.80	*0.000034*
C42CA009	15.00 W		0.0002830	5.981	0.0008110	34.108	0.0008674	3.075	0.0649030	0.260	0.2152705	0.130	2.02867 ± 0.15480	118.9 ± 9.1	61.16	4.70	40.8 ± 27.8	0.731	10.50	*0.000015*
C42CA015	15.00 W		0.0002091	7.906	0.0000319	948.328	0.0005817	3.541	0.0441039	0.413	0.1525570	0.182	2.05717 ± 0.22263	120.6 ± 13.1	59.47	3.19	705.8 ± 13387.2	0.502	10.39	*0.000016*
C42CA016	15.00 W		0.0003825	4.044	0.0002671	83.326	0.0007009	2.662	0.0529337	0.380	0.2231804	0.148	2.08055 ± 0.17404	122.0 ± 10.2	49.35	3.83	101.1 ± 168.4	0.601	10.42	*0.000024*
C42CA018	15.00 W		0.0003355	4.591	0.0006196	38.810	0.0006625	2.554	0.0492108	0.401	0.2046747	0.153	2.14479 ± 0.18635	125.8 ± 10.9	51.57	3.56	40.5 ± 31.4	0.626	9.30	*0.000021*
C42CA021	15.00 W		0.0002192	5.643	0.0000929	289.221	0.0006929	2.357	0.0547618	0.314	0.1844838	0.208	2.18563 ± 0.13498	128.1 ± 7.9	64.88	3.97	300.7 ± 1739.2	0.665	9.74	*0.000013*
C42CA014	15.00 W		0.0002691	5.871	0.0000768	458.371	0.0003438	4.867	0.0236969	0.617	0.1314599	0.190	2.19183 ± 0.39564	128.5 ± 23.2	39.51	1.72	157.3 ± 1441.9	0.269	10.42	*0.000038*
C42CA028	15.00 W		0.0000468	31.093	0.0003467	73.000	0.0002892	5.112	0.0252534	0.548	0.0697005	0.430	2.21256 ± 0.34241	129.7 ± 20.1	80.16	1.83	37.1 ± 54.2	0.290	10.30	*0.000006*
C42CA031	15.00 W		0.0001732	8.081	0.0001676	191.402	0.0004021	3.955	0.0309640	0.573	0.1198061	0.323	2.21468 ± 0.26966	129.8 ± 15.8	57.24	2.24	94.2 ± 360.7	0.286	12.81	*0.000023*
C42CA005	15.00 W		0.0003194	4.121	0.0001057	273.681	0.0005266	3.437	0.0398075	0.436	0.1833641	0.234	2.23512 ± 0.19771	131.0 ± 11.6	48.52	2.88	192.0 ± 1051.1	0.481	9.79	*0.000026*
C42CA019	15.00 W		0.0004578	4.343	0.0002353	139.490	0.0004452	3.456	0.0301134	0.416	0.2028674	0.206	2.24312 ± 0.39193	131.5 ± 23.0	33.30	2.18	65.3 ± 182.1	0.346	10.30	*0.000051*
C42CA012	15.00 W		0.0004726	3.505	0.0008417	32.770	0.0006485	2.603	0.0487357	0.333	0.2502243	0.146	2.26950 ± 0.20226	133.1 ± 11.9	44.20	3.53	29.5 ± 19.4	0.582	9.91	*0.000031*
C42CA039	15.00 W		0.0003285	5.668	0.0002707	103.328	0.0002032	7.187	0.0116813	0.741	0.1235608	0.233	2.26969 ± 0.94435	133.1 ± 55.4	21.46	0.85	22.0 ± 45.5	0.121	11.42	0.000104
C42CA035	15.00 W		0.0001595	10.540	0.0000001	242790.132	0.0001572	8.357	0.0111502	0.903	0.0725834	0.426	2.28168 ± 0.89391	133.8 ± 52.4	35.05	0.81	52657.6 ± 255694805.2	0.135	9.77	*0.000045*
C42CA020	15.00 W		0.0002897	5.830	0.0000494	457.248	0.0004735	3.442	0.0335717	0.386	0.1628042	0.163	2.29842 ± 0.29844	134.8 ± 17.5	47.40	2.43	346.4 ± 3168.0	0.396	10.03	*0.000028*
C42CA001	15.00 W		0.0004558	4.795	0.0010981	20.347	0.0010096	1.819	0.0743865	0.326	0.3088732	0.086	2.34225 ± 0.17458	137.3 ± 10.2	56.41	5.39	34.5 ± 14.1	0.930	9.46	*0.000019*
C42CA045	15.00 W		0.0002238	6.294	0.0002342	97.634	0.0001987	8.748	0.0135331	0.662	0.0979320	0.307	2.34854 ± 0.61763	137.7 ± 36.2	32.45	0.98	29.5 ± 57.5	0.176	9.10	*0.000049*
C42CA008	15.00 W		0.0004190	4.758	0.0008676	42.833	0.0005880	2.523	0.0415750	0.477	0.2229663	0.155	2.38597 ± 0.28501	139.9 ± 16.7	44.49	3.01	24.4 ± 20.9	0.488	10.08	*0.000033*
C42CA042	15.00 W		0.0001456	11.659	0.0000256	933.822	0.0001941	8.777	0.0138771	0.635	0.0763033	0.423	2.39692 ± 0.72530	140.5 ± 42.5	43.59	1.01	276.0 ± 5154.6	0.087	18.87	0.000064
C42CA011	15.00 W		0.0040898	1.101	0.0004348	58.710	0.0014391	1.644	0.0522977	0.349	1.3354483	0.058	2.42662 ± 0.51647	142.3 ± 30.3	9.50	3.79	61.3 ± 72.0	0.588	10.52	0.000267
C42CA036	15.00 W		0.0002950	6.002	0.0005121	58.537	0.0003298	4.043	0.0224722	0.520	0.1428625	0.263	2.47971 ± 0.46774	145.4 ± 27.4	39.01	1.63	22.4 ± 26.2	0.253	10.51	*0.000045*
C42CA002	15.00 W		0.0004984	3.443	0.0009538	24.673	0.0015049	1.955	0.1179117	0.251	0.4499508	0.125	2.56689 ± 0.08760	150.5 ± 5.1	67.27	8.54	63.0 ± 31.1	1.378	10.12	*0.000014*
C42CA013	15.00 W		0.0003183	4.355	0.0004122	58.825	0.0007076	2.592	0.0555017	0.311	0.2373992	0.176	2.58242 ± 0.14936	151.4 ± 8.8	60.37	4.02	68.7 ± 80.8	0.682	9.63	*0.000018*
C42CA024	15.00 W		0.0004706	4.118	0.0005780	42.414	0.0003398	4.837	0.0232772	0.534	0.1998156	0.148	2.61125 ± 0.49393	153.1 ± 29.0	30.42	1.69	20.5 ± 17.4	0.280	9.84	0.000065
C42CA032	15.00 W		0.0000762	22.373	0.0000582	586.743	0.0001913	7.126	0.0140208	0.470	0.0604148	0.535	2.70314 ± 0.72034	158.5 ± 42.2	62.73	1.02	122.9 ± 1442.4	0.179	9.27	*0.000016*
C42CA023	15.00 W		0.0002562	6.829	0.0000866	324.496	0.0004072	3.902	0.0292334	0.385	0.1555886	0.189	2.73209 ± 0.35502	160.2 ± 20.8	51.33	2.12	172.2 ± 1117.5	0.359	9.63	*0.000027*
C42CA004	15.00 W		0.0004786	3.357	0.0002833	98.172	0.0007261	2.820	0.0532770	0.362	0.2961972	0.075	2.90453 ± 0.17992	170.3 ± 10.5	52.24	3.86	95.9 ± 188.3	0.605	10.42	*0.000030*
C42CA006	15.00 W		0.0004252	3.931	0.0001278	305.987	0.0008782	2.373	0.0683398	0.326	0.3615703	0.091	3.45185 ± 0.14673	202.4 ± 8.6	65.24	4.95	272.8 ± 1669.2	0.810	9.98	*0.000020*
C42CA017	15.00 W		0.0006449	3.002	0.0001367	203.078	0.0005234	4.285	0.0293871	0.316	0.3399504	0.061	5.08303 ± 0.39156	298.0 ± 23.0	43.94	2.13	109.7 ± 445.4	0.359	9.68	*0.000069*
C42CA010	15.00 W		0.0002298	5.652	0.0007061	45.416	0.0003454	4.354	0.0223781	0.488	0.2010611	0.116	5.95245 ± 0.34866	349.0 ± 20.4	66.25	1.62	16.2 ± 14.7	0.294	9.01	*0.000030*
		Σ	0.0153310	0.723	0.0119250	14.995	0.0194818	0.585	1.3806707	0.068	7.9062493	0.028								

Procedure Blanks	Laser power	36Ar [V]	1σ	37Ar [V]	1σ	38Ar [V]	1σ	39Ar [V]	1σ	40Ar [V]	1σ
C42CA034	15.00 W	0.0002009	0.0000101	0.0017610	0.0000255	0.0000891	0.0000089	0.0001285	0.0000089	0.0031981	0.0002594
C42CA030	15.00 W	0.0002066	0.0000101	0.0017431	0.0000255	0.0000962	0.0000089	0.0001186	0.0000089	0.0031837	0.0002594
C42CA043	15.00 W	0.0001911	0.0000101	0.0017777	0.0000255	0.0000899	0.0000089	0.0001025	0.0000089	0.0031890	0.0002594
C42CA037	15.00 W	0.0001963	0.0000101	0.0017653	0.0000255	0.0000875	0.0000089	0.0001234	0.0000089	0.0032243	0.0002594
C42CA033	15.00 W	0.0002033	0.0000101	0.0017568	0.0000255	0.0000909	0.0000089	0.0001281	0.0000089	0.0031861	0.0002594
C42CA027	15.00 W	0.0002072	0.0000101	0.0017117	0.0000255	0.0001065	0.0000089	0.0000869	0.0000089	0.0032413	0.0002594
C42CA026	15.00 W	0.0002064	0.0000101	0.0016994	0.0000255	0.0001102	0.0000089	0.0000734	0.0000089	0.0032737	0.0002594
C42CA041	15.00 W	0.0001913	0.0000101	0.0017706	0.0000255	0.0000883	0.0000089	0.0001091	0.0000089	0.0032311	0.0002594
C42CA003	15.00 W	0.0001628	0.0000095	0.0014838	0.0000268	0.0000722	0.0000091	0.0001325	0.0000110	0.0036056	0.0001192
C42CA022	15.00 W	0.0001824	0.0000095	0.0017331	0.0000268	0.0000814	0.0000091	0.0000970	0.0000110	0.0030101	0.0001192
C42CA038	15.00 W	0.0001950	0.0000101	0.0017662	0.0000255	0.0000874	0.0000089	0.0001207	0.0000089	0.0032311	0.0002594
C42CA009	15.00 W	0.0001772	0.0000095	0.0015955	0.0000268	0.0000788	0.0000091	0.0001166	0.0000110	0.0032524	0.0001192
C42CA015	15.00 W	0.0001839	0.0000095	0.0016767	0.0000268	0.0000819	0.0000091	0.0001050	0.0000110	0.0030527	0.0001192
C42CA016	15.00 W	0.0001843	0.0000095	0.0016863	0.0000268	0.0000821	0.0000091	0.0001037	0.0000110	0.0030357	0.0001192
C42CA018	15.00 W	0.0001845	0.0000095	0.0017087	0.0000268	0.0000822	0.0000091	0.0001005	0.0000110	0.0030073	0.0001192
C42CA021	15.00 W	0.0001832	0.0000095	0.0017280	0.0000268	0.0000817	0.0000091	0.0000977	0.0000110	0.0030043	0.0001192
C42CA014	15.00 W	0.0001834	0.0000095	0.0016663	0.0000268	0.0000817	0.0000091	0.0001065	0.0000110	0.0030732	0.0001192
C42CA028	15.00 W	0.0002075	0.0000101	0.0017220	0.0000255	0.0001032	0.0000089	0.0000979	0.0000089	0.0032174	0.0002594
C42CA031	15.00 W	0.0002057	0.0000101	0.0017487	0.0000255	0.0000941	0.0000089	0.0001232	0.0000089	0.0031807	0.0002594
C42CA005	15.00 W	0.0001679	0.0000095	0.0015206	0.0000268	0.0000746	0.0000091	0.0001273	0.0000110	0.0034834	0.0001192
C42CA019	15.00 W	0.0001842	0.0000095	0.0017156	0.0000268	0.0000821	0.0000091	0.0000995	0.0000110	0.0030030	0.0001192
C42CA012	15.00 W	0.0001818	0.0000095	0.0016436	0.0000268	0.0000809	0.0000091	0.0001098	0.0000110	0.0031245	0.0001192
C42CA039	15.00 W	0.0001929	0.0000101	0.0017678	0.0000255	0.0000876	0.0000089	0.0001155	0.0000089	0.0032372	0.0002594
C42CA035	15.00 W	0.0001994	0.0000101	0.0017628	0.0000255	0.0000884	0.0000089	0.0001275	0.0000089	0.0032069	0.0002594
C42CA020	15.00 W	0.0001838	0.0000095	0.0017221	0.0000268	0.0000820	0.0000091	0.0000986	0.0000110	0.0030019	0.0001192
C42CA001	15.00 W	0.0001550	0.0000095	0.0014309	0.0000268	0.0000687	0.0000091	0.0001400	0.0000110	0.0037892	0.0001192
C42CA045	15.00 W	0.0001929	0.0000101	0.0017870	0.0000255	0.0000914	0.0000089	0.0001005	0.0000089	0.0031233	0.0002594
C42CA008	15.00 W	0.0001755	0.0000095	0.0015807	0.0000268	0.0000780	0.0000091	0.0001187	0.0000110	0.0032957	0.0001192
C42CA042	15.00 W	0.0001909	0.0000101	0.0017727	0.0000255	0.0000888	0.0000089	0.0001062	0.0000089	0.0032205	0.0002594
C42CA011	15.00 W	0.0001800	0.0000095	0.0016227	0.0000268	0.0000800	0.0000091	0.0001127	0.0000110	0.0031773	0.0001192
C42CA036	15.00 W	0.0001978	0.0000101	0.0017642	0.0000255	0.0000879	0.0000089	0.0001258	0.0000089	0.0032159	0.0002594
C42CA002	15.00 W	0.0001600	0.0000095	0.0014645	0.0000268	0.0000710	0.0000091	0.0001353	0.0000110	0.0036719	0.0001192
C42CA013	15.00 W	0.0001827	0.0000095	0.0016553	0.0000268	0.0000813	0.0000091	0.0001081	0.0000110	0.0030971	0.0001192
C42CA024	15.00 W	0.0002034	0.0000101	0.0016690	0.0000255	0.0001188	0.0000089	0.0000391	0.0000089	0.0033656	0.0002594
C42CA032	15.00 W	0.0002046	0.0000101	0.0017532	0.0000255	0.0000924	0.0000089	0.0001263	0.0000089	0.0031818	0.0002594
C42CA023	15.00 W	0.0001815	0.0000095	0.0017376	0.0000268	0.0000810	0.0000091	0.0000964	0.0000110	0.0030194	0.0001192
C42CA004	15.00 W	0.0001655	0.0000095	0.0015025	0.0000268	0.0000734	0.0000091	0.0001298	0.0000110	0.0035428	0.0001192
C42CA006	15.00 W	0.0001702	0.0000095	0.0015379	0.0000268	0.0000756	0.0000091	0.0001248	0.0000110	0.0034275	0.0001192
C42CA017	15.00 W	0.0001845	0.0000095	0.0016953	0.0000268	0.0000822	0.0000091	0.0001024	0.0000110	0.0030221	0.0001192
C42CA010	15.00 W	0.0001786	0.0000095	0.0016092	0.0000268	0.0000794	0.0000091	0.0001146	0.0000110	0.0032139	0.0001192

Sample Parameters	Laser power	Material	Location	Analyst	Power	%1σ	J	%1σ	MDF	%1σ	Volume Ratio	Sensitivity (mol/volt)	Day	Month	Year	Hour	Min	Resist	Irradiation	Project	Experiment	Nmb	Standard Name
C42CA034	15.00 W	K-feldspar (0.25-0.5 mm)	Cadamosto, Cape Verde	Jan Sticklus	15	0.14	0.0000325	0.15	1.0098	0.21	1	1.203E-14	23	MAR	2017	5	6	1	can42	Examples	C42CA024	02	TCS2
C42CA030	15.00 W	K-feldspar (0.25-0.5 mm)	Cadamosto, Cape Verde	Jan Sticklus	15	0.14	0.0000325	0.15	1.0098	0.21	1	1.203E-14	23	MAR	2017	2	51	1	can42	Examples	C42CA024	02	TCS2
C42CA043	15.00 W	K-feldspar (0.25-0.5 mm)	Cadamosto, Cape Verde	Jan Sticklus	15	0.14	0.0000325	0.15	1.0098	0.21	1	1.203E-14	23	MAR	2017	10	4	1	can42	Examples	C42CA024	02	TCS2
C42CA037	15.00 W	K-feldspar (0.25-0.5 mm)	Cadamosto, Cape Verde	Jan Sticklus	15	0.14	0.0000325	0.15	1.0098	0.21	1	1.203E-14	23	MAR	2017	6	33	1	can42	Examples	C42CA024	02	TCS2
C42CA033	15.00 W	K-feldspar (0.25-0.5 mm)	Cadamosto, Cape Verde	Jan Sticklus	15	0.14	0.0000325	0.15	1.0098	0.21	1	1.203E-14	23	MAR	2017	4	18	1	can42	Examples	C42CA024	02	TCS2
C42CA027	15.00 W	K-feldspar (0.25-0.5 mm)	Cadamosto, Cape Verde	Jan Sticklus	15	0.14	0.0000325	0.15	1.0098	0.21	1	1.203E-14	23	MAR	2017	1	6	1	can42	Examples	C42CA024	02	TCS2
C42CA026	15.00 W	K-feldspar (0.25-0.5 mm)	Cadamosto, Cape Verde	Jan Sticklus	15	0.14	0.0000325	0.15	1.0098	0.21	1	1.203E-14	23	MAR	2017	0	37	1	can42	Examples	C42CA024	02	TCS2
C42CA041	15.00 W	K-feldspar (0.25-0.5 mm)	Cadamosto, Cape Verde	Jan Sticklus	15	0.14	0.0000325	0.15	1.0098	0.21	1	1.203E-14	23	MAR	2017	8	47	1	can42	Examples	C42CA024	02	TCS2
C42CA003	15.00 W	K-feldspar (0.5-1 mm)	Cadamosto, Cape Verde	Jan Sticklus	15	0.14	0.0000325	0.15	1.0098	0.21	1	1.203E-14	22	MAR	2017	12	16	1	can42	Examples	c42it13ip2_DR2CF	01	TCS2
C42CA022	15.00 W	K-feldspar (0.5-1 mm)	Cadamosto, Cape Verde	Jan Sticklus	15	0.14	0.0000325	0.15	1.0098	0.21	1	1.203E-14	22	MAR	2017	22	22	1	can42	Examples	c42it13ip2_DR2CF	01	TCS2
C42CA038	15.00 W	K-feldspar (0.25-0.5 mm)	Cadamosto, Cape Verde	Jan Sticklus	15	0.14	0.0000325	0.15	1.0098	0.21	1	1.203E-14	23	MAR	2017	7	1	1	can42	Examples	C42CA024	02	TCS2
C42CA009	15.00 W	K-feldspar (0.5-1 mm)	Cadamosto, Cape Verde	Jan Sticklus	15	0.14	0.0000325	0.15	1.0098	0.21	1	1.203E-14	22	MAR	2017	15	29	1	can42	Examples	c42it13ip2_DR2CF	01	TCS2
C42CA015	15.00 W	K-feldspar (0.5-1 mm)	Cadamosto, Cape Verde	Jan Sticklus	15	0.14	0.0000325	0.15	1.0098	0.21	1	1.203E-14	22	MAR	2017	18	41	1	can42	Examples	c42it13ip2_DR2CF	01	TCS2
C42CA016	15.00 W	K-feldspar (0.5-1 mm)	Cadamosto, Cape Verde	Jan Sticklus	15	0.14	0.0000325	0.15	1.0098	0.21	1	1.203E-14	22	MAR	2017	19	10	1	can42	Examples	c42it13ip2_DR2CF	01	TCS2
C42CA018	15.00 W	K-feldspar (0.5-1 mm)	Cadamosto, Cape Verde	Jan Sticklus	15	0.14	0.0000325	0.15	1.0098	0.21	1	1.203E-14	22	MAR	2017	20	27	1	can42	Examples	c42it13ip2_DR2CF	01	TCS2
C42CA021	15.00 W	K-feldspar (0.5-1 mm)	Cadamosto, Cape Verde	Jan Sticklus	15	0.14	0.0000325	0.15	1.0098	0.21	1	1.203E-14	22	MAR	2017	21	53	1	can42	Examples	c42it13ip2_DR2CF	01	TCS2
C42CA014	15.00 W	K-feldspar (0.5-1 mm)	Cadamosto, Cape Verde	Jan Sticklus	15	0.14	0.0000325	0.15	1.0098	0.21	1	1.203E-14	22	MAR	2017	18	12	1	can42	Examples	c42it13ip2_DR2CF	01	TCS2
C42CA028	15.00 W	K-feldspar (0.25-0.5 mm)	Cadamosto, Cape Verde	Jan Sticklus	15	0.14	0.0000325	0.15	1.0098	0.21	1	1.203E-14	23	MAR	2017	1	34	1	can42	Examples	C42CA024	02	TCS2
C42CA031	15.00 W	K-feldspar (0.25-0.5 mm)	Cadamosto, Cape Verde	Jan Sticklus	15	0.14	0.0000325	0.15	1.0098	0.21	1	1.203E-14	23	MAR	2017	3	20	1	can42	Examples	C42CA024	02	TCS2
C42CA005	15.00 W	K-feldspar (0.5-1 mm)	Cadamosto, Cape Verde	Jan Sticklus	15	0.14	0.0000325	0.15	1.0098	0.21	1	1.203E-14	22	MAR	2017	13	14	1	can42	Examples	c42it13ip2_DR2CF	01	TCS2
C42CA019	15.00 W	K-feldspar (0.5-1 mm)	Cadamosto, Cape Verde	Jan Sticklus	15	0.14	0.0000325	0.15	1.0098	0.21	1	1.203E-14	22	MAR	2017	20	55	1	can42	Examples	c42it13ip2_DR2CF	01	TCS2
C42CA012	15.00 W	K-feldspar (0.5-1 mm)	Cadamosto, Cape Verde	Jan Sticklus	15	0.14	0.0000325	0.15	1.0098	0.21	1	1.203E-14	22	MAR	2017	17	14	1	can42	Examples	c42it13ip2_DR2CF	01	TCS2
C42CA039	15.00 W	K-feldspar (0.25-0.5 mm)	Cadamosto, Cape Verde	Jan Sticklus	15	0.14	0.0000325	0.15	1.0098	0.21	1	1.203E-14	23	MAR	2017	7	49	1	can42	Examples	C42CA024	02	TCS2
C42CA035	15.00 W	K-feldspar (0.25-0.5 mm)	Cadamosto, Cape Verde	Jan Sticklus	15	0.14	0.0000325	0.15	1.0098	0.21	1	1.203E-14	23	MAR	2017	5	35	1	can42	Examples	C42CA024	02	TCS2
C42CA020	15.00 W	K-feldspar (0.5-1 mm)	Cadamosto, Cape Verde	Jan Sticklus	15	0.14	0.0000325	0.15	1.0098	0.21	1	1.203E-14	22	MAR	2017	21	24	1	can42	Examples	c42it13ip2_DR2CF	01	TCS2
C42CA001	15.00 W	K-feldspar (0.5-1 mm)	Cadamosto, Cape Verde	Jan Sticklus	15	0.14	0.0000325	0.15	1.0098	0.21	1	1.203E-14	22	MAR	2017	10	59	1	can42	Examples	c42it13ip2_DR2CF	01	TCS2
C42CA045	15.00 W	K-feldspar (0.25-0.5 mm)	Cadamosto, Cape Verde	Jan Sticklus	15	0.14	0.0000325	0.15	1.0098	0.21	1	1.203E-14	23	MAR	2017	11	2	1	can42	Examples	C42CA024	02	TCS2
C42CA008	15.00 W	K-feldspar (0.5-1 mm)	Cadamosto, Cape Verde	Jan Sticklus	15	0.14	0.0000325	0.15	1.0098	0.21	1	1.203E-14	22	MAR	2017	15	0	1	can42	Examples	c42it13ip2_DR2CF	01	TCS2
C42CA042	15.00 W	K-feldspar (0.25-0.5 mm)	Cadamosto, Cape Verde	Jan Sticklus	15	0.14	0.0000325	0.15	1.0098	0.21	1	1.203E-14	23	MAR	2017	9	16	1	can42	Examples	C42CA024	02	TCS2
C42CA011	15.00 W	K-feldspar (0.5-1 mm)	Cadamosto, Cape Verde	Jan Sticklus	15	0.14	0.0000325	0.15	1.0098	0.21	1	1.203E-14	22	MAR	2017	16	26	1	can42	Examples	c42it13ip2_DR2CF	01	TCS2
C42CA036	15.00 W	K-feldspar (0.25-0.5 mm)	Cadamosto, Cape Verde	Jan Sticklus	15	0.14	0.0000325	0.15	1.0098	0.21	1	1.203E-14	23	MAR	2017	6	4	1	can42	Examples	C42CA024	02	TCS2
C42CA002	15.00 W	K-feldspar (0.5-1 mm)	Cadamosto, Cape Verde	Jan Sticklus	15	0.14	0.0000325	0.15	1.0098	0.21	1	1.203E-14	22	MAR	2017	11	47	1	can42	Examples	c42it13ip2_DR2CF	01	TCS2
C42CA013	15.00 W	K-feldspar (0.5-1 mm)	Cadamosto, Cape Verde	Jan Sticklus	15	0.14	0.0000325	0.15	1.0098	0.21	1	1.203E-14	22	MAR	2017	17	43	1	can42	Examples	c42it13ip2_DR2CF	01	TCS2
C42CA024	15.00 W	K-feldspar (0.25-0.5 mm)	Cadamosto, Cape Verde	Jan Sticklus	15	0.14	0.0000325	0.15	1.0098	0.21	1	1.203E-14	22	MAR	2017	23	39	1	can42	Examples	C42CA024	02	TCS2
C42CA032	15.00 W	K-feldspar (0.25-0.5 mm)	Cadamosto, Cape Verde	Jan Sticklus	15	0.14	0.0000325	0.15	1.0098	0.21	1	1.203E-14	23	MAR	2017	3	49	1	can42	Examples	C42CA024	02	TCS2
C42CA023	15.00 W	K-feldspar (0.5-1 mm)	Cadamosto, Cape Verde	Jan Sticklus	15	0.14	0.0000325	0.15	1.0098	0.21	1	1.203E-14	22	MAR	2017	22	51	1	can42	Examples	c42it13ip2_DR2CF	01	TCS2
C42CA004	15.00 W	K-feldspar (0.5-1 mm)	Cadamosto, Cape Verde	Jan Sticklus	15	0.14	0.0000325	0.15	1.0098	0.21	1	1.203E-14	22	MAR	2017	12	45	1	can42	Examples	c42it13ip2_DR2CF	01	TCS2
C42CA006	15.00 W	K-feldspar (0.5-1 mm)	Cadamosto, Cape Verde	Jan Sticklus	15	0.14	0.0000325	0.15	1.0098	0.21	1	1.203E-14	22	MAR	2017	13	43	1	can42	Examples	c42it13ip2_DR2CF	01	TCS2
C42CA017	15.00 W	K-feldspar (0.5-1 mm)	Cadamosto, Cape Verde	Jan Sticklus	15	0.14	0.0000325	0.15	1.0098	0.21	1	1.203E-14	22	MAR	2017	19	39	1	can42	Examples	c42it13ip2_DR2CF	01	TCS2
C42CA010	15.00 W	K-feldspar (0.5-1 mm)	Cadamosto, Cape Verde	Jan Sticklus	15	0.14	0.0000325	0.15	1.0098	0.21	1	1.203E-14	22	MAR	2017	15	57	1	can42	Examples	c42it13ip2_DR2CF	01	TCS2

Irradiation Constants	Laser power	40/36(a)	%1σ	40/36(c)	%1σ	38/36(a)	%1σ	38/36(c)	%1σ	39/37(ca)	%1σ	38/37(ca)	%1σ	36/37(ca)	%1σ	40/39(k)	%1σ	38/39(k)	%1σ	36/38(cl)	%1σ	K/Ca	%1σ	K/Cl	%1σ	Ca/Cl	%1σ
C42CA034	15.00 W	295.5	0.178	0.018	35	0.1869	0.107	1.493	3	0.000702	1.71	0.000196	0.41	0.0002702	0.15	0.00073	12.33	0.01215	0.25	262.8	0.65	0.51	0	0	0	0	0
C42CA030	15.00 W	295.5	0.178	0.018	35	0.1869	0.107	1.493	3	0.000702	1.71	0.000196	0.41	0.0002702	0.15	0.00073	12.33	0.01215	0.25	262.8	0.65	0.51	0	0	0	0	0
C42CA043	15.00 W	295.5	0.178	0.018	35	0.1869	0.107	1.493	3	0.000702	1.71	0.000196	0.41	0.0002702	0.15	0.00073	12.33	0.01215	0.25	262.8	0.65	0.51	0	0	0	0	0
C42CA037	15.00 W	295.5	0.178	0.018	35	0.1869	0.107	1.493	3	0.000702	1.71	0.000196	0.41	0.0002702	0.15	0.00073	12.33	0.01215	0.25	262.8	0.65	0.51	0	0	0	0	0
C42CA033	15.00 W	295.5	0.178	0.018	35	0.1869	0.107	1.493	3	0.000702	1.71	0.000196	0.41	0.0002702	0.15	0.00073	12.33	0.01215	0.25	262.8	0.65	0.51	0	0	0	0	0
C42CA027	15.00 W	295.5	0.178	0.018	35	0.1869	0.107	1.493	3	0.000702	1.71	0.000196	0.41	0.0002702	0.15	0.00073	12.33	0.01215	0.25	262.8	0.65	0.51	0	0	0	0	0
C42CA026	15.00 W	295.5	0.178	0.018	35	0.1869	0.107	1.493	3	0.000702	1.71	0.000196	0.41	0.0002702	0.15	0.00073	12.33	0.01215	0.25	262.8	0.65	0.51	0	0	0	0	0
C42CA041	15.00 W	295.5	0.178	0.018	35	0.1869	0.107	1.493	3	0.000702	1.71	0.000196	0.41	0.0002702	0.15	0.00073	12.33	0.01215	0.25	262.8	0.65	0.51	0	0	0	0	0
C42CA003	15.00 W	295.5	0.178	0.018	35	0.1869	0.107	1.493	3	0.000702	1.71	0.000196	0.41	0.0002702	0.15	0.00073	12.33	0.01215	0.25	262.8	0.65	0.51	0	0	0	0	0
C42CA022	15.00 W	295.5	0.178	0.018	35	0.1869	0.107	1.493	3	0.000702	1.71	0.000196	0.41	0.0002702	0.15	0.00073	12.33	0.01215	0.25	262.8	0.65	0.51	0	0	0	0	0
C42CA038	15.00 W	295.5	0.178	0.018	35	0.1869	0.107	1.493	3	0.000702	1.71	0.000196	0.41	0.0002702	0.15	0.00073	12.33	0.01215	0.25	262.8	0.65	0.51	0	0	0	0	0
C42CA009	15.00 W	295.5	0.178	0.018	35	0.1869	0.107	1.493	3	0.000702	1.71	0.000196	0.41	0.0002702	0.15	0.00073	12.33	0.01215	0.25	262.8	0.65	0.51	0	0	0	0	0
C42CA015	15.00 W	295.5	0.178	0.018	35	0.1869	0.107	1.493	3	0.000702	1.71	0.000196	0.41	0.0002702	0.15	0.00073	12.33	0.01215	0.25	262.8	0.65	0.51	0	0	0	0	0
C42CA016	15.00 W	295.5	0.178	0.018	35	0.1869	0.107	1.493	3	0.000702	1.71	0.000196	0.41	0.0002702	0.15	0.00073	12.33	0.01215	0.25	262.8	0.65	0.51	0	0	0	0	0
C42CA018	15.00 W	295.5	0.178	0.018	35	0.1869	0.107	1.493	3	0.000702	1.71	0.000196	0.41	0.0002702	0.15	0.00073	12.33	0.01215	0.25	262.8	0.65	0.51	0	0	0	0	0
C42CA021	15.00 W	295.5	0.178	0.018	35	0.1869	0.107	1.493	3	0.000702	1.71	0.000196	0.41	0.0002702	0.15	0.00073	12.33	0.01215	0.25	262.8	0.65	0.51	0	0	0	0	0
C42CA014	15.00 W	295.5	0.178	0.018	35	0.1869	0.107	1.493	3	0.000702	1.71	0.000196	0.41	0.0002702	0.15	0.00073	12.33	0.01215	0.25	262.8	0.65	0.51	0	0	0	0	0
C42CA028	15.00 W	295.5	0.178	0.018	35	0.1869	0.107	1.493	3	0.000702	1.71	0.000196	0.41	0.0002702	0.15	0.00073	12.33	0.01215	0.25	262.8	0.65	0.51	0	0	0	0	0
C42CA031	15.00 W	295.5	0.178	0.018	35	0.1869	0.107	1.493	3	0.000702	1.71	0.000196	0.41	0.0002702	0.15	0.00073	12.33	0.01215	0.25	262.8	0.65	0.51	0	0	0	0	0
C42CA005	15.00 W	295.5	0.178	0.018	35	0.1869	0.107	1.493	3	0.000702	1.71	0.000196	0.41	0.0002702	0.15	0.00073	12.33	0.01215	0.25	262.8	0.65	0.51	0	0	0	0	0
C42CA019	15.00 W	295.5	0.178	0.018	35	0.1869	0.107	1.493	3	0.000702	1.71	0.000196	0.41	0.0002702	0.15	0.00073	12.33	0.01215	0.25	262.8	0.65	0.51	0	0	0	0	0
C42CA012	15.00 W	295.5	0.178	0.018	35	0.1869	0.107	1.493	3	0.000702	1.71	0.000196	0.41	0.0002702	0.15	0.00073	12.33	0.01215	0.25	262.8	0.65	0.51	0	0	0	0	0
C42CA039	15.00 W	295.5	0.178	0.018	35	0.1869	0.107	1.493	3	0.000702	1.71	0.000196	0.41	0.0002702	0.15	0.00073	12.33	0.01215	0.25	262.8	0.65	0.51	0	0	0	0	0
C42CA035	15.00 W	295.5	0.178	0.018	35	0.1869	0.107	1.493	3	0.000702	1.71	0.000196	0.41	0.0002702	0.15	0.00073	12.33	0.01215	0.25	262.8	0.65	0.51	0	0	0	0	0
C42CA020	15.00 W	295.5	0.178	0.018	35	0.1869	0.107	1.493	3	0.000702	1.71	0.000196	0.41	0.0002702	0.15	0.00073	12.33	0.01215	0.25	262.8	0.65	0.51	0	0	0	0	0
C42CA001	15.00 W	295.5	0.178	0.018	35	0.1869	0.107	1.493	3	0.000702	1.71	0.000196	0.41	0.0002702	0.15	0.00073	12.33	0.01215	0.25	262.8	0.65	0.51	0	0	0	0	0
C42CA045	15.00 W	295.5	0.178	0.018	35	0.1869	0.107	1.493	3	0.000702	1.71	0.000196	0.41	0.0002702	0.15	0.00073	12.33	0.01215	0.25	262.8	0.65	0.51	0	0	0	0	0
C42CA008	15.00 W	295.5	0.178	0.018	35	0.1869	0.107	1.493	3	0.000702	1.71	0.000196	0.41	0.0002702	0.15	0.00073	12.33	0.01215	0.25	262.8	0.65	0.51	0	0	0	0	0
C42CA042	15.00 W	295.5	0.178	0.018	35	0.1869	0.107	1.493	3	0.000702	1.71	0.000196	0.41	0.0002702	0.15	0.00073	12.33	0.01215	0.25	262.8	0.65	0.51	0	0	0	0	0
C42CA011	15.00 W	295.5	0.178	0.018	35	0.1869	0.107	1.493	3	0.000702	1.71	0.000196	0.41	0.0002702	0.15	0.00073	12.33	0.01215	0.25	262.8	0.65	0.51	0	0	0	0	0
C42CA036	15.00 W	295.5	0.178	0.018	35	0.1869	0.107	1.493	3	0.000702	1.71	0.000196	0.41	0.0002702	0.15	0.00073	12.33	0.01215	0.25	262.8	0.65	0.51	0	0	0	0	0
C42CA002	15.00 W	295.5	0.178	0.018	35	0.1869	0.107	1.493	3	0.000702	1.71	0.000196	0.41	0.0002702	0.15	0.00073	12.33	0.01215	0.25	262.8	0.65	0.51	0	0	0	0	0
C42CA013	15.00 W	295.5	0.178	0.018	35	0.1869	0.107	1.493	3	0.000702	1.71	0.000196	0.41	0.0002702	0.15	0.00073	12.33	0.01215	0.25	262.8	0.65	0.51	0	0	0	0	0
C42CA024	15.00 W	295.5	0.178	0.018	35	0.1869	0.107	1.493	3	0.000702	1.71	0.000196	0.41	0.0002702	0.15	0.00073	12.33	0.01215	0.25	262.8	0.65	0.51	0	0	0	0	0
C42CA032	15.00 W	295.5	0.178	0.018	35	0.1869	0.107	1.493	3	0.000702	1.71	0.000196	0.41	0.0002702	0.15	0.00073	12.33	0.01215	0.25	262.8	0.65	0.51	0	0	0	0	0
C42CA023	15.00 W	295.5	0.178	0.018	35	0.1869	0.107	1.493	3	0.000702	1.71	0.000196	0.41	0.0002702	0.15	0.00073	12.33	0.01215	0.25	262.8	0.65	0.51	0	0	0	0	0
C42CA004	15.00 W	295.5	0.178	0.018	35	0.1869	0.107	1.493	3	0.000702	1.71	0.000196	0.41	0.0002702	0.15	0.00073	12.33	0.01215	0.25	262.8	0.65	0.51	0	0	0	0	0
C42CA006	15.00 W	295.5	0.178	0.018	35	0.1869	0.107	1.493	3	0.000702	1.71	0.000196	0.41	0.0002702	0.15	0.00073	12.33	0.01215	0.25	262.8	0.65	0.51	0	0	0	0	0
C42CA017	15.00 W	295.5	0.178	0.018	35	0.1869	0.107	1.493	3	0.000702	1.71	0.000196	0.41	0.0002702	0.15	0.00073	12.33	0.01215	0.25	262.8	0.65	0.51	0	0	0	0	0
C42CA010	15.00 W	295.5	0.178	0.018	35	0.1869	0.107	1.493	3	0.000702	1.71	0.000196	0.41	0.0002702	0.15	0.00073	12.33	0.01215	0.25	262.8	0.65	0.51	0	0	0	0	0

Information on Analysis and Constants Used in Calculations

Sample = DR2FF (M80/3 037DR-2)
Material = K-feldspar 0.25-0.5 mm
Location = Cadamosto, Cape Verde
Analyst = Jan Sticklus
Project = EXAMPLES
Mass Discrimination Law = POW
Irradiation = can42
J = 0.00003250 ± 0.00000005
TCS2 = 27.870 ± 0.039 Ma
Heating = 45 sec
Instrument = MAP216

Age Equations = Conventional
Negative Intensities = Allowed
Decay Constant 40K = 5.543 ± 0.009 E-10 1/a
Decay Constant 39Ar = 2.940 ± 0.016 E-07 1/h
Decay Constant 37Ar = 8.230 ± 0.012 E-04 1/h
Decay Constant 36Cl = 2.257 ± 0.015 E-06 1/a
Atmospheric Ratio 40/36(a) = 295.50 ± 0.53
Atmospheric Ratio 38/36(a) = 0.1869 ± 0.0002
Production Ratio 39/37(ca) = 0.000702 ± 0.000012
Production Ratio 38/37(ca) = 0.000196 ± 0.000001
Production Ratio 36/37(ca) = 0.000270 ± 0.000000
Production Ratio 40/39(k) = 0.000730 ± 0.000090
Production Ratio 38/39(k) = 0.012150 ± 0.000030
Production Ratio 36/38(cl) = 262.80
Scaling Ratio K/Ca = 0.510

Results	40(a)/36(a) ± 2σ	40(r)/39(k) ± 2σ	Age ± 2σ (Ka)	MSWD	39Ar(k) (%,n)	K/Ca ± 2σ
Age Plateau		1.65742 ± 0.24209	97.2 ± 14.2	0.10	5.82	12.7 ± 9.0
Overestimated Error		± 14.61%	± 14.61%	98%	5	
		Minimal External Error	± 14.2	2.41	2σ Confidence Limit	
		Analytical Error	± 14.2	1.0000	Error Magnification	
Total Fusion Age		2.44512 ± 0.04781	143.4 ± 2.8		40	59.0 ± 17.7
		± 1.96%	± 1.98%			
		Minimal External Error	± 2.9			
		Analytical Error	± 2.8			
Normal Isochron	305.44 ± 60.62	1.53074 ± 0.79662	89.7 ± 46.7	0.09	5.82	
Overestimated Error	± 19.85%	± 52.04%	± 52.04%	96%	5	
		Minimal External Error	± 46.7	2.63	2σ Confidence Limit	
		Analytical Error	± 46.7	1.0000	Error Magnification	
				10	Number of Iterations	
				0.0000134069	Convergence	
Inverse Isochron	305.84 ± 60.66	1.52852 ± 0.78296	89.6 ± 45.9	0.09	5.82	
Overestimated Error	± 19.83%	± 51.22%	± 51.22%	96%	5	
		Minimal External Error	± 45.9	2.63	2σ Confidence Limit	
		Analytical Error	± 45.9	1.0000	Error Magnification	
				3	Number of Iterations	
				0.0000269224	Convergence	
				20%	Spreading Factor	

[a] Blue dots in table indicate selected steps used to calculate the weighted mean and inverse isochron ages.
[b] Weight % K values calculated from $^{39}Ar_K$ values and weights of individual grains.
[c] Alteration Index values in italics indicate analyses from fresh material, normal font is from altered material (Baksi, 2007; van den Bogaard, 2013).
Values shown in red are negative values.
Abbreviations used in tables: (r) = radiogenic ^{40}Ar; (k) = Ar derived from K; (a) = atmospheric Ar; (ca) = Ar derived from Ca; (cl) = Ar derived from Ca; (c) = cosmogenic Ar; MDF = Mass Discrimination Factor.
Green squares in the inverse isochron plots indicate selected steps (blue dots in table), and blue squares are non-selected steps. Pink lines in the inverse isochron plot indicate a line fit through selected data, and the purple lines incidate a fit through an air $^{40}Ar/^{36}Ar$ ratio (295.5).
Stacked probability plot produced using Isoplot (Ludwig, 2011), where filled and unfilled 2σ error bars indicate selected/not selected data to calculate inverse-variance weighted mean age (black line), respectively.

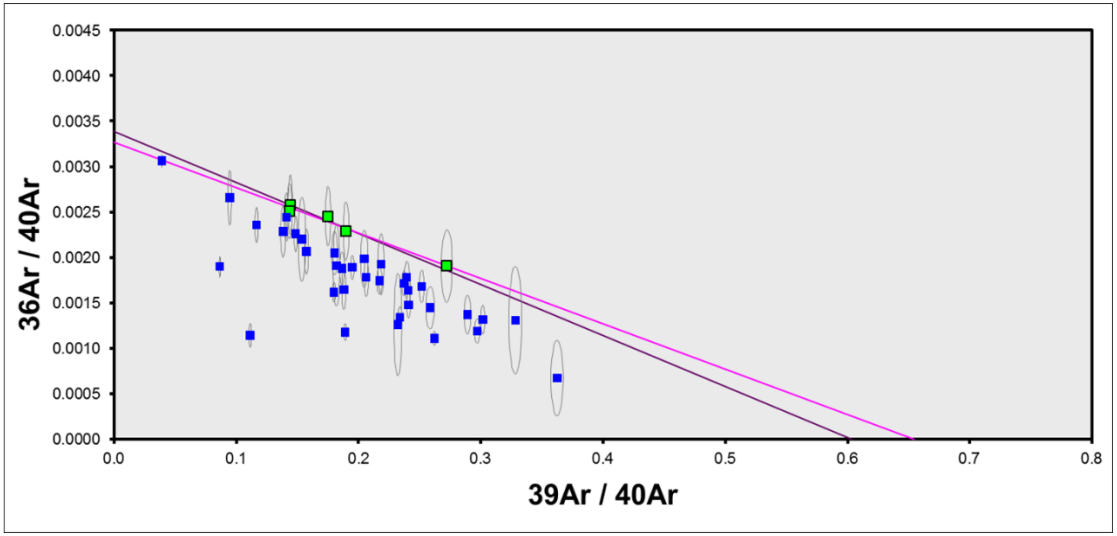
36Ar / 40Ar
39Ar / 40Ar
0.0045
0.0040
0.0035
0.0030
0.0025
0.0020
0.0015
0.0010
0.0005
0.0000
0.0
0.1
0.2
0.3
0.4
0.5
0.6
0.7
0.8

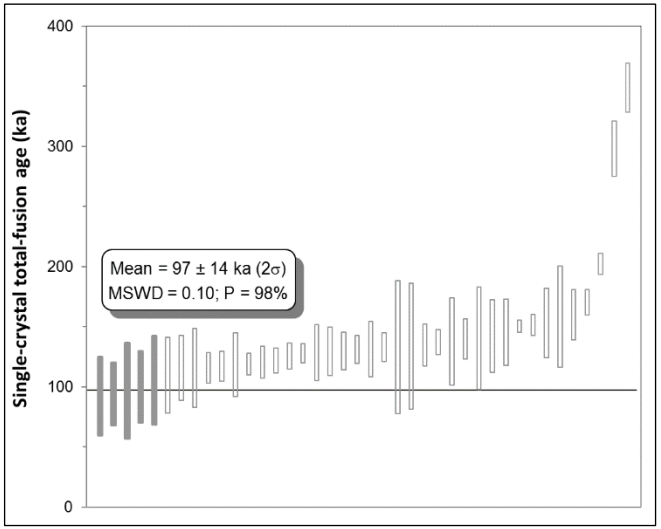
Single-crystal total-fusion age (ka)
Mean = 97 ± 14 ka (2σ)
MSWD = 0.10; P = 98%
400
300
200
100
0

Combined data – total fusion

Combined weighted mean ages, inverse isochron ages, and inverse isochron plots from samples 149-2, 149-6, 152-2, 035ROV-12 and 037DR-2, organized according to group ages.

21 ka group

Analysis #	Sample #	Mineral	Age (ka)	± 2σ (ka)	± % 2σ (ka)	Weighted mean age ± 2σ	Inverse isochron age ± 2σ
C36HA091	149-6	K-feldspar	11.5	6.5	56.2	21.14 ± 0.62 ka	20.56 ± 0.90 ka
C42BA078	149-2	K-feldspar	12.5	8.0	64.4	MSWD = 1.30, P = 7.3%, n = 53	MSWD = 1.27, P = 9.1%, SF = 74%, n = 53
C42BB003	149-2	K-feldspar	13.7	10.7	78.1		Initial $^{40}Ar/^{36}Ar$ = 299.1 ± 5.3
C36HA121	149-6	K-feldspar	15.1	3.6	24.0		
C42BA087	149-2	K-feldspar	15.4	10.3	66.8		
C42BB001	149-2	K-feldspar	15.9	8.2	51.5		
C42BA073	149-2	K-feldspar	16.5	8.7	53.0		
C42BB002	149-2	K-feldspar	17.2	13.8	80.5		
C42BA082	149-2	K-feldspar	17.4	17.5	100.7		
C42BA074	149-2	K-feldspar	17.7	9.8	55.5		
C36HA120	149-6	K-feldspar	17.8	5.7	31.8		
C42CA051	152-2	K-feldspar	18.5	5.3	28.8		
C42BA077	149-2	K-feldspar	18.6	9.5	50.9		
C36GC005	149-6	K-feldspar	18.9	15.0	79.1		
C36HA119	149-6	K-feldspar	19.5	5.9	30.3		
C42CA054	152-2	K-feldspar	19.5	6.3	32.6		
C36GC100	149-6	K-feldspar	19.7	5.3	26.8		
C42BB006	149-2	K-feldspar	19.8	12.8	64.8		
C42CA050	152-2	K-feldspar	19.8	4.8	24.3		
C42CA060	152-2	K-feldspar	20.0	3.7	18.5		
C42CA062	152-2	K-feldspar	20.1	3.7	18.2		
C42CA057	152-2	K-feldspar	20.1	2.9	14.2		
C42CA048	152-2	K-feldspar	20.2	3.7	18.2		
C42CA058	152-2	K-feldspar	20.6	2.5	12.0		
C42BA080	149-2	K-feldspar	20.6	10.9	53.1		
C42CA065	152-2	K-feldspar	20.6	4.2	20.2		

C36GC104	149-6	K-feldspar	20.8	1.9	9.0
C36GC106	149-6	K-feldspar	20.8	3.5	16.8
C42CA049	152-2	K-feldspar	20.9	2.8	13.4
C42BA075	149-2	K-feldspar	21.0	20.8	99.0
C42CA052	152-2	K-feldspar	21.2	2.1	9.7
C36HA122	149-6	K-feldspar	21.3	1.2	5.7
C42CA067	152-2	K-feldspar	21.3	5.2	24.4
C42BA083	149-2	K-feldspar	21.3	8.7	40.7
C36HA117	149-6	K-feldspar	21.3	6.5	30.4
C42CA056	152-2	K-feldspar	21.5	3.0	14.1
C36GC103	149-6	K-feldspar	21.7	2.5	11.3
C42BA079	149-2	K-feldspar	22.1	13.4	60.7
C42BA081	149-2	K-feldspar	22.1	12.0	54.2
C42CA063	152-2	K-feldspar	22.7	5.0	22.2
C36HA118	149-6	K-feldspar	22.7	2.6	11.7
C42BB005	149-2	K-feldspar	22.9	7.0	30.6
C42CA064	152-2	K-feldspar	23.5	4.9	21.0
C36GC101	149-6	K-feldspar	23.8	3.3	13.8
C42CA047	152-2	K-feldspar	23.9	3.2	13.4
C42BB004	149-2	K-feldspar	24.5	5.6	22.9
C42BA076	149-2	K-feldspar	24.8	8.6	34.6
C42BA072	149-2	K-feldspar	25.6	6.6	25.7
C42CA053	152-2	K-feldspar	26.0	3.7	14.3
C36GC105	149-6	K-feldspar	26.5	6.4	24.1
C42BA088	149-2	K-feldspar	27.3	5.9	21.6
C42BA084	149-2	K-feldspar	28.0	14.0	50.0
C42BA085	149-2	K-feldspar	28.4	9.3	32.8

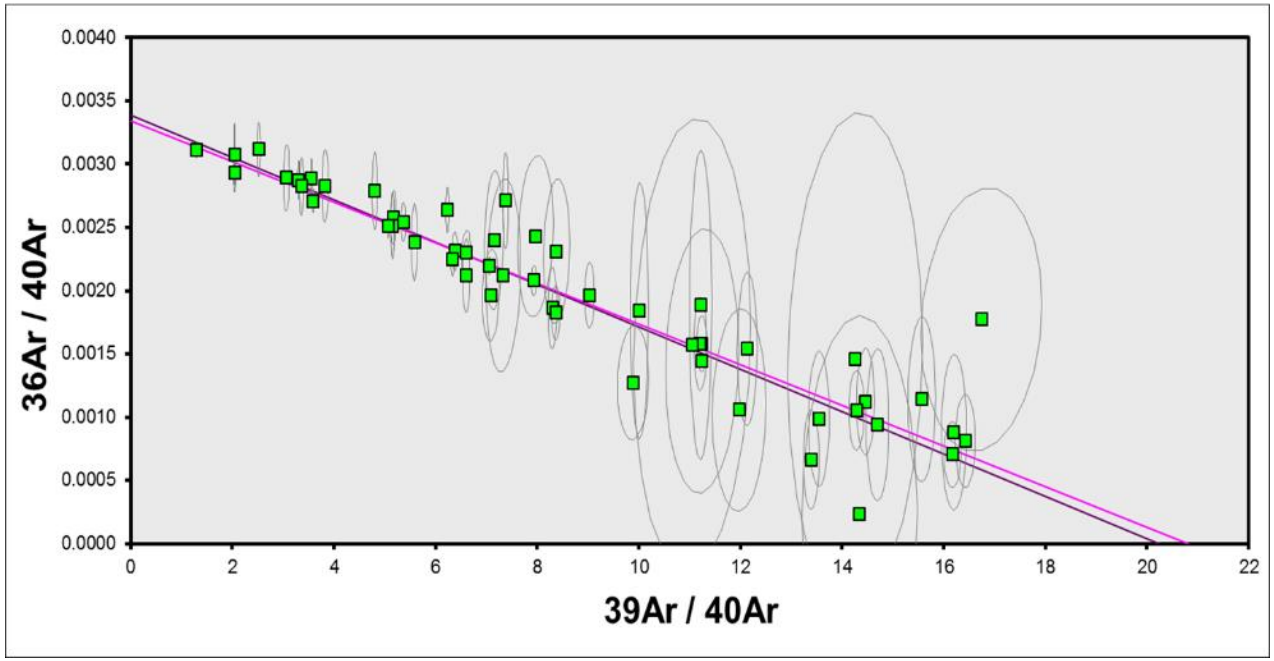

Inverse isochron plots: 2σ error ellipses; green squares = selected analyses; pink line = fit to data (green squares), purple line = line fit through atmospheric $^{40}Ar/^{36}Ar$ ratio.

149-2 step-heating

Relative Abundances	Laser power	[a]	36Ar [V]	%1σ	37Ar [V]	%1σ	38Ar [V]	%1σ	39Ar [V]	%1σ	40Ar [V]	%1σ	40(r)/39(k) ± 2σ	Age ± 2σ (Ka)	40Ar(r) (%)	39Ar(k) (%)	K/Ca ± 2σ	Step #	$^{36}Ar/^{39}Ar$ Alt. Index[b]
C47GA002	4.00 W	•	0.0000094	185.134	0.0000087	238.835	0.0000391	38.446	0.0042402	0.807	0.0088821	1.464	1.44112 ± 2.41768	83.7 ± 140.4	68.80	0.64	247 ± 1182	1	*0.000006*
C47GA003	5.00 W	•	0.0000111	124.544	0.0000120	168.770	0.0000002	9678.776	0.0005203	4.402	0.0093833	1.456	11.72245 ± 15.76064	680.8 ± 915.2	65.00	0.08	22 ± 75	2	*0.000054*
C47GA004	6.00 W	•	0.0000465	28.448	0.0000152	152.973	0.0000220	70.407	0.0022272	1.873	0.0117639	0.863	0.88678 ± 3.51039	51.5 ± 203.9	16.79	0.34	75 ± 229	3	*0.000053*
C47GA005	7.00 W	•	0.0000440	28.671	0.0000161	118.576	0.0000308	39.569	0.0048532	0.852	0.0151488	0.601	0.44434 ± 1.53501	25.8 ± 89.2	14.24	0.73	153 ± 364	4	*0.000023*
C47GA006	8.00 W	•	0.0000685	23.533	0.0000155	141.516	0.0001122	18.128	0.0094467	0.867	0.0225288	0.496	0.23989 ± 1.00945	13.9 ± 58.6	10.06	1.43	310 ± 879	5	*0.000018*
C47GA007	9.00 W	•	0.0000353	39.445	0.0000053	379.332	0.0001154	12.624	0.0105580	0.707	0.0180922	0.674	0.72351 ± 0.78089	42.0 ± 45.4	42.22	1.59	1014 ± 7692	6	*0.000009*
C47GA008	10.00 W	•	0.0001321	11.861	0.0000064	351.443	0.0009053	2.808	0.0802419	0.247	0.0629546	0.309	0.29725 ± 0.11556	17.3 ± 6.7	37.89	12.11	6414 ± 45082	7	*0.000004*
C47GA009	15.00 W	•	0.0006373	4.608	0.0000013	1711.997	0.0051964	0.771	0.4410198	0.235	0.3443535	0.054	0.35305 ± 0.03943	20.5 ± 2.3	45.22	66.56	174555 ± 5976749	8	*0.000004*
C47GA010	25.00 W	•	0.0000796	18.503	0.0000159	119.862	0.0012690	1.645	0.1094710	0.250	0.0606994	0.287	0.33894 ± 0.07958	19.7 ± 4.6	61.13	16.52	3513 ± 8422	9	*0.000002*
		Σ	0.0010638	4.798	0.0000493	128.152	0.0076903	0.848	0.6625783	0.166	0.5538065	0.077							

Procedure Blanks	Laser power	36Ar [V]	1σ	37Ar [V]	1σ	38Ar [V]	1σ	39Ar [V]	1σ	40Ar [V]	1σ
C47GA002	4.00 W	0.0000922	0.0000112	0.0001450	0.0000188	0.0000505	0.0000112	0.0000508	0.0000121	0.0021640	0.0000717
C47GA003	5.00 W	0.0000942	0.0000112	0.0001453	0.0000188	0.0000508	0.0000112	0.0000493	0.0000121	0.0022038	0.0000717
C47GA004	6.00 W	0.0000957	0.0000112	0.0001450	0.0000188	0.0000506	0.0000112	0.0000533	0.0000121	0.0022395	0.0000717
C47GA005	7.00 W	0.0000967	0.0000112	0.0001440	0.0000188	0.0000499	0.0000112	0.0000628	0.0000121	0.0022713	0.0000717
C47GA006	8.00 W	0.0000973	0.0000112	0.0001411	0.0000188	0.0000476	0.0000112	0.0000907	0.0000121	0.0023151	0.0000717
C47GA007	9.00 W	0.0000969	0.0000112	0.0001387	0.0000188	0.0000457	0.0000112	0.0001141	0.0000121	0.0023356	0.0000717
C47GA008	10.00 W	0.0000961	0.0000112	0.0001355	0.0000188	0.0000432	0.0000112	0.0001437	0.0000121	0.0023529	0.0000717
C47GA009	15.00 W	0.0000947	0.0000112	0.0001318	0.0000188	0.0000403	0.0000112	0.0001789	0.0000121	0.0023662	0.0000717
C47GA010	25.00 W	0.0000928	0.0000112	0.0001274	0.0000188	0.0000368	0.0000112	0.0002196	0.0000121	0.0023756	0.0000717

Sample Parameters	Laser power	Sample	Material	Location	Analyst	Standard (in Ma)	%1σ	J	%1σ	MDF	%1σ	Volume Ratio	Sensitivity (mol/volt)	Day	Month	Year	Hour	Min	Resist	Irradiation	Project	Experiment	Nmb	Standard Name
C47GA002	4.00 W	POS 320/2 149-2 (1492f)	K-feldspar (0.5-1 mm)	Cadamosto Smt, Cape Verde	Jan Sticklus	27.87	0.14	0.0000322	0.311	1.0098	0.21	1	1.211E-14	25	OCT	2018	11	54	1	can42	Examples	c42it14ip2_1492f	01	TCS2
C47GA003	5.00 W	POS 320/2 149-2 (1492f)	K-feldspar (0.5-1 mm)	Cadamosto Smt, Cape Verde	Jan Sticklus	27.87	0.14	0.0000322	0.311	1.0098	0.21	1	1.211E-14	25	OCT	2018	12	23	1	can42	Examples	c42it14ip2_1492f	01	TCS2
C47GA004	6.00 W	POS 320/2 149-2 (1492f)	K-feldspar (0.5-1 mm)	Cadamosto Smt, Cape Verde	Jan Sticklus	27.87	0.14	0.0000322	0.311	1.0098	0.21	1	1.211E-14	25	OCT	2018	12	52	1	can42	Examples	c42it14ip2_1492f	01	TCS2
C47GA005	7.00 W	POS 320/2 149-2 (1492f)	K-feldspar (0.5-1 mm)	Cadamosto Smt, Cape Verde	Jan Sticklus	27.87	0.14	0.0000322	0.311	1.0098	0.21	1	1.211E-14	25	OCT	2018	13	21	1	can42	Examples	c42it14ip2_1492f	01	TCS2
C47GA006	8.00 W	POS 320/2 149-2 (1492f)	K-feldspar (0.5-1 mm)	Cadamosto Smt, Cape Verde	Jan Sticklus	27.87	0.14	0.0000322	0.311	1.0098	0.21	1	1.211E-14	25	OCT	2018	14	9	1	can42	Examples	c42it14ip2_1492f	01	TCS2
C47GA007	9.00 W	POS 320/2 149-2 (1492f)	K-feldspar (0.5-1 mm)	Cadamosto Smt, Cape Verde	Jan Sticklus	27.87	0.14	0.0000322	0.311	1.0098	0.21	1	1.211E-14	25	OCT	2018	14	37	1	can42	Examples	c42it14ip2_1492f	01	TCS2
C47GA008	10.00 W	POS 320/2 149-2 (1492f)	K-feldspar (0.5-1 mm)	Cadamosto Smt, Cape Verde	Jan Sticklus	27.87	0.14	0.0000322	0.311	1.0098	0.21	1	1.211E-14	25	OCT	2018	15	6	1	can42	Examples	c42it14ip2_1492f	01	TCS2
C47GA009	15.00 W	POS 320/2 149-2 (1492f)	K-feldspar (0.5-1 mm)	Cadamosto Smt, Cape Verde	Jan Sticklus	27.87	0.14	0.0000322	0.311	1.0098	0.21	1	1.211E-14	25	OCT	2018	15	35	1	can42	Examples	c42it14ip2_1492f	01	TCS2
C47GA010	25.00 W	POS 320/2 149-2 (1492f)	K-feldspar (0.5-1 mm)	Cadamosto Smt, Cape Verde	Jan Sticklus	27.87	0.14	0.0000322	0.311	1.0098	0.21	1	1.211E-14	25	OCT	2018	16	4	1	can42	Examples	c42it14ip2_1492f	01	TCS2

Irradiation Constants	Laser power	40/36(a)	%1σ	40/36(c)	%1σ	38/36(a)	%1σ	38/36(c)	%1σ	39/37(ca)	%1σ	38/37(ca)	%1σ	36/37(ca)	%1σ	40/39(k)	%1σ	38/39(k)	%1σ	36/38(cl)	%1σ	K/Ca	%1σ	K/Cl	%1σ	Ca/Cl	%1σ
C47GA002	4.00 W	295.5	0.178	0.018	35	0.1869	0.107	1.493	3	0.000702	1.71	0.000196	4.08	0.0002702	0.15	0.00073	12.33	0.01215	0.27	262.8	0.65	0.51	0	0	0	0	0
C47GA003	5.00 W	295.5	0.178	0.018	35	0.1869	0.107	1.493	3	0.000702	1.71	0.000196	4.08	0.0002702	0.15	0.00073	12.33	0.01215	0.27	262.8	0.65	0.51	0	0	0	0	0
C47GA004	6.00 W	295.5	0.178	0.018	35	0.1869	0.107	1.493	3	0.000702	1.71	0.000196	4.08	0.0002702	0.15	0.00073	12.33	0.01215	0.27	262.8	0.65	0.51	0	0	0	0	0
C47GA005	7.00 W	295.5	0.178	0.018	35	0.1869	0.107	1.493	3	0.000702	1.71	0.000196	4.08	0.0002702	0.15	0.00073	12.33	0.01215	0.27	262.8	0.65	0.51	0	0	0	0	0
C47GA006	8.00 W	295.5	0.178	0.018	35	0.1869	0.107	1.493	3	0.000702	1.71	0.000196	4.08	0.0002702	0.15	0.00073	12.33	0.01215	0.27	262.8	0.65	0.51	0	0	0	0	0
C47GA007	9.00 W	295.5	0.178	0.018	35	0.1869	0.107	1.493	3	0.000702	1.71	0.000196	4.08	0.0002702	0.15	0.00073	12.33	0.01215	0.27	262.8	0.65	0.51	0	0	0	0	0
C47GA008	10.00 W	295.5	0.178	0.018	35	0.1869	0.107	1.493	3	0.000702	1.71	0.000196	4.08	0.0002702	0.15	0.00073	12.33	0.01215	0.27	262.8	0.65	0.51	0	0	0	0	0
C47GA009	15.00 W	295.5	0.178	0.018	35	0.1869	0.107	1.493	3	0.000702	1.71	0.000196	4.08	0.0002702	0.15	0.00073	12.33	0.01215	0.27	262.8	0.65	0.51	0	0	0	0	0
C47GA010	25.00 W	295.5	0.178	0.018	35	0.1869	0.107	1.493	3	0.000702	1.71	0.000196	4.08	0.0002702	0.15	0.00073	12.33	0.01215	0.27	262.8	0.65	0.51	0	0	0	0	0

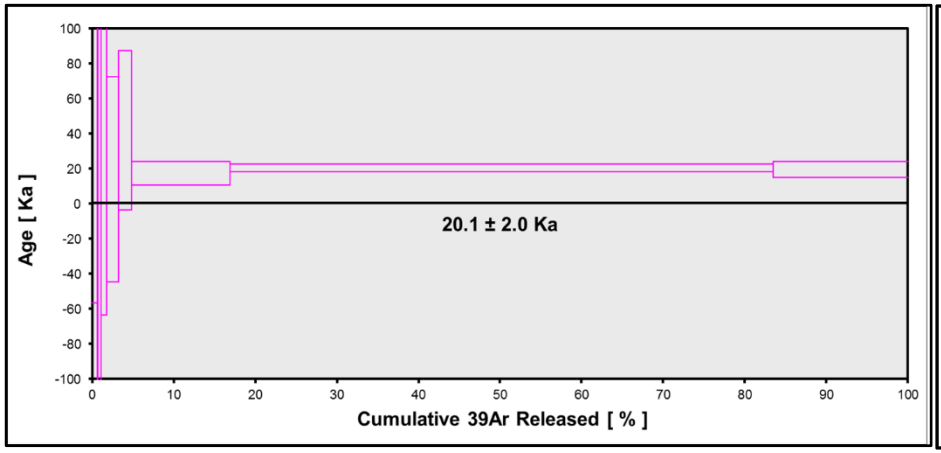
Age [Ka]
20.1 ± 2.0 Ka
Cumulative 39Ar Released [%]

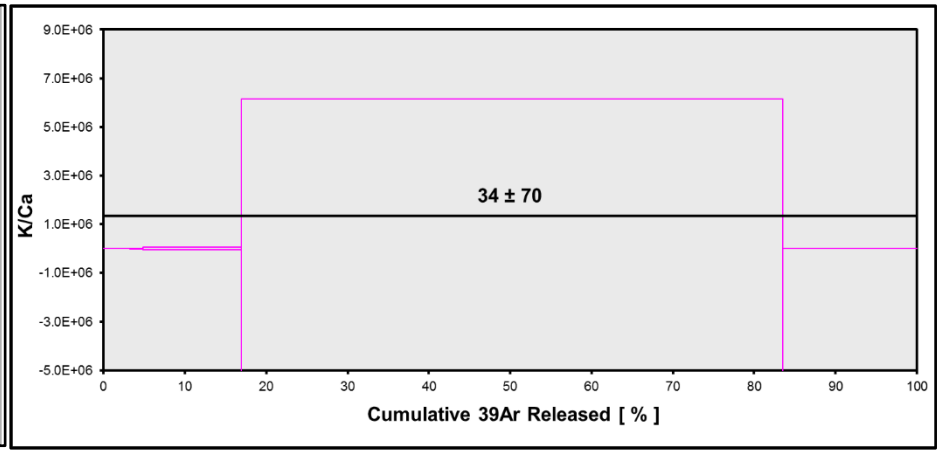
K/Ca
34 ± 70
Cumulative 39Ar Released [%]

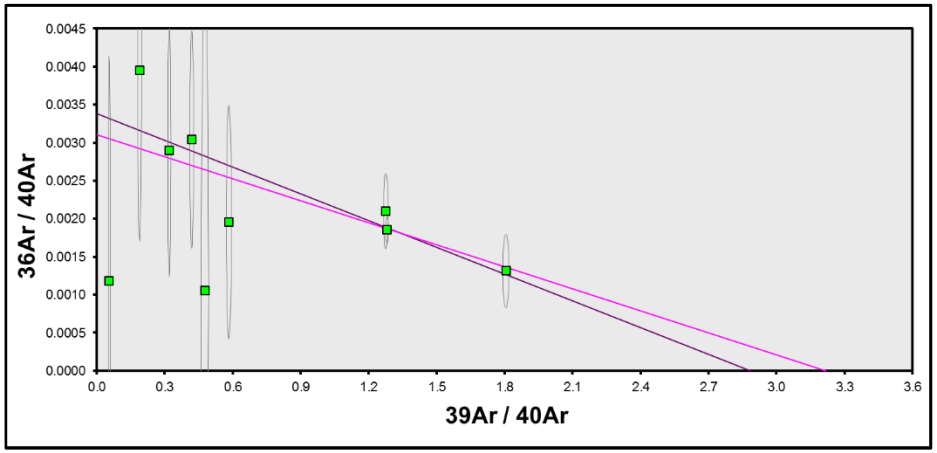
36Ar / 40Ar
39Ar / 40Ar

Information on Analysis and Constants Used in Calculations

Sample = POS 320/2 149-2 (1492F)
Material = K-feldspar
Location = Cadamosto Smt, Cape Verde
Analyst = Jan Sticklus
Project = EXAMPLES
Mass Discrimination Law = POW
Irradiation = can42
J = 0.00003220 ± 0.00000010
TCS2 = 27.870 ± 0.039 Ma
Heating = 45 sec
Instrument = MAP216
Weight = 10.092 mg

Age Equations = Conventional
Negative Intensities = Allowed
Decay Constant 40K = 5.543 ± 0.009 E-10 1/a
Decay Constant 39Ar = 2.940 ± 0.016 E-07 1/h
No 37Ar Decay Correction
Decay Constant 36Cl = 2.257 ± 0.015 E-06 1/a
Atmospheric Ratio 40/36(a) = 295.50 ± 0.53
Atmospheric Ratio 38/36(a) = 0.1869 ± 0.0002
Production Ratio 39/37(ca) = 0.000702 ± 0.0000
Production Ratio 38/37(ca) = 0.000196 ± 0.0000
Production Ratio 36/37(ca) = 0.000270 ± 0.0000
Production Ratio 40/39(k) = 0.000730 ± 0.00009
Production Ratio 38/39(k) = 0.012150 ± 0.00003
Production Ratio 36/38(cl) = 262.80
Scaling Ratio K/Ca = 0.510

Results	40(a)/36(a) ± 2σ	40(r)/39(k) ± 2σ	Age ± 2σ (Ka)	MSWD	39Ar(k) (%,n)	K/Ca ± 2σ
Age Plateau		0.34652 ± 0.03373 ± 9.73%	20.1 ± 2.0 ± 9.75%	0.66	100.00	34 ± 70
				73%	9	
		Minimal External Error ± 2.0		2.00	2σ Confidence Limit	
		Analytical Error ± 2.0		1.0000	Error Magnification	
Total Fusion Age		0.36064 ± 0.04558 ± 12.64%	20.9 ± 2.7 ± 12.65%		9	6857 ± 17575
		Minimal External Error ± 2.7				
		Analytical Error ± 2.6				
Normal Isochron	287.06 ± 70.74 ± 24.64%	0.35502 ± 0.10019 ± 28.22%	20.6 ± 5.8 ± 28.23%	0.38	100.00	
				91%	9	
		Minimal External Error ± 5.8		2.07	2σ Confidence Limit	
		Analytical Error ± 5.8		1.0000	Error Magnification	
				22	Number of Iterations	
				0.0000025351	Convergence	
Inverse Isochron	322.00 ± 86.53 ± 26.87%	0.31077 ± 0.09971 ± 32.09%	18.1 ± 5.8 ± 32.09%	0.69	100.00	
				68%	9	
		Minimal External Error ± 5.8		2.07	2σ Confidence Limit	
		Analytical Error ± 5.8		1.0000	Error Magnification	
				3	Number of Iterations	
				0.0005326868	Convergence	
				54%	Spreading Factor	

[a] Blue dots in table indicate selected steps used to calculate the plateau and inverse isochron ages.

[b] Alteration Index values in italics indicate analyses from fresh material, normal font is from altered material (Baksi, 2007; van den Bogaard, 2013).

Values shown in red are negative values.

Abbreviations used in tables: (r) = radiogenic ^{40}Ar; (k) = Ar derived from K; (a) = atmospheric Ar; (ca) = Ar derived from Ca; (cl) = Ar derived from Ca; (c) = cosmogenic Ar; MDF = Mass Discrimination Factor.

Green squares in the inverse isochron plots indicate selected steps (blue dots in table), and blue squares are non-selected steps. Pink lines in the inverse isochron plot indicate a line fit through selected data, and the purple lines incidate a fit through an air ^{40}Ar/^{36}Ar ratio (295.5).

152-1 step heating

Relative Abundances	Laser power	a	36Ar [V]	%1σ	37Ar [V]	%1σ	38Ar [V]	%1σ	39Ar [V]	%1σ	40Ar [V]	%1σ	40(r)/39(k) ± 2σ	Age ± 2σ (Ka)	40Ar(r) (%)	39Ar(k) (%)	K/Ca ± 2σ	Step #	$^{36}Ar/^{39}Ar$ Alt. Index[b]
C47GA033	5.00 W		0.0000152	77.356	0.0000070	224.317	0.0000054	222.026	0.0008535	5.067	0.0026737	6.691	8.40913 ± 8.22083	497.5 ± 486.3	268.45	0.12	63 ± 281	1	*-0.000048*
C47GA034	6.00 W		0.0001299	9.874	0.0000170	75.231	0.0000661	28.366	0.0032136	1.699	0.0364722	0.908	0.59278 ± 2.36783	35.1 ± 140.1	5.22	0.45	96 ± 145	2	0.000108
C47GA035	7.00 W		0.0000463	28.476	0.0000144	113.294	0.0001007	21.280	0.0090864	0.860	0.0136881	1.533	0.00139 ± 0.85793	0.1 ± 50.8	0.09	1.27	322 ± 730	3	*0.000014*
C47GA036	8.00 W		0.0000329	42.382	0.0000040	400.542	0.0004449	3.777	0.0364931	0.427	0.0329437	0.474	0.63540 ± 0.22623	37.6 ± 13.4	70.39	5.10	4681 ± 37497	4	*0.000002*
C47GA037	9.00 W	•	0.0000029	493.333	0.0000103	172.920	0.0000705	20.817	0.0058089	0.845	0.0063782	2.324	1.24513 ± 1.45825	73.7 ± 86.3	113.40	0.81	289 ± 999	5	*-0.000001*
C47GA038	10.00 W	•	0.0000081	186.247	0.0000257	69.541	0.0000610	23.934	0.0062478	1.187	0.0059829	2.420	0.57325 ± 1.42855	33.9 ± 84.5	59.86	0.87	124 ± 173	6	*0.000003*
C47GA039	15.00 W	•	0.0001101	14.410	0.0000015	1246.812	0.0063518	0.682	0.5448409	0.223	0.2395073	0.147	0.37914 ± 0.01735	22.4 ± 1.0	86.25	76.21	187394 ± 4672908	7	*0.000001*
C47GA040	25.00 W	•	0.0000593	22.347	0.0000178	87.174	0.0012940	1.982	0.1083944	0.259	0.0527113	0.270	0.32389 ± 0.07233	19.2 ± 4.3	66.60	15.16	3113 ± 5427	8	*0.000001*
		Σ	0.0003684	10.624	0.0000035	1336.062	0.0083836	0.773	0.7149386	0.177	0.3903574	0.162							

Procedure Blanks	Laser power	36Ar [V]	1σ	37Ar [V]	1σ	38Ar [V]	1σ	39Ar [V]	1σ	40Ar [V]	1σ
C47GA033	5.00 W	0.0001045	0.0000094	0.0001401	0.0000113	0.0000471	0.0000095	0.0000890	0.0000406	0.0027046	0.0001011
C47GA034	6.00 W	0.0001048	0.0000094	0.0001379	0.0000113	0.0000463	0.0000095	0.0000958	0.0000406	0.0026781	0.0001011
C47GA035	7.00 W	0.0001052	0.0000094	0.0001358	0.0000113	0.0000456	0.0000095	0.0001024	0.0000406	0.0026524	0.0001011
C47GA036	8.00 W	0.0001057	0.0000094	0.0001322	0.0000113	0.0000443	0.0000095	0.0001138	0.0000406	0.0026085	0.0001011
C47GA037	9.00 W	0.0001060	0.0000094	0.0001300	0.0000113	0.0000435	0.0000095	0.0001206	0.0000406	0.0025819	0.0001011
C47GA038	10.00 W	0.0001063	0.0000094	0.0001278	0.0000113	0.0000428	0.0000095	0.0001275	0.0000406	0.0025553	0.0001011
C47GA039	15.00 W	0.0001066	0.0000094	0.0001256	0.0000113	0.0000420	0.0000095	0.0001343	0.0000406	0.0025288	0.0001011
C47GA040	25.00 W	0.0001070	0.0000094	0.0001234	0.0000113	0.0000412	0.0000095	0.0001411	0.0000406	0.0025022	0.0001011

Sample Parameters	Laser power	Sample	Material	Location	Analyst	Standard (in Ma)	%1σ	J	%1σ	MDF	%1σ	Volume Ratio	Sensitivity (mol/volt)	Day	Month	Year	Hour	Min	Resist	Irradiation	Project	Experiment	Nmb	Standard Name
C47GA033	5.00 W	POS 320/2 152-1 (1521f)	K-feldspar	Cadamosto Smt, Cape Verde	Jan Sticklus	27.87	0.14	0.0000328	0.305	1.0098	0.21	1	1.211E-14	26	OCT	2018	4	44	1	can42	Examples	c42it7ip3_1521f	01	TCS2
C47GA034	6.00 W	POS 320/2 152-1 (1521f)	K-feldspar	Cadamosto Smt, Cape Verde	Jan Sticklus	27.87	0.14	0.0000328	0.305	1.0098	0.21	1	1.211E-14	26	OCT	2018	5	13	1	can42	Examples	c42it7ip3_1521f	01	TCS2
C47GA035	7.00 W	POS 320/2 152-1 (1521f)	K-feldspar	Cadamosto Smt, Cape Verde	Jan Sticklus	27.87	0.14	0.0000328	0.305	1.0098	0.21	1	1.211E-14	26	OCT	2018	5	41	1	can42	Examples	c42it7ip3_1521f	01	TCS2
C47GA036	8.00 W	POS 320/2 152-1 (1521f)	K-feldspar	Cadamosto Smt, Cape Verde	Jan Sticklus	27.87	0.14	0.0000328	0.305	1.0098	0.21	1	1.211E-14	26	OCT	2018	6	29	1	can42	Examples	c42it7ip3_1521f	01	TCS2
C47GA037	9.00 W	POS 320/2 152-1 (1521f)	K-feldspar	Cadamosto Smt, Cape Verde	Jan Sticklus	27.87	0.14	0.0000328	0.305	1.0098	0.21	1	1.211E-14	26	OCT	2018	6	58	1	can42	Examples	c42it7ip3_1521f	01	TCS2
C47GA038	10.00 W	POS 320/2 152-1 (1521f)	K-feldspar	Cadamosto Smt, Cape Verde	Jan Sticklus	27.87	0.14	0.0000328	0.305	1.0098	0.21	1	1.211E-14	26	OCT	2018	7	27	1	can42	Examples	c42it7ip3_1521f	01	TCS2
C47GA039	15.00 W	POS 320/2 152-1 (1521f)	K-feldspar	Cadamosto Smt, Cape Verde	Jan Sticklus	27.87	0.14	0.0000328	0.305	1.0098	0.21	1	1.211E-14	26	OCT	2018	7	56	1	can42	Examples	c42it7ip3_1521f	01	TCS2
C47GA040	25.00 W	POS 320/2 152-1 (1521f)	K-feldspar	Cadamosto Smt, Cape Verde	Jan Sticklus	27.87	0.14	0.0000328	0.305	1.0098	0.21	1	1.211E-14	26	OCT	2018	8	25	1	can42	Examples	c42it7ip3_1521f	01	TCS2

Irradiation Constants	Laser power	40/36(a)	%1σ	40/36(c)	%1σ	38/36(a)	%1σ	38/36(c)	%1σ	39/37(ca)	%1σ	38/37(ca)	%1σ	36/37(ca)	%1σ	40/39(k)	%1σ	38/39(k)	%1σ	36/38(cl)	%1σ	K/Ca	%1σ	K/Cl	%1σ	Ca/Cl	%1σ
C47GA033	5.00 W	295.5	0.178	0.018	35	0.1869	0.107	1.493	3	0.000702	1.71	0.000196	4.08	0.0002702	0.15	0.00073	12.33	0.01215	0.27	262.8	0.65	0.51	0	0	0	0	0
C47GA034	6.00 W	295.5	0.178	0.018	35	0.1869	0.107	1.493	3	0.000702	1.71	0.000196	4.08	0.0002702	0.15	0.00073	12.33	0.01215	0.27	262.8	0.65	0.51	0	0	0	0	0
C47GA035	7.00 W	295.5	0.178	0.018	35	0.1869	0.107	1.493	3	0.000702	1.71	0.000196	4.08	0.0002702	0.15	0.00073	12.33	0.01215	0.27	262.8	0.65	0.51	0	0	0	0	0
C47GA036	8.00 W	295.5	0.178	0.018	35	0.1869	0.107	1.493	3	0.000702	1.71	0.000196	4.08	0.0002702	0.15	0.00073	12.33	0.01215	0.27	262.8	0.65	0.51	0	0	0	0	0
C47GA037	9.00 W	295.5	0.178	0.018	35	0.1869	0.107	1.493	3	0.000702	1.71	0.000196	4.08	0.0002702	0.15	0.00073	12.33	0.01215	0.27	262.8	0.65	0.51	0	0	0	0	0
C47GA038	10.00 W	295.5	0.178	0.018	35	0.1869	0.107	1.493	3	0.000702	1.71	0.000196	4.08	0.0002702	0.15	0.00073	12.33	0.01215	0.27	262.8	0.65	0.51	0	0	0	0	0
C47GA039	15.00 W	295.5	0.178	0.018	35	0.1869	0.107	1.493	3	0.000702	1.71	0.000196	4.08	0.0002702	0.15	0.00073	12.33	0.01215	0.27	262.8	0.65	0.51	0	0	0	0	0
C47GA040	25.00 W	295.5	0.178	0.018	35	0.1869	0.107	1.493	3	0.000702	1.71	0.000196	4.08	0.0002702	0.15	0.00073	12.33	0.01215	0.27	262.8	0.65	0.51	0	0	0	0	0

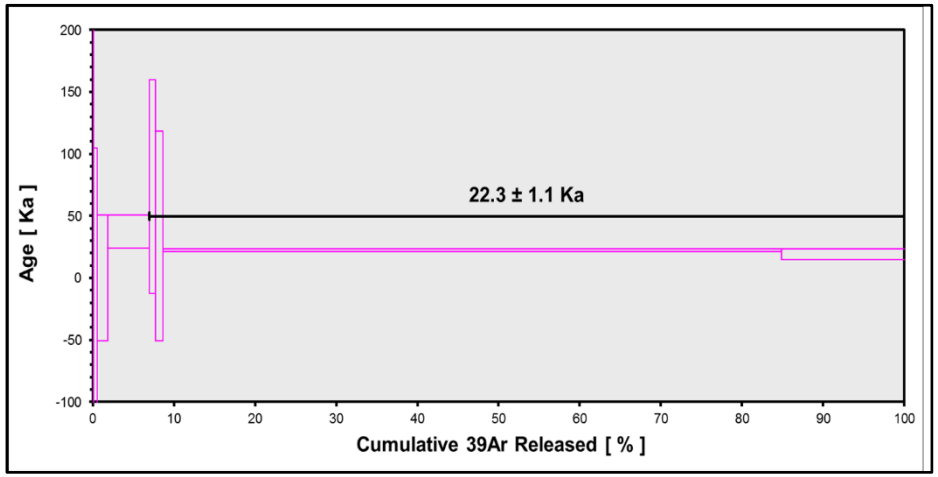

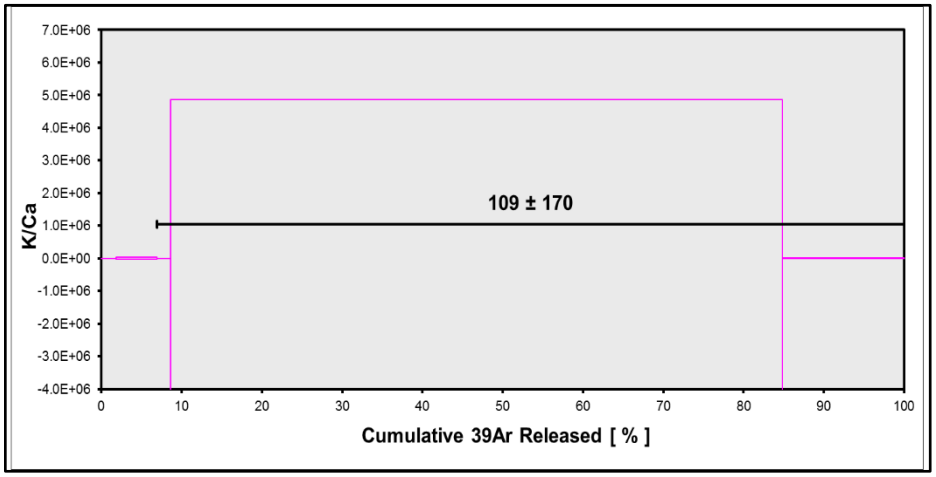

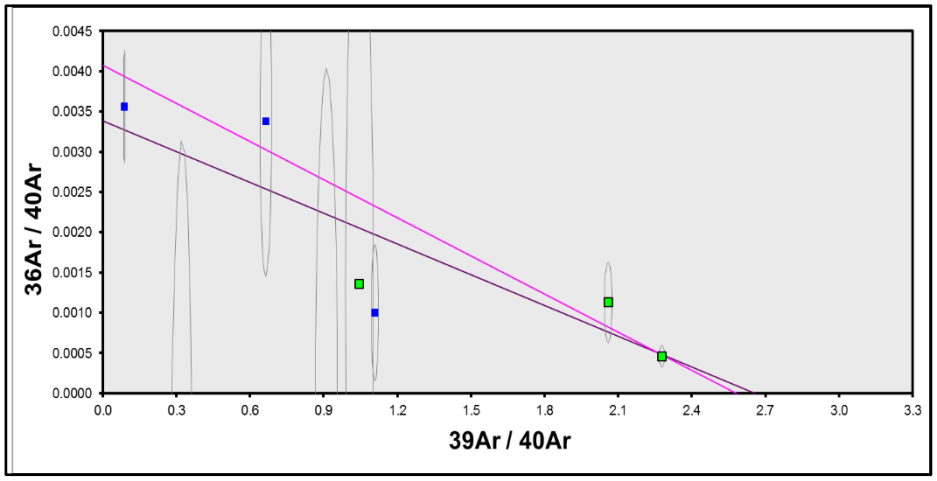
36Ar / 40Ar
0.0045
0.0040
0.0035
0.0030
0.0025
0.0020
0.0015
0.0010
0.0005
0.0000
0.0
0.3
0.6
0.9
1.2
1.5
1.8
2.1
2.4
2.7
3.0
3.3
39Ar / 40Ar

Information on Analysis and Constants Used in Calculations

Sample = POS 320/2 152-1 (1521F)
Material = K-feldspar
Location = Cadamosto Smt, Cape Verde
Analyst = Jan Sticklus
Project = EXAMPLES
Mass Discrimination Law = POW
Irradiation = can42
J = 0.00003280 ± 0.00000010
TCS2 = 27.870 ± 0.039 Ma
Heating = 45 sec
Instrument = MAP216
Weight = 10.325 mg

Age Equations = Conventional
Negative Intensities = Allowed
Decay Constant 40K = 5.543 ± 0.009 E-10 1/a
Decay Constant 39Ar = 2.940 ± 0.016 E-07 1/h
No 37Ar Decay Correction
Decay Constant 36Cl = 2.257 ± 0.015 E-06 1/a
Atmospheric Ratio 40/36(a) = 295.50 ± 0.53
Atmospheric Ratio 38/36(a) = 0.1869 ± 0.0002
Production Ratio 39/37(ca) = 0.000702 ± 0.000012
Production Ratio 38/37(ca) = 0.000196 ± 0.000008
Production Ratio 36/37(ca) = 0.000270 ± 0.000000
Production Ratio 40/39(k) = 0.000730 ± 0.000090
Production Ratio 38/39(k) = 0.012150 ± 0.000033
Production Ratio 36/38(cl) = 262.80
Scaling Ratio K/Ca = 0.510

Results	40(a)/36(a) ± 2σ	40(r)/39(k) ± 2σ	Age ± 2σ (Ka)	MSWD	39Ar(k) (%,n)	K/Ca ± 2σ
Age Plateau		0.37628 ± 0.01874 ± 4.98%	22.3 ± 1.1 ± 5.02%	1.23	93.06	109 ± 170
			Minimal External Error ± 1.1	30%	4	
			Analytical Error ± 1.1	2.63	2σ Confidence Limit	
				1.1110	Error Magnification	
Total Fusion Age		0.39299 ± 0.03244 ± 8.25%	23.3 ± 1.9 ± 8.28%		8	105267 ± 2812877
			Minimal External Error ± 1.9			
			Analytical Error ± 1.9			
Normal Isochron	430.18 ± 940.14 ± 218.54%	0.65792 ± 0.36124 ± 54.91%	38.9 ± 21.4 ± 54.91%	11.26	93.06	
Error Chron			Minimal External Error ± 21.4	0%	4	
			Analytical Error ± 21.4	3.00	2σ Confidence Limit	
				3.3554	Error Magnification	
				37	Number of Iterations	
				0.0000054194	Convergence	
Inverse Isochron	245.21 ± 319.50 ± 130.30%	0.38738 ± 0.05181 ± 13.38%	22.9 ± 3.1 ± 13.39%	1.79	93.06	
			Minimal External Error ± 3.1	17%	4	
			Analytical Error ± 3.1	3.00	2σ Confidence Limit	
				1.3380	Error Magnification	
				4	Number of Iterations	
				0.0003347420	Convergence	
				53%	Spreading Factor	

[a] Blue dots in table indicate selected steps used to calculate the plateau and inverse isochron ages.
[b] Alteration Index values in italics indicate analyses from fresh material, normal font is from altered material (Baksi, 2007; van den Bogaard, 2013).
Values shown in red are negative values.
Abbreviations used in tables: (r) = radiogenic ^{40}Ar; (k) = Ar derived from K; (a) = atmospheric Ar; (ca) = Ar derived from Ca; (cl) = Ar derived from Ca; (c) = cosmogenic Ar; MDF = Mass Discrimination Factor.
Green squares in the inverse isochron plots indicate selected steps (blue dots in table), and blue squares are non-selected steps. Pink lines in the inverse isochron plot indicate a line fit through selected data, and the purple lines incidate a fit through an air $^{40}Ar/^{36}Ar$ ratio (295.5).

035ROV-12 step heating

Relative Abundance	Laser power	[a]	36Ar [V]	%1σ	37Ar [V]	%1σ	38Ar [V]	%1σ	39Ar [V]	%1σ	40Ar [V]	%1σ	40(r)/39(k) ± 2σ	Age ± 2σ (Ka)	40Ar(r) (%)	39Ar(k) (%)	K/Ca ± 2σ	Step #	$^{36}Ar/^{39}Ar$ Alt. Index[b]
C47FB116	6.00 W	•	0.0000264	72.687	0.0000069	319.367	0.0000182	78.771	0.0001734	15.511	0.0029187	36.761	28.19519 ± 67.21102	1669.2 ± 3980.8	167.52	0.06	13 ± 82	1	0.0003509
C47FB117	8.00 W	•	0.0000159	123.763	0.0000004	5229.683	0.0000306	51.273	0.0009286	4.320	0.0026452	40.513	7.91795 ± 12.76037	468.5 ± 754.9	277.97	0.33	1308 ± 136814	2	*-0.0000394*
C47FB118	12.00 W	•	0.0000932	19.482	0.0000216	81.524	0.0016026	2.312	0.1346333	0.281	0.1593010	0.684	0.97793 ± 0.08152	57.9 ± 4.8	82.65	47.15	3182 ± 5188	3	*0.0000016*
C47FB119	20.00 W	•	0.0000090	207.513	0.0000022	955.317	0.0008175	2.715	0.0676207	0.300	0.0623084	1.725	0.88138 ± 0.16636	52.2 ± 9.8	95.65	23.68	15658 ± 299160	4	*0.0000003*
C47FB120	25.00 W		0.0000574	33.215	0.0000123	211.143	0.0009961	2.324	0.0821880	0.255	0.0764911	1.408	0.72356 ± 0.13965	42.8 ± 8.3	77.74	28.78	3397 ± 14345	5	*0.0000016*
		Σ	0.0001701	24.930	0.0000187	255.261	0.0034650	1.541	0.2855440	0.168	0.3036644	0.793							

Procedure Blanks	Laser power	36Ar [V]	1σ	37Ar [V]	1σ	38Ar [V]	1σ	39Ar [V]	1σ	40Ar [V]	1σ
C47FB116	6.00 W	0.0002733	0.0000136	0.0001592	0.0000128	0.0001168	0.0000119	0.0002497	0.0000242	0.0030616	0.0010683
C47FB117	8.00 W	0.0002725	0.0000136	0.0001587	0.0000128	0.0001132	0.0000119	0.0002416	0.0000242	0.0030661	0.0010683
C47FB118	12.00 W	0.0002716	0.0000136	0.0001582	0.0000128	0.0001094	0.0000119	0.0002332	0.0000242	0.0030709	0.0010683
C47FB119	20.00 W	0.0002708	0.0000136	0.0001576	0.0000128	0.0001056	0.0000119	0.0002248	0.0000242	0.0030756	0.0010683
C47FB120	25.00 W	0.0002699	0.0000136	0.0001571	0.0000128	0.0001019	0.0000119	0.0002165	0.0000242	0.0030803	0.0010683

Sample Parameters	Laser power	Sample	Material	Location	Analyst	Standard (in Ma)	%1σ	J	%1σ	MDF	%1σ	Volume Ratio	Sensitivity (mol/volt)	Day	Month	Year	Hour	Min	Resist	Irradiation	Project	Experiment	Nmb	Standard Name
C47FB116	6.00 W	M80/3 035ROV-12 (3512f)	K-feldspar (1 >1 mm crystal)	Cadamosto Smt, Cape Verde	Jan Sticklus	27.87	0.14	0.0000328	0.305	1.0098	0.21	1	1.211E-14	28	SEP	2018	23	6	1	can42	Examples	c42it7ip5_3512f	01	TCS2
C47FB117	8.00 W	M80/3 035ROV-12 (3512f)	K-feldspar (1 >1 mm crystal)	Cadamosto Smt, Cape Verde	Jan Sticklus	27.87	0.14	0.0000328	0.305	1.0098	0.21	1	1.211E-14	28	SEP	2018	23	34	1	can42	Examples	c42it7ip5_3512f	01	TCS2
C47FB118	12.00 W	M80/3 035ROV-12 (3512f)	K-feldspar (1 >1 mm crystal)	Cadamosto Smt, Cape Verde	Jan Sticklus	27.87	0.14	0.0000328	0.305	1.0098	0.21	1	1.211E-14	29	SEP	2018	0	3	1	can42	Examples	c42it7ip5_3512f	01	TCS2
C47FB119	20.00 W	M80/3 035ROV-12 (3512f)	K-feldspar (1 >1 mm crystal)	Cadamosto Smt, Cape Verde	Jan Sticklus	27.87	0.14	0.0000328	0.305	1.0098	0.21	1	1.211E-14	29	SEP	2018	0	32	1	can42	Examples	c42it7ip5_3512f	01	TCS2
C47FB120	25.00 W	M80/3 035ROV-12 (3512f)	K-feldspar (1 >1 mm crystal)	Cadamosto Smt, Cape Verde	Jan Sticklus	27.87	0.14	0.0000328	0.305	1.0098	0.21	1	1.211E-14	29	SEP	2018	1	1	1	can42	Examples	c42it7ip5_3512f	01	TCS2

Irradiation Constants	Laser power	40/36(a)	%1σ	40/36(c)	%1σ	38/36(a)	%1σ	38/36(c)	%1σ	39/37(ca)	%1σ	38/37(ca)	%1σ	36/37(ca)	%1σ	40/39(k)	%1σ	38/39(k)	%1σ	36/38(cl)	%1σ	K/Ca	%1σ	K/Cl	%1σ	Ca/Cl	%1σ
C47FB116	6.00 W	295.5	0.178	0.018	35	0.1869	0.107	1.493	3	0.000702	1.71	0.000196	4.08	0.0002702	0.15	0.00073	12.33	0.01215	0.27	262.8	0.65	0.51	0	0	0	0	0
C47FB117	8.00 W	295.5	0.178	0.018	35	0.1869	0.107	1.493	3	0.000702	1.71	0.000196	4.08	0.0002702	0.15	0.00073	12.33	0.01215	0.27	262.8	0.65	0.51	0	0	0	0	0
C47FB118	12.00 W	295.5	0.178	0.018	35	0.1869	0.107	1.493	3	0.000702	1.71	0.000196	4.08	0.0002702	0.15	0.00073	12.33	0.01215	0.27	262.8	0.65	0.51	0	0	0	0	0
C47FB119	20.00 W	295.5	0.178	0.018	35	0.1869	0.107	1.493	3	0.000702	1.71	0.000196	4.08	0.0002702	0.15	0.00073	12.33	0.01215	0.27	262.8	0.65	0.51	0	0	0	0	0
C47FB120	25.00 W	295.5	0.178	0.018	35	0.1869	0.107	1.493	3	0.000702	1.71	0.000196	4.08	0.0002702	0.15	0.00073	12.33	0.01215	0.27	262.8	0.65	0.51	0	0	0	0	0

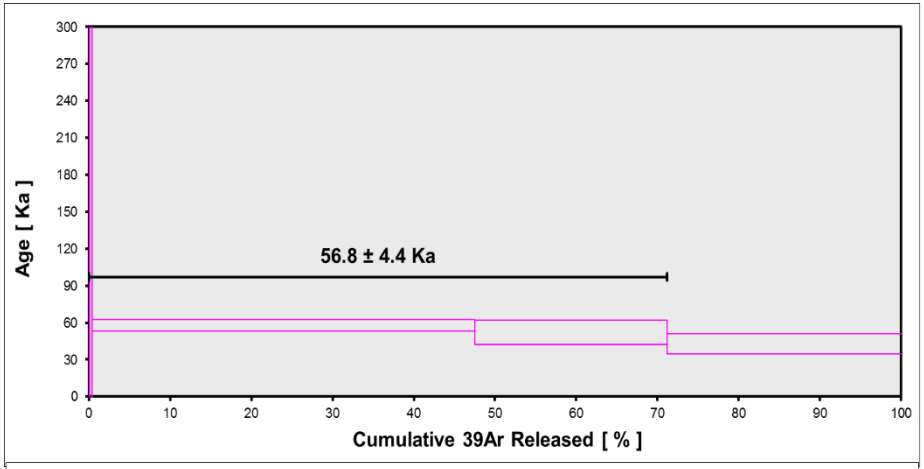

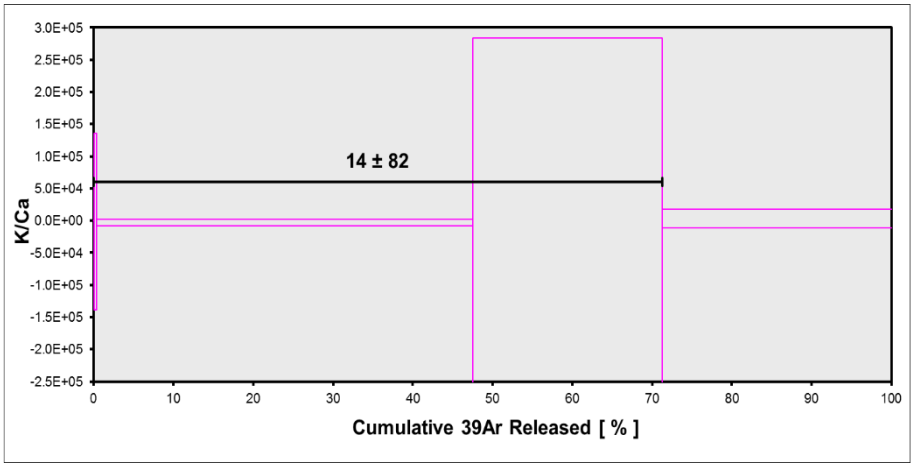

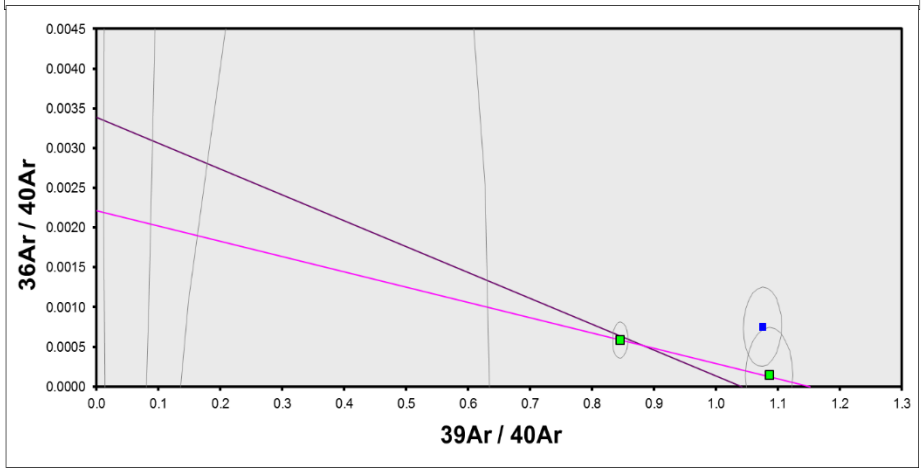

Information on Analysis and Constants Used in Calculations

Sample = M80/3 035ROV-12 (3512F)
Material = K-feldspar (1 crystal)
Location = Cadamosto Smt, Cape Verde
Analyst = Jan Sticklus
Project = EXAMPLES
Mass Discrimination Law = POW
Irradiation = can42
J = 0.00003280 ± 0.00000010
TCS2 = 27.870 ± 0.039 Ma
Heating = 45 sec
Instrument = MAP216
Weight = 4.968 mg (1 grain = 2.8 x 1.5 x 0.5 mm)

Age Equations = Conventional
Negative Intensities = Allowed
Decay Constant 40K = 5.543 ± 0.009 E-10 1/a
Decay Constant 39Ar = 2.940 ± 0.016 E-07 1/h
No 37Ar Decay Correction
Decay Constant 36Cl = 2.257 ± 0.015 E-06 1/a
Atmospheric Ratio 40/36(a) = 295.50 ± 0.53
Atmospheric Ratio 38/36(a) = 0.1869 ± 0.0002
Production Ratio 39/37(ca) = 0.000702 ± 0.000012
Production Ratio 38/37(ca) = 0.000196 ± 0.000008
Production Ratio 36/37(ca) = 0.000270 ± 0.000000
Production Ratio 40/39(k) = 0.000730 ± 0.000090
Production Ratio 38/39(k) = 0.012150 ± 0.000033
Production Ratio 36/38(cl) = 262.80
Scaling Ratio K/Ca = 0.510

Results	40(a)/36(a) ± 2σ	40(r)/39(k) ± 2σ	Age ± 2σ (Ka)	MSWD	39Ar(k) (%,n)	K/Ca ± 2σ
Age Plateau		0.95943 ± 0.07355 ± 7.67%	56.8 ± 4.4 ± 7.69%	1.01	71.22	14 ± 82
				39%	4	
		Minimal External Error ± 4.4		2.63	2σ Confidence Limit	
		Analytical Error ± 4.4		1.0047	Error Magnification	
Total Fusion Age		0.88670 ± 0.08944 ± 10.09%	52.5 ± 5.3 ± 10.11%		5	7804 ± 39840
		Minimal External Error ± 5.3				
		Analytical Error ± 5.3				
Normal Isochron	201.50 ± 298.90 ± 148.34%	0.91370 ± 0.11773 ± 12.88%	54.1 ± 7.0 ± 12.90%	6.08	71.22	
Error Chron				0%	4	
		Minimal External Error ± 7.0		3.00	2σ Confidence Limit	
		Analytical Error ± 7.0		2.4667	Error Magnification	
				1	Number of Iterations	
				0.0000067842	Convergence	
Inverse Isochron	452.19 ± 477.06 ± 105.50%	0.86802 ± 0.22787 ± 26.25%	51.4 ± 13.5 ± 26.26%	0.90	71.22	
				41%	4	
		Minimal External Error ± 13.5		3.00	2σ Confidence Limit	
		Analytical Error ± 13.5		1.0000	Error Magnification	
				5	Number of Iterations	
				0.0000197789	Convergence	
				89%	Spreading Factor	

[a] Blue dots in table indicate selected steps used to calculate the plateau and inverse isochron ages.
[b] Alteration Index values in italics indicate analyses from fresh material, normal font is from altered material (Baksi, 2007; van den Bogaard, 2013).
Values shown in red are negative values.
Abbreviations used in tables: (r) = radiogenic ^{40}Ar; (k) = Ar derived from K; (a) = atmospheric Ar; (ca) = Ar derived from Ca; (cl) = Ar derived from Cl; (c) = cosmogenic Ar; MDF = Mass Discrimination Factor.
Green squares in the inverse isochron plots indicate selected steps (blue dots in table), and blue squares are non-selected steps. Pink lines in the inverse isochron plot indicate a line fit through selected data, and the purple lines incidate a fit through an air $^{40}Ar/^{36}Ar$ ratio (295.5).

037DR-2 fine step-heating

Relative Abundance	Laser power	[a]	36Ar [V]	%1σ	37Ar [V]	%1σ	38Ar [V]	%1σ	39Ar [V]	%1σ	40Ar [V]	%1σ	40(r)/39(k) ± 2σ	Age ± 2σ (Ka)	40Ar(r) (%)	39Ar(k) (%)	K/Ca ± 2σ	Step #	$^{36}Ar/^{39}Ar$ Alt. Index[b]
C47GA021	1.50 W		0.0010084	3.542	0.0000770	22.717	0.0005685	4.427	0.0245604	0.819	0.4157476	0.416	4.79553 ± 0.87540	281.2 ± 51.3	28.33	3.76	163 ± 74	1	0.000098
C47GA022	4.00 W		0.0022348	1.356	0.0000672	26.284	0.0029405	0.889	0.2084602	0.221	1.2216327	0.081	2.69163 ± 0.08796	157.8 ± 5.2	45.93	31.93	1581 ± 831	2	*0.000026*
C47GA023	5.00 W		0.0000624	21.763	0.0000180	91.008	0.0000579	28.955	0.0043373	0.954	0.0207519	0.935	0.52888 ± 1.85413	31.0 ± 108.7	11.05	0.66	123 ± 223	3	*0.000034*
C47GA024	6.00 W		0.0002914	5.002	0.0000180	71.861	0.0012672	2.403	0.1075524	0.246	0.3890665	0.072	2.81616 ± 0.08148	165.1 ± 4.8	77.85	16.48	3045 ± 4377	4	*0.000006*
C47GA025	7.00 W	•	0.0001874	7.472	0.0000116	117.659	0.0016649	1.617	0.1410894	0.247	0.3751250	0.107	2.26560 ± 0.05999	132.8 ± 3.5	85.21	21.61	6181 ± 14544	5	*0.000003*
C47GA026	8.00 W	•	0.0000593	28.955	0.0000127	136.085	0.0002431	6.267	0.0222357	0.501	0.0598032	0.353	1.90101 ± 0.45697	111.5 ± 26.8	70.68	3.41	896 ± 2439	6	*0.000006*
C47GA027	9.00 W	•	0.0000548	24.872	0.0000161	85.724	0.0005224	4.015	0.0449442	0.338	0.1132153	0.236	2.15807 ± 0.18017	126.5 ± 10.6	85.67	6.88	1425 ± 2443	7	*0.000003*
C47GA028	10.00 W	•	0.0000040	369.140	0.0000039	427.800	0.0000838	24.233	0.0073781	0.550	0.0164708	1.148	2.07249 ± 1.17612	121.5 ± 69.0	92.84	1.13	958 ± 8196	8	*0.000001*
C47GA029	15.00 W		0.0001023	14.429	0.0000111	133.037	0.0009499	1.774	0.0812682	0.320	0.1986853	0.219	2.07219 ± 0.10866	121.5 ± 6.4	84.76	12.45	3737 ± 9944	9	*0.000003*
C47GA030	25.00 W		0.0000555	30.567	0.0000060	258.310	0.0001478	8.185	0.0109944	0.531	0.0358488	0.551	1.76909 ± 0.91241	103.7 ± 53.5	54.26	1.68	942 ± 4866	10	*0.000012*
		Σ	0.0040602	1.555	0.0000820	60.548	0.0084459	0.817	0.6528203	0.114	2.8463471	0.076							

Procedure Blanks	Laser power	36Ar [V]	1σ	37Ar [V]	1σ	38Ar [V]	1σ	39Ar [V]	1σ	40Ar [V]	1σ
C47GA021	1.50 W	0.0000839	0.0000111	0.0001482	0.0000118	0.0000612	0.0000097	0.0001424	0.0000200	0.0029186	0.0001818
C47GA022	4.00 W	0.0000855	0.0000111	0.0001476	0.0000118	0.0000597	0.0000097	0.0001380	0.0000200	0.0028943	0.0001818
C47GA023	5.00 W	0.0000870	0.0000111	0.0001469	0.0000118	0.0000583	0.0000097	0.0001336	0.0000200	0.0028699	0.0001818
C47GA024	6.00 W	0.0000886	0.0000111	0.0001463	0.0000118	0.0000569	0.0000097	0.0001292	0.0000200	0.0028455	0.0001818
C47GA025	7.00 W	0.0000901	0.0000111	0.0001457	0.0000118	0.0000555	0.0000097	0.0001249	0.0000200	0.0028220	0.0001818
C47GA026	8.00 W	0.0000927	0.0000111	0.0001446	0.0000118	0.0000532	0.0000097	0.0001176	0.0000200	0.0027816	0.0001818
C47GA027	9.00 W	0.0000943	0.0000111	0.0001440	0.0000118	0.0000517	0.0000097	0.0001132	0.0000200	0.0027573	0.0001818
C47GA028	10.00 W	0.0000958	0.0000111	0.0001433	0.0000118	0.0000503	0.0000097	0.0001088	0.0000200	0.0027329	0.0001818
C47GA029	15.00 W	0.0000974	0.0000111	0.0001427	0.0000118	0.0000489	0.0000097	0.0001044	0.0000200	0.0027085	0.0001818
C47GA030	25.00 W	0.0000989	0.0000111	0.0001421	0.0000118	0.0000475	0.0000097	0.0001000	0.0000200	0.0026841	0.0001818

Sample Parameters	Laser power	Sample	Material	Location	Analyst	Standard (in Ma)	%1σ	J	%1σ	MDF	%1σ	Volume Ratio	Sensitivity (mol/volt)	Day	Month	Year	Hour	Min	Resist	Irradiation	Project	Experiment	Nmb	Standard Name
C47GA021	1.50 W	M80/3 037DR-2 (0.25-0.5 mm; DR2ff)	K-feldspar	Cadamosto Smt, Cape Verde	Jan Sticklus	27.87	0.14	0.0000325	0.154	1.0098	0.21	1	1.211E-14	25	OCT	2018	22	19	1	can42	Examples	c42it13ip4_DR2ff	01	TCS2
C47GA022	4.00 W	M80/3 037DR-2 (0.25-0.5 mm; DR2ff)	K-feldspar	Cadamosto Smt, Cape Verde	Jan Sticklus	27.87	0.14	0.0000325	0.154	1.0098	0.21	1	1.211E-14	25	OCT	2018	22	48	1	can42	Examples	c42it13ip4_DR2ff	01	TCS2
C47GA023	5.00 W	M80/3 037DR-2 (0.25-0.5 mm; DR2ff)	K-feldspar	Cadamosto Smt, Cape Verde	Jan Sticklus	27.87	0.14	0.0000325	0.154	1.0098	0.21	1	1.211E-14	25	OCT	2018	23	17	1	can42	Examples	c42it13ip4_DR2ff	01	TCS2
C47GA024	6.00 W	M80/3 037DR-2 (0.25-0.5 mm; DR2ff)	K-feldspar	Cadamosto Smt, Cape Verde	Jan Sticklus	27.87	0.14	0.0000325	0.154	1.0098	0.21	1	1.211E-14	25	OCT	2018	23	46	1	can42	Examples	c42it13ip4_DR2ff	01	TCS2
C47GA025	7.00 W	M80/3 037DR-2 (0.25-0.5 mm; DR2ff)	K-feldspar	Cadamosto Smt, Cape Verde	Jan Sticklus	27.87	0.14	0.0000325	0.154	1.0098	0.21	1	1.211E-14	26	OCT	2018	0	14	1	can42	Examples	c42it13ip4_DR2ff	01	TCS2
C47GA026	8.00 W	M80/3 037DR-2 (0.25-0.5 mm; DR2ff)	K-feldspar	Cadamosto Smt, Cape Verde	Jan Sticklus	27.87	0.14	0.0000325	0.154	1.0098	0.21	1	1.211E-14	26	OCT	2018	1	2	1	can42	Examples	c42it13ip4_DR2ff	01	TCS2
C47GA027	9.00 W	M80/3 037DR-2 (0.25-0.5 mm; DR2ff)	K-feldspar	Cadamosto Smt, Cape Verde	Jan Sticklus	27.87	0.14	0.0000325	0.154	1.0098	0.21	1	1.211E-14	26	OCT	2018	1	31	1	can42	Examples	c42it13ip4_DR2ff	01	TCS2
C47GA028	10.00 W	M80/3 037DR-2 (0.25-0.5 mm; DR2ff)	K-feldspar	Cadamosto Smt, Cape Verde	Jan Sticklus	27.87	0.14	0.0000325	0.154	1.0098	0.21	1	1.211E-14	26	OCT	2018	2	0	1	can42	Examples	c42it13ip4_DR2ff	01	TCS2
C47GA029	15.00 W	M80/3 037DR-2 (0.25-0.5 mm; DR2ff)	K-feldspar	Cadamosto Smt, Cape Verde	Jan Sticklus	27.87	0.14	0.0000325	0.154	1.0098	0.21	1	1.211E-14	26	OCT	2018	2	29	1	can42	Examples	c42it13ip4_DR2ff	01	TCS2
C47GA030	25.00 W	M80/3 037DR-2 (0.25-0.5 mm; DR2ff)	K-feldspar	Cadamosto Smt, Cape Verde	Jan Sticklus	27.87	0.14	0.0000325	0.154	1.0098	0.21	1	1.211E-14	26	OCT	2018	2	58	1	can42	Examples	c42it13ip4_DR2ff	01	TCS2

Irradiation Constants	Laser power	40/36(a)	%1σ	40/36(c)	%1σ	38/36(a)	%1σ	38/36(c)	%1σ	39/37(ca)	%1σ	38/37(ca)	%1σ	36/37(ca)	%1σ	40/39(k)	%1σ	38/39(k)	%1σ	36/38(cl)	%1σ	K/Ca	%1σ	K/Cl	%1σ	Ca/Cl	%1σ
C47GA021	1.50 W	295.5	0.178	0.018	35	0.1869	0.107	1.493	3	0.000702	1.71	0.000196	4.08	0.0002702	0.15	0.00073	12.33	0.01215	0.27	262.8	0.65	0.51	0	0	0	0	0
C47GA022	4.00 W	295.5	0.178	0.018	35	0.1869	0.107	1.493	3	0.000702	1.71	0.000196	4.08	0.0002702	0.15	0.00073	12.33	0.01215	0.27	262.8	0.65	0.51	0	0	0	0	0
C47GA023	5.00 W	295.5	0.178	0.018	35	0.1869	0.107	1.493	3	0.000702	1.71	0.000196	4.08	0.0002702	0.15	0.00073	12.33	0.01215	0.27	262.8	0.65	0.51	0	0	0	0	0
C47GA024	6.00 W	295.5	0.178	0.018	35	0.1869	0.107	1.493	3	0.000702	1.71	0.000196	4.08	0.0002702	0.15	0.00073	12.33	0.01215	0.27	262.8	0.65	0.51	0	0	0	0	0
C47GA025	7.00 W	295.5	0.178	0.018	35	0.1869	0.107	1.493	3	0.000702	1.71	0.000196	4.08	0.0002702	0.15	0.00073	12.33	0.01215	0.27	262.8	0.65	0.51	0	0	0	0	0
C47GA026	8.00 W	295.5	0.178	0.018	35	0.1869	0.107	1.493	3	0.000702	1.71	0.000196	4.08	0.0002702	0.15	0.00073	12.33	0.01215	0.27	262.8	0.65	0.51	0	0	0	0	0
C47GA027	9.00 W	295.5	0.178	0.018	35	0.1869	0.107	1.493	3	0.000702	1.71	0.000196	4.08	0.0002702	0.15	0.00073	12.33	0.01215	0.27	262.8	0.65	0.51	0	0	0	0	0
C47GA028	10.00 W	295.5	0.178	0.018	35	0.1869	0.107	1.493	3	0.000702	1.71	0.000196	4.08	0.0002702	0.15	0.00073	12.33	0.01215	0.27	262.8	0.65	0.51	0	0	0	0	0
C47GA029	15.00 W	295.5	0.178	0.018	35	0.1869	0.107	1.493	3	0.000702	1.71	0.000196	4.08	0.0002702	0.15	0.00073	12.33	0.01215	0.27	262.8	0.65	0.51	0	0	0	0	0
C47GA030	25.00 W	295.5	0.178	0.018	35	0.1869	0.107	1.493	3	0.000702	1.71	0.000196	4.08	0.0002702	0.15	0.00073	12.33	0.01215	0.27	262.8	0.65	0.51	0	0	0	0	0

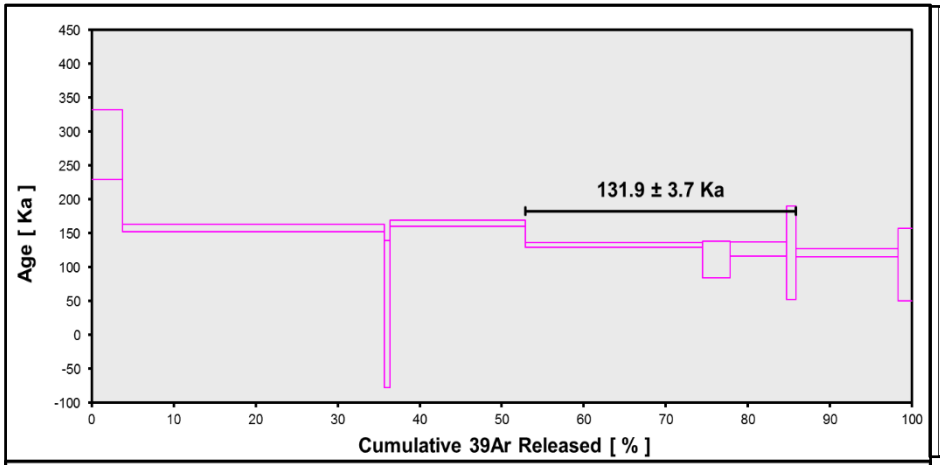
Age [Ka]
131.9 ± 3.7 Ka
Cumulative 39Ar Released [%]

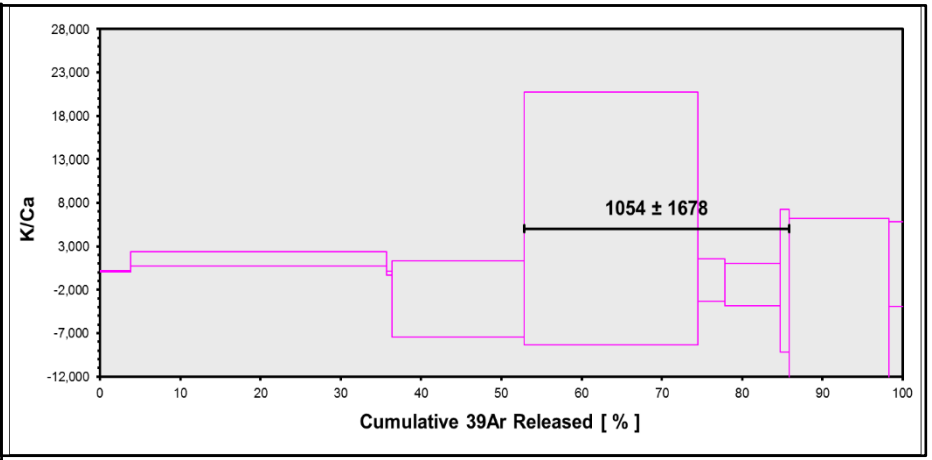
K/Ca
1054 ± 1678
Cumulative 39Ar Released [%]

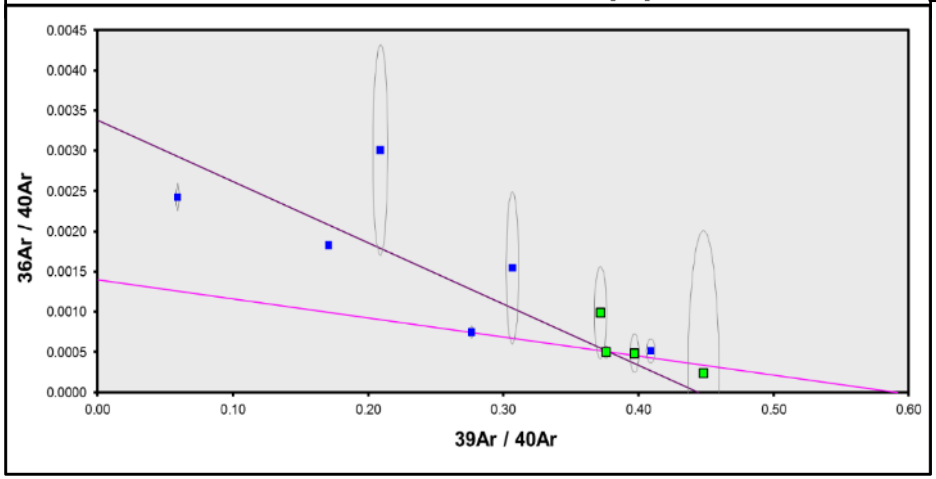
36Ar / 40Ar
39Ar / 40Ar

Information on Analysis and Constants Used in Calculations

Sample = M80/3 037DR-2 (DR2FF)
Material = K-feldspar
Location = Cadamosto Smt, Cape Verde
Analyst = Jan Sticklus
Project = EXAMPLES
Mass Discrimination Law = POW
Irradiation = can42
J = 0.00003250 ± 0.00000005
TCS2 = 27.870 ± 0.039 Ma
Heating = 45 sec
Instrument = MAP216
Weight = 10.575 mg

Age Equations = Conventional
Negative Intensities = Allowed
Decay Constant 40K = 5.543 ± 0.009 E-10 1/a
Decay Constant 39Ar = 2.940 ± 0.016 E-07 1/h
No 37Ar Decay Correction
Decay Constant 36Cl = 2.257 ± 0.015 E-06 1/a
Atmospheric Ratio 40/36(a) = 295.50 ± 0.53
Atmospheric Ratio 38/36(a) = 0.1869 ± 0.0002
Production Ratio 39/37(ca) = 0.000702 ± 0.000012
Production Ratio 38/37(ca) = 0.000196 ± 0.000008
Production Ratio 36/37(ca) = 0.000270 ± 0.000000
Production Ratio 40/39(k) = 0.000730 ± 0.000090
Production Ratio 38/39(k) = 0.012150 ± 0.000033
Production Ratio 36/38(cl) = 262.80
Scaling Ratio K/Ca = 0.510

Results	40(a)/36(a) ± 2σ	40(r)/39(k) ± 2σ	Age ± 2σ (Ka)	MSWD	39Ar(k) (%,n)	K/Ca ± 2σ
Age Plateau		2.24906 ± 0.06295 ± 2.80%	131.9 ± 3.7 ± 2.82%	1.25	33.03	1054 ± 1678
				29%	4	
		Minimal External Error ± 3.7		2.63	2σ Confidence Limit	
		Analytical Error ± 3.7		1.1158	Error Magnification	
Total Fusion Age		2.52155 ± 0.05797 ± 2.30%	147.8 ± 3.4 ± 2.32%		10	4060 ± 4917
		Minimal External Error ± 3.5				
		Analytical Error ± 3.4				
Normal Isochron	377.37 ± 501.30 ± 132.84%	2.09982 ± 0.70563 ± 33.60%	123.1 ± 41.4 ± 33.60%	3.98	33.03	
No Convergence				2%	4	
		Minimal External Error ± 41.4		3.00	2σ Confidence Limit	
		Analytical Error ± 41.4		1.9943	Error Magnification	
				100	Number of Iterations	
				0.0000976702	Convergence	
Inverse Isochron	713.72 ± 2479.91 ± 347.46%	1.69097 ± 0.84138 ± 49.76%	99.1 ± 49.3 ± 49.76%	1.41	33.03	
				24%	4	
		Minimal External Error ± 49.3		3.00	2σ Confidence Limit	
		Analytical Error ± 49.3		1.1875	Error Magnification	
				4	Number of Iterations	
				0.0025086480	Convergence	
				13%	Spreading Factor	

[a] Blue dots in table indicate selected steps used to calculate the weighted mean and inverse isochron ages.
[b] Alteration Index values in italics indicate analyses from fresh material, normal font is from altered material (Baksi, 2007; van den Bogaard, 2013).
Values shown in red are negative values.
Abbreviations used in tables: (r) = radiogenic ^{40}Ar; (k) = Ar derived from K; (a) = atmospheric Ar; (ca) = Ar derived from Ca; (cl) = Ar derived from Ca; (c) = cosmogenic Ar; MDF = Mass Discrimination Factor.
Green squares in the inverse isochron plots indicate selected steps (blue dots in table), and blue squares are non-selected steps. Pink lines in the inverse isochron plot indicate a line fit through selected data, and the purple lines incidate a fit through an air $^{40}Ar/^{36}Ar$ ratio (295.5).

037DR-2 coarse step-heating

Relative Abundance	Laser power	[a]	36Ar [V]	%1σ	37Ar [V]	%1σ	38Ar [V]	%1σ	39Ar [V]	%1σ	40Ar [V]	%1σ	40(r)/39(k) ± 2σ	Age ± 2σ (Ka)	40Ar(r) (%)	39Ar(k) (%)	K/Ca ± 2σ	Step #	$^{36}Ar/^{39}Ar$ Alt. Index[b]
C47GA011	1.50 W		0.0013019	2.073	0.0000127	129.804	0.0002995	5.837	0.0043212	1.226	0.4069045	0.118	5.13833 ± 3.71331	301.2 ± 217.7	5.46	0.66	173 ± 449	1	0.000714
C47GA012	4.00 W		0.0016833	1.625	0.0000829	26.520	0.0010033	1.983	0.0554224	0.502	0.6515288	0.163	2.78037 ± 0.29730	163.0 ± 17.4	23.65	8.47	341 ± 181	2	0.000072
C47GA013	5.00 W	•	0.0001296	17.497	0.0000217	71.041	0.0004763	3.885	0.0410444	0.329	0.1362186	0.242	2.38508 ± 0.32730	139.8 ± 19.2	71.87	6.27	966 ± 1373	3	*0.000007*
C47GA014	6.00 W	•	0.0000519	34.055	0.0000063	265.837	0.0002568	6.641	0.0185084	0.374	0.0548453	0.553	2.13485 ± 0.56518	125.2 ± 33.1	72.04	2.83	1489 ± 7915	4	*0.000007*
C47GA015	7.00 W	•	0.0004758	4.771	0.0000078	203.695	0.0015541	2.091	0.1280448	0.244	0.4239581	0.113	2.21218 ± 0.10567	129.7 ± 6.2	66.81	19.57	8376 ± 34124	5	*0.000009*
C47GA016	8.00 W	•	0.0000156	125.620	0.0000025	613.119	0.0001179	12.541	0.0106842	0.453	0.0383668	0.767	3.15749 ± 1.08898	185.1 ± 63.8	87.93	1.63	2199 ± 26964	6	*0.000003*
C47GA017	9.00 W	•	0.0000266	73.559	0.0000287	55.060	0.0002168	6.099	0.0202680	0.364	0.0531855	0.566	2.23576 ± 0.57108	131.1 ± 33.5	85.20	3.10	360 ± 396	7	*0.000003*
C47GA018	10.00 W	•	0.0000125	161.281	0.0000184	98.384	0.0000476	30.947	0.0063024	1.204	0.0155998	1.865	1.89009 ± 1.88710	110.8 ± 110.6	76.36	0.96	175 ± 344	8	*0.000005*
C47GA019	15.00 W	•	0.0020648	1.635	0.0000014	1286.014	0.0043570	1.188	0.3456744	0.226	1.3468116	0.050	2.13033 ± 0.05897	124.9 ± 3.5	54.68	52.82	121697 ± 3130081	9	*0.000014*
C47GA020	25.00 W		0.0001224	17.983	0.0000115	147.596	0.0002707	7.479	0.0241660	0.389	0.0800342	0.419	1.81411 ± 0.53934	106.4 ± 31.6	54.78	3.69	1069 ± 3156	10	*0.000012*
		Σ	0.0058844	1.273	0.0000591	92.267	0.0086002	0.907	0.6544362	0.139	3.2074533	0.051							

Procedure Blanks	Laser power	36Ar [V]	1σ	37Ar [V]	1σ	38Ar [V]	1σ	39Ar [V]	1σ	40Ar [V]	1σ
C47GA011	1.50 W	0.0000977	0.0000175	0.0001260	0.0000134	0.0000388	0.0000099	0.0002479	0.0000269	0.0025349	0.0002722
C47GA012	4.00 W	0.0000973	0.0000175	0.0001283	0.0000134	0.0000416	0.0000099	0.0002364	0.0000269	0.0025900	0.0002722
C47GA013	5.00 W	0.0000969	0.0000175	0.0001307	0.0000134	0.0000444	0.0000099	0.0002250	0.0000269	0.0026450	0.0002722
C47GA014	6.00 W	0.0000965	0.0000175	0.0001330	0.0000134	0.0000472	0.0000099	0.0002135	0.0000269	0.0027001	0.0002722
C47GA015	7.00 W	0.0000961	0.0000175	0.0001353	0.0000134	0.0000500	0.0000099	0.0002021	0.0000269	0.0027552	0.0002722
C47GA016	8.00 W	0.0000954	0.0000175	0.0001391	0.0000134	0.0000545	0.0000099	0.0001835	0.0000269	0.0028445	0.0002722
C47GA017	9.00 W	0.0000950	0.0000175	0.0001414	0.0000134	0.0000573	0.0000099	0.0001720	0.0000269	0.0028995	0.0002722
C47GA018	10.00 W	0.0000946	0.0000175	0.0001438	0.0000134	0.0000601	0.0000099	0.0001605	0.0000269	0.0029546	0.0002722
C47GA019	15.00 W	0.0000942	0.0000175	0.0001461	0.0000134	0.0000629	0.0000099	0.0001491	0.0000269	0.0030097	0.0002722
C47GA020	25.00 W	0.0000938	0.0000175	0.0001484	0.0000134	0.0000657	0.0000099	0.0001376	0.0000269	0.0030648	0.0002722

Sample Parameter	Laser power	Sample	Material	Location	Analyst	Standard (in Ma)	%1σ	J	%1σ	MDF	%1σ	Volume Ratio	Sensitivity (mol/volt)	Day	Month	Year	Hour	Min	Resist	Irradiation	Project	Experiment	Nmb	Standard Name
C47GA011	1.50 W	M80/3 037DR-2 (0.5-1 mm; DR2fc)	K-feldspar	Cadamosto Smt, Cape Verde	Jan Sticklus	27.87	0.14	0.0000325	0.154	1.0098	0.21	1	1.211E-14	25	OCT	2018	16	52	1	can42	Examples	c42it13ip2_DR2fc	01	TCS2
C47GA012	4.00 W	M80/3 037DR-2 (0.5-1 mm; DR2fc)	K-feldspar	Cadamosto Smt, Cape Verde	Jan Sticklus	27.87	0.14	0.0000325	0.154	1.0098	0.21	1	1.211E-14	25	OCT	2018	17	21	1	can42	Examples	c42it13ip2_DR2fc	01	TCS2
C47GA013	5.00 W	M80/3 037DR-2 (0.5-1 mm; DR2fc)	K-feldspar	Cadamosto Smt, Cape Verde	Jan Sticklus	27.87	0.14	0.0000325	0.154	1.0098	0.21	1	1.211E-14	25	OCT	2018	17	50	1	can42	Examples	c42it13ip2_DR2fc	01	TCS2
C47GA014	6.00 W	M80/3 037DR-2 (0.5-1 mm; DR2fc)	K-feldspar	Cadamosto Smt, Cape Verde	Jan Sticklus	27.87	0.14	0.0000325	0.154	1.0098	0.21	1	1.211E-14	25	OCT	2018	18	19	1	can42	Examples	c42it13ip2_DR2fc	01	TCS2
C47GA015	7.00 W	M80/3 037DR-2 (0.5-1 mm; DR2fc)	K-feldspar	Cadamosto Smt, Cape Verde	Jan Sticklus	27.87	0.14	0.0000325	0.154	1.0098	0.21	1	1.211E-14	25	OCT	2018	18	48	1	can42	Examples	c42it13ip2_DR2fc	01	TCS2
C47GA016	8.00 W	M80/3 037DR-2 (0.5-1 mm; DR2fc)	K-feldspar	Cadamosto Smt, Cape Verde	Jan Sticklus	27.87	0.14	0.0000325	0.154	1.0098	0.21	1	1.211E-14	25	OCT	2018	19	35	1	can42	Examples	c42it13ip2_DR2fc	01	TCS2
C47GA017	9.00 W	M80/3 037DR-2 (0.5-1 mm; DR2fc)	K-feldspar	Cadamosto Smt, Cape Verde	Jan Sticklus	27.87	0.14	0.0000325	0.154	1.0098	0.21	1	1.211E-14	25	OCT	2018	20	4	1	can42	Examples	c42it13ip2_DR2fc	01	TCS2
C47GA018	10.00 W	M80/3 037DR-2 (0.5-1 mm; DR2fc)	K-feldspar	Cadamosto Smt, Cape Verde	Jan Sticklus	27.87	0.14	0.0000325	0.154	1.0098	0.21	1	1.211E-14	25	OCT	2018	20	33	1	can42	Examples	c42it13ip2_DR2fc	01	TCS2
C47GA019	15.00 W	M80/3 037DR-2 (0.5-1 mm; DR2fc)	K-feldspar	Cadamosto Smt, Cape Verde	Jan Sticklus	27.87	0.14	0.0000325	0.154	1.0098	0.21	1	1.211E-14	25	OCT	2018	21	2	1	can42	Examples	c42it13ip2_DR2fc	01	TCS2
C47GA020	25.00 W	M80/3 037DR-2 (0.5-1 mm; DR2fc)	K-feldspar	Cadamosto Smt, Cape Verde	Jan Sticklus	27.87	0.14	0.0000325	0.154	1.0098	0.21	1	1.211E-14	25	OCT	2018	21	31	1	can42	Examples	c42it13ip2_DR2fc	01	TCS2

Irradiation Constants	Laser power	40/36(a)	%1σ	40/36(c)	%1σ	38/36(a)	%1σ	38/36(c)	%1σ	39/37(ca)	%1σ	38/37(ca)	%1σ	36/37(ca)	%1σ	40/39(k)	%1σ	38/39(k)	%1σ	36/38(cl)	%1σ	K/Ca	%1σ	K/Cl	%1σ	Ca/Cl	%1σ
C47GA011	1.50 W	295.5	0.178	0.018	35	0.1869	0.107	1.493	3	0.000702	1.71	0.000196	4.08	0.0002702	0.15	0.00073	12.33	0.01215	0.27	262.8	0.65	0.51	0	0	0	0	0
C47GA012	4.00 W	295.5	0.178	0.018	35	0.1869	0.107	1.493	3	0.000702	1.71	0.000196	4.08	0.0002702	0.15	0.00073	12.33	0.01215	0.27	262.8	0.65	0.51	0	0	0	0	0
C47GA013	5.00 W	295.5	0.178	0.018	35	0.1869	0.107	1.493	3	0.000702	1.71	0.000196	4.08	0.0002702	0.15	0.00073	12.33	0.01215	0.27	262.8	0.65	0.51	0	0	0	0	0
C47GA014	6.00 W	295.5	0.178	0.018	35	0.1869	0.107	1.493	3	0.000702	1.71	0.000196	4.08	0.0002702	0.15	0.00073	12.33	0.01215	0.27	262.8	0.65	0.51	0	0	0	0	0
C47GA015	7.00 W	295.5	0.178	0.018	35	0.1869	0.107	1.493	3	0.000702	1.71	0.000196	4.08	0.0002702	0.15	0.00073	12.33	0.01215	0.27	262.8	0.65	0.51	0	0	0	0	0
C47GA016	8.00 W	295.5	0.178	0.018	35	0.1869	0.107	1.493	3	0.000702	1.71	0.000196	4.08	0.0002702	0.15	0.00073	12.33	0.01215	0.27	262.8	0.65	0.51	0	0	0	0	0
C47GA017	9.00 W	295.5	0.178	0.018	35	0.1869	0.107	1.493	3	0.000702	1.71	0.000196	4.08	0.0002702	0.15	0.00073	12.33	0.01215	0.27	262.8	0.65	0.51	0	0	0	0	0
C47GA018	10.00 W	295.5	0.178	0.018	35	0.1869	0.107	1.493	3	0.000702	1.71	0.000196	4.08	0.0002702	0.15	0.00073	12.33	0.01215	0.27	262.8	0.65	0.51	0	0	0	0	0
C47GA019	15.00 W	295.5	0.178	0.018	35	0.1869	0.107	1.493	3	0.000702	1.71	0.000196	4.08	0.0002702	0.15	0.00073	12.33	0.01215	0.27	262.8	0.65	0.51	0	0	0	0	0
C47GA020	25.00 W	295.5	0.178	0.018	35	0.1869	0.107	1.493	3	0.000702	1.71	0.000196	4.08	0.0002702	0.15	0.00073	12.33	0.01215	0.27	262.8	0.65	0.51	0	0	0	0	0

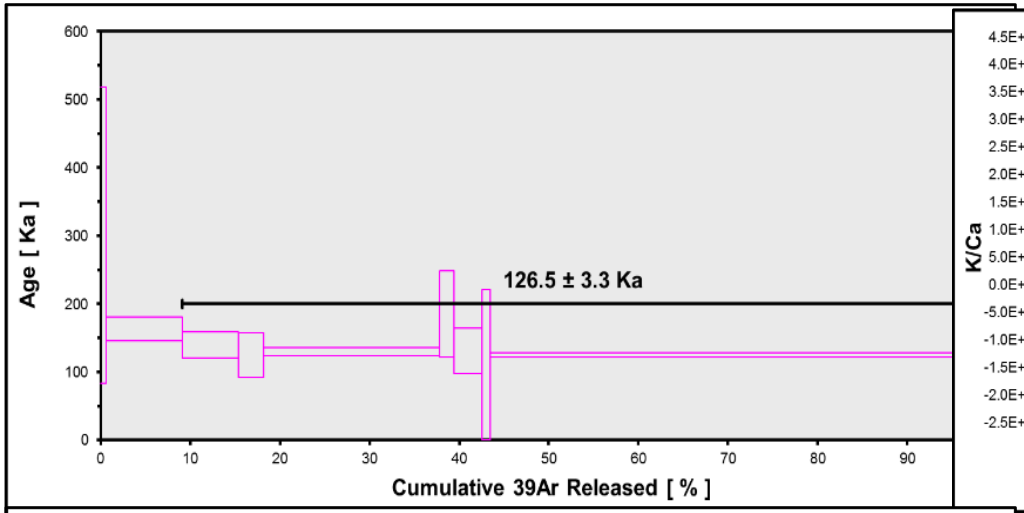
Age [Ka]
600
500
400
300
200
100
0
126.5 ± 3.3 Ka
0
10
20
30
40
50
60
70
80
90
Cumulative 39Ar Released [%]

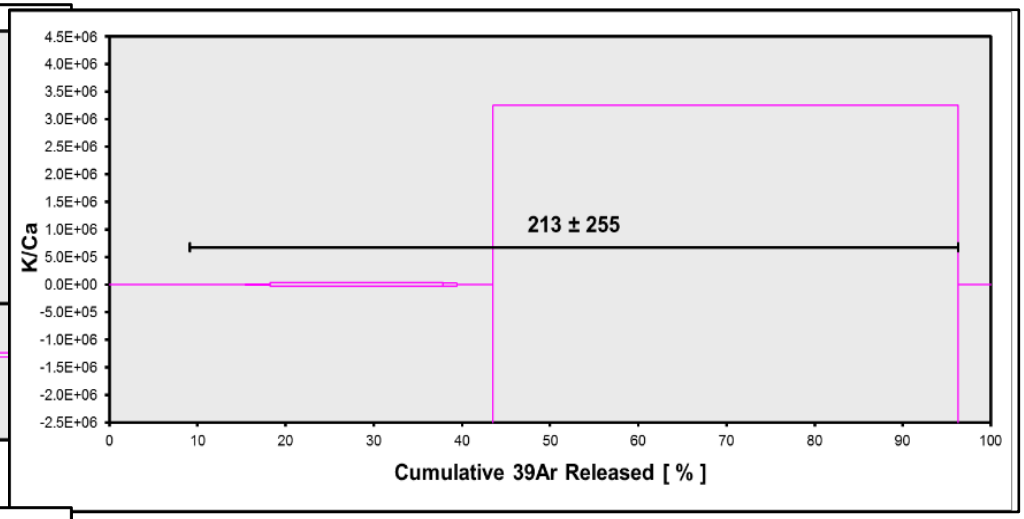
K/Ca
4.5E+06
4.0E+06
3.5E+06
3.0E+06
2.5E+06
2.0E+06
1.5E+06
1.0E+06
5.0E+05
0.0E+00
-5.0E+05
-1.0E+06
-1.5E+06
-2.0E+06
-2.5E+06
213 ± 255
0
10
20
30
40
50
60
70
80
90
100
Cumulative 39Ar Released [%]

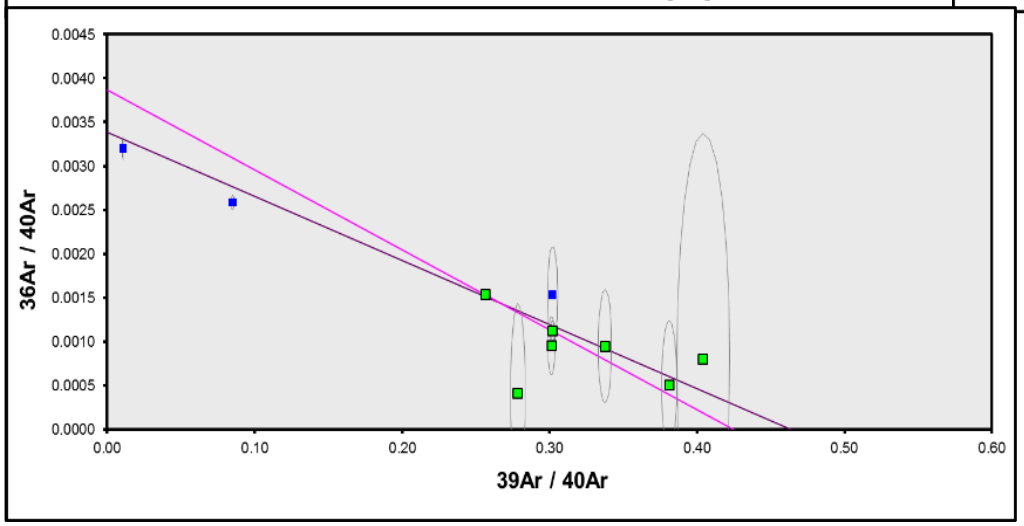
36Ar / 40Ar
0.0045
0.0040
0.0035
0.0030
0.0025
0.0020
0.0015
0.0010
0.0005
0.0000
0.00
0.10
0.20
0.30
0.40
0.50
0.60
39Ar / 40Ar

Information on Analysis and Constants Used in Calculations

Sample = M80/3 037DR-2 (DR2FC)
Material = K-feldspar
Location = Cadamosto Smt, Cape Verde
Analyst = Jan Sticklus
Project = EXAMPLES
Mass Discrimination Law = POW
Irradiation = can42
J = 0.00003250 ± 0.00000005
TCS2 = 27.870 ± 0.039 Ma
Heating = 45 sec
Instrument = MAP216
Weight = 10.583 mg

Age Equations = Conventional
Negative Intensities = Allowed
Decay Constant 40K = 5.543 ± 0.009 E-10 1/a
Decay Constant 39Ar = 2.940 ± 0.016 E-07 1/h
No 37Ar Decay Correction
Decay Constant 36Cl = 2.257 ± 0.015 E-06 1/a
Atmospheric Ratio 40/36(a) = 295.50 ± 0.53
Atmospheric Ratio 38/36(a) = 0.1869 ± 0.0002
Production Ratio 39/37(ca) = 0.000702 ± 0.000012
Production Ratio 38/37(ca) = 0.000196 ± 0.000008
Production Ratio 36/37(ca) = 0.000270 ± 0.000000
Production Ratio 40/39(k) = 0.000730 ± 0.000090
Production Ratio 38/39(k) = 0.012150 ± 0.000033
Production Ratio 36/38(cl) = 262.80
Scaling Ratio K/Ca = 0.510

Results

Results	40(a)/36(a) ± 2σ		40(r)/39(k) ± 2σ		Age ± 2σ (Ka)		MSWD	39Ar(k) (%,n)	K/Ca ± 2σ
Age Plateau			2.15787	± 0.05592	126.5	± 3.3	1.23	87.18	213 ± 255
				± 2.59%		± 2.61%	29%	7	
				Minimal External Error		± 3.3	2.15	2σ Confidence Limit	
				Analytical Error		± 3.3	1.1097	Error Magnification	
Total Fusion Age			2.24340	± 0.06831	131.5	± 4.0		10	5647 ± 10421
				± 3.04%		± 3.06%			
				Minimal External Error		± 4.0			
				Analytical Error		± 4.0			
Normal Isochron	187.77	± 76.68	2.72578	± 0.39262	159.8	± 23.0	11.22	87.18	
Error Chron		± 40.84%		± 14.40%		± 14.41%	0%	7	
				Minimal External Error		± 23.0	2.26	2σ Confidence Limit	
				Analytical Error		± 23.0	3.3492	Error Magnification	
							34	Number of Iterations	
							0.0000263811	Convergence	
Inverse Isochron	258.61	± 40.55	2.35414	± 0.21248	138.0	± 12.5	0.97	87.18	
		± 15.68%		± 9.03%		± 9.03%	43%	7	
				Minimal External Error		± 12.5	2.26	2σ Confidence Limit	
				Analytical Error		± 12.5	1.0000	Error Magnification	
							3	Number of Iterations	
							0.0001550396	Convergence	
							35%	Spreading Factor	

[a] Blue dots in table indicate selected steps used to calculate the plateau and inverse isochron ages.

[b] Alteration Index values in italics indicate analyses from fresh material, normal font is from altered material (Baksi, 2007; van den Bogaard, 2013).

Values shown in red are negative values.

Abbreviations used in tables: (r) = radiogenic ^{40}Ar; (k) = Ar derived from K; (a) = atmospheric Ar; (ca) = Ar derived from Ca; (cl) = Ar derived from Ca; (c) = cosmogenic Ar; MDF = Mass Discrimination Factor.

Green squares in the inverse isochron plots indicate selected steps (blue dots in table), and blue squares are non-selected steps. Pink lines in the inverse isochron plot indicate a line fit through selected data, and the purple lines incidate a fit through an air $^{40}Ar/^{36}Ar$ ratio (295.5).

9.2.4 *Appendix D – $^{40}Ar^*$ diffusive loss and ^{40}Ar-^{39}Ar reset age modelling based on minimum, maximum, and average crystal rim growth measurements from Cadamosto Seamount sanidine samples 035ROV-12 and 037DR-2*

Total overgrowth phenocrystic rim thickness

Sample	Estimated grain diameter (mm)	Min.-max. rim thickness (mm)	Magma residence duration (days)	% $^{40}Ar^*$ loss[a]	Antecryst age (ka)	Eruption age (ka)	Modeled reset age (ka)[b]
035ROV-12	5	0.005	48	18	611.9	51.8	511
035ROV-12	5	1.64	15.799	100	611.9	51.8	52
037DR-2	4	0.025	241	46	349.0	97.2	234
037DR-2	4	0.96	9.259	100	349.0	97.2	97

Final overgrowth phenocrystic rim thickness

Sample	Estimated grain diameter (mm)	Min.-max. rim thickness (mm)	Magma residence duration (days)	% $^{40}Ar^*$ loss[a]	Antecryst age (ka)	Eruption age (ka)	Modeled reset age (ka)[b]
035ROV-12	5	0.005	48	18	611.9	51.8	511
035ROV-12	5	0.02	193	34	611.9	51.8	420
037DR-2	4	0.025	241	46	349.0	97.2	234
037DR-2	4	0.085	820	73	349.0	97.2	166

[a]Using Benson Mines orthoclase Ar diffusion parameters (Cassata and Renne, 2013).

[b]Modelled reset ages calculated using $^{40}Ar^*$ losses for the oldest SCTF ages: 035ROV-12 = 611.9 ± 8.8 ka, and 037DR-2 = 349.0 ± 20.4 ka.

9.3 Appendices and supplementary data to Chapter 3

The data was published with the article (Samrock et al. 2022). The material is available online at https://doi.org/10.1007/s00531-022-02160-x.

9.3.1 Appendix A: Sample descriptions

Sample 17-16/3: Lat/Long: 15.200262, -23.123276

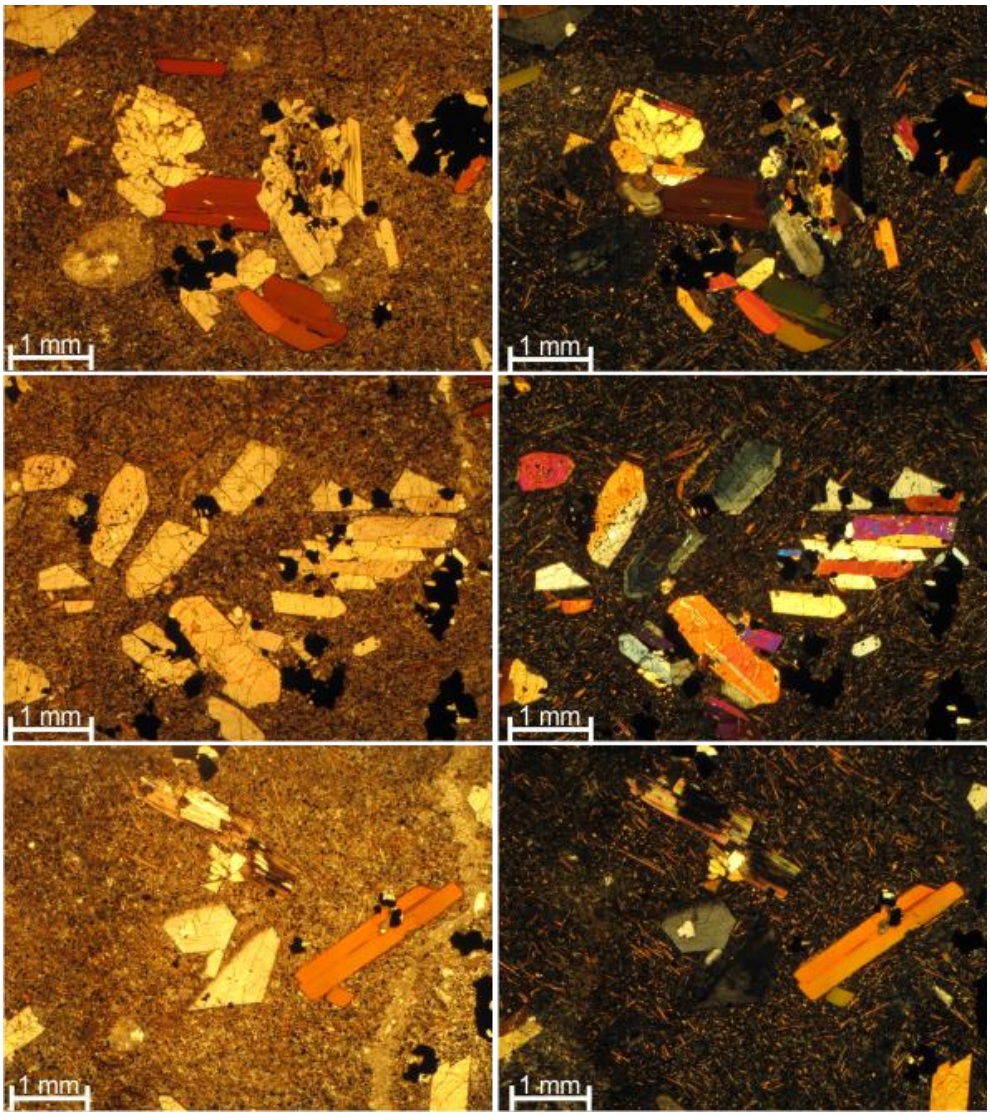

Sample 17-16/3 was collected from a dyke that intruded the Morro Formation limestones on the SW flank of Mte Branco. This nosean-nephelinite sample is fresh and glassy and contains macrocrysts of clinopyroxene, phlogopite and Fe-Ti oxides, and to lesser extents nepheline, nosean and apatite. Crystals make up ~30% of the rock volume and are up to 3 mm in size. Crystals are idiomorphic to hypidiomorphic, and some crystals form glomerocrysts. Clinopyroxenes are optically zoned and contain mineral inclusions (biotite, Fe-Ti oxides and feldspathoids). The glassy groundmass comprises abundant phlogopite microphenocrysts. Veins are unfilled. The images shown above are thin section photographs in plain (left) and crossed (right) polarized light.

Sample 17-73: Lat/Long:15.202839, -23.117849

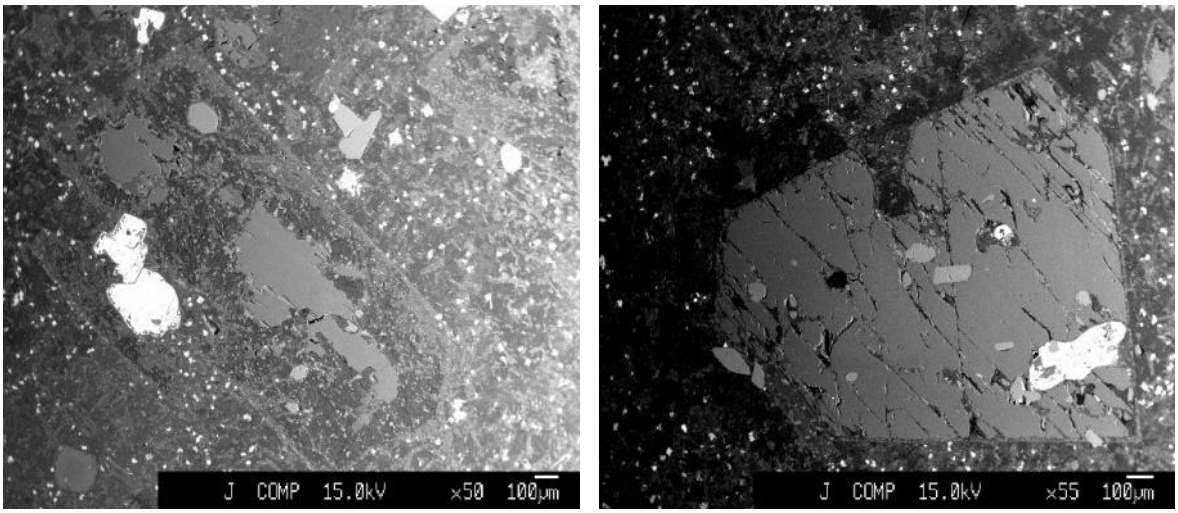

This sample is a nephelinite dyke that intruded the Batalha Formation pillow lavas below the Mte Branco Thrust. The sample is moderately altered, and comprises partly fresh phlogopite and clinopyroxene and lesser amphibole and Fe-Ti oxides as macrocrysts (macrocrysts ca. 7%), and minor nephelinie and titanite. Crystals are up to 2 mm in size, and are idiomorphic to xenomorphic in shape. Clinopyroxenes are mainly replaced by zeolite and chlorite, and form pseudomorphs that only preserve former clinopyroxene cores (see left Secondary Electron Microscope – Backscattered Electron (SEM-BSE) image above). Biotite crystals are often skeletal and contain inclusions (feldspathoids, Fe-Ti oxides, titanite and apatite; see right SEM-BSE image above). The sample further contains several sizeable, rounded and polymineralic glomerocrysts, which comprise minerals optically similar to the macrocryst minerals. Glomercryst minerals comprise phlogopite, amphibole, clinopyroxene, titanite, Fe-Ti oxides and trace apatite. The groundmass comprises calcium carbonate fillings in vesicles and minor cracks.

Sample 17-74: Lat/Long: 15.203719, -23.118145

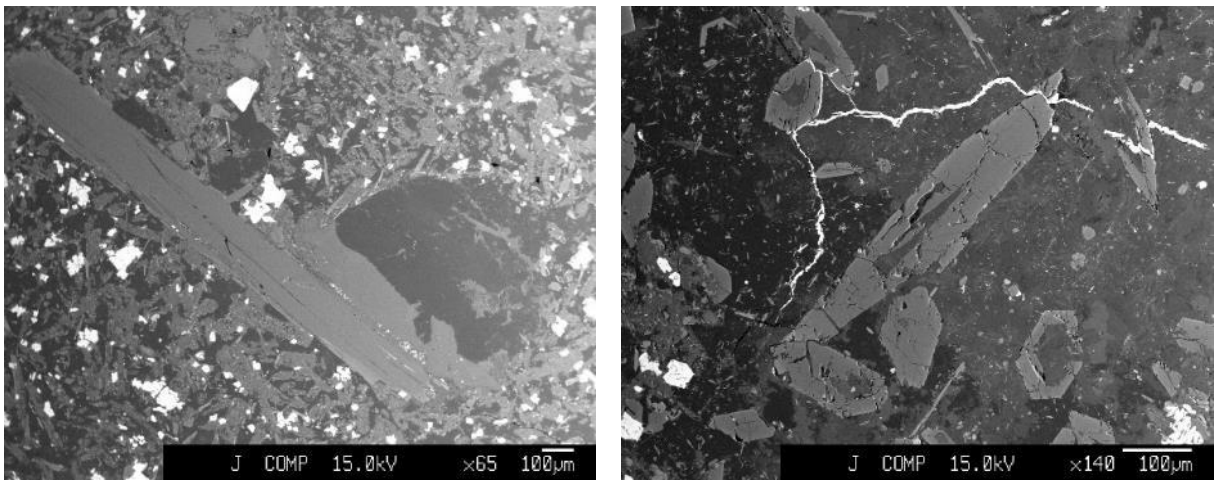

This sample is a NE-SW striking nephelinite dyke that intrude pillow lavas of the Batalha Formation. The sample is moderately altered, and macrocrysts (about 1% and up to 4 mm in diameter) comprise partly fresh phlogopite and clinopyroxene, some Fe-Ti oxides, and minor nepheline. Former clinopyroxene crystals were replaced by zeolite and calcite pseudomorphs, and only a few remnants of clinopyroxene were found. The comparatively coarse groundmass contains abundant phlogopite and nepheline, and comprises calcium carbonate fillings in vesicles.

Sample 18-32: Lat/Long: 15.224898, -23.134683

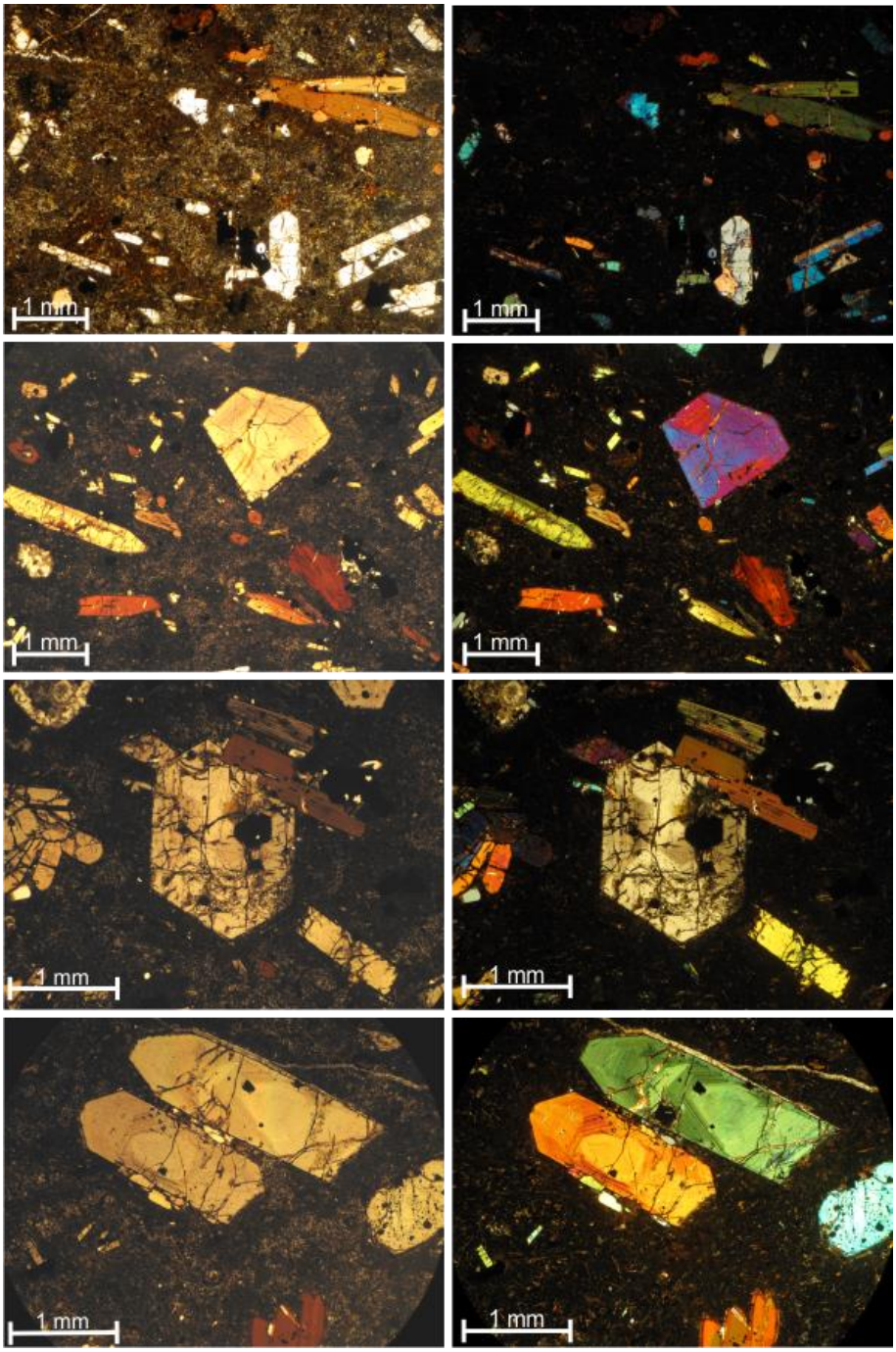

This sample is a moderately altered nosean-nephelinite conglomerate clast from the base of Mte Penoso. The main macrocysts (about 10%) are clinopyroxene, phlogopite and Fe-Ti oxides, lesser nepheline, and minor nosean and apatite. The brown microcrystalline groundmass contains abundant phlogopite and Fe-Ti oxides, and comprises calcium-carbonate fillings in vesicles and minor cracks. The groundmass shows signs of alteration in some places. Crystals are idiomorphic to hypidiomorphic and up to 3 mm in size. Phlogopite crystals re up to 2 mm in diameter and dominantly idiomorphic, but some are rounded. Some phlogopites include groundmass minerals and pyrite. Some phlogopites, especially rounded crystals, are surrounded by reaction rims with groundmass minerals. Clinopyroxenes are optically zoned (e.g., hourglass zoning) and contained mineral inclusions of Fe-Ti oxides. Some show signs of alteration along cracks. Glomerocrysts of clinopyroxene, phlogopite, Fe-Ti oxides and minor apatite also occur. The images above show thin section images in plain (left) and crossed (right) polarized light.

9.3.2 *Appendix B: 40Ar-39Ar data tables and plots for individual samples*

ARGO Laboratory

GEOMAR Helmholtz Centre for Oceanographic Research Kiel, Kiel, Germany

Sample 17-73 step-heating results (1773b)

Relative Abundances	Laser power		36Ar [V]	%1σ	37Ar [V]	%1σ	38Ar [V]	%1σ	39Ar [V]	%1σ	40Ar [V]	%1σ	40(r)/39(k) ± 2σ	Age ± 2σ (Ma)	40Ar(r) (%)	39Ar(k) (%)	K/Ca ± 2σ	Step #	$^{36}Ar/^{39}Ar$ Alt. Index*
C47GA101	0.15 W		0.0037138	1.146	0.0267668	4.408	0.0018543	2.847	0.0894186	0.307	1.472659	0.067	4.22052 ± 0.28669	8.04 ± 0.55	25.62	1.47	1.7 ± 0.2	1	0.003230
C47GA102	0.20 W		0.0029475	1.593	0.0230239	4.790	0.0037403	1.670	0.2591214	0.256	2.129845	0.041	4.86488 ± 0.11084	9.27 ± 0.21	59.18	4.26	5.7 ± 0.6	2	0.000885
C47GA103	0.25 W		0.0020740	1.469	0.0472020	2.716	0.0054961	1.174	0.4260611	0.229	2.906921	0.061	5.39288 ± 0.04994	10.27 ± 0.09	79.04	7.00	4.6 ± 0.3	3	*0.000377*
C47GA104	0.30 W		0.0020366	2.337	0.0237992	4.727	0.0075847	0.937	0.5911000	0.230	3.786746	0.054	5.39079 ± 0.05426	10.27 ± 0.10	84.15	9.71	12.7 ± 1.2	4	*0.000268*
C47GA105	0.35 W		0.0014441	2.273	0.0243486	5.033	0.0067972	1.118	0.5366419	0.232	3.329901	0.018	5.41292 ± 0.04415	10.31 ± 0.08	87.23	8.82	11.2 ± 1.1	5	*0.000209*
C47GA106	0.40 W		0.0007657	3.462	0.0211111	6.095	0.0054851	1.218	0.4397842	0.244	2.623702	0.080	5.45471 ± 0.04549	10.39 ± 0.09	91.43	7.22	10.6 ± 1.3	6	*0.000135*
C47GA107	0.45 W		0.0009664	3.246	0.0163529	7.430	0.0057330	1.143	0.4619901	0.233	2.802987	0.018	5.45128 ± 0.04757	10.38 ± 0.09	89.85	7.59	14.4 ± 2.1	7	*0.000162*
C47GA108	0.50 W		0.0007213	5.366	0.0089780	13.531	0.0041410	1.583	0.3317440	0.238	1.963197	0.161	5.27685 ± 0.07586	10.05 ± 0.14	89.17	5.45	18.8 ± 5.1	8	*0.000169*
C47GA109	0.55 W		0.0003730	6.625	0.0059177	19.108	0.0030237	2.030	0.2399928	0.235	1.403919	0.144	5.39192 ± 0.06806	10.27 ± 0.13	92.17	3.94	20.7 ± 7.9	9	*0.000121*
C47GA110	0.60 W		0.0003030	7.690	0.0059329	20.130	0.0036747	1.586	0.3113407	0.247	1.768772	0.046	5.39445 ± 0.05191	10.27 ± 0.10	94.95	5.11	26.8 ± 10.8	10	*0.000075*
C47GA111	0.70 W		0.0005693	5.042	0.0096038	12.437	0.0049086	1.363	0.4011162	0.219	2.309903	0.035	5.34060 ± 0.04854	10.17 ± 0.09	92.74	6.59	21.3 ± 5.3	11	*0.000110*
C47GA112	0.80 W		0.0004826	4.976	0.0302375	4.269	0.0035468	1.806	0.2913622	0.236	1.721944	0.045	5.42846 ± 0.05534	10.34 ± 0.11	91.85	4.79	4.9 ± 0.4	12	*0.000127*
C47GA113	0.90 W		0.0003089	6.852	0.0045251	24.513	0.0038723	1.499	0.3228467	0.233	1.853503	0.024	5.45883 ± 0.04642	10.39 ± 0.09	95.08	5.30	36.4 ± 17.8	13	*0.000074*
C47GA114	1.00 W		0.0004700	5.197	0.0044279	25.808	0.0030748	1.930	0.2484066	0.233	1.502135	0.053	5.48878 ± 0.06383	10.45 ± 0.12	90.77	4.08	28.6 ± 14.8	14	*0.000147*
C47GA115	1.10 W	•	0.0000727	35.187	0.0010152	112.615	0.0015441	3.458	0.1333139	0.279	0.769624	0.141	5.61169 ± 0.11883	10.68 ± 0.23	97.21	2.19	67.0 ± 150.8	15	*0.000042*
C47GA116	1.20 W	•	0.0000698	33.178	0.0008736	124.926	0.0007371	7.090	0.0662818	0.508	0.396712	0.157	5.67436 ± 0.21527	10.80 ± 0.41	94.81	1.09	38.7 ± 96.7	16	*0.000082*
C47GA117	1.50 W	•	0.0003417	7.101	0.0026137	42.712	0.0026212	1.942	0.2232670	0.234	1.326521	0.060	5.48938 ± 0.06956	10.45 ± 0.13	92.39	3.67	43.6 ± 37.2	17	*0.000119*
C47GA118	3.00 W	•	0.0004614	4.635	0.0044682	25.806	0.0042800	1.490	0.3642460	0.252	2.190043	0.066	5.63849 ± 0.04556	10.74 ± 0.09	93.78	5.98	41.6 ± 21.5	18	*0.000098*
C47GA119	10.00 W	•	0.0004683	5.392	0.0027580	40.885	0.0022616	2.465	0.1903006	0.236	1.191282	0.071	5.53326 ± 0.08317	10.54 ± 0.16	88.39	3.13	35.2 ± 28.8	19	*0.000191*
C47GA120	15.00 W	•	0.0003944	6.911	0.0017053	65.789	0.0019417	3.470	0.1586392	0.254	0.980650	0.041	5.44712 ± 0.10541	10.37 ± 0.20	88.12	2.61	47.4 ± 62.4	20	*0.000194*
		Σ	0.0189845	0.720	0.2656614	1.976	0.0763184	0.364	6.0869753	0.058	38.430965	0.016							

Procedure Blanks	Laser power	36Ar [V]	1σ	37Ar [V]	1σ	38Ar [V]	1σ	39Ar [V]	1σ	40Ar [V]	1σ
C47GA101	0.15 W	0.0002192	0.0000179	0.0001902	0.0000431	0.0001316	0.0000483	0.0003886	0.0001400	0.0033566	0.0001776
C47GA102	0.20 W	0.0002443	0.0000179	0.0002077	0.0000431	0.0001600	0.0000483	0.0004597	0.0001400	0.0033475	0.0001776
C47GA103	0.25 W	0.0002672	0.0000179	0.0002236	0.0000431	0.0001858	0.0000483	0.0005241	0.0001400	0.0033338	0.0001776
C47GA104	0.30 W	0.0002879	0.0000179	0.0002378	0.0000431	0.0002090	0.0000483	0.0005815	0.0001400	0.0033156	0.0001776
C47GA105	0.35 W	0.0003065	0.0000179	0.0002504	0.0000431	0.0002295	0.0000483	0.0006322	0.0001400	0.0032927	0.0001776
C47GA106	0.40 W	0.0003326	0.0000179	0.0002676	0.0000431	0.0002576	0.0000483	0.0007010	0.0001400	0.0032448	0.0001776
C47GA107	0.45 W	0.0003455	0.0000179	0.0002758	0.0000431	0.0002710	0.0000483	0.0007335	0.0001400	0.0032097	0.0001776
C47GA108	0.50 W	0.0003563	0.0000179	0.0002824	0.0000431	0.0002819	0.0000483	0.0007591	0.0001400	0.0031701	0.0001776
C47GA109	0.55 W	0.0003646	0.0000179	0.0002872	0.0000431	0.0002898	0.0000483	0.0007774	0.0001400	0.0031274	0.0001776
C47GA110	0.60 W	0.0003712	0.0000179	0.0002906	0.0000431	0.0002955	0.0000483	0.0007896	0.0001400	0.0030788	0.0001776
C47GA111	0.70 W	0.0003773	0.0000179	0.0002926	0.0000431	0.0002990	0.0000483	0.0007949	0.0001400	0.0029881	0.0001776
C47GA112	0.80 W	0.0003782	0.0000179	0.0002916	0.0000431	0.0002976	0.0000483	0.0007890	0.0001400	0.0029272	0.0001776
C47GA113	0.90 W	0.0003769	0.0000179	0.0002890	0.0000431	0.0002936	0.0000483	0.0007762	0.0001400	0.0028617	0.0001776
C47GA114	1.00 W	0.0003734	0.0000179	0.0002848	0.0000431	0.0002869	0.0000483	0.0007566	0.0001400	0.0027917	0.0001776
C47GA115	1.10 W	0.0003678	0.0000179	0.0002789	0.0000431	0.0002776	0.0000483	0.0007302	0.0001400	0.0027170	0.0001776
C47GA116	1.20 W	0.0003539	0.0000179	0.0002655	0.0000431	0.0002564	0.0000483	0.0006715	0.0001400	0.0025833	0.0001776
C47GA117	1.50 W	0.0003426	0.0000179	0.0002553	0.0000431	0.0002401	0.0000483	0.0006269	0.0001400	0.0024964	0.0001776
C47GA118	3.00 W	0.0003292	0.0000179	0.0002434	0.0000431	0.0002211	0.0000483	0.0005755	0.0001400	0.0024050	0.0001776
C47GA119	10.00 W	0.0003142	0.0000179	0.0002304	0.0000431	0.0002003	0.0000483	0.0005194	0.0001400	0.0023123	0.0001776
C47GA120	15.00 W	0.0002965	0.0000179	0.0002153	0.0000431	0.0001761	0.0000483	0.0004545	0.0001400	0.0022118	0.0001776

Sample Parameters	Laser power	Sample	Material	Location	Analyst	Standard (in Ma)	%1σ	J	%1σ	MDF	%1σ	Volume Ratio	Sensitivity (mol/volt)
C47GA101	0.15 W	17-73 (1773b)	Phlogopite	Maio, Cape Verdes	Jan Sticklus	28.344	0.039	1.06E-03	0.08	1.0098	0.21	1	1.211E-14
C47GA102	0.20 W	17-73 (1773b)	Phlogopite	Maio, Cape Verdes	Jan Sticklus	28.344	0.039	1.06E-03	0.08	1.0098	0.21	1	1.211E-14
C47GA103	0.25 W	17-73 (1773b)	Phlogopite	Maio, Cape Verdes	Jan Sticklus	28.344	0.039	1.06E-03	0.08	1.0098	0.21	1	1.211E-14
C47GA104	0.30 W	17-73 (1773b)	Phlogopite	Maio, Cape Verdes	Jan Sticklus	28.344	0.039	1.06E-03	0.08	1.0098	0.21	1	1.211E-14
C47GA105	0.35 W	17-73 (1773b)	Phlogopite	Maio, Cape Verdes	Jan Sticklus	28.344	0.039	1.06E-03	0.08	1.0098	0.21	1	1.211E-14
C47GA106	0.40 W	17-73 (1773b)	Phlogopite	Maio, Cape Verdes	Jan Sticklus	28.344	0.039	1.06E-03	0.08	1.0098	0.21	1	1.211E-14
C47GA107	0.45 W	17-73 (1773b)	Phlogopite	Maio, Cape Verdes	Jan Sticklus	28.344	0.039	1.06E-03	0.08	1.0098	0.21	1	1.211E-14
C47GA108	0.50 W	17-73 (1773b)	Phlogopite	Maio, Cape Verdes	Jan Sticklus	28.344	0.039	1.06E-03	0.08	1.0098	0.21	1	1.211E-14
C47GA109	0.55 W	17-73 (1773b)	Phlogopite	Maio, Cape Verdes	Jan Sticklus	28.344	0.039	1.06E-03	0.08	1.0098	0.21	1	1.211E-14
C47GA110	0.60 W	17-73 (1773b)	Phlogopite	Maio, Cape Verdes	Jan Sticklus	28.344	0.039	1.06E-03	0.08	1.0098	0.21	1	1.211E-14
C47GA111	0.70 W	17-73 (1773b)	Phlogopite	Maio, Cape Verdes	Jan Sticklus	28.344	0.039	1.06E-03	0.08	1.0098	0.21	1	1.211E-14
C47GA112	0.80 W	17-73 (1773b)	Phlogopite	Maio, Cape Verdes	Jan Sticklus	28.344	0.039	1.06E-03	0.08	1.0098	0.21	1	1.211E-14
C47GA113	0.90 W	17-73 (1773b)	Phlogopite	Maio, Cape Verdes	Jan Sticklus	28.344	0.039	1.06E-03	0.08	1.0098	0.21	1	1.211E-14
C47GA114	1.00 W	17-73 (1773b)	Phlogopite	Maio, Cape Verdes	Jan Sticklus	28.344	0.039	1.06E-03	0.08	1.0098	0.21	1	1.211E-14
C47GA115	1.10 W	17-73 (1773b)	Phlogopite	Maio, Cape Verdes	Jan Sticklus	28.344	0.039	1.06E-03	0.08	1.0098	0.21	1	1.211E-14
C47GA116	1.20 W	17-73 (1773b)	Phlogopite	Maio, Cape Verdes	Jan Sticklus	28.344	0.039	1.06E-03	0.08	1.0098	0.21	1	1.211E-14
C47GA117	1.50 W	17-73 (1773b)	Phlogopite	Maio, Cape Verdes	Jan Sticklus	28.344	0.039	1.06E-03	0.08	1.0098	0.21	1	1.211E-14
C47GA118	3.00 W	17-73 (1773b)	Phlogopite	Maio, Cape Verdes	Jan Sticklus	28.344	0.039	1.06E-03	0.08	1.0098	0.21	1	1.211E-14
C47GA119	10.00 W	17-73 (1773b)	Phlogopite	Maio, Cape Verdes	Jan Sticklus	28.344	0.039	1.06E-03	0.08	1.0098	0.21	1	1.211E-14
C47GA120	15.00 W	17-73 (1773b)	Phlogopite	Maio, Cape Verdes	Jan Sticklus	28.344	0.039	1.06E-03	0.08	1.0098	0.21	1	1.211E-14

Day	Month	Year	Hour	Min	Resist	Irradiation	Project	Experiment	Nmb	Standard Name
27	OCT	2018	17	54	1	can47	Examples	c47it5ip3_1773b	01	TCS2
27	OCT	2018	18	23	1	can47	Examples	c47it5ip3_1773b	01	TCS2
27	OCT	2018	18	52	1	can47	Examples	c47it5ip3_1773b	01	TCS2
27	OCT	2018	19	21	1	can47	Examples	c47it5ip3_1773b	01	TCS2
27	OCT	2018	19	50	1	can47	Examples	c47it5ip3_1773b	01	TCS2
27	OCT	2018	20	38	1	can47	Examples	c47it5ip3_1773b	01	TCS2
27	OCT	2018	21	7	1	can47	Examples	c47it5ip3_1773b	01	TCS2
27	OCT	2018	21	36	1	can47	Examples	c47it5ip3_1773b	01	TCS2
27	OCT	2018	22	4	1	can47	Examples	c47it5ip3_1773b	01	TCS2
27	OCT	2018	22	33	1	can47	Examples	c47it5ip3_1773b	01	TCS2
27	OCT	2018	23	21	1	can47	Examples	c47it5ip3_1773b	01	TCS2
27	OCT	2018	23	50	1	can47	Examples	c47it5ip3_1773b	01	TCS2
28	OCT	2018	0	19	1	can47	Examples	c47it5ip3_1773b	01	TCS2
28	OCT	2018	0	48	1	can47	Examples	c47it5ip3_1773b	01	TCS2
28	OCT	2018	1	17	1	can47	Examples	c47it5ip3_1773b	01	TCS2
28	OCT	2018	2	5	1	can47	Examples	c47it5ip3_1773b	01	TCS2
28	OCT	2018	2	34	1	can47	Examples	c47it5ip3_1773b	01	TCS2
28	OCT	2018	3	3	1	can47	Examples	c47it5ip3_1773b	01	TCS2
28	OCT	2018	3	31	1	can47	Examples	c47it5ip3_1773b	01	TCS2
28	OCT	2018	4	0	1	can47	Examples	c47it5ip3_1773b	01	TCS2

Irradiation Constants	Laser power	40/36(a)	%1σ	40/36(c)	%1σ	38/36(a)	%1σ	38/36(c)	%1σ	39/37(ca)	%1σ	38/37(ca)	%1σ	36/37(ca)	%1σ	40/39(k)	%1σ	38/39(k)	%1σ	36/38(cl)	%1σ	K/Ca	%1σ	K/Cl	%1σ	Ca/Cl	%1σ
C47GA101	0.15 W	295.5	0.178	0.018	35	0.1869	0.107	1.493	3	0.000702	1.71	0.000196	4.08	0.0002702	0.15	0.00073	12.33	0.01215	0.27	262.8	0.65	0.51	0	0	0	0	0
C47GA102	0.20 W	295.5	0.178	0.018	35	0.1869	0.107	1.493	3	0.000702	1.71	0.000196	4.08	0.0002702	0.15	0.00073	12.33	0.01215	0.27	262.8	0.65	0.51	0	0	0	0	0
C47GA103	0.25 W	295.5	0.178	0.018	35	0.1869	0.107	1.493	3	0.000702	1.71	0.000196	4.08	0.0002702	0.15	0.00073	12.33	0.01215	0.27	262.8	0.65	0.51	0	0	0	0	0
C47GA104	0.30 W	295.5	0.178	0.018	35	0.1869	0.107	1.493	3	0.000702	1.71	0.000196	4.08	0.0002702	0.15	0.00073	12.33	0.01215	0.27	262.8	0.65	0.51	0	0	0	0	0
C47GA105	0.35 W	295.5	0.178	0.018	35	0.1869	0.107	1.493	3	0.000702	1.71	0.000196	4.08	0.0002702	0.15	0.00073	12.33	0.01215	0.27	262.8	0.65	0.51	0	0	0	0	0
C47GA106	0.40 W	295.5	0.178	0.018	35	0.1869	0.107	1.493	3	0.000702	1.71	0.000196	4.08	0.0002702	0.15	0.00073	12.33	0.01215	0.27	262.8	0.65	0.51	0	0	0	0	0
C47GA107	0.45 W	295.5	0.178	0.018	35	0.1869	0.107	1.493	3	0.000702	1.71	0.000196	4.08	0.0002702	0.15	0.00073	12.33	0.01215	0.27	262.8	0.65	0.51	0	0	0	0	0
C47GA108	0.50 W	295.5	0.178	0.018	35	0.1869	0.107	1.493	3	0.000702	1.71	0.000196	4.08	0.0002702	0.15	0.00073	12.33	0.01215	0.27	262.8	0.65	0.51	0	0	0	0	0
C47GA109	0.55 W	295.5	0.178	0.018	35	0.1869	0.107	1.493	3	0.000702	1.71	0.000196	4.08	0.0002702	0.15	0.00073	12.33	0.01215	0.27	262.8	0.65	0.51	0	0	0	0	0
C47GA110	0.60 W	295.5	0.178	0.018	35	0.1869	0.107	1.493	3	0.000702	1.71	0.000196	4.08	0.0002702	0.15	0.00073	12.33	0.01215	0.27	262.8	0.65	0.51	0	0	0	0	0
C47GA111	0.70 W	295.5	0.178	0.018	35	0.1869	0.107	1.493	3	0.000702	1.71	0.000196	4.08	0.0002702	0.15	0.00073	12.33	0.01215	0.27	262.8	0.65	0.51	0	0	0	0	0
C47GA112	0.80 W	295.5	0.178	0.018	35	0.1869	0.107	1.493	3	0.000702	1.71	0.000196	4.08	0.0002702	0.15	0.00073	12.33	0.01215	0.27	262.8	0.65	0.51	0	0	0	0	0
C47GA113	0.90 W	295.5	0.178	0.018	35	0.1869	0.107	1.493	3	0.000702	1.71	0.000196	4.08	0.0002702	0.15	0.00073	12.33	0.01215	0.27	262.8	0.65	0.51	0	0	0	0	0
C47GA114	1.00 W	295.5	0.178	0.018	35	0.1869	0.107	1.493	3	0.000702	1.71	0.000196	4.08	0.0002702	0.15	0.00073	12.33	0.01215	0.27	262.8	0.65	0.51	0	0	0	0	0
C47GA115	1.10 W	295.5	0.178	0.018	35	0.1869	0.107	1.493	3	0.000702	1.71	0.000196	4.08	0.0002702	0.15	0.00073	12.33	0.01215	0.27	262.8	0.65	0.51	0	0	0	0	0
C47GA116	1.20 W	295.5	0.178	0.018	35	0.1869	0.107	1.493	3	0.000702	1.71	0.000196	4.08	0.0002702	0.15	0.00073	12.33	0.01215	0.27	262.8	0.65	0.51	0	0	0	0	0
C47GA117	1.50 W	295.5	0.178	0.018	35	0.1869	0.107	1.493	3	0.000702	1.71	0.000196	4.08	0.0002702	0.15	0.00073	12.33	0.01215	0.27	262.8	0.65	0.51	0	0	0	0	0
C47GA118	3.00 W	295.5	0.178	0.018	35	0.1869	0.107	1.493	3	0.000702	1.71	0.000196	4.08	0.0002702	0.15	0.00073	12.33	0.01215	0.27	262.8	0.65	0.51	0	0	0	0	0
C47GA119	10.00 W	295.5	0.178	0.018	35	0.1869	0.107	1.493	3	0.000702	1.71	0.000196	4.08	0.0002702	0.15	0.00073	12.33	0.01215	0.27	262.8	0.65	0.51	0	0	0	0	0
C47GA120	15.00 W	295.5	0.178	0.018	35	0.1869	0.107	1.493	3	0.000702	1.71	0.000196	4.08	0.0002702	0.15	0.00073	12.33	0.01215	0.27	262.8	0.65	0.51	0	0	0	0	0

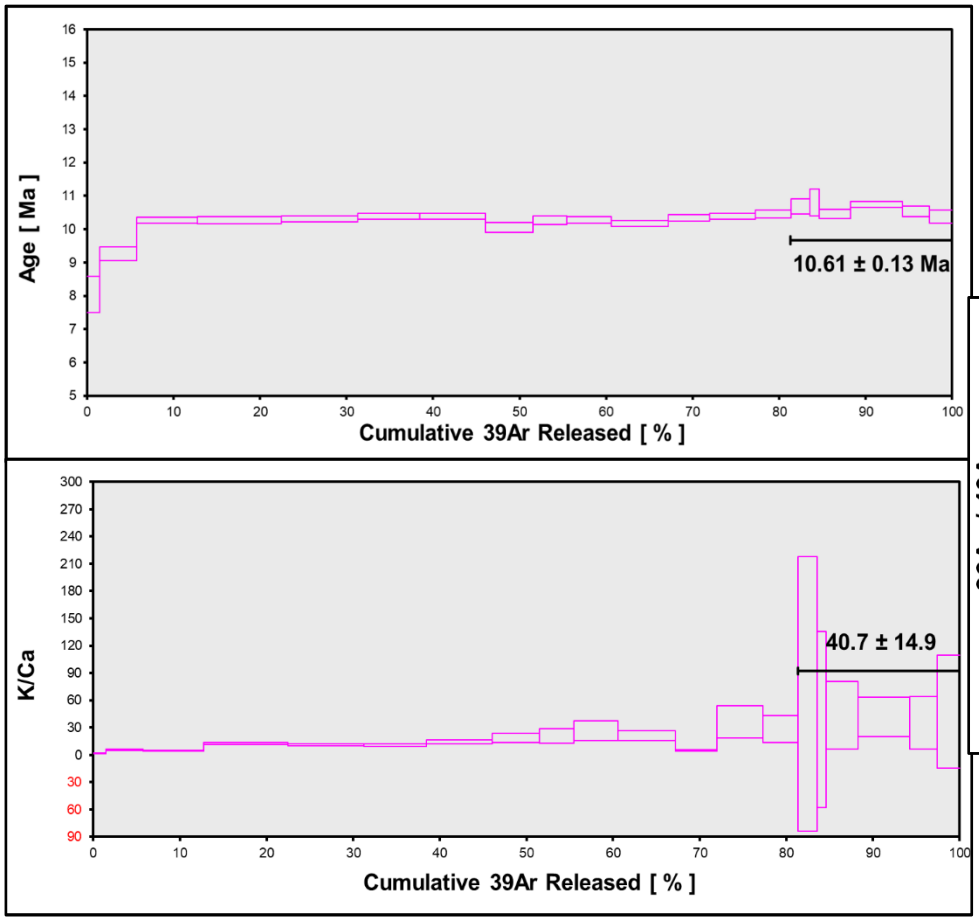
Age [Ma]
Cumulative 39Ar Released [%]
10.61 ± 0.13 Ma
K/Ca
Cumulative 39Ar Released [%]
40.7 ± 14.9

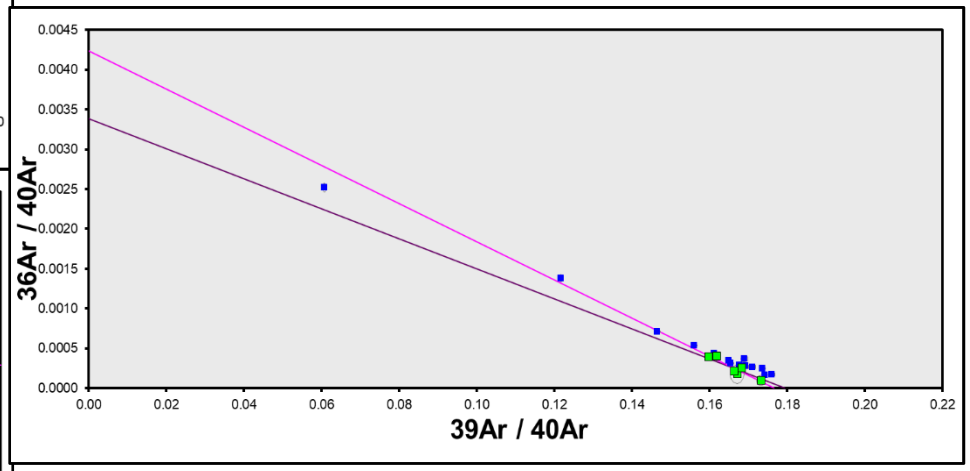
36Ar / 40Ar
39Ar / 40Ar

Information on Analysis and Constants Used in Calculations

Sample = 17-73 (1773B)
Material = Phlogopite
Location = Maio, Cape Verde
Analyst = Jan Sticklus
Project = EXAMPLES
Mass Discrimination Law = POW
Irradiation = can47
J = 0.00105850 ± 0.00000085
TCS2 = 28.344 ± 0.011 Ma
Experiment Type = SAMPLE
Heating = 45 sec
Isolation = 15.00 min
Instrument = MAP216
Weight = 3.779 mg
Weight %K = 5.9

Age Equations = Conventional
Negative Intensities = Allowed
Decay Constant 40K = 5.543 ± 0.009 E-10 1/a
Decay Constant 39Ar = 2.940 ± 0.016 E-07 1/h
Decay Constant 37Ar = 8.230 ± 0.012 E-04 1/h
Decay Constant 36Cl = 2.257 ± 0.015 E-06 1/a
Atmospheric Ratio 40/36(a) = 295.50 ± 0.53
Atmospheric Ratio 38/36(a) = 0.1869 ± 0.0002
Production Ratio 39/37(ca) = 0.000702 ± 0.000012
Production Ratio 38/37(ca) = 0.000196 ± 0.000008
Production Ratio 36/37(ca) = 0.000270 ± 0.000000
Production Ratio 40/39(k) = 0.000730 ± 0.000090
Production Ratio 38/39(k) = 0.012150 ± 0.000033
Production Ratio 36/38(cl) = 262.80
Scaling Ratio K/Ca = 0.510

Results	40(a)/36(a) ± 2σ	40(r)/39(k) ± 2σ	Age ± 2σ (Ma)	MSWD	39Ar(k) (%,n)	K/Ca ± 2σ
SH Weighted Mean		5.57509 ± 0.06576	10.61 ± 0.13	4.39	18.66	40.7 ± 14.9
Error Mean		± 1.18%	± 1.19%	0%	6	
		Minimal External Error	± 0.13	2.26	2σ Confidence Limit	
		Analytical Error	± 0.12	2.0955	Error Magnification	
Total Fusion Age		5.39493 ± 0.01486	10.273 0.033		20	11.7 ± 0.5
		± 0.28%	± 0.32%			
		Minimal External Error	0.046			
		Analytical Error	0.028			
Normal Isochron	230.02 ± 100.33	5.65613 ± 0.16872	10.77 ± 0.32	4.81	18.66	
Error Chron	± 43.62%	± 2.98%	± 2.98%	0%	6	
		Minimal External Error	± 0.32	2.41	2σ Confidence Limit	
		Analytical Error	± 0.32	2.1934	Error Magnification	
				1	Number of Iterations	
				0.0000243115	Convergence	
Inverse Isochron	235.91 ± 102.22	5.66409 ± 0.16330	10.78 ± 0.31	4.48	18.66	
Error Chron	± 43.33%	± 2.88%	± 2.88%	0%	6	
		Minimal External Error	± 0.31	2.41	2σ Confidence Limit	
		Analytical Error	± 0.31	2.1163	Error Magnification	
				3	Number of Iterations	
				0.0000208288	Convergence	
				8%	Spreading Factor	

Blue dots in table indicate selected steps used to calculate the weighted mean, isochron and inverse isochron ages.
* Alteration Index values in italics indicate analyses from fresh material, normal font is from altered material (Baksi, 2007).
Values shown in red are negative values.
Abbreviations used in tables: (r) = radiogenic ^{40}Ar; (k) = Ar derived from K; (a) = atmospheric Ar; (ca) = Ar derived from Ca; (cl) = Ar derived from Ca; (c) = cosmogenic Ar; MDF = Mass Discrimination Factor.
Green squares in the inverse isochron plots indicate selected steps (blue dots in table), and blue squares are non-selected steps. Pink lines in the inverse isochron plot indicate a line fit through selected data, and the purple lines incidate a fit through an air ^{40}Ar/^{36}Ar ratio (295.5).

Sample 17-73 single-/multi-crystal total-fusion resutls (1-2 crystals; 0.25-0.5 mm; 1773b)

Relative Abundances	Laser power		36Ar [V]	%1σ	37Ar [V]	%1σ	38Ar [V]	%1σ	39Ar [V]	%1σ	40Ar [V]	%1σ	40(r)/39(k) ± 2σ	Age ± 2σ (Ma)	40Ar(r) (%)	39Ar(k) (%)	K/Ca ± 2σ	Sample weight (mg)	$^{36}Ar/^{39}Ar$ Alt. Index	Wt. % K
C47AB109	5.00 W		0.0017098	1.341	0.0029085	1.465	0.0019506	0.926	0.1377496	0.266	1.152280	0.103	4.69830 ± 0.10374	8.95 ± 0.20	56.17	6.31	24.2 ± 0.7	0.086	*0.000961*	5.8
C47AB112	5.00 W		0.0020919	1.128	0.0069704	1.258	0.0019319	1.407	0.1276137	0.284	1.237517	0.102	4.85730 ± 0.11573	9.25 ± 0.22	50.09	5.84	9.3 ± 0.2	0.072	0.001404	6.5
C47AB108	5.00 W		0.0002137	5.355	0.0002108	14.688	0.0005271	3.788	0.0400933	0.333	0.258560	0.228	4.87361 ± 0.17437	9.28 ± 0.33	75.57	1.84	97.0 ± 28.5	0.020	*0.000517*	7.3
C47AB113	5.00 W		0.0001050	10.171	0.0020786	1.986	0.0011188	2.432	0.0945863	0.336	0.508361	0.090	5.04778 ± 0.07547	9.61 ± 0.14	93.92	4.33	23.2 ± 0.9	0.044	*0.000115*	7.8
C47BC006	5.00 W	•	0.0004767	3.154	0.0014535	2.646	0.0010015	1.478	0.0754598	0.337	0.546140	0.056	5.37171 ± 0.12362	10.23 ± 0.23	74.22	3.45	26.5 ± 1.4	0.042	*0.000549*	6.6
C47AB114	5.00 W	•	0.0001667	8.186	0.0011155	3.037	0.0012229	1.946	0.1013266	0.228	0.603465	0.093	5.46980 ± 0.08415	10.42 ± 0.16	91.84	4.64	46.3 ± 2.8	0.044	*0.000183*	8.4
C47BC004	5.00 W	•	0.0002525	6.287	0.0116939	1.106	0.0015490	1.522	0.1265653	0.346	0.769268	0.114	5.49560 ± 0.08449	10.46 ± 0.16	90.41	5.79	5.5 ± 0.1	0.069	*0.000175*	6.7
C47AB107	5.00 W	•	0.0001361	9.083	0.0031341	1.268	0.0010571	3.535	0.0852352	0.298	0.509128	0.103	5.50366 ± 0.09264	10.48 ± 0.18	92.14	3.90	13.9 ± 0.4	0.043	*0.000152*	7.2
C47BC005	5.00 W	•	0.0000853	15.370	0.0015234	3.450	0.0009255	2.556	0.0776121	0.264	0.452682	0.067	5.50863 ± 0.10431	10.49 ± 0.20	94.44	3.55	26.0 ± 1.8	0.040	*0.000103*	7.1
C47AB105	5.00 W	•	0.0004168	4.190	0.0161622	0.935	0.0007618	2.332	0.0586647	0.270	0.445194	0.131	5.51179 ± 0.17972	10.49 ± 0.34	72.62	2.69	1.9 ± 0.0	0.036	*0.000554*	5.9
C47BC008	5.00 W	•	0.0001871	7.871	0.0004814	7.708	0.0007660	1.982	0.0617139	0.349	0.396495	0.097	5.52864 ± 0.14679	10.53 ± 0.28	86.05	2.83	65.4 ± 10.1	0.031	*0.000292*	7.3
C47BC009	5.00 W	•	0.0000988	14.082	0.0004801	8.705	0.0004946	3.849	0.0400654	0.389	0.250710	0.191	5.52929 ± 0.21101	10.53 ± 0.40	88.36	1.83	42.6 ± 7.4	0.022	*0.000217*	6.7
C47AB111	5.00 W	•	0.0001862	6.894	0.0021963	1.968	0.0012965	2.493	0.1083928	0.264	0.656316	0.087	5.54825 ± 0.07662	10.56 ± 0.15	91.63	4.96	25.2 ± 1.0	0.054	*0.000166*	7.3
C47BC003	5.00 W	•	0.0000639	17.582	0.0008151	6.262	0.0010012	2.273	0.0860575	0.314	0.496950	0.060	5.55516 ± 0.08501	10.58 ± 0.16	96.20	3.94	53.8 ± 6.8	0.044	*0.000070*	7.1
C47AB115	5.00 W	•	0.0002613	4.601	0.0116132	0.800	0.0022764	1.488	0.1910219	0.279	1.138635	0.078	5.56087 ± 0.04937	10.59 ± 0.09	93.29	8.74	8.4 ± 0.1	0.094	*0.000133*	7.4
C47AB104	5.00 W	•	0.0001021	13.664	0.0025739	2.485	0.0012506	1.642	0.1059707	0.237	0.619421	0.096	5.56194 ± 0.08290	10.59 ± 0.16	95.15	4.85	21.0 ± 1.0	0.059	*0.000083*	6.6
C47BC007	5.00 W	•	0.0000399	41.511	0.0023167	3.024	0.0007100	2.683	0.0586437	0.285	0.338351	0.088	5.57116 ± 0.17019	10.61 ± 0.32	96.56	2.68	12.9 ± 0.8	0.029	*0.000066*	7.4
C47BC001	5.00 W	•	0.0000568	25.431	0.0023892	2.259	0.0009237	2.061	0.0763464	0.269	0.442213	0.111	5.57421 ± 0.11652	10.61 ± 0.22	96.23	3.50	16.3 ± 0.7	0.040	*0.000068*	7.0
C47BB006	5.00 W	•	0.0000480	34.784	0.0010403	6.229	0.0007427	1.486	0.0642461	0.336	0.372796	0.111	5.58228 ± 0.15876	10.63 ± 0.30	96.20	2.94	31.5 ± 3.9	0.037	*0.000062*	6.3
C47BC002	5.00 W	•	0.0001313	12.534	0.0013006	3.556	0.0011113	2.082	0.0907155	0.278	0.545597	0.115	5.58710 ± 0.11251	10.64 ± 0.21	92.89	4.15	35.6 ± 2.5	0.048	*0.000132*	6.9
C47AB106	5.00 W	•	0.0007114	2.464	0.0755566	0.693	0.0019760	1.457	0.1549249	0.252	1.073958	0.105	5.61541 ± 0.07422	10.69 ± 0.14	80.98	7.09	1.0 ± 0.0	0.043	*0.000321*	5.4
C47BB007	5.00 W	•	0.0000315	49.715	0.0007402	5.972	0.0012014	1.859	0.0961353	0.330	0.549915	0.096	5.62329 ± 0.10380	10.71 ± 0.20	98.30	4.40	66.2 ± 7.9	0.054	*0.000028*	6.5
C47BB008	5.00 W	•	0.0001082	16.795	0.0081954	1.252	0.0008629	2.791	0.0709730	0.311	0.431252	0.128	5.63463 ± 0.15615	10.73 ± 0.30	92.72	3.25	4.4 ± 0.1	0.043	*0.000119*	6.0
C47AB110	5.00 W	•	0.0002188	4.787	0.0004742	5.589	0.0006957	1.771	0.0543310	0.255	0.373695	0.124	5.68809 ± 0.11888	10.83 ± 0.23	82.70	2.49	58.4 ± 6.5	0.021	*0.000504*	9.4
		Σ	0.0078997	0.955	0.1574239	0.392	0.0273551	0.417	2.1844445	0.063	14.168897	0.023								

Procedure Blanks	Laser power	36Ar [V]	1σ	37Ar [V]	1σ	38Ar [V]	1σ	39Ar [V]	1σ	40Ar [V]	1σ
C47AB109	5.00 W	0.0000800	0.0000092	0.0001767	0.0000081	0.0000378	0.0000066	0.0001790	0.0000263	0.0033145	0.0003812
C47AB112	5.00 W	0.0000857	0.0000092	0.0001821	0.0000081	0.0000390	0.0000066	0.0001608	0.0000263	0.0033877	0.0003812
C47AB108	5.00 W	0.0000784	0.0000092	0.0001752	0.0000081	0.0000375	0.0000066	0.0001840	0.0000263	0.0032945	0.0003812
C47AB113	5.00 W	0.0000873	0.0000092	0.0001835	0.0000081	0.0000393	0.0000066	0.0001558	0.0000263	0.0034077	0.0003812
C47BC006	5.00 W	0.0001628	0.0000093	0.0002495	0.0000102	0.0000689	0.0000070	0.0001287	0.0000126	0.0028468	0.0000971
C47AB114	5.00 W	0.0000889	0.0000092	0.0001850	0.0000081	0.0000397	0.0000066	0.0001508	0.0000263	0.0034277	0.0003812
C47BC004	5.00 W	0.0001575	0.0000093	0.0002444	0.0000102	0.0000634	0.0000070	0.0001168	0.0000126	0.0027219	0.0000971
C47AB107	5.00 W	0.0000769	0.0000092	0.0001738	0.0000081	0.0000372	0.0000066	0.0001890	0.0000263	0.0032745	0.0003812
C47BC005	5.00 W	0.0001596	0.0000093	0.0002460	0.0000102	0.0000658	0.0000070	0.0001228	0.0000126	0.0027803	0.0000971
C47AB105	5.00 W	0.0000738	0.0000092	0.0001709	0.0000081	0.0000365	0.0000066	0.0001989	0.0000263	0.0032352	0.0003812
C47BC008	5.00 W	0.0001723	0.0000093	0.0002616	0.0000102	0.0000769	0.0000070	0.0001396	0.0000126	0.0030044	0.0000971
C47BC009	5.00 W	0.0001786	0.0000093	0.0002704	0.0000102	0.0000819	0.0000070	0.0001447	0.0000126	0.0030954	0.0000971
C47AB111	5.00 W	0.0000842	0.0000092	0.0001806	0.0000081	0.0000387	0.0000066	0.0001658	0.0000263	0.0033677	0.0003812
C47BC003	5.00 W	0.0001562	0.0000093	0.0002457	0.0000102	0.0000608	0.0000070	0.0001062	0.0000126	0.0026432	0.0000971
C47AB115	5.00 W	0.0000904	0.0000092	0.0001864	0.0000081	0.0000400	0.0000066	0.0001459	0.0000263	0.0034471	0.0003812
C47AB104	5.00 W	0.0000722	0.0000092	0.0001694	0.0000081	0.0000362	0.0000066	0.0002039	0.0000263	0.0032151	0.0003812
C47BC007	5.00 W	0.0001670	0.0000093	0.0002546	0.0000102	0.0000726	0.0000070	0.0001343	0.0000126	0.0029215	0.0000971
C47BC001	5.00 W	0.0001602	0.0000093	0.0002577	0.0000102	0.0000604	0.0000070	0.0000880	0.0000126	0.0025643	0.0000971
C47BB006	5.00 W	0.0002983	0.0000136	0.0003338	0.0000148	0.0001377	0.0000057	0.0003512	0.0000307	0.0043365	0.0003575
C47BC002	5.00 W	0.0001569	0.0000093	0.0002487	0.0000102	0.0000602	0.0000070	0.0000997	0.0000126	0.0026076	0.0000971
C47AB106	5.00 W	0.0000753	0.0000092	0.0001723	0.0000081	0.0000369	0.0000066	0.0001940	0.0000263	0.0032545	0.0003812
C47BB007	5.00 W	0.0002983	0.0000136	0.0003338	0.0000148	0.0001377	0.0000057	0.0003512	0.0000307	0.0043365	0.0003575
C47BB008	5.00 W	0.0002983	0.0000136	0.0003338	0.0000148	0.0001377	0.0000057	0.0003512	0.0000307	0.0043365	0.0003575
C47AB110	5.00 W	0.0000826	0.0000092	0.0001791	0.0000081	0.0000384	0.0000066	0.0001708	0.0000263	0.0033477	0.0003812

Sample Parameters	Laser power	Sample	Material	Location	Analyst	Standard (in Ma)	%1σ	J	%1σ	MDF	%1σ	Volume Ratio	Sensitivity (mol/volt)
C47AB109	5.00 W	17-73 (1773b) 2 crystals	Phlogopite (0.25-0.5 mm)	Maio, Cape Verdes	Jan Sticklus	28.344	0.039	1.06E-03	0.08	1.0098	0.21	1	1.211E-14
C47AB112	5.00 W	17-73 (1773b) 2 crystals	Phlogopite (0.25-0.5 mm)	Maio, Cape Verdes	Jan Sticklus	28.344	0.039	1.06E-03	0.08	1.0098	0.21	1	1.211E-14
C47AB108	5.00 W	17-73 (1773b) 2 crystals	Phlogopite (0.25-0.5 mm)	Maio, Cape Verdes	Jan Sticklus	28.344	0.039	1.06E-03	0.08	1.0098	0.21	1	1.211E-14
C47AB113	5.00 W	17-73 (1773b) 2 crystals	Phlogopite (0.25-0.5 mm)	Maio, Cape Verdes	Jan Sticklus	28.344	0.039	1.06E-03	0.08	1.0098	0.21	1	1.211E-14
C47BC006	5.00 W	17-73 (1773b) 1 crystal	Phlogopite (0.25-0.5 mm)	Maio, Cape Verdes	Jan Sticklus	28.344	0.039	1.06E-03	0.08	1.0098	0.21	1	1.211E-14
C47AB114	5.00 W	17-73 (1773b) 2 crystals	Phlogopite (0.25-0.5 mm)	Maio, Cape Verdes	Jan Sticklus	28.344	0.039	1.06E-03	0.08	1.0098	0.21	1	1.211E-14
C47BC004	5.00 W	17-73 (1773b) 1 crystal	Phlogopite (0.25-0.5 mm)	Maio, Cape Verdes	Jan Sticklus	28.344	0.039	1.06E-03	0.08	1.0098	0.21	1	1.211E-14
C47AB107	5.00 W	17-73 (1773b) 1 crystal	Phlogopite (0.25-0.5 mm)	Maio, Cape Verdes	Jan Sticklus	28.344	0.039	1.06E-03	0.08	1.0098	0.21	1	1.211E-14
C47BC005	5.00 W	17-73 (1773b) 1 crystal	Phlogopite (0.25-0.5 mm)	Maio, Cape Verdes	Jan Sticklus	28.344	0.039	1.06E-03	0.08	1.0098	0.21	1	1.211E-14
C47AB105	5.00 W	17-73 (1773b) 1 crystal	Phlogopite (0.25-0.5 mm)	Maio, Cape Verdes	Jan Sticklus	28.344	0.039	1.06E-03	0.08	1.0098	0.21	1	1.211E-14
C47BC008	5.00 W	17-73 (1773b) 1 crystal	Phlogopite (0.25-0.5 mm)	Maio, Cape Verdes	Jan Sticklus	28.344	0.039	1.06E-03	0.08	1.0098	0.21	1	1.211E-14
C47BC009	5.00 W	17-73 (1773b) 1 crystal	Phlogopite (0.25-0.5 mm)	Maio, Cape Verdes	Jan Sticklus	28.344	0.039	1.06E-03	0.08	1.0098	0.21	1	1.211E-14
C47AB111	5.00 W	17-73 (1773b) 2 crystals	Phlogopite (0.25-0.5 mm)	Maio, Cape Verdes	Jan Sticklus	28.344	0.039	1.06E-03	0.08	1.0098	0.21	1	1.211E-14
C47BC003	5.00 W	17-73 (1773b) 1 crystal	Phlogopite (0.25-0.5 mm)	Maio, Cape Verdes	Jan Sticklus	28.344	0.039	1.06E-03	0.08	1.0098	0.21	1	1.211E-14
C47AB115	5.00 W	17-73 (1773b) 2 crystals	Phlogopite (0.25-0.5 mm)	Maio, Cape Verdes	Jan Sticklus	28.344	0.039	1.06E-03	0.08	1.0098	0.21	1	1.211E-14
C47AB104	5.00 W	17-73 (1773b) 1 crystal	Phlogopite (0.25-0.5 mm)	Maio, Cape Verdes	Jan Sticklus	28.344	0.039	1.06E-03	0.08	1.0098	0.21	1	1.211E-14
C47BC007	5.00 W	17-73 (1773b) 1 crystal	Phlogopite (0.25-0.5 mm)	Maio, Cape Verdes	Jan Sticklus	28.344	0.039	1.06E-03	0.08	1.0098	0.21	1	1.211E-14
C47BC001	5.00 W	17-73 (1773b) 1 crystal	Phlogopite (0.25-0.5 mm)	Maio, Cape Verdes	Jan Sticklus	28.344	0.039	1.06E-03	0.08	1.0098	0.21	1	1.211E-14
C47BB006	5.00 W	17-73 (1773b) 1 crystal	Phlogopite (0.25-0.5 mm)	Maio, Cape Verdes	Jan Sticklus	28.344	0.039	1.06E-03	0.08	1.0098	0.21	1	1.211E-14
C47BC002	5.00 W	17-73 (1773b) 1 crystal	Phlogopite (0.25-0.5 mm)	Maio, Cape Verdes	Jan Sticklus	28.344	0.039	1.06E-03	0.08	1.0098	0.21	1	1.211E-14
C47AB106	5.00 W	17-73 (1773b) 1 crystal	Phlogopite (0.25-0.5 mm)	Maio, Cape Verdes	Jan Sticklus	28.344	0.039	1.06E-03	0.08	1.0098	0.21	1	1.211E-14
C47BB007	5.00 W	17-73 (1773b) 1 crystal	Phlogopite (0.25-0.5 mm)	Maio, Cape Verdes	Jan Sticklus	28.344	0.039	1.06E-03	0.08	1.0098	0.21	1	1.211E-14
C47BB008	5.00 W	17-73 (1773b) 1 crystal	Phlogopite (0.25-0.5 mm)	Maio, Cape Verdes	Jan Sticklus	28.344	0.039	1.06E-03	0.08	1.0098	0.21	1	1.211E-14
C47AB110	5.00 W	17-73 (1773b) 2 crystals	Phlogopite (0.25-0.5 mm)	Maio, Cape Verdes	Jan Sticklus	28.344	0.039	1.06E-03	0.08	1.0098	0.21	1	1.211E-14

Day	Month	Year	Hour	Min	Resist	Irradiation	Project	Experiment	Nmb	Standard Name
24	JUN	2018	18	7	1	can47	Examples	C47AB109	02	TCS2
24	JUN	2018	19	53	1	can47	Examples	C47AB109	02	TCS2
24	JUN	2018	17	38	1	can47	Examples	C47AB109	02	TCS2
24	JUN	2018	20	22	1	can47	Examples	C47AB109	02	TCS2
2	JUL	2018	14	4	1	can47	Examples	c47it5ip3_1773b	01	TCS2
24	JUN	2018	20	51	1	can47	Examples	C47AB109	02	TCS2
2	JUL	2018	13	6	1	can47	Examples	c47it5ip3_1773b	01	TCS2
24	JUN	2018	17	9	1	can47	Examples	C47AB109	02	TCS2
2	JUL	2018	13	35	1	can47	Examples	c47it5ip3_1773b	01	TCS2
24	JUN	2018	16	12	1	can47	Examples	C47AB109	02	TCS2
2	JUL	2018	15	2	1	can47	Examples	c47it5ip3_1773b	01	TCS2
2	JUL	2018	15	31	1	can47	Examples	c47it5ip3_1773b	01	TCS2
24	JUN	2018	19	24	1	can47	Examples	C47AB109	02	TCS2
2	JUL	2018	12	18	1	can47	Examples	c47it5ip3_1773b	01	TCS2
24	JUN	2018	21	19	1	can47	Examples	C47AB109	02	TCS2
24	JUN	2018	15	43	1	can47	Examples	C47AB109	02	TCS2
2	JUL	2018	14	33	1	can47	Examples	c47it5ip3_1773b	01	TCS2
2	JUL	2018	11	2	1	can47	Examples	c47it5ip3_1773b	01	TCS2
30	JUN	2018	21	5	1	can47	Examples	c47it5ip3_1773b	01	TCS2
2	JUL	2018	11	50	1	can47	Examples	c47it5ip3_1773b	01	TCS2
24	JUN	2018	16	40	1	can47	Examples	C47AB109	02	TCS2
30	JUN	2018	21	34	1	can47	Examples	c47it5ip3_1773b	01	TCS2
30	JUN	2018	22	3	1	can47	Examples	c47it5ip3_1773b	01	TCS2
24	JUN	2018	18	55	1	can47	Examples	C47AB109	02	TCS2

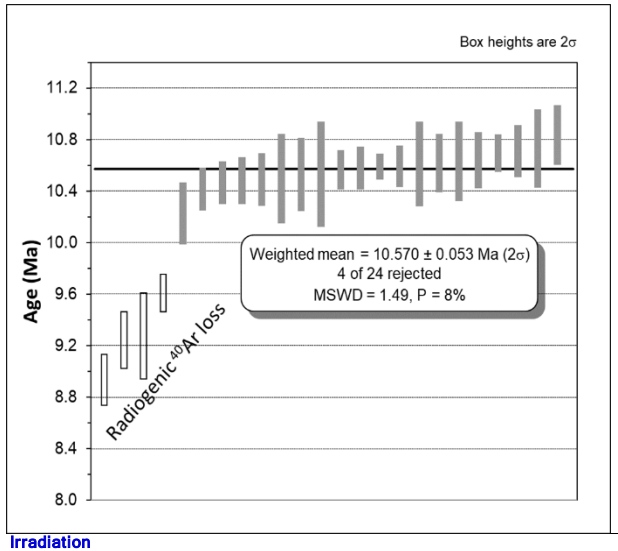

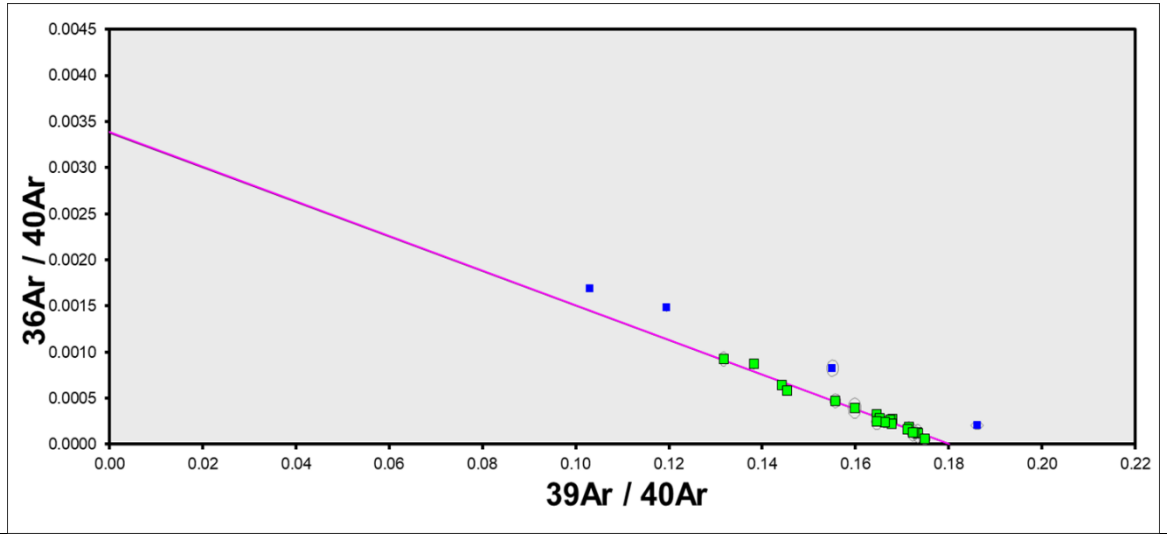

Irradiation Constants	Laser power	40/36(a)	%1σ	40/36(c)	%1σ	38/36(a)	%1σ	38/36(c)	%1σ	39/37(ca)	%1σ	38/37(ca)	%1σ	36/37(ca)	%1σ	40/39(k)	%1σ	38/39(k)	%1σ	36/38(cl)	%1σ	K/Ca	%1σ	K/Cl	%1σ	Ca/Cl	%1σ
C47AB109	5.00 W	295.5	0.178	0.018	35	0.1869	0.107	1.493	3	0.000702	1.71	0.000196	4.08	0.0002702	0.15	0.00073	12.33	0.01215	0.27	262.8	0.65	0.51	0	0	0	0	0
C47AB112	5.00 W	295.5	0.178	0.018	35	0.1869	0.107	1.493	3	0.000702	1.71	0.000196	4.08	0.0002702	0.15	0.00073	12.33	0.01215	0.27	262.8	0.65	0.51	0	0	0	0	0
C47AB108	5.00 W	295.5	0.178	0.018	35	0.1869	0.107	1.493	3	0.000702	1.71	0.000196	4.08	0.0002702	0.15	0.00073	12.33	0.01215	0.27	262.8	0.65	0.51	0	0	0	0	0
C47AB113	5.00 W	295.5	0.178	0.018	35	0.1869	0.107	1.493	3	0.000702	1.71	0.000196	4.08	0.0002702	0.15	0.00073	12.33	0.01215	0.27	262.8	0.65	0.51	0	0	0	0	0
C47BC006	5.00 W	295.5	0.178	0.018	35	0.1869	0.107	1.493	3	0.000702	1.71	0.000196	4.08	0.0002702	0.15	0.00073	12.33	0.01215	0.27	262.8	0.65	0.51	0	0	0	0	0
C47AB114	5.00 W	295.5	0.178	0.018	35	0.1869	0.107	1.493	3	0.000702	1.71	0.000196	4.08	0.0002702	0.15	0.00073	12.33	0.01215	0.27	262.8	0.65	0.51	0	0	0	0	0
C47BC004	5.00 W	295.5	0.178	0.018	35	0.1869	0.107	1.493	3	0.000702	1.71	0.000196	4.08	0.0002702	0.15	0.00073	12.33	0.01215	0.27	262.8	0.65	0.51	0	0	0	0	0
C47AB107	5.00 W	295.5	0.178	0.018	35	0.1869	0.107	1.493	3	0.000702	1.71	0.000196	4.08	0.0002702	0.15	0.00073	12.33	0.01215	0.27	262.8	0.65	0.51	0	0	0	0	0
C47BC005	5.00 W	295.5	0.178	0.018	35	0.1869	0.107	1.493	3	0.000702	1.71	0.000196	4.08	0.0002702	0.15	0.00073	12.33	0.01215	0.27	262.8	0.65	0.51	0	0	0	0	0
C47AB105	5.00 W	295.5	0.178	0.018	35	0.1869	0.107	1.493	3	0.000702	1.71	0.000196	4.08	0.0002702	0.15	0.00073	12.33	0.01215	0.27	262.8	0.65	0.51	0	0	0	0	0
C47BC008	5.00 W	295.5	0.178	0.018	35	0.1869	0.107	1.493	3	0.000702	1.71	0.000196	4.08	0.0002702	0.15	0.00073	12.33	0.01215	0.27	262.8	0.65	0.51	0	0	0	0	0
C47BC009	5.00 W	295.5	0.178	0.018	35	0.1869	0.107	1.493	3	0.000702	1.71	0.000196	4.08	0.0002702	0.15	0.00073	12.33	0.01215	0.27	262.8	0.65	0.51	0	0	0	0	0
C47AB111	5.00 W	295.5	0.178	0.018	35	0.1869	0.107	1.493	3	0.000702	1.71	0.000196	4.08	0.0002702	0.15	0.00073	12.33	0.01215	0.27	262.8	0.65	0.51	0	0	0	0	0
C47BC003	5.00 W	295.5	0.178	0.018	35	0.1869	0.107	1.493	3	0.000702	1.71	0.000196	4.08	0.0002702	0.15	0.00073	12.33	0.01215	0.27	262.8	0.65	0.51	0	0	0	0	0
C47AB115	5.00 W	295.5	0.178	0.018	35	0.1869	0.107	1.493	3	0.000702	1.71	0.000196	4.08	0.0002702	0.15	0.00073	12.33	0.01215	0.27	262.8	0.65	0.51	0	0	0	0	0
C47AB104	5.00 W	295.5	0.178	0.018	35	0.1869	0.107	1.493	3	0.000702	1.71	0.000196	4.08	0.0002702	0.15	0.00073	12.33	0.01215	0.27	262.8	0.65	0.51	0	0	0	0	0
C47BC007	5.00 W	295.5	0.178	0.018	35	0.1869	0.107	1.493	3	0.000702	1.71	0.000196	4.08	0.0002702	0.15	0.00073	12.33	0.01215	0.27	262.8	0.65	0.51	0	0	0	0	0
C47BC001	5.00 W	295.5	0.178	0.018	35	0.1869	0.107	1.493	3	0.000702	1.71	0.000196	4.08	0.0002702	0.15	0.00073	12.33	0.01215	0.27	262.8	0.65	0.51	0	0	0	0	0
C47BB006	5.00 W	295.5	0.178	0.018	35	0.1869	0.107	1.493	3	0.000702	1.71	0.000196	4.08	0.0002702	0.15	0.00073	12.33	0.01215	0.27	262.8	0.65	0.51	0	0	0	0	0
C47BC002	5.00 W	295.5	0.178	0.018	35	0.1869	0.107	1.493	3	0.000702	1.71	0.000196	4.08	0.0002702	0.15	0.00073	12.33	0.01215	0.27	262.8	0.65	0.51	0	0	0	0	0
C47AB106	5.00 W	295.5	0.178	0.018	35	0.1869	0.107	1.493	3	0.000702	1.71	0.000196	4.08	0.0002702	0.15	0.00073	12.33	0.01215	0.27	262.8	0.65	0.51	0	0	0	0	0
C47BB007	5.00 W	295.5	0.178	0.018	35	0.1869	0.107	1.493	3	0.000702	1.71	0.000196	4.08	0.0002702	0.15	0.00073	12.33	0.01215	0.27	262.8	0.65	0.51	0	0	0	0	0
C47BB008	5.00 W	295.5	0.178	0.018	35	0.1869	0.107	1.493	3	0.000702	1.71	0.000196	4.08	0.0002702	0.15	0.00073	12.33	0.01215	0.27	262.8	0.65	0.51	0	0	0	0	0
C47AB110	5.00 W	295.5	0.178	0.018	35	0.1869	0.107	1.493	3	0.000702	1.71	0.000196	4.08	0.0002702	0.15	0.00073	12.33	0.01215	0.27	262.8	0.65	0.51	0	0	0	0	0

Information on Analysis and Constants Used in Calculations

Sample = 17-73 (1773B)
Material = Phlogopite (0.25-0.5 mm)
Location = Maio, Cape Verdes
Analyst = Jan Sticklus
Project = EXAMPLES
Mass Discrimination Law = POW
Irradiation = can47
J = 0.00105850 ± 0.00000085
TCS2 = 28.344 ± 0.011 Ma
Experiment Type = SAMPLE
Heating = 45 sec
Isolation = 15.00 min
Instrument = MAP216

Age Equations = Conventional
Negative Intensities = Allowed
Decay Constant 40K = 5.543 ± 0.009 E-10 1/a
Decay Constant 39Ar = 2.940 ± 0.016 E-07 1/h
Decay Constant 37Ar = 8.230 ± 0.012 E-04 1/h
Decay Constant 36Cl = 2.257 ± 0.015 E-06 1/a
Atmospheric Ratio 40/36(a) = 295.50 ± 0.53
Atmospheric Ratio 38/36(a) = 0.1869 ± 0.0002
Production Ratio 39/37(ca) = 0.000702 ± 0.000012
Production Ratio 38/37(ca) = 0.000196 ± 0.000008
Production Ratio 36/37(ca) = 0.000270 ± 0.000000
Production Ratio 40/39(k) = 0.000730 ± 0.000090
Production Ratio 38/39(k) = 0.012150 ± 0.000033
Production Ratio 36/38(cl) = 262.80
Scaling Ratio K/Ca = 0.510

Results	40(a)/36(a) ± 2σ	40(r)/39(k) ± 2σ	Age ± 2σ (Ma)	MSWD	39Ar(k) (%,n)	K/Ca ± 2σ
SCTF/MGTF Weighted Mean		5.55131 ± 0.02644 ± 0.48%	10.570 0.053 ± 0.50%	1.49	81.69	1.4 ± 0.6
				8%	20	
		Minimal External Error	0.063	1.65	2σ Confidence Limit	
		Analytical Error	0.050	1.2212	Error Magnification	
Total Fusion Age		5.42294 ± 0.02177 ± 0.40%	10.326 0.044 ± 0.43%		24	7.1 ± 0.1
		Minimal External Error	0.055			
		Analytical Error	0.041			
Normal Isochron	272.77 ± 20.77 ± 7.62%	5.60221 ± 0.04835 ± 0.86%	10.666 0.093 ± 0.88%	2.25	81.69	
No Convergence				0%	20	
		Minimal External Error	0.099	1.67	2σ Confidence Limit	
		Analytical Error	0.092	1.4985	Error Magnification	
				100	Number of Iterations	
				0.0001445546	Convergence	
Inverse Isochron	295.05 ± 18.48 ± 6.26%	5.55238 ± 0.04457 ± 0.80%	10.572 0.086 ± 0.82%	1.57	81.69	
				6%	20	
		Minimal External Error	0.093	1.67	2σ Confidence Limit	
		Analytical Error	0.085	1.2548	Error Magnification	
				3	Number of Iterations	
				0.0000300534	Convergence	
				24%	Spreading Factor	

Blue dots in table indicate selected analyses used to calculate the weighted mean, isochron and inverse isochron ages.
* Alteration Index values in italics indicate analyses from fresh material, normal font is from altered material (Baksi, 2007).
Values shown in red are negative values.
Abbreviations used in tables: (r) = radiogenic ^{40}Ar; (k) = Ar derived from K; (a) = atmospheric Ar; (ca) = Ar derived from Ca; (cl) = Ar derived from Ca; (c) = cosmogenic Ar; MDF = Mass Discrimination Factor.
Green squares in the inverse isochron plots indicate selected steps (blue dots in table), and blue squares are non-selected steps. Pink lines in the inverse isochron plot indicate a line fit through selected data, and the purple lines incidate a fit through an air ^{40}Ar/^{36}Ar ratio (295.5).

Sample 17-74 step-heating results (1774b)

Relative Abundances	Laser power		36Ar [V]	%1σ	37Ar [V]	%1σ	38Ar [V]	%1σ	39Ar [V]	%1σ	40Ar [V]	%1σ	40(r)/39(k) ± 2σ	Age ± 2σ (Ma)	40Ar(r) (%)	39Ar(k) (%)	K/Ca ± 2σ	Step #	$^{36}Ar/^{39}Ar$ Alt. Index*
C47GA121	0.15 W		0.0015721	2.682	0.0052228	13.558	0.0006459	10.910	0.0222650	1.285	0.538969	0.178	3.36134 ± 1.12846	6.41 ± 2.15	13.88	0.34	2.2 ± 0.6	1	0.005510
C47GA122	0.20 W		0.0009602	4.187	0.0073264	9.882	0.0007087	10.547	0.0392881	0.833	0.459354	0.144	4.48465 ± 0.61095	8.54 ± 1.16	38.35	0.59	2.7 ± 0.5	2	0.001905
C47GA123	0.25 W		0.0012465	2.233	0.0066539	10.974	0.0015155	4.750	0.1043083	0.338	0.898379	0.101	5.08598 ± 0.16284	9.69 ± 0.31	59.05	1.57	8.0 ± 1.8	3	0.000932
C47GA124	0.30 W		0.0014086	2.836	0.0069484	9.636	0.0024353	3.233	0.1763223	0.284	1.331749	0.091	5.19479 ± 0.13806	9.89 ± 0.26	68.78	2.66	12.9 ± 2.5	4	0.000623
C47GA125	0.35 W		0.0013770	2.605	0.0112008	7.674	0.0038018	2.004	0.2917418	0.236	1.966166	0.075	5.34717 ± 0.07775	10.18 ± 0.15	79.34	4.40	13.3 ± 2.0	5	*0.000368*
C47GA126	0.40 W		0.0011014	2.770	0.0108074	8.453	0.0049123	1.689	0.3870874	0.245	2.397885	0.063	5.35550 ± 0.05409	10.20 ± 0.10	86.45	5.83	18.3 ± 3.1	6	*0.000222*
C47GA127	0.45 W		0.0011180	2.858	0.0218870	3.897	0.0046257	1.969	0.3652729	0.253	2.305928	0.049	5.41275 ± 0.05891	10.31 ± 0.11	85.74	5.51	8.5 ± 0.7	7	*0.000238*
C47GA128	0.50 W		0.0016134	2.259	0.0255729	4.006	0.0043136	1.805	0.3255684	0.237	2.245717	0.054	5.43928 ± 0.07159	10.36 ± 0.14	78.85	4.91	6.5 ± 0.5	8	*0.000385*
C47GA129	0.55 W		0.0014044	2.108	0.0397751	2.455	0.0067627	1.140	0.5394953	0.238	3.337097	0.048	5.42177 ± 0.04200	10.32 ± 0.08	87.65	8.13	6.9 ± 0.3	9	*0.000202*
C47GA130	0.60 W		0.0015079	2.070	0.0237311	5.359	0.0073145	1.412	0.5801135	0.227	3.559218	0.071	5.36995 ± 0.04109	10.23 ± 0.08	87.52	8.74	12.5 ± 1.3	10	*0.000202*
C47GA131	0.70 W		0.0009633	4.601	0.0177969	4.484	0.0081437	1.079	0.6519269	0.239	3.833380	0.089	5.44499 ± 0.04902	10.37 ± 0.09	92.60	9.83	18.7 ± 1.7	11	*0.000115*
C47GA132	0.80 W		0.0015038	2.615	0.0136894	6.037	0.0080096	1.037	0.6220272	0.223	3.800481	0.074	5.39659 ± 0.04542	10.28 ± 0.09	88.32	9.38	23.2 ± 2.8	12	*0.000188*
C47GA133	0.90 W		0.0012577	3.138	0.0105608	9.687	0.0069039	1.248	0.5431806	0.306	3.314913	0.081	5.41946 ± 0.05522	10.32 ± 0.10	88.80	8.19	26.2 ± 5.1	13	*0.000180*
C47GA134	1.00 W	•	0.0006351	6.652	0.0091939	10.020	0.0074388	1.177	0.6090448	0.217	3.503448	0.049	5.44474 ± 0.04766	10.37 ± 0.09	94.65	9.18	33.8 ± 6.8	14	*0.000081*
C47GA135	1.10 W	•	0.0004485	6.545	0.0031436	22.986	0.0036287	2.348	0.2913290	0.261	1.738348	0.107	5.51217 ± 0.06738	10.50 ± 0.13	92.38	4.39	47.3 ± 21.7	15	*0.000120*
C47GA136	1.20 W	•	0.0002765	10.605	0.0017208	40.809	0.0037333	2.074	0.3134177	0.251	1.806283	0.074	5.50222 ± 0.06240	10.48 ± 0.12	95.47	4.72	92.9 ± 75.8	16	*0.000069*
C47GA137	1.50 W	•	0.0000638	46.021	0.0005113	121.312	0.0020236	3.762	0.1750052	0.286	0.988739	0.083	5.54115 ± 0.10445	10.55 ± 0.20	98.08	2.64	174.6 ± 423.5	17	*0.000029*
C47GA138	3.00 W	•	0.0001166	23.831	0.0010869	69.176	0.0051384	1.712	0.4454081	0.235	2.488875	0.047	5.50999 ± 0.04533	10.49 ± 0.09	98.61	6.71	209.0 ± 289.2	18	*0.000020*
C47GA139	10.00 W	•	0.0004102	7.584	0.0005850	119.483	0.0010410	7.006	0.0885395	0.474	0.627776	0.109	5.72012 ± 0.21523	10.89 ± 0.41	80.68	1.33	77.2 ± 184.5	19	*0.000362*
C47GA140	15.00 W	•	0.0001987	13.310	0.0014429	47.551	0.0007218	9.714	0.0634986	0.515	0.416660	0.145	5.63827 ± 0.25363	10.73 ± 0.48	85.93	0.96	22.4 ± 21.3	20	*0.000244*

Procedure Blanks	Laser power	36Ar [V]	1σ	37Ar [V]	1σ	38Ar [V]	1σ	39Ar [V]	1σ	40Ar [V]	1σ
C47GA121	0.15 W	0.0002830	0.0000241	0.0002165	0.0000243	0.0001650	0.0000702	0.0004066	0.0002458	0.0022067	0.0004708
C47GA122	0.20 W	0.0002938	0.0000241	0.0002236	0.0000243	0.0001722	0.0000702	0.0004165	0.0002458	0.0023262	0.0004708
C47GA123	0.25 W	0.0003087	0.0000241	0.0002339	0.0000243	0.0001855	0.0000702	0.0004506	0.0002458	0.0024492	0.0004708
C47GA124	0.30 W	0.0003270	0.0000241	0.0002470	0.0000243	0.0002038	0.0000702	0.0005053	0.0002458	0.0025738	0.0004708
C47GA125	0.35 W	0.0003481	0.0000241	0.0002621	0.0000243	0.0002262	0.0000702	0.0005766	0.0002458	0.0026975	0.0004708
C47GA126	0.40 W	0.0003874	0.0000241	0.0002905	0.0000243	0.0002699	0.0000702	0.0007214	0.0002458	0.0028947	0.0004708
C47GA127	0.45 W	0.0004126	0.0000241	0.0003086	0.0000243	0.0002987	0.0000702	0.0008189	0.0002458	0.0030057	0.0004708
C47GA128	0.50 W	0.0004374	0.0000241	0.0003262	0.0000243	0.0003272	0.0000702	0.0009160	0.0002458	0.0031045	0.0004708
C47GA129	0.55 W	0.0004628	0.0000241	0.0003440	0.0000243	0.0003564	0.0000702	0.0010159	0.0002458	0.0031962	0.0004708
C47GA130	0.60 W	0.0004872	0.0000241	0.0003608	0.0000243	0.0003844	0.0000702	0.0011115	0.0002458	0.0032747	0.0004708
C47GA131	0.70 W	0.0005239	0.0000241	0.0003847	0.0000243	0.0004257	0.0000702	0.0012500	0.0002458	0.0033699	0.0004708
C47GA132	0.80 W	0.0005427	0.0000241	0.0003959	0.0000243	0.0004460	0.0000702	0.0013158	0.0002458	0.0034029	0.0004708
C47GA133	0.90 W	0.0005582	0.0000241	0.0004041	0.0000243	0.0004616	0.0000702	0.0013634	0.0002458	0.0034148	0.0004708
C47GA134	1.00 W	0.0005697	0.0000241	0.0004085	0.0000243	0.0004716	0.0000702	0.0013893	0.0002458	0.0034034	0.0004708
C47GA135	1.10 W	0.0005765	0.0000241	0.0004088	0.0000243	0.0004751	0.0000702	0.0013896	0.0002458	0.0033664	0.0004708
C47GA136	1.20 W	0.0005758	0.0000241	0.0003984	0.0000243	0.0004640	0.0000702	0.0013238	0.0002458	0.0032433	0.0004708
C47GA137	1.50 W	0.0005671	0.0000241	0.0003846	0.0000243	0.0004455	0.0000702	0.0012380	0.0002458	0.0031279	0.0004708
C47GA138	3.00 W	0.0005513	0.0000241	0.0003646	0.0000243	0.0004170	0.0000702	0.0011128	0.0002458	0.0029790	0.0004708
C47GA139	10.00 W	0.0005278	0.0000241	0.0003377	0.0000243	0.0003775	0.0000702	0.0009447	0.0002458	0.0027943	0.0004708
C47GA140	15.00 W	0.0004971	0.0000241	0.0003046	0.0000243	0.0003282	0.0000702	0.0007379	0.0002458	0.0025800	0.0004708

Sample Parameters	Laser power	Sample	Material	Location	Analyst	Standard (in Ma)	%1σ	J	%1σ	MDF	%1σ	Volume Ratio	Sensitivity (mol/volt)
C47GA121	0.15 W	17-74 (1774b)	Phlogopite	Maio, Cape Verdes	Jan Sticklus	28.344	0.039	1.06E-03	0.08	1.0098	0.21	1	1.211E-14
C47GA122	0.20 W	17-74 (1774b)	Phlogopite	Maio, Cape Verdes	Jan Sticklus	28.344	0.039	1.06E-03	0.08	1.0098	0.21	1	1.211E-14
C47GA123	0.25 W	17-74 (1774b)	Phlogopite	Maio, Cape Verdes	Jan Sticklus	28.344	0.039	1.06E-03	0.08	1.0098	0.21	1	1.211E-14
C47GA124	0.30 W	17-74 (1774b)	Phlogopite	Maio, Cape Verdes	Jan Sticklus	28.344	0.039	1.06E-03	0.08	1.0098	0.21	1	1.211E-14
C47GA125	0.35 W	17-74 (1774b)	Phlogopite	Maio, Cape Verdes	Jan Sticklus	28.344	0.039	1.06E-03	0.08	1.0098	0.21	1	1.211E-14
C47GA126	0.40 W	17-74 (1774b)	Phlogopite	Maio, Cape Verdes	Jan Sticklus	28.344	0.039	1.06E-03	0.08	1.0098	0.21	1	1.211E-14
C47GA127	0.45 W	17-74 (1774b)	Phlogopite	Maio, Cape Verdes	Jan Sticklus	28.344	0.039	1.06E-03	0.08	1.0098	0.21	1	1.211E-14
C47GA128	0.50 W	17-74 (1774b)	Phlogopite	Maio, Cape Verdes	Jan Sticklus	28.344	0.039	1.06E-03	0.08	1.0098	0.21	1	1.211E-14
C47GA129	0.55 W	17-74 (1774b)	Phlogopite	Maio, Cape Verdes	Jan Sticklus	28.344	0.039	1.06E-03	0.08	1.0098	0.21	1	1.211E-14
C47GA130	0.60 W	17-74 (1774b)	Phlogopite	Maio, Cape Verdes	Jan Sticklus	28.344	0.039	1.06E-03	0.08	1.0098	0.21	1	1.211E-14
C47GA131	0.70 W	17-74 (1774b)	Phlogopite	Maio, Cape Verdes	Jan Sticklus	28.344	0.039	1.06E-03	0.08	1.0098	0.21	1	1.211E-14
C47GA132	0.80 W	17-74 (1774b)	Phlogopite	Maio, Cape Verdes	Jan Sticklus	28.344	0.039	1.06E-03	0.08	1.0098	0.21	1	1.211E-14
C47GA133	0.90 W	17-74 (1774b)	Phlogopite	Maio, Cape Verdes	Jan Sticklus	28.344	0.039	1.06E-03	0.08	1.0098	0.21	1	1.211E-14
C47GA134	1.00 W	17-74 (1774b)	Phlogopite	Maio, Cape Verdes	Jan Sticklus	28.344	0.039	1.06E-03	0.08	1.0098	0.21	1	1.211E-14
C47GA135	1.10 W	17-74 (1774b)	Phlogopite	Maio, Cape Verdes	Jan Sticklus	28.344	0.039	1.06E-03	0.08	1.0098	0.21	1	1.211E-14
C47GA136	1.20 W	17-74 (1774b)	Phlogopite	Maio, Cape Verdes	Jan Sticklus	28.344	0.039	1.06E-03	0.08	1.0098	0.21	1	1.211E-14
C47GA137	1.50 W	17-74 (1774b)	Phlogopite	Maio, Cape Verdes	Jan Sticklus	28.344	0.039	1.06E-03	0.08	1.0098	0.21	1	1.211E-14
C47GA138	3.00 W	17-74 (1774b)	Phlogopite	Maio, Cape Verdes	Jan Sticklus	28.344	0.039	1.06E-03	0.08	1.0098	0.21	1	1.211E-14
C47GA139	10.00 W	17-74 (1774b)	Phlogopite	Maio, Cape Verdes	Jan Sticklus	28.344	0.039	1.06E-03	0.08	1.0098	0.21	1	1.211E-14
C47GA140	15.00 W	17-74 (1774b)	Phlogopite	Maio, Cape Verdes	Jan Sticklus	28.344	0.039	1.06E-03	0.08	1.0098	0.21	1	1.211E-14

Day	Month	Year	Hour	Min	Resist	Irradiation	Project	Experiment	Nmb	Standard Name
28	OCT	2018	4	48	1	can47	Examples	c47it5ip4_1774b	01	TCS2
28	OCT	2018	5	17	1	can47	Examples	c47it5ip4_1774b	01	TCS2
28	OCT	2018	5	46	1	can47	Examples	c47it5ip4_1774b	01	TCS2
28	OCT	2018	6	15	1	can47	Examples	c47it5ip4_1774b	01	TCS2
28	OCT	2018	6	44	1	can47	Examples	c47it5ip4_1774b	01	TCS2
28	OCT	2018	7	32	1	can47	Examples	c47it5ip4_1774b	01	TCS2
28	OCT	2018	8	1	1	can47	Examples	c47it5ip4_1774b	01	TCS2
28	OCT	2018	8	29	1	can47	Examples	c47it5ip4_1774b	01	TCS2
28	OCT	2018	8	58	1	can47	Examples	c47it5ip4_1774b	01	TCS2
28	OCT	2018	9	27	1	can47	Examples	c47it5ip4_1774b	01	TCS2
28	OCT	2018	10	15	1	can47	Examples	c47it5ip4_1774b	01	TCS2
28	OCT	2018	10	44	1	can47	Examples	c47it5ip4_1774b	01	TCS2
28	OCT	2018	11	13	1	can47	Examples	c47it5ip4_1774b	01	TCS2
28	OCT	2018	11	42	1	can47	Examples	c47it5ip4_1774b	01	TCS2
28	OCT	2018	12	11	1	can47	Examples	c47it5ip4_1774b	01	TCS2
28	OCT	2018	12	59	1	can47	Examples	c47it5ip4_1774b	01	TCS2
28	OCT	2018	13	28	1	can47	Examples	c47it5ip4_1774b	01	TCS2
28	OCT	2018	13	57	1	can47	Examples	c47it5ip4_1774b	01	TCS2
28	OCT	2018	14	26	1	can47	Examples	c47it5ip4_1774b	01	TCS2
28	OCT	2018	14	54	1	can47	Examples	c47it5ip4_1774b	01	TCS2

Irradiation Constants	Laser power	40/36(a)	%1σ	40/36(c)	%1σ	38/36(a)	%1σ	38/36(c)	%1σ	39/37(ca)	%1σ	38/37(ca)	%1σ	36/37(ca)	%1σ	40/39(k)	%1σ	38/39(k)	%1σ	36/38(cl)	%1σ	K/Ca	%1σ	K/Cl	%1σ	Ca/Cl	%1σ
C47GA121	0.15 W	295.5	0.178	0.018	35	0.1869	0.107	1.493	3	0.000702	1.71	0.000196	4.08	0.0002702	0.15	0.00073	12.33	0.01215	0.27	262.8	0.65	0.51	0	0	0	0	0
C47GA122	0.20 W	295.5	0.178	0.018	35	0.1869	0.107	1.493	3	0.000702	1.71	0.000196	4.08	0.0002702	0.15	0.00073	12.33	0.01215	0.27	262.8	0.65	0.51	0	0	0	0	0
C47GA123	0.25 W	295.5	0.178	0.018	35	0.1869	0.107	1.493	3	0.000702	1.71	0.000196	4.08	0.0002702	0.15	0.00073	12.33	0.01215	0.27	262.8	0.65	0.51	0	0	0	0	0
C47GA124	0.30 W	295.5	0.178	0.018	35	0.1869	0.107	1.493	3	0.000702	1.71	0.000196	4.08	0.0002702	0.15	0.00073	12.33	0.01215	0.27	262.8	0.65	0.51	0	0	0	0	0
C47GA125	0.35 W	295.5	0.178	0.018	35	0.1869	0.107	1.493	3	0.000702	1.71	0.000196	4.08	0.0002702	0.15	0.00073	12.33	0.01215	0.27	262.8	0.65	0.51	0	0	0	0	0
C47GA126	0.40 W	295.5	0.178	0.018	35	0.1869	0.107	1.493	3	0.000702	1.71	0.000196	4.08	0.0002702	0.15	0.00073	12.33	0.01215	0.27	262.8	0.65	0.51	0	0	0	0	0
C47GA127	0.45 W	295.5	0.178	0.018	35	0.1869	0.107	1.493	3	0.000702	1.71	0.000196	4.08	0.0002702	0.15	0.00073	12.33	0.01215	0.27	262.8	0.65	0.51	0	0	0	0	0
C47GA128	0.50 W	295.5	0.178	0.018	35	0.1869	0.107	1.493	3	0.000702	1.71	0.000196	4.08	0.0002702	0.15	0.00073	12.33	0.01215	0.27	262.8	0.65	0.51	0	0	0	0	0
C47GA129	0.55 W	295.5	0.178	0.018	35	0.1869	0.107	1.493	3	0.000702	1.71	0.000196	4.08	0.0002702	0.15	0.00073	12.33	0.01215	0.27	262.8	0.65	0.51	0	0	0	0	0
C47GA130	0.60 W	295.5	0.178	0.018	35	0.1869	0.107	1.493	3	0.000702	1.71	0.000196	4.08	0.0002702	0.15	0.00073	12.33	0.01215	0.27	262.8	0.65	0.51	0	0	0	0	0
C47GA131	0.70 W	295.5	0.178	0.018	35	0.1869	0.107	1.493	3	0.000702	1.71	0.000196	4.08	0.0002702	0.15	0.00073	12.33	0.01215	0.27	262.8	0.65	0.51	0	0	0	0	0
C47GA132	0.80 W	295.5	0.178	0.018	35	0.1869	0.107	1.493	3	0.000702	1.71	0.000196	4.08	0.0002702	0.15	0.00073	12.33	0.01215	0.27	262.8	0.65	0.51	0	0	0	0	0
C47GA133	0.90 W	295.5	0.178	0.018	35	0.1869	0.107	1.493	3	0.000702	1.71	0.000196	4.08	0.0002702	0.15	0.00073	12.33	0.01215	0.27	262.8	0.65	0.51	0	0	0	0	0
C47GA134	1.00 W	295.5	0.178	0.018	35	0.1869	0.107	1.493	3	0.000702	1.71	0.000196	4.08	0.0002702	0.15	0.00073	12.33	0.01215	0.27	262.8	0.65	0.51	0	0	0	0	0
C47GA135	1.10 W	295.5	0.178	0.018	35	0.1869	0.107	1.493	3	0.000702	1.71	0.000196	4.08	0.0002702	0.15	0.00073	12.33	0.01215	0.27	262.8	0.65	0.51	0	0	0	0	0
C47GA136	1.20 W	295.5	0.178	0.018	35	0.1869	0.107	1.493	3	0.000702	1.71	0.000196	4.08	0.0002702	0.15	0.00073	12.33	0.01215	0.27	262.8	0.65	0.51	0	0	0	0	0
C47GA137	1.50 W	295.5	0.178	0.018	35	0.1869	0.107	1.493	3	0.000702	1.71	0.000196	4.08	0.0002702	0.15	0.00073	12.33	0.01215	0.27	262.8	0.65	0.51	0	0	0	0	0
C47GA138	3.00 W	295.5	0.178	0.018	35	0.1869	0.107	1.493	3	0.000702	1.71	0.000196	4.08	0.0002702	0.15	0.00073	12.33	0.01215	0.27	262.8	0.65	0.51	0	0	0	0	0
C47GA139	10.00 W	295.5	0.178	0.018	35	0.1869	0.107	1.493	3	0.000702	1.71	0.000196	4.08	0.0002702	0.15	0.00073	12.33	0.01215	0.27	262.8	0.65	0.51	0	0	0	0	0
C47GA140	15.00 W	295.5	0.178	0.018	35	0.1869	0.107	1.493	3	0.000702	1.71	0.000196	4.08	0.0002702	0.15	0.00073	12.33	0.01215	0.27	262.8	0.65	0.51	0	0	0	0	0

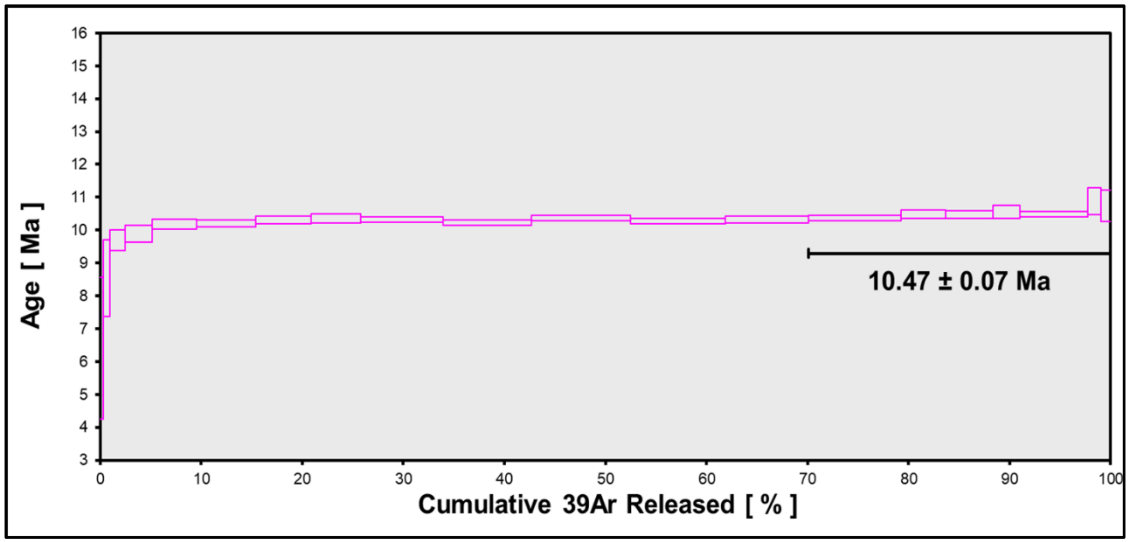

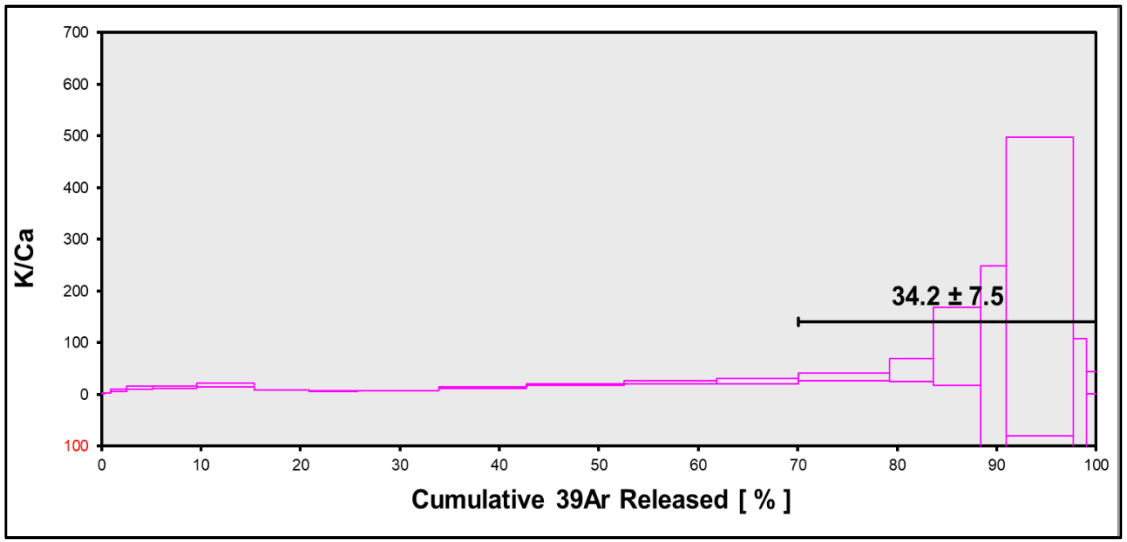
K/Ca
700
600
500
400
300
200
100
0
100
34.2 ± 7.5
0
10
20
30
40
50
60
70
80
90
100
Cumulative 39Ar Released [%]

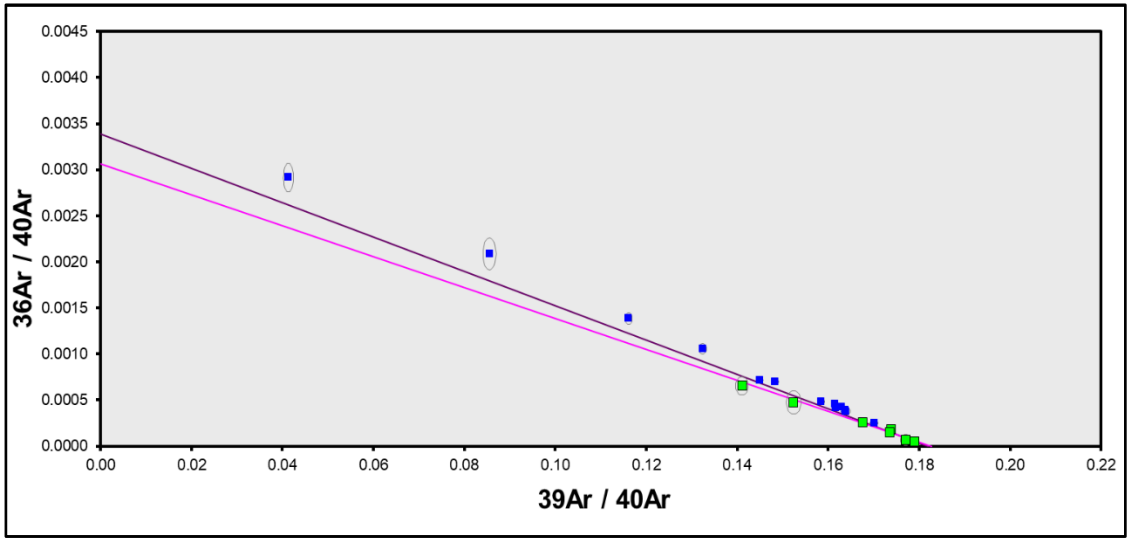
36Ar / 40Ar
0.0045
0.0040
0.0035
0.0030
0.0025
0.0020
0.0015
0.0010
0.0005
0.0000
0.00
0.02
0.04
0.06
0.08
0.10
0.12
0.14
0.16
0.18
0.20
0.22
39Ar / 40Ar

Information on Analysis and Constants Used in Calculations

Sample = 17-74 (1774B)
Material = Phlogopite
Location = Maio, Cape Verde
Analyst = Jan Sticklus
Project = EXAMPLES
Mass Discrimination Law = POW
Irradiation = can47
J = 0.00105850 ± 0.00000085
TCS2 = 28.344 ± 0.011 Ma
Experiment Type = SAMPLE
Heating = 45 sec
Isolation = 15.00 min
Instrument = MAP216
Weight = 4.110 mg
Weight %K = 6.0

Age Equations = Conventional
Negative Intensities = Allowed
Decay Constant 40K = 5.543 ± 0.009 E-10 1/a
Decay Constant 39Ar = 2.940 ± 0.016 E-07 1/h
Decay Constant 37Ar = 8.230 ± 0.012 E-04 1/h
Decay Constant 36Cl = 2.257 ± 0.015 E-06 1/a
Atmospheric Ratio 40/36(a) = 295.50 ± 0.53
Atmospheric Ratio 38/36(a) = 0.1869 ± 0.0002
Production Ratio 39/37(ca) = 0.000702 ± 0.000012
Production Ratio 38/37(ca) = 0.000196 ± 0.000008
Production Ratio 36/37(ca) = 0.000270 ± 0.000000
Production Ratio 40/39(k) = 0.000730 ± 0.000090
Production Ratio 38/39(k) = 0.012150 ± 0.000033
Production Ratio 36/38(cl) = 262.80
Scaling Ratio K/Ca = 0.510

Results

Results	40(a)/36(a) ± 2σ	40(r)/39(k) ± 2σ	Age ± 2σ (Ma)	MSWD	39Ar(k) (%,n)	K/Ca ± 2σ
SH Weighted Mean		5.49638 ± 0.03555	10.466 0.070	1.94	29.94	34.2 ± 7.5
		± 0.65%	± 0.66%	7%	7	
		Minimal External Error	0.077	2.15	2σ Confidence Limit	
		Analytical Error	0.067	1.3918	Error Magnification	
Total Fusion Age		5.41142 ± 0.01568	10.304 ± 0.034		20	15.6 ± 0.5
		± 0.29%	± 0.33%			
		Minimal External Error	± 0.047			
		Analytical Error	± 0.030			
Normal Isochron	281.30 ± 67.75	5.51395 ± 0.07155	10.50 ± 0.14	2.86	29.94	
Error Chron	± 24.08%	± 1.30%	± 1.30%	1%	7	
		Minimal External Error	± 0.14	2.26	2σ Confidence Limit	
		Analytical Error	± 0.14	1.6913	Error Magnification	
				1	Number of Iterations	
				0.0000211181	Convergence	
Inverse Isochron	326.11 ± 55.46	5.46991 ± 0.05987	10.42 ± 0.11	1.79	29.94	
	± 17.01%	± 1.09%	± 1.10%	11%	7	
		Minimal External Error	± 0.12	2.26	2σ Confidence Limit	
		Analytical Error	± 0.11	1.3375	Error Magnification	
				4	Number of Iterations	
				0.0000769806	Convergence	
				21%	Spreading Factor	

Blue dots in table indicate selected steps used to calculate the weighted mean, isochron and inverse isochron ages.
* Alteration Index values in italics indicate analyses from fresh material, normal font is from altered material (Baksi, 2007).
Values shown in red are negative values.
Abbreviations used in tables: (r) = radiogenic ^{40}Ar; (k) = Ar derived from K; (a) = atmospheric Ar; (ca) = Ar derived from Ca; (cl) = Ar derived from Cl; (c) = cosmogenic Ar; MDF = Mass Discrimination Factor.
Green squares in the inverse isochron plots indicate selected steps (blue dots in table), and blue squares are non-selected steps. Pink lines in the inverse isochron plot indicate a line fit through selected data, and the purple lines incidate a fit through an air ^{40}Ar/^{36}Ar ratio (295.5).

Sample 17-74 single-crystal total-fusion results (1774b)

Relative Abundances	Laser power		36Ar [V]	%1σ	37Ar [V]	%1σ	38Ar [V]	%1σ	39Ar [V]	%1σ	40Ar [V]	%1σ	40(r)/39(k) ± 2σ	Age ± 2σ (Ma)	40Ar(r) (%)	39Ar(k) (%)	K/Ca ± 2σ	Sample weight (mg)	$^{36}Ar/^{39}Ar$ Alt. Index	Wt. % K
C47BA047	5.00 W		0.0007627	2.908	0.0019899	2.361	0.0016559	1.962	0.1247220	0.312	0.860786	0.110	5.09524 ± 0.11104	9.70 ± 0.21	73.83	2.01	32.0 ± 1.5	0.075	*0.000492*	6.1
C47BA045	5.00 W		0.0009257	2.276	0.0022417	1.754	0.0024569	1.069	0.1898658	0.273	1.285962	0.089	5.33258 ± 0.07293	10.15 ± 0.14	78.73	3.06	43.2 ± 1.5	0.109	*0.000411*	6.4
C47BA044	5.00 W	•	0.0009031	2.537	0.0018851	2.161	0.0030405	1.263	0.2375934	0.302	1.539508	0.119	5.35636 ± 0.06746	10.20 ± 0.13	82.66	3.83	64.3 ± 2.8	0.134	*0.000326*	6.5
C47BC020	5.00 W	•	0.0045839	1.173	0.0108973	1.200	0.0066712	0.871	0.4766490	0.250	3.929507	0.094	5.40341 ± 0.07426	10.29 ± 0.14	65.54	7.68	22.3 ± 0.5	0.295	*0.000751*	5.9
C47BC016	5.00 W	•	0.0028295	1.918	0.0009254	4.223	0.0027890	2.035	0.1897898	0.265	1.863577	0.125	5.41338 ± 0.17388	10.31 ± 0.33	55.13	3.06	104.6 ± 8.9	0.102	0.001342	6.8
C47BC019	5.00 W	•	0.0014528	2.705	0.0053395	1.552	0.0054519	1.089	0.4316481	0.228	2.775467	0.085	5.43565 ± 0.06032	10.35 ± 0.11	84.54	6.95	41.2 ± 1.3	0.266	*0.000264*	5.9
C47BA036	5.00 W	•	0.0001536	10.114	0.0015951	2.314	0.0019309	1.090	0.1605770	0.241	0.918829	0.074	5.43940 ± 0.06348	10.36 ± 0.12	95.06	2.59	51.3 ± 2.4	0.086	*0.000086*	6.8
C47BC017	5.00 W	•	0.0008856	3.424	0.0005538	7.981	0.0020595	2.127	0.1638042	0.256	1.153138	0.156	5.44166 ± 0.11517	10.36 ± 0.22	77.30	2.64	150.8 ± 24.1	0.091	*0.000471*	6.6
C47BA040	5.00 W	•	0.0033635	1.315	0.0009352	4.358	0.0032139	1.077	0.2189715	0.251	2.186499	0.097	5.44592 ± 0.12508	10.37 ± 0.24	54.54	3.53	119.4 ± 10.4	0.123	0.001323	6.5
C47BA037	5.00 W	•	0.0006550	3.313	0.0014627	3.516	0.0028807	1.626	0.2314692	0.266	1.456715	0.133	5.45701 ± 0.06483	10.39 ± 0.12	86.71	3.73	80.7 ± 5.7	0.129	*0.000246*	6.6
C47BC010	5.00 W	•	0.0031445	1.302	0.0024419	2.167	0.0038694	1.587	0.2733444	0.222	2.420862	0.108	5.45712 ± 0.09456	10.39 ± 0.18	61.62	4.40	57.1 ± 2.5	0.148	*0.001028*	6.7
C47BC014	5.00 W	•	0.0002907	8.544	0.0113558	0.876	0.0049917	1.355	0.4180138	0.231	2.366895	0.085	5.45830 ± 0.04427	10.39 ± 0.08	96.40	6.73	18.8 ± 0.3	0.239	*0.000058*	6.4
C47BA039	5.00 W	•	0.0010300	3.131	0.0004900	6.389	0.0017162	1.875	0.1295291	0.288	1.011756	0.110	5.46080 ± 0.15168	10.40 ± 0.29	69.91	2.09	134.8 ± 17.2	0.071	*0.000702*	6.7
C47BC013	5.00 W	•	0.0004277	5.490	0.0097881	1.253	0.0048207	1.186	0.4024799	0.224	2.327339	0.090	5.46979 ± 0.04361	10.42 ± 0.08	94.59	6.48	21.0 ± 0.5	0.227	*0.000091*	6.5
C47BA038	5.00 W	•	0.0013896	2.068	0.0014432	2.913	0.0024400	1.622	0.1825014	0.229	1.409061	0.161	5.47078 ± 0.09982	10.42 ± 0.19	70.86	2.94	64.5 ± 3.8	0.101	*0.000665*	6.6
C47BC011	5.00 W	•	0.0007158	3.591	0.0013399	3.727	0.0038078	1.647	0.3067607	0.225	1.890586	0.125	5.47319 ± 0.05750	10.42 ± 0.11	88.81	4.94	116.8 ± 8.7	0.170	*0.000204*	6.6
C47BC018	5.00 W	•	0.0004017	5.913	0.0062398	1.154	0.0061498	1.088	0.5119374	0.252	2.922309	0.109	5.47673 ± 0.04082	10.43 ± 0.08	95.94	8.24	41.8 ± 1.0	0.298	*0.000065*	6.3
C47BC012	5.00 W	•	0.0015620	1.978	0.0011702	3.897	0.0047594	1.322	0.3772496	0.252	2.528162	0.071	5.47757 ± 0.05670	10.43 ± 0.11	81.74	6.08	164.4 ± 12.8	0.208	*0.000363*	6.6
C47BC021	5.00 W	•	0.0010645	2.791	0.0027008	1.912	0.0035140	1.586	0.2740552	0.254	1.815895	0.114	5.47834 ± 0.07157	10.43 ± 0.14	82.68	4.41	51.7 ± 2.0	0.159	*0.000324*	6.3
C47BA046	5.00 W	•	0.0008242	1.980	0.0014225	3.179	0.0025239	1.237	0.1998984	0.250	1.340965	0.053	5.48979 ± 0.05615	10.45 ± 0.11	81.84	3.22	71.7 ± 4.6	0.112	*0.000356*	6.5
C47BA042	5.00 W	•	0.0004980	3.605	0.0026203	1.954	0.0024806	1.515	0.2015879	0.271	1.255295	0.120	5.49739 ± 0.06236	10.47 ± 0.12	88.28	3.25	39.2 ± 1.5	0.110	*0.000219*	6.7
C47BA041	5.00 W	•	0.0011856	2.176	0.0008310	4.970	0.0017234	1.745	0.1273254	0.279	1.052108	0.103	5.51129 ± 0.12517	10.49 ± 0.24	66.70	2.05	78.1 ± 7.8	0.072	*0.000797*	6.5
C47BA043	5.00 W	•	0.0015687	1.541	0.0007769	5.569	0.0034750	1.331	0.2733843	0.228	1.973668	0.080	5.52333 ± 0.05947	10.52 ± 0.11	76.51	4.40	179.5 ± 20.0	0.152	*0.000499*	6.6
C47BC015	5.00 W	•	0.0000885	23.422	0.0003458	12.329	0.0012524	3.449	0.1066739	0.392	0.615532	0.265	5.52469 ± 0.12646	10.52 ± 0.24	95.74	1.72	157.3 ± 38.8	0.055	*0.000078*	7.1
		Σ	0.0307067	0.488	0.0707922	0.427	0.0796746	0.297	6.2098314	0.055	42.900422	0.023								

Procedure Blanks	Laser power	36Ar [V]	1σ	37Ar [V]	1σ	38Ar [V]	1σ	39Ar [V]	1σ	40Ar [V]	1σ
C47BA047	5.00 W	0.0001696	0.0000109	0.0002472	0.0000096	0.0000896	0.0000140	0.0004178	0.0000337	0.0061090	0.0004987
C47BA045	5.00 W	0.0001653	0.0000109	0.0002458	0.0000096	0.0000856	0.0000140	0.0003878	0.0000337	0.0058566	0.0004987
C47BA044	5.00 W	0.0001631	0.0000109	0.0002451	0.0000096	0.0000836	0.0000140	0.0003726	0.0000337	0.0057281	0.0004987
C47BC020	5.00 W	0.0002599	0.0000190	0.0003312	0.0000106	0.0001588	0.0000380	0.0005468	0.0001478	0.0055566	0.0014613
C47BC016	5.00 W	0.0002309	0.0000190	0.0003117	0.0000106	0.0001280	0.0000380	0.0003844	0.0001478	0.0045068	0.0014613
C47BC019	5.00 W	0.0002526	0.0000190	0.0003263	0.0000106	0.0001511	0.0000380	0.0005062	0.0001478	0.0052941	0.0014613
C47BA036	5.00 W	0.0001443	0.0000109	0.0002389	0.0000096	0.0000660	0.0000140	0.0002409	0.0000337	0.0046209	0.0004987
C47BC017	5.00 W	0.0002381	0.0000190	0.0003166	0.0000106	0.0001357	0.0000380	0.0004250	0.0001478	0.0047692	0.0014613
C47BA040	5.00 W	0.0001530	0.0000109	0.0002418	0.0000096	0.0000741	0.0000140	0.0003015	0.0000337	0.0051302	0.0004987
C47BA037	5.00 W	0.0001464	0.0000109	0.0002396	0.0000096	0.0000680	0.0000140	0.0002557	0.0000337	0.0047449	0.0004987
C47BC010	5.00 W	0.0001830	0.0000190	0.0002795	0.0000106	0.0000770	0.0000380	0.0001155	0.0001478	0.0027691	0.0014613
C47BC014	5.00 W	0.0002117	0.0000190	0.0002988	0.0000106	0.0001075	0.0000380	0.0002765	0.0001478	0.0038099	0.0014613
C47BA039	5.00 W	0.0001508	0.0000109	0.0002410	0.0000096	0.0000721	0.0000140	0.0002862	0.0000337	0.0050018	0.0004987
C47BC013	5.00 W	0.0002044	0.0000190	0.0002940	0.0000106	0.0000998	0.0000380	0.0002359	0.0001478	0.0035474	0.0014613
C47BA038	5.00 W	0.0001486	0.0000109	0.0002403	0.0000096	0.0000700	0.0000140	0.0002709	0.0000337	0.0048734	0.0004987
C47BC011	5.00 W	0.0001902	0.0000190	0.0002844	0.0000106	0.0000847	0.0000380	0.0001561	0.0001478	0.0030316	0.0014613
C47BC018	5.00 W	0.0002454	0.0000190	0.0003214	0.0000106	0.0001434	0.0000380	0.0004656	0.0001478	0.0050317	0.0014613
C47BC012	5.00 W	0.0001972	0.0000190	0.0002891	0.0000106	0.0000921	0.0000380	0.0001953	0.0001478	0.0032850	0.0014613
C47BC021	5.00 W	0.0002668	0.0000190	0.0003359	0.0000106	0.0001663	0.0000380	0.0005860	0.0001478	0.0058100	0.0014613
C47BA046	5.00 W	0.0001674	0.0000109	0.0002465	0.0000096	0.0000876	0.0000140	0.0004026	0.0000337	0.0059806	0.0004987
C47BA042	5.00 W	0.0001588	0.0000109	0.0002437	0.0000096	0.0000795	0.0000140	0.0003420	0.0000337	0.0054713	0.0004987
C47BA041	5.00 W	0.0001552	0.0000109	0.0002425	0.0000096	0.0000761	0.0000140	0.0003167	0.0000337	0.0052587	0.0004987
C47BA043	5.00 W	0.0001610	0.0000109	0.0002444	0.0000096	0.0000816	0.0000140	0.0003573	0.0000337	0.0055997	0.0004987
C47BC015	5.00 W	0.0002189	0.0000190	0.0003037	0.0000106	0.0001153	0.0000380	0.0003171	0.0001478	0.0040723	0.0014613

Sample Parameters	Laser power	Sample	Material	Location	Analyst	Standard (in Ma)	%1σ	J	%1σ	MDF	%1σ	Volume Ratio	Sensitivity (mol/volt)
C47BA047	5.00 W	17-74 (1774b)	Phlogopite	Maio, Cape Verdes	Jan Sticklus	28.344	0.039	1.06E-03	0.08	1.0098	0.21	1	1.211E-14
C47BA045	5.00 W	17-74 (1774b)	Phlogopite	Maio, Cape Verdes	Jan Sticklus	28.344	0.039	1.06E-03	0.08	1.0098	0.21	1	1.211E-14
C47BA044	5.00 W	17-74 (1774b)	Phlogopite	Maio, Cape Verdes	Jan Sticklus	28.344	0.039	1.06E-03	0.08	1.0098	0.21	1	1.211E-14
C47BC020	5.00 W	17-74 (1774b)	Phlogopite	Maio, Cape Verdes	Jan Sticklus	28.344	0.039	1.06E-03	0.08	1.0098	0.21	1	1.211E-14
C47BC016	5.00 W	17-74 (1774b)	Phlogopite	Maio, Cape Verdes	Jan Sticklus	28.344	0.039	1.06E-03	0.08	1.0098	0.21	1	1.211E-14
C47BC019	5.00 W	17-74 (1774b)	Phlogopite	Maio, Cape Verdes	Jan Sticklus	28.344	0.039	1.06E-03	0.08	1.0098	0.21	1	1.211E-14
C47BA036	5.00 W	17-74 (1774b)	Phlogopite	Maio, Cape Verdes	Jan Sticklus	28.344	0.039	1.06E-03	0.08	1.0098	0.21	1	1.211E-14
C47BC017	5.00 W	17-74 (1774b)	Phlogopite	Maio, Cape Verdes	Jan Sticklus	28.344	0.039	1.06E-03	0.08	1.0098	0.21	1	1.211E-14
C47BA040	5.00 W	17-74 (1774b)	Phlogopite	Maio, Cape Verdes	Jan Sticklus	28.344	0.039	1.06E-03	0.08	1.0098	0.21	1	1.211E-14
C47BA037	5.00 W	17-74 (1774b)	Phlogopite	Maio, Cape Verdes	Jan Sticklus	28.344	0.039	1.06E-03	0.08	1.0098	0.21	1	1.211E-14
C47BC010	5.00 W	17-74 (1774b)	Phlogopite	Maio, Cape Verdes	Jan Sticklus	28.344	0.039	1.06E-03	0.08	1.0098	0.21	1	1.211E-14
C47BC014	5.00 W	17-74 (1774b)	Phlogopite	Maio, Cape Verdes	Jan Sticklus	28.344	0.039	1.06E-03	0.08	1.0098	0.21	1	1.211E-14
C47BA039	5.00 W	17-74 (1774b)	Phlogopite	Maio, Cape Verdes	Jan Sticklus	28.344	0.039	1.06E-03	0.08	1.0098	0.21	1	1.211E-14
C47BC013	5.00 W	17-74 (1774b)	Phlogopite	Maio, Cape Verdes	Jan Sticklus	28.344	0.039	1.06E-03	0.08	1.0098	0.21	1	1.211E-14
C47BA038	5.00 W	17-74 (1774b)	Phlogopite	Maio, Cape Verdes	Jan Sticklus	28.344	0.039	1.06E-03	0.08	1.0098	0.21	1	1.211E-14
C47BC011	5.00 W	17-74 (1774b)	Phlogopite	Maio, Cape Verdes	Jan Sticklus	28.344	0.039	1.06E-03	0.08	1.0098	0.21	1	1.211E-14
C47BC018	5.00 W	17-74 (1774b)	Phlogopite	Maio, Cape Verdes	Jan Sticklus	28.344	0.039	1.06E-03	0.08	1.0098	0.21	1	1.211E-14
C47BC012	5.00 W	17-74 (1774b)	Phlogopite	Maio, Cape Verdes	Jan Sticklus	28.344	0.039	1.06E-03	0.08	1.0098	0.21	1	1.211E-14
C47BC021	5.00 W	17-74 (1774b)	Phlogopite	Maio, Cape Verdes	Jan Sticklus	28.344	0.039	1.06E-03	0.08	1.0098	0.21	1	1.211E-14
C47BA046	5.00 W	17-74 (1774b)	Phlogopite	Maio, Cape Verdes	Jan Sticklus	28.344	0.039	1.06E-03	0.08	1.0098	0.21	1	1.211E-14
C47BA042	5.00 W	17-74 (1774b)	Phlogopite	Maio, Cape Verdes	Jan Sticklus	28.344	0.039	1.06E-03	0.08	1.0098	0.21	1	1.211E-14
C47BA041	5.00 W	17-74 (1774b)	Phlogopite	Maio, Cape Verdes	Jan Sticklus	28.344	0.039	1.06E-03	0.08	1.0098	0.21	1	1.211E-14
C47BA043	5.00 W	17-74 (1774b)	Phlogopite	Maio, Cape Verdes	Jan Sticklus	28.344	0.039	1.06E-03	0.08	1.0098	0.21	1	1.211E-14
C47BC015	5.00 W	17-74 (1774b)	Phlogopite	Maio, Cape Verdes	Jan Sticklus	28.344	0.039	1.06E-03	0.08	1.0098	0.21	1	1.211E-14

Day	Month	Year	Hour	Min	Resist	Irradiation	Project	Experiment	Nmb	Standard Name
29	JUN	2018	10	20	1	can47	Examples	c47it5ip4_1774b	01	TCS2
29	JUN	2018	9	23	1	can47	Examples	c47it5ip4_1774b	01	TCS2
29	JUN	2018	8	54	1	can47	Examples	c47it5ip4_1774b	01	TCS2
2	JUL	2018	21	27	1	can47	Examples	c47it5ip4_1774b	01	TCS2
2	JUL	2018	19	31	1	can47	Examples	c47it5ip4_1774b	01	TCS2
2	JUL	2018	20	58	1	can47	Examples	c47it5ip4_1774b	01	TCS2
29	JUN	2018	4	44	1	can47	Examples	c47it5ip4_1774b	01	TCS2
2	JUL	2018	20	0	1	can47	Examples	c47it5ip4_1774b	01	TCS2
29	JUN	2018	6	39	1	can47	Examples	c47it5ip4_1774b	01	TCS2
29	JUN	2018	5	12	1	can47	Examples	c47it5ip4_1774b	01	TCS2
2	JUL	2018	16	19	1	can47	Examples	c47it5ip4_1774b	01	TCS2
2	JUL	2018	18	14	1	can47	Examples	c47it5ip4_1774b	01	TCS2
29	JUN	2018	6	10	1	can47	Examples	c47it5ip4_1774b	01	TCS2
2	JUL	2018	17	45	1	can47	Examples	c47it5ip4_1774b	01	TCS2
29	JUN	2018	5	41	1	can47	Examples	c47it5ip4_1774b	01	TCS2
2	JUL	2018	16	48	1	can47	Examples	c47it5ip4_1774b	01	TCS2
2	JUL	2018	20	29	1	can47	Examples	c47it5ip4_1774b	01	TCS2
2	JUL	2018	17	16	1	can47	Examples	c47it5ip4_1774b	01	TCS2
2	JUL	2018	21	55	1	can47	Examples	c47it5ip4_1774b	01	TCS2
29	JUN	2018	9	51	1	can47	Examples	c47it5ip4_1774b	01	TCS2
29	JUN	2018	7	56	1	can47	Examples	c47it5ip4_1774b	01	TCS2
29	JUN	2018	7	8	1	can47	Examples	c47it5ip4_1774b	01	TCS2
29	JUN	2018	8	25	1	can47	Examples	c47it5ip4_1774b	01	TCS2
2	JUL	2018	18	43	1	can47	Examples	c47it5ip4_1774b	01	TCS2

Irradiation Constants	Laser power	40/36(a)	%1σ	40/36(c)	%1σ	38/36(a)	%1σ	38/36(c)	%1σ	39/37(ca)	%1σ	38/37(ca)	%1σ	36/37(ca)	%1σ	40/39(k)	%1σ	38/39(k)	%1σ	36/38(cl)	%1σ	K/Ca	%1σ	K/Cl	%1σ	Ca/Cl	%1σ
C47BA047	5.00 W	295.5	0.178	0.018	35	0.1869	0.107	1.493	3	0.000702	1.71	0.000196	4.08	0.0002702	0.15	0.00073	12.33	0.01215	0.27	262.8	0.65	0.51	0	0	0	0	0
C47BA045	5.00 W	295.5	0.178	0.018	35	0.1869	0.107	1.493	3	0.000702	1.71	0.000196	4.08	0.0002702	0.15	0.00073	12.33	0.01215	0.27	262.8	0.65	0.51	0	0	0	0	0
C47BA044	5.00 W	295.5	0.178	0.018	35	0.1869	0.107	1.493	3	0.000702	1.71	0.000196	4.08	0.0002702	0.15	0.00073	12.33	0.01215	0.27	262.8	0.65	0.51	0	0	0	0	0
C47BC020	5.00 W	295.5	0.178	0.018	35	0.1869	0.107	1.493	3	0.000702	1.71	0.000196	4.08	0.0002702	0.15	0.00073	12.33	0.01215	0.27	262.8	0.65	0.51	0	0	0	0	0
C47BC016	5.00 W	295.5	0.178	0.018	35	0.1869	0.107	1.493	3	0.000702	1.71	0.000196	4.08	0.0002702	0.15	0.00073	12.33	0.01215	0.27	262.8	0.65	0.51	0	0	0	0	0
C47BC019	5.00 W	295.5	0.178	0.018	35	0.1869	0.107	1.493	3	0.000702	1.71	0.000196	4.08	0.0002702	0.15	0.00073	12.33	0.01215	0.27	262.8	0.65	0.51	0	0	0	0	0
C47BA036	5.00 W	295.5	0.178	0.018	35	0.1869	0.107	1.493	3	0.000702	1.71	0.000196	4.08	0.0002702	0.15	0.00073	12.33	0.01215	0.27	262.8	0.65	0.51	0	0	0	0	0
C47BC017	5.00 W	295.5	0.178	0.018	35	0.1869	0.107	1.493	3	0.000702	1.71	0.000196	4.08	0.0002702	0.15	0.00073	12.33	0.01215	0.27	262.8	0.65	0.51	0	0	0	0	0
C47BA040	5.00 W	295.5	0.178	0.018	35	0.1869	0.107	1.493	3	0.000702	1.71	0.000196	4.08	0.0002702	0.15	0.00073	12.33	0.01215	0.27	262.8	0.65	0.51	0	0	0	0	0
C47BA037	5.00 W	295.5	0.178	0.018	35	0.1869	0.107	1.493	3	0.000702	1.71	0.000196	4.08	0.0002702	0.15	0.00073	12.33	0.01215	0.27	262.8	0.65	0.51	0	0	0	0	0
C47BC010	5.00 W	295.5	0.178	0.018	35	0.1869	0.107	1.493	3	0.000702	1.71	0.000196	4.08	0.0002702	0.15	0.00073	12.33	0.01215	0.27	262.8	0.65	0.51	0	0	0	0	0
C47BC014	5.00 W	295.5	0.178	0.018	35	0.1869	0.107	1.493	3	0.000702	1.71	0.000196	4.08	0.0002702	0.15	0.00073	12.33	0.01215	0.27	262.8	0.65	0.51	0	0	0	0	0
C47BA039	5.00 W	295.5	0.178	0.018	35	0.1869	0.107	1.493	3	0.000702	1.71	0.000196	4.08	0.0002702	0.15	0.00073	12.33	0.01215	0.27	262.8	0.65	0.51	0	0	0	0	0
C47BC013	5.00 W	295.5	0.178	0.018	35	0.1869	0.107	1.493	3	0.000702	1.71	0.000196	4.08	0.0002702	0.15	0.00073	12.33	0.01215	0.27	262.8	0.65	0.51	0	0	0	0	0
C47BA038	5.00 W	295.5	0.178	0.018	35	0.1869	0.107	1.493	3	0.000702	1.71	0.000196	4.08	0.0002702	0.15	0.00073	12.33	0.01215	0.27	262.8	0.65	0.51	0	0	0	0	0
C47BC011	5.00 W	295.5	0.178	0.018	35	0.1869	0.107	1.493	3	0.000702	1.71	0.000196	4.08	0.0002702	0.15	0.00073	12.33	0.01215	0.27	262.8	0.65	0.51	0	0	0	0	0
C47BC018	5.00 W	295.5	0.178	0.018	35	0.1869	0.107	1.493	3	0.000702	1.71	0.000196	4.08	0.0002702	0.15	0.00073	12.33	0.01215	0.27	262.8	0.65	0.51	0	0	0	0	0
C47BC012	5.00 W	295.5	0.178	0.018	35	0.1869	0.107	1.493	3	0.000702	1.71	0.000196	4.08	0.0002702	0.15	0.00073	12.33	0.01215	0.27	262.8	0.65	0.51	0	0	0	0	0
C47BC021	5.00 W	295.5	0.178	0.018	35	0.1869	0.107	1.493	3	0.000702	1.71	0.000196	4.08	0.0002702	0.15	0.00073	12.33	0.01215	0.27	262.8	0.65	0.51	0	0	0	0	0
C47BA046	5.00 W	295.5	0.178	0.018	35	0.1869	0.107	1.493	3	0.000702	1.71	0.000196	4.08	0.0002702	0.15	0.00073	12.33	0.01215	0.27	262.8	0.65	0.51	0	0	0	0	0
C47BA042	5.00 W	295.5	0.178	0.018	35	0.1869	0.107	1.493	3	0.000702	1.71	0.000196	4.08	0.0002702	0.15	0.00073	12.33	0.01215	0.27	262.8	0.65	0.51	0	0	0	0	0
C47BA041	5.00 W	295.5	0.178	0.018	35	0.1869	0.107	1.493	3	0.000702	1.71	0.000196	4.08	0.0002702	0.15	0.00073	12.33	0.01215	0.27	262.8	0.65	0.51	0	0	0	0	0
C47BA043	5.00 W	295.5	0.178	0.018	35	0.1869	0.107	1.493	3	0.000702	1.71	0.000196	4.08	0.0002702	0.15	0.00073	12.33	0.01215	0.27	262.8	0.65	0.51	0	0	0	0	0
C47BC015	5.00 W	295.5	0.178	0.018	35	0.1869	0.107	1.493	3	0.000702	1.71	0.000196	4.08	0.0002702	0.15	0.00073	12.33	0.01215	0.27	262.8	0.65	0.51	0	0	0	0	0

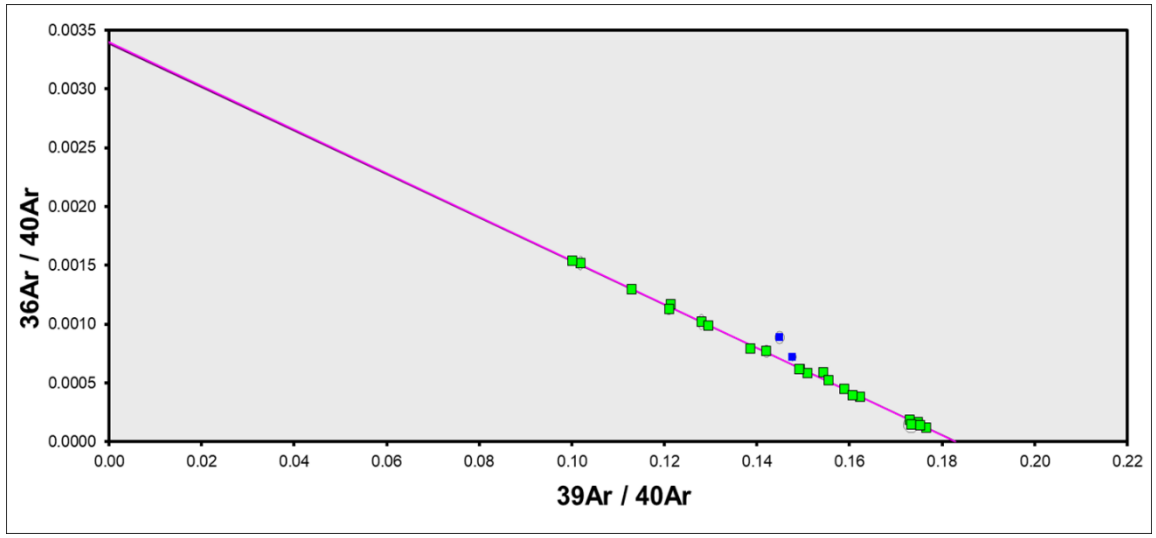

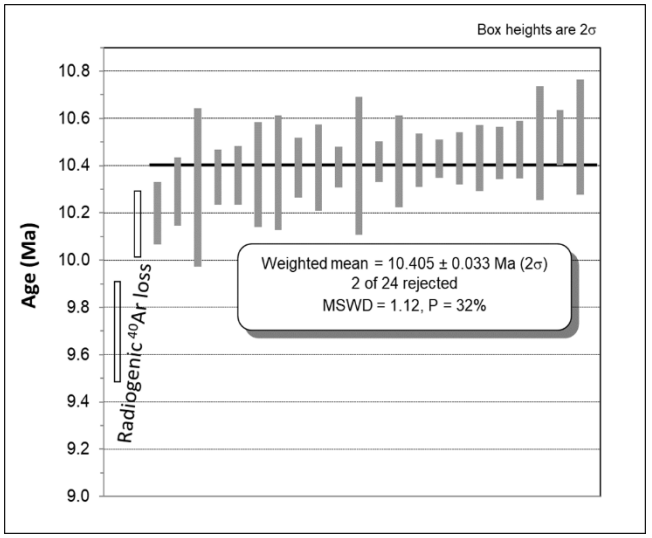

Information on Analysis and Constants Used in Calculations

Sample = 17-74 (1774B)
Material = Phlogopite
Location = Maio, Cape Verde
Analyst = Jan Sticklus
Project = EXAMPLES
Mass Discrimination Law = POW
Irradiation = can47
J = 0.00105850 ± 0.00000085
TCS2 = 28.344 ± 0.011 Ma
Experiment Type = SAMPLE
Heating = 45 sec
Isolation = 15.00 min
Instrument = MAP216

Age Equations = Conventional
Negative Intensities = Allowed
Decay Constant 40K = 5.543 ± 0.009 E-10 1/a
Decay Constant 39Ar = 2.940 ± 0.016 E-07 1/h
Decay Constant 37Ar = 8.230 ± 0.012 E-04 1/h
Decay Constant 36Cl = 2.257 ± 0.015 E-06 1/a
Atmospheric Ratio 40/36(a) = 295.50 ± 0.53
Atmospheric Ratio 38/36(a) = 0.1869 ± 0.0002
Production Ratio 39/37(ca) = 0.000702 ± 0.000012
Production Ratio 38/37(ca) = 0.000196 ± 0.000008
Production Ratio 36/37(ca) = 0.000270 ± 0.000000
Production Ratio 40/39(k) = 0.000730 ± 0.000090
Production Ratio 38/39(k) = 0.012150 ± 0.000033
Production Ratio 36/38(cl) = 262.80
Scaling Ratio K/Ca = 0.510

Results

Results	40(a)/36(a) ± 2σ	40(r)/39(k) ± 2σ	Age ± 2σ (Ma)	MSWD	39Ar(k) (%,n)	K/Ca ± 2σ
SCTF Weighted Mean		5.46460 ± 0.01492 (± 0.27%)	10.405 ± 0.033 (± 0.32%)	1.12	94.93	24.5 ± 5.1
				32%	22	
		Minimal External Error ± 0.047		1.62	2σ Confidence Limit	
		Analytical Error ± 0.028		1.0571	Error Magnification	
Total Fusion Age		5.44749 ± 0.01587 (± 0.29%)	10.373 ± 0.034 (± 0.33%)		24	44.7 ± 0.4
		Minimal External Error ± 0.048				
		Analytical Error ± 0.030				
Normal Isochron	292.53 ± 5.03 (± 1.72%)	5.47694 ± 0.02300 (± 0.42%)	10.429 ± 0.047 (± 0.45%)	1.27	94.93	
				19%	22	
		Minimal External Error ± 0.057		1.63	2σ Confidence Limit	
		Analytical Error ± 0.044		1.1270	Error Magnification	
				1	Number of Iterations	
				0.0000479385	Convergence	
Inverse Isochron	294.24 ± 4.86 (± 1.65%)	5.46901 ± 0.02243 (± 0.41%)	10.414 ± 0.046 (± 0.44%)	1.16	94.93	
				28%	22	
		Minimal External Error ± 0.057		1.63	2σ Confidence Limit	
		Analytical Error ± 0.043		1.0772	Error Magnification	
				3	Number of Iterations	
				0.0000075541	Convergence	
				42%	Spreading Factor	

Blue dots in table indicate selected analyses used to calculate the weighted mean, isochron and inverse isochron ages.
* Alteration Index values in italics indicate analyses from fresh material, normal font is from altered material (Baksi, 2007).
Values shown in red are negative values.
Abbreviations used in tables: (r) = radiogenic ^{40}Ar; (k) = Ar derived from K; (a) = atmospheric Ar; (ca) = Ar derived from Ca; (cl) = Ar derived from Ca; (c) = cosmogenic Ar; MDF = Mass Discrimination Factor.
Green squares in the inverse isochron plots indicate selected steps (blue dots in table), and blue squares are non-selected steps. Pink lines in the inverse isochron plot indicate a line fit through selected data, and the purple lines incidate a fit through an air $^{40}Ar/^{36}Ar$ ratio (295.5).

Sample 17-16/3 step-heating results (0.25-0.5 mm; 163bs)

Relative Abundances	Laser power		36Ar [V]	%1σ	37Ar [V]	%1σ	38Ar [V]	%1σ	39Ar [V]	%1σ	40Ar [V]	%1σ	40(r)/39(k) ± 2σ	Age ± 2σ (Ma)	40Ar(r) (%)	39Ar(k) (%)	K/Ca ± 2σ	Step #	$^{36}Ar/^{39}Ar$ Alt. Index*
C47GA081	0.15 W	•	0.0034016	1.525	0.0033043	14.637	0.0009601	3.970	0.0256927	0.568	1.117965	0.098	4.40053 ± 1.20533	8.38 ± 2.29	10.11	0.34	4.0 ± 1.2	1	0.010238
C47GA082	0.20 W	•	0.0008759	2.287	0.0010586	40.417	0.0006114	5.799	0.0373276	0.381	0.429437	0.085	4.57243 ± 0.32058	8.71 ± 0.61	39.74	0.49	18.0 ± 14.5	2	0.001814
C47GA083	0.25 W	•	0.0011453	1.606	0.0041798	10.835	0.0013371	2.770	0.0943790	0.275	0.799542	0.092	4.88878 ± 0.12003	9.31 ± 0.23	57.71	1.25	11.5 ± 2.5	3	0.000938
C47GA084	0.30 W	•	0.0011617	1.958	0.0073226	6.983	0.0024231	1.854	0.1808792	0.221	1.229317	0.143	4.90106 ± 0.08009	9.33 ± 0.15	72.11	2.39	12.6 ± 1.8	4	*0.000496*
C47GA085	0.35 W	•	0.0009325	2.741	0.0089779	5.156	0.0032728	1.690	0.2621108	0.277	1.546677	0.103	4.85170 ± 0.06484	9.24 ± 0.12	82.22	3.46	14.9 ± 1.5	5	*0.000274*
C47GA086	0.40 W	•	0.0008139	3.715	0.0063957	8.715	0.0036771	1.374	0.2996332	0.327	1.697887	0.072	4.86496 ± 0.06812	9.27 ± 0.13	85.85	3.95	23.9 ± 4.2	6	*0.000210*
C47GA087	0.45 W	•	0.0007113	3.286	0.0069136	8.494	0.0041503	1.302	0.3391896	0.233	1.863445	0.086	4.87508 ± 0.04766	9.29 ± 0.09	88.74	4.48	25.0 ± 4.3	7	*0.000162*
C47GA088	0.50 W	•	0.0007853	3.313	0.0088969	5.745	0.0046538	1.282	0.3749047	0.223	2.057761	0.036	4.87099 ± 0.04664	9.28 ± 0.09	88.74	4.95	21.5 ± 2.5	8	*0.000162*
C47GA089	0.55 W	•	0.0004362	3.634	0.0100130	5.978	0.0047299	1.387	0.3848549	0.225	1.996124	0.072	4.85319 ± 0.03357	9.24 ± 0.06	93.57	5.08	19.6 ± 2.3	9	*0.000087*
C47GA090	0.60 W	•	0.0004534	4.316	0.0116053	5.230	0.0041393	1.231	0.3422638	0.219	1.795292	0.077	4.85598 ± 0.04078	9.25 ± 0.08	92.57	4.52	15.0 ± 1.6	10	*0.000102*
C47GA091	0.70 W	•	0.0009965	2.377	0.0120344	3.442	0.0065566	0.884	0.5364902	0.217	2.900345	0.048	4.85839 ± 0.03401	9.25 ± 0.06	89.87	7.08	22.7 ± 1.6	11	*0.000143*
C47GA092	0.80 W	•	0.0007231	2.600	0.0086548	5.738	0.0055019	1.219	0.4507644	0.216	2.395890	0.065	4.84203 ± 0.03311	9.22 ± 0.06	91.10	5.95	26.6 ± 3.1	12	*0.000124*
C47GA093	0.90 W	•	0.0007381	2.382	0.0069129	8.348	0.0063728	1.017	0.5188808	0.229	2.729594	0.048	4.84056 ± 0.03033	9.22 ± 0.06	92.02	6.85	38.3 ± 6.4	13	*0.000110*
C47GA094	1.00 W	•	0.0008515	2.995	0.0062262	9.677	0.0061232	1.063	0.5017659	0.222	2.686995	0.070	4.85392 ± 0.03776	9.25 ± 0.07	90.64	6.62	41.1 ± 8.0	14	*0.000131*
C47GA095	1.10 W	•	0.0002055	9.593	0.0058456	7.703	0.0045041	1.152	0.3827154	0.229	1.945257	0.120	4.92468 ± 0.03981	9.38 ± 0.08	96.89	5.05	33.4 ± 5.1	15	*0.000041*
C47GA096	1.20 W	•	0.0002091	10.466	0.0042702	9.436	0.0042052	1.241	0.3506128	0.245	1.772008	0.093	4.87806 ± 0.04497	9.29 ± 0.09	96.52	4.63	41.9 ± 7.9	16	*0.000046*
C47GA097	1.50 W	•	0.0004353	4.590	0.0079676	4.695	0.0074479	0.871	0.6230178	0.233	3.166823	0.065	4.87691 ± 0.03033	9.29 ± 0.06	95.94	8.22	39.9 ± 3.7	17	*0.000054*
C47GA098	3.00 W	•	0.0007439	2.118	0.0117254	4.500	0.0162152	0.676	1.3618193	0.223	6.825102	0.078	4.85033 ± 0.02402	9.24 ± 0.05	96.78	17.97	59.2 ± 5.3	18	*0.000042*
C47GA099	10.00 W	•	0.0001675	9.440	0.0035122	15.332	0.0056358	1.242	0.4724452	0.229	2.354553	0.049	4.87886 ± 0.03025	9.29 ± 0.06	97.89	6.23	68.6 ± 21.0	19	*0.000027*
C47GA100	15.00 W	•	0.0000933	15.218	0.0005990	100.612	0.0004498	8.228	0.0380759	0.422	0.213398	0.134	4.88112 ± 0.22471	9.30 ± 0.43	87.09	0.50	32.4 ± 65.2	20	*0.000189*
		Σ	0.0158808	0.667	0.1364159	1.686	0.0929675	0.283	7.5778234	0.064	41.523411	0.020							

Procedure Blanks	Laser power	36Ar [V]	1σ	37Ar [V]	1σ	38Ar [V]	1σ	39Ar [V]	1σ	40Ar [V]	1σ
C47GA081	0.15 W	0.0000821	0.0000106	0.0001223	0.0000132	0.0000413	0.0000326	0.0000685	0.0000171	0.0024314	0.0002241
C47GA082	0.20 W	0.0000869	0.0000106	0.0001255	0.0000132	0.0000442	0.0000326	0.0000919	0.0000171	0.0024991	0.0002241
C47GA083	0.25 W	0.0000929	0.0000106	0.0001295	0.0000132	0.0000480	0.0000326	0.0001183	0.0000171	0.0025544	0.0002241
C47GA084	0.30 W	0.0000999	0.0000106	0.0001339	0.0000132	0.0000526	0.0000326	0.0001466	0.0000171	0.0025963	0.0002241
C47GA085	0.35 W	0.0001077	0.0000106	0.0001386	0.0000132	0.0000578	0.0000326	0.0001760	0.0000171	0.0026269	0.0002241
C47GA086	0.40 W	0.0001218	0.0000106	0.0001469	0.0000132	0.0000674	0.0000326	0.0002259	0.0000171	0.0026571	0.0002241
C47GA087	0.45 W	0.0001308	0.0000106	0.0001520	0.0000132	0.0000735	0.0000326	0.0002558	0.0000171	0.0026661	0.0002241
C47GA088	0.50 W	0.0001400	0.0000106	0.0001570	0.0000132	0.0000797	0.0000326	0.0002849	0.0000171	0.0026703	0.0002241
C47GA089	0.55 W	0.0001492	0.0000106	0.0001619	0.0000132	0.0000859	0.0000326	0.0003125	0.0000171	0.0026715	0.0002241
C47GA090	0.60 W	0.0001582	0.0000106	0.0001665	0.0000132	0.0000919	0.0000326	0.0003382	0.0000171	0.0026716	0.0002241
C47GA091	0.70 W	0.0001721	0.0000106	0.0001730	0.0000132	0.0001008	0.0000326	0.0003742	0.0000171	0.0026741	0.0002241
C47GA092	0.80 W	0.0001799	0.0000106	0.0001763	0.0000132	0.0001057	0.0000326	0.0003920	0.0000171	0.0026799	0.0002241
C47GA093	0.90 W	0.0001870	0.0000106	0.0001789	0.0000132	0.0001099	0.0000326	0.0004059	0.0000171	0.0026913	0.0002241
C47GA094	1.00 W	0.0001931	0.0000106	0.0001807	0.0000132	0.0001132	0.0000326	0.0004151	0.0000171	0.0027099	0.0002241
C47GA095	1.10 W	0.0001982	0.0000106	0.0001816	0.0000132	0.0001155	0.0000326	0.0004193	0.0000171	0.0027377	0.0002241
C47GA096	1.20 W	0.0002037	0.0000106	0.0001808	0.0000132	0.0001169	0.0000326	0.0004133	0.0000171	0.0028088	0.0002241
C47GA097	1.50 W	0.0002051	0.0000106	0.0001787	0.0000132	0.0001161	0.0000326	0.0004010	0.0000171	0.0028697	0.0002241
C47GA098	3.00 W	0.0002048	0.0000106	0.0001753	0.0000132	0.0001137	0.0000326	0.0003816	0.0000171	0.0029465	0.0002241
C47GA099	10.00 W	0.0002026	0.0000106	0.0001705	0.0000132	0.0001097	0.0000326	0.0003544	0.0000171	0.0030410	0.0002241
C47GA100	15.00 W	0.0001985	0.0000106	0.0001644	0.0000132	0.0001042	0.0000326	0.0003203	0.0000171	0.0031507	0.0002241

Sample Parameters	Laser power	Sample	Material	Location	Analyst	Standard (in Ma)	%1σ	J	%1σ	MDF	%1σ	Volume Ratio	Sensitivity (mol/volt)
C47GA081	0.15 W	17-16/3 (163bs)	Phlogopite	Maio, Cape Verdes	Jan Sticklus	28.344	0.039	0.0010585	0.08	1.0098	0.21	1	1.211E-14
C47GA082	0.20 W	17-16/3 (163bs)	Phlogopite	Maio, Cape Verdes	Jan Sticklus	28.344	0.039	0.0010585	0.08	1.0098	0.21	1	1.211E-14
C47GA083	0.25 W	17-16/3 (163bs)	Phlogopite	Maio, Cape Verdes	Jan Sticklus	28.344	0.039	0.0010585	0.08	1.0098	0.21	1	1.211E-14
C47GA084	0.30 W	17-16/3 (163bs)	Phlogopite	Maio, Cape Verdes	Jan Sticklus	28.344	0.039	0.0010585	0.08	1.0098	0.21	1	1.211E-14
C47GA085	0.35 W	17-16/3 (163bs)	Phlogopite	Maio, Cape Verdes	Jan Sticklus	28.344	0.039	0.0010585	0.08	1.0098	0.21	1	1.211E-14
C47GA086	0.40 W	17-16/3 (163bs)	Phlogopite	Maio, Cape Verdes	Jan Sticklus	28.344	0.039	0.0010585	0.08	1.0098	0.21	1	1.211E-14
C47GA087	0.45 W	17-16/3 (163bs)	Phlogopite	Maio, Cape Verdes	Jan Sticklus	28.344	0.039	0.0010585	0.08	1.0098	0.21	1	1.211E-14
C47GA088	0.50 W	17-16/3 (163bs)	Phlogopite	Maio, Cape Verdes	Jan Sticklus	28.344	0.039	0.0010585	0.08	1.0098	0.21	1	1.211E-14
C47GA089	0.55 W	17-16/3 (163bs)	Phlogopite	Maio, Cape Verdes	Jan Sticklus	28.344	0.039	0.0010585	0.08	1.0098	0.21	1	1.211E-14
C47GA090	0.60 W	17-16/3 (163bs)	Phlogopite	Maio, Cape Verdes	Jan Sticklus	28.344	0.039	0.0010585	0.08	1.0098	0.21	1	1.211E-14
C47GA091	0.70 W	17-16/3 (163bs)	Phlogopite	Maio, Cape Verdes	Jan Sticklus	28.344	0.039	0.0010585	0.08	1.0098	0.21	1	1.211E-14
C47GA092	0.80 W	17-16/3 (163bs)	Phlogopite	Maio, Cape Verdes	Jan Sticklus	28.344	0.039	0.0010585	0.08	1.0098	0.21	1	1.211E-14
C47GA093	0.90 W	17-16/3 (163bs)	Phlogopite	Maio, Cape Verdes	Jan Sticklus	28.344	0.039	0.0010585	0.08	1.0098	0.21	1	1.211E-14
C47GA094	1.00 W	17-16/3 (163bs)	Phlogopite	Maio, Cape Verdes	Jan Sticklus	28.344	0.039	0.0010585	0.08	1.0098	0.21	1	1.211E-14
C47GA095	1.10 W	17-16/3 (163bs)	Phlogopite	Maio, Cape Verdes	Jan Sticklus	28.344	0.039	0.0010585	0.08	1.0098	0.21	1	1.211E-14
C47GA096	1.20 W	17-16/3 (163bs)	Phlogopite	Maio, Cape Verdes	Jan Sticklus	28.344	0.039	0.0010585	0.08	1.0098	0.21	1	1.211E-14
C47GA097	1.50 W	17-16/3 (163bs)	Phlogopite	Maio, Cape Verdes	Jan Sticklus	28.344	0.039	0.0010585	0.08	1.0098	0.21	1	1.211E-14
C47GA098	3.00 W	17-16/3 (163bs)	Phlogopite	Maio, Cape Verdes	Jan Sticklus	28.344	0.039	0.0010585	0.08	1.0098	0.21	1	1.211E-14
C47GA099	10.00 W	17-16/3 (163bs)	Phlogopite	Maio, Cape Verdes	Jan Sticklus	28.344	0.039	0.0010585	0.08	1.0098	0.21	1	1.211E-14
C47GA100	15.00 W	17-16/3 (163bs)	Phlogopite	Maio, Cape Verdes	Jan Sticklus	28.344	0.039	0.0010585	0.08	1.0098	0.21	1	1.211E-14

Day	Month	Year	Hour	Min	Resist	Irradiation	Project	Experiment	Nmb	Standard Name
27	OCT	2018	7	1	1	can47	Examples	c47it5ip2_163bs	01	TCS2
27	OCT	2018	7	29	1	can47	Examples	c47it5ip2_163bs	01	TCS2
27	OCT	2018	7	58	1	can47	Examples	c47it5ip2_163bs	01	TCS2
27	OCT	2018	8	27	1	can47	Examples	c47it5ip2_163bs	01	TCS2
27	OCT	2018	8	56	1	can47	Examples	c47it5ip2_163bs	01	TCS2
27	OCT	2018	9	44	1	can47	Examples	c47it5ip2_163bs	01	TCS2
27	OCT	2018	10	13	1	can47	Examples	c47it5ip2_163bs	01	TCS2
27	OCT	2018	10	42	1	can47	Examples	c47it5ip2_163bs	01	TCS2
27	OCT	2018	11	11	1	can47	Examples	c47it5ip2_163bs	01	TCS2
27	OCT	2018	11	40	1	can47	Examples	c47it5ip2_163bs	01	TCS2
27	OCT	2018	12	27	1	can47	Examples	c47it5ip2_163bs	01	TCS2
27	OCT	2018	12	56	1	can47	Examples	c47it5ip2_163bs	01	TCS2
27	OCT	2018	13	25	1	can47	Examples	c47it5ip2_163bs	01	TCS2
27	OCT	2018	13	54	1	can47	Examples	c47it5ip2_163bs	01	TCS2
27	OCT	2018	14	23	1	can47	Examples	c47it5ip2_163bs	01	TCS2
27	OCT	2018	15	11	1	can47	Examples	c47it5ip2_163bs	01	TCS2
27	OCT	2018	15	40	1	can47	Examples	c47it5ip2_163bs	01	TCS2
27	OCT	2018	16	9	1	can47	Examples	c47it5ip2_163bs	01	TCS2
27	OCT	2018	16	38	1	can47	Examples	c47it5ip2_163bs	01	TCS2
27	OCT	2018	17	6	1	can47	Examples	c47it5ip2_163bs	01	TCS2

Irradiation Constants	Laser power	40/36(a)	%1σ	40/36(c)	%1σ	38/36(a)	%1σ	38/36(c)	%1σ	39/37(ca)	%1σ	38/37(ca)	%1σ	36/37(ca)	%1σ	40/39(k)	%1σ	38/39(k)	%1σ	36/38(cl)	%1σ	K/Ca	%1σ	K/Cl	%1σ	Ca/Cl	%1σ
C47GA081	0.15 W	295.5	0.178	0.018	35	0.1869	0.107	1.493	3	0.000702	1.71	0.000196	4.08	0.0002702	0.15	0.00073	12.33	0.01215	0.27	262.8	0.65	0.51	0	0	0	0	0
C47GA082	0.20 W	295.5	0.178	0.018	35	0.1869	0.107	1.493	3	0.000702	1.71	0.000196	4.08	0.0002702	0.15	0.00073	12.33	0.01215	0.27	262.8	0.65	0.51	0	0	0	0	0
C47GA083	0.25 W	295.5	0.178	0.018	35	0.1869	0.107	1.493	3	0.000702	1.71	0.000196	4.08	0.0002702	0.15	0.00073	12.33	0.01215	0.27	262.8	0.65	0.51	0	0	0	0	0
C47GA084	0.30 W	295.5	0.178	0.018	35	0.1869	0.107	1.493	3	0.000702	1.71	0.000196	4.08	0.0002702	0.15	0.00073	12.33	0.01215	0.27	262.8	0.65	0.51	0	0	0	0	0
C47GA085	0.35 W	295.5	0.178	0.018	35	0.1869	0.107	1.493	3	0.000702	1.71	0.000196	4.08	0.0002702	0.15	0.00073	12.33	0.01215	0.27	262.8	0.65	0.51	0	0	0	0	0
C47GA086	0.40 W	295.5	0.178	0.018	35	0.1869	0.107	1.493	3	0.000702	1.71	0.000196	4.08	0.0002702	0.15	0.00073	12.33	0.01215	0.27	262.8	0.65	0.51	0	0	0	0	0
C47GA087	0.45 W	295.5	0.178	0.018	35	0.1869	0.107	1.493	3	0.000702	1.71	0.000196	4.08	0.0002702	0.15	0.00073	12.33	0.01215	0.27	262.8	0.65	0.51	0	0	0	0	0
C47GA088	0.50 W	295.5	0.178	0.018	35	0.1869	0.107	1.493	3	0.000702	1.71	0.000196	4.08	0.0002702	0.15	0.00073	12.33	0.01215	0.27	262.8	0.65	0.51	0	0	0	0	0
C47GA089	0.55 W	295.5	0.178	0.018	35	0.1869	0.107	1.493	3	0.000702	1.71	0.000196	4.08	0.0002702	0.15	0.00073	12.33	0.01215	0.27	262.8	0.65	0.51	0	0	0	0	0
C47GA090	0.60 W	295.5	0.178	0.018	35	0.1869	0.107	1.493	3	0.000702	1.71	0.000196	4.08	0.0002702	0.15	0.00073	12.33	0.01215	0.27	262.8	0.65	0.51	0	0	0	0	0
C47GA091	0.70 W	295.5	0.178	0.018	35	0.1869	0.107	1.493	3	0.000702	1.71	0.000196	4.08	0.0002702	0.15	0.00073	12.33	0.01215	0.27	262.8	0.65	0.51	0	0	0	0	0
C47GA092	0.80 W	295.5	0.178	0.018	35	0.1869	0.107	1.493	3	0.000702	1.71	0.000196	4.08	0.0002702	0.15	0.00073	12.33	0.01215	0.27	262.8	0.65	0.51	0	0	0	0	0
C47GA093	0.90 W	295.5	0.178	0.018	35	0.1869	0.107	1.493	3	0.000702	1.71	0.000196	4.08	0.0002702	0.15	0.00073	12.33	0.01215	0.27	262.8	0.65	0.51	0	0	0	0	0
C47GA094	1.00 W	295.5	0.178	0.018	35	0.1869	0.107	1.493	3	0.000702	1.71	0.000196	4.08	0.0002702	0.15	0.00073	12.33	0.01215	0.27	262.8	0.65	0.51	0	0	0	0	0
C47GA095	1.10 W	295.5	0.178	0.018	35	0.1869	0.107	1.493	3	0.000702	1.71	0.000196	4.08	0.0002702	0.15	0.00073	12.33	0.01215	0.27	262.8	0.65	0.51	0	0	0	0	0
C47GA096	1.20 W	295.5	0.178	0.018	35	0.1869	0.107	1.493	3	0.000702	1.71	0.000196	4.08	0.0002702	0.15	0.00073	12.33	0.01215	0.27	262.8	0.65	0.51	0	0	0	0	0
C47GA097	1.50 W	295.5	0.178	0.018	35	0.1869	0.107	1.493	3	0.000702	1.71	0.000196	4.08	0.0002702	0.15	0.00073	12.33	0.01215	0.27	262.8	0.65	0.51	0	0	0	0	0
C47GA098	3.00 W	295.5	0.178	0.018	35	0.1869	0.107	1.493	3	0.000702	1.71	0.000196	4.08	0.0002702	0.15	0.00073	12.33	0.01215	0.27	262.8	0.65	0.51	0	0	0	0	0
C47GA099	10.00 W	295.5	0.178	0.018	35	0.1869	0.107	1.493	3	0.000702	1.71	0.000196	4.08	0.0002702	0.15	0.00073	12.33	0.01215	0.27	262.8	0.65	0.51	0	0	0	0	0
C47GA100	15.00 W	295.5	0.178	0.018	35	0.1869	0.107	1.493	3	0.000702	1.71	0.000196	4.08	0.0002702	0.15	0.00073	12.33	0.01215	0.27	262.8	0.65	0.51	0	0	0	0	0

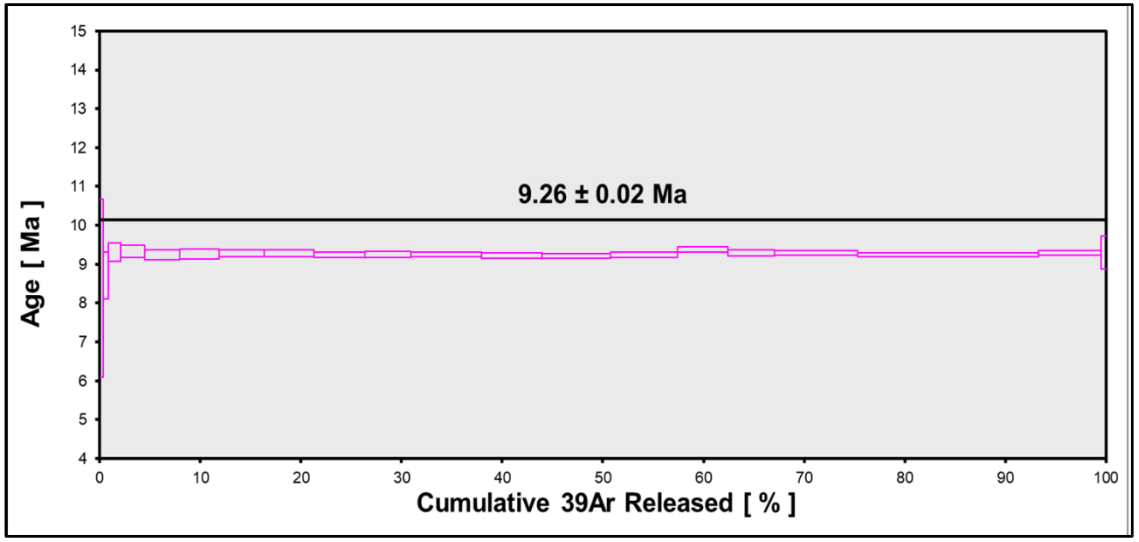

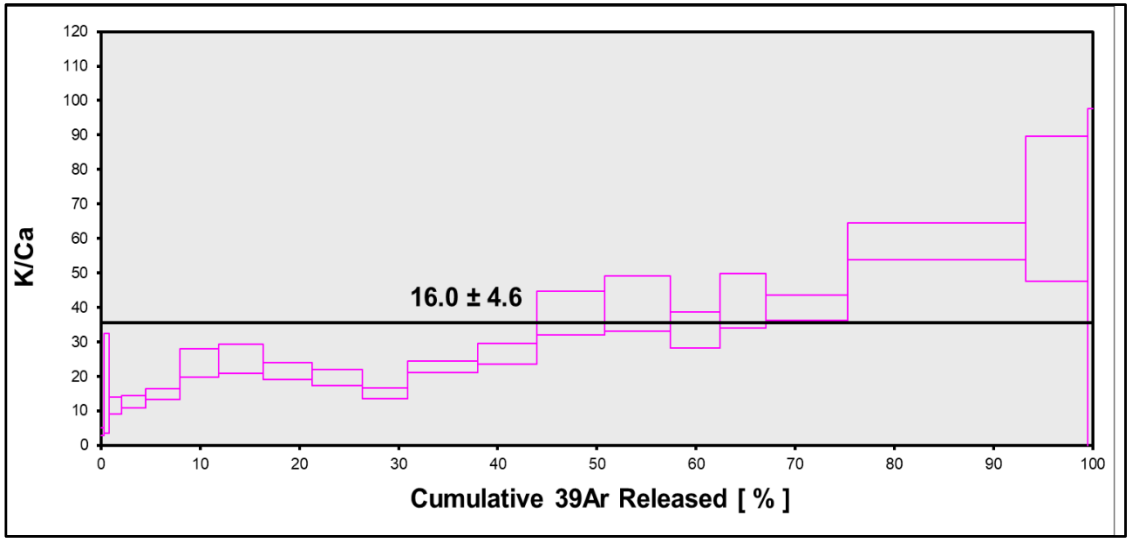
K/Ca
16.0 ± 4.6
Cumulative 39Ar Released [%]

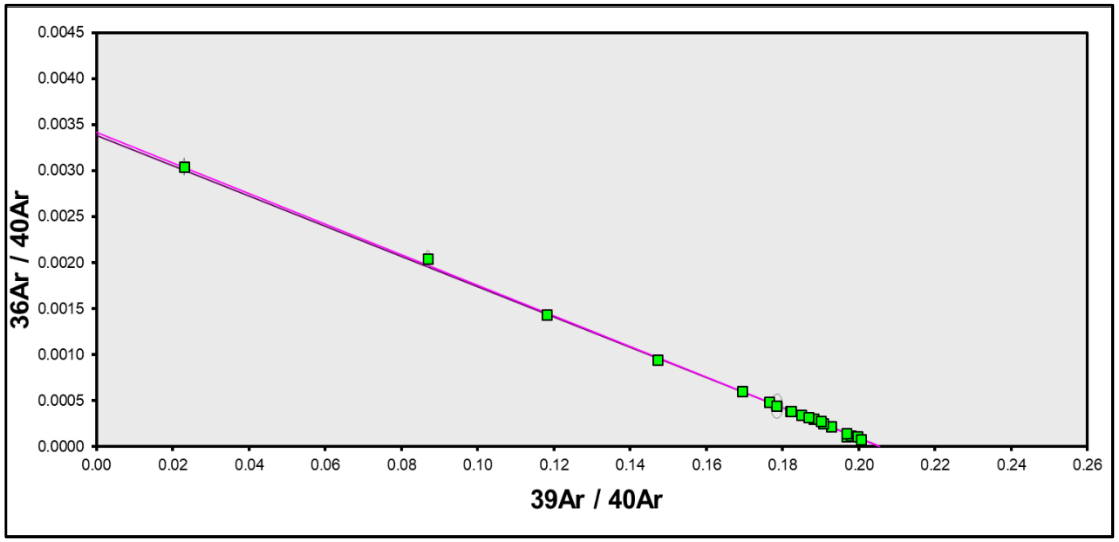
36Ar / 40Ar
39Ar / 40Ar

Information on Analysis and Constants Used in Calculations

Sample = 17-16/3 (163BS)
Material = Phlogopite
Location = Maio, Cape Verde
Analyst = Jan Sticklus
Project = EXAMPLES
Mass Discrimination Law = POW
Irradiation = can47
J = 0.00105850 ± 0.00000085
TCS2 = 28.344 ± 0.011 Ma
Experiment Type = SAMPLE
Heating = 45 sec
Isolation = 15.00 min
Instrument = MAP216
Weight = 4.740 mg
Weight %K = 5.9

Age Equations = Conventional
Negative Intensities = Allowed
Decay Constant 40K = 5.543 ± 0.009 E-10 1/a
Decay Constant 39Ar = 2.940 ± 0.016 E-07 1/h
Decay Constant 37Ar = 8.230 ± 0.012 E-04 1/h
Decay Constant 36Cl = 2.257 ± 0.015 E-06 1/a
Atmospheric Ratio 40/36(a) = 295.50 ± 0.53
Atmospheric Ratio 38/36(a) = 0.1869 ± 0.0002
Production Ratio 39/37(ca) = 0.000702 ± 0.000012
Production Ratio 38/37(ca) = 0.000196 ± 0.000008
Production Ratio 36/37(ca) = 0.000270 ± 0.000000
Production Ratio 40/39(k) = 0.000730 ± 0.000090
Production Ratio 38/39(k) = 0.012150 ± 0.000033
Production Ratio 36/38(cl) = 262.80
Scaling Ratio K/Ca = 0.510

Results	40(a)/36(a) ± 2σ	40(r)/39(k) ± 2σ	Age ± 2σ (Ma)	MSWD	39Ar(k) (%,n)	K/Ca ± 2σ
Age Plateau		4.86315 ± 0.01020	9.263 ± 0.024	1.22	100.00	16.0 ± 4.6
		± 0.21%	± 0.26%	23%	20	
		Minimal External Error	± 0.038	1.65	2σ Confidence Limit	
		Analytical Error	± 0.019	1.1039	Error Magnification	
Total Fusion Age		4.86109 ± 0.01058	9.259 ± 0.025		20	28.3 ± 1.0
		± 0.22%	± 0.27%			
		Minimal External Error	± 0.039			
		Analytical Error	± 0.020			
Normal Isochron	289.08 ± 6.13	4.87778 ± 0.01349	9.291 ± 0.030	1.33	100.00	
No Convergence	± 2.12%	± 0.28%	± 0.32%	16%	20	
		Minimal External Error	± 0.042	1.67	2σ Confidence Limit	
		Analytical Error	± 0.026	1.1527	Error Magnification	
				100	Number of Iterations	
				0.0000589297	Convergence	
Inverse Isochron	292.66 ± 5.90	4.86713 ± 0.01297	9.270 ± 0.029	1.23	100.00	
	± 2.02%	± 0.27%	± 0.31%	22%	20	
		Minimal External Error	± 0.041	1.67	2σ Confidence Limit	
		Analytical Error	± 0.025	1.1096	Error Magnification	
				3	Number of Iterations	
				0.0000014217	Convergence	
				86%	Spreading Factor	

Blue dots in table indicate selected steps used to calculate the weighted mean, isochron and inverse isochron ages.
* Alteration Index values in italics indicate analyses from fresh material, normal font is from altered material (Baksi, 2007).
Values shown in red are negative values.
Abbreviations used in tables: (r) = radiogenic ^{40}Ar; (k) = Ar derived from K; (a) = atmospheric Ar; (ca) = Ar derived from Ca; (cl) = Ar derived from Ca; (c) = cosmogenic Ar; MDF = Mass Discrimination Factor.
Green squares in the inverse isochron plots indicate selected steps (blue dots in table), and blue squares are non-selected steps. Pink lines in the inverse isochron plot indicate a line fit through selected data, and the purple lines incidate a fit through an air ^{40}Ar/^{36}Ar ratio (295.5).

Sample 17-16/3 single-crystal total-fusion results (0.25-0.5 mm fraction; 163bs)

Relative Abundances	Laser power		36Ar [V]	%1σ	37Ar [V]	%1σ	38Ar [V]	%1σ	39Ar [V]	%1σ	40Ar [V]	%1σ	40(r)/39(k) ± 2σ	Age ± 2σ (Ma)	40Ar(r) (%)	39Ar(k) (%)	K/Ca ± 2σ	Sample weight (mg)	$^{36}Ar/^{39}Ar$ Alt. Index	Wt. % K
C47AB096	5.00 W	•	0.0001245	8.666	0.0019725	1.805	0.0014676	1.699	0.1243642	0.279	0.635929	0.081	4.81812 ± 0.05850	9.18 ± 0.11	94.22	2.62	32.2 ± 1.2	0.071	*0.000085*	6.4
C47BA097	5.00 W	•	0.0006046	4.159	0.0019610	3.005	0.0027825	1.398	0.2202591	0.244	1.240497	0.091	4.82083 ± 0.07224	9.18 ± 0.14	85.60	4.64	57.3 ± 3.5	0.131	*0.000223*	6.1
C47BA096	5.00 W	•	0.0002748	8.170	0.0029355	2.562	0.0030929	1.164	0.2494115	0.247	1.288637	0.056	4.84143 ± 0.05861	9.22 ± 0.11	93.70	5.25	43.3 ± 2.2	0.148	*0.000090*	6.2
C47BB004	5.00 W	•	0.0002673	7.331	0.0067027	1.758	0.0020341	1.652	0.1655865	0.237	0.880318	0.106	4.84190 ± 0.07451	9.22 ± 0.14	91.07	3.49	12.6 ± 0.4	0.106	*0.000121*	5.7
C47BA100	5.00 W	•	0.0003975	5.880	0.0065834	1.205	0.0020598	1.839	0.1647677	0.276	0.915198	0.103	4.84420 ± 0.08878	9.23 ± 0.17	87.21	3.47	12.8 ± 0.3	0.100	*0.000191*	6.0
C47BB002	5.00 W	•	0.0002350	6.951	0.0024184	3.725	0.0027852	1.112	0.2353714	0.254	1.211661	0.103	4.85292 ± 0.04902	9.24 ± 0.09	94.27	4.96	49.6 ± 3.7	0.145	*0.000078*	5.9
C47BA095	5.00 W	•	0.0002159	12.453	0.0008822	7.535	0.0020953	1.256	0.1722052	0.296	0.899699	0.104	4.85373 ± 0.09728	9.25 ± 0.18	92.90	3.63	99.6 ± 15.0	0.106	*0.000098*	5.9
C47AB103	5.00 W	•	0.0002746	3.851	0.0010874	3.836	0.0018447	1.157	0.1516327	0.229	0.818057	0.070	4.85967 ± 0.04749	9.26 ± 0.09	90.08	3.19	71.1 ± 5.5	0.087	*0.000153*	6.4
C47AB094	5.00 W	•	0.0002084	7.736	0.0034301	1.831	0.0027880	1.370	0.2346537	0.220	1.203149	0.044	4.86536 ± 0.04612	9.27 ± 0.09	94.89	4.94	34.9 ± 1.3	0.146	*0.000069*	5.9
C47AB092	5.00 W	•	0.0003034	3.729	0.0125629	0.993	0.0043509	0.714	0.3683386	0.217	1.881989	0.033	4.86814 ± 0.02809	9.27 ± 0.05	95.28	7.76	15.0 ± 0.3	0.230	*0.000063*	5.9
C47AB098	5.00 W	•	0.0005304	3.047	0.0013077	2.237	0.0033485	1.437	0.2811414	0.248	1.527249	0.067	4.87451 ± 0.04235	9.28 ± 0.08	89.73	5.92	109.6 ± 4.9	0.165	*0.000155*	6.2
C47BA101	5.00 W	•	0.0002186	9.000	0.0014764	4.018	0.0018929	1.308	0.1563646	0.248	0.826844	0.145	4.87496 ± 0.07967	9.29 ± 0.15	92.19	3.29	54.0 ± 4.3	0.098	*0.000108*	5.8
C47BB003	5.00 W	•	0.0003001	6.250	0.0039720	2.159	0.0024703	1.280	0.1973605	0.246	1.051466	0.111	4.87926 ± 0.06226	9.29 ± 0.12	91.58	4.16	25.3 ± 1.1	0.126	*0.000115*	5.7
C47AB102	5.00 W	•	0.0003051	3.973	0.0013446	1.901	0.0014798	1.581	0.1204672	0.217	0.678530	0.053	4.88439 ± 0.06346	9.30 ± 0.12	86.72	2.54	45.7 ± 1.7	0.067	*0.000220*	6.6
C47AB099	5.00 W	•	0.0002641	5.652	0.0082763	1.113	0.0013024	1.741	0.1081167	0.229	0.605801	0.069	4.88698 ± 0.08500	9.31 ± 0.16	87.21	2.28	6.7 ± 0.2	0.062	*0.000204*	6.4
C47BB001	5.00 W	•	0.0006371	4.311	0.0010591	8.227	0.0025741	0.866	0.2018931	0.230	1.175526	0.092	4.88980 ± 0.08423	9.31 ± 0.16	83.98	4.25	97.2 ± 16.0	0.123	*0.000250*	6.0
C47BA099	5.00 W	•	0.0002620	7.576	0.0017502	3.201	0.0027933	1.027	0.2278958	0.232	1.192482	0.097	4.89275 ± 0.05719	9.32 ± 0.11	93.51	4.80	66.4 ± 4.3	0.136	*0.000093*	6.1
C47AB097	5.00 W	•	0.0006117	2.349	0.0024972	1.423	0.0023756	1.717	0.1932993	0.214	1.127131	0.056	4.89618 ± 0.04924	9.33 ± 0.09	83.97	4.07	39.5 ± 1.1	0.113	*0.000262*	6.3
C47BA098	5.00 W	•	0.0004780	4.109	0.0054949	1.902	0.0036770	1.057	0.2952157	0.229	1.586567	0.054	4.89664 ± 0.04565	9.33 ± 0.09	91.11	6.22	27.4 ± 1.0	0.196	*0.000118*	5.5
C47BB005	5.00 W	•	0.0003008	6.389	0.0036956	2.288	0.0034436	1.268	0.2784494	0.245	1.452803	0.080	4.89867 ± 0.04807	9.33 ± 0.09	93.89	5.86	38.4 ± 1.8	0.173	*0.000084*	5.9
C47AB101	5.00 W	•	0.0009053	1.802	0.0027725	1.891	0.0032096	0.807	0.2640990	0.231	1.564073	0.033	4.90950 ± 0.04330	9.35 ± 0.08	82.90	5.56	48.6 ± 1.9	0.159	*0.000275*	6.1
C47AB100	5.00 W	•	0.0001996	5.327	0.0034998	1.746	0.0014538	1.343	0.1195814	0.269	0.647095	0.084	4.91982 ± 0.05955	9.37 ± 0.11	90.92	2.52	17.4 ± 0.6	0.069	*0.000139*	6.3
C47AB095	5.00 W	•	0.0006768	3.181	0.0022353	2.227	0.0012859	1.674	0.0971126	0.236	0.681420	0.066	4.95858 ± 0.13361	9.44 ± 0.25	70.67	2.04	22.2 ± 1.0	0.051	*0.000642*	7.0
C47AB093	5.00 W	•	0.0002387	3.943	0.0038994	1.365	0.0014770	1.202	0.1212295	0.257	0.671731	0.080	4.96113 ± 0.05329	9.45 ± 0.10	89.53	2.55	15.9 ± 0.4	0.070	*0.000164*	6.3
		Σ	0.0088343	1.018	0.0838171	0.425	0.0580850	0.265	4.7488167	0.052	25.763852	0.016								

Procedure Blanks	Laser power	36Ar [V]	1σ	37Ar [V]	1σ	38Ar [V]	1σ	39Ar [V]	1σ	40Ar [V]	1σ
C47AB096	5.00 W	0.0000730	0.0000071	0.0001618	0.0000076	0.0000371	0.0000082	0.0002723	0.0000165	0.0035460	0.0001233
C47BA097	5.00 W	0.0003206	0.0000161	0.0003713	0.0000164	0.0001780	0.0000166	0.0004956	0.0000381	0.0052904	0.0005542
C47BA096	5.00 W	0.0003206	0.0000161	0.0003713	0.0000164	0.0001780	0.0000166	0.0004956	0.0000381	0.0052904	0.0005542
C47BB004	5.00 W	0.0002915	0.0000143	0.0003323	0.0000286	0.0001389	0.0000078	0.0003542	0.0000210	0.0043949	0.0003288
C47BA100	5.00 W	0.0003206	0.0000161	0.0003713	0.0000164	0.0001780	0.0000166	0.0004956	0.0000381	0.0052904	0.0005542
C47BB002	5.00 W	0.0002877	0.0000143	0.0003366	0.0000286	0.0001401	0.0000078	0.0003529	0.0000210	0.0045027	0.0003288
C47BA095	5.00 W	0.0003206	0.0000161	0.0003713	0.0000164	0.0001780	0.0000166	0.0004956	0.0000381	0.0052904	0.0005542
C47AB103	5.00 W	0.0000767	0.0000071	0.0001704	0.0000076	0.0000336	0.0000082	0.0002112	0.0000165	0.0031288	0.0001233
C47AB094	5.00 W	0.0000720	0.0000071	0.0001595	0.0000076	0.0000380	0.0000082	0.0002883	0.0000165	0.0036555	0.0001233
C47AB092	5.00 W	0.0000710	0.0000071	0.0001573	0.0000076	0.0000389	0.0000082	0.0003044	0.0000165	0.0037650	0.0001233
C47AB098	5.00 W	0.0000743	0.0000071	0.0001647	0.0000076	0.0000359	0.0000082	0.0002513	0.0000165	0.0034025	0.0001233
C47BA101	5.00 W	0.0003206	0.0000161	0.0003713	0.0000164	0.0001780	0.0000166	0.0004956	0.0000381	0.0052904	0.0005542
C47BB003	5.00 W	0.0002895	0.0000143	0.0003345	0.0000286	0.0001395	0.0000078	0.0003535	0.0000210	0.0044497	0.0003288
C47AB102	5.00 W	0.0000762	0.0000071	0.0001692	0.0000076	0.0000341	0.0000082	0.0002192	0.0000165	0.0031836	0.0001233
C47AB099	5.00 W	0.0000747	0.0000071	0.0001659	0.0000076	0.0000354	0.0000082	0.0002433	0.0000165	0.0033478	0.0001233
C47BB001	5.00 W	0.0002845	0.0000143	0.0003402	0.0000286	0.0001412	0.0000078	0.0003518	0.0000210	0.0045934	0.0003288
C47BA099	5.00 W	0.0003206	0.0000161	0.0003713	0.0000164	0.0001780	0.0000166	0.0004956	0.0000381	0.0052904	0.0005542
C47AB097	5.00 W	0.0000735	0.0000071	0.0001629	0.0000076	0.0000366	0.0000082	0.0002646	0.0000165	0.0034931	0.0001233
C47BA098	5.00 W	0.0003206	0.0000161	0.0003713	0.0000164	0.0001780	0.0000166	0.0004956	0.0000381	0.0052904	0.0005542
C47BB005	5.00 W	0.0002934	0.0000143	0.0003301	0.0000286	0.0001382	0.0000078	0.0003549	0.0000210	0.0043401	0.0003288
C47AB101	5.00 W	0.0000757	0.0000071	0.0001681	0.0000076	0.0000345	0.0000082	0.0002272	0.0000165	0.0032383	0.0001233
C47AB100	5.00 W	0.0000752	0.0000071	0.0001670	0.0000076	0.0000350	0.0000082	0.0002352	0.0000165	0.0032931	0.0001233
C47AB095	5.00 W	0.0000725	0.0000071	0.0001606	0.0000076	0.0000375	0.0000082	0.0002803	0.0000165	0.0036007	0.0001233
C47AB093	5.00 W	0.0000715	0.0000071	0.0001584	0.0000076	0.0000384	0.0000082	0.0002963	0.0000165	0.0037102	0.0001233

Sample Parameters	Laser power	Sample	Material	Location	Analyst	Standard (in Ma)	%1σ	J	%1σ	MDF	%1σ	Volume Ratio	Sensitivity (mol/volt)
C47AB096	5.00 W	17-16/3 (163bs)	Phlogopite (0.25-0.5 mm)	Maio, Cape Verdes	Jan Sticklus	28.344	0.039	1.06E-03	0.08	1.0098	0.21	1	1.211E-14
C47BA097	5.00 W	17-16/3 (163bs)	Phlogopite (0.25-0.5 mm)	Maio, Cape Verdes	Jan Sticklus	28.344	0.039	1.06E-03	0.08	1.0098	0.21	1	1.211E-14
C47BA096	5.00 W	17-16/3 (163bs)	Phlogopite (0.25-0.5 mm)	Maio, Cape Verdes	Jan Sticklus	28.344	0.039	1.06E-03	0.08	1.0098	0.21	1	1.211E-14
C47BB004	5.00 W	17-16/3 (163bs)	Phlogopite (0.25-0.5 mm)	Maio, Cape Verdes	Jan Sticklus	28.344	0.039	1.06E-03	0.08	1.0098	0.21	1	1.211E-14
C47BA100	5.00 W	17-16/3 (163bs)	Phlogopite (0.25-0.5 mm)	Maio, Cape Verdes	Jan Sticklus	28.344	0.039	1.06E-03	0.08	1.0098	0.21	1	1.211E-14
C47BB002	5.00 W	17-16/3 (163bs)	Phlogopite (0.25-0.5 mm)	Maio, Cape Verdes	Jan Sticklus	28.344	0.039	1.06E-03	0.08	1.0098	0.21	1	1.211E-14
C47BA095	5.00 W	17-16/3 (163bs)	Phlogopite (0.25-0.5 mm)	Maio, Cape Verdes	Jan Sticklus	28.344	0.039	1.06E-03	0.08	1.0098	0.21	1	1.211E-14
C47AB103	5.00 W	17-16/3 (163bs)	Phlogopite (0.25-0.5 mm)	Maio, Cape Verdes	Jan Sticklus	28.344	0.039	1.06E-03	0.08	1.0098	0.21	1	1.211E-14
C47AB094	5.00 W	17-16/3 (163bs)	Phlogopite (0.25-0.5 mm)	Maio, Cape Verdes	Jan Sticklus	28.344	0.039	1.06E-03	0.08	1.0098	0.21	1	1.211E-14
C47AB092	5.00 W	17-16/3 (163bs)	Phlogopite (0.25-0.5 mm)	Maio, Cape Verdes	Jan Sticklus	28.344	0.039	1.06E-03	0.08	1.0098	0.21	1	1.211E-14
C47AB098	5.00 W	17-16/3 (163bs)	Phlogopite (0.25-0.5 mm)	Maio, Cape Verdes	Jan Sticklus	28.344	0.039	1.06E-03	0.08	1.0098	0.21	1	1.211E-14
C47BA101	5.00 W	17-16/3 (163bs)	Phlogopite (0.25-0.5 mm)	Maio, Cape Verdes	Jan Sticklus	28.344	0.039	1.06E-03	0.08	1.0098	0.21	1	1.211E-14
C47BB003	5.00 W	17-16/3 (163bs)	Phlogopite (0.25-0.5 mm)	Maio, Cape Verdes	Jan Sticklus	28.344	0.039	1.06E-03	0.08	1.0098	0.21	1	1.211E-14
C47AB102	5.00 W	17-16/3 (163bs)	Phlogopite (0.25-0.5 mm)	Maio, Cape Verdes	Jan Sticklus	28.344	0.039	1.06E-03	0.08	1.0098	0.21	1	1.211E-14
C47AB099	5.00 W	17-16/3 (163bs)	Phlogopite (0.25-0.5 mm)	Maio, Cape Verdes	Jan Sticklus	28.344	0.039	1.06E-03	0.08	1.0098	0.21	1	1.211E-14
C47BB001	5.00 W	17-16/3 (163bs)	Phlogopite (0.25-0.5 mm)	Maio, Cape Verdes	Jan Sticklus	28.344	0.039	1.06E-03	0.08	1.0098	0.21	1	1.211E-14
C47BA099	5.00 W	17-16/3 (163bs)	Phlogopite (0.25-0.5 mm)	Maio, Cape Verdes	Jan Sticklus	28.344	0.039	1.06E-03	0.08	1.0098	0.21	1	1.211E-14
C47AB097	5.00 W	17-16/3 (163bs)	Phlogopite (0.25-0.5 mm)	Maio, Cape Verdes	Jan Sticklus	28.344	0.039	1.06E-03	0.08	1.0098	0.21	1	1.211E-14
C47BA098	5.00 W	17-16/3 (163bs)	Phlogopite (0.25-0.5 mm)	Maio, Cape Verdes	Jan Sticklus	28.344	0.039	1.06E-03	0.08	1.0098	0.21	1	1.211E-14
C47BB005	5.00 W	17-16/3 (163bs)	Phlogopite (0.25-0.5 mm)	Maio, Cape Verdes	Jan Sticklus	28.344	0.039	1.06E-03	0.08	1.0098	0.21	1	1.211E-14
C47AB101	5.00 W	17-16/3 (163bs)	Phlogopite (0.25-0.5 mm)	Maio, Cape Verdes	Jan Sticklus	28.344	0.039	1.06E-03	0.08	1.0098	0.21	1	1.211E-14
C47AB100	5.00 W	17-16/3 (163bs)	Phlogopite (0.25-0.5 mm)	Maio, Cape Verdes	Jan Sticklus	28.344	0.039	1.06E-03	0.08	1.0098	0.21	1	1.211E-14
C47AB095	5.00 W	17-16/3 (163bs)	Phlogopite (0.25-0.5 mm)	Maio, Cape Verdes	Jan Sticklus	28.344	0.039	1.06E-03	0.08	1.0098	0.21	1	1.211E-14
C47AB093	5.00 W	17-16/3 (163bs)	Phlogopite (0.25-0.5 mm)	Maio, Cape Verdes	Jan Sticklus	28.344	0.039	1.06E-03	0.08	1.0098	0.21	1	1.211E-14

Day	Month	Year	Hour	Min	Resist	Irradiation	Project	Experiment	Nmb	Standard Name
24	JUN	2018	11	14	1	can47	Examples	C47AB092	02	TCS2
30	JUN	2018	13	16	1	can47	Examples	c47it5ip2_163bs	01	TCS2
30	JUN	2018	12	47	1	can47	Examples	c47it5ip2_163bs	01	TCS2
30	JUN	2018	19	48	1	can47	Examples	c47it5ip2_163bs	01	TCS2
30	JUN	2018	14	43	1	can47	Examples	c47it5ip2_163bs	01	TCS2
30	JUN	2018	18	51	1	can47	Examples	c47it5ip2_163bs	01	TCS2
30	JUN	2018	12	18	1	can47	Examples	c47it5ip2_163bs	01	TCS2
24	JUN	2018	14	55	1	can47	Examples	C47AB092	02	TCS2
24	JUN	2018	10	16	1	can47	Examples	C47AB092	02	TCS2
24	JUN	2018	9	18	1	can47	Examples	C47AB092	02	TCS2
24	JUN	2018	12	30	1	can47	Examples	C47AB092	02	TCS2
30	JUN	2018	15	31	1	can47	Examples	c47it5ip2_163bs	01	TCS2
30	JUN	2018	19	19	1	can47	Examples	c47it5ip2_163bs	01	TCS2
24	JUN	2018	14	26	1	can47	Examples	C47AB092	02	TCS2
24	JUN	2018	12	59	1	can47	Examples	C47AB092	02	TCS2
30	JUN	2018	18	3	1	can47	Examples	c47it5ip2_163bs	01	TCS2
30	JUN	2018	14	14	1	can47	Examples	c47it5ip2_163bs	01	TCS2
24	JUN	2018	11	42	1	can47	Examples	C47AB092	02	TCS2
30	JUN	2018	13	45	1	can47	Examples	c47it5ip2_163bs	01	TCS2
30	JUN	2018	20	17	1	can47	Examples	c47it5ip2_163bs	01	TCS2
24	JUN	2018	13	57	1	can47	Examples	C47AB092	02	TCS2
24	JUN	2018	13	28	1	can47	Examples	C47AB092	02	TCS2
24	JUN	2018	10	45	1	can47	Examples	C47AB092	02	TCS2
24	JUN	2018	9	47	1	can47	Examples	C47AB092	02	TCS2

Irradiation Constants	Laser power	40/36(a)	%1σ	40/36(c)	%1σ	38/36(a)	%1σ	38/36(c)	%1σ	39/37(ca)	%1σ	38/37(ca)	%1σ	36/37(ca)	%1σ	40/39(k)	%1σ	38/39(k)	%1σ	36/38(cl)	%1σ	K/Ca	%1σ	K/Cl	%1σ	Ca/Cl	%1σ
C47AB096	5.00 W	295.5	0.178	0.018	35	0.1869	0.107	1.493	3	0.000702	1.71	0.000196	4.08	0.0002702	0.15	0.00073	12.33	0.01215	0.27	262.8	0.65	0.51	0	0	0	0	0
C47BA097	5.00 W	295.5	0.178	0.018	35	0.1869	0.107	1.493	3	0.000702	1.71	0.000196	4.08	0.0002702	0.15	0.00073	12.33	0.01215	0.27	262.8	0.65	0.51	0	0	0	0	0
C47BA096	5.00 W	295.5	0.178	0.018	35	0.1869	0.107	1.493	3	0.000702	1.71	0.000196	4.08	0.0002702	0.15	0.00073	12.33	0.01215	0.27	262.8	0.65	0.51	0	0	0	0	0
C47BB004	5.00 W	295.5	0.178	0.018	35	0.1869	0.107	1.493	3	0.000702	1.71	0.000196	4.08	0.0002702	0.15	0.00073	12.33	0.01215	0.27	262.8	0.65	0.51	0	0	0	0	0
C47BA100	5.00 W	295.5	0.178	0.018	35	0.1869	0.107	1.493	3	0.000702	1.71	0.000196	4.08	0.0002702	0.15	0.00073	12.33	0.01215	0.27	262.8	0.65	0.51	0	0	0	0	0
C47BB002	5.00 W	295.5	0.178	0.018	35	0.1869	0.107	1.493	3	0.000702	1.71	0.000196	4.08	0.0002702	0.15	0.00073	12.33	0.01215	0.27	262.8	0.65	0.51	0	0	0	0	0
C47BA095	5.00 W	295.5	0.178	0.018	35	0.1869	0.107	1.493	3	0.000702	1.71	0.000196	4.08	0.0002702	0.15	0.00073	12.33	0.01215	0.27	262.8	0.65	0.51	0	0	0	0	0
C47AB103	5.00 W	295.5	0.178	0.018	35	0.1869	0.107	1.493	3	0.000702	1.71	0.000196	4.08	0.0002702	0.15	0.00073	12.33	0.01215	0.27	262.8	0.65	0.51	0	0	0	0	0
C47AB094	5.00 W	295.5	0.178	0.018	35	0.1869	0.107	1.493	3	0.000702	1.71	0.000196	4.08	0.0002702	0.15	0.00073	12.33	0.01215	0.27	262.8	0.65	0.51	0	0	0	0	0
C47AB092	5.00 W	295.5	0.178	0.018	35	0.1869	0.107	1.493	3	0.000702	1.71	0.000196	4.08	0.0002702	0.15	0.00073	12.33	0.01215	0.27	262.8	0.65	0.51	0	0	0	0	0
C47AB098	5.00 W	295.5	0.178	0.018	35	0.1869	0.107	1.493	3	0.000702	1.71	0.000196	4.08	0.0002702	0.15	0.00073	12.33	0.01215	0.27	262.8	0.65	0.51	0	0	0	0	0
C47BA101	5.00 W	295.5	0.178	0.018	35	0.1869	0.107	1.493	3	0.000702	1.71	0.000196	4.08	0.0002702	0.15	0.00073	12.33	0.01215	0.27	262.8	0.65	0.51	0	0	0	0	0
C47BB003	5.00 W	295.5	0.178	0.018	35	0.1869	0.107	1.493	3	0.000702	1.71	0.000196	4.08	0.0002702	0.15	0.00073	12.33	0.01215	0.27	262.8	0.65	0.51	0	0	0	0	0
C47AB102	5.00 W	295.5	0.178	0.018	35	0.1869	0.107	1.493	3	0.000702	1.71	0.000196	4.08	0.0002702	0.15	0.00073	12.33	0.01215	0.27	262.8	0.65	0.51	0	0	0	0	0
C47AB099	5.00 W	295.5	0.178	0.018	35	0.1869	0.107	1.493	3	0.000702	1.71	0.000196	4.08	0.0002702	0.15	0.00073	12.33	0.01215	0.27	262.8	0.65	0.51	0	0	0	0	0
C47BB001	5.00 W	295.5	0.178	0.018	35	0.1869	0.107	1.493	3	0.000702	1.71	0.000196	4.08	0.0002702	0.15	0.00073	12.33	0.01215	0.27	262.8	0.65	0.51	0	0	0	0	0
C47BA099	5.00 W	295.5	0.178	0.018	35	0.1869	0.107	1.493	3	0.000702	1.71	0.000196	4.08	0.0002702	0.15	0.00073	12.33	0.01215	0.27	262.8	0.65	0.51	0	0	0	0	0
C47AB097	5.00 W	295.5	0.178	0.018	35	0.1869	0.107	1.493	3	0.000702	1.71	0.000196	4.08	0.0002702	0.15	0.00073	12.33	0.01215	0.27	262.8	0.65	0.51	0	0	0	0	0
C47BA098	5.00 W	295.5	0.178	0.018	35	0.1869	0.107	1.493	3	0.000702	1.71	0.000196	4.08	0.0002702	0.15	0.00073	12.33	0.01215	0.27	262.8	0.65	0.51	0	0	0	0	0
C47BB005	5.00 W	295.5	0.178	0.018	35	0.1869	0.107	1.493	3	0.000702	1.71	0.000196	4.08	0.0002702	0.15	0.00073	12.33	0.01215	0.27	262.8	0.65	0.51	0	0	0	0	0
C47AB101	5.00 W	295.5	0.178	0.018	35	0.1869	0.107	1.493	3	0.000702	1.71	0.000196	4.08	0.0002702	0.15	0.00073	12.33	0.01215	0.27	262.8	0.65	0.51	0	0	0	0	0
C47AB100	5.00 W	295.5	0.178	0.018	35	0.1869	0.107	1.493	3	0.000702	1.71	0.000196	4.08	0.0002702	0.15	0.00073	12.33	0.01215	0.27	262.8	0.65	0.51	0	0	0	0	0
C47AB095	5.00 W	295.5	0.178	0.018	35	0.1869	0.107	1.493	3	0.000702	1.71	0.000196	4.08	0.0002702	0.15	0.00073	12.33	0.01215	0.27	262.8	0.65	0.51	0	0	0	0	0
C47AB093	5.00 W	295.5	0.178	0.018	35	0.1869	0.107	1.493	3	0.000702	1.71	0.000196	4.08	0.0002702	0.15	0.00073	12.33	0.01215	0.27	262.8	0.65	0.51	0	0	0	0	0

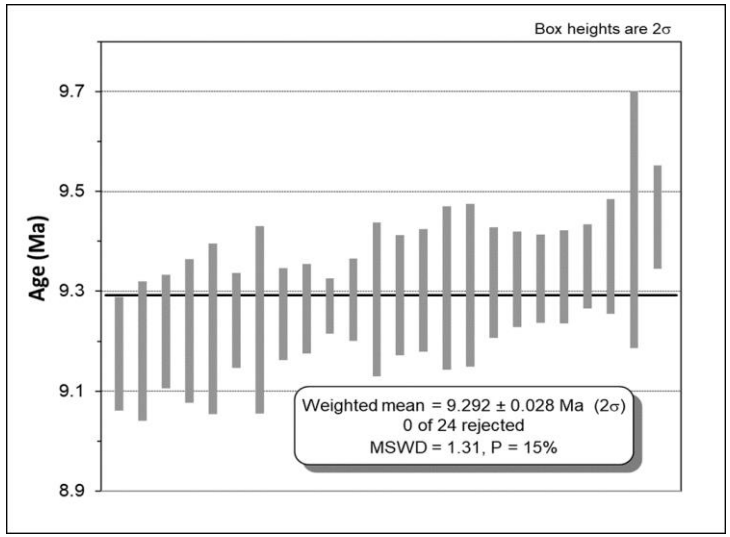

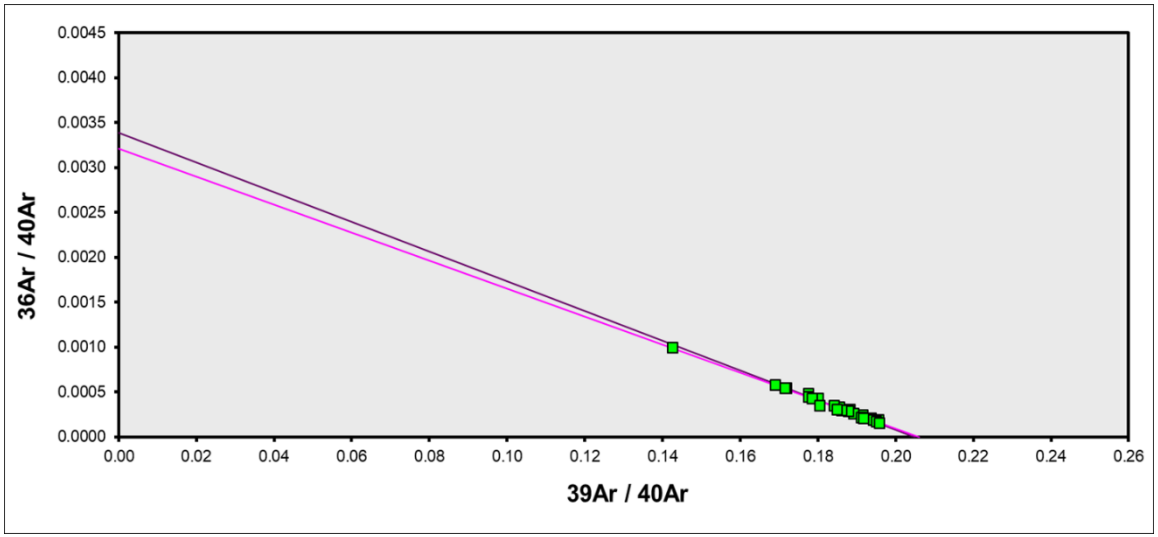

Information on Analysis and Constants Used in Calculations

Sample = 17-16/3 (163BS)
Material = Phlogopite (0.25-0.5 mm)
Location = Maio, Cape Verdes
Analyst = Jan Sticklus
Project = EXAMPLES
Mass Discrimination Law = POW
Irradiation = can47
J = 0.00105850 ± 0.00000085
TCS2 = 28.344 ± 0.011 Ma
Experiment Type = SAMPLE
Heating = 45 sec
Isolation = 15.00 min
Instrument = MAP216

Age Equations = Conventional
Negative Intensities = Allowed
Decay Constant 40K = 5.543 ± 0.009 E-10 1/a
Decay Constant 39Ar = 2.940 ± 0.016 E-07 1/h
Decay Constant 37Ar = 8.230 ± 0.012 E-04 1/h
Decay Constant 36Cl = 2.257 ± 0.015 E-06 1/a
Atmospheric Ratio 40/36(a) = 295.50 ± 0.53
Atmospheric Ratio 38/36(a) = 0.1869 ± 0.0002
Production Ratio 39/37(ca) = 0.000702 ± 0.000012
Production Ratio 38/37(ca) = 0.000196 ± 0.000008
Production Ratio 36/37(ca) = 0.000270 ± 0.000000
Production Ratio 40/39(k) = 0.000730 ± 0.000090
Production Ratio 38/39(k) = 0.012150 ± 0.000033
Production Ratio 36/38(cl) = 262.80
Scaling Ratio K/Ca = 0.510

Results	40(a)/36(a) ± 2σ	40(r)/39(k) ± 2σ	Age ± 2σ (Ma)	MSWD	39Ar(k) (%,n)	K/Ca ± 2σ
SCTF Weighted Mean		4.87864 ± 0.01269 ± 0.26%	9.292 ± 0.028 ± 0.30%	1.31	100.00	11.8 ± 3.4
				15%	24	
		Minimal External Error ± 0.041		1.59	2σ Confidence Limit	
		Analytical Error ± 0.024		1.1447	Error Magnification	
Total Fusion Age		4.87634 ± 0.01240 ± 0.25%	9.288 ± 0.028 ± 0.30%		24	28.9 ± 0.2
		Minimal External Error ± 0.041				
		Analytical Error ± 0.024				
Normal Isochron	311.60 ± 12.66 ± 4.06%	4.84783 ± 0.02453 ± 0.51%	9.234 ± 0.049 ± 0.53%	1.04	100.00	
				41%	24	
		Minimal External Error ± 0.057		1.60	2σ Confidence Limit	
		Analytical Error ± 0.047		1.0186	Error Magnification	
				1	Number of Iterations	
				0.0000011495	Convergence	
Inverse Isochron	311.43 ± 12.83 ± 4.12%	4.85167 ± 0.02471 ± 0.51%	9.241 ± 0.049 ± 0.53%	1.06	100.00	
				39%	24	
		Minimal External Error ± 0.057		1.60	2σ Confidence Limit	
		Analytical Error ± 0.047		1.0274	Error Magnification	
				3	Number of Iterations	
				0.0000011185	Convergence	
				26%	Spreading Factor	

Sample 17-16/3 single-crystal total-fusion results (0.5-1 mm fraction; 163bl)

Relative Abundances	Laser power		36Ar [V]	%1σ	37Ar [V]	%1σ	38Ar [V]	%1σ	39Ar [V]	%1σ	40Ar [V]	%1σ	40(r)/39(k) ± 2σ	Age ± 2σ (Ma)	40Ar(r) (%)	39Ar(k) (%)	K/Ca ± 2σ	Sample weight (mg)	$^{36}Ar/^{39}Ar$ Alt. Index	Wt. % K
C47AB090	5.00 W	•	0.0005596	1.903	0.0025374	1.650	0.0021978	0.998	0.1782450	0.240	1.024185	0.192	4.81865 ± 0.04772	9.18 ± 0.09	83.86	3.49	35.8 ± 1.2	0.117	*0.000231*	5.6
C47AB080	5.00 W	•	0.0007516	1.873	0.0023129	1.440	0.0023688	1.266	0.1920618	0.276	1.148288	0.175	4.82270 ± 0.05512	9.19 ± 0.10	80.66	3.76	42.4 ± 1.2	0.126	*0.000288*	5.6
C47BA083	5.00 W	•	0.0002480	13.361	0.0029248	4.738	0.0024097	3.743	0.1990880	0.394	1.035075	0.335	4.83146 ± 0.11109	9.20 ± 0.21	92.93	3.89	34.7 ± 3.3	0.135	*0.000089*	5.4
C47BA084	5.00 W	•	0.0005357	5.008	0.0063031	2.406	0.0029570	3.120	0.2458222	0.281	1.346455	0.248	4.83478 ± 0.07515	9.21 ± 0.14	88.27	4.81	19.9 ± 1.0	0.169	*0.000153*	5.3
C47BA094	5.00 W	•	0.0017141	1.874	0.0010562	12.061	0.0025880	3.669	0.1911745	0.304	1.432022	0.233	4.84094 ± 0.10969	9.22 ± 0.21	64.63	3.74	92.3 ± 22.3	0.070	*0.001185*	10.0
C47AB084	5.00 W	•	0.0003773	4.748	0.0038906	1.866	0.0027768	0.907	0.2332288	0.272	1.242933	0.166	4.85190 ± 0.05545	9.24 ± 0.11	91.04	4.56	30.6 ± 1.2	0.151	*0.000121*	5.6
C47AB081	5.00 W	•	0.0001117	11.508	0.0007471	5.084	0.0022738	1.318	0.1942529	0.264	0.976736	0.205	4.85778 ± 0.05112	9.25 ± 0.10	96.61	3.80	132.6 ± 13.5	0.123	*0.000044*	5.8
C47AB089	5.00 W	•	0.0004159	3.147	0.0015323	2.490	0.0019871	1.429	0.1624178	0.240	0.911934	0.215	4.85809 ± 0.05833	9.25 ± 0.11	86.52	3.18	54.1 ± 2.7	0.114	*0.000176*	5.2
C47AB083	5.00 W	•	0.0007218	2.185	0.0017587	1.795	0.0026258	1.239	0.2101043	0.246	1.234513	0.164	4.86053 ± 0.05410	9.26 ± 0.10	82.72	4.11	60.9 ± 2.2	0.138	*0.000253*	5.6
C47AB085	5.00 W	•	0.0003510	3.265	0.0011101	4.039	0.0027303	0.793	0.2288435	0.243	1.216391	0.165	4.86187 ± 0.04174	9.26 ± 0.08	91.47	4.47	105.1 ± 8.5	0.144	*0.000118*	5.8
C47AB086	5.00 W	•	0.0006248	2.763	0.0060815	0.815	0.0037311	1.275	0.3088143	0.227	1.686661	0.119	4.86476 ± 0.04189	9.27 ± 0.08	89.07	6.04	25.9 ± 0.4	0.200	*0.000151*	5.6
C47AB082	5.00 W	•	0.0003743	3.400	0.0011274	2.765	0.0031388	0.832	0.2660445	0.228	1.406001	0.151	4.86876 ± 0.03932	9.27 ± 0.07	92.13	5.20	120.3 ± 6.7	0.172	*0.000105*	5.7
C47BA089	5.00 W	•	0.0004406	5.786	0.0091437	1.606	0.0036396	2.468	0.2993346	0.269	1.587249	0.211	4.86943 ± 0.06105	9.27 ± 0.12	91.83	5.85	16.7 ± 0.5	0.193	*0.000110*	5.7
C47BA087	5.00 W	•	0.0002853	9.103	0.0022225	6.043	0.0067157	1.470	0.5590528	0.223	2.808199	0.129	4.87191 ± 0.03734	9.28 ± 0.07	96.99	10.93	128.3 ± 15.5	0.357	*0.000039*	5.7
C47AB091	5.00 W	•	0.0008449	2.344	0.0035912	1.777	0.0033989	1.243	0.2731216	0.235	1.583861	0.125	4.88535 ± 0.05083	9.31 ± 0.10	84.24	5.34	38.8 ± 1.4	0.175	*0.000233*	5.7
C47AB088	5.00 W	•	0.0004085	4.151	0.0006521	5.974	0.0012922	1.495	0.1038990	0.261	0.628409	0.310	4.88622 ± 0.10667	9.31 ± 0.20	80.79	2.03	81.3 ± 9.7	0.072	*0.000274*	5.3
C47BA085	5.00 W	•	0.0002094	12.153	0.0004429	28.993	0.0016171	5.622	0.1380415	0.374	0.738317	0.463	4.89969 ± 0.12521	9.33 ± 0.24	91.61	2.70	159.0 ± 92.2	0.094	*0.000108*	5.4
C47BA092	5.00 W	•	0.0009635	2.777	0.0009486	13.838	0.0017007	5.445	0.1267502	0.392	0.906821	0.374	4.90806 ± 0.14132	9.35 ± 0.27	68.60	2.48	68.1 ± 18.9	0.083	*0.000562*	5.6
C47BA090	5.00 W	•	0.0018733	1.715	0.0005282	24.051	0.0021544	4.219	0.1535987	0.352	1.308814	0.258	4.91670 ± 0.13625	9.36 ± 0.26	57.70	3.00	148.3 ± 71.3	0.101	*0.000897*	5.6
C47AB087	5.00 W	•	0.0025732	1.174	0.0045150	1.223	0.0048907	0.786	0.3772426	0.222	2.617428	0.082	4.92294 ± 0.05385	9.38 ± 0.10	70.95	7.38	42.6 ± 1.1	0.244	*0.000510*	5.7
C47BA091	5.00 W	•	0.0006664	4.214	0.0005176	25.136	0.0015173	5.835	0.1184228	0.411	0.780353	0.427	4.92636 ± 0.15647	9.38 ± 0.30	74.76	2.32	116.7 ± 58.7	0.113	*0.000285*	3.8
C47BA088	5.00 W	•	0.0005343	4.953	0.0005935	21.498	0.0029595	3.170	0.2457031	0.280	1.368682	0.254	4.92731 ± 0.07494	9.38 ± 0.14	88.45	4.80	211.1 ± 90.8	0.157	*0.000165*	5.7
C47BA093	5.00 W	•	0.0012615	2.340	0.0014915	9.012	0.0015258	5.923	0.1092933	0.476	0.915840	0.361	4.96936 ± 0.17755	9.46 ± 0.34	59.30	2.14	37.4 ± 6.7	0.087	*0.000701*	4.6
		Σ	0.0168467	0.659	0.0560289	0.847	0.0631967	0.513	5.1145577	0.060	29.905167	0.044								

Procedure Blanks	Laser power	36Ar [V]	1σ	37Ar [V]	1σ	38Ar [V]	1σ	39Ar [V]	1σ	40Ar [V]	1σ
C47AB090	5.00 W	0.0000687	0.0000067	0.0001597	0.0000110	0.0000420	0.0000071	0.0003290	0.0001105	0.0037562	0.0019254
C47AB080	5.00 W	0.0000638	0.0000067	0.0001624	0.0000110	0.0000455	0.0000071	0.0002279	0.0001105	0.0078516	0.0019254
C47BA083	5.00 W	0.0004368	0.0000235	0.0004843	0.0000535	0.0003897	0.0000889	0.0014608	0.0003687	0.0126660	0.0032401
C47BA084	5.00 W	0.0004260	0.0000235	0.0004745	0.0000535	0.0003710	0.0000889	0.0013720	0.0003687	0.0119578	0.0032401
C47BA094	5.00 W	0.0003105	0.0000235	0.0003708	0.0000535	0.0001721	0.0000889	0.0004293	0.0003687	0.0044358	0.0032401
C47AB084	5.00 W	0.0000656	0.0000067	0.0001614	0.0000110	0.0000442	0.0000071	0.0002660	0.0001105	0.0063092	0.0019254
C47AB081	5.00 W	0.0000643	0.0000067	0.0001621	0.0000110	0.0000452	0.0000071	0.0002374	0.0001105	0.0074660	0.0019254
C47AB089	5.00 W	0.0000682	0.0000067	0.0001599	0.0000110	0.0000424	0.0000071	0.0003195	0.0001105	0.0041418	0.0019254
C47AB083	5.00 W	0.0000652	0.0000067	0.0001616	0.0000110	0.0000445	0.0000071	0.0002565	0.0001105	0.0066948	0.0019254
C47AB085	5.00 W	0.0000661	0.0000067	0.0001611	0.0000110	0.0000439	0.0000071	0.0002755	0.0001105	0.0059236	0.0019254
C47AB086	5.00 W	0.0000668	0.0000067	0.0001607	0.0000110	0.0000433	0.0000071	0.0002913	0.0001105	0.0052853	0.0019254
C47AB082	5.00 W	0.0000647	0.0000067	0.0001619	0.0000110	0.0000449	0.0000071	0.0002469	0.0001105	0.0070804	0.0019254
C47BA089	5.00 W	0.0003645	0.0000235	0.0004193	0.0000535	0.0002651	0.0000889	0.0008700	0.0003687	0.0079526	0.0032401
C47BA087	5.00 W	0.0003933	0.0000235	0.0004452	0.0000535	0.0003148	0.0000889	0.0011057	0.0003687	0.0098331	0.0032401
C47AB091	5.00 W	0.0000691	0.0000067	0.0001594	0.0000110	0.0000417	0.0000071	0.0003386	0.0001105	0.0033706	0.0019254
C47AB088	5.00 W	0.0000677	0.0000067	0.0001602	0.0000110	0.0000427	0.0000071	0.0003100	0.0001105	0.0045274	0.0019254
C47BA085	5.00 W	0.0004151	0.0000235	0.0004647	0.0000535	0.0003523	0.0000889	0.0012833	0.0003687	0.0112496	0.0032401
C47BA092	5.00 W	0.0003322	0.0000235	0.0003903	0.0000535	0.0002096	0.0000889	0.0006068	0.0003687	0.0058523	0.0032401
C47BA090	5.00 W	0.0003536	0.0000235	0.0004095	0.0000535	0.0002464	0.0000889	0.0007813	0.0003687	0.0072444	0.0032401
C47AB087	5.00 W	0.0000673	0.0000067	0.0001604	0.0000110	0.0000430	0.0000071	0.0003008	0.0001105	0.0048997	0.0019254
C47BA091	5.00 W	0.0003427	0.0000235	0.0003997	0.0000535	0.0002276	0.0000889	0.0006925	0.0003687	0.0065361	0.0032401
C47BA088	5.00 W	0.0003825	0.0000235	0.0004354	0.0000535	0.0002961	0.0000889	0.0010170	0.0003687	0.0091249	0.0032401
C47BA093	5.00 W	0.0003213	0.0000235	0.0003805	0.0000535	0.0001908	0.0000889	0.0005180	0.0003687	0.0051441	0.0032401

Sample Parameters	Laser power	Sample	Material	Location	Analyst	Standard (in Ma)	%1σ	J	%1σ	MDF	%1σ	Volume Ratio	Sensitivity (mol/volt)
C47AB090	5.00 W	17/16-3 (163bl)	Phlogopite (0.5-1 mm)	Maio, Cape Verdes	Jan Sticklus	28.344	0.039	1.06E-03	0.08	1.0098	0.21	1	1.211E-14
C47AB080	5.00 W	17/16-3 (163bl)	Phlogopite (0.5-1 mm)	Maio, Cape Verdes	Jan Sticklus	28.344	0.039	1.06E-03	0.08	1.0098	0.21	1	1.211E-14
C47BA083	5.00 W	17/16-3 (163bl)	Phlogopite (0.5-1 mm)	Maio, Cape Verdes	Jan Sticklus	28.344	0.039	1.06E-03	0.08	1.0098	0.21	1	1.211E-14
C47BA084	5.00 W	17/16-3 (163bl)	Phlogopite (0.5-1 mm)	Maio, Cape Verdes	Jan Sticklus	28.344	0.039	1.06E-03	0.08	1.0098	0.21	1	1.211E-14
C47BA094	5.00 W	17/16-3 (163bl)	Phlogopite (0.5-1 mm)	Maio, Cape Verdes	Jan Sticklus	28.344	0.039	1.06E-03	0.08	1.0098	0.21	1	1.211E-14
C47AB084	5.00 W	17/16-3 (163bl)	Phlogopite (0.5-1 mm)	Maio, Cape Verdes	Jan Sticklus	28.344	0.039	1.06E-03	0.08	1.0098	0.21	1	1.211E-14
C47AB081	5.00 W	17/16-3 (163bl)	Phlogopite (0.5-1 mm)	Maio, Cape Verdes	Jan Sticklus	28.344	0.039	1.06E-03	0.08	1.0098	0.21	1	1.211E-14
C47AB089	5.00 W	17/16-3 (163bl)	Phlogopite (0.5-1 mm)	Maio, Cape Verdes	Jan Sticklus	28.344	0.039	1.06E-03	0.08	1.0098	0.21	1	1.211E-14
C47AB083	5.00 W	17/16-3 (163bl)	Phlogopite (0.5-1 mm)	Maio, Cape Verdes	Jan Sticklus	28.344	0.039	1.06E-03	0.08	1.0098	0.21	1	1.211E-14
C47AB085	5.00 W	17/16-3 (163bl)	Phlogopite (0.5-1 mm)	Maio, Cape Verdes	Jan Sticklus	28.344	0.039	1.06E-03	0.08	1.0098	0.21	1	1.211E-14
C47AB086	5.00 W	17/16-3 (163bl)	Phlogopite (0.5-1 mm)	Maio, Cape Verdes	Jan Sticklus	28.344	0.039	1.06E-03	0.08	1.0098	0.21	1	1.211E-14
C47AB082	5.00 W	17/16-3 (163bl)	Phlogopite (0.5-1 mm)	Maio, Cape Verdes	Jan Sticklus	28.344	0.039	1.06E-03	0.08	1.0098	0.21	1	1.211E-14
C47BA089	5.00 W	17/16-3 (163bl)	Phlogopite (0.5-1 mm)	Maio, Cape Verdes	Jan Sticklus	28.344	0.039	1.06E-03	0.08	1.0098	0.21	1	1.211E-14
C47BA087	5.00 W	17/16-3 (163bl)	Phlogopite (0.5-1 mm)	Maio, Cape Verdes	Jan Sticklus	28.344	0.039	1.06E-03	0.08	1.0098	0.21	1	1.211E-14
C47AB091	5.00 W	17/16-3 (163bl)	Phlogopite (0.5-1 mm)	Maio, Cape Verdes	Jan Sticklus	28.344	0.039	1.06E-03	0.08	1.0098	0.21	1	1.211E-14
C47AB088	5.00 W	17/16-3 (163bl)	Phlogopite (0.5-1 mm)	Maio, Cape Verdes	Jan Sticklus	28.344	0.039	1.06E-03	0.08	1.0098	0.21	1	1.211E-14
C47BA085	5.00 W	17/16-3 (163bl)	Phlogopite (0.5-1 mm)	Maio, Cape Verdes	Jan Sticklus	28.344	0.039	1.06E-03	0.08	1.0098	0.21	1	1.211E-14
C47BA092	5.00 W	17/16-3 (163bl)	Phlogopite (0.5-1 mm)	Maio, Cape Verdes	Jan Sticklus	28.344	0.039	1.06E-03	0.08	1.0098	0.21	1	1.211E-14
C47BA090	5.00 W	17/16-3 (163bl)	Phlogopite (0.5-1 mm)	Maio, Cape Verdes	Jan Sticklus	28.344	0.039	1.06E-03	0.08	1.0098	0.21	1	1.211E-14
C47AB087	5.00 W	17/16-3 (163bl)	Phlogopite (0.5-1 mm)	Maio, Cape Verdes	Jan Sticklus	28.344	0.039	1.06E-03	0.08	1.0098	0.21	1	1.211E-14
C47BA091	5.00 W	17/16-3 (163bl)	Phlogopite (0.5-1 mm)	Maio, Cape Verdes	Jan Sticklus	28.344	0.039	1.06E-03	0.08	1.0098	0.21	1	1.211E-14
C47BA088	5.00 W	17/16-3 (163bl)	Phlogopite (0.5-1 mm)	Maio, Cape Verdes	Jan Sticklus	28.344	0.039	1.06E-03	0.08	1.0098	0.21	1	1.211E-14
C47BA093	5.00 W	17/16-3 (163bl)	Phlogopite (0.5-1 mm)	Maio, Cape Verdes	Jan Sticklus	28.344	0.039	1.06E-03	0.08	1.0098	0.21	1	1.211E-14

Day	Month	Year	Hour	Min	Resist	Irradiation	Project	Experiment	Nmb	Standard Name
24	JUN	2018	8	1	1	can47	Examples	c47it5ip1_163bl	01	TCS2
24	JUN	2018	2	53	1	can47	Examples	c47it5ip1_163bl	01	TCS2
30	JUN	2018	5	53	1	can47	Examples	c47it5ip1_163bl	01	TCS2
30	JUN	2018	6	22	1	can47	Examples	c47it5ip1_163bl	01	TCS2
30	JUN	2018	11	30	1	can47	Examples	c47it5ip1_163bl	01	TCS2
24	JUN	2018	4	49	1	can47	Examples	c47it5ip1_163bl	01	TCS2
24	JUN	2018	3	22	1	can47	Examples	c47it5ip1_163bl	01	TCS2
24	JUN	2018	7	32	1	can47	Examples	c47it5ip1_163bl	01	TCS2
24	JUN	2018	4	20	1	can47	Examples	c47it5ip1_163bl	01	TCS2
24	JUN	2018	5	18	1	can47	Examples	c47it5ip1_163bl	01	TCS2
24	JUN	2018	6	6	1	can47	Examples	c47it5ip1_163bl	01	TCS2
24	JUN	2018	3	51	1	can47	Examples	c47it5ip1_163bl	01	TCS2
30	JUN	2018	9	6	1	can47	Examples	c47it5ip1_163bl	01	TCS2
30	JUN	2018	7	49	1	can47	Examples	c47it5ip1_163bl	01	TCS2
24	JUN	2018	8	30	1	can47	Examples	c47it5ip1_163bl	01	TCS2
24	JUN	2018	7	3	1	can47	Examples	c47it5ip1_163bl	01	TCS2
30	JUN	2018	6	51	1	can47	Examples	c47it5ip1_163bl	01	TCS2
30	JUN	2018	10	32	1	can47	Examples	c47it5ip1_163bl	01	TCS2
30	JUN	2018	9	35	1	can47	Examples	c47it5ip1_163bl	01	TCS2
24	JUN	2018	6	35	1	can47	Examples	c47it5ip1_163bl	01	TCS2
30	JUN	2018	10	4	1	can47	Examples	c47it5ip1_163bl	01	TCS2
30	JUN	2018	8	18	1	can47	Examples	c47it5ip1_163bl	01	TCS2
30	JUN	2018	11	1	1	can47	Examples	c47it5ip1_163bl	01	TCS2

Irradiation Constants	Laser power	40/36(a)	%1σ	40/36(c)	%1σ	38/36(a)	%1σ	38/36(c)	%1σ	39/37(ca)	%1σ	38/37(ca)	%1σ	36/37(ca)	%1σ	40/39(k)	%1σ	38/39(k)	%1σ	36/38(cl)	%1σ	K/Ca	%1σ	K/Cl	%1σ	Ca/Cl	%1σ
C47AB090	5.00 W	295.5	0.178	0.018	35	0.1869	0.107	1.493	3	0.000702	1.71	0.000196	4.08	0.0002702	0.15	0.00073	12.33	0.01215	0.27	262.8	0.65	0.51	0	0	0	0	0
C47AB080	5.00 W	295.5	0.178	0.018	35	0.1869	0.107	1.493	3	0.000702	1.71	0.000196	4.08	0.0002702	0.15	0.00073	12.33	0.01215	0.27	262.8	0.65	0.51	0	0	0	0	0
C47BA083	5.00 W	295.5	0.178	0.018	35	0.1869	0.107	1.493	3	0.000702	1.71	0.000196	4.08	0.0002702	0.15	0.00073	12.33	0.01215	0.27	262.8	0.65	0.51	0	0	0	0	0
C47BA084	5.00 W	295.5	0.178	0.018	35	0.1869	0.107	1.493	3	0.000702	1.71	0.000196	4.08	0.0002702	0.15	0.00073	12.33	0.01215	0.27	262.8	0.65	0.51	0	0	0	0	0
C47BA094	5.00 W	295.5	0.178	0.018	35	0.1869	0.107	1.493	3	0.000702	1.71	0.000196	4.08	0.0002702	0.15	0.00073	12.33	0.01215	0.27	262.8	0.65	0.51	0	0	0	0	0
C47AB084	5.00 W	295.5	0.178	0.018	35	0.1869	0.107	1.493	3	0.000702	1.71	0.000196	4.08	0.0002702	0.15	0.00073	12.33	0.01215	0.27	262.8	0.65	0.51	0	0	0	0	0
C47AB081	5.00 W	295.5	0.178	0.018	35	0.1869	0.107	1.493	3	0.000702	1.71	0.000196	4.08	0.0002702	0.15	0.00073	12.33	0.01215	0.27	262.8	0.65	0.51	0	0	0	0	0
C47AB089	5.00 W	295.5	0.178	0.018	35	0.1869	0.107	1.493	3	0.000702	1.71	0.000196	4.08	0.0002702	0.15	0.00073	12.33	0.01215	0.27	262.8	0.65	0.51	0	0	0	0	0
C47AB083	5.00 W	295.5	0.178	0.018	35	0.1869	0.107	1.493	3	0.000702	1.71	0.000196	4.08	0.0002702	0.15	0.00073	12.33	0.01215	0.27	262.8	0.65	0.51	0	0	0	0	0
C47AB085	5.00 W	295.5	0.178	0.018	35	0.1869	0.107	1.493	3	0.000702	1.71	0.000196	4.08	0.0002702	0.15	0.00073	12.33	0.01215	0.27	262.8	0.65	0.51	0	0	0	0	0
C47AB086	5.00 W	295.5	0.178	0.018	35	0.1869	0.107	1.493	3	0.000702	1.71	0.000196	4.08	0.0002702	0.15	0.00073	12.33	0.01215	0.27	262.8	0.65	0.51	0	0	0	0	0
C47AB082	5.00 W	295.5	0.178	0.018	35	0.1869	0.107	1.493	3	0.000702	1.71	0.000196	4.08	0.0002702	0.15	0.00073	12.33	0.01215	0.27	262.8	0.65	0.51	0	0	0	0	0
C47BA089	5.00 W	295.5	0.178	0.018	35	0.1869	0.107	1.493	3	0.000702	1.71	0.000196	4.08	0.0002702	0.15	0.00073	12.33	0.01215	0.27	262.8	0.65	0.51	0	0	0	0	0
C47BA087	5.00 W	295.5	0.178	0.018	35	0.1869	0.107	1.493	3	0.000702	1.71	0.000196	4.08	0.0002702	0.15	0.00073	12.33	0.01215	0.27	262.8	0.65	0.51	0	0	0	0	0
C47AB091	5.00 W	295.5	0.178	0.018	35	0.1869	0.107	1.493	3	0.000702	1.71	0.000196	4.08	0.0002702	0.15	0.00073	12.33	0.01215	0.27	262.8	0.65	0.51	0	0	0	0	0
C47AB088	5.00 W	295.5	0.178	0.018	35	0.1869	0.107	1.493	3	0.000702	1.71	0.000196	4.08	0.0002702	0.15	0.00073	12.33	0.01215	0.27	262.8	0.65	0.51	0	0	0	0	0
C47BA085	5.00 W	295.5	0.178	0.018	35	0.1869	0.107	1.493	3	0.000702	1.71	0.000196	4.08	0.0002702	0.15	0.00073	12.33	0.01215	0.27	262.8	0.65	0.51	0	0	0	0	0
C47BA092	5.00 W	295.5	0.178	0.018	35	0.1869	0.107	1.493	3	0.000702	1.71	0.000196	4.08	0.0002702	0.15	0.00073	12.33	0.01215	0.27	262.8	0.65	0.51	0	0	0	0	0
C47BA090	5.00 W	295.5	0.178	0.018	35	0.1869	0.107	1.493	3	0.000702	1.71	0.000196	4.08	0.0002702	0.15	0.00073	12.33	0.01215	0.27	262.8	0.65	0.51	0	0	0	0	0
C47AB087	5.00 W	295.5	0.178	0.018	35	0.1869	0.107	1.493	3	0.000702	1.71	0.000196	4.08	0.0002702	0.15	0.00073	12.33	0.01215	0.27	262.8	0.65	0.51	0	0	0	0	0
C47BA091	5.00 W	295.5	0.178	0.018	35	0.1869	0.107	1.493	3	0.000702	1.71	0.000196	4.08	0.0002702	0.15	0.00073	12.33	0.01215	0.27	262.8	0.65	0.51	0	0	0	0	0
C47BA088	5.00 W	295.5	0.178	0.018	35	0.1869	0.107	1.493	3	0.000702	1.71	0.000196	4.08	0.0002702	0.15	0.00073	12.33	0.01215	0.27	262.8	0.65	0.51	0	0	0	0	0
C47BA093	5.00 W	295.5	0.178	0.018	35	0.1869	0.107	1.493	3	0.000702	1.71	0.000196	4.08	0.0002702	0.15	0.00073	12.33	0.01215	0.27	262.8	0.65	0.51	0	0	0	0	0

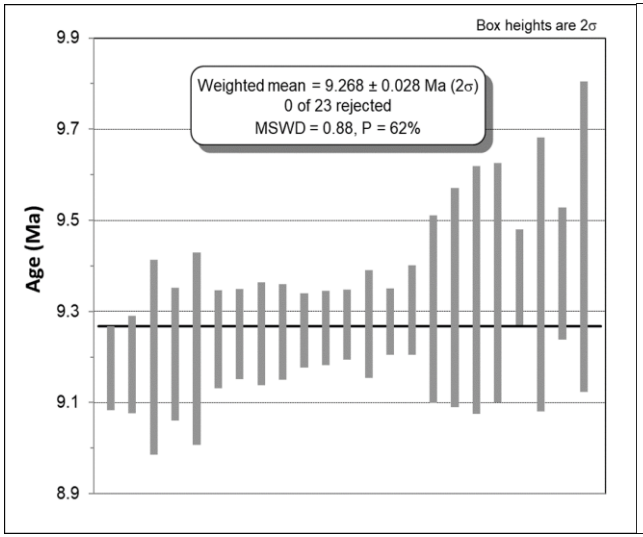

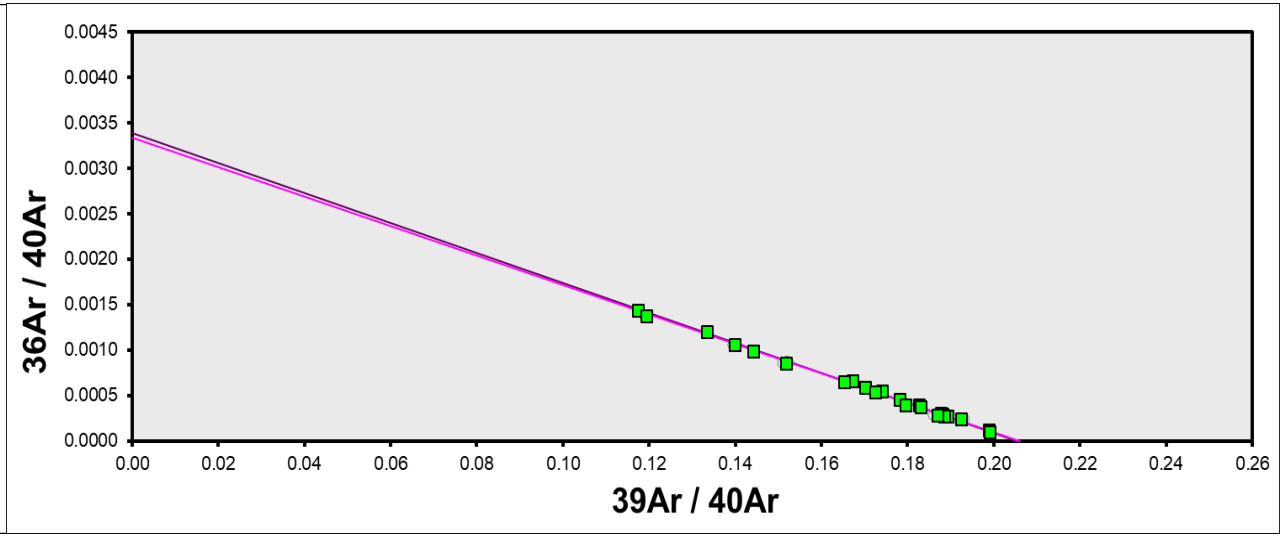

Information on Analysis and Constants Used in Calculations

Sample = 17/16-3 (163BL)
Material = Phlogopite
Location = Maio Cape Verde
Analyst = Jan Sticklus
Project = EXAMPLES
Mass Discrimination Law = POW
Irradiation = can47
J = 0.00105850 ± 0.00000085
TCS2 = 28.344 ± 0.011 Ma
Experiment Type = SAMPLE
Heating = 45 sec
Isolation = 15.00 min
Instrument = MAP216

Age Equations = Conventional
Negative Intensities = Allowed
Decay Constant 40K = 5.543 ± 0.009 E-10 1/a
Decay Constant 39Ar = 2.940 ± 0.016 E-07 1/h
Decay Constant 37Ar = 8.230 ± 0.012 E-04 1/h
Decay Constant 36Cl = 2.257 ± 0.015 E-06 1/a
Atmospheric Ratio 40/36(a) = 295.50 ± 0.53
Atmospheric Ratio 38/36(a) = 0.1869 ± 0.0002
Production Ratio 39/37(ca) = 0.000702 ± 0.000012
Production Ratio 38/37(ca) = 0.000196 ± 0.000008
Production Ratio 36/37(ca) = 0.000270 ± 0.000000
Production Ratio 40/39(k) = 0.000730 ± 0.000090
Production Ratio 38/39(k) = 0.012150 ± 0.000033
Production Ratio 36/38(cl) = 262.80
Scaling Ratio K/Ca = 0.510

Results	40(a)/36(a) ± 2σ	40(r)/39(k) ± 2σ	Age ± 2σ (Ma)	MSWD	39Ar(k) (%,n)	K/Ca ± 2σ
SCTF Weighted Mean		4.86585 ± 0.01243	9.268 ± 0.028	0.88	100.00	27.5 ± 4.8
		± 0.26%	± 0.30%	62%	23	
		Minimal External Error	± 0.041	1.60	2σ Confidence Limit	
		Analytical Error	± 0.024	1.0000	Error Magnification	
Total Fusion Age		4.87391 ± 0.01504	9.283 ± 0.032		23	46.6 ± 0.8
		± 0.31%	± 0.35%			
		Minimal External Error	± 0.044			
		Analytical Error	± 0.029			
Normal Isochron	297.71 ± 6.11	4.86273 ± 0.01981	9.262 ± 0.040	0.86	100.00	
	± 2.05%	± 0.41%	± 0.44%	65%	23	
		Minimal External Error	± 0.050	1.62	2σ Confidence Limit	
		Analytical Error	± 0.038	1.0000	Error Magnification	
				1	Number of Iterations	
				0.0000482759	Convergence	
Inverse Isochron	300.25 ± 6.11	4.85402 ± 0.01983	9.246 ± 0.040	0.81	100.00	
	± 2.03%	± 0.41%	± 0.44%	71%	23	
		Minimal External Error	± 0.050	1.62	2σ Confidence Limit	
		Analytical Error	± 0.038	1.0000	Error Magnification	
				3	Number of Iterations	
				0.0000903644	Convergence	
				40%	Spreading Factor	

Sample 17-16/3 single-crystal total-fusion results (0.25-0.5 and 0.5-1 mm fractions; 163bs and 163bl combined)

Relative Abundances	Laser power		36Ar [V]	%1σ	37Ar [V]	%1σ	38Ar [V]	%1σ	39Ar [V]	%1σ	40Ar [V]	%1σ	40(r)/39(k) ± 2σ	Age ± 2σ (Ma)	40Ar(r) (%)	39Ar(k) (%)	K/Ca ± 2σ	Sample weight (mg)	$^{36}Ar/^{39}Ar$ Alt. Index	Wt. % K
C47AB096	5.00 W	•	0.0001245	8.666	0.0019725	1.805	0.0014676	1.699	0.1243642	0.279	0.635929	0.081	4.81812 ± 0.05850	9.18 ± 0.11	94.22	1.26	32.2 ± 1.2	0.071	*0.000085*	6.4
C47AB090	5.00 W	•	0.0005596	1.903	0.0025374	1.650	0.0021978	0.998	0.1782450	0.240	1.024185	0.192	4.81865 ± 0.04772	9.18 ± 0.09	83.86	1.81	35.8 ± 1.2	0.117	*0.000231*	5.6
C47BA097	5.00 W	•	0.0006046	4.159	0.0019610	3.005	0.0027825	1.398	0.2202591	0.244	1.240497	0.091	4.82083 ± 0.07224	9.18 ± 0.14	85.60	2.23	57.3 ± 3.5	0.131	*0.000223*	6.1
C47AB080	5.00 W	•	0.0007516	1.873	0.0023129	1.440	0.0023688	1.266	0.1920618	0.276	1.148288	0.175	4.82270 ± 0.05512	9.19 ± 0.10	80.66	1.95	42.4 ± 1.2	0.126	*0.000288*	5.6
C47BA083	5.00 W	•	0.0002480	13.361	0.0029248	4.738	0.0024097	3.743	0.1990880	0.394	1.035075	0.335	4.83146 ± 0.11109	9.20 ± 0.21	92.93	2.02	34.7 ± 3.3	0.135	*0.000089*	5.4
C47BA084	5.00 W	•	0.0005357	5.008	0.0063031	2.406	0.0029570	3.120	0.2458222	0.281	1.346455	0.248	4.83478 ± 0.07515	9.21 ± 0.14	88.27	2.49	19.9 ± 1.0	0.169	*0.000153*	5.3
C47BA094	5.00 W	•	0.0017141	1.874	0.0010562	12.061	0.0025880	3.669	0.1911745	0.304	1.432022	0.233	4.84094 ± 0.10969	9.22 ± 0.21	64.63	1.94	92.3 ± 22.3	0.070	*0.001185*	10.0
C47BA096	5.00 W	•	0.0002748	8.170	0.0029355	2.562	0.0030929	1.164	0.2494115	0.247	1.288637	0.056	4.84143 ± 0.05861	9.22 ± 0.11	93.70	2.53	43.3 ± 2.2	0.148	*0.000090*	6.2
C47BB004	5.00 W	•	0.0002673	7.331	0.0067027	1.758	0.0020341	1.652	0.1655865	0.237	0.880318	0.106	4.84190 ± 0.07451	9.22 ± 0.14	91.07	1.68	12.6 ± 0.4	0.106	*0.000121*	5.7
C47BA100	5.00 W	•	0.0003975	5.880	0.0065834	1.205	0.0020598	1.839	0.1647677	0.276	0.915198	0.103	4.84420 ± 0.08878	9.23 ± 0.17	87.21	1.67	12.8 ± 0.3	0.100	*0.000191*	6.0
C47AB084	5.00 W	•	0.0003773	4.748	0.0038906	1.866	0.0027768	0.907	0.2332288	0.272	1.242933	0.166	4.85190 ± 0.05545	9.24 ± 0.11	91.04	2.36	30.6 ± 1.2	0.151	*0.000121*	5.6
C47BB002	5.00 W	•	0.0002350	6.951	0.0024184	3.725	0.0027852	1.112	0.2353714	0.254	1.211661	0.103	4.85292 ± 0.04902	9.24 ± 0.09	94.27	2.39	49.6 ± 3.7	0.145	*0.000078*	5.9
C47BA095	5.00 W	•	0.0002159	12.453	0.0008822	7.535	0.0020953	1.256	0.1722052	0.296	0.899699	0.104	4.85373 ± 0.09728	9.25 ± 0.18	92.90	1.75	99.6 ± 15.0	0.106	*0.000098*	5.9
C47AB081	5.00 W	•	0.0001117	11.508	0.0007471	5.084	0.0022738	1.318	0.1942529	0.264	0.976736	0.205	4.85778 ± 0.05112	9.25 ± 0.10	96.61	1.97	132.6 ± 13.5	0.123	*0.000044*	5.8
C47AB089	5.00 W	•	0.0004159	3.147	0.0015323	2.490	0.0019871	1.429	0.1624178	0.240	0.911934	0.215	4.85809 ± 0.05833	9.25 ± 0.11	86.52	1.65	54.1 ± 2.7	0.114	*0.000176*	5.2
C47AB103	5.00 W	•	0.0002746	3.851	0.0010874	3.836	0.0018447	1.157	0.1516327	0.229	0.818057	0.070	4.85967 ± 0.04749	9.26 ± 0.09	90.08	1.54	71.1 ± 5.5	0.087	*0.000153*	6.4
C47AB083	5.00 W	•	0.0007218	2.185	0.0017587	1.795	0.0026258	1.239	0.2101043	0.246	1.234513	0.164	4.86053 ± 0.05410	9.26 ± 0.10	82.72	2.13	60.9 ± 2.2	0.138	*0.000253*	5.6
C47AB085	5.00 W	•	0.0003510	3.265	0.0011101	4.039	0.0027303	0.793	0.2288435	0.243	1.216391	0.165	4.86187 ± 0.04174	9.26 ± 0.08	91.47	2.32	105.1 ± 8.5	0.144	*0.000118*	5.8
C47AB086	5.00 W	•	0.0006248	2.763	0.0060815	0.815	0.0037311	1.275	0.3088143	0.227	1.686661	0.119	4.86476 ± 0.04189	9.27 ± 0.08	89.07	3.13	25.9 ± 0.4	0.200	*0.000151*	5.6
C47AB094	5.00 W	•	0.0002084	7.736	0.0034301	1.831	0.0027880	1.370	0.2346537	0.220	1.203149	0.044	4.86536 ± 0.04612	9.27 ± 0.09	94.89	2.38	34.9 ± 1.3	0.146	*0.000069*	5.9
C47AB092	5.00 W	•	0.0003034	3.729	0.0125629	0.993	0.0043509	0.714	0.3683386	0.217	1.881989	0.033	4.86814 ± 0.02809	9.27 ± 0.05	95.28	3.73	15.0 ± 0.3	0.230	*0.000063*	5.9
C47AB082	5.00 W	•	0.0003743	3.400	0.0011274	2.765	0.0031388	0.832	0.2660445	0.228	1.406001	0.151	4.86876 ± 0.03932	9.27 ± 0.07	92.13	2.70	120.3 ± 6.7	0.172	*0.000105*	5.7
C47BA089	5.00 W	•	0.0004406	5.786	0.0091437	1.606	0.0036396	2.468	0.2993346	0.269	1.587249	0.211	4.86943 ± 0.06105	9.27 ± 0.12	91.83	3.03	16.7 ± 0.5	0.193	*0.000110*	5.7
C47BA087	5.00 W	•	0.0002853	9.103	0.0022225	6.043	0.0067157	1.470	0.5590528	0.223	2.808199	0.129	4.87191 ± 0.03734	9.28 ± 0.07	96.99	5.67	128.3 ± 15.5	0.357	*0.000039*	5.7
C47AB098	5.00 W	•	0.0005304	3.047	0.0013077	2.237	0.0033485	1.437	0.2811414	0.248	1.527249	0.067	4.87451 ± 0.04235	9.28 ± 0.08	89.73	2.85	109.6 ± 4.9	0.165	*0.000155*	6.2
C47BA101	5.00 W	•	0.0002186	9.000	0.0014764	4.018	0.0018929	1.308	0.1563646	0.248	0.826844	0.145	4.87496 ± 0.07967	9.29 ± 0.15	92.19	1.59	54.0 ± 4.3	0.098	*0.000108*	5.8
C47BB003	5.00 W	•	0.0003001	6.250	0.0039720	2.159	0.0024703	1.280	0.1973605	0.246	1.051466	0.111	4.87926 ± 0.06226	9.29 ± 0.12	91.58	2.00	25.3 ± 1.1	0.126	*0.000115*	5.7
C47AB102	5.00 W	•	0.0003051	3.973	0.0013446	1.901	0.0014798	1.581	0.1204672	0.217	0.678530	0.053	4.88439 ± 0.06346	9.30 ± 0.12	86.72	1.22	45.7 ± 1.7	0.067	*0.000220*	6.6
C47AB091	5.00 W	•	0.0008449	2.344	0.0035912	1.777	0.0033989	1.243	0.2731216	0.235	1.583861	0.125	4.88535 ± 0.05083	9.31 ± 0.10	84.24	2.77	38.8 ± 1.4	0.175	*0.000233*	5.7
C47AB088	5.00 W	•	0.0004085	4.151	0.0006521	5.974	0.0012922	1.495	0.1038990	0.261	0.628409	0.310	4.88622 ± 0.10667	9.31 ± 0.20	80.79	1.05	81.3 ± 9.7	0.072	*0.000274*	5.3
C47AB099	5.00 W	•	0.0002641	5.652	0.0082763	1.113	0.0013024	1.741	0.1081167	0.229	0.605801	0.069	4.88698 ± 0.08500	9.31 ± 0.16	87.21	1.10	6.7 ± 0.2	0.062	*0.000204*	6.4
C47BB001	5.00 W	•	0.0006371	4.311	0.0010591	8.227	0.0025741	0.866	0.2018931	0.230	1.175526	0.092	4.88980 ± 0.08423	9.31 ± 0.16	83.98	2.05	97.2 ± 16.0	0.123	*0.000250*	6.0
C47BA099	5.00 W	•	0.0002620	7.576	0.0017502	3.201	0.0027933	1.027	0.2278958	0.232	1.192482	0.097	4.89275 ± 0.05719	9.32 ± 0.11	93.51	2.31	66.4 ± 4.3	0.136	*0.000093*	6.1
C47AB097	5.00 W	•	0.0006117	2.349	0.0024972	1.423	0.0023756	1.717	0.1932993	0.214	1.127131	0.056	4.89618 ± 0.04924	9.33 ± 0.09	83.97	1.96	39.5 ± 1.1	0.113	*0.000262*	6.3
C47BA098	5.00 W	•	0.0004780	4.109	0.0054949	1.902	0.0036770	1.057	0.2952157	0.229	1.586567	0.054	4.89664 ± 0.04565	9.33 ± 0.09	91.11	2.99	27.4 ± 1.0	0.196	*0.000118*	5.5
C47BB005	5.00 W	•	0.0003008	6.389	0.0036956	2.288	0.0034436	1.268	0.2784494	0.245	1.452803	0.080	4.89867 ± 0.04807	9.33 ± 0.09	93.89	2.82	38.4 ± 1.8	0.173	*0.000084*	5.9
C47BA085	5.00 W	•	0.0002094	12.153	0.0004429	28.993	0.0016171	5.622	0.1380415	0.374	0.738317	0.463	4.89969 ± 0.12521	9.33 ± 0.24	91.61	1.40	159.0 ± 92.2	0.094	*0.000108*	5.4
C47BA092	5.00 W	•	0.0009635	2.777	0.0009486	13.838	0.0017007	5.445	0.1267502	0.392	0.906821	0.374	4.90806 ± 0.14132	9.35 ± 0.27	68.60	1.29	68.1 ± 18.9	0.083	*0.000562*	5.6
C47AB101	5.00 W	•	0.0009053	1.802	0.0027725	1.891	0.0032096	0.807	0.2640990	0.231	1.564073	0.033	4.90950 ± 0.04330	9.35 ± 0.08	82.90	2.68	48.6 ± 1.9	0.159	*0.000275*	6.1
C47BA090	5.00 W	•	0.0018733	1.715	0.0005282	24.051	0.0021544	4.219	0.1535987	0.352	1.308814	0.258	4.91670 ± 0.13625	9.36 ± 0.26	57.70	1.56	148.3 ± 71.3	0.101	*0.000897*	5.6
C47AB100	5.00 W	•	0.0001996	5.327	0.0034998	1.746	0.0014538	1.343	0.1195814	0.269	0.647095	0.084	4.91982 ± 0.05955	9.37 ± 0.11	90.92	1.21	17.4 ± 0.6	0.069	*0.000139*	6.3
C47AB087	5.00 W	•	0.0025732	1.174	0.0045150	1.223	0.0048907	0.786	0.3772426	0.222	2.617428	0.082	4.92294 ± 0.05385	9.38 ± 0.10	70.95	3.82	42.6 ± 1.1	0.244	*0.000510*	5.7
C47BA091	5.00 W	•	0.0006664	4.214	0.0005176	25.136	0.0015173	5.835	0.1184228	0.411	0.780353	0.427	4.92636 ± 0.15647	9.38 ± 0.30	74.76	1.20	116.7 ± 58.7	0.113	*0.000285*	3.8
C47BA088	5.00 W	•	0.0005343	4.953	0.0005935	21.498	0.0029595	3.170	0.2457031	0.280	1.368682	0.254	4.92731 ± 0.07494	9.38 ± 0.14	88.45	2.49	211.1 ± 90.8	0.157	*0.000165*	5.7
C47AB095	5.00 W	•	0.0006768	3.181	0.0022353	2.227	0.0012859	1.674	0.0971126	0.236	0.681420	0.066	4.95858 ± 0.13361	9.44 ± 0.25	70.67	0.98	22.2 ± 1.0	0.051	*0.000642*	7.0
C47AB093	5.00 W	•	0.0002387	3.943	0.0038994	1.365	0.0014770	1.202	0.1212295	0.257	0.671731	0.080	4.96113 ± 0.05329	9.45 ± 0.10	89.53	1.23	15.9 ± 0.4	0.070	*0.000164*	6.3
C47BA093	5.00 W	•	0.0012615	2.340	0.0014915	9.012	0.0015258	5.923	0.1092933	0.476	0.915840	0.361	4.96936 ± 0.17755	9.46 ± 0.34	59.30	1.11	37.4 ± 6.7	0.087	*0.000701*	4.6
		Σ	0.0256810	0.556	0.1398460	0.424	0.1212817	0.296	9.8633744	0.040	55.669019	0.025								

Procedure Blanks	Laser power	36Ar [V]	1σ	37Ar [V]	1σ	38Ar [V]	1σ	39Ar [V]	1σ	40Ar [V]	1σ
C47AB096	5.00 W	0.0000730	0.0000071	0.0001618	0.0000076	0.0000371	0.0000082	0.0002723	0.0000165	0.0035460	0.0001233
C47AB090	5.00 W	0.0000687	0.0000067	0.0001597	0.0000110	0.0000420	0.0000071	0.0003290	0.0001105	0.0037562	0.0019254
C47BA097	5.00 W	0.0003206	0.0000161	0.0003713	0.0000164	0.0001780	0.0000166	0.0004956	0.0000381	0.0052904	0.0005542
C47AB080	5.00 W	0.0000638	0.0000067	0.0001624	0.0000110	0.0000455	0.0000071	0.0002279	0.0001105	0.0078516	0.0019254
C47BA083	5.00 W	0.0004368	0.0000235	0.0004843	0.0000535	0.0003897	0.0000889	0.0014608	0.0003687	0.0126660	0.0032401
C47BA084	5.00 W	0.0004260	0.0000235	0.0004745	0.0000535	0.0003710	0.0000889	0.0013720	0.0003687	0.0119578	0.0032401
C47BA094	5.00 W	0.0003105	0.0000235	0.0003708	0.0000535	0.0001721	0.0000889	0.0004293	0.0003687	0.0044358	0.0032401
C47BA096	5.00 W	0.0003206	0.0000161	0.0003713	0.0000164	0.0001780	0.0000166	0.0004956	0.0000381	0.0052904	0.0005542
C47BB004	5.00 W	0.0002915	0.0000143	0.0003323	0.0000286	0.0001389	0.0000078	0.0003542	0.0000210	0.0043949	0.0003288
C47BA100	5.00 W	0.0003206	0.0000161	0.0003713	0.0000164	0.0001780	0.0000166	0.0004956	0.0000381	0.0052904	0.0005542
C47AB084	5.00 W	0.0000656	0.0000067	0.0001614	0.0000110	0.0000442	0.0000071	0.0002660	0.0001105	0.0063092	0.0019254
C47BB002	5.00 W	0.0002877	0.0000143	0.0003366	0.0000286	0.0001401	0.0000078	0.0003529	0.0000210	0.0045027	0.0003288
C47BA095	5.00 W	0.0003206	0.0000161	0.0003713	0.0000164	0.0001780	0.0000166	0.0004956	0.0000381	0.0052904	0.0005542
C47AB081	5.00 W	0.0000643	0.0000067	0.0001621	0.0000110	0.0000452	0.0000071	0.0002374	0.0001105	0.0074660	0.0019254
C47AB089	5.00 W	0.0000682	0.0000067	0.0001599	0.0000110	0.0000424	0.0000071	0.0003195	0.0001105	0.0041418	0.0019254
C47AB103	5.00 W	0.0000767	0.0000071	0.0001704	0.0000076	0.0000336	0.0000082	0.0002112	0.0000165	0.0031288	0.0001233
C47AB083	5.00 W	0.0000652	0.0000067	0.0001616	0.0000110	0.0000445	0.0000071	0.0002565	0.0001105	0.0066948	0.0019254
C47AB085	5.00 W	0.0000661	0.0000067	0.0001611	0.0000110	0.0000439	0.0000071	0.0002755	0.0001105	0.0059236	0.0019254
C47AB086	5.00 W	0.0000668	0.0000067	0.0001607	0.0000110	0.0000433	0.0000071	0.0002913	0.0001105	0.0052853	0.0019254
C47AB094	5.00 W	0.0000720	0.0000071	0.0001595	0.0000076	0.0000380	0.0000082	0.0002883	0.0000165	0.0036555	0.0001233
C47AB092	5.00 W	0.0000710	0.0000071	0.0001573	0.0000076	0.0000389	0.0000082	0.0003044	0.0000165	0.0037650	0.0001233
C47AB082	5.00 W	0.0000647	0.0000067	0.0001619	0.0000110	0.0000449	0.0000071	0.0002469	0.0001105	0.0070804	0.0019254
C47BA089	5.00 W	0.0003645	0.0000235	0.0004193	0.0000535	0.0002651	0.0000889	0.0008700	0.0003687	0.0079526	0.0032401
C47BA087	5.00 W	0.0003933	0.0000235	0.0004452	0.0000535	0.0003148	0.0000889	0.0011057	0.0003687	0.0098331	0.0032401
C47AB098	5.00 W	0.0000743	0.0000071	0.0001647	0.0000076	0.0000359	0.0000082	0.0002513	0.0000165	0.0034025	0.0001233
C47BA101	5.00 W	0.0003206	0.0000161	0.0003713	0.0000164	0.0001780	0.0000166	0.0004956	0.0000381	0.0052904	0.0005542
C47BB003	5.00 W	0.0002895	0.0000143	0.0003345	0.0000286	0.0001395	0.0000078	0.0003535	0.0000210	0.0044497	0.0003288
C47AB102	5.00 W	0.0000762	0.0000071	0.0001692	0.0000076	0.0000341	0.0000082	0.0002192	0.0000165	0.0031836	0.0001233
C47AB091	5.00 W	0.0000691	0.0000067	0.0001594	0.0000110	0.0000417	0.0000071	0.0003386	0.0001105	0.0033706	0.0019254
C47AB088	5.00 W	0.0000677	0.0000067	0.0001602	0.0000110	0.0000427	0.0000071	0.0003100	0.0001105	0.0045274	0.0019254
C47AB099	5.00 W	0.0000747	0.0000071	0.0001659	0.0000076	0.0000354	0.0000082	0.0002433	0.0000165	0.0033478	0.0001233
C47BB001	5.00 W	0.0002845	0.0000143	0.0003402	0.0000286	0.0001412	0.0000078	0.0003518	0.0000210	0.0045934	0.0003288
C47BA099	5.00 W	0.0003206	0.0000161	0.0003713	0.0000164	0.0001780	0.0000166	0.0004956	0.0000381	0.0052904	0.0005542
C47AB097	5.00 W	0.0000735	0.0000071	0.0001629	0.0000076	0.0000366	0.0000082	0.0002646	0.0000165	0.0034931	0.0001233
C47BA098	5.00 W	0.0003206	0.0000161	0.0003713	0.0000164	0.0001780	0.0000166	0.0004956	0.0000381	0.0052904	0.0005542
C47BB005	5.00 W	0.0002934	0.0000143	0.0003301	0.0000286	0.0001382	0.0000078	0.0003549	0.0000210	0.0043401	0.0003288
C47BA085	5.00 W	0.0004151	0.0000235	0.0004647	0.0000535	0.0003523	0.0000889	0.0012833	0.0003687	0.0112496	0.0032401
C47BA092	5.00 W	0.0003322	0.0000235	0.0003903	0.0000535	0.0002096	0.0000889	0.0006068	0.0003687	0.0058523	0.0032401
C47AB101	5.00 W	0.0000757	0.0000071	0.0001681	0.0000076	0.0000345	0.0000082	0.0002272	0.0000165	0.0032383	0.0001233
C47BA090	5.00 W	0.0003536	0.0000235	0.0004095	0.0000535	0.0002464	0.0000889	0.0007813	0.0003687	0.0072444	0.0032401
C47AB100	5.00 W	0.0000752	0.0000071	0.0001670	0.0000076	0.0000350	0.0000082	0.0002352	0.0000165	0.0032931	0.0001233
C47AB087	5.00 W	0.0000673	0.0000067	0.0001604	0.0000110	0.0000430	0.0000071	0.0003008	0.0001105	0.0048997	0.0019254
C47BA091	5.00 W	0.0003427	0.0000235	0.0003997	0.0000535	0.0002276	0.0000889	0.0006925	0.0003687	0.0065361	0.0032401
C47BA088	5.00 W	0.0003825	0.0000235	0.0004354	0.0000535	0.0002961	0.0000889	0.0010170	0.0003687	0.0091249	0.0032401
C47AB095	5.00 W	0.0000725	0.0000071	0.0001606	0.0000076	0.0000375	0.0000082	0.0002803	0.0000165	0.0036007	0.0001233
C47AB093	5.00 W	0.0000715	0.0000071	0.0001584	0.0000076	0.0000384	0.0000082	0.0002963	0.0000165	0.0037102	0.0001233
C47BA093	5.00 W	0.0003213	0.0000235	0.0003805	0.0000535	0.0001908	0.0000889	0.0005180	0.0003687	0.0051441	0.0032401

Sample Parameters	Laser power	Sample	Material	Location	Analyst	Standard (in Ma)	%1σ	J	%1σ	MDF	%1σ	Volume Ratio	Sensitivity (mol/volt)
C47AB096	5.00 W	17-16/3 (163bs)	Phlogopite (0.25-0.5 mm)	Maio, Cape Verdes	Jan Sticklus	28.344	0.039	1.06E-03	0.08	1.0098	0.21	1	1.211E-14
C47AB090	5.00 W	17/16-3 (163bl)	Phlogopite (0.5-1 mm)	Maio, Cape Verdes	Jan Sticklus	28.344	0.039	1.06E-03	0.08	1.0098	0.21	1	1.211E-14
C47BA097	5.00 W	17-16/3 (163bs)	Phlogopite (0.25-0.5 mm)	Maio, Cape Verdes	Jan Sticklus	28.344	0.039	1.06E-03	0.08	1.0098	0.21	1	1.211E-14
C47AB080	5.00 W	17/16-3 (163bl)	Phlogopite (0.5-1 mm)	Maio, Cape Verdes	Jan Sticklus	28.344	0.039	1.06E-03	0.08	1.0098	0.21	1	1.211E-14
C47BA083	5.00 W	17/16-3 (163bl)	Phlogopite (0.5-1 mm)	Maio, Cape Verdes	Jan Sticklus	28.344	0.039	1.06E-03	0.08	1.0098	0.21	1	1.211E-14
C47BA084	5.00 W	17/16-3 (163bl)	Phlogopite (0.5-1 mm)	Maio, Cape Verdes	Jan Sticklus	28.344	0.039	1.06E-03	0.08	1.0098	0.21	1	1.211E-14
C47BA094	5.00 W	17/16-3 (163bl)	Phlogopite (0.5-1 mm)	Maio, Cape Verdes	Jan Sticklus	28.344	0.039	1.06E-03	0.08	1.0098	0.21	1	1.211E-14
C47BA096	5.00 W	17-16/3 (163bs)	Phlogopite (0.25-0.5 mm)	Maio, Cape Verdes	Jan Sticklus	28.344	0.039	1.06E-03	0.08	1.0098	0.21	1	1.211E-14
C47BB004	5.00 W	17-16/3 (163bs)	Phlogopite (0.25-0.5 mm)	Maio, Cape Verdes	Jan Sticklus	28.344	0.039	1.06E-03	0.08	1.0098	0.21	1	1.211E-14
C47BA100	5.00 W	17-16/3 (163bs)	Phlogopite (0.25-0.5 mm)	Maio, Cape Verdes	Jan Sticklus	28.344	0.039	1.06E-03	0.08	1.0098	0.21	1	1.211E-14
C47AB084	5.00 W	17/16-3 (163bl)	Phlogopite (0.5-1 mm)	Maio, Cape Verdes	Jan Sticklus	28.344	0.039	1.06E-03	0.08	1.0098	0.21	1	1.211E-14
C47BB002	5.00 W	17-16/3 (163bs)	Phlogopite (0.25-0.5 mm)	Maio, Cape Verdes	Jan Sticklus	28.344	0.039	1.06E-03	0.08	1.0098	0.21	1	1.211E-14
C47BA095	5.00 W	17-16/3 (163bs)	Phlogopite (0.25-0.5 mm)	Maio, Cape Verdes	Jan Sticklus	28.344	0.039	1.06E-03	0.08	1.0098	0.21	1	1.211E-14
C47AB081	5.00 W	17/16-3 (163bl)	Phlogopite (0.5-1 mm)	Maio, Cape Verdes	Jan Sticklus	28.344	0.039	1.06E-03	0.08	1.0098	0.21	1	1.211E-14
C47AB089	5.00 W	17/16-3 (163bl)	Phlogopite (0.5-1 mm)	Maio, Cape Verdes	Jan Sticklus	28.344	0.039	1.06E-03	0.08	1.0098	0.21	1	1.211E-14
C47AB103	5.00 W	17-16/3 (163bs)	Phlogopite (0.25-0.5 mm)	Maio, Cape Verdes	Jan Sticklus	28.344	0.039	1.06E-03	0.08	1.0098	0.21	1	1.211E-14
C47AB083	5.00 W	17/16-3 (163bl)	Phlogopite (0.5-1 mm)	Maio, Cape Verdes	Jan Sticklus	28.344	0.039	1.06E-03	0.08	1.0098	0.21	1	1.211E-14
C47AB085	5.00 W	17/16-3 (163bl)	Phlogopite (0.5-1 mm)	Maio, Cape Verdes	Jan Sticklus	28.344	0.039	1.06E-03	0.08	1.0098	0.21	1	1.211E-14
C47AB086	5.00 W	17/16-3 (163bl)	Phlogopite (0.5-1 mm)	Maio, Cape Verdes	Jan Sticklus	28.344	0.039	1.06E-03	0.08	1.0098	0.21	1	1.211E-14
C47AB094	5.00 W	17-16/3 (163bs)	Phlogopite (0.25-0.5 mm)	Maio, Cape Verdes	Jan Sticklus	28.344	0.039	1.06E-03	0.08	1.0098	0.21	1	1.211E-14
C47AB092	5.00 W	17-16/3 (163bs)	Phlogopite (0.25-0.5 mm)	Maio, Cape Verdes	Jan Sticklus	28.344	0.039	1.06E-03	0.08	1.0098	0.21	1	1.211E-14
C47AB082	5.00 W	17/16-3 (163bl)	Phlogopite (0.5-1 mm)	Maio, Cape Verdes	Jan Sticklus	28.344	0.039	1.06E-03	0.08	1.0098	0.21	1	1.211E-14
C47BA089	5.00 W	17/16-3 (163bl)	Phlogopite (0.5-1 mm)	Maio, Cape Verdes	Jan Sticklus	28.344	0.039	1.06E-03	0.08	1.0098	0.21	1	1.211E-14
C47BA087	5.00 W	17/16-3 (163bl)	Phlogopite (0.5-1 mm)	Maio, Cape Verdes	Jan Sticklus	28.344	0.039	1.06E-03	0.08	1.0098	0.21	1	1.211E-14
C47AB098	5.00 W	17-16/3 (163bs)	Phlogopite (0.25-0.5 mm)	Maio, Cape Verdes	Jan Sticklus	28.344	0.039	1.06E-03	0.08	1.0098	0.21	1	1.211E-14
C47BA101	5.00 W	17-16/3 (163bs)	Phlogopite (0.25-0.5 mm)	Maio, Cape Verdes	Jan Sticklus	28.344	0.039	1.06E-03	0.08	1.0098	0.21	1	1.211E-14
C47BB003	5.00 W	17-16/3 (163bs)	Phlogopite (0.25-0.5 mm)	Maio, Cape Verdes	Jan Sticklus	28.344	0.039	1.06E-03	0.08	1.0098	0.21	1	1.211E-14
C47AB102	5.00 W	17-16/3 (163bs)	Phlogopite (0.25-0.5 mm)	Maio, Cape Verdes	Jan Sticklus	28.344	0.039	1.06E-03	0.08	1.0098	0.21	1	1.211E-14
C47AB091	5.00 W	17/16-3 (163bl)	Phlogopite (0.5-1 mm)	Maio, Cape Verdes	Jan Sticklus	28.344	0.039	1.06E-03	0.08	1.0098	0.21	1	1.211E-14
C47AB088	5.00 W	17/16-3 (163bl)	Phlogopite (0.5-1 mm)	Maio, Cape Verdes	Jan Sticklus	28.344	0.039	1.06E-03	0.08	1.0098	0.21	1	1.211E-14
C47AB099	5.00 W	17-16/3 (163bs)	Phlogopite (0.25-0.5 mm)	Maio, Cape Verdes	Jan Sticklus	28.344	0.039	1.06E-03	0.08	1.0098	0.21	1	1.211E-14
C47BB001	5.00 W	17-16/3 (163bs)	Phlogopite (0.25-0.5 mm)	Maio, Cape Verdes	Jan Sticklus	28.344	0.039	1.06E-03	0.08	1.0098	0.21	1	1.211E-14
C47BA099	5.00 W	17-16/3 (163bs)	Phlogopite (0.25-0.5 mm)	Maio, Cape Verdes	Jan Sticklus	28.344	0.039	1.06E-03	0.08	1.0098	0.21	1	1.211E-14
C47AB097	5.00 W	17-16/3 (163bs)	Phlogopite (0.25-0.5 mm)	Maio, Cape Verdes	Jan Sticklus	28.344	0.039	1.06E-03	0.08	1.0098	0.21	1	1.211E-14
C47BA098	5.00 W	17-16/3 (163bs)	Phlogopite (0.25-0.5 mm)	Maio, Cape Verdes	Jan Sticklus	28.344	0.039	1.06E-03	0.08	1.0098	0.21	1	1.211E-14
C47BB005	5.00 W	17-16/3 (163bs)	Phlogopite (0.25-0.5 mm)	Maio, Cape Verdes	Jan Sticklus	28.344	0.039	1.06E-03	0.08	1.0098	0.21	1	1.211E-14
C47BA085	5.00 W	17/16-3 (163bl)	Phlogopite (0.5-1 mm)	Maio, Cape Verdes	Jan Sticklus	28.344	0.039	1.06E-03	0.08	1.0098	0.21	1	1.211E-14
C47BA092	5.00 W	17/16-3 (163bl)	Phlogopite (0.5-1 mm)	Maio, Cape Verdes	Jan Sticklus	28.344	0.039	1.06E-03	0.08	1.0098	0.21	1	1.211E-14
C47AB101	5.00 W	17-16/3 (163bs)	Phlogopite (0.25-0.5 mm)	Maio, Cape Verdes	Jan Sticklus	28.344	0.039	1.06E-03	0.08	1.0098	0.21	1	1.211E-14
C47BA090	5.00 W	17/16-3 (163bl)	Phlogopite (0.5-1 mm)	Maio, Cape Verdes	Jan Sticklus	28.344	0.039	1.06E-03	0.08	1.0098	0.21	1	1.211E-14
C47AB100	5.00 W	17-16/3 (163bs)	Phlogopite (0.25-0.5 mm)	Maio, Cape Verdes	Jan Sticklus	28.344	0.039	1.06E-03	0.08	1.0098	0.21	1	1.211E-14
C47AB087	5.00 W	17/16-3 (163bl)	Phlogopite (0.5-1 mm)	Maio, Cape Verdes	Jan Sticklus	28.344	0.039	1.06E-03	0.08	1.0098	0.21	1	1.211E-14
C47BA091	5.00 W	17/16-3 (163bl)	Phlogopite (0.5-1 mm)	Maio, Cape Verdes	Jan Sticklus	28.344	0.039	1.06E-03	0.08	1.0098	0.21	1	1.211E-14
C47BA088	5.00 W	17/16-3 (163bl)	Phlogopite (0.5-1 mm)	Maio, Cape Verdes	Jan Sticklus	28.344	0.039	1.06E-03	0.08	1.0098	0.21	1	1.211E-14
C47AB095	5.00 W	17-16/3 (163bs)	Phlogopite (0.25-0.5 mm)	Maio, Cape Verdes	Jan Sticklus	28.344	0.039	1.06E-03	0.08	1.0098	0.21	1	1.211E-14
C47AB093	5.00 W	17-16/3 (163bs)	Phlogopite (0.25-0.5 mm)	Maio, Cape Verdes	Jan Sticklus	28.344	0.039	1.06E-03	0.08	1.0098	0.21	1	1.211E-14
C47BA093	5.00 W	17/16-3 (163bl)	Phlogopite (0.5-1 mm)	Maio, Cape Verdes	Jan Sticklus	28.344	0.039	1.06E-03	0.08	1.0098	0.21	1	1.211E-14

Day	Month	Year	Hour	Min	Resist	Irradiation	Project	Experiment	Nmb	Standard Name
24	JUN	2018	11	14	1	can47	Examples	C47AB092	02	TCS2
24	JUN	2018	8	1	1	can47	Examples	C47AB080	03	TCS2
30	JUN	2018	13	16	1	can47	Examples	c47it5ip2_163bs	01	TCS2
24	JUN	2018	2	53	1	can47	Examples	C47AB080	03	TCS2
30	JUN	2018	5	53	1	can47	Examples	C47AB080	03	TCS2
30	JUN	2018	6	22	1	can47	Examples	C47AB080	03	TCS2
30	JUN	2018	11	30	1	can47	Examples	C47AB080	03	TCS2
30	JUN	2018	12	47	1	can47	Examples	c47it5ip2_163bs	01	TCS2
30	JUN	2018	19	48	1	can47	Examples	c47it5ip2_163bs	01	TCS2
30	JUN	2018	14	43	1	can47	Examples	c47it5ip2_163bs	01	TCS2
24	JUN	2018	4	49	1	can47	Examples	C47AB080	03	TCS2
30	JUN	2018	18	51	1	can47	Examples	c47it5ip2_163bs	01	TCS2
30	JUN	2018	12	18	1	can47	Examples	c47it5ip2_163bs	01	TCS2
24	JUN	2018	3	22	1	can47	Examples	C47AB080	03	TCS2
24	JUN	2018	7	32	1	can47	Examples	C47AB080	03	TCS2
24	JUN	2018	14	55	1	can47	Examples	C47AB092	02	TCS2
24	JUN	2018	4	20	1	can47	Examples	C47AB080	03	TCS2
24	JUN	2018	5	18	1	can47	Examples	C47AB080	03	TCS2
24	JUN	2018	6	6	1	can47	Examples	C47AB080	03	TCS2
24	JUN	2018	10	16	1	can47	Examples	C47AB092	02	TCS2
24	JUN	2018	9	18	1	can47	Examples	C47AB092	02	TCS2
24	JUN	2018	3	51	1	can47	Examples	C47AB080	03	TCS2
30	JUN	2018	9	6	1	can47	Examples	C47AB080	03	TCS2
30	JUN	2018	7	49	1	can47	Examples	C47AB080	03	TCS2
24	JUN	2018	12	30	1	can47	Examples	C47AB092	02	TCS2
30	JUN	2018	15	31	1	can47	Examples	c47it5ip2_163bs	01	TCS2
30	JUN	2018	19	19	1	can47	Examples	c47it5ip2_163bs	01	TCS2
24	JUN	2018	14	26	1	can47	Examples	C47AB092	02	TCS2
24	JUN	2018	8	30	1	can47	Examples	C47AB080	03	TCS2
24	JUN	2018	7	3	1	can47	Examples	C47AB080	03	TCS2
24	JUN	2018	12	59	1	can47	Examples	C47AB092	02	TCS2
30	JUN	2018	18	3	1	can47	Examples	c47it5ip2_163bs	01	TCS2
30	JUN	2018	14	14	1	can47	Examples	c47it5ip2_163bs	01	TCS2
24	JUN	2018	11	42	1	can47	Examples	C47AB092	02	TCS2
30	JUN	2018	13	45	1	can47	Examples	c47it5ip2_163bs	01	TCS2
30	JUN	2018	20	17	1	can47	Examples	c47it5ip2_163bs	01	TCS2
30	JUN	2018	6	51	1	can47	Examples	C47AB080	03	TCS2
30	JUN	2018	10	32	1	can47	Examples	C47AB080	03	TCS2
24	JUN	2018	13	57	1	can47	Examples	C47AB092	02	TCS2
30	JUN	2018	9	35	1	can47	Examples	C47AB080	03	TCS2
24	JUN	2018	13	28	1	can47	Examples	C47AB092	02	TCS2
24	JUN	2018	6	35	1	can47	Examples	C47AB080	03	TCS2
30	JUN	2018	10	4	1	can47	Examples	C47AB080	03	TCS2
30	JUN	2018	8	18	1	can47	Examples	C47AB080	03	TCS2
24	JUN	2018	10	45	1	can47	Examples	C47AB092	02	TCS2
24	JUN	2018	9	47	1	can47	Examples	C47AB092	02	TCS2
30	JUN	2018	11	1	1	can47	Examples	C47AB080	03	TCS2

Irradiation Constants	Laser power	40/36(a)	%1σ	40/36(c)	%1σ	38/36(a)	%1σ	38/36(c)	%1σ	39/37(ca)	%1σ	38/37(ca)	%1σ	36/37(ca)	%1σ	40/39(k)	%1σ	38/39(k)	%1σ	36/38(cl)	%1σ	K/Ca	%1σ	K/Cl	%1σ	Ca/Cl	%1σ
C47AB096	5.00 W	295.5	0.178	0.018	35	0.1869	0.107	1.493	3	0.000702	1.71	0.000196	4.08	0.0002702	0.15	0.00073	12.33	0.01215	0.27	262.8	0.65	0.51	0	0	0	0	0
C47BA090	5.00 W	295.5	0.178	0.018	35	0.1869	0.107	1.493	3	0.000702	1.71	0.000196	4.08	0.0002702	0.15	0.00073	12.33	0.01215	0.27	262.8	0.65	0.51	0	0	0	0	0
C47BA097	5.00 W	295.5	0.178	0.018	35	0.1869	0.107	1.493	3	0.000702	1.71	0.000196	4.08	0.0002702	0.15	0.00073	12.33	0.01215	0.27	262.8	0.65	0.51	0	0	0	0	0
C47AB080	5.00 W	295.5	0.178	0.018	35	0.1869	0.107	1.493	3	0.000702	1.71	0.000196	4.08	0.0002702	0.15	0.00073	12.33	0.01215	0.27	262.8	0.65	0.51	0	0	0	0	0
C47BA083	5.00 W	295.5	0.178	0.018	35	0.1869	0.107	1.493	3	0.000702	1.71	0.000196	4.08	0.0002702	0.15	0.00073	12.33	0.01215	0.27	262.8	0.65	0.51	0	0	0	0	0
C47BA084	5.00 W	295.5	0.178	0.018	35	0.1869	0.107	1.493	3	0.000702	1.71	0.000196	4.08	0.0002702	0.15	0.00073	12.33	0.01215	0.27	262.8	0.65	0.51	0	0	0	0	0
C47BA094	5.00 W	295.5	0.178	0.018	35	0.1869	0.107	1.493	3	0.000702	1.71	0.000196	4.08	0.0002702	0.15	0.00073	12.33	0.01215	0.27	262.8	0.65	0.51	0	0	0	0	0
C47BA096	5.00 W	295.5	0.178	0.018	35	0.1869	0.107	1.493	3	0.000702	1.71	0.000196	4.08	0.0002702	0.15	0.00073	12.33	0.01215	0.27	262.8	0.65	0.51	0	0	0	0	0
C47BB004	5.00 W	295.5	0.178	0.018	35	0.1869	0.107	1.493	3	0.000702	1.71	0.000196	4.08	0.0002702	0.15	0.00073	12.33	0.01215	0.27	262.8	0.65	0.51	0	0	0	0	0
C47BA100	5.00 W	295.5	0.178	0.018	35	0.1869	0.107	1.493	3	0.000702	1.71	0.000196	4.08	0.0002702	0.15	0.00073	12.33	0.01215	0.27	262.8	0.65	0.51	0	0	0	0	0
C47AB084	5.00 W	295.5	0.178	0.018	35	0.1869	0.107	1.493	3	0.000702	1.71	0.000196	4.08	0.0002702	0.15	0.00073	12.33	0.01215	0.27	262.8	0.65	0.51	0	0	0	0	0
C47BB002	5.00 W	295.5	0.178	0.018	35	0.1869	0.107	1.493	3	0.000702	1.71	0.000196	4.08	0.0002702	0.15	0.00073	12.33	0.01215	0.27	262.8	0.65	0.51	0	0	0	0	0
C47BA095	5.00 W	295.5	0.178	0.018	35	0.1869	0.107	1.493	3	0.000702	1.71	0.000196	4.08	0.0002702	0.15	0.00073	12.33	0.01215	0.27	262.8	0.65	0.51	0	0	0	0	0
C47AB081	5.00 W	295.5	0.178	0.018	35	0.1869	0.107	1.493	3	0.000702	1.71	0.000196	4.08	0.0002702	0.15	0.00073	12.33	0.01215	0.27	262.8	0.65	0.51	0	0	0	0	0
C47AB089	5.00 W	295.5	0.178	0.018	35	0.1869	0.107	1.493	3	0.000702	1.71	0.000196	4.08	0.0002702	0.15	0.00073	12.33	0.01215	0.27	262.8	0.65	0.51	0	0	0	0	0
C47AB103	5.00 W	295.5	0.178	0.018	35	0.1869	0.107	1.493	3	0.000702	1.71	0.000196	4.08	0.0002702	0.15	0.00073	12.33	0.01215	0.27	262.8	0.65	0.51	0	0	0	0	0
C47AB083	5.00 W	295.5	0.178	0.018	35	0.1869	0.107	1.493	3	0.000702	1.71	0.000196	4.08	0.0002702	0.15	0.00073	12.33	0.01215	0.27	262.8	0.65	0.51	0	0	0	0	0
C47AB085	5.00 W	295.5	0.178	0.018	35	0.1869	0.107	1.493	3	0.000702	1.71	0.000196	4.08	0.0002702	0.15	0.00073	12.33	0.01215	0.27	262.8	0.65	0.51	0	0	0	0	0
C47AB086	5.00 W	295.5	0.178	0.018	35	0.1869	0.107	1.493	3	0.000702	1.71	0.000196	4.08	0.0002702	0.15	0.00073	12.33	0.01215	0.27	262.8	0.65	0.51	0	0	0	0	0
C47AB094	5.00 W	295.5	0.178	0.018	35	0.1869	0.107	1.493	3	0.000702	1.71	0.000196	4.08	0.0002702	0.15	0.00073	12.33	0.01215	0.27	262.8	0.65	0.51	0	0	0	0	0
C47AB092	5.00 W	295.5	0.178	0.018	35	0.1869	0.107	1.493	3	0.000702	1.71	0.000196	4.08	0.0002702	0.15	0.00073	12.33	0.01215	0.27	262.8	0.65	0.51	0	0	0	0	0
C47AB082	5.00 W	295.5	0.178	0.018	35	0.1869	0.107	1.493	3	0.000702	1.71	0.000196	4.08	0.0002702	0.15	0.00073	12.33	0.01215	0.27	262.8	0.65	0.51	0	0	0	0	0
C47BA089	5.00 W	295.5	0.178	0.018	35	0.1869	0.107	1.493	3	0.000702	1.71	0.000196	4.08	0.0002702	0.15	0.00073	12.33	0.01215	0.27	262.8	0.65	0.51	0	0	0	0	0
C47BA087	5.00 W	295.5	0.178	0.018	35	0.1869	0.107	1.493	3	0.000702	1.71	0.000196	4.08	0.0002702	0.15	0.00073	12.33	0.01215	0.27	262.8	0.65	0.51	0	0	0	0	0
C47AB098	5.00 W	295.5	0.178	0.018	35	0.1869	0.107	1.493	3	0.000702	1.71	0.000196	4.08	0.0002702	0.15	0.00073	12.33	0.01215	0.27	262.8	0.65	0.51	0	0	0	0	0
C47BA101	5.00 W	295.5	0.178	0.018	35	0.1869	0.107	1.493	3	0.000702	1.71	0.000196	4.08	0.0002702	0.15	0.00073	12.33	0.01215	0.27	262.8	0.65	0.51	0	0	0	0	0
C47BB003	5.00 W	295.5	0.178	0.018	35	0.1869	0.107	1.493	3	0.000702	1.71	0.000196	4.08	0.0002702	0.15	0.00073	12.33	0.01215	0.27	262.8	0.65	0.51	0	0	0	0	0
C47AB102	5.00 W	295.5	0.178	0.018	35	0.1869	0.107	1.493	3	0.000702	1.71	0.000196	4.08	0.0002702	0.15	0.00073	12.33	0.01215	0.27	262.8	0.65	0.51	0	0	0	0	0
C47AB091	5.00 W	295.5	0.178	0.018	35	0.1869	0.107	1.493	3	0.000702	1.71	0.000196	4.08	0.0002702	0.15	0.00073	12.33	0.01215	0.27	262.8	0.65	0.51	0	0	0	0	0
C47AB088	5.00 W	295.5	0.178	0.018	35	0.1869	0.107	1.493	3	0.000702	1.71	0.000196	4.08	0.0002702	0.15	0.00073	12.33	0.01215	0.27	262.8	0.65	0.51	0	0	0	0	0
C47AB099	5.00 W	295.5	0.178	0.018	35	0.1869	0.107	1.493	3	0.000702	1.71	0.000196	4.08	0.0002702	0.15	0.00073	12.33	0.01215	0.27	262.8	0.65	0.51	0	0	0	0	0
C47BB001	5.00 W	295.5	0.178	0.018	35	0.1869	0.107	1.493	3	0.000702	1.71	0.000196	4.08	0.0002702	0.15	0.00073	12.33	0.01215	0.27	262.8	0.65	0.51	0	0	0	0	0
C47BA099	5.00 W	295.5	0.178	0.018	35	0.1869	0.107	1.493	3	0.000702	1.71	0.000196	4.08	0.0002702	0.15	0.00073	12.33	0.01215	0.27	262.8	0.65	0.51	0	0	0	0	0
C47AB097	5.00 W	295.5	0.178	0.018	35	0.1869	0.107	1.493	3	0.000702	1.71	0.000196	4.08	0.0002702	0.15	0.00073	12.33	0.01215	0.27	262.8	0.65	0.51	0	0	0	0	0
C47BA098	5.00 W	295.5	0.178	0.018	35	0.1869	0.107	1.493	3	0.000702	1.71	0.000196	4.08	0.0002702	0.15	0.00073	12.33	0.01215	0.27	262.8	0.65	0.51	0	0	0	0	0
C47BB005	5.00 W	295.5	0.178	0.018	35	0.1869	0.107	1.493	3	0.000702	1.71	0.000196	4.08	0.0002702	0.15	0.00073	12.33	0.01215	0.27	262.8	0.65	0.51	0	0	0	0	0
C47BA085	5.00 W	295.5	0.178	0.018	35	0.1869	0.107	1.493	3	0.000702	1.71	0.000196	4.08	0.0002702	0.15	0.00073	12.33	0.01215	0.27	262.8	0.65	0.51	0	0	0	0	0
C47BA092	5.00 W	295.5	0.178	0.018	35	0.1869	0.107	1.493	3	0.000702	1.71	0.000196	4.08	0.0002702	0.15	0.00073	12.33	0.01215	0.27	262.8	0.65	0.51	0	0	0	0	0
C47AB101	5.00 W	295.5	0.178	0.018	35	0.1869	0.107	1.493	3	0.000702	1.71	0.000196	4.08	0.0002702	0.15	0.00073	12.33	0.01215	0.27	262.8	0.65	0.51	0	0	0	0	0
C47BA090	5.00 W	295.5	0.178	0.018	35	0.1869	0.107	1.493	3	0.000702	1.71	0.000196	4.08	0.0002702	0.15	0.00073	12.33	0.01215	0.27	262.8	0.65	0.51	0	0	0	0	0
C47AB100	5.00 W	295.5	0.178	0.018	35	0.1869	0.107	1.493	3	0.000702	1.71	0.000196	4.08	0.0002702	0.15	0.00073	12.33	0.01215	0.27	262.8	0.65	0.51	0	0	0	0	0
C47AB087	5.00 W	295.5	0.178	0.018	35	0.1869	0.107	1.493	3	0.000702	1.71	0.000196	4.08	0.0002702	0.15	0.00073	12.33	0.01215	0.27	262.8	0.65	0.51	0	0	0	0	0
C47BA091	5.00 W	295.5	0.178	0.018	35	0.1869	0.107	1.493	3	0.000702	1.71	0.000196	4.08	0.0002702	0.15	0.00073	12.33	0.01215	0.27	262.8	0.65	0.51	0	0	0	0	0
C47BA088	5.00 W	295.5	0.178	0.018	35	0.1869	0.107	1.493	3	0.000702	1.71	0.000196	4.08	0.0002702	0.15	0.00073	12.33	0.01215	0.27	262.8	0.65	0.51	0	0	0	0	0
C47AB095	5.00 W	295.5	0.178	0.018	35	0.1869	0.107	1.493	3	0.000702	1.71	0.000196	4.08	0.0002702	0.15	0.00073	12.33	0.01215	0.27	262.8	0.65	0.51	0	0	0	0	0
C47AB093	5.00 W	295.5	0.178	0.018	35	0.1869	0.107	1.493	3	0.000702	1.71	0.000196	4.08	0.0002702	0.15	0.00073	12.33	0.01215	0.27	262.8	0.65	0.51	0	0	0	0	0
C47BA093	5.00 W	295.5	0.178	0.018	35	0.1869	0.107	1.493	3	0.000702	1.71	0.000196	4.08	0.0002702	0.15	0.00073	12.33	0.01215	0.27	262.8	0.65	0.51	0	0	0	0	0

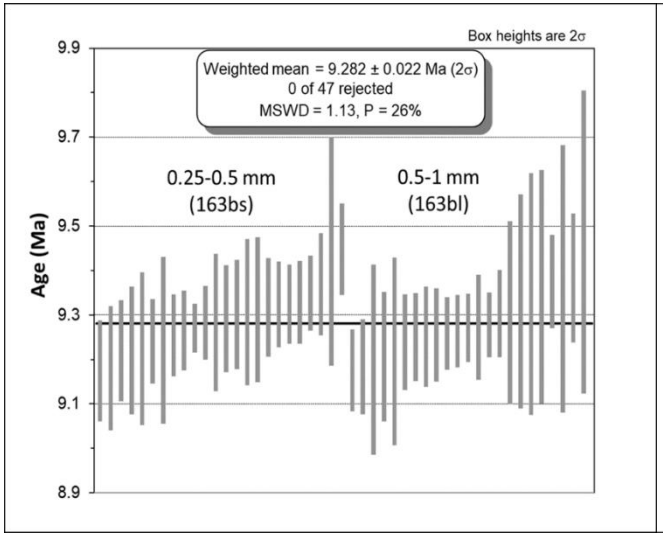

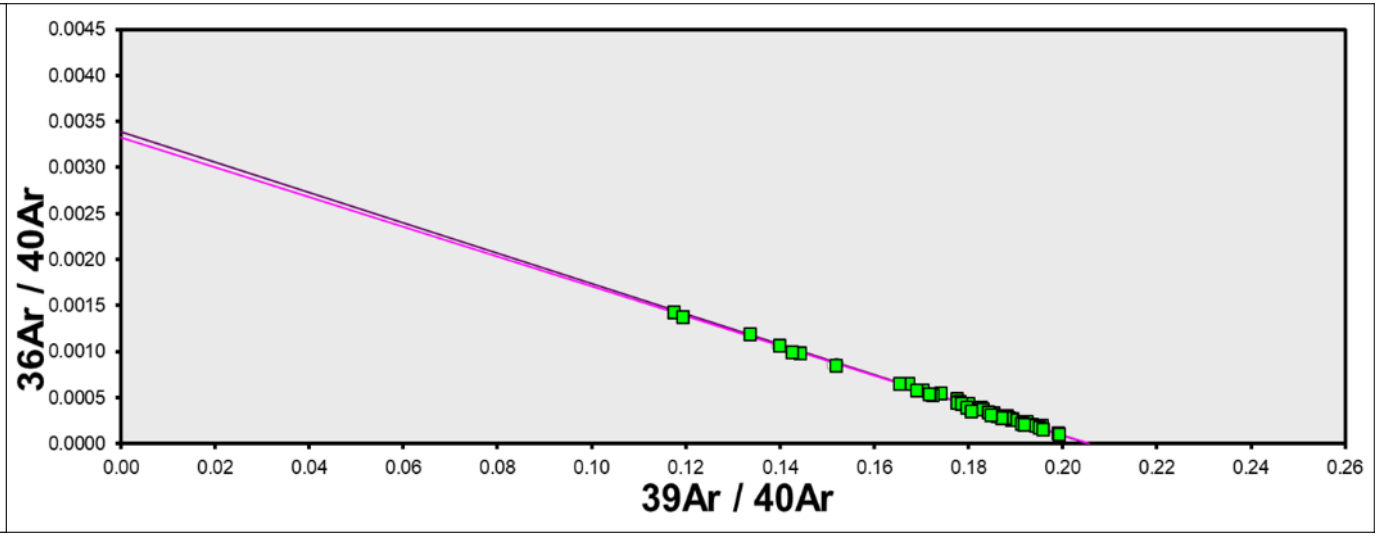

Information on Analysis and Constants Used in Calculations

Sample = 17-16/3 (163BS)
Material = Phlogopite (0.25-0.5 mm)
Location = Maio, Cape Verdes
Analyst = Jan Sticklus
Project = EXAMPLES
Mass Discrimination Law = POW
Irradiation = can47
J = 0.00105850 ± 0.00000085
TCS2 = 28.344 ± 0.011 Ma
Experiment Type = SAMPLE
Heating = 45 sec
Isolation = 15.00 min
Instrument = MAP216

Age Equations = Conventional
Negative Intensities = Allowed
Decay Constant 40K = 5.543 ± 0.009 E-10 1/a
Decay Constant 39Ar = 2.940 ± 0.016 E-07 1/h
Decay Constant 37Ar = 8.230 ± 0.012 E-04 1/h
Decay Constant 36Cl = 2.257 ± 0.015 E-06 1/a
Atmospheric Ratio 40/36(a) = 295.50 ± 0.53
Atmospheric Ratio 38/36(a) = 0.1869 ± 0.0002
Production Ratio 39/37(ca) = 0.000702 ± 0.000012
Production Ratio 38/37(ca) = 0.000196 ± 0.000008
Production Ratio 36/37(ca) = 0.000270 ± 0.000000
Production Ratio 40/39(k) = 0.000730 ± 0.000090
Production Ratio 38/39(k) = 0.012150 ± 0.000033
Production Ratio 36/38(cl) = 262.80
Scaling Ratio K/Ca = 0.510

Results	40(a)/36(a) ± 2σ	40(r)/39(k) ± 2σ	Age ± 2σ (Ma)	MSWD	39Ar(k) (%,n)	K/Ca ± 2σ
SCTF Weighted Mean		4.87298 ± 0.00879 ± 0.18%	9.282 ± 0.022 ± 0.24%	1.13	100.00	14.0 ± 3.0
				26%	47	
		Minimal External Error ± 0.037		1.42	2σ Confidence Limit	
		Analytical Error ± 0.017		1.0618	Error Magnification	
Total Fusion Age		4.87508 ± 0.00982 ± 0.20%	9.286 ± 0.024 ± 0.26%		47	36.0 ± 0.3
		Minimal External Error ± 0.038				
		Analytical Error ± 0.019				
Normal Isochron	300.83 ± 5.36 ± 1.78%	4.85950 ± 0.01396 ± 0.29%	9.256 ± 0.030 ± 0.33%	1.03	100.00	
				42%	47	
		Minimal External Error ± 0.042		1.42	2σ Confidence Limit	
		Analytical Error ± 0.027		1.0128	Error Magnification	
				1	Number of Iterations	
				0.0000061562	Convergence	
Inverse Isochron	301.12 ± 5.43 ± 1.80%	4.86149 ± 0.01411 ± 0.29%	9.260 ± 0.031 ± 0.33%	1.05	100.00	
				37%	47	
		Minimal External Error ± 0.043		1.42	2σ Confidence Limit	
		Analytical Error ± 0.027		1.0266	Error Magnification	
				3	Number of Iterations	
				0.0000336030	Convergence	
				40%	Spreading Factor	

Blue dots in table indicate selected analyses used to calculate the weighted mean, isochron and inverse isochron ages.
* Alteration Index values in italics indicate analyses from fresh material, normal font is from altered material (Baksi, 2007).
Values shown in red are negative values.
Abbreviations used in tables: (r) = radiogenic ^{40}Ar; (k) = Ar derived from K; (a) = atmospheric Ar; (ca) = Ar derived from Ca; (cl) = Ar derived from Ca; (c) = cosmogenic Ar; MDF = Mass Discrimination Factor.
Green squares in the inverse isochron plots indicate selected steps (blue dots in table), and blue squares are non-selected steps. Pink lines in the inverse isochron plot indicate a line fit through selected data, and the purple lines incidate a fit through an air $^{40}Ar/^{36}Ar$ ratio (295.5).

Sample 17-16/3 combined single-crystal total-fusion and step-heating plateau $^{40}Ar^*/^{39}Ar$ age calculation (0.25-0.5 and 0.5-1 mm fractions; SCTF 163bs, 163bl, and SH 163bs)

Weighted mean age calculated using $^{40}Ar^*/^{39}Ar$ ratios from SH plateau steps and SCTF analyses (including J value error; Heath et al. 2018)

Sample	$^{40}Ar^*/^{39}Ar$	± 2σ
163bs SCTF	4.81812	± 0.05850
163bs SCTF	4.82083	± 0.07224
163bs SCTF	4.84143	± 0.05861
163bs SCTF	4.84190	± 0.07451
163bs SCTF	4.84420	± 0.08878
163bs SCTF	4.85292	± 0.04902
163bs SCTF	4.85373	± 0.09728
163bs SCTF	4.85967	± 0.04749
163bs SCTF	4.86536	± 0.04612
163bs SCTF	4.86814	± 0.02809
163bs SCTF	4.87451	± 0.04235
163bs SCTF	4.87496	± 0.07967
163bs SCTF	4.87926	± 0.06226
163bs SCTF	4.88439	± 0.06346
163bs SCTF	4.88698	± 0.08500
163bs SCTF	4.88980	± 0.08423
163bs SCTF	4.89275	± 0.05719
163bs SCTF	4.89618	± 0.04924
163bs SCTF	4.89664	± 0.04565
163bs SCTF	4.89867	± 0.04807
163bs SCTF	4.90950	± 0.04330
163bs SCTF	4.91982	± 0.05955
163bs SCTF	4.95858	± 0.13361
163bs SCTF	4.96113	± 0.05329
163bl SCTF	4.81865	± 0.04772
163bl SCTF	4.82270	± 0.05512
163bl SCTF	4.83146	± 0.11109
163bl SCTF	4.83478	± 0.07515
163bl SCTF	4.84094	± 0.10969
163bl SCTF	4.85190	± 0.05545
163bl SCTF	4.85778	± 0.05112
163bl SCTF	4.85809	± 0.05833
163bl SCTF	4.86053	± 0.05410
163bl SCTF	4.86187	± 0.04174
163bl SCTF	4.86476	± 0.04189
163bl SCTF	4.86876	± 0.03932
163bl SCTF	4.86943	± 0.06105
163bl SCTF	4.87191	± 0.03734
163bl SCTF	4.88535	± 0.05083
163bl SCTF	4.88622	± 0.10667
163bl SCTF	4.89969	± 0.12521
163bl SCTF	4.90806	± 0.14132
163bl SCTF	4.91670	± 0.13625
163bl SCTF	4.92294	± 0.05385
163bl SCTF	4.92636	± 0.15647
163bl SCTF	4.92731	± 0.07494
163bl SCTF	4.96936	± 0.17755
163 SH	4.40053	± 1.20533
163 SH	4.57243	± 0.32058
163 SH	4.88878	± 0.12003
163 SH	4.90106	± 0.08009
163 SH	4.85170	± 0.06484
163 SH	4.86496	± 0.06812
163 SH	4.87508	± 0.04766
163 SH	4.87099	± 0.04664
163 SH	4.85319	± 0.03357
163 SH	4.85598	± 0.04078
163 SH	4.85839	± 0.03401
163 SH	4.84203	± 0.03311
163 SH	4.84056	± 0.03033
163 SH	4.85392	± 0.03776
163 SH	4.92468	± 0.03981
163 SH	4.87806	± 0.04497
163 SH	4.87691	± 0.03033
163 SH	4.85033	± 0.02402
163 SH	4.87886	± 0.03025
163 SH	4.88112	± 0.22471

	$^{40}Ar^*/^{39}Ar$ weighted mean	± 2σ	± 1σ	± 1σ (%)
	4.8686	0.0062	0.0031	0.06
Total K λ (Steiger	5.543E-10			
J value	0.0010585		8.997E-07	0.085

$^{40}Ar^*/^{39}Ar$ age (Ma)	±2σ (Ma)	±1σ (Ma)	± 1σ (%)
9.273	0.020	0.010	0.11

$^{40}Ar^*/^{39}Ar$ weighted mean = 4.8686 ± 0.0062 (2σ)
Weighted by data-point errors only, 0 of 67 rejected

Sample 18-32/3 single-crystal total-fusion results (0.25-0.5 mm fraction; 323bs)

Relative Abundances	Laser power		36Ar [V]	%1σ	37Ar [V]	%1σ	38Ar [V]	%1σ	39Ar [V]	%1σ	40Ar [V]	%1σ	40(r)/39(k) ± 2σ	Age ± 2σ (Ma)	40Ar(r) (%)	39Ar(k) (%)	K/Ca ± 2σ	Sample weight (mg)	$^{36}Ar/^{39}Ar$ Alt. Index	Wt. % K
C47BA057	5.00 W	•	0.0001106	12.973	0.0025421	2.762	0.0011065	2.282	0.0909780	0.298	0.4401839	0.157	4.48079 ± 0.09814	8.54 ± 0.19	92.61	5.46	18.3 ± 1.0	0.044	*0.000121*	7.6
C47BA056	5.00 W	•	0.0001433	11.992	0.0003146	17.911	0.0009348	2.438	0.0767728	0.334	0.3897905	0.148	4.52509 ± 0.13658	8.62 ± 0.26	89.13	4.61	124.5 ± 44.6	0.038	*0.000182*	7.4
C47BA052	5.00 W	•	0.0003613	4.314	0.0021234	2.818	0.0014686	1.848	0.1200503	0.266	0.6501049	0.146	4.52668 ± 0.08205	8.62 ± 0.16	83.59	7.21	28.8 ± 1.6	0.068	*0.000257*	6.4
C47BA053	5.00 W	•	0.0001184	12.079	0.0022461	2.463	0.0015215	1.850	0.1274949	0.236	0.6130835	0.104	4.53493 ± 0.07039	8.64 ± 0.13	94.31	7.66	28.9 ± 1.4	0.073	*0.000078*	6.4
C47BA051	5.00 W	•	0.0003765	5.146	0.0096604	1.370	0.0019039	1.287	0.1526686	0.265	0.8034404	0.099	4.53835 ± 0.07950	8.65 ± 0.15	86.23	9.17	8.1 ± 0.2	0.088	*0.000206*	6.3
C47BA050	5.00 W	•	0.0001508	10.190	0.0076153	1.660	0.0023484	1.274	0.1949916	0.237	0.9328708	0.148	4.55812 ± 0.05328	8.68 ± 0.10	95.27	11.71	13.1 ± 0.4	0.101	*0.000077*	6.3
C47BA054	5.00 W	•	0.0012177	1.956	0.0128235	1.173	0.0027978	1.363	0.2167929	0.240	1.3513440	0.085	4.57770 ± 0.06960	8.72 ± 0.13	73.44	13.02	8.6 ± 0.2	0.113	*0.000064*	6.3
C47BA048	5.00 W	•	0.0001351	10.198	0.0013331	4.270	0.0015276	1.806	0.1253603	0.323	0.6149970	0.173	4.58745 ± 0.07342	8.74 ± 0.14	93.51	7.53	48.0 ± 4.1	0.125	*0.000470*	6.3
C47BA058	5.00 W	•	0.0005094	3.089	0.0010906	6.400	0.0026961	1.357	0.2215624	0.262	1.1675350	0.119	4.58988 ± 0.05002	8.74 ± 0.10	87.10	13.31	103.6 ± 13.3	0.074	*0.000088*	6.2
C47BA055	5.00 W	•	0.0001755	10.622	0.0011932	4.998	0.0009719	3.163	0.0819602	0.420	0.4301473	0.214	4.61608 ± 0.14170	8.79 ± 0.27	87.95	4.92	35.0 ± 3.5	0.123	*0.000200*	6.6
C47BA059	5.00 W	•	0.0001507	8.600	0.0006647	8.285	0.0022582	1.625	0.1878851	0.247	0.9120383	0.109	4.61677 ± 0.04792	8.79 ± 0.09	95.11	11.28	144.2 ± 23.9	0.038	*0.000223*	7.9
C47BA049	5.00 W		0.0007885	3.142	0.0042664	2.052	0.0009834	2.168	0.0684919	0.403	0.6243843	0.120	5.71898 ± 0.22015	10.89 ± 0.42	62.73	4.11	8.2 ± 0.3	0.104	*0.000070*	6.6
		Σ	0.0042379	1.434	0.0458734	0.666	0.0205186	0.499	1.6650092	0.083	8.9299198	0.038								

Procedure Blanks	Laser power	36Ar [V]	1σ	37Ar [V]	1σ	38Ar [V]	1σ	39Ar [V]	1σ	40Ar [V]	1σ
C47BA057	5.00 W	0.0001805	0.0000126	0.0002627	0.0000216	0.0000883	0.0000177	0.0003187	0.0000274	0.0049793	0.0005227
C47BA056	5.00 W	0.0001797	0.0000126	0.0002618	0.0000216	0.0000887	0.0000177	0.0003285	0.0000274	0.0050824	0.0005227
C47BA052	5.00 W	0.0001761	0.0000126	0.0002579	0.0000216	0.0000909	0.0000177	0.0003741	0.0000274	0.0055585	0.0005227
C47BA053	5.00 W	0.0001769	0.0000126	0.0002588	0.0000216	0.0000905	0.0000177	0.0003642	0.0000274	0.0054555	0.0005227
C47BA051	5.00 W	0.0001753	0.0000126	0.0002571	0.0000216	0.0000914	0.0000177	0.0003840	0.0000274	0.0056615	0.0005227
C47BA050	5.00 W	0.0001746	0.0000126	0.0002563	0.0000216	0.0000919	0.0000177	0.0003938	0.0000274	0.0057646	0.0005227
C47BA054	5.00 W	0.0001782	0.0000126	0.0002602	0.0000216	0.0000897	0.0000177	0.0003479	0.0000274	0.0052849	0.0005227
C47BA048	5.00 W	0.0001730	0.0000126	0.0002546	0.0000216	0.0000928	0.0000177	0.0004135	0.0000274	0.0059707	0.0005227
C47BA058	5.00 W	0.0001813	0.0000126	0.0002635	0.0000216	0.0000878	0.0000177	0.0003088	0.0000274	0.0048763	0.0005227
C47BA055	5.00 W	0.0001789	0.0000126	0.0002610	0.0000216	0.0000892	0.0000177	0.0003384	0.0000274	0.0051854	0.0005227
C47BA059	5.00 W	0.0001820	0.0000126	0.0002643	0.0000216	0.0000873	0.0000177	0.0002990	0.0000274	0.0047732	0.0005227
C47BA049	5.00 W	0.0001738	0.0000126	0.0002554	0.0000216	0.0000924	0.0000177	0.0004037	0.0000274	0.0058676	0.0005227

Sample Parameters	Laser power	Sample	Material	Location	Analyst	Standard (in Ma)	%1σ	J	%1σ	MDF	%1σ	Volume Ratio	Sensitivity (mol/volt)
C47BA057	5.00 W	18-32/3 (323bs)	Phlogopite (0.25-0.5 mm)	Maio, Cape Verdes	Jan Sticklus	28.344	0.039	1.06E-03	0.08	1.0098	0.21	1	1.211E-14
C47BA056	5.00 W	18-32/3 (323bs)	Phlogopite (0.25-0.5 mm)	Maio, Cape Verdes	Jan Sticklus	28.344	0.039	1.06E-03	0.08	1.0098	0.21	1	1.211E-14
C47BA052	5.00 W	18-32/3 (323bs)	Phlogopite (0.25-0.5 mm)	Maio, Cape Verdes	Jan Sticklus	28.344	0.039	1.06E-03	0.08	1.0098	0.21	1	1.211E-14
C47BA053	5.00 W	18-32/3 (323bs)	Phlogopite (0.25-0.5 mm)	Maio, Cape Verdes	Jan Sticklus	28.344	0.039	1.06E-03	0.08	1.0098	0.21	1	1.211E-14
C47BA051	5.00 W	18-32/3 (323bs)	Phlogopite (0.25-0.5 mm)	Maio, Cape Verdes	Jan Sticklus	28.344	0.039	1.06E-03	0.08	1.0098	0.21	1	1.211E-14
C47BA050	5.00 W	18-32/3 (323bs)	Phlogopite (0.25-0.5 mm)	Maio, Cape Verdes	Jan Sticklus	28.344	0.039	1.06E-03	0.08	1.0098	0.21	1	1.211E-14
C47BA054	5.00 W	18-32/3 (323bs)	Phlogopite (0.25-0.5 mm)	Maio, Cape Verdes	Jan Sticklus	28.344	0.039	1.06E-03	0.08	1.0098	0.21	1	1.211E-14
C47BA048	5.00 W	18-32/3 (323bs)	Phlogopite (0.25-0.5 mm)	Maio, Cape Verdes	Jan Sticklus	28.344	0.039	1.06E-03	0.08	1.0098	0.21	1	1.211E-14
C47BA058	5.00 W	18-32/3 (323bs)	Phlogopite (0.25-0.5 mm)	Maio, Cape Verdes	Jan Sticklus	28.344	0.039	1.06E-03	0.08	1.0098	0.21	1	1.211E-14
C47BA055	5.00 W	18-32/3 (323bs)	Phlogopite (0.25-0.5 mm)	Maio, Cape Verdes	Jan Sticklus	28.344	0.039	1.06E-03	0.08	1.0098	0.21	1	1.211E-14
C47BA059	5.00 W	18-32/3 (323bs)	Phlogopite (0.25-0.5 mm)	Maio, Cape Verdes	Jan Sticklus	28.344	0.039	1.06E-03	0.08	1.0098	0.21	1	1.211E-14
C47BA049	5.00 W	18-32/3 (323bs)	Phlogopite (0.25-0.5 mm)	Maio, Cape Verdes	Jan Sticklus	28.344	0.039	1.06E-03	0.08	1.0098	0.21	1	1.211E-14

Day	Month	Year	Hour	Min	Resist	Irradiation	Project	Experiment	Nmb	Standard Name
29	JUN	2018	15	47	1	can47	Examples	C47BA057	02	TCS2
29	JUN	2018	15	18	1	can47	Examples	C47BA057	02	TCS2
29	JUN	2018	13	4	1	can47	Examples	C47BA057	02	TCS2
29	JUN	2018	13	33	1	can47	Examples	C47BA057	02	TCS2
29	JUN	2018	12	35	1	can47	Examples	C47BA057	02	TCS2
29	JUN	2018	12	6	1	can47	Examples	C47BA057	02	TCS2
29	JUN	2018	14	21	1	can47	Examples	C47BA057	02	TCS2
29	JUN	2018	11	8	1	can47	Examples	C47BA057	02	TCS2
29	JUN	2018	16	16	1	can47	Examples	C47BA057	02	TCS2
29	JUN	2018	14	49	1	can47	Examples	C47BA057	02	TCS2
29	JUN	2018	16	45	1	can47	Examples	C47BA057	02	TCS2
29	JUN	2018	11	37	1	can47	Examples	C47BA057	02	TCS2

Irradiation Constants	Laser power	40/36(a)	%1σ	40/36(c)	%1σ	38/36(a)	%1σ	38/36(c)	%1σ	39/37(ca)	%1σ	38/37(ca)	%1σ	36/37(ca)	%1σ	40/39(k)	%1σ	38/39(k)	%1σ	36/38(cl)	%1σ	K/Ca	%1σ	K/Cl	%1σ	Ca/Cl	%1σ
C47BA057	5.00 W	295.5	0.178	0.018	35	0.1869	0.107	1.493	3	0.000702	1.71	0.000196	4.08	0.0002702	0.15	0.00073	12.33	0.01215	0.27	262.8	0.65	0.51	0	0	0	0	0
C47BA056	5.00 W	295.5	0.178	0.018	35	0.1869	0.107	1.493	3	0.000702	1.71	0.000196	4.08	0.0002702	0.15	0.00073	12.33	0.01215	0.27	262.8	0.65	0.51	0	0	0	0	0
C47BA052	5.00 W	295.5	0.178	0.018	35	0.1869	0.107	1.493	3	0.000702	1.71	0.000196	4.08	0.0002702	0.15	0.00073	12.33	0.01215	0.27	262.8	0.65	0.51	0	0	0	0	0
C47BA053	5.00 W	295.5	0.178	0.018	35	0.1869	0.107	1.493	3	0.000702	1.71	0.000196	4.08	0.0002702	0.15	0.00073	12.33	0.01215	0.27	262.8	0.65	0.51	0	0	0	0	0
C47BA051	5.00 W	295.5	0.178	0.018	35	0.1869	0.107	1.493	3	0.000702	1.71	0.000196	4.08	0.0002702	0.15	0.00073	12.33	0.01215	0.27	262.8	0.65	0.51	0	0	0	0	0
C47BA050	5.00 W	295.5	0.178	0.018	35	0.1869	0.107	1.493	3	0.000702	1.71	0.000196	4.08	0.0002702	0.15	0.00073	12.33	0.01215	0.27	262.8	0.65	0.51	0	0	0	0	0
C47BA054	5.00 W	295.5	0.178	0.018	35	0.1869	0.107	1.493	3	0.000702	1.71	0.000196	4.08	0.0002702	0.15	0.00073	12.33	0.01215	0.27	262.8	0.65	0.51	0	0	0	0	0
C47BA048	5.00 W	295.5	0.178	0.018	35	0.1869	0.107	1.493	3	0.000702	1.71	0.000196	4.08	0.0002702	0.15	0.00073	12.33	0.01215	0.27	262.8	0.65	0.51	0	0	0	0	0
C47BA058	5.00 W	295.5	0.178	0.018	35	0.1869	0.107	1.493	3	0.000702	1.71	0.000196	4.08	0.0002702	0.15	0.00073	12.33	0.01215	0.27	262.8	0.65	0.51	0	0	0	0	0
C47BA055	5.00 W	295.5	0.178	0.018	35	0.1869	0.107	1.493	3	0.000702	1.71	0.000196	4.08	0.0002702	0.15	0.00073	12.33	0.01215	0.27	262.8	0.65	0.51	0	0	0	0	0
C47BA059	5.00 W	295.5	0.178	0.018	35	0.1869	0.107	1.493	3	0.000702	1.71	0.000196	4.08	0.0002702	0.15	0.00073	12.33	0.01215	0.27	262.8	0.65	0.51	0	0	0	0	0
C47BA049	5.00 W	295.5	0.178	0.018	35	0.1869	0.107	1.493	3	0.000702	1.71	0.000196	4.08	0.0002702	0.15	0.00073	12.33	0.01215	0.27	262.8	0.65	0.51	0	0	0	0	0

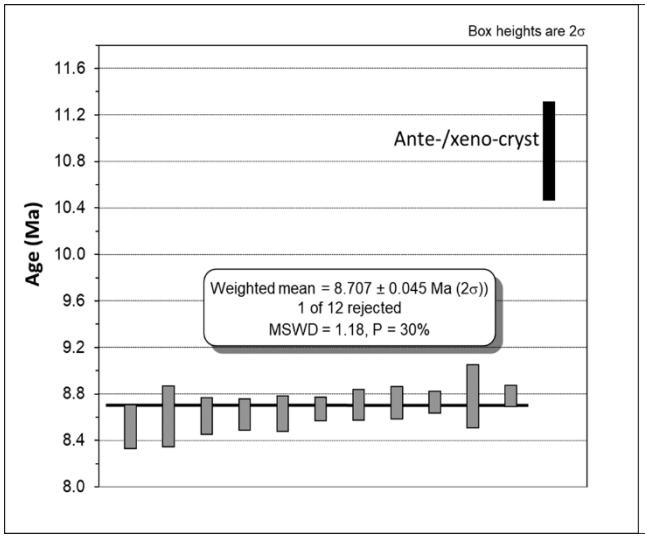

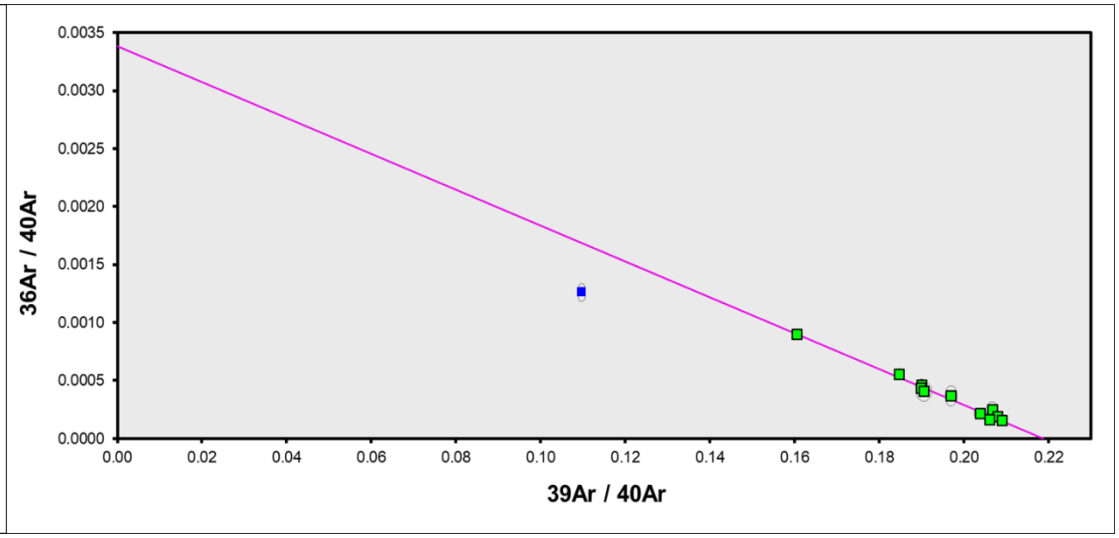

Information on Analysis and Constants Used in Calculations

Sample = 18-32/3 (323BS)
Material = Phlogopite
Location = Maio Cape Verde
Analyst = Jan Sticklus
Project = EXAMPLES
Mass Discrimination Law = POW
Irradiation = can47
J = 0.00105850 ± 0.00000085
TCS2 = 28.344 ± 0.011 Ma
Experiment Type = SAMPLE
Heating = 45 sec
Isolation = 15.00 min
Instrument = MAP216

Age Equations = Conventional
Negative Intensities = Allowed
Decay Constant 40K = 5.543 ± 0.009 E-10 1/a
Decay Constant 39Ar = 2.940 ± 0.016 E-07 1/h
Decay Constant 37Ar = 8.230 ± 0.012 E-04 1/h
Decay Constant 36Cl = 2.257 ± 0.015 E-06 1/a
Atmospheric Ratio 40/36(a) = 295.50 ± 0.53
Atmospheric Ratio 38/36(a) = 0.1869 ± 0.0002
Production Ratio 39/37(ca) = 0.000702 ± 0.000012
Production Ratio 38/37(ca) = 0.000196 ± 0.000008
Production Ratio 36/37(ca) = 0.000270 ± 0.000000
Production Ratio 40/39(k) = 0.000730 ± 0.000090
Production Ratio 38/39(k) = 0.012150 ± 0.000033
Production Ratio 36/38(cl) = 262.80
Scaling Ratio K/Ca = 0.510

Results	40(a)/36(a) ± 2σ	40(r)/39(k) ± 2σ	Age ± 2σ (Ma)	MSWD	39Ar(k) (%,n)	K/Ca ± 2σ
SCTF Weighted Mean		4.57046 ± 0.02269 ± 0.50%	8.707 ± 0.045 ± 0.52%	1.18	95.89	9.5 ± 2.4
				30%	11	
		Minimal External Error ± 0.053		1.89	2σ Confidence Limit	
		Analytical Error ± 0.043		1.0871	Error Magnification	
Total Fusion Age		4.61272 ± 0.02326 ± 0.50%	8.787 ± 0.046 ± 0.53%		12	18.5 ± 0.2
		Minimal External Error ± 0.054				
		Analytical Error ± 0.044				
Normal Isochron	294.79 ± 18.02 ± 6.11%	4.56668 ± 0.04180 ± 0.92%	8.700 ± 0.081 ± 0.93%	1.44	95.89	
No Convergence				16%	11	
		Minimal External Error ± 0.085		1.94	2σ Confidence Limit	
		Analytical Error ± 0.079		1.1998	Error Magnification	
				100	Number of Iterations	
				0.0000657915	Convergence	
Inverse Isochron	295.70 ± 17.16 ± 5.80%	4.57024 ± 0.03966 ± 0.87%	8.706 ± 0.077 ± 0.88%	1.31	95.89	
				22%	11	
		Minimal External Error ± 0.082		1.94	2σ Confidence Limit	
		Analytical Error ± 0.075		1.1464	Error Magnification	
				3	Number of Iterations	
				0.0000285741	Convergence	
				22%	Spreading Factor	

Sample 18-32/3 single-crystal total-fusion results (0.5-1 mm fraction; 323bl)

Relative Abundances	Laser power		36Ar [V]	%1σ	37Ar [V]	%1σ	38Ar [V]	%1σ	39Ar [V]	%1σ	40Ar [V]	%1σ	40(r)/39(k) ± 2σ	Age ± 2σ (Ma)	40Ar(r) (%)	39Ar(k) (%)	K/Ca ± 2σ	Sample weight (mg)	$^{36}Ar/^{39}Ar$ Alt. Index	Wt. % K
C47BC027	5.00 W	•	0.0008506	4.028	0.0062254	2.079	0.0043061	1.914	0.3418945	0.260	1.778060	0.109	4.46620 ± 0.06466	8.51 ± 0.12	85.88	4.55	28.0 ± 1.2	0.214	*0.000192*	5.8
C47BC028	5.00 W	•	0.0003503	8.849	0.0056031	2.387	0.0034006	2.503	0.2807664	0.263	1.367982	0.124	4.50460 ± 0.07047	8.58 ± 0.13	92.45	3.73	25.6 ± 1.2	0.170	*0.000099*	6.0
C47BC031	5.00 W	•	0.0011454	2.867	0.0190233	0.953	0.0052091	1.529	0.4248298	0.233	2.251424	0.078	4.50585 ± 0.05104	8.58 ± 0.10	85.02	5.65	11.4 ± 0.2	0.262	*0.000211*	5.9
C47BA065	5.00 W	•	0.0003566	3.924	0.0120675	1.039	0.0039146	1.071	0.3335962	0.241	1.610610	0.127	4.51445 ± 0.03520	8.60 ± 0.07	93.50	4.44	14.1 ± 0.3	0.202	*0.000085*	6.0
C47BC026	5.00 W	•	0.0008036	4.857	0.0166358	0.957	0.0047605	1.662	0.3837478	0.294	1.969952	0.104	4.51755 ± 0.06661	8.61 ± 0.13	88.00	5.10	11.8 ± 0.2	0.240	*0.000161*	5.8
C47BC032	5.00 W	•	0.0005021	6.023	0.0088125	1.762	0.0074571	1.260	0.6147770	0.225	2.929746	0.079	4.52465 ± 0.03630	8.62 ± 0.07	94.94	8.17	35.6 ± 1.3	0.377	*0.000064*	6.0
C47BA060	5.00 W	•	0.0001609	7.391	0.0038432	2.183	0.0020915	1.863	0.1749213	0.234	0.841251	0.115	4.53861 ± 0.04679	8.65 ± 0.09	94.37	2.33	23.2 ± 1.0	0.267	*0.000154*	5.6
C47BC030	5.00 W	•	0.0008631	3.815	0.0564032	0.795	0.0050370	1.679	0.4080901	0.225	2.103991	0.101	4.54145 ± 0.05296	8.65 ± 0.10	88.08	5.43	3.7 ± 0.1	0.262	*0.000079*	6.0
C47BC022	5.00 W	•	0.0004289	7.152	0.0065333	2.275	0.0050130	1.670	0.4287534	0.259	2.073707	0.101	4.54156 ± 0.04937	8.65 ± 0.09	93.90	5.70	33.5 ± 1.5	0.176	*0.000121*	5.9
C47BA070	5.00 W	•	0.0004396	2.967	0.0015559	4.732	0.0034397	1.380	0.2838548	0.248	1.419365	0.138	4.54240 ± 0.03795	8.65 ± 0.07	90.84	3.77	93.0 ± 8.8	0.163	*0.000050*	6.0
C47BC033	5.00 W	•	0.0001718	16.277	0.0076065	1.844	0.0032219	2.339	0.2666895	0.250	1.263741	0.138	4.54987 ± 0.06732	8.67 ± 0.13	96.01	3.55	17.9 ± 0.7	0.177	*0.000056*	6.1
C47BC029	5.00 W	•	0.0002039	14.224	0.0019517	6.177	0.0036027	2.063	0.2938408	0.267	1.397879	0.138	4.55208 ± 0.06456	8.67 ± 0.12	95.69	3.91	76.8 ± 9.5	0.183	*0.000071*	6.1
C47BA067	5.00 W	•	0.0002705	4.837	0.0056017	1.772	0.0036530	0.784	0.3053351	0.248	1.471331	0.120	4.55779 ± 0.03590	8.68 ± 0.07	94.58	4.06	27.8 ± 1.0	0.186	*0.000107*	6.1
C47BA061	5.00 W	•	0.0004143	4.900	0.0115170	1.099	0.0037269	1.161	0.3116192	0.257	1.542526	0.116	4.55952 ± 0.04653	8.69 ± 0.09	92.11	4.14	13.8 ± 0.3	0.254	*0.000282*	6.1
C47BA066	5.00 W	•	0.0014820	1.782	0.0020971	3.293	0.0052263	1.011	0.4213082	0.224	2.361538	0.072	4.56551 ± 0.04324	8.70 ± 0.08	81.45	5.60	102.5 ± 6.8	0.094	*0.000085*	6.3
C47BA068	5.00 W	•	0.0001668	6.863	0.0029788	2.719	0.0019216	1.912	0.1616278	0.311	0.790161	0.165	4.58459 ± 0.05316	8.73 ± 0.10	93.78	2.15	27.7 ± 1.5	0.142	*0.000100*	6.0
C47BA063	5.00 W	•	0.0003039	4.383	0.0370964	0.869	0.0027537	0.937	0.2343199	0.311	1.161235	0.091	4.58495 ± 0.04501	8.73 ± 0.09	92.51	3.12	3.2 ± 0.1	0.138	*0.000089*	6.3
C47BA064	5.00 W	•	0.0002539	6.921	0.0039122	2.009	0.0029037	1.623	0.2364027	0.295	1.158874	0.129	4.58542 ± 0.05313	8.74 ± 0.10	93.54	3.14	30.8 ± 1.3	0.290	*0.000080*	5.5
C47BC023	5.00 W		0.0004876	6.167	0.0394745	0.875	0.0052691	1.585	0.4376629	0.229	2.164826	0.100	4.62389 ± 0.04686	8.81 ± 0.09	93.48	5.82	5.7 ± 0.1	0.122	*0.000338*	6.1
C47BA062	5.00 W		0.0008545	2.097	0.0038444	2.015	0.0025930	1.664	0.2043671	0.276	1.199385	0.113	4.63406 ± 0.05944	8.83 ± 0.11	78.96	2.72	27.1 ± 1.1	0.078	*0.000284*	6.3
C47BA071	5.00 W		0.0004588	2.598	0.0014587	5.328	0.0017306	2.042	0.1336751	0.293	0.756797	0.156	4.64753 ± 0.06200	8.85 ± 0.12	82.09	1.78	46.7 ± 5.0	0.321	*0.000295*	4.5
C47BC024	5.00 W		0.0019587	2.124	0.0125558	1.286	0.0052038	1.785	0.3999605	0.250	2.611820	0.094	5.08492 ± 0.06787	9.68 ± 0.13	77.87	5.32	16.2 ± 0.4	0.063	*0.000605*	4.0
C47BC025	5.00 W		0.0036589	1.537	0.0171296	0.986	0.0040672	2.203	0.2664333	0.244	2.645033	0.115	5.87420 ± 0.13084	11.18 ± 0.25	59.17	3.54	7.9 ± 0.2	0.308	*0.000574*	3.2
C47BA069	5.00 W		0.0031070	1.655	0.0143540	1.216	0.0027686	1.251	0.1727141	0.246	1.983063	0.080	6.17230 ± 0.18045	11.75 ± 0.34	53.75	2.30	6.1 ± 0.2	0.213	*0.000705*	3.0
		Σ	0.0196934	0.729	0.2982815	0.293	0.0932712	0.346	7.5211873	0.054	40.854297	0.022								

Procedure Blanks	Laser power	36Ar [V]	1σ	37Ar [V]	1σ	38Ar [V]	1σ	39Ar [V]	1σ	40Ar [V]	1σ
C47BC027	5.00 W	0.0003133	0.0000278	0.0003687	0.0000411	0.0002163	0.0000699	0.0007450	0.0002185	0.0067064	0.0015147
C47BC028	5.00 W	0.0003192	0.0000278	0.0003707	0.0000411	0.0002158	0.0000699	0.0007359	0.0002185	0.0065368	0.0015147
C47BC031	5.00 W	0.0003298	0.0000278	0.0003743	0.0000411	0.0002149	0.0000699	0.0007197	0.0002185	0.0062330	0.0015147
C47BA065	5.00 W	0.0002004	0.0000087	0.0002788	0.0000264	0.0001015	0.0000125	0.0003853	0.0000555	0.0055898	0.0006449
C47BC026	5.00 W	0.0003098	0.0000278	0.0003674	0.0000411	0.0002166	0.0000699	0.0007504	0.0002185	0.0068088	0.0015147
C47BC032	5.00 W	0.0003334	0.0000278	0.0003755	0.0000411	0.0002146	0.0000699	0.0007142	0.0002185	0.0061306	0.0015147
C47BA060	5.00 W	0.0001814	0.0000087	0.0002685	0.0000264	0.0000867	0.0000125	0.0003212	0.0000555	0.0050746	0.0006449
C47BC030	5.00 W	0.0003264	0.0000278	0.0003731	0.0000411	0.0002152	0.0000699	0.0007250	0.0002185	0.0063319	0.0015147
C47BC022	5.00 W	0.0002955	0.0000278	0.0003626	0.0000411	0.0002178	0.0000699	0.0007723	0.0002185	0.0072186	0.0015147
C47BA070	5.00 W	0.0002220	0.0000087	0.0002906	0.0000264	0.0001184	0.0000125	0.0004584	0.0000555	0.0061765	0.0006449
C47BC033	5.00 W	0.0003369	0.0000278	0.0003767	0.0000411	0.0002143	0.0000699	0.0007087	0.0002185	0.0060281	0.0015147
C47BC029	5.00 W	0.0003228	0.0000278	0.0003719	0.0000411	0.0002155	0.0000699	0.0007304	0.0002185	0.0064344	0.0015147
C47BA067	5.00 W	0.0002105	0.0000087	0.0002843	0.0000264	0.0001095	0.0000125	0.0004196	0.0000555	0.0058653	0.0006449
C47BA061	5.00 W	0.0001852	0.0000087	0.0002706	0.0000264	0.0000896	0.0000125	0.0003341	0.0000555	0.0051783	0.0006449
C47BA066	5.00 W	0.0002067	0.0000087	0.0002823	0.0000264	0.0001065	0.0000125	0.0004067	0.0000555	0.0057615	0.0006449
C47BA068	5.00 W	0.0002143	0.0000087	0.0002864	0.0000264	0.0001124	0.0000125	0.0004325	0.0000555	0.0059690	0.0006449
C47BA063	5.00 W	0.0001928	0.0000087	0.0002748	0.0000264	0.0000956	0.0000125	0.0003600	0.0000555	0.0053859	0.0006449
C47BA064	5.00 W	0.0001965	0.0000087	0.0002768	0.0000264	0.0000985	0.0000125	0.0003724	0.0000555	0.0054860	0.0006449
C47BC023	5.00 W	0.0002991	0.0000278	0.0003638	0.0000411	0.0002175	0.0000699	0.0007668	0.0002185	0.0071162	0.0015147
C47BA062	5.00 W	0.0001890	0.0000087	0.0002727	0.0000264	0.0000926	0.0000125	0.0003470	0.0000555	0.0052821	0.0006449
C47BA071	5.00 W	0.0002258	0.0000087	0.0002926	0.0000264	0.0001214	0.0000125	0.0004713	0.0000555	0.0062803	0.0006449
C47BC024	5.00 W	0.0003026	0.0000278	0.0003650	0.0000411	0.0002172	0.0000699	0.0007614	0.0002185	0.0070137	0.0015147
C47BC025	5.00 W	0.0003062	0.0000278	0.0003662	0.0000411	0.0002169	0.0000699	0.0007559	0.0002185	0.0069113	0.0015147
C47BA069	5.00 W	0.0002182	0.0000087	0.0002885	0.0000264	0.0001154	0.0000125	0.0004455	0.0000555	0.0060728	0.0006449

Sample Parameters	Laser power	Sample	Material	Location	Analyst	Standard (in Ma)	%1σ	J	%1σ	MDF	%1σ	Volume Ratio	Sensitivity (mol/volt)
C47BC027	5.00 W	18-32/3 (323bl)	Phlogopite (0.5-1 mm)	Maio, Cape Verdes	Jan Sticklus	28.344	0.039	1.06E-03	0.08	1.0098	0.21	1	1.211E-14
C47BC028	5.00 W	18-32/3 (323bl)	Phlogopite (0.5-1 mm)	Maio, Cape Verdes	Jan Sticklus	28.344	0.039	1.06E-03	0.08	1.0098	0.21	1	1.211E-14
C47BC031	5.00 W	18-32/3 (323bl)	Phlogopite (0.5-1 mm)	Maio, Cape Verdes	Jan Sticklus	28.344	0.039	1.06E-03	0.08	1.0098	0.21	1	1.211E-14
C47BA065	5.00 W	18-32/3 (323bl)	Phlogopite (0.5-1 mm)	Maio, Cape Verdes	Jan Sticklus	28.344	0.039	1.06E-03	0.08	1.0098	0.21	1	1.211E-14
C47BC026	5.00 W	18-32/3 (323bl)	Phlogopite (0.5-1 mm)	Maio, Cape Verdes	Jan Sticklus	28.344	0.039	1.06E-03	0.08	1.0098	0.21	1	1.211E-14
C47BC032	5.00 W	18-32/3 (323bl)	Phlogopite (0.5-1 mm)	Maio, Cape Verdes	Jan Sticklus	28.344	0.039	1.06E-03	0.08	1.0098	0.21	1	1.211E-14
C47BA060	5.00 W	18-32/3 (323bl)	Phlogopite (0.5-1 mm)	Maio, Cape Verdes	Jan Sticklus	28.344	0.039	1.06E-03	0.08	1.0098	0.21	1	1.211E-14
C47BC030	5.00 W	18-32/3 (323bl)	Phlogopite (0.5-1 mm)	Maio, Cape Verdes	Jan Sticklus	28.344	0.039	1.06E-03	0.08	1.0098	0.21	1	1.211E-14
C47BC022	5.00 W	18-32/3 (323bl)	Phlogopite (0.5-1 mm)	Maio, Cape Verdes	Jan Sticklus	28.344	0.039	1.06E-03	0.08	1.0098	0.21	1	1.211E-14
C47BA070	5.00 W	18-32/3 (323bl)	Phlogopite (0.5-1 mm)	Maio, Cape Verdes	Jan Sticklus	28.344	0.039	1.06E-03	0.08	1.0098	0.21	1	1.211E-14
C47BC033	5.00 W	18-32/3 (323bl)	Phlogopite (0.5-1 mm)	Maio, Cape Verdes	Jan Sticklus	28.344	0.039	1.06E-03	0.08	1.0098	0.21	1	1.211E-14
C47BC029	5.00 W	18-32/3 (323bl)	Phlogopite (0.5-1 mm)	Maio, Cape Verdes	Jan Sticklus	28.344	0.039	1.06E-03	0.08	1.0098	0.21	1	1.211E-14
C47BA067	5.00 W	18-32/3 (323bl)	Phlogopite (0.5-1 mm)	Maio, Cape Verdes	Jan Sticklus	28.344	0.039	1.06E-03	0.08	1.0098	0.21	1	1.211E-14
C47BA061	5.00 W	18-32/3 (323bl)	Phlogopite (0.5-1 mm)	Maio, Cape Verdes	Jan Sticklus	28.344	0.039	1.06E-03	0.08	1.0098	0.21	1	1.211E-14
C47BA066	5.00 W	18-32/3 (323bl)	Phlogopite (0.5-1 mm)	Maio, Cape Verdes	Jan Sticklus	28.344	0.039	1.06E-03	0.08	1.0098	0.21	1	1.211E-14
C47BA068	5.00 W	18-32/3 (323bl)	Phlogopite (0.5-1 mm)	Maio, Cape Verdes	Jan Sticklus	28.344	0.039	1.06E-03	0.08	1.0098	0.21	1	1.211E-14
C47BA063	5.00 W	18-32/3 (323bl)	Phlogopite (0.5-1 mm)	Maio, Cape Verdes	Jan Sticklus	28.344	0.039	1.06E-03	0.08	1.0098	0.21	1	1.211E-14
C47BA064	5.00 W	18-32/3 (323bl)	Phlogopite (0.5-1 mm)	Maio, Cape Verdes	Jan Sticklus	28.344	0.039	1.06E-03	0.08	1.0098	0.21	1	1.211E-14
C47BC023	5.00 W	18-32/3 (323bl)	Phlogopite (0.5-1 mm)	Maio, Cape Verdes	Jan Sticklus	28.344	0.039	1.06E-03	0.08	1.0098	0.21	1	1.211E-14
C47BA062	5.00 W	18-32/3 (323bl)	Phlogopite (0.5-1 mm)	Maio, Cape Verdes	Jan Sticklus	28.344	0.039	1.06E-03	0.08	1.0098	0.21	1	1.211E-14
C47BA071	5.00 W	18-32/3 (323bl)	Phlogopite (0.5-1 mm)	Maio, Cape Verdes	Jan Sticklus	28.344	0.039	1.06E-03	0.08	1.0098	0.21	1	1.211E-14
C47BC024	5.00 W	18-32/3 (323bl)	Phlogopite (0.5-1 mm)	Maio, Cape Verdes	Jan Sticklus	28.344	0.039	1.06E-03	0.08	1.0098	0.21	1	1.211E-14
C47BC025	5.00 W	18-32/3 (323bl)	Phlogopite (0.5-1 mm)	Maio, Cape Verdes	Jan Sticklus	28.344	0.039	1.06E-03	0.08	1.0098	0.21	1	1.211E-14
C47BA069	5.00 W	18-32/3 (323bl)	Phlogopite (0.5-1 mm)	Maio, Cape Verdes	Jan Sticklus	28.344	0.039	1.06E-03	0.08	1.0098	0.21	1	1.211E-14

Day	Month	Year	Hour	Min	Resist	Irradiation	Project	Experiment	Nmb	Standard Name
3	JUL	2018	1	8	1	can47	Examples	c47it5ip6_323bl	01	TCS2
3	JUL	2018	1	56	1	can47	Examples	c47it5ip6_323bl	01	TCS2
3	JUL	2018	3	22	1	can47	Examples	c47it5ip6_323bl	01	TCS2
29	JUN	2018	19	57	1	can47	Examples	c47it5ip6_323bl	01	TCS2
3	JUL	2018	0	39	1	can47	Examples	c47it5ip6_323bl	01	TCS2
3	JUL	2018	3	51	1	can47	Examples	c47it5ip6_323bl	01	TCS2
29	JUN	2018	17	33	1	can47	Examples	c47it5ip6_323bl	01	TCS2
3	JUL	2018	2	54	1	can47	Examples	c47it5ip6_323bl	01	TCS2
2	JUL	2018	22	43	1	can47	Examples	c47it5ip6_323bl	01	TCS2
29	JUN	2018	22	41	1	can47	Examples	c47it5ip6_323bl	01	TCS2
3	JUL	2018	4	20	1	can47	Examples	c47it5ip6_323bl	01	TCS2
3	JUL	2018	2	25	1	can47	Examples	c47it5ip6_323bl	01	TCS2
29	JUN	2018	21	14	1	can47	Examples	c47it5ip6_323bl	01	TCS2
29	JUN	2018	18	2	1	can47	Examples	c47it5ip6_323bl	01	TCS2
29	JUN	2018	20	45	1	can47	Examples	c47it5ip6_323bl	01	TCS2
29	JUN	2018	21	43	1	can47	Examples	c47it5ip6_323bl	01	TCS2
29	JUN	2018	19	0	1	can47	Examples	c47it5ip6_323bl	01	TCS2
29	JUN	2018	19	28	1	can47	Examples	c47it5ip6_323bl	01	TCS2
2	JUL	2018	23	12	1	can47	Examples	c47it5ip6_323bl	01	TCS2
29	JUN	2018	18	31	1	can47	Examples	c47it5ip6_323bl	01	TCS2
29	JUN	2018	23	10	1	can47	Examples	c47it5ip6_323bl	01	TCS2
2	JUL	2018	23	41	1	can47	Examples	c47it5ip6_323bl	01	TCS2
3	JUL	2018	0	10	1	can47	Examples	c47it5ip6_323bl	01	TCS2
29	JUN	2018	22	12	1	can47	Examples	c47it5ip6_323bl	01	TCS2

Irradiation Constants	Laser power	40/36(a)	%1σ	40/36(c)	%1σ	38/36(a)	%1σ	38/36(c)	%1σ	39/37(ca)	%1σ	38/37(ca)	%1σ	36/37(ca)	%1σ	40/39(k)	%1σ	38/39(k)	%1σ	36/38(cl)	%1σ	K/Ca	%1σ	K/Cl	%1σ	Ca/Cl	%1σ
C47BC027	5.00 W	295.5	0.178	0.018	35	0.1869	0.107	1.493	3	0.000702	1.71	0.000196	4.08	0.0002702	0.15	0.00073	12.33	0.01215	0.27	262.8	0.65	0.51	0	0	0	0	0
C47BC028	5.00 W	295.5	0.178	0.018	35	0.1869	0.107	1.493	3	0.000702	1.71	0.000196	4.08	0.0002702	0.15	0.00073	12.33	0.01215	0.27	262.8	0.65	0.51	0	0	0	0	0
C47BC031	5.00 W	295.5	0.178	0.018	35	0.1869	0.107	1.493	3	0.000702	1.71	0.000196	4.08	0.0002702	0.15	0.00073	12.33	0.01215	0.27	262.8	0.65	0.51	0	0	0	0	0
C47BA065	5.00 W	295.5	0.178	0.018	35	0.1869	0.107	1.493	3	0.000702	1.71	0.000196	4.08	0.0002702	0.15	0.00073	12.33	0.01215	0.27	262.8	0.65	0.51	0	0	0	0	0
C47BC026	5.00 W	295.5	0.178	0.018	35	0.1869	0.107	1.493	3	0.000702	1.71	0.000196	4.08	0.0002702	0.15	0.00073	12.33	0.01215	0.27	262.8	0.65	0.51	0	0	0	0	0
C47BC032	5.00 W	295.5	0.178	0.018	35	0.1869	0.107	1.493	3	0.000702	1.71	0.000196	4.08	0.0002702	0.15	0.00073	12.33	0.01215	0.27	262.8	0.65	0.51	0	0	0	0	0
C47BA060	5.00 W	295.5	0.178	0.018	35	0.1869	0.107	1.493	3	0.000702	1.71	0.000196	4.08	0.0002702	0.15	0.00073	12.33	0.01215	0.27	262.8	0.65	0.51	0	0	0	0	0
C47BC030	5.00 W	295.5	0.178	0.018	35	0.1869	0.107	1.493	3	0.000702	1.71	0.000196	4.08	0.0002702	0.15	0.00073	12.33	0.01215	0.27	262.8	0.65	0.51	0	0	0	0	0
C47BC022	5.00 W	295.5	0.178	0.018	35	0.1869	0.107	1.493	3	0.000702	1.71	0.000196	4.08	0.0002702	0.15	0.00073	12.33	0.01215	0.27	262.8	0.65	0.51	0	0	0	0	0
C47BA070	5.00 W	295.5	0.178	0.018	35	0.1869	0.107	1.493	3	0.000702	1.71	0.000196	4.08	0.0002702	0.15	0.00073	12.33	0.01215	0.27	262.8	0.65	0.51	0	0	0	0	0
C47BC033	5.00 W	295.5	0.178	0.018	35	0.1869	0.107	1.493	3	0.000702	1.71	0.000196	4.08	0.0002702	0.15	0.00073	12.33	0.01215	0.27	262.8	0.65	0.51	0	0	0	0	0
C47BC029	5.00 W	295.5	0.178	0.018	35	0.1869	0.107	1.493	3	0.000702	1.71	0.000196	4.08	0.0002702	0.15	0.00073	12.33	0.01215	0.27	262.8	0.65	0.51	0	0	0	0	0
C47BA067	5.00 W	295.5	0.178	0.018	35	0.1869	0.107	1.493	3	0.000702	1.71	0.000196	4.08	0.0002702	0.15	0.00073	12.33	0.01215	0.27	262.8	0.65	0.51	0	0	0	0	0
C47BA061	5.00 W	295.5	0.178	0.018	35	0.1869	0.107	1.493	3	0.000702	1.71	0.000196	4.08	0.0002702	0.15	0.00073	12.33	0.01215	0.27	262.8	0.65	0.51	0	0	0	0	0
C47BA066	5.00 W	295.5	0.178	0.018	35	0.1869	0.107	1.493	3	0.000702	1.71	0.000196	4.08	0.0002702	0.15	0.00073	12.33	0.01215	0.27	262.8	0.65	0.51	0	0	0	0	0
C47BA068	5.00 W	295.5	0.178	0.018	35	0.1869	0.107	1.493	3	0.000702	1.71	0.000196	4.08	0.0002702	0.15	0.00073	12.33	0.01215	0.27	262.8	0.65	0.51	0	0	0	0	0
C47BA063	5.00 W	295.5	0.178	0.018	35	0.1869	0.107	1.493	3	0.000702	1.71	0.000196	4.08	0.0002702	0.15	0.00073	12.33	0.01215	0.27	262.8	0.65	0.51	0	0	0	0	0
C47BA064	5.00 W	295.5	0.178	0.018	35	0.1869	0.107	1.493	3	0.000702	1.71	0.000196	4.08	0.0002702	0.15	0.00073	12.33	0.01215	0.27	262.8	0.65	0.51	0	0	0	0	0
C47BC023	5.00 W	295.5	0.178	0.018	35	0.1869	0.107	1.493	3	0.000702	1.71	0.000196	4.08	0.0002702	0.15	0.00073	12.33	0.01215	0.27	262.8	0.65	0.51	0	0	0	0	0
C47BA062	5.00 W	295.5	0.178	0.018	35	0.1869	0.107	1.493	3	0.000702	1.71	0.000196	4.08	0.0002702	0.15	0.00073	12.33	0.01215	0.27	262.8	0.65	0.51	0	0	0	0	0
C47BA071	5.00 W	295.5	0.178	0.018	35	0.1869	0.107	1.493	3	0.000702	1.71	0.000196	4.08	0.0002702	0.15	0.00073	12.33	0.01215	0.27	262.8	0.65	0.51	0	0	0	0	0
C47BC024	5.00 W	295.5	0.178	0.018	35	0.1869	0.107	1.493	3	0.000702	1.71	0.000196	4.08	0.0002702	0.15	0.00073	12.33	0.01215	0.27	262.8	0.65	0.51	0	0	0	0	0
C47BC025	5.00 W	295.5	0.178	0.018	35	0.1869	0.107	1.493	3	0.000702	1.71	0.000196	4.08	0.0002702	0.15	0.00073	12.33	0.01215	0.27	262.8	0.65	0.51	0	0	0	0	0
C47BA069	5.00 W	295.5	0.178	0.018	35	0.1869	0.107	1.493	3	0.000702	1.71	0.000196	4.08	0.0002702	0.15	0.00073	12.33	0.01215	0.27	262.8	0.65	0.51	0	0	0	0	0

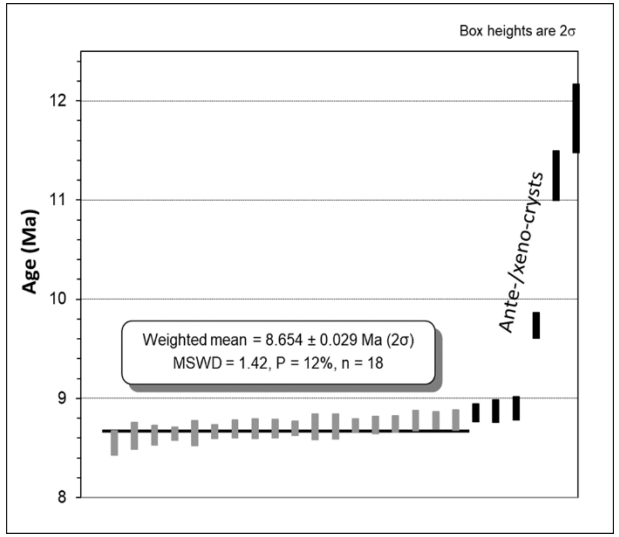

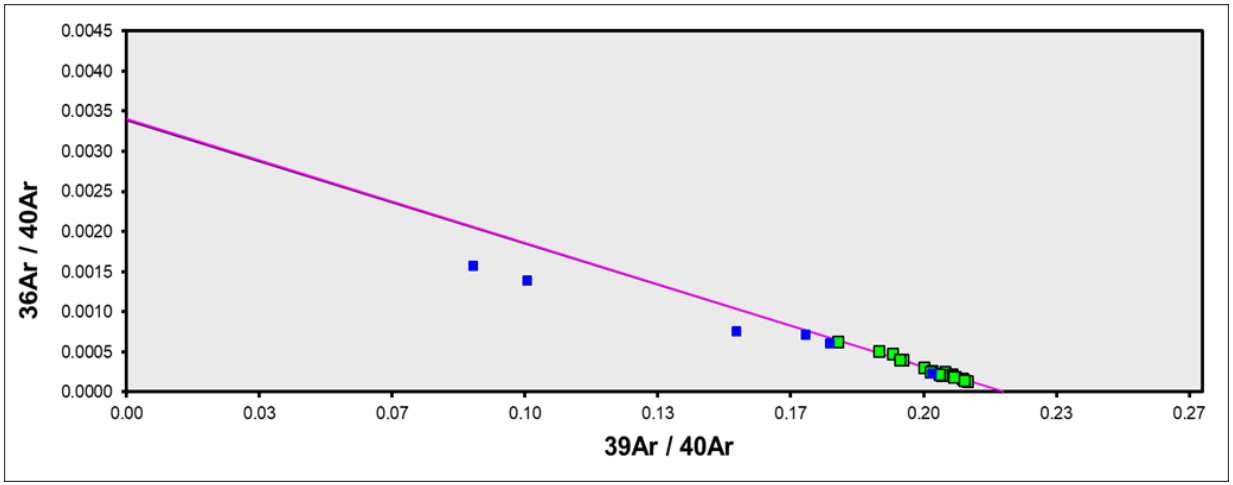

Information on Analysis and Constants Used in Calculations

Sample = 18-32/3 (323BL)
Material = Phlogopite
Location = Maio Cape Verdes
Analyst = Jan Sticklus
Project = EXAMPLES
Mass Discrimination Law = POW
Irradiation = can47
J = 0.00105850 ± 0.00000085
TCS2 = 28.344 ± 0.011 Ma
Experiment Type = SAMPLE
Heating = 45 sec
Isolation = 15.00 min
Instrument = MAP216

Age Equations = Conventional
Negative Intensities = Allowed
Decay Constant 40K = 5.543 ± 0.009 E-10 1/a
Decay Constant 39Ar = 2.940 ± 0.016 E-07 1/h
Decay Constant 37Ar = 8.230 ± 0.012 E-04 1/h
Decay Constant 36Cl = 2.257 ± 0.015 E-06 1/a
Atmospheric Ratio 40/36(a) = 295.50 ± 0.53
Atmospheric Ratio 38/36(a) = 0.1869 ± 0.0002
Production Ratio 39/37(ca) = 0.000702 ± 0.000012
Production Ratio 38/37(ca) = 0.000196 ± 0.000008
Production Ratio 36/37(ca) = 0.000270 ± 0.000000
Production Ratio 40/39(k) = 0.000730 ± 0.000090
Production Ratio 38/39(k) = 0.012150 ± 0.000033
Production Ratio 36/38(cl) = 262.80
Scaling Ratio K/Ca = 0.510

Results	40(a)/36(a) ± 2σ	40(r)/39(k) ± 2σ	Age ± 2σ (Ma)	MSWD	39Ar(k) (%,n)	K/Ca ± 2σ
SCTF Weighted Mean		4.54283 ± 0.01334 ± 0.29%	8.654 ± 0.029 ± 0.33%	1.42 12% 1.69 1.1904	78.53 18 2σ Confidence Limit Error Magnification	4.6 ± 1.8
			Minimal External Error ± 0.040 Analytical Error ± 0.025			
Total Fusion Age		4.66073 ± 0.01261 ± 0.27%	8.878 ± 0.028 ± 0.31%		24	12.9 ± 0.1
			Minimal External Error ± 0.040 Analytical Error ± 0.024			
Normal Isochron No Convergence	288.43 ± 17.91 ± 6.21%	4.55142 ± 0.02890 ± 0.64%	8.671 ± 0.057 ± 0.65%	1.55 7% 1.71 1.2462 100 0.0000555896	78.53 18 2σ Confidence Limit Error Magnification Number of Iterations Convergence	
			Minimal External Error ± 0.063 Analytical Error ± 0.055			
Inverse Isochron	293.86 ± 17.85 ± 6.08%	4.54530 ± 0.02872 ± 0.63%	8.659 ± 0.056 ± 0.65%	1.51 9% 1.71 1.2268 3 0.0001311746 15%	78.53 18 2σ Confidence Limit Error Magnification Number of Iterations Convergence Spreading Factor	
			Minimal External Error ± 0.063 Analytical Error ± 0.055			

Sample 18-32/3 single-crystal total-fusion results (combined 0.25-0.5 mm and 0.5-1 mm fractions; 323 and 323bl)

Relative Abundances	Laser power	Group	36Ar [V]	%1σ	37Ar [V]	%1σ	38Ar [V]	%1σ	39Ar [V]	%1σ	40Ar [V]	%1σ	40(r)/39(k) ± 2σ	Age ± 2σ (Ma)	40Ar(r) (%)	39Ar(k) (%)	K/Ca ± 2σ	Sample weight (mg)	$^{36}Ar/^{39}Ar$ Alt. Index	Wt. % K
C47BC027	5.00 W	1	0.0008506	4.028	0.0062254	2.079	0.0043061	1.914	0.3418945	0.260	1.778060	0.109	4.46620 ± 0.06466	8.51 ± 0.12	85.88	3.72	28.0 ± 1.2	0.214	*0.000192*	5.8
C47BA057	5.00 W	1	0.0001106	12.973	0.0025421	2.762	0.0011065	2.282	0.0909780	0.298	0.440184	0.157	4.48079 ± 0.09814	8.54 ± 0.19	92.61	0.99	18.3 ± 1.0	0.044	*0.000121*	7.6
C47BC028	5.00 W	1	0.0003503	8.849	0.0056031	2.387	0.0034006	2.503	0.2807664	0.263	1.367982	0.124	4.50460 ± 0.07047	8.58 ± 0.13	92.45	3.06	25.6 ± 1.2	0.170	*0.000099*	6.0
C47BC031	5.00 W	1	0.0011454	2.867	0.0190233	0.953	0.0052091	1.529	0.4248298	0.233	2.251424	0.078	4.50585 ± 0.05104	8.58 ± 0.10	85.02	4.62	11.4 ± 0.2	0.262	*0.000211*	5.9
C47BA065	5.00 W	1	0.0003566	3.924	0.0120675	1.039	0.0039146	1.071	0.3335962	0.241	1.610610	0.127	4.51445 ± 0.03520	8.60 ± 0.07	93.50	3.63	14.1 ± 0.3	0.202	*0.000085*	6.0
C47BC026	5.00 W	1	0.0008036	4.857	0.0166358	0.957	0.0047605	1.662	0.3837478	0.294	1.969952	0.104	4.51755 ± 0.06661	8.61 ± 0.13	88.00	4.18	11.8 ± 0.2	0.240	*0.000161*	5.8
C47BC032	5.00 W	1	0.0005021	6.023	0.0088125	1.762	0.0074571	1.260	0.6147770	0.225	2.929746	0.079	4.52465 ± 0.03630	8.62 ± 0.07	94.94	6.69	35.6 ± 1.3	0.377	*0.000064*	6.0
C47BA056	5.00 W	1	0.0001433	11.992	0.0003146	17.911	0.0009348	2.438	0.0767728	0.334	0.389790	0.148	4.52509 ± 0.13658	8.62 ± 0.26	89.13	0.84	124.5 ± 44.6	0.038	*0.000182*	7.4
C47BA052	5.00 W	1	0.0003613	4.314	0.0021234	2.818	0.0014686	1.848	0.1200503	0.266	0.650105	0.146	4.52668 ± 0.08205	8.62 ± 0.16	83.59	1.31	28.8 ± 1.6	0.068	*0.000257*	6.4
C47BA053	5.00 W	1	0.0001184	12.079	0.0022461	2.463	0.0015215	1.850	0.1274949	0.236	0.613083	0.104	4.53493 ± 0.07039	8.64 ± 0.13	94.31	1.39	28.9 ± 1.4	0.073	*0.000078*	6.4
C47BA051	5.00 W	1	0.0003765	5.146	0.0096604	1.370	0.0019039	1.287	0.1526686	0.265	0.803440	0.099	4.53835 ± 0.07950	8.65 ± 0.15	86.23	1.66	8.1 ± 0.2	0.088	*0.000206*	6.3
C47BA060	5.00 W	1	0.0001609	7.391	0.0038432	2.183	0.0020915	1.863	0.1749213	0.234	0.841251	0.115	4.53861 ± 0.04679	8.65 ± 0.09	94.37	1.90	23.2 ± 1.0	0.101	*0.000077*	6.3
C47BC030	5.00 W	1	0.0008631	3.815	0.0564032	0.795	0.0050370	1.679	0.4080901	0.225	2.103991	0.101	4.54145 ± 0.05296	8.65 ± 0.10	88.08	4.44	3.7 ± 0.1	0.267	*0.000154*	5.6
C47BC022	5.00 W	1	0.0004289	7.152	0.0065333	2.275	0.0050130	1.670	0.4287534	0.259	2.073707	0.101	4.54156 ± 0.04937	8.65 ± 0.09	93.90	4.67	33.5 ± 1.5	0.262	*0.000079*	6.0
C47BA070	5.00 W	1	0.0004396	2.967	0.0015559	4.732	0.0034397	1.380	0.2838548	0.248	1.419365	0.138	4.54240 ± 0.03795	8.65 ± 0.07	90.84	3.09	93.0 ± 8.8	0.176	*0.000121*	5.9
C47BC033	5.00 W	1	0.0001718	16.277	0.0076065	1.844	0.0032219	2.339	0.2666895	0.250	1.263741	0.138	4.54987 ± 0.06732	8.67 ± 0.13	96.01	2.90	17.9 ± 0.7	0.163	*0.000050*	6.0
C47BC029	5.00 W	1	0.0002039	14.224	0.0019517	6.177	0.0036027	2.063	0.2938408	0.267	1.397879	0.138	4.55208 ± 0.06456	8.67 ± 0.12	95.69	3.20	76.8 ± 9.5	0.177	*0.000056*	6.1
C47BA067	5.00 W	1	0.0002705	4.837	0.0056017	1.772	0.0036530	0.784	0.3053351	0.248	1.471331	0.120	4.55779 ± 0.03590	8.68 ± 0.07	94.58	3.32	27.8 ± 1.0	0.183	*0.000071*	6.1
C47BA050	5.00 W	1	0.0001508	10.190	0.0076153	1.660	0.0023484	1.274	0.1949916	0.237	0.932871	0.148	4.55812 ± 0.05328	8.68 ± 0.10	95.27	2.12	13.1 ± 0.4	0.113	*0.000064*	6.3
C47BA061	5.00 W	1	0.0004143	4.900	0.0115170	1.099	0.0037269	1.161	0.3116192	0.257	1.542526	0.116	4.55952 ± 0.04653	8.69 ± 0.09	92.11	3.39	13.8 ± 0.3	0.186	*0.000107*	6.1
C47BA066	5.00 W	1	0.0014820	1.782	0.0020971	3.293	0.0052263	1.011	0.4213082	0.224	2.361538	0.072	4.56551 ± 0.04324	8.70 ± 0.08	81.45	4.59	102.5 ± 6.8	0.254	*0.000282*	6.1
C47BA054	5.00 W	1	0.0012177	1.956	0.0128235	1.173	0.0027978	1.363	0.2167929	0.240	1.351344	0.085	4.57770 ± 0.06960	8.72 ± 0.13	73.44	2.36	8.6 ± 0.2	0.125	*0.000470*	6.3
C47BA068	5.00 W	1	0.0001668	6.863	0.0029788	2.719	0.0019216	1.912	0.1616278	0.311	0.790161	0.165	4.58459 ± 0.05316	8.73 ± 0.10	93.78	1.76	27.7 ± 1.5	0.094	*0.000085*	6.3
C47BA063	5.00 W	1	0.0003039	4.383	0.0370964	0.869	0.0027537	0.937	0.2343199	0.311	1.161235	0.091	4.58495 ± 0.04501	8.73 ± 0.09	92.51	2.55	3.2 ± 0.1	0.142	*0.000100*	6.0
C47BA064	5.00 W	1	0.0002539	6.921	0.0039122	2.009	0.0029037	1.623	0.2364027	0.295	1.158874	0.129	4.58542 ± 0.05313	8.74 ± 0.10	93.54	2.57	30.8 ± 1.3	0.138	*0.000089*	6.3
C47BA048	5.00 W	1	0.0001351	10.198	0.0013331	4.270	0.0015276	1.806	0.1253603	0.323	0.614997	0.173	4.58745 ± 0.07342	8.74 ± 0.14	93.51	1.36	48.0 ± 4.1	0.074	*0.000088*	6.2
C47BA058	5.00 W	1	0.0005094	3.089	0.0010906	6.400	0.0026961	1.357	0.2215624	0.262	1.167535	0.119	4.58988 ± 0.05002	8.74 ± 0.10	87.10	2.41	103.6 ± 13.3	0.123	*0.000200*	6.6
C47BA055	5.00 W	1	0.0001755	10.622	0.0011932	4.998	0.0009719	3.163	0.0819602	0.420	0.430147	0.214	4.61608 ± 0.14170	8.79 ± 0.27	87.95	0.89	35.0 ± 3.5	0.038	*0.000223*	7.9
C47BA059	5.00 W	1	0.0001507	8.600	0.0006647	8.285	0.0022582	1.625	0.1878851	0.247	0.912038	0.109	4.61677 ± 0.04792	8.79 ± 0.09	95.11	2.05	144.2 ± 23.9	0.104	*0.000070*	6.6
C47BC023	5.00 W	2	0.0004876	6.167	0.0394745	0.875	0.0052691	1.585	0.4376629	0.229	2.164826	0.100	4.62389 ± 0.04686	8.81 ± 0.09	93.48	4.76	5.7 ± 0.1	0.290	*0.000080*	5.5
C47BA062	5.00 W	2	0.0008545	2.097	0.0038444	2.015	0.0025930	1.664	0.2043671	0.276	1.199385	0.113	4.63406 ± 0.05944	8.83 ± 0.11	78.96	2.22	27.1 ± 1.1	0.122	*0.000338*	6.1
C47BA071	5.00 W	2	0.0004588	2.598	0.0014587	5.328	0.0017306	2.042	0.1336751	0.293	0.756797	0.156	4.64753 ± 0.06200	8.85 ± 0.12	82.09	1.46	46.7 ± 5.0	0.078	*0.000284*	6.3
C47BC024	5.00 W	3	0.0019587	2.124	0.0125558	1.286	0.0052038	1.785	0.3999605	0.250	2.611820	0.094	5.08492 ± 0.06787	9.68 ± 0.13	77.87	4.35	16.2 ± 0.4	0.321	*0.000295*	4.5
C47BA049	5.00 W	3	0.0007885	3.142	0.0042664	2.052	0.0009834	2.168	0.0684919	0.403	0.624384	0.120	5.71898 ± 0.22015	10.89 ± 0.42	62.73	0.75	8.2 ± 0.3	0.063	*0.000605*	4.0
C47BC025	5.00 W	3	0.0036589	1.537	0.0171296	0.986	0.0040672	2.203	0.2664333	0.244	2.645033	0.115	5.87420 ± 0.13084	11.18 ± 0.25	59.17	2.90	7.9 ± 0.2	0.308	*0.000574*	3.2
C47BA069	5.00 W	3	0.0031070	1.655	0.0143540	1.216	0.0027686	1.251	0.1727141	0.246	1.983063	0.080	6.17230 ± 0.18045	11.75 ± 0.34	53.75	1.88	6.1 ± 0.2	0.213	*0.000705*	3.0
		Σ	0.0239313	0.651	0.3441548	0.269	0.1137897	0.297	9.1861965	0.047	49.784216	0.020								

Procedure Blanks	Laser power	36Ar [V]	1σ	37Ar [V]	1σ	38Ar [V]	1σ	39Ar [V]	1σ	40Ar [V]	1σ
C47BC027	5.00 W	0.0003133	0.0000278	0.0003687	0.0000411	0.0002163	0.0000699	0.0007450	0.0002185	0.0067064	0.0015147
C47BA057	5.00 W	0.0001805	0.0000126	0.0002627	0.0000216	0.0000883	0.0000177	0.0003187	0.0000274	0.0049793	0.0005227
C47BC028	5.00 W	0.0003192	0.0000278	0.0003707	0.0000411	0.0002158	0.0000699	0.0007359	0.0002185	0.0065368	0.0015147
C47BC031	5.00 W	0.0003298	0.0000278	0.0003743	0.0000411	0.0002149	0.0000699	0.0007197	0.0002185	0.0062330	0.0015147
C47BA065	5.00 W	0.0002004	0.0000087	0.0002788	0.0000264	0.0001015	0.0000125	0.0003853	0.0000555	0.0055898	0.0006449
C47BC026	5.00 W	0.0003098	0.0000278	0.0003674	0.0000411	0.0002166	0.0000699	0.0007504	0.0002185	0.0068088	0.0015147
C47BC032	5.00 W	0.0003334	0.0000278	0.0003755	0.0000411	0.0002146	0.0000699	0.0007142	0.0002185	0.0061306	0.0015147
C47BA056	5.00 W	0.0001797	0.0000126	0.0002618	0.0000216	0.0000887	0.0000177	0.0003285	0.0000274	0.0050824	0.0005227
C47BA052	5.00 W	0.0001761	0.0000126	0.0002579	0.0000216	0.0000909	0.0000177	0.0003741	0.0000274	0.0055585	0.0005227
C47BA053	5.00 W	0.0001769	0.0000126	0.0002588	0.0000216	0.0000905	0.0000177	0.0003642	0.0000274	0.0054555	0.0005227
C47BA051	5.00 W	0.0001753	0.0000126	0.0002571	0.0000216	0.0000914	0.0000177	0.0003840	0.0000274	0.0056615	0.0005227
C47BA060	5.00 W	0.0001814	0.0000087	0.0002685	0.0000264	0.0000867	0.0000125	0.0003212	0.0000555	0.0050746	0.0006449
C47BC030	5.00 W	0.0003264	0.0000278	0.0003731	0.0000411	0.0002152	0.0000699	0.0007250	0.0002185	0.0063319	0.0015147
C47BC022	5.00 W	0.0002955	0.0000278	0.0003626	0.0000411	0.0002178	0.0000699	0.0007723	0.0002185	0.0072186	0.0015147
C47BA070	5.00 W	0.0002220	0.0000087	0.0002906	0.0000264	0.0001184	0.0000125	0.0004584	0.0000555	0.0061765	0.0006449
C47BC033	5.00 W	0.0003369	0.0000278	0.0003767	0.0000411	0.0002143	0.0000699	0.0007087	0.0002185	0.0060281	0.0015147
C47BC029	5.00 W	0.0003228	0.0000278	0.0003719	0.0000411	0.0002155	0.0000699	0.0007304	0.0002185	0.0064344	0.0015147
C47BA067	5.00 W	0.0002105	0.0000087	0.0002843	0.0000264	0.0001095	0.0000125	0.0004196	0.0000555	0.0058653	0.0006449
C47BA050	5.00 W	0.0001746	0.0000126	0.0002563	0.0000216	0.0000919	0.0000177	0.0003938	0.0000274	0.0057646	0.0005227
C47BA061	5.00 W	0.0001852	0.0000087	0.0002706	0.0000264	0.0000896	0.0000125	0.0003341	0.0000555	0.0051783	0.0006449
C47BA066	5.00 W	0.0002067	0.0000087	0.0002823	0.0000264	0.0001065	0.0000125	0.0004067	0.0000555	0.0057615	0.0006449
C47BA054	5.00 W	0.0001782	0.0000126	0.0002602	0.0000216	0.0000897	0.0000177	0.0003479	0.0000274	0.0052849	0.0005227
C47BA068	5.00 W	0.0002143	0.0000087	0.0002864	0.0000264	0.0001124	0.0000125	0.0004325	0.0000555	0.0059690	0.0006449
C47BA063	5.00 W	0.0001928	0.0000087	0.0002748	0.0000264	0.0000956	0.0000125	0.0003600	0.0000555	0.0053859	0.0006449
C47BA064	5.00 W	0.0001965	0.0000087	0.0002768	0.0000264	0.0000985	0.0000125	0.0003724	0.0000555	0.0054860	0.0006449
C47BA048	5.00 W	0.0001730	0.0000126	0.0002546	0.0000216	0.0000928	0.0000177	0.0004135	0.0000274	0.0059707	0.0005227
C47BA058	5.00 W	0.0001813	0.0000126	0.0002635	0.0000216	0.0000878	0.0000177	0.0003088	0.0000274	0.0048763	0.0005227
C47BA055	5.00 W	0.0001789	0.0000126	0.0002610	0.0000216	0.0000892	0.0000177	0.0003384	0.0000274	0.0051854	0.0005227
C47BA059	5.00 W	0.0001820	0.0000126	0.0002643	0.0000216	0.0000873	0.0000177	0.0002990	0.0000274	0.0047732	0.0005227
C47BC023	5.00 W	0.0002991	0.0000278	0.0003638	0.0000411	0.0002175	0.0000699	0.0007668	0.0002185	0.0071162	0.0015147
C47BA062	5.00 W	0.0001890	0.0000087	0.0002727	0.0000264	0.0000926	0.0000125	0.0003470	0.0000555	0.0052821	0.0006449
C47BA071	5.00 W	0.0002258	0.0000087	0.0002926	0.0000264	0.0001214	0.0000125	0.0004713	0.0000555	0.0062803	0.0006449
C47BC024	5.00 W	0.0003026	0.0000278	0.0003650	0.0000411	0.0002172	0.0000699	0.0007614	0.0002185	0.0070137	0.0015147
C47BA049	5.00 W	0.0001738	0.0000126	0.0002554	0.0000216	0.0000924	0.0000177	0.0004037	0.0000274	0.0058676	0.0005227
C47BC025	5.00 W	0.0003062	0.0000278	0.0003662	0.0000411	0.0002169	0.0000699	0.0007559	0.0002185	0.0069113	0.0015147
C47BA069	5.00 W	0.0002182	0.0000087	0.0002885	0.0000264	0.0001154	0.0000125	0.0004455	0.0000555	0.0060728	0.0006449

Sample Parameters	Laser power	Sample	Material	Location	Analyst	Standard (in Ma)	%1σ	J	%1σ	MDF	%1σ	Volume Ratio	Sensitivity (mol/volt)
C47BC027	5.00 W	18-32/3 (323bl)	Phlogopite (0.5-1 mm)	Maio, Cape Verdes	Jan Sticklus	28.344	0.039	1.06E-03	0.08	1.0098	0.21	1	1.211E-14
C47BA057	5.00 W	18-32/3 (323bs)	Phlogopite (0.25-0.5 mm)	Maio, Cape Verdes	Jan Sticklus	28.344	0.039	1.06E-03	0.08	1.0098	0.21	1	1.211E-14
C47BC028	5.00 W	18-32/3 (323bl)	Phlogopite (0.5-1 mm)	Maio, Cape Verdes	Jan Sticklus	28.344	0.039	1.06E-03	0.08	1.0098	0.21	1	1.211E-14
C47BC031	5.00 W	18-32/3 (323bl)	Phlogopite (0.5-1 mm)	Maio, Cape Verdes	Jan Sticklus	28.344	0.039	1.06E-03	0.08	1.0098	0.21	1	1.211E-14
C47BA065	5.00 W	18-32/3 (323bl)	Phlogopite (0.5-1 mm)	Maio, Cape Verdes	Jan Sticklus	28.344	0.039	1.06E-03	0.08	1.0098	0.21	1	1.211E-14
C47BC026	5.00 W	18-32/3 (323bl)	Phlogopite (0.5-1 mm)	Maio, Cape Verdes	Jan Sticklus	28.344	0.039	1.06E-03	0.08	1.0098	0.21	1	1.211E-14
C47BC032	5.00 W	18-32/3 (323bl)	Phlogopite (0.5-1 mm)	Maio, Cape Verdes	Jan Sticklus	28.344	0.039	1.06E-03	0.08	1.0098	0.21	1	1.211E-14
C47BA056	5.00 W	18-32/3 (323bs)	Phlogopite (0.25-0.5 mm)	Maio, Cape Verdes	Jan Sticklus	28.344	0.039	1.06E-03	0.08	1.0098	0.21	1	1.211E-14
C47BA052	5.00 W	18-32/3 (323bs)	Phlogopite (0.25-0.5 mm)	Maio, Cape Verdes	Jan Sticklus	28.344	0.039	1.06E-03	0.08	1.0098	0.21	1	1.211E-14
C47BA053	5.00 W	18-32/3 (323bs)	Phlogopite (0.25-0.5 mm)	Maio, Cape Verdes	Jan Sticklus	28.344	0.039	1.06E-03	0.08	1.0098	0.21	1	1.211E-14
C47BA051	5.00 W	18-32/3 (323bs)	Phlogopite (0.25-0.5 mm)	Maio, Cape Verdes	Jan Sticklus	28.344	0.039	1.06E-03	0.08	1.0098	0.21	1	1.211E-14
C47BA060	5.00 W	18-32/3 (323bl)	Phlogopite (0.5-1 mm)	Maio, Cape Verdes	Jan Sticklus	28.344	0.039	1.06E-03	0.08	1.0098	0.21	1	1.211E-14
C47BC030	5.00 W	18-32/3 (323bl)	Phlogopite (0.5-1 mm)	Maio, Cape Verdes	Jan Sticklus	28.344	0.039	1.06E-03	0.08	1.0098	0.21	1	1.211E-14
C47BC022	5.00 W	18-32/3 (323bl)	Phlogopite (0.5-1 mm)	Maio, Cape Verdes	Jan Sticklus	28.344	0.039	1.06E-03	0.08	1.0098	0.21	1	1.211E-14
C47BA070	5.00 W	18-32/3 (323bl)	Phlogopite (0.5-1 mm)	Maio, Cape Verdes	Jan Sticklus	28.344	0.039	1.06E-03	0.08	1.0098	0.21	1	1.211E-14
C47BC033	5.00 W	18-32/3 (323bl)	Phlogopite (0.5-1 mm)	Maio, Cape Verdes	Jan Sticklus	28.344	0.039	1.06E-03	0.08	1.0098	0.21	1	1.211E-14
C47BC029	5.00 W	18-32/3 (323bl)	Phlogopite (0.5-1 mm)	Maio, Cape Verdes	Jan Sticklus	28.344	0.039	1.06E-03	0.08	1.0098	0.21	1	1.211E-14
C47BA067	5.00 W	18-32/3 (323bl)	Phlogopite (0.5-1 mm)	Maio, Cape Verdes	Jan Sticklus	28.344	0.039	1.06E-03	0.08	1.0098	0.21	1	1.211E-14
C47BA050	5.00 W	18-32/3 (323bs)	Phlogopite (0.25-0.5 mm)	Maio, Cape Verdes	Jan Sticklus	28.344	0.039	1.06E-03	0.08	1.0098	0.21	1	1.211E-14
C47BA061	5.00 W	18-32/3 (323bl)	Phlogopite (0.5-1 mm)	Maio, Cape Verdes	Jan Sticklus	28.344	0.039	1.06E-03	0.08	1.0098	0.21	1	1.211E-14
C47BA066	5.00 W	18-32/3 (323bl)	Phlogopite (0.5-1 mm)	Maio, Cape Verdes	Jan Sticklus	28.344	0.039	1.06E-03	0.08	1.0098	0.21	1	1.211E-14
C47BA054	5.00 W	18-32/3 (323bs)	Phlogopite (0.25-0.5 mm)	Maio, Cape Verdes	Jan Sticklus	28.344	0.039	1.06E-03	0.08	1.0098	0.21	1	1.211E-14
C47BA068	5.00 W	18-32/3 (323bl)	Phlogopite (0.5-1 mm)	Maio, Cape Verdes	Jan Sticklus	28.344	0.039	1.06E-03	0.08	1.0098	0.21	1	1.211E-14
C47BA063	5.00 W	18-32/3 (323bl)	Phlogopite (0.5-1 mm)	Maio, Cape Verdes	Jan Sticklus	28.344	0.039	1.06E-03	0.08	1.0098	0.21	1	1.211E-14
C47BA064	5.00 W	18-32/3 (323bl)	Phlogopite (0.5-1 mm)	Maio, Cape Verdes	Jan Sticklus	28.344	0.039	1.06E-03	0.08	1.0098	0.21	1	1.211E-14
C47BA048	5.00 W	18-32/3 (323bs)	Phlogopite (0.25-0.5 mm)	Maio, Cape Verdes	Jan Sticklus	28.344	0.039	1.06E-03	0.08	1.0098	0.21	1	1.211E-14
C47BA058	5.00 W	18-32/3 (323bs)	Phlogopite (0.25-0.5 mm)	Maio, Cape Verdes	Jan Sticklus	28.344	0.039	1.06E-03	0.08	1.0098	0.21	1	1.211E-14
C47BA055	5.00 W	18-32/3 (323bs)	Phlogopite (0.25-0.5 mm)	Maio, Cape Verdes	Jan Sticklus	28.344	0.039	1.06E-03	0.08	1.0098	0.21	1	1.211E-14
C47BA059	5.00 W	18-32/3 (323bs)	Phlogopite (0.25-0.5 mm)	Maio, Cape Verdes	Jan Sticklus	28.344	0.039	1.06E-03	0.08	1.0098	0.21	1	1.211E-14
C47BC023	5.00 W	18-32/3 (323bl)	Phlogopite (0.5-1 mm)	Maio, Cape Verdes	Jan Sticklus	28.344	0.039	1.06E-03	0.08	1.0098	0.21	1	1.211E-14
C47BA062	5.00 W	18-32/3 (323bl)	Phlogopite (0.5-1 mm)	Maio, Cape Verdes	Jan Sticklus	28.344	0.039	1.06E-03	0.08	1.0098	0.21	1	1.211E-14
C47BA071	5.00 W	18-32/3 (323bl)	Phlogopite (0.5-1 mm)	Maio, Cape Verdes	Jan Sticklus	28.344	0.039	1.06E-03	0.08	1.0098	0.21	1	1.211E-14
C47BC024	5.00 W	18-32/3 (323bl)	Phlogopite (0.5-1 mm)	Maio, Cape Verdes	Jan Sticklus	28.344	0.039	1.06E-03	0.08	1.0098	0.21	1	1.211E-14
C47BA049	5.00 W	18-32/3 (323bs)	Phlogopite (0.25-0.5 mm)	Maio, Cape Verdes	Jan Sticklus	28.344	0.039	1.06E-03	0.08	1.0098	0.21	1	1.211E-14
C47BC025	5.00 W	18-32/3 (323bl)	Phlogopite (0.5-1 mm)	Maio, Cape Verdes	Jan Sticklus	28.344	0.039	1.06E-03	0.08	1.0098	0.21	1	1.211E-14
C47BA069	5.00 W	18-32/3 (323bl)	Phlogopite (0.5-1 mm)	Maio, Cape Verdes	Jan Sticklus	28.344	0.039	1.06E-03	0.08	1.0098	0.21	1	1.211E-14

Day	Month	Year	Hour	Min	Resist	Irradiation	Project	Experiment	Nmb	Standard Name
3	JUL	2018	1	8	1	can47	Examples	c47it5ip6_323bl	01	TCS2
29	JUN	2018	15	47	1	can47	Examples	C47BA057	02	TCS2
3	JUL	2018	1	56	1	can47	Examples	c47it5ip6_323bl	01	TCS2
3	JUL	2018	3	22	1	can47	Examples	c47it5ip6_323bl	01	TCS2
29	JUN	2018	19	57	1	can47	Examples	c47it5ip6_323bl	01	TCS2
3	JUL	2018	0	39	1	can47	Examples	c47it5ip6_323bl	01	TCS2
3	JUL	2018	3	51	1	can47	Examples	c47it5ip6_323bl	01	TCS2
29	JUN	2018	15	18	1	can47	Examples	C47BA057	02	TCS2
29	JUN	2018	13	4	1	can47	Examples	C47BA057	02	TCS2
29	JUN	2018	13	33	1	can47	Examples	C47BA057	02	TCS2
29	JUN	2018	12	35	1	can47	Examples	C47BA057	02	TCS2
29	JUN	2018	17	33	1	can47	Examples	c47it5ip6_323bl	01	TCS2
3	JUL	2018	2	54	1	can47	Examples	c47it5ip6_323bl	01	TCS2
2	JUL	2018	22	43	1	can47	Examples	c47it5ip6_323bl	01	TCS2
29	JUN	2018	22	41	1	can47	Examples	c47it5ip6_323bl	01	TCS2
3	JUL	2018	4	20	1	can47	Examples	c47it5ip6_323bl	01	TCS2
3	JUL	2018	2	25	1	can47	Examples	c47it5ip6_323bl	01	TCS2
29	JUN	2018	21	14	1	can47	Examples	c47it5ip6_323bl	01	TCS2
29	JUN	2018	12	6	1	can47	Examples	C47BA057	02	TCS2
29	JUN	2018	18	2	1	can47	Examples	c47it5ip6_323bl	01	TCS2
29	JUN	2018	20	45	1	can47	Examples	c47it5ip6_323bl	01	TCS2
29	JUN	2018	14	21	1	can47	Examples	C47BA057	02	TCS2
29	JUN	2018	21	43	1	can47	Examples	c47it5ip6_323bl	01	TCS2
29	JUN	2018	19	0	1	can47	Examples	c47it5ip6_323bl	01	TCS2
29	JUN	2018	19	28	1	can47	Examples	c47it5ip6_323bl	01	TCS2
29	JUN	2018	11	8	1	can47	Examples	C47BA057	02	TCS2
29	JUN	2018	16	16	1	can47	Examples	C47BA057	02	TCS2
29	JUN	2018	14	49	1	can47	Examples	C47BA057	02	TCS2
29	JUN	2018	16	45	1	can47	Examples	C47BA057	02	TCS2
2	JUL	2018	23	12	1	can47	Examples	c47it5ip6_323bl	01	TCS2
29	JUN	2018	18	31	1	can47	Examples	c47it5ip6_323bl	01	TCS2
29	JUN	2018	23	10	1	can47	Examples	c47it5ip6_323bl	01	TCS2
2	JUL	2018	23	41	1	can47	Examples	c47it5ip6_323bl	01	TCS2
29	JUN	2018	11	37	1	can47	Examples	C47BA057	02	TCS2
3	JUL	2018	0	10	1	can47	Examples	c47it5ip6_323bl	01	TCS2
29	JUN	2018	22	12	1	can47	Examples	c47it5ip6_323bl	01	TCS2

Irradiation Constants	Laser power	40/36(a)	%1σ	40/36(c)	%1σ	38/36(a)	%1σ	38/36(c)	%1σ	39/37(ca)	%1σ	38/37(ca)	%1σ	36/37(ca)	%1σ	40/39(k)	%1σ	38/39(k)	%1σ	36/38(cl)	%1σ	K/Ca	%1σ	K/Cl	%1σ	Ca/Cl	%1σ
C47BC027	5.00 W	295.5	0.178	0.018	35	0.1869	0.107	1.493	3	0.000702	1.71	0.000196	4.08	0.0002702	0.15	0.00073	12.33	0.01215	0.27	262.8	0.65	0.51	0	0	0	0	0
C47BA057	5.00 W	295.5	0.178	0.018	35	0.1869	0.107	1.493	3	0.000702	1.71	0.000196	4.08	0.0002702	0.15	0.00073	12.33	0.01215	0.27	262.8	0.65	0.51	0	0	0	0	0
C47BC028	5.00 W	295.5	0.178	0.018	35	0.1869	0.107	1.493	3	0.000702	1.71	0.000196	4.08	0.0002702	0.15	0.00073	12.33	0.01215	0.27	262.8	0.65	0.51	0	0	0	0	0
C47BC031	5.00 W	295.5	0.178	0.018	35	0.1869	0.107	1.493	3	0.000702	1.71	0.000196	4.08	0.0002702	0.15	0.00073	12.33	0.01215	0.27	262.8	0.65	0.51	0	0	0	0	0
C47BA065	5.00 W	295.5	0.178	0.018	35	0.1869	0.107	1.493	3	0.000702	1.71	0.000196	4.08	0.0002702	0.15	0.00073	12.33	0.01215	0.27	262.8	0.65	0.51	0	0	0	0	0
C47BC026	5.00 W	295.5	0.178	0.018	35	0.1869	0.107	1.493	3	0.000702	1.71	0.000196	4.08	0.0002702	0.15	0.00073	12.33	0.01215	0.27	262.8	0.65	0.51	0	0	0	0	0
C47BC032	5.00 W	295.5	0.178	0.018	35	0.1869	0.107	1.493	3	0.000702	1.71	0.000196	4.08	0.0002702	0.15	0.00073	12.33	0.01215	0.27	262.8	0.65	0.51	0	0	0	0	0
C47BA056	5.00 W	295.5	0.178	0.018	35	0.1869	0.107	1.493	3	0.000702	1.71	0.000196	4.08	0.0002702	0.15	0.00073	12.33	0.01215	0.27	262.8	0.65	0.51	0	0	0	0	0
C47BA052	5.00 W	295.5	0.178	0.018	35	0.1869	0.107	1.493	3	0.000702	1.71	0.000196	4.08	0.0002702	0.15	0.00073	12.33	0.01215	0.27	262.8	0.65	0.51	0	0	0	0	0
C47BA053	5.00 W	295.5	0.178	0.018	35	0.1869	0.107	1.493	3	0.000702	1.71	0.000196	4.08	0.0002702	0.15	0.00073	12.33	0.01215	0.27	262.8	0.65	0.51	0	0	0	0	0
C47BA051	5.00 W	295.5	0.178	0.018	35	0.1869	0.107	1.493	3	0.000702	1.71	0.000196	4.08	0.0002702	0.15	0.00073	12.33	0.01215	0.27	262.8	0.65	0.51	0	0	0	0	0
C47BA060	5.00 W	295.5	0.178	0.018	35	0.1869	0.107	1.493	3	0.000702	1.71	0.000196	4.08	0.0002702	0.15	0.00073	12.33	0.01215	0.27	262.8	0.65	0.51	0	0	0	0	0
C47BC030	5.00 W	295.5	0.178	0.018	35	0.1869	0.107	1.493	3	0.000702	1.71	0.000196	4.08	0.0002702	0.15	0.00073	12.33	0.01215	0.27	262.8	0.65	0.51	0	0	0	0	0
C47BC022	5.00 W	295.5	0.178	0.018	35	0.1869	0.107	1.493	3	0.000702	1.71	0.000196	4.08	0.0002702	0.15	0.00073	12.33	0.01215	0.27	262.8	0.65	0.51	0	0	0	0	0
C47BA070	5.00 W	295.5	0.178	0.018	35	0.1869	0.107	1.493	3	0.000702	1.71	0.000196	4.08	0.0002702	0.15	0.00073	12.33	0.01215	0.27	262.8	0.65	0.51	0	0	0	0	0
C47BC033	5.00 W	295.5	0.178	0.018	35	0.1869	0.107	1.493	3	0.000702	1.71	0.000196	4.08	0.0002702	0.15	0.00073	12.33	0.01215	0.27	262.8	0.65	0.51	0	0	0	0	0
C47BC029	5.00 W	295.5	0.178	0.018	35	0.1869	0.107	1.493	3	0.000702	1.71	0.000196	4.08	0.0002702	0.15	0.00073	12.33	0.01215	0.27	262.8	0.65	0.51	0	0	0	0	0
C47BA067	5.00 W	295.5	0.178	0.018	35	0.1869	0.107	1.493	3	0.000702	1.71	0.000196	4.08	0.0002702	0.15	0.00073	12.33	0.01215	0.27	262.8	0.65	0.51	0	0	0	0	0
C47BA050	5.00 W	295.5	0.178	0.018	35	0.1869	0.107	1.493	3	0.000702	1.71	0.000196	4.08	0.0002702	0.15	0.00073	12.33	0.01215	0.27	262.8	0.65	0.51	0	0	0	0	0
C47BA061	5.00 W	295.5	0.178	0.018	35	0.1869	0.107	1.493	3	0.000702	1.71	0.000196	4.08	0.0002702	0.15	0.00073	12.33	0.01215	0.27	262.8	0.65	0.51	0	0	0	0	0
C47BA066	5.00 W	295.5	0.178	0.018	35	0.1869	0.107	1.493	3	0.000702	1.71	0.000196	4.08	0.0002702	0.15	0.00073	12.33	0.01215	0.27	262.8	0.65	0.51	0	0	0	0	0
C47BA054	5.00 W	295.5	0.178	0.018	35	0.1869	0.107	1.493	3	0.000702	1.71	0.000196	4.08	0.0002702	0.15	0.00073	12.33	0.01215	0.27	262.8	0.65	0.51	0	0	0	0	0
C47BA068	5.00 W	295.5	0.178	0.018	35	0.1869	0.107	1.493	3	0.000702	1.71	0.000196	4.08	0.0002702	0.15	0.00073	12.33	0.01215	0.27	262.8	0.65	0.51	0	0	0	0	0
C47BA063	5.00 W	295.5	0.178	0.018	35	0.1869	0.107	1.493	3	0.000702	1.71	0.000196	4.08	0.0002702	0.15	0.00073	12.33	0.01215	0.27	262.8	0.65	0.51	0	0	0	0	0
C47BA064	5.00 W	295.5	0.178	0.018	35	0.1869	0.107	1.493	3	0.000702	1.71	0.000196	4.08	0.0002702	0.15	0.00073	12.33	0.01215	0.27	262.8	0.65	0.51	0	0	0	0	0
C47BA048	5.00 W	295.5	0.178	0.018	35	0.1869	0.107	1.493	3	0.000702	1.71	0.000196	4.08	0.0002702	0.15	0.00073	12.33	0.01215	0.27	262.8	0.65	0.51	0	0	0	0	0
C47BA058	5.00 W	295.5	0.178	0.018	35	0.1869	0.107	1.493	3	0.000702	1.71	0.000196	4.08	0.0002702	0.15	0.00073	12.33	0.01215	0.27	262.8	0.65	0.51	0	0	0	0	0
C47BA055	5.00 W	295.5	0.178	0.018	35	0.1869	0.107	1.493	3	0.000702	1.71	0.000196	4.08	0.0002702	0.15	0.00073	12.33	0.01215	0.27	262.8	0.65	0.51	0	0	0	0	0
C47BA059	5.00 W	295.5	0.178	0.018	35	0.1869	0.107	1.493	3	0.000702	1.71	0.000196	4.08	0.0002702	0.15	0.00073	12.33	0.01215	0.27	262.8	0.65	0.51	0	0	0	0	0
C47BC023	5.00 W	295.5	0.178	0.018	35	0.1869	0.107	1.493	3	0.000702	1.71	0.000196	4.08	0.0002702	0.15	0.00073	12.33	0.01215	0.27	262.8	0.65	0.51	0	0	0	0	0
C47BA062	5.00 W	295.5	0.178	0.018	35	0.1869	0.107	1.493	3	0.000702	1.71	0.000196	4.08	0.0002702	0.15	0.00073	12.33	0.01215	0.27	262.8	0.65	0.51	0	0	0	0	0
C47BA071	5.00 W	295.5	0.178	0.018	35	0.1869	0.107	1.493	3	0.000702	1.71	0.000196	4.08	0.0002702	0.15	0.00073	12.33	0.01215	0.27	262.8	0.65	0.51	0	0	0	0	0
C47BC024	5.00 W	295.5	0.178	0.018	35	0.1869	0.107	1.493	3	0.000702	1.71	0.000196	4.08	0.0002702	0.15	0.00073	12.33	0.01215	0.27	262.8	0.65	0.51	0	0	0	0	0
C47BA049	5.00 W	295.5	0.178	0.018	35	0.1869	0.107	1.493	3	0.000702	1.71	0.000196	4.08	0.0002702	0.15	0.00073	12.33	0.01215	0.27	262.8	0.65	0.51	0	0	0	0	0
C47BC025	5.00 W	295.5	0.178	0.018	35	0.1869	0.107	1.493	3	0.000702	1.71	0.000196	4.08	0.0002702	0.15	0.00073	12.33	0.01215	0.27	262.8	0.65	0.51	0	0	0	0	0
C47BA069	5.00 W	295.5	0.178	0.018	35	0.1869	0.107	1.493	3	0.000702	1.71	0.000196	4.08	0.0002702	0.15	0.00073	12.33	0.01215	0.27	262.8	0.65	0.51	0	0	0	0	0

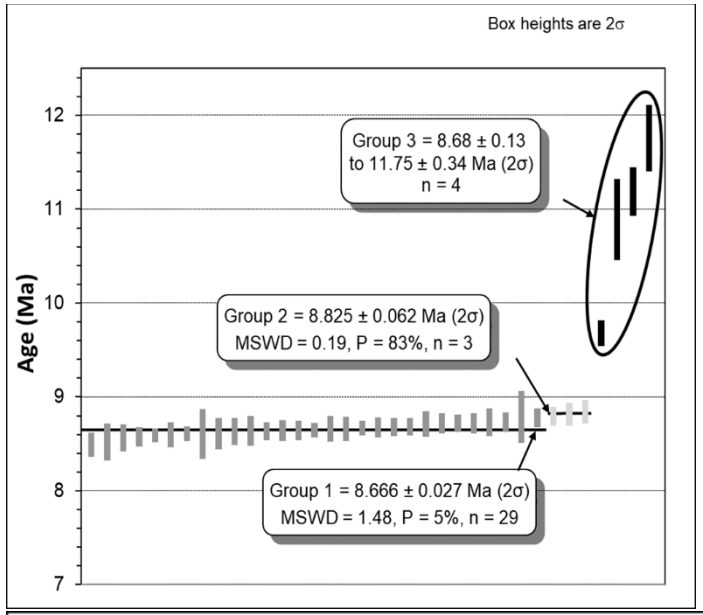
Box heights are 2σ
Age (Ma)
12
11
10
9
8
7
Group 3 = 8.68 ± 0.13
to 11.75 ± 0.34 Ma (2σ)
n = 4
Group 2 = 8.825 ± 0.062 Ma (2σ)
MSWD = 0.19, P = 83%, n = 3
Group 1 = 8.666 ± 0.027 Ma (2σ)
MSWD = 1.48, P = 5%, n = 29

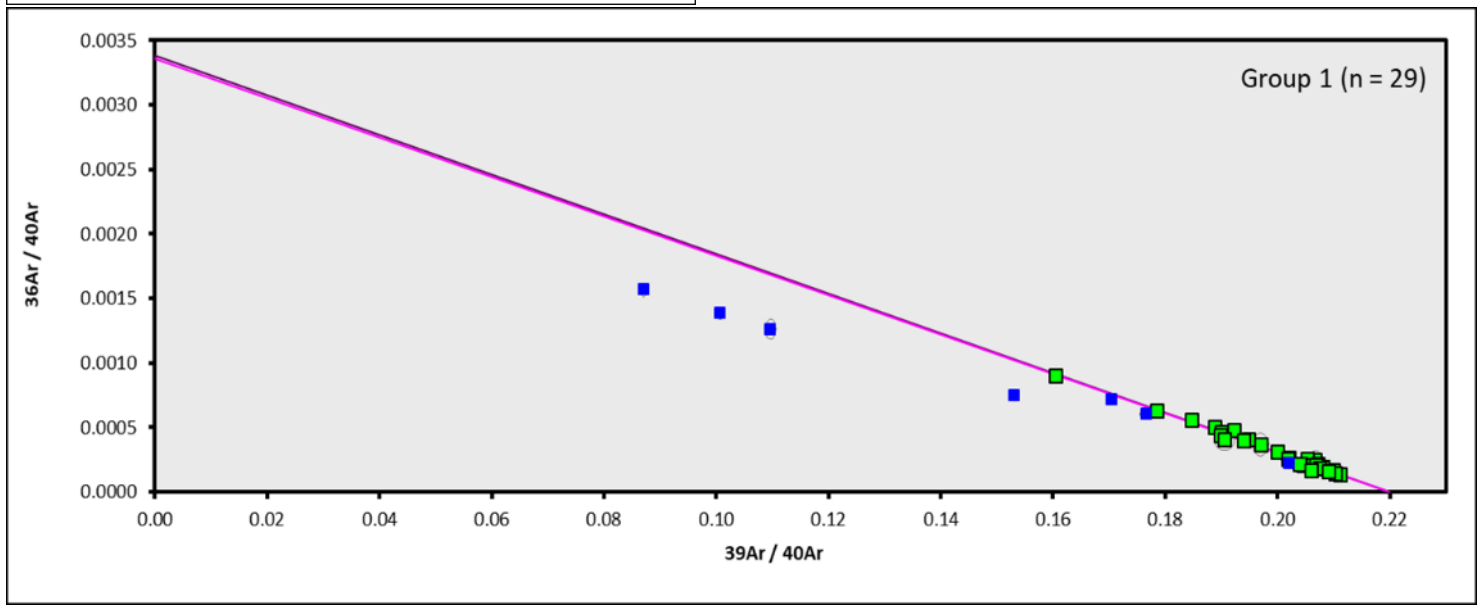
Group 1 (n = 29)
36Ar / 40Ar
0.0035
0.0030
0.0025
0.0020
0.0015
0.0010
0.0005
0.0000
0.00
0.02
0.04
0.06
0.08
0.10
0.12
0.14
0.16
0.18
0.20
0.22
39Ar / 40Ar

Information on Analysis and Constants Used in Calculations

Sample = 18-32/3 (323BL)
Material = Phlogopite
Location = Maio Cape Verdes
Analyst = Jan Sticklus
Project = EXAMPLES
Mass Discrimination Law = POW
Irradiation = can47
J = 0.00105850 ± 0.00000085
TCS2 = 28.344 ± 0.011 Ma
Experiment Type = SAMPLE
Heating = 45 sec
Isolation = 15.00 min
Instrument = MAP216

Age Equations = Conventional
Negative Intensities = Allowed
Decay Constant 40K = 5.543 ± 0.009 E-10 1/a
Decay Constant 39Ar = 2.940 ± 0.016 E-07 1/h
Decay Constant 37Ar = 8.230 ± 0.012 E-04 1/h
Decay Constant 36Cl = 2.257 ± 0.015 E-06 1/a
Atmospheric Ratio 40/36(a) = 295.50 ± 0.53
Atmospheric Ratio 38/36(a) = 0.1869 ± 0.0002
Production Ratio 39/37(ca) = 0.000702 ± 0.000012
Production Ratio 38/37(ca) = 0.000196 ± 0.000008
Production Ratio 36/37(ca) = 0.000270 ± 0.000000
Production Ratio 40/39(k) = 0.000730 ± 0.000090
Production Ratio 38/39(k) = 0.012150 ± 0.000033
Production Ratio 36/38(cl) = 262.80
Scaling Ratio K/Ca = 0.510

Results (Group 1)	40(a)/36(a) ± 2σ	40(r)/39(k) ± 2σ	Age ± 2σ (Ma)	MSWD	39Ar(k) (%,n)	K/Ca ± 2σ
SCTF Weighted Mean		4.54901 ± 0.01199 ± 0.26%	8.666 ± 0.027 ± 0.31%	1.48	81.68	5.0 ± 1.5
		Minimal External Error ± 0.038		5%	29	
		Analytical Error ± 0.023		1.53	2σ Confidence Limit	
				1.2152	Error Magnification	
Total Fusion Age		4.65203 ± 0.01115 ± 0.24%	8.862 ± 0.025 ± 0.29%		36	13.6 ± 0.1
		Minimal External Error ± 0.038				
		Analytical Error ± 0.021				
Normal Isochron	292.46 ± 12.72 ± 4.35%	4.55175 ± 0.02283 ± 0.50%	8.671 ± 0.046 ± 0.53%	1.54	81.68	
No Convergence		Minimal External Error ± 0.053		4%	29	
		Analytical Error ± 0.043		1.54	2σ Confidence Limit	
				1.2404	Error Magnification	
				100	Number of Iterations	
				0.0000750635	Convergence	
Inverse Isochron	297.37 ± 12.76 ± 4.29%	4.54635 ± 0.02282 ± 0.50%	8.661 ± 0.046 ± 0.53%	1.53	81.68	
		Minimal External Error ± 0.053		4%	29	
		Analytical Error ± 0.043		1.54	2σ Confidence Limit	
				1.2367	Error Magnification	
				3	Number of Iterations	
				0.0000005816	Convergence	
				23%	Spreading Factor	

Results (Group 2)	40(a)/36(a) ± 2σ	40(r)/39(k) ± 2σ	Age ± 2σ (Ma)	MSWD	39Ar(k) (%,n)	K/Ca ± 2σ
SCTF Weighted Mean		4.63293 ± 0.03165 ± 0.68%	8.825 ± 0.062 ± 0.70%	0.19	8.44	5.9 ± 3.0
Overestimated Error		Minimal External Error ± 0.068		83%	3	
		Analytical Error ± 0.060		3.00	2σ Confidence Limit	
				1.0000	Error Magnification	
Total Fusion Age		4.65203 ± 0.01115 ± 0.24%	8.862 ± 0.025 ± 0.29%		36	13.6 ± 0.1
		Minimal External Error ± 0.038				
		Analytical Error ± 0.021				
Normal Isochron	301.38 ± 23.11 ± 7.67%	4.61720 ± 0.06769 ± 1.47%	8.80 ± 0.13 ± 1.47%	0.17	8.44	
Overestimated Error		Minimal External Error ± 0.13		68%	3	
		Analytical Error ± 0.13		3.83	2σ Confidence Limit	
				1.0000	Error Magnification	
				1	Number of Iterations	
				0.0000163311	Convergence	
Inverse Isochron	300.69 ± 23.09 ± 7.68%	4.61957 ± 0.06756 ± 1.46%	8.80 ± 0.13 ± 1.47%	0.17	8.44	
Overestimated Error		Minimal External Error ± 0.13		68%	3	
		Analytical Error ± 0.13		3.83	2σ Confidence Limit	
				1.0000	Error Magnification	
				2	Number of Iterations	
				0.0000165924	Convergence	
				15%	Spreading Factor	

Group numbers (1-3) in table indicate selected analyses used to calculate the weighted mean, isochron and inverse isochron ages.
* Alteration Index values in *italics* indicate analyses from fresh material, normal font is from altered material (Baksi, 2007).
Values shown in red are negative values.
Abbreviations used in tables: (r) = radiogenic ^{40}Ar; (k) = Ar derived from K; (a) = atmospheric Ar; (ca) = Ar derived from Ca; (cl) = Ar derived from Cl; (c) = cosmogenic Ar; MDF = Mass Discrimination Factor.
Green squares in the inverse isochron plots indicate selected steps (blue dots in table), and blue squares are non-selected steps. Pink lines in the inverse isochron plot indicate a line fit through selected data, and the purple lines incidate a fit through an air $^{40}Ar/^{36}Ar$ ratio (295.5).

9.3.3 *Appendix C: Images of sedimentary rocks and fossils from Maio Island*

In the following section, we present field images of rocks of the Batalha, Morro, Carqueijo and Coruja Formations, as well as photographs of macrofossils, thin section images, and SEM secondary electron (SE) images of the respective rocks. The SEM images were recorded at the Institute of Geosciences and the Institute of Material Sciences at the Christian-Albrecht University of Kiel, Germany. To identify the nannofossils, we used the Nannotax3, Fossilworks and Global Biodiversity Information Facility websites (Young et al. 2017, Fossilworks.org, GBIF Secretariat 2017). The identification of the calpionellids was based on Grün and Blau (1997).

Batalha Formation

Sampling locations for the Batalha Formation intercalated sedimentary rocks

Sample	Location	Description	Coordinates	
			Latitude	Longitude
18-51	N of Mte Esgrovere	Red intercalated sediments	15°09'57.25"N	23°10'53.72"W
18-53	N of Mte Esgrovere	Brecciated dyke	15°09'54.85"N	23°11'01.81"W

Fossil content of the Batalha Formation intercalated sedimentary rocks

?*Calpionellites darderi* (Colom, 1934) Colom, 1948 (**Fig. C1f**).

Field and thin section images

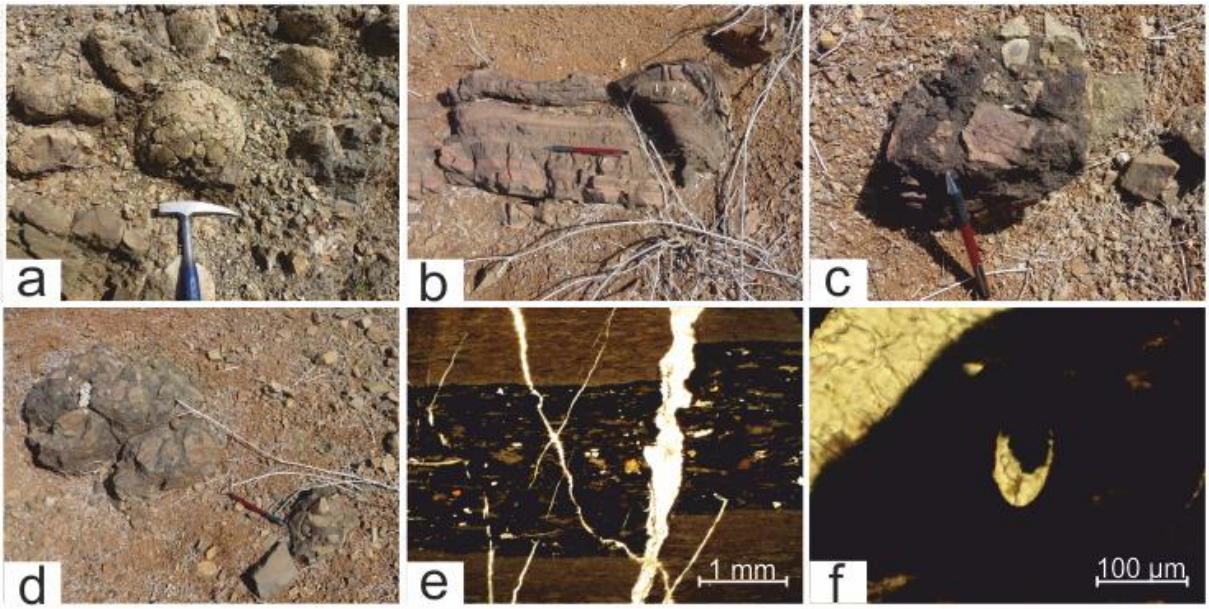

FigureC1: Batalha Formation. **a**: Pillow lava on the northern flank of Mte Branco, with hammer for scale. **b**: Red intercalated sediments in the upper Batalha Formation, N of Mte Esgrovere, with pencil for scale. **c, d**: Breccia in the upper part of the Batalha Formation, N of Mte Esgrovere, with angular fragments of altered sedimentary rocks. Pencil is shown for scale. **e, f**: Thin section images of organic-rich red intercalated sediment (Mte Esgrovere), showing a micro-fault (**e**) and ?*Calpionellites darderi* (Colom 1934) Colom 1948 (**f**).

Morro Formation

Sampling locations for the Morro Formation sedimentary rocks

Sample	Location	Description	Coordinates		Bedding (dip direction/dip)
			Latitude	Longitude	
17-75/5	N of Mte Branco	Pebble of Morro Formation limestone	15°12'14.09"N	23°07'6.78"W	
18-6	S of Mte Branco	Limestone with macrofossils	15°11'44.20"N	23°07'31.57"W	
18-14	Mte Branco	Pelagic limestone	15°11'42.47"N	23°07'14.28"W	076/36
18-42	Rib da Baia	Massive limestone with chert bands	15°11'19.85"N	23°06'30.63"W	074/23
18-62	Mte Esgrovere	Limestone with ammonites and aptychi	15°09'46.57"N	23°10'55.98"W	251/64
18-63	Mte Esgrovere	Limestone with ammonites and aptychi	15°09'38.37"N	23°10'51.74"W	245/70
18-64	Mte Esgrovere	Limestone, bioturbatetd	15°09'35.43"N	23°10'57.58"W	231/30
18-65	Rib do Morro	Limestone with ammonite remnants	15°11'1.08"N	23°12'8.58"W	264/43

Fossil content of Morro Formation rocks

Macrofossils:

- Aptychi **(Fig. C2g).**
- Ammonites:
  - *Phylloceras* cf. *infundibulum* (d'Orbigny 1840); **Fig. C2h.**
  - *Neocomites neocomiensis* (d'Orbigny 1841); **Fig. C2i.**
- Gastropods (**Fig. C3a**).
- Sponge spicule fragments.
- Echinoid fragments.
- Bivalce fragments.

Micro- and nannofossils:

- Radiolaria.
- Foraminifera.
- Calpionellids (*Tintinnopsella* cf. gr. *carpathica* (Murgeanu & Filipescu 1933) Colom 1948; **Fig. C3c**).
- *Cadosina* sp. (**Fig. C3g**).
- *Nannoconus sp.* (**Fig. C4a**).
- *Watznaueria fossacincta* (Black 1971) Bown in Bown & Cooper 1989 (**Fig. C4b**).
- *Watznaueria britannica* (Stradner 1963) Reinhardt 1964 (**Fig. C4d**).
- *Cyclagelosphaera* cf. *argoensis* Bown 1992 (**Fig. C4c).**

Images of Morro Formation rocks and samples

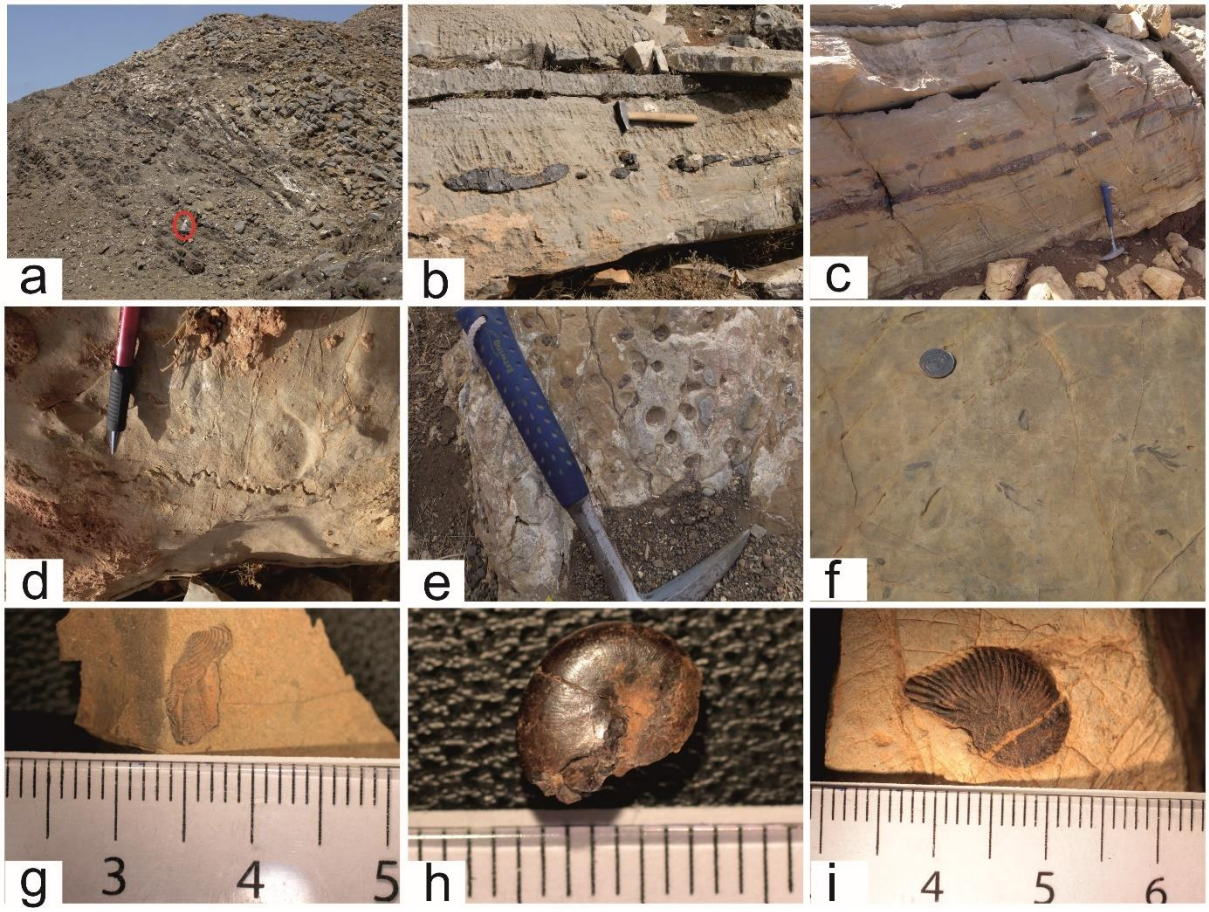

Figure C2: Morro Formation **a**: Massive pelagic limestones, intruded by dykes (left side) at Mte Branco. Person encircled in red for scale. **b, c**: Chert lenses in Morro Formation limestones at Mte Branco (**b**) and Mte Esgrovere (**c**). **d**: Stylolites in Morro limestones. **e**: Remnants of ammonites at Rib do Morro. **f**: Macrofossils at Mte Branco. **g**: Aptychus. **h, i**: Ammonites *Phylloceras* cf. *infundibulum* (d'Orbigny 1840) (**h**) and *Neocomites neocomiensis* (d'Orbigny 1841) in **i**. Hammers (**b**, **c** and **e**), a pen (**d**), and a coin (**f**) are shown for scale. In **g-i,** cm-scale (**g, i**) and mm-scale (**h**) bars are shown.

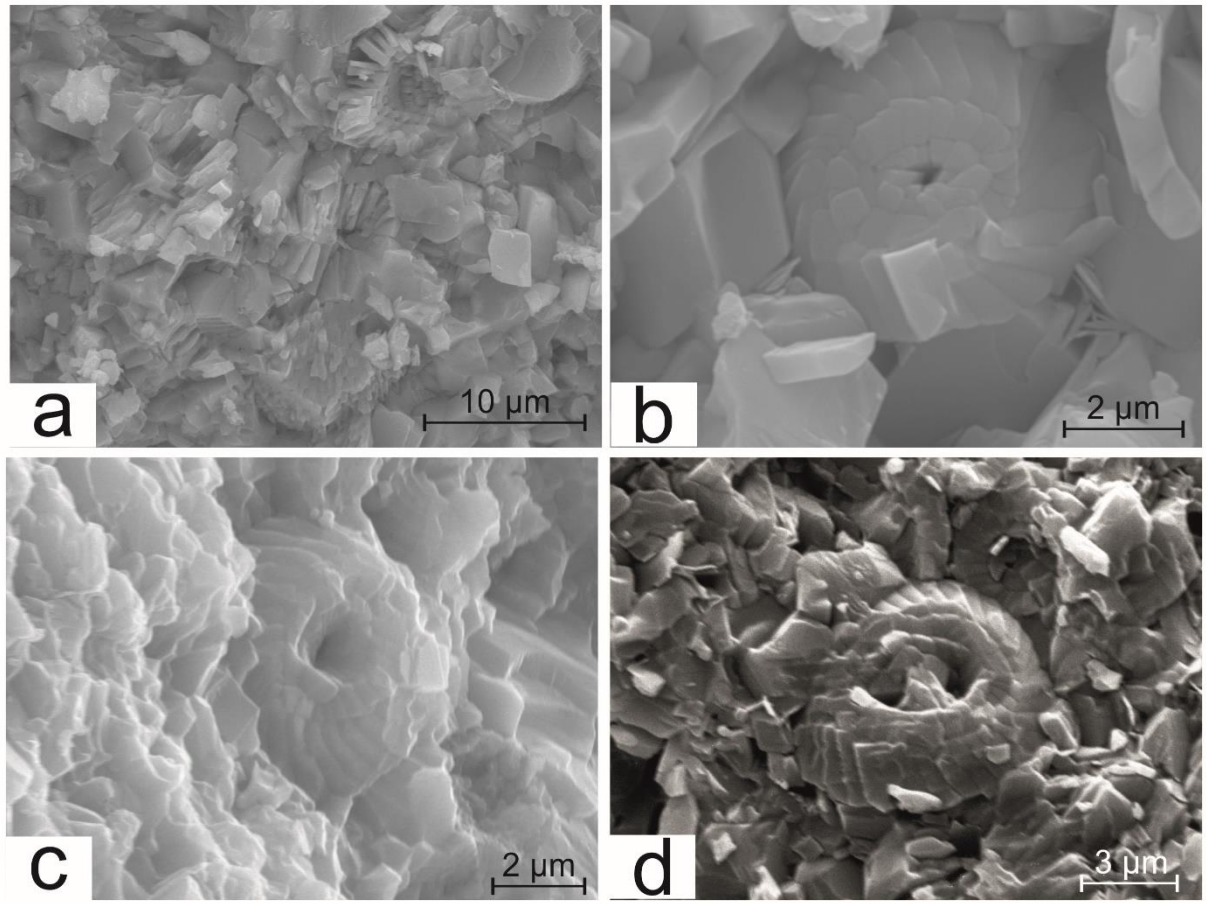

Figure C3: Thin section images of Morro Formation limestones. **a:** Gastropod and stylolites. **b**: radiolarians. **c-f**: calpionellids (*Tintinnopsella* cf. gr. *carpathica* (Murgeanu & Filipescu 1933) Colom 1948) in **c**). **g**: *Cadosina* sp. **h**: foraminifera and organic-rich seam. **i**: Radiolaria and bioturbation, containing dolomite rhombs. **Figure C4**: SEM-SE images of microfossils from the Morro Formation limestones. **a**: Remnants of *Nannoconus* sp. **b**: *Watznaueria fossacincta* (Black 1971) Bown in Bown & Cooper 1989. **c**: *Cylcagelosphaera* cf. *argoensis* Bown 1992. **d**: *Watznaueria britannica* (Stradner 1963) Reinhardt, 1964.

Carqueijo Formation and Coruja Formation

Sampling locations for the Carqueijo Formation sedimentary rocks:

Sample	Location	Description	Coordinates		Bedding (dip direction/dip)
			Latitude	Longitude	
18-40/8	N of Lomba da Vigia	Marl with iron stones above upper beds of Morro Formation	15°11'37.42"N	23°06'37.07"W	078/36
18-69	Rib do Morro	Marl with ironstones and nannofossils, just above Morro Formation	15°11'3.66"N	23°12'16.20"W	279/70

Fossil content of Carqueijo Formation rocks

Macrofossils

- Radiolaria.

Micro- and nannofossils:

- *Cyclagelospahera* cf. *argoensis* Bown 1992 (**Fig. C6a**).
- *Prediscosphaera* cf. *cretacea* (Arkhangelsky 1912) Gartner 1968 (**Fig. C6i**).
- *Zeugarhabdotus* cf. *diplogrammus* (Deflandre in Deflandre & Fert 1954) Burnett in Gale et al. 1996 (**Fig. C6h**).
- *Watznaueria* cf. *britannica* (Stradner 1963) Reinhardt 1964 (**Fig. C6b**).
- *Watznaueria* cf. *ovata* Bukry 1969 (**Fig. C6f**).
- *Watznaueria fossacincta* (Black 1971) Bown in Bown & Cooper 1989 (**Fig. C6**).
- *Watznaueria* cf. *manivitae* Bukry 1973.

Images of Carqueijo Formation and Coruja Formation rocks

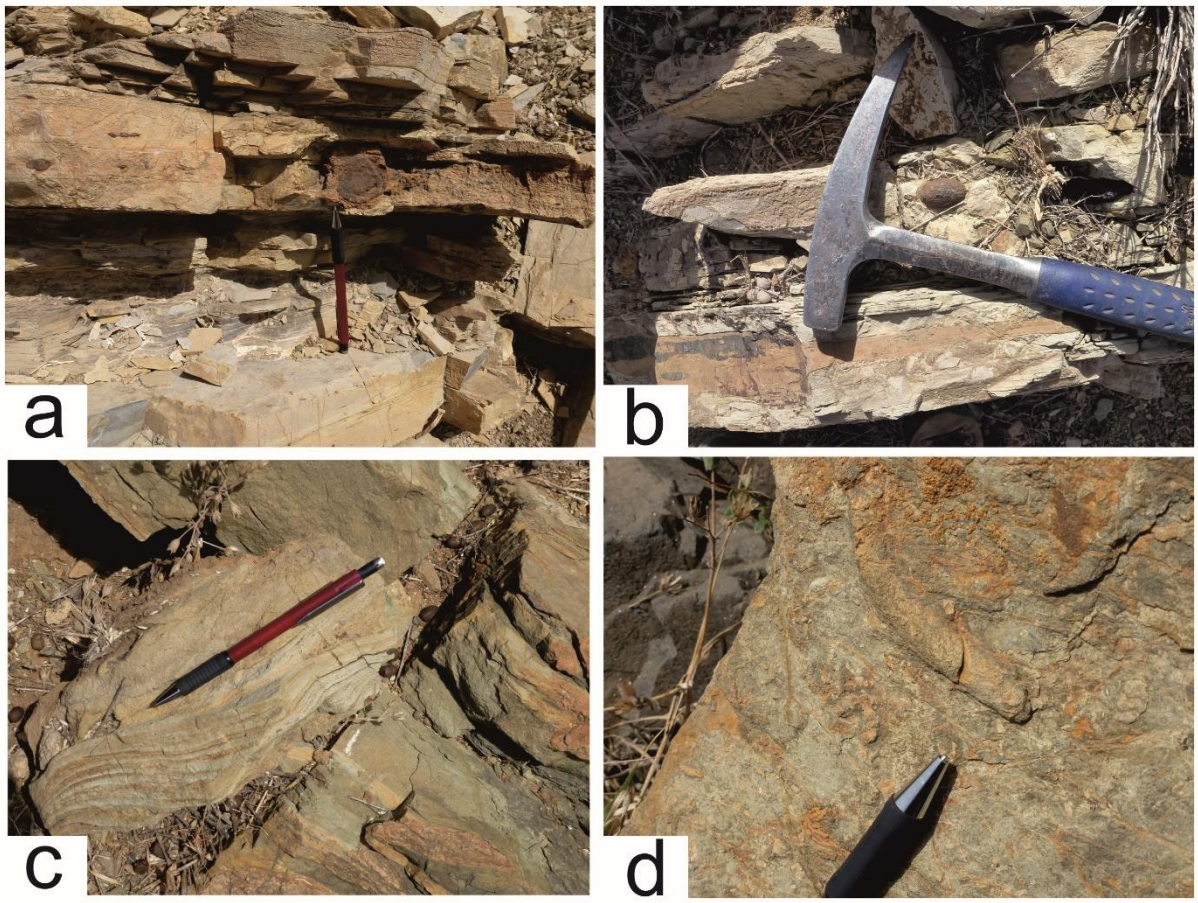

Figure C5: Marls and lime-mudstones of the Carqueijo Formation, including iron-sulfide concretions (**a, b**); and images of Coruja Formation sandstones, including burrows (**c, d**). Pens (a**, c** and d**)** and a hammer (**b**) are shown for scale.

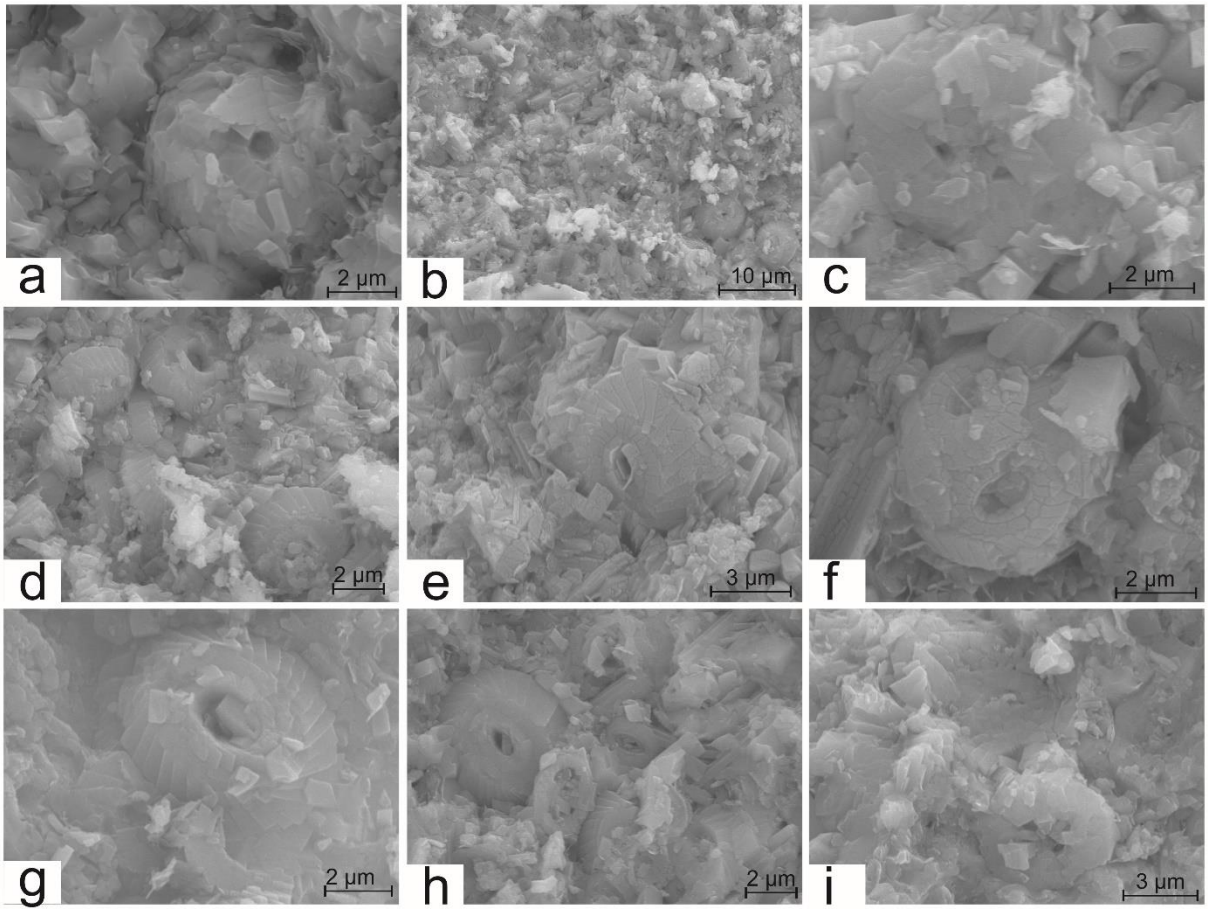

Figure C6: SEM-SE images of microfossils from the Carqueijo Formation. **a**: *Cyclagelosphaera* cf. *argoensis* Bown 1992 (Lomba da Vigia); **b**: *Watznaueria britannica* (Stradner 1963) Reinhardt 1964 (enlarged in **c**); **d**: *Watznaueria* cf. *britannica* (Stradner 1963) Reinhardt 1964 and *Watznaueria fossacincta* (Black 1971) Bown in Bown & Cooper 1989; **f**: *Watznaueria* cf. *ovata* Bukry 1969; **e, g**: *Watznaueria fossacincta* (Black 1971) Bown in Bown & Cooper 1989, **h**: *Watznaueria fossacincta* (Black 1971) Bown in Bown & Cooper, 1989 and *Zeugrhabdotus* cf. *diplogrammus* (Deflandre in Deflandre & Fert 1954) Burnett in Gale et al. 1996; **i**: *Prediscosphaera* cf. *cretacea* (Arkhangelsky 1912) Gartner 1968.

References

Fossilworks.org Paleobiology Database Fossilworks. http://fossilworks.org/bridge.pl?a=home. Accessed 25 Mar 2019

GBIF Secretariat (2017) GBIF Backbone Taxnomy. https://doi.org/10.15468/39omei. Accessed via gbif.org on 17 Jul 2021

Grün B, Blau J (1997) New aspects of calpionellid biochronology: proposal for a revised calpionellid zonal and subzonal division. Revue Paléobiol (Revue de Paléobiologie) 16(1):197–214

Young JR, Bown PR, Lees JA (2017) Nannotax3 website. http://www.mikrotax.org/Nannotax3/. Accessed 01 Apr 2019

9.3.4 *Appendix D: Lambert structural data*

Location	Type	Measurement #	Azimuth	Dip	Latitude	Longitude	Comments
Batalha Fm dykes	Batalha Fm dyke	62	322	88	15.202651	-23.1174	
Batalha Fm dykes	Batalha Fm dyke	63	129	73	15.202715	-23.1174	
Batalha Fm dykes	Batalha Fm dyke	64	333	82	15.202706	-23.1174	
Batalha Fm dykes	Batalha Fm dyke	65	34	25	15.202764	-23.1175	
Batalha Fm dykes	Batalha Fm dyke	66	79	27	15.202805	-23.1175	
Batalha Fm dykes	Batalha Fm dyke	67	57	27	15.202805	-23.1175	
Batalha Fm dykes	Batalha Fm dyke	68	56	37	15.202786	-23.1174	
Batalha Fm dykes	Batalha Fm dyke	69	70	35	15.202802	-23.1174	
Batalha Fm dykes	Batalha Fm dyke	70	327	60	15.202747	-23.1174	
Batalha Fm dykes	Batalha Fm dyke	71	328	63	15.202735	-23.1174	
Batalha Fm dykes	Batalha Fm dyke	72	92	55	15.202761	-23.1175	
Batalha Fm dykes	Batalha Fm dyke	73	310	90	15.202829	-23.1174	
Batalha Fm dykes	Batalha Fm dyke	74	60	65	15.202836	-23.1174	
Batalha Fm dykes	Batalha Fm dyke	75	56	66	15.202836	-23.1174	
Batalha Fm dykes	Batalha Fm dyke	76	48	71	15.202839	-23.1174	
Batalha Fm dykes	Batalha Fm dyke	77	27	62	15.202834	-23.1174	
Batalha Fm dykes	Batalha Fm dyke	78	47	53	15.202784	-23.1174	
Batalha Fm dykes	Batalha Fm dyke	79	135	79	15.202787	-23.1173	
Batalha Fm dykes	Batalha Fm dyke	80	103	81	15.202807	-23.1173	
Batalha Fm dykes	Batalha Fm dyke	81	114	84	15.202811	-23.1173	
Batalha Fm dykes	Batalha Fm dyke	82	104	77	15.202818	-23.1173	
Batalha Fm dykes	Batalha Fm dyke	83	93	81	15.202876	-23.1173	
Batalha Fm dykes	Batalha Fm dyke	84	92	77	15.202876	-23.1173	
Batalha Fm dykes	Batalha Fm dyke	85	287	54	15.202876	-23.1173	
Batalha Fm dykes	Batalha Fm dyke	86	278	59	15.202876	-23.1173	
Batalha Fm dykes	Batalha Fm dyke	87	287	49	15.202857	-23.1173	
Batalha Fm dykes	Batalha Fm dyke	88	110	71	15.202857	-23.1173	
Batalha Fm dykes	Batalha Fm dyke	89	10	80	15.202935	-23.1173	

Batalha Fm dykes	Batalha Fm dyke	90	339	82	15.20301	-23.1173
Batalha Fm dykes	Batalha Fm dyke	91	322	45	15.203048	-23.1173
Batalha Fm dykes	Batalha Fm dyke	92	334	53	15.203063	-23.1173
Batalha Fm dykes	Batalha Fm dyke	93	327	50	15.203063	-23.1173
Batalha Fm dykes	Batalha Fm dyke	94	335	47	15.203063	-23.1173
Batalha Fm dykes	Batalha Fm dyke	95	163	75	15.203209	-23.1173
Batalha Fm dykes	Batalha Fm dyke	96	76	41	15.203232	-23.1172
Batalha Fm dykes	Batalha Fm dyke	97	86	57	15.20323	-23.1172
Batalha Fm dykes	Batalha Fm dyke	98	93	58	15.20323	-23.1172
Batalha Fm dykes	Batalha Fm dyke	99	341	88	15.203265	-23.1172
Batalha Fm dykes	Batalha Fm dyke	100	91	51	15.203378	-23.1172
Batalha Fm dykes	Batalha Fm dyke	101	82	55	15.203378	-23.1172
Batalha Fm dykes	Batalha Fm dyke	102	79	57	15.203441	-23.1172
Batalha Fm dykes	Batalha Fm dyke	103	71	66	15.20345	-23.1172
Batalha Fm dykes	Batalha Fm dyke	104	187	71	15.203491	-23.1172
Batalha Fm dykes	Batalha Fm dyke	105	186	72	15.203491	-23.1172
Batalha Fm dykes	Batalha Fm dyke	108	90	56	15.203493	-23.1172
Batalha Fm dykes	Batalha Fm dyke	109	80	60	15.203512	-23.1171
Batalha Fm dykes	Batalha Fm dyke	110	92	77	15.203412	-23.1171
Batalha Fm dykes	Batalha Fm dyke	111	17	80	15.203318	-23.1171
Batalha Fm dykes	Batalha Fm dyke	112	8	79	15.203318	-23.1171
Batalha Fm dykes	Batalha Fm dyke	113	22	86	15.203327	-23.1171
Batalha Fm dykes	Batalha Fm dyke	114	19	83	15.203342	-23.1171
Batalha Fm dykes	Batalha Fm dyke	115	115	79	15.203336	-23.1171
Batalha Fm dykes	Batalha Fm dyke	116	122	65	15.203338	-23.1171
Batalha Fm dykes	Batalha Fm dyke	117	120	59	15.203332	-23.1171
Batalha Fm dykes	Batalha Fm dyke	118	112	68	15.203307	-23.1171
Batalha Fm dykes	Batalha Fm dyke	119	169	68	15.203307	-23.1171
Batalha Fm dykes	Batalha Fm dyke	120	167	81	15.203307	-23.1171
Batalha Fm dykes	Batalha Fm dyke	121	161	81	15.203309	-23.1171
Batalha Fm dykes	Batalha Fm dyke	122	172	82	15.203314	-23.1171

Batalha Fm dykes	Batalha Fm dyke	123	169	75	15.203274	-23.1171
Batalha Fm dykes	Batalha Fm dyke	124	171	76	15.203274	-23.1171
Batalha Fm dykes	Batalha Fm dyke	125	156	74	15.203146	-23.1171
Batalha Fm dykes	Batalha Fm dyke	126	144	78	15.203139	-23.1171
Batalha Fm dykes	Batalha Fm dyke	127	277	85	15.20315	-23.117
Batalha Fm dykes	Batalha Fm dyke	132	161	80	15.202971	-23.1171
Batalha Fm dykes	Batalha Fm dyke	133	144	82	15.202898	-23.1171
Batalha Fm dykes	Batalha Fm dyke	135	353	69	15.203017	-23.1171
Batalha Fm dykes	Batalha Fm dyke	136	355	90	15.202916	-23.1171
Batalha Fm dykes	Batalha Fm dyke	137	75	60	15.202676	-23.1172
Batalha Fm dykes	Batalha Fm dyke	138	77	59	15.202679	-23.1172
Batalha Fm dykes	Batalha Fm dyke	139	316	80	15.202637	-23.1171
Batalha Fm dykes	Batalha Fm dyke	140	77	65	15.202644	-23.1171
Batalha Fm dykes	Batalha Fm dyke	141	297	68	15.202614	-23.1173
Batalha Fm dykes	Batalha Fm dyke	142	302	52	15.202633	-23.1173
Batalha Fm dykes	Batalha Fm dyke	143	298	59	15.202633	-23.1173
Batalha Fm dykes	Batalha Fm dyke	144	301	62	15.202649	-23.1173
Batalha Fm dykes	Batalha Fm dyke	145	163	77	15.20268	-23.1173
Batalha Fm dykes	Batalha Fm dyke	146	159	85	15.202658	-23.1173
Batalha Fm dykes	Batalha Fm dyke	147	158	87	15.202658	-23.1173
Batalha Fm dykes	Batalha Fm dyke	148	155	79	15.202651	-23.1174
Batalha Fm dykes	Batalha Fm dyke	149	328	80	15.202642	-23.1174
Batalha Fm dykes	Batalha Fm dyke	150	329	86	15.202642	-23.1174
Batalha Fm dykes	Batalha Fm dyke	151	166	82	15.202681	-23.1174
Batalha Fm dykes	Batalha Fm dyke	152	148	75	15.202693	-23.1174
Batalha Fm dykes	Batalha Fm dyke	153	150	80	15.202696	-23.1174
Batalha Fm dykes	Batalha Fm dyke	154	311	71	15.202715	-23.1174
Batalha Fm dykes	Batalha Fm dyke	155	323	83	15.202748	-23.1174
Batalha Fm dykes	Batalha Fm dyke	156	325	75	15.202757	-23.1174
Batalha Fm dykes	Batalha Fm dyke	157	309	61	15.202766	-23.1174
Batalha Fm dykes	Batalha Fm dyke	158	309	65	15.202778	-23.1174

Batalha Fm dykes	Batalha Fm dyke	159	60	82	15.202827	-23.1174	
Batalha Fm dykes	Batalha Fm dyke	160	37	84	15.202826	-23.1174	
Batalha Fm dykes	Batalha Fm dyke	161	40	85	15.202826	-23.1174	
Batalha Fm dykes	Batalha Fm dyke	162	322	78	15.202782	-23.1174	
Batalha Fm dykes	Batalha Fm dyke	163	321	79	15.202782	-23.1174	
Batalha Fm dykes	Batalha Fm dyke	164	304	62	15.202782	-23.1174	
Batalha Fm dykes	Batalha Fm dyke	168	53	53	15.203926	-23.1186	Younger dyke, offsets dyke measurement # 169.
Batalha Fm dykes	Batalha Fm dyke	169	275	58	15.203905	-23.1186	Older dyke, is offset by dyke measurement # 168.
Batalha Fm dykes	Batalha Fm dyke	170	341	63	15.203132	-23.1183	Older dyke, is crosscut by dyke measurement # 171.
Batalha Fm dykes	Batalha Fm dyke	171	44	59	15.203148	-23.1182	Younger dyke that offsets dyke measuerement #170.
Mte Branco	Morro Fm bedding	18	42	44	15.196034	-23.123	
Mte Branco	Morro Fm bedding	19	32	18	15.196805	-23.1228	
Mte Branco	Morro Fm bedding	20	33	18	15.197727	-23.1226	
Mte Branco	Morro Fm bedding	22	54	29	15.199214	-23.1234	
Mte Branco	Moro Fm dyke	23	336	10	15.199719	-23.1238	
Mte Branco	Moro Fm dyke	24	7	24	15.19988	-23.1237	
Mte Branco	Morro Fm bedding	25	44	32	15.200056	-23.1238	
Mte Branco	Morro Fm bedding	26	46	28	15.200016	-23.1238	
Mte Branco	Morro Fm bedding	27	51	25	15.200148	-23.124	
Mte Branco	Morro Fm bedding	28	35	22	15.201018	-23.1242	
Mte Branco	Moro Fm dyke	29	358	21	15.20103	-23.1244	
Mte Branco	Morro Fm bedding	30	51	30	15.201402	-23.1242	
Mte Branco	Morro Fm bedding	31	35	21	15.201477	-23.1238	
Mte Branco	Morro Fm bedding	32	53	33	15.202739	-23.1247	
Mte Branco	Morro Fm bedding	33	54	44	15.194423	-23.1176	